CORA Cork Open Research Archive
Cartlann Taighde Oscailte Chorcaí

Title	The taphonomy of anurans from the Eocene Geiseltal Konservat-Lagerstätte
Authors	Falk, Daniel
Publication date	2024
Original Citation	Falk, D. 2024. The taphonomy of anurans from the Eocene Geiseltal Konservat-Lagerstätte. PhD Thesis, University College Cork.
Type of publication	Doctoral thesis
Rights	© 2024, Daniel Falk. - https://creativecommons.org/licenses/by-nc-nd/4.0/
Download date	2026-10-26 10:15:41
Item downloaded from	https://hdl.handle.net/10468/16976

UCC
University College Cork, Ireland
Coláiste na hOllscoile Corcaigh

Ollscoil na hÉireann, Corcaigh
National University of Ireland, Cork



The taphonomy of anurans from the Eocene Geiseltal Konservat-Lagerstätte

Thesis presented by

Daniel Falk, MSc
ORCiD: 0000-0001-7502-6844

for the degree of

Doctor of Philosophy

University College Cork
School of Biological, Earth and Environmental Sciences
Head of School: Prof. Astrid Wingler

Supervisors:

Prof. Maria McNamara (University College Cork, Ireland)

Dr Oliver Wings (Natural History Museum Bamberg, Germany)

2024

In unendlicher Dankbarkeit widme ich diese Arbeit zu gleichen Teilen

meinen Großeltern, Hannelore & Udo Falk und Erika & Eberhard Lenz,

und meinen Eltern, Christiane & Dirk Falk.

With infinite gratitude I dedicate this work in equal parts to

my grandparents Hannelore & Udo Falk and Erika & Eberhard Lenz

and to my parents Christiane & Dirk Falk.

Die Zeit bis zur Vervollständigung dieser Arbeit war voller Gegensätze: Deutsch and English. Heim- und Fernweh. Freude und Leid. Tag und Nacht. Freunde und Feinde. Theorie und Praxis. Diskutieren und Akzeptieren. Kampf und Frieden. Glück und Unglück. Geburt und Beerdigung. Speichern und Löschen.

Sonnenaufgang

Nächtlich Kälte ungewiss,
those icy nights, so painful cold,
hours left before the kiss.
Trauer, Tränen, Ungeduld.

Wenn sonnig Gruß erhellt den Tag,
sunshine sprinkles eyes to eyes,
no more time to chance the luck.
Ein Abschied, der im Herzen bleibt.

Auf jeden Tag geht Nacht einher.
In darkness, faith and memories,
this silent place, you'll find me there.
Mit Freude auf den Tag verwies.

Und so die Sonne strahlt aufs Neu',
sending smiles into the world.
This tiny human full of joy,
ist was ein Menschenleben währt.

Daniel Falk
May 2024

Declaration

This is to certify that the work I am submitting is my own and has not been submitted for another degree, either at University College Cork or elsewhere. All external references and sources are clearly acknowledged and identified within the contents. I have read and understood the regulations of University College Cork concerning plagiarism and intellectual property.

Digital signature of the candidate: 

Abstract

The Eocene Geiseltal fossil site is represented by ca. 50,000 fossil specimens that were recovered from open-cast lignite mines in central Germany in the early to mid-20th century. The fossils were excavated primarily from organic-rich sediments of lacustrine and fluvial deposits and are curated in the Geiseltal Collection of the Natural Sciences Collections of the Martin Luther University Halle-Wittenberg in Halle (Saale). The fossil collection includes vertebrates, invertebrates, plants and trace fossils. Despite its rich fauna and flora, the taphonomy of the biota is poorly understood. This is because the primary fossil collections, studied extensively in the early 20th century, were not accessible for study using modern techniques. The Geiseltal biota is famous for reports of three dimensionally preserved soft tissues; the subcellular anatomical details described for various soft tissues in different vertebrate groups and in the anurans in particular, represent a fidelity of preservation that is among the highest known for any Konservat-Lagerstätte. Intriguingly, the proposed mode of preservation, direct replication in silica, is not known in other fossils, but has not been verified using modern approaches. This thesis addresses these issues using quantitative taphonomic approaches, microbeam techniques (scanning electron microscopy, micro-Fourier transform infrared spectroscopy, micro-Raman spectroscopy, X-ray diffraction and synchrotron rapid scanning-X-ray fluorescence) and statistical analysis to elucidate the taphonomy of the Geiseltal anurans (i.e., frogs and toads). Critical assessment of trends in the articulation and completeness of the fossil anurans reveals a hierarchy of taphonomic controls, whereby preservation is controlled at the specimen level by the size and location of bones, by the three-dimensional configuration of joints, by the impact of predators and scavengers, by the duration of pre-depositional transport and the impact of bottom currents on the lake floor. The studied Geiseltal anurans lack most of the soft tissues reported originally; there is no evidence for preservation in silica. Instead, the only soft tissue features present are melanosome films and the anuran-specific mid-dermal Eberth-Katschenko (E-K) layer, preserved as sulfurised organic remains and as a phosphatised replacement, respectively. Multivariate analysis of geometry data of melanosomes preserved in

anurans from Geiseltal, other fossil biotas and extant anurans reveals that the evolution of melanosomes in the skin is decoupled from that of melanosomes in the eyes and internal tissues. This most likely reflects disparate physiological constraints on melanosome function since the Middle Eocene. In summary, comparison of the taphonomy of the Geiseltal anurans with fossils from other lacustrine Konservat-Lagerstätten reveals that the skeletal and soft tissue features of the Geiseltal anurans are not unique. The mode of preservation of the Geiseltal anurans also applies to anurans from other lacustrine Konservat-Lagerstätten, revealing high-level controls on the preservation of anurans in the fossil record. The major controls on skeletal taphonomy are the broad palaeoclimatic setting, which controls lake water temperature, lake physiography, which controls the lake depth and lake size and anatomy, which control the size and location, respectively, of bones. These results potentially apply to other vertebrate groups. The major controls on the preservation of anuran soft tissues are the availability of phosphate ions and reduced sulfur species, the development of microenvironments during decay and the tissue chemistry. This thesis highlights the power of combining quantitative, analytical and comparative approaches to assess the skeletal and soft tissue taphonomy of fossil vertebrates in order to develop models for the preservation of fossil vertebrates in lacustrine environments. This thesis also demonstrates that comparative analysis of melanosome data from fossil and extant specimens in a single vertebrate group can inform on the evolution of melanin in that group. Finally, scientific investigation of fossil collections using modern analytical techniques is essential to critically re-evaluate both historical fossil interpretations and established scientific paradigms.

Contents

Declaration **3**

Abstract **4**

List of figures **9**

List of tables **15**

Foreword and acknowledgements **16**

Outline **24**

1. Introduction **26**

1.1 Taphonomy 26

1.2 Lagerstätten 30

1.3 Soft tissue preservation 33

1.3.1 Modes of soft tissue preservation 33

1.3.2 Melanosomes in the fossil record 36

1.3.3 Vertebrate integument in the fossil record 40

1.4 Fossil anurans 42

1.5 The Geiseltal Konservat-Lagerstätte and Geiseltal Collection 46

1.6 Aims of this thesis 51

1.6.1 Identification of patterns in skeletal taphonomy 51

1.6.2 Testing the historic taphonomic models for soft tissue preservation 52

1.6.3 Investigating the anuran melanosomes 52

2. Material and methods **54**

2.1 Fossil specimens 54

2.2 Light microscopy 56

2.3 Sampling and sample preparation 57

2.4 Scanning electron microscopy (SEM) and energy-dispersive X-ray spectroscopy (EDS) 60

2.5 Micro-Fourier-transform infrared spectroscopy (μ-FTIR) 64

2.6 Micro-Raman spectroscopy (μ-RS) 67

2.7 Electron probe microanalysis (EPMA) 70

2.8 X-ray diffraction (XRD) 72

2.9 Synchrotron rapid scanning-X-ray fluorescence (SRS-XRF) 74

2.10 Quantitative taphonomy 76

2.11 Statistical analysis 77

2.12 Melanosome measurements 79

3. The skeletal taphonomy of anurans from the Eocene Geiseltal Konservat-Lagerstätte, Germany: insights into the controls on fossil anuran preservation 81

3.1 Introduction 83

3.2 Geological setting 85

3.3 Material and method 90

3.4 Results 102

3.5 Discussion 114

3.6 Conclusion 133

3.7 Data archiving statement 134

3.8 Acknowledgements 134

3.9 Author contributions 134

3.10 References 135

3.11 Supporting information 152

4. Fossilized anuran soft tissues reveal a new taphonomic model for the Eocene Geiseltal Konservat-Lagerstätte, Germany 175

4.1 Introduction 176

4.2 Results 179

4.3 Discussion 185

4.4 Methods 197

4.5 Data availability 201

4.6 References 201

4.7 Acknowledgements 210

4.8 Author contributions 211

4.9 Competing interests 211

4.10 Supplementary information 211

5. Evolutionary constraints on anuran melanin for 45 million years 232

5.1 Introduction 233

5.2 Results 237

5.3 Discussion 250

5.4 Limitations of the study 255

5.5 Acknowledgements 255

5.6 Author contributions 256

5.7 Declaration of interests 256

5.8 References 256

5.9 Star Methods 266

5.10 Supplemental information 273
6. Discussion 314
6.1 Recurring taphonomic trends in anuran preservation 314
6.2 The death of the Geiseltal anurans was likely mating-related 316
6.3 The soft tissues from the Geiseltal anurans are sulfurised and replicated in calcium phosphate 318
6.4 Melanosomes from the Geiseltal anurans show tissue-specific geometries 324
6.5 Melanosomes show evolutionarily conserved geometries 328
6.6 Comparative taphonomy of anurans from Geiseltal and Libros 330
6.7 Limitations and biases 334
7. Concluding remarks 344
7.1 Conclusions 344
7.2 Future perspectives 346
7.3 Closing words: Long live the frog king! 349
8. References 352
Appendix 379
Appendix I – Lists
Sample list
Geiseltal Collection specimen requests
Appendix II – Supplementary papers
Supplementary paper 1: Die eozänen Froschlurche der Geiseltal-Sammlung – Interdisziplinäre Zugänge zum Rätsel der Fossilerhaltung
Supplementary paper 2: Der mysteriöse Tod der Frösche des Geiseltales/Sachsen-Anhalt im Mitteleozän
Appendix III – Datasets
Supplementary datasets 1–3

List of figures

Figure 1.1: Anuran anatomy. A, Schematic of skeletal elements and soft tissues of the anuran body. B, Photograph in false colours of the skeleton of the largest anuran specimen (Pelobatidae; GMH Ce II-4949-1930) in the Geiseltal Collection. The skeleton of this specimen is near-complete and well-articulated. Photograph: D. Falk. Modified after Falk & Stache 2021..... 43

Figure 1.2: Photographs of fossil anurans from several Palaeogene and Neogene biotas. A, Anuran from the Geiseltal biota (Eocene, Germany) conserved in nitrocellulose lacquer, Palaeobatrachidae, Natural Sciences Collections, Halle (Saale), Germany. B, Anuran from the Bechlejovice biota (Oligocene, Czech Republic) conserved in host sediment, Palaeobatrachidae, National Museum, Prague, Czech Republic. C, Anuran from the Messel biota (Eocene, Germany) conserved in resin, Pelobatidae, Natural History Museum, Brussels, Belgium. D, Anuran from the Libros biota (Miocene, Spain) conserved in host sediment, Ranidae, Natural History Museum, London, United Kingdom. Photographs: A, C, D. Falk. B, M. McNamara. D, V. Rossi. 45

Figure 1.3: Photographs of fossil specimens from the Geiseltal Collection. A, Alligatoroid crocodilian (Diplocynodon) in paraffin wax; the arrowhead indicates a cluster of gastroliths (stomach stones). B, Fish (Thaumaturus spannuthi) with soft tissue preservation in the eyespot and the body cavity; the specimen is conserved in nitrocellulose lacquer. C, Near-complete and articulated skeleton of the tapir-like ungulate (Lophiodon); the specimen is conserved in gypsum. D, Angiosperm leaf with insect feeding traces on the lower left leaf margin; the specimen is conserved in the original sediment. E, Artiodactyl mammal (Amphirhagatherium) with preserved soft tissues in the body cavity; the specimen is conserved in paraffin wax; Photographs: A, O. Wings. B–E, D. Falk. 49

Figure 2.1: Photograph, X-ray image and hand drawing of an incomplete anuran from the Geiseltal Collection (Pelobatidae), GMH Ce III-6728-1932. A, Photograph showing the specimen conserved in nitrocellulose lacquer with dark body outline in the torso, abdomen and limbs. B, X-ray image of the specimen reveals the skeletal elements. C, Schematic hand drawing of the specimen skeleton with notes on the soft tissue textures and sediment patches that are present on the slab. Modified after Falk & Stache 2021. Photograph and drawing: D. Falk. X-ray image from Kuhn (1941). 56

Figure 2.2: Photographs of the sampling of fossil soft tissues from the Geiseltal anurans, of the sediment sample preparation and of certain sediment and soft tissue samples. A, Sampling of fossil anuran soft tissues performed by D. Falk using sterile metal scalpels and forceps. B, Scanning electron microscope aluminium stubs with fossil soft tissue samples, each ca. 0.5 x 0.5 mm, on carbon sticky tape. C, Homogenisation of sediment samples with an agate pestle and mortar. D, Selected sediment samples in glass vials. Photographs: D. Falk. 59

Figure 2.3: A selection of photographs of in-house techniques that were used for the analysis of the Geiseltal fossils in this thesis; Mary Ward Microbeam Laboratory, School of Biological, Earth and Environmental Sciences. A, Scanning Electron Microscope with BSE and EDS detector; JEOL JSM IT100 VP-SEM. B, Au sputter coater (left) and C sputter coater (right); both Agar Scientific SEM Sputter Coater with pumping system. C, Fourier-transform infrared spectrometer with attenuated total reflectance

attachment; Perkin Elmer Spotlight 400i ATR-FTIR. D, Raman spectrometer; Renishaw InVia Qontor. Photographs: D. Falk. 64

Fig. 3.1: Palaeogeography of the Eocene Geiseltal Lagerstätte (modified after Storch 1986; Hastings & Hellmund 2015b; Scotese 2016). 85

Figure 3.2: Stratigraphy of the Geiseltal Lagerstätte (modified after Haubold & Hellmund 1998). Geiseltal sequence and anuran sites. Inset shows stratigraphic section of the interval containing site CeII ('dying field 1'), drawn using data from Raupach (1948). *Note that CeII/CeIII was originally assigned to UMC by Krumbiegel (1962a). Also note that the mammal biochronology data for the Geiseltal strata (MP) are not universally accepted (Ring et al. 2020). Abbreviations: BC, basal coal; BHM, basal 'Hauptmittel' ('Hauptmittel': intercalated sandy and silty successions); Ce, 'Cecilie' pit; Gr., Grauvian; IL, 'Geiselröhlitz' site; Leo, 'Leonhard' pit; LHM, lower 'Hauptmittel'; LLC, lower lower coal; LMC, lower middle coal; LUC, lower upper coal; MHM, middle 'Hauptmittel'; MUC, middle upper coal; Ns, 'Neumark-South' pit; Nw, 'Neumark-West' pit; UHM, upper 'Hauptmittel'; ULC, upper lower coal; UMC, upper middle coal; UUC, upper upper coal; v, varve-like; Ypr., Ypresian. 1; 6, carbonate bed; 2, dark lignites rich in insect fossils ('black coal'); 3, lignites rich in vertebrate fossils (site CeII, dying field 1); 4, lignites; 5, laminated lignites/dysodile coal ('Blätterkohle'). Scale bar in inset represents 0.3 m. 87

Figure 3.3: Variation in completeness and articulation among the Geiseltal anurans. Some specimens are truncated by the edge of the slab or embedding medium (arrows). Specimens belong to truncation categories T0–T4; untruncated specimens were assigned to a taphonomic state (for details see text). All slabs retain patches of dark organic-rich host sediment. Interpretative line drawings are shown in Fig. S3.2. A, Ce III-6735-1932; incomplete, near-fully-articulated, T2. B, Ce II-4949-1930; near-complete, near-fully articulated with patches of sediment (apparent as dark polygons), T0, States 1, 9. C, Ce III-6728-1932; near-complete, partially articulated (the urostyle is shifted to the left), potential coprolite (star), T0, States 1, 7, 8. D, Ce IV-4953-1933; accumulation of mostly disarticulated bones, T0, States 4, 9. E, Ce III-6720-1932; incomplete, partially articulated anterior body, T0, States 3, 9. F, Ce III-6719-1932; near-complete, near-fully articulated, T2. G, Ce I-4947-1930; incomplete, lacking limbs, near-fully articulated, T0, States 2, 9. H, Ce III-6742-1932; incomplete, near-fully articulated, T4. I, IL 17A-1969; disarticulated and reorientated vertebrae and possible limb elements, T0, States 5, 9. J, Ce III-6737-1932; incomplete, near-fully-articulated foot showing digits I to V and several phalanges, States 6, 9. All scale bars represent 10 mm. 92

Figure 3.4: Truncation. A–E, Truncation categories for the Geiseltal anurans. A, T0: no bones truncated. B, T1: 0.1–24.9% of bones truncated. C, T2: 25–49.9% truncation. D, T3: 50–74.9% truncation. E, T4:75–100% truncation). F–H, Impact of truncation on completeness and articulation. F, hand is not truncated and includes ten phalanges (in black outline). G, H, hand is truncated by the edge of the slab (thick zigzag line). G, truncated hand lacks five phalanges, which are omitted from the study. The presence of five out of a measurable total of five phalanges thus results in a completeness value of 100%; this is the preferred approach for calculating completeness used in this study. The alternative approach is to include the bones truncated by the slab in the study but code them as 'absent' (Fig. S3), in which case the presence of five of ten phalanges yields a completeness value of 50%. This approach potentially biases specimen completeness to lower values and is rejected in this study. H, edge passes through three phalanges; these bones are coded as present, whereas bones beyond the edge are omitted... 98

Figure 3.5: Impact of truncation on the percentage completeness of individual specimens. A–C, specimen completeness for the entire dataset; D–H, specimen completeness for truncation categories. A, no elements omitted from the dataset. B, phalanges omitted. C, entire hands and feet omitted. D, T0 (no truncation). E, T1 (0.1–24.9% truncation). F, T2 (25%–49.9% truncation). G, T3 (50%–74.9% truncation). H, T4 (75%–100% truncation). Horizontal lines in boxplots denote median value. 103

Figure 3.6: Schematic frog skeleton summarizing the percentage completeness and articulation values for each type of skeletal element in the Geiseltal anurans (n = 140); a black and white version of this figure is provided in the Supporting Information (Fig. S3.6). 106

Figure 3.7: Percentage completeness of skeletal elements. A, percentage of specimens in the dataset for which each skeletal element is complete, i.e. represented by at least one element. For example, the completeness value for the femur is 93%; this indicates that 93% of specimens have at least one femur. B, percentage of skeletal elements present (i.e., complete), based on the total number of those elements in the dataset. For example, the completeness value for the femur is 84%; this indicates that 84% of all femura are present..... 107

Figure 3.8: Impact of truncation on the percentage articulation of individual specimens. A–C, specimen articulation for the entire dataset; D–H, specimen articulation for truncation categories. A, no elements omitted from the dataset. B, phalanges omitted. C, entire hands and feet omitted. D–H, Specimens in truncation categories T0 (no truncation; D), T1 (0.1–24.9% truncation; E), T2 (25%–49.9% truncation; F), T3 (50%–74.9% truncation; G), T4 (75%–100% truncation; H). Horizontal lines in boxplots denote median value. 109

Figure 3.9: Percentage articulation versus percentage completeness for each specimen (n = 140). . 110

Figure 3.10: Percentage articulation of joints. A, percentage of specimens in the dataset for which each joint is articulated, i.e. represented by at least one articulated element. For example, the articulation value for the femur-tibiofibula (knee joint) is 96%; this indicates that at least one knee joint is articulated in 96% of specimens. B, percentage of articulated joints, based on the total number of those joints in the dataset. For example, the value for the femur-tibiofibula joint is 80%; this indicates that 80% of all knee joints in the dataset are articulated..... 112

Figure 3.11: Distinct qualitative patterns in disarticulation and loss of skeletal elements in Geiseltal specimens reveal the controls on preservation and taphonomic pathways (A–E) in sinkhole and dying field deposits. See text for detailed characterisation of taphonomic states (1–9). States 1 to 3 form a genetically related sequence that represents the progressive disarticulation and loss of elements from distal to proximal body regions with potential transitions to States 4, 5 and / or 6. States 7, 8 and 9 may be superimposed on any of the other taphonomic states. 115

Figure 3.12: Controls on preservation for anurans in lacustrine-hosted Cenozoic biotas. A, fossils are more complete and articulated when carcasses were deposited during cooler climatic phases in deep, cool lakes, with inhibited scavenging, bank vegetation and / or post-depositional disturbance. B, fossils are usually less complete and articulated when carcasses were deposited during warmer climatic phases in shallow, warm lakes, with scavengers present, pronounced bank vegetation and powerful post-depositional disturbance. 132

Figure 4.1: Soft tissue preservation in anurans from the Eocene Geiseltal biota. (a–b) Photographs of specimens showing extensive soft tissues, visible as a cream-colored friable material and/or a dark brown material. Boxes indicate regions shown in (c), (d) and (f). Insets show color-coded line drawings of the bones; Legend in (a) also applies to (b). (a) GMH CeIII-6698-1932 (Pelobatidae). The two parallel linear features crossing the torso are preparation artefacts. (b) GMH CeIII-6743-1932 (Pelobatidae). (c–f) Light micrographs showing details of the soft tissues. (c) Cream-colored, friable material overlain by thin brown material. (d) Dark grey-brown sediment (s) overlain by brown material and, in turn, the cream-colored material. Sediment and brown material are superficially similar in hand specimen but are readily distinguished using light microscopy and especially SEM. (e) GMH CeIII-4936a-1932 (Pelobatidae). Orange material with a striking honeycomb texture occurs in two layers, separated by a thick, blocky, dark brown material. (f) Pale, homogenous material in the cranium. b, bone, br, brown material, r, resin, s, sediment, sr, region sampled by Voigt. 181

Figure 4.2: Succession of soft tissue layers in the Geiseltal anurans. (a) CeIII-4967-1932 (Pelobatidae). Backscatter electron image of a fractured sample of soft tissue. Not all soft tissue layers are continuous across the entire area of the sample. Bright-toned region in left center of image shows Layer 2 in ventral aspect, overlain by dark-toned Layer 1 (in right of image), which, in turn, is overlain by Layer 2. (b) Schematic vertical section of soft tissues. Layer 1 is sandwiched between two layers of Layer 2. Layer 2 comprises a thin, outer, amorphous sublayer (2a) underlain by a thicker fibrous sublayer (2b) and, in turn, an innermost sublayer defined by closely spaced crystal globules (2c). Layer 1 comprises an outer amorphous sublayer (1a) and an inner sublayer with zones of densely packed microbodies alternating with zones with rare microbodies (1b). c, position of centrifugal fibers. 183

Figure 4.3: Electron micrographs of soft tissues in the Geiseltal anurans. (a–c), Backscatter electron images showing Layer 1 (dark tones) and Layer 2 (bright tones). (d–n), Secondary electron images (d,e,i,j,k,m,n) and backscatter electron images (f,g,h,l) showing microstructures. (a) Successive layers showing continuous amorphous outer surface of Layer 2 (Sublayer 2a) underlain by Sublayer 1a, in turn underlain by Sublayer 1b; Sublayers 1a and 1b show polygonal cracking. The plane of splitting has exposed Sublayer 2c locally where Sublayers 2a and 2b separated into the counterpart. (b) Inner surface of Layer 2 showing curved to sinuous fibers of Sublayer 2b, overlain by Sublayer 1b (top of image). (c) Layer 2 underlain by Layer 1. (d) Detail of region indicated in c showing Layer 2 underlain by Layer 1. Layer 2 comprises small irregular granules that are often juxtaposed or conjoined. Layer 1 comprises round microbodies. (e) Detail of region indicated in (a), showing outer surface of Layer 2 with distinctive dimpled texture; see (i) for detail. Microbodies occur on the layer surface and in surface cavities. (f) Sinuous fibers of Layer 2 (Sublayer 2b) crudely defined by irregular globules of calcium phosphate (see j and k). (g) Detail of region indicated in (b). (h) Backscatter electron micrograph showing alternating microbody-poor (arrows) and microbody-rich sublayers in Layer 1 in the torso. (i) Detail of region indicated in e showing dimpled outer surface of Layer 2. (j) Detail of the fibers in Sublayer 2b showing closely spaced to juxtaposed, irregular, poorly defined globules with similar nanotexture to those in Sublayer 2c. (k) Close-up of individual globule from Sublayer 2c showing irregular surface and margins, with a poorly defined fibrillar nanotexture. (l), Detail of (h). Transition of microbody-rich to -poor sublayer in Layer 1. (m) Microbodies from Layer 1 in the torso. (n) Densely packed euhedral crystals comprising pale material in cranium. (a,e,f,i,k,m) GMH CeIII-4967-1932; (c,b,d,g,n) GMH CeIII-6698-1932; (h,j,l), GMH CeIII-4936a-1932. 186

Figure 4.4: Chemical mapping of the soft tissues of GMH CeIII-4967-1932; see Methods for analytical parameters. (a–b) Backscatter electron images showing Layers 1 and 2. (a) shows Sublayers 1b, 2b and 2c. (b) shows Sublayers 1a and 2c. Elongate features on the sample surface are interpreted as fungal

contaminants (arrowheads). (a) Sublayers 2b and 2c are enriched in Ca, P and O and, to a lesser extent, F. Sublayer 1b is enriched in C and S. (b) Irregular globules of Sublayer 2c (see also Fig. 4.3k) are enriched in Ca, P and O and, to a lesser extent, F. Sublayer 1a is enriched in C and S. 190

Figure 4.5: FTIR spectroscopy of the mineral phase that replicates the E-K Layer (GMH CeIII-4936a-1932; Pelobatidae). The FTIR spectrum of the E-K layer (red) shares several bands with spectra of carbonated hydroxyapatite (CHAp25M) and carbonated fluorhydroxyapatite (CFAp530). The peaks at 1509 cm^{-1}, 1242 cm^{-1}, 1180 cm^{-1}, and 828 cm^{-1} probably derive from the embedding resin (modified from Antonakos et al.[30]). 193

Figure 4.6: Taphonomic model for the preservation of the E-K layer in the Geiseltal anurans. 195

Figure 5.1: Electron micrographs of melanosomes preserved in fossil anuran soft tissues. (A–L) Fossil melanosomes from different body regions of specimens from Geiseltal (Eocene, Germany, A–F), Bechlejovice (Oligocene, Czech Republic, G–H) and Libros (Miocene, Spain, I–L). (A–C, G, I) Fossil melanosomes from the eyespots. (D, J) Fossil melanosomes from the torso. (E, K) Fossil melanosomes from the abdomen. (F, H, L) Fossil melanosomes from the skin. (A) Layer of ovoid melanosomes overlain by a layer of rod-shaped melanosomes, GMH CeIII-4983-1932. (B) Rod-shaped melanosomes and ovoid melanosomes, GMH CeIII-4983-1932. (C) Ovoid melanosomes, GMH CeIII-6698-1932. (D) Spheroidal melanosomes, GMH CeIII-4967-1932. (E) Spheroidal and ovoid melanosomes, GMH CeIII-4967-1932. (F) Ovoid melanosomes, GMH CeIII-4967-1932. (G) Ovoid melanosomes, NHML-OR35184. (H) Ovoid melanosomes (arrowheads), NHML-OR35184. (I) Rod-shaped melanosomes and ovoid melanosomes, NHML-R4982. (J) Ovoid melanosomes, NHML-R4982. (K) Ovoid melanosomes, NHML-R4982. (L) Ovoid melanosomes, MNCN 63798. 234

Figure 5.2: Melanosomes from soft tissues of extant anurans. (A) Eye, Bombina variegata. (B) Eye, Rhaebo guttatus. (C) Gonads, Bombina variegata. (D) Gonads, Rhaebo guttatus. (E) Liver, Xenopus laevis. (F) Liver, Rhaebo guttatus. (G) Lungs, Xenopus laevis. (H) Skin, Rhaebo guttatus. (I) Skin, Xenopus laevis. 236

Figure 5.3: Scatterplots showing the morphospace for melanosomes from fossil and extant anurans. Fossil data are for various body regions of fossil anurans from the Geiseltal, Bechlejovice and Libros biotas; extant data are for various organs. (A–B) Convex hulls are used to visualise the morphospace for the total dataset and for the eyes/eyespots. (C–F) 95% confidence ellipses are used to visualise the morphospace for each tissue / body region. Schematic frog skeleton indicates the sampling region for melanosomes from fossil anurans. (A) Morphospace of the total dataset. (B) Morphospace of melanosomes from the eyespots of fossil specimens and eyes of extant specimens. (C) Morphospace of melanosomes from fossil skin and skin from extant anurans. (D) Morphospace of melanosomes from the torso of fossil specimens and from the lungs of extant specimens. (E) Morphospace of melanosomes from the abdomen of fossil specimens and from the liver of extant specimens. (F) Morphospace of melanosomes from the abdomen of fossil specimens and from the gonads of extant specimens. 241

Figure 5.4: Principal Components Analysis (PCA) of geometry data for melanosomes from different body regions of fossil and extant anurans. Data point labels use upper case to denote biota and lower case, body region as indicated in (C), e.g., Ge denotes Geiseltal eyespot. pop1, population 1; pop2, population 2. Data for specimen GMH CeIII-4967-1932 are included in the Geiseltal data and are shown

separately. (A) Non-standardised dataset; the biplot in the bottom of the morphospace plot shows that most of the morphological variation is driven by the mean and interquartile range of melanosome length. The vectors for the variables 1, 3, 4, 5, 7 and 8 are too small to be displayed at this scale. (B) Standardised dataset; the biplot in the bottom of the morphospace plot shows that most of the morphological variation is driven by the skew, mean and kurtosis of melanosome aspect ratio. Most data points plot closely to each other and the morphospace of abdomen, skin and torso show an extensive overlap. Discrimination between skin and non-integumentary tissues is only possible for eye tissues / eyespots. This PCA does not yield meaningful results. (C) Legend for (A) and (B). 244

Figure 5.5: Synchrotron rapid scanning-X-ray fluorescence (SRS-XRF) analysis of GMH CeIII-4967-1932 from the Eocene Geiseltal biota. (A) Truncated photograph of the specimen showing extensive soft tissues, visible as a beige-coloured material and/or a dark brown material in the torso and around the hindlimbs. Arrowheads indicate sample locations; s, sediment, St1, sampling location 1 in torso, St2 sampling location 2 in torso, l, lacquer. Scale in (A) also applies to (B–H). (B, C) SRS-XRF tricolour maps of the region shown in (A). (D–H) Maps for selected principal components (PCs) identified during principal component analysis of the SRS-XRF data (see Methods). PC 1 corresponds primarily to Ca, Ni and Sb. PC 2 corresponds primarily to Fe. PC 4 corresponds to Co and Cu. PC 5 corresponds primarily to Zn. PC 6 corresponds primarily to Ti, V, Cr and Mn. The map in (H) shows horizontal bands that differ in tone; these features are artefacts generated during data acquisition. (I) Line drawing of the skeleton. 247

Figure 5.6: SRS-XRF maps of GMH CeIII-4967-1932. Bones are enriched in K, Ca, Mn, Co, Ni, Cu and Sb relative to the host sediment and embedding lacquer. The soft tissues in the torso are enriched in Zn relative to the bones, host sediment and lacquer. K, Ca, Mn, Co, Ni, and Sb are associated with soft tissues in the torso, in the abdomen and in the hindlimbs. The map for Cu shows horizontal bands that differ in tone; these features are artefacts generated during data acquisition. Scale in map for K applies to all figure parts..... 248

Figure 5.7: Linear discriminant analysis (LDA) of the metal chemistry of selected regions of interest (ROI) in SRS-XRF maps of GMH CeIII-4967-1932 (Figure S5.19). The chemospace for each ROI is represented by 95% confidence ellipses. The biplot in the bottom left of the chemospace plot shows that most of the chemical variation in the dataset is driven by Ca, Ni, and Zn. 249

Figure 6.1: Mating Geiseltal anurans form a mating ball. Drawing: A. Pieri. 317

Figure 6.2: A dead Geiseltal frog with disarticulated bones in arms and legs on the bottom of a pond. Most of the skin is still intact. Drawing: A. Pieri. 321

Figure 6.3: SEM image of fossil melanosomes (coloured) from an anuran eyespot. Image: D. Falk ... 326

Figure 7.1: Lang lebe der Froschkönig/long live the frog king! Photograph: P. Chung, modified. 350

List of tables

Table 2.1: Significance tests and assumptions for test validity. 79

Table 3.1: Percentage of Libros specimens for which each skeletal element is complete or joint is articulated (data from McNamara et al. 2012a) 126

Table 3.2: Significance tests on skeletal completeness data. 156

Table 3.3: Significance tests on specimen articulation data. 158

Table 5.1: Soft tissue samples from extant and fossil anurans used in this study. 269

Foreword and acknowledgements

(English version below)

„Es lief alles nach Plan, aber der Plan war scheiße!“

Diesen Spruch habe ich einst an der Pinnwand meines Mentors, dem Paläontologen „Prof“ Jörg W. Schneider (Technische Universität Bergakademie Freiberg), gesehen und entschieden, ihn als mein Lebensmotto zu übernehmen. Pläne waren schon immer Teil meines Lebens. Jeder, der mich kennt, beschreibt mich wohl als geplant und zielstrebig.

Vom Kleinkindesalter an, hatte ich einen Plan: Dinoforscher zu werden. Mit dem Abschluss des Masters of Science in Angewandter Paläontologie und Stratigraphie schien der Plan abgeschlossen zu sein. Doch nicht ganz. Denn in der Kindertagesstätte sagte mir meine damalige Betreuerin, Frau Wulff, dass ich meiner unleserlichen Handschrift nach, Doktor werden Würde. Sie kannte mich, meinen Ehrgeiz und meine Selbstmotivation gut, und letztlich hatte sie wohl Recht: in 2018 startete ich nach einer Reihe „geplanter“ und glücklicher Zufälle meine Promotion. Dass ich dafür nach Cork, Irland ausreise und Jahre dort verbringe, hatte ich bis dahin nicht erwartet. Auch nicht, dass ich eine wundervolle Familie auf der grünen Insel gründe...

Ich liebe Herausforderungen. Auch diese sind Teil meiner Pläne – manchmal bewusst, manchmal unbewusst. Das Leben in einem anderen Land, ist nicht immer unbeschwert. Alltag ist kein Urlaub. Familie und altbekannte Freunde sind fern. Freunde zu finden, ist mühselig und zeitaufwendig. Es ist ein Neuanfang in einer anderen Kultur mit weit mehr als nur einer anderen Sprache. Die Zeit im Ausland ist geprägt von Neugier und Abenteuer, aber auch von Missverständnissen, Verlust und dem Gefühl „zwischen“ dem Heimatland und dem ausländischen Aufenthaltsort zu stehen. Es ist ein Akzeptieren von neuen Traditionen, ein Neuerlernen von zwischenmenschlichen Umgängen und das Rechtfertigen und manchmal auch Aufgeben von Altbekanntem aus Deutschland. Das tagtägliche Erlernen und Verarbeiten der englischen Sprache zum Beispiel verlangsamten meine Muttersprache. Und dennoch, die Iren sind ein warmherziges, geselliges Gute-Laune-Volk, dass man schnell liebgewinnt. Dem gegenüber stehen die Eigenarten, Probleme auf die „lange Strecke“ zu schieben, bis das Problem Alltag ist und damit kein Problem mehr ist. Oft werden Probleme auch ohne einen Plan gelöst, was dann langfristig in weiteren Problemen mündet.

Das Leben im Ausland regt daher auch zur Selbstreflexion der eigenen Kultur an und ich kann schmunzelnd sagen, dass ich mich noch nie so „deutsch“ gefühlt habe – in positiven als auch nervigen Aspekten. Geplant zu sein, kann beiden Kategorien zugeordnet werden.

Zurück zu meinen Plänen. Vier Jahre Doktorarbeit, dann zurück nach Deutschland. Ein klar abgegrenztes Arbeitsthema. Was kann da schon schief gehen!?

Doch diese Doktorarbeit verlangte einiges ab. Es war nicht ein Thema zu bearbeiten, sondern es waren viele Themen, die flexibel ineinandergriffen. Der strukturierte Zeitplan war mehr ein Leitfaden als ein verbindliches Regelwerk. Das Einarbeiten in die neuen Themen kostete war mühselig. Ebenso die Aufgabe der Selbstständigkeit, denn in Irland ist der Doktorand ein Student und wird dementsprechend vom System bevormundet. Es kostete mich viel Zeit und Kraft, mich anzupassen, ohne mich komplett zu ändern. Dann kam die COVID-19 Pandemie und plötzlich fühlte ich mich festgesetzt auf einer Insel. Aus vier Jahren, wurden mindestens fünf, am Ende sogar fast sechs. War der Plan der Doktorarbeit zu viel für mich? Hatte ich mich verplant?

Trotz aller Schwierigkeiten, Aufgeben war keine Alternative. Ein Lebensmotto, dass ich stolz von meinen Eltern und Großeltern übernommen habe. Die wichtigste Lektion für mich war daher, dass Pläne nicht starr sind – Pläne sind anpassbar. Sowohl inhaltlich als auch zeitlich. Das ist Leben!

Die schönsten Planänderungen traten mit der Liebe zu Aileen und der Geburt von Klara in mein Leben. Beides war und ist tausendfach mehr Freude als ich mir je erdachte. Jetzt, ein paar Jahre später, ist die Doktorarbeit geschrieben. Die Herausforderung ist bestanden. Entscheidend ist, dass irgendwie doch alles nach Plan lief…

Ich bedanke mich zutiefst bei einem nichtsahnenden Mentor, der mich mit seiner Erfahrung, sein Wissen, seinem Scharfsinn, seiner Fitness, seinem Witz und seiner Junggebliebenheit seit meinem Studium in Freiberg zu neuen Herausforderungen motiviert hat. Vielen Dank Prof. em. Dr. Jörg W. Schneider, kurz „Prof“.
Mein Dank richtet sich auch an Dr. Ute Gebhardt, welche mir erlaubte, mit ihren Projektmitteln nach Südafrika zu einer Konferenz zu reisen. Auf jener Konferenz hörte ich von der Doktorandenstelle in Irland und das Spiel nahm seinen Lauf.

Meine vier Großeltern erlebten den Startschuss dieser Arbeit und ich weiß, dass sie von Anfang an den Abschluss dieses Studienabschnitts stolz hervorsahen. Auch, wenn einige diesen Abschluss nicht mehr erleben konnten, sind sie alle Teil dieser Arbeit. Ich möchte mich bei euch bedanken, dass ihr mein Leben und Studien mit Interesse und stolz verfolgt habt und mich bei allen Vorhaben unterstützt habt. Ich danke meinen Eltern Christiane und Dirk, die mich bekräftigt und ermutigt habt, von früh-auf selbstständig zu sein und meinen Zielen zu folgen. Von euch habe ich gelernt, dass Aufgeben keine Alternative ist. Nie hattet ihr Zweifel an meinen Plänen, dass ich an meinen Grenzen komme oder meine Vorhaben abbreche. Für eure Erziehung, die Förderung meiner Neugier, das Vertrauen in mich, das

vermittelte Wissen, das jahrelange Studentenfutter und die vielen Pakete mit regionalen Köstlichkeiten kann ich euch gar nicht genug danken.

Danke auch an meinem Bruder Georg, der mich immer bestens mit Humor und KFZ-Sachverstand versorgt hat und die Computerprobleme von Mama und Papa löst, seitdem ich außer Landes bin. Die gemeinsamen Leidenschaften für Star Wars, Herr der Ringe, Action- und Horrorfilme machen die Doktorandenzeit deutlich angenehmer.

Ich bedanke mich bei allen Wegbereitern, die mich inspiriert und/oder in schwierigen Zeiten akzeptiert und ausgehalten haben, allen voran bei meiner Liebe, Aileen. Ehrgeiz, Zielstrebigkeit und Verbissenheit sind nicht immer ein Garant für Harmonie. Überschrittene Deadlines, Planungsunsicherheit, Stress und einsame Wochenenden schon gar nicht. Vielen Dank für deine Geduld, deine Gelassenheit, deine Positivität und dein Verständnis. Vielen Dank fuer deine Liebe, deine Empathie, deine Hilfe bei Problemen und die alleinerziehende Betreuung von Klara an so manchen Tagen.
Auch Klara hat zu dieser Arbeit beigetragen. Ich danke der kleinen Made für die vielen schönen Stunden, in denen sie mich zum Lachen gebracht hat, mit mir Fahrrad gefahren ist, mich aus dem Alltagstrott herausgeholt hat und mich hat (temporär) wieder Kind werden lassen.

Ein ganz besonderer Dank geht an meine Schwimmsportsfreunde des SV Stahl Hennigsdorf e.V., insbesondere an meinen ehemaligen Schwimmtrainer Dietmar Losensky und den jetzigen Abteilungsleiter Ingo Meitzner. Dank euch wurde ich nicht nur positiv auf den Geruch von Chlor konditioniert, sondern habe auch die Liebe zum Schwimmsport und Trainern entdeckt. Den erlangten sportlichen Ehrgeiz, die anhaltende Selbstmotivation und die fachlichen Grundlagen, um mich selbst zu trainieren habe ich euch zu verdanken. Diese Eigenschaften sind der Schlüssel, auch nach 25 Jahren noch Freude am Sport- und Wettkampf-Schwimmen zu empfinden. Schwimmen hilft mir, mein mentales und körperliches Gleichgewicht im Einklang zu halten. Während der Promotion war das Schwimmtraining, egal ob allein oder mit Kameraden, eine Zeit der körperlichen Belastung und der geistigen Entspannung. Die Zeit im Becken half mir, in schwierigen Zeiten nicht dem Wahnsinn zu verfallen. Ich wünsche allen Schwimmkameraden, die mich auf dem Weg in Deutschland und Irland begleitet haben, ein schnelles Wasser, für ein Leben lang.

Die COVID-lockdowns in Irland hätte ich nicht ohne Hilfe überstanden. Für innige, anhaltende Freundschaft, Ehrlichkeit und das Teilen und Akzeptieren von kulturellen Eigenarten bin ich meinen ehemaligen Mitbewohnern Teresa und Juan zu tiefem Dank verpflichtet. Ihr seid Familie.

Besonderer Dank geht an Naomi, die mir über all die Jahre den Rücken freigehalten hat, wenn es um zähflüssige Administration in der Universität ging, und Peter, der dafür sorgte, dass die technischen Geräte reibungslos funktionierten und mir immer freundlich und positiv zur Seite stand.

Ein herzliches Dankeschön für fachlichen Rat und tatkräftige Unterstützung bei der Arbeit geht an meine Kollegen in Cork und extern: Aaron, Aidan, Aude, Bea, Dan, Dirleane, Gerard, Hannah, Hollie, Holly-Anne, Jess, John, Jürgen, Larissa, Luke, Marcos, Michael, Miriam, Ninon, Odhran, Paulina, Tiffany, Tuhin, Valentina und Zixiao.

Meinen Freunden Alex, Andrew, Anna, Ciara, Elke, Eric, Jan, Konrad, Resi und Tessa danke ich für offene Ohren und Ratschläge.

Für die zur Verfügungstellung ihrer auf meine Doktorarbeitsthemen abgestimmte Paläo-Kunst, danke ich meiner italienischen Ausgrabungskollegin und Präparatorin Alice Pieri von der Universität Pisa.

Ich bedanke mich bei dem gesamten Team des Zentralmagazins Naturwissenschaftlicher Sammlungen, insbesondere Bianca Bernstein (jetzt Museum Weißenfels), Arila Perl, Michael Stache und Dr. Frank Steinheimer, für Insiderwissen zu Administration, Froschthemen und Geiseltalfossilien, aber auch für das entgegengebrachte Vertrauen bei meiner selbstständigen Arbeit in der Sammlung und die warmherzige Aufnahme in die Arbeitsgruppe.

Ein Dankeschön geht auch an meine Prüfer Dr. Chris Mays (Naturhistorisches Museum Wien), Dr. Duncan Murdock (University of Oxford) und Dr. Marguerite Nyhan (University College Cork), die diese Doktorarbeit, neben ihrer eigentlichen wissenschaftlichen Tätigkeit, unabhängig und kritisch geprüft haben.

Schlussendlich bedanke ich mich bei meinen akademischen Betreuern Prof. Maria McNamara (University College Cork) und Dr. Oliver Wings (Naturkundemuseum Bamberg). Vielen Dank für eure Kooperation, die diese Doktorarbeit möglich gemacht hat, für zahlreiche Änderungsvorschläge, für eure Unterstützung und für eure wissenschaftliche Begleitung.

(English version)

"Everything went according to plan, but the plan sucked!"

I once saw this saying on the pinboard of my mentor, the palaeontologist 'Prof' Jörg W. Schneider (Freiberg University of Mining and Technology) and decided to adopt it as my motto for life. Plans have always been part of my life. Everyone who knows me probably describes me as planned and determined.

From an early age, I had a plan: to become a dinosaur scientist. When I graduated as a Master of Science in Applied Palaeontology and Stratigraphy, the plan seemed to be complete. But not quite. In playschool, my childminder at the time, Mrs Wulff, told me that, judging by my illegible handwriting, I would become a doctor. She knew me, my ambition and my self-motivation well, and in the end she was probably right: in 2018, after a series of 'planned' and lucky coincidences, I started my doctorate. Until then, I neither thought about travelling to Cork, Ireland, and spending years there nor would I have thought about starting a wonderful family on the Emerald Isle...

I love challenges. These are also part of my plans – sometimes consciously, sometimes unconsciously. Life in another country is not always easy. Everyday life is not a holiday. Family and familiar friends are far away. Making friends is difficult and time-consuming. It is a new start in a different culture with far more than just a different language. The time abroad is characterised by curiosity and adventure, but also by misunderstandings, loss and the feeling of being 'between' the home country and the foreign location. Life in a foreign country includes accepting new traditions, to learn (again) how to deal with people and to justify and/or abandon familiar things from home. The daily learning and processing of the English language, for example, slowed down my mother tongue. And yet, the Irish are warm-hearted, sociable, funny people that you quickly keep in your heart. On the other hand, they have a tendency to put problems out of sight until the problem becomes part of everyday life and is therefore no longer a problem anymore. On the other hand, problems can be solved without a plan, which then leads to further problems in the long term.

Living abroad therefore also encourages self-reflection on one's own culture and I can say with a smile that I have never felt so 'German' – in both positive and annoying aspects. Being a planner can be assigned to both categories.

Back to my plans. Four years of doctoral research, then back to Germany. A clearly defined work topic. What could possibly go wrong?

This doctoral thesis demanded a lot. There wasn't just one topic to work on, but many flexible topics that related to each other. The structured timetable was more of a guide than a binding set of rules. Getting into the new topics was tedious. Further, it was difficult to work independently, because in Ireland the doctoral student is a student and is therefore patronised by the system. It took me a lot of time and energy to adapt without changing completely. Then the COVID-19 pandemic came and suddenly I felt stuck on an island. Four years turned into at least five and in the end almost six. Was the doctoral thesis too much for me? Did I plan this challenge badly?

Despite all the difficulties, giving up was not an option. I proudly adopted this life motto from my parents and grandparents. The most important lesson for me was therefore that plans are not rigid – plans are adaptable. Both in terms of content and time. That is life!
The best changes to my plans came with the love for Aileen and the birth of Klara. Both were and are a thousand times more joyful than I ever imagined. Now, a few years later, I've written my doctoral thesis. The challenge has been completed and the important thing is, that somehow everything went according to plan...

I would like to express my deepest gratitude to an unsuspecting mentor who has motivated me to take on new challenges with his experience, knowledge, acumen, fitness, brilliancy and youthfulness since my studies in Freiberg. Many thanks to Prof. em. Dr Jörg W. Schneider, or in short, “Prof”.

My thanks go to Dr Ute Gebhardt, who allowed me to travel to a conference in South Africa with her project funds. At that conference I heard about the PhD project in Ireland and that is how everything started.

My four grandparents witnessed the start of this work and I know that from the beginning on they proudly looked forward to seeing me completing this study. Even though some of them did not get the chance to see me graduating, they are all part of this work. I would like to thank you for being proud and interested in my life and in my studies and for supporting me in all my ambitions.

I would like to thank my parents, Christiane and Dirk, who encouraged me to be independent from an early age and to pursue my goals. I learnt from you that giving up is not an option. You never had any doubts about my plans, doubts that I would reach my limits or that I abandon my plans. I can't thank you enough for your education, the encouragement of my curiosity, the trust you placed in me, the knowledge you imparted, the years of funding and the many parcels of regional delicacies.

Thanks also to my brother Georg, who has always provided me with the humour and car-repair-skills and has been fixing my mum and dad's computers since I left the country. Our shared passions for Star

Wars, Lord of the Rings and action and horror movies made my time as a PhD candidate much more enjoyable.

I would like to thank all those who have inspired me and/or accepted and tolerated me in difficult times, with Aileen, my love, leading the way. Ambition, determination and doggedness are not always a guarantee for harmony. Missed deadlines, planning uncertainty, stress and lonely weekends are certainly not romantic. Thank you for your patience, your calmness, your positivity and your understanding. Thank you for your love, your empathy, your help with problems and for looking after Klara as a single parent on plenty of days.
Klara has also contributed to this work. I would like to thank my “little maggot” for the many wonderful hours in which she made me laugh, rode my bike with me, got me out of the daily grind and allowed me to (temporarily) become a child again.

A very special thank you goes to my swimming friends at SV Stahl Hennigsdorf e.V., especially to my former swimming coach Dietmar Losensky and the current head of club Ingo Meitzner. Thanks to you, I was not only positively conditioned to the smell of chlorine, but also discovered my love for swimming and coaching. Thanks to you I kept alive my sports ambition and self-motivation and learned the technical foundations to train myself. These qualities are the key to enjoy competitive swimming even after 25 years. Swimming helps me to keep my mental and physical balance in harmony. During my PhD project, swim training, whether alone or with friends, was a time of physical exercise and mental relaxation. In difficult times the time in the pool prevented me from falling into madness. I wish all my swimming colleagues who have accompanied me on my journey in Germany and Ireland a life full of “fast water”.

I would not have survived the COVID lockdowns in Ireland without help. I am incredible grateful for my former flatmates Teresa and Juan for their intimate and enduring friendship, for honesty and the sharing and tolerating of cultural quirks. You are family.

Special thanks go to Naomi, who kept my back clear all these years when it came to tough administration at the university. I am also grateful for Peters help in using the technical appliances and his always friendly and positive attitude.

A big thank you for professional advice and active support to my colleagues in Cork and other parts of the world: Aaron, Aidan, Aude, Bea, Dan, Dirleane, Gerard, Hannah, Hollie, Holly-Anne, Jess, John, Jürgen, Larissa, Luke, Marcos, Michael, Miriam, Ninon, Odhran, Paulina, Tiffany, Tuhin, Valentina and Zixiao.

I would like to thank my friends Alex, Andrew, Anna, Ciara, Elke, Eric, Jan, Konrad, Resi and Tessa for their open ears and advice.

I would also like to thank my Italian excavation colleague and taxidermist Alice Pieri from the University of Pisa for making her palaeoart available to this thesis.

I would like to thank the entire team of the Zentralmagazin Naturwissenschaftlicher Sammlungen (Natural Sciences Collections), especially Bianca Bernstein (now Museum Weißenfels), Arila Perl, Michael Stache and Dr Frank Steinheimer, for their insider knowledge on administration, frogs and Geiseltal fossils, but also for their trust during my independent work in the collection and for their warm welcome into the working group.

I am grateful for the work of my examiners Dr Chris Mays (Vienna Natural History Museum), Dr Duncan Murdock (University of Oxford) and Dr Marguerite Nyhan (University College Cork), who examined this doctoral thesis independently and critically in addition to their current scientific work.

Finally, I would like to thank my academic supervisors Prof Maria McNamara (University College Cork) and Dr Oliver Wings (Bamberg Natural History Museum). Thank you for your co-operation in making this thesis possible, for your numerous suggestions for changes, for your support and for your scientific guidance.

Outline

This thesis comprises eight chapters.

Chapter 1 contains several discrete parts. The first part provides definitions for key terms and an overview of soft tissues in the fossil record, with particular emphasis on modes of the soft tissue preservation in fossils, especially the preservation of melanosomes and integument. These introductory sections are followed by a synopsis of anuran biology and the anuran fossil record. The chapter then introduces the Geiseltal Lagerstätte and the Geiseltal Collection in Halle (Salle); the collection hosts the fossil material studied for this thesis. The chapter concludes with an outline of the aims of this thesis.

Chapter 2 details the fossil material and methods used in this thesis. The first part of the chapter provides information on: 1) the fossil specimens; 2) the sites from which the specimens were excavated; 3) the excavation methods; and 4) the conservation of the fossil slabs. The following sections introduce the techniques used in this study including the sampling and sample preparation protocols. For each technique, the functional principles, applications and limitations are described. These technical sections are followed by a synopsis of quantitative taphonomy and an overview of the statistical analyses used in this study. The chapter concludes with a summary of the measurements on melanosomes.

Chapters 3–5 follow the formatting requirements of specific journals for publication. Each of these chapters (i.e., Chapters 3–5) is an independent study. In each case, the main text is followed by references and supplementary information.

Chapter 3 presents a manuscript published in *Papers of Palaeontology.* This paper investigates the completeness and articulation of anuran skeletons from Geiseltal. Comparison with anurans from other Cenozoic Lagerstätten reveal repeated patterns in the skeletal element preservation in the anuran fossil

record. The patterns elucidate the ultimate controls on preservation of anurans from diverse lacustrine-hosted biotas.

Chapter 4 presents a manuscript published in *Scientific Reports.* The study comprises the first comprehensive analysis of soft tissues and sediment of any fossil from Geiseltal using a suite of modern electron beam (scanning electron microscopy and X-ray diffraction) and spectroscopic techniques (energy-dispersive X-ray spectroscopy, electron probe microanalysis, Fourier transform infrared spectroscopy and Raman spectroscopy). It demonstrates that existing models for the preservation of soft tissues in anurans from Geiseltal are incorrect. The paper introduces a new model for the preservation of the Geiseltal anuran soft tissues.

Chapter 5 presents a study that has been submitted for publication in *iScience.* The paper includes an analysis of the geometry and chemistry of the fossil melanosomes preserved in the soft tissues from the Geiseltal anurans. Further, the data on the geometry of the melanosomes from the Geiseltal anurans was combined with the geometry data of melanosomes from anurans from Palaeogene and Neogene biotas and from extant anurans. It is the first study that compares the geometry of fossil melanosomes with the geometry of tissue-specific melanosomes from extant anurans. The study results infer on the biology of ancient anurans and the evolution of melanosomes in anurans and potentially other vertebrates.

Chapter 6 provides discussion of the findings and Chapter 7 comprises the conclusions, an outlook for future research and closing words. References cited in Chapters 1, 2, 6 and 7 are provided in Chapter 8.

Appendix I comprises a list of the specimens and samples that were analysed in this thesis and a list of Geiseltal specimens, that are curated in collections outside the Geiseltal Collection following an international request. Appendix II provides two popular science articles in German. Falk & Stache (2021) summarise the history of the Geiseltal site and offer an insight into the material and methods that were used for this study. Falk *et al.* (2022a) provide examples for mating-related deaths of extant anurans in central Germany. Appendix III comprises the datasets for Chapter 3.

1. Introduction

This chapter presents essential background information for this thesis. It comprises six sections. Section 1.1 focuses on the scientific field of taphonomy and elucidates the link between taphonomy and palaeontology. This is followed by Section 1.2, which focuses on the term Lagerstätten and the classification model of Lagerstätten. Section 1.3 presents a summary of the preservation of fossil soft tissues and Section 1.4 summarises the anuran fossil record. Collectively, these sections provide the foundation for a summary of the Geiseltal Konservat-Lagerstätte (Section 1.5). Section 1.6 outlines the aims of this thesis.

1.1 Taphonomy

After death, most organisms degrade completely. The remaining organisms, or parts thereof, are transformed to fossils. Taphonomy (Greek: taphos, “burial”; nomos “laws”) is the study of death and postmortem processes that lead to the transition of organisms into the lithosphere (Efremov 1940; Martin 1999). The taphonomy of organisms typically includes six steps (Allison 2001; Anderson 2001; Wilson 2001; Purnell *et al.* 2018): death, decay, transport, deposition, burial and diagenesis (i.e., post-burial processes such as compaction, mineralisation and cementation). The order of these steps is not fixed, e.g. the transport, deposition and/or burial of an organism can take place before its death. Further, transport and deposition do not apply to organisms that are sessile and/or buried *in situ*. Taphonomic processes are often discussed in relation to two broad-scale processes: those that occur before burial (e.g., transport and deposition, i.e., biostratinomy) and those that occur after burial (i.e., diagenesis). Biological controls that impact taphonomy of an organism include tissue structure, tissue chemistry and autolysis (the destruction of cells or tissues by their own enzymes).

Taphonomy is an interdisciplinary science that combines certain fields of the bio- and geosciences and various aspects of chemistry and physics (Wuttke & Reisdorf 2012). The concept of taphonomy is used by several fields including palaeontology, geology, biology, mineralogy, archaeology, forensics and material sciences.

The physical mechanisms (e.g., fluid dynamics and gravity) that underpin most taphonomic processes (e.g., transport and deposition) are generally well characterised (Dodson 1973; Weigelt 1989; Anderson 2001; Reisdorf & Wuttke 2012; Baumjohann & Benecke 2022). Further, the chemical mechanisms of decay are well understood (Aturaliya & Lukasewycz 1999; Allison 2001; Purnell *et al.* 2018). This thesis is written in the context of this understanding. Our understanding of the chemical mechanisms of preservation processes, however, is incomplete (Briggs & McMahon 2016; Purnell *et al.* 2018); in particular, it is unclear in which tissues preservation is initiated and which mechanisms lead to the preservation of certain tissue types (e.g., connective tissues). Further, the effects of changes in certain chemical parameters (e.g., pH and the concentrations of inorganic ions) inside and outside the carcass on tissue preservation is not resolved (Purnell *et al.* 2018). It is also unclear how biological controls (e.g., tissue structure, tissue chemistry) affect tissue preservation.

The preservation of different tissue types as carbon-based remains is biased towards lipids (Briggs 2001; Evershed & Lockheart 2001). It is not known, however, whether this bias is introduced by the analysis techniques we currently use (e.g., gas chromatography-mass spectrometry). Different analytical approaches may be more effective in the detection of non-lipid components in fossils.

In palaeontology, taphonomic processes are investigated by studying the biological information that is extracted from the anatomy of fossils and the mode of preservation (including the chemical compositions of the studied fossils; Purnell *et al.* 2018). Other ways to investigate taphonomic processes include: 1) the study of the chemistry and the composition of the rocks that host the fossils

and 2) lab experiments, e.g., to replicate modes of preservation of fossils. In turn, an understanding of taphonomy can inform on the biology of ancient organisms (i.e. their characteristics as living organisms), on biological, physical and chemical characteristics of the depositional setting and on syndepositional and postdepositional processes. This knowledge is essential to understand the formation of fossil deposits.

The skeletal taphonomy reveals the postmortem changes of the skeleton. Skeletal taphonomy can inform on our understanding of extrinsic taphonomic factors (i.e., characteristics of the depositional setting) and intrinsic taphonomic factors (i.e., characteristics of the organisms' biology and chemistry, e.g., tissue chemistry). The skeletal taphonomy of an organism is commonly investigated using metrics (Driscoll *et al.* 2019; also see Chapter 3) such as the skeletal completeness metric (Mannion & Upchurch 2010; Cashmore *et al.* 2020), the character completeness metric (Mannion & Upchurch 2010), the taphonomic completeness metric (Beardmore *et al.* 2012) or the completeness score (Fountaine *et al.* 2005). Analysis of the skeletal taphonomy of a particular taxon in different fossil biotas may reveal variations in preservation through space and time. Such analysis can reveal sampling biases, e.g., the variations in preservation follow a clearly anthropogenic induced pattern, or if skeletal taphonomic data from different localities are compared, e.g., the theropod remains from the Northern Hemisphere are more complete and more abundant than those from the Southern Hemisphere, probably due to a historical focus in sampling activity on the Northern Hemisphere (Cashmore & Butler 2019). The analysis of the skeletal taphonomy can also reveal how fossil discoveries through history have altered our interpretations of the fossil record (Kidwell 2001; Brocklehurst & Fröbisch 2014; Cleary *et al.* 2015; Dean *et al.* 2016; Whitaker & Kimmig 2020), e.g., the change of phylogenetic relations between taxa with the discovery of new taxa (Bernard *et al.* 2010) and the recognition of synonymy in dinosaur taxa (Benton 2008).

Skeletal taphonomic data have been investigated for numerous fossil vertebrates including the early tetrapod *Acanthostega* (Devonian, Greenland; Coates 1996), the aquatic reptile *Serpianosaurus* (Triassic, Switzerland; Beardmore *et al.* 2012; Beardmore & Furrer 2018), the bird *Archaeopteryx* (Jurassic, Germany; Kemp & Unwin 1997), the dinosaur *Juravenator* (Jurassic, Germany; Reisdorf & Wuttke 2012), multituberculate mammals (Cretaceous, China; Kielan-Jaworowska & Hurum 2006), the frog *Pelophylax pueyoi* (Miocene, Spain; McNamara *et al.* 2012a), salamanders (Miocene, Spain; McNamara *et al.* 2012b) and other frogs of the genus *Pelophylax* (Pliocene, Spain; Blain *et al.* 2023).

In Chapter 3 of this thesis, skeletal taphonomy metrics are used to interpret the processes involved in the preservation of anurans from the Eocene of Geiseltal.

In contrast to the use of fossil specimens, taphonomic processes can also be investigated in controlled laboratory experiments (Purnell *et al.* 2018). These experiments are designed to control extrinsic and intrinsic taphonomic factors (Briggs *et al.* 1993; Briggs 2003; Briggs & McMahon 2016) and are often focused on decay (Carter *et al.* 2008; Gäb *et al.* 2020; Carlisle *et al.* 2021), mineralisation (Briggs 1995; Sagemann *et al.* 1999; Toporski *et al.* 2002b; Briggs 2003) and/or maturation (e.g., the impacts of diagenesis; Gupta *et al.* 2008; McNamara *et al*. 2013; Slater *et al.* 2020; Slater *et al.* 2023).

The fossil record is biased. Most species are entirely absent from the fossil record and most individuals of those species that are present in the record are also not preserved. Further, the process of fossilisation is biased towards preservation of hard tissues (biomineralised tissues) due to the preferential decay of soft tissues (Allison 2001). An understanding of taphonomic processes can therefore inform on our knowledge of gaps and biases in the fossil record and also biases related to sampling techniques and human behaviour (Kidwell 2001; Brocklehurst & Fröbisch 2014; Cleary *et al.* 2015; Dean *et al.* 2016; Purnell *et al.* 2018; Cashmore *et al.* 2020; Whitaker & Kimmig 2020). An

understanding of taphonomic biases is needed to accurately interpret the palaeobiology of ancient organisms.

In sum, taphonomy is essential to our understanding of the processes involved in fossil preservation including the formation of fossil deposits. Taphonomy can also improve our understanding of biases in the fossil record and about what fossils reveal about the history of biodiversity and evolution.

1.2 Lagerstätten

Lagerstätten (German: Lager, “storage”; Stätte “place”) are fossil deposits that preserve an unusually rich amount of qualitative and/or quantitative palaeobiological information (Seilacher 1970). This information provides insights into the biology of ancient ecosystems, the morphology of ancient organisms and, as a result, the evolutionary history of life (Allison 1988; Briggs 2014). It is notable that in the German language, the term Lagerstätten includes not only fossil deposits but also (geological) placer and ore deposits. As a result, the term Fossil-Lagerstätten is used interchangeably with “Lagerstätten” in the literature.

Lagerstätten are heterogeneously distributed through geological time and space (Allison & Briggs 1993; Muscente *et al.* 2017). Lagerstätten can be classified as Konservat-Lagerstätten and/or Konzentrat-Lagerstätten (Seilacher 1970; Seilacher & Westphal 1971; Seilacher *et al.* 1985; Briggs 2014).

Konzentrat-Lagerstätten are fossil deposits that comprise concentrated and abundant, usually disarticulated, skeletal elements of organisms. Three deposit types can be distinguished (Seilacher & Westphal 1971; Seilacher *et al.* 1985; Kidwell *et al.* 1986): (1) Condensation deposits are localities that preserve skeletal elements that accumulate over time, in conjunction with low sedimentation rates, e.g., the cave system of Richards Spur (Permian, USA; MacDougall *et al.* 2017). (2) Placer deposits are

characterised by the deposition of skeletal elements in a restricted area due to physical laws (usually due to fluid dynamics and gravity), e.g. storm-generated beds of gastropods (Triassic, USA; Nützel & Schulbert 2005) and crinoids (Cretaceous, Poland; Salamon *et al.* 2009), but also bone beds (e.g., generated by fluvial processes) that can contain skeletal elements of e.g., dinosaurs (Jurassic, USA; Storrs *et al.* 2012), turtles (Jurassic, China; Wings *et al.* 2012) and pterosaurs (Cretaceous, Morocco; Smith *et al.* 2023). (3) Concentration traps are localities that trap organisms and preserve their skeletal elements, e.g., in fissure fillings (Permian, Germany; Sues & Boy 1988). In concentration traps skeletal elements accumulate over a shorter time than in condensation deposits. The three deposit types represent end-members of a gradational series.

In contrast, Konservat-Lagerstätten are characterised by the high-quality preservation of fossils. Fossils in Konservat-Lagerstätten are usually well-articulated skeletons and/or preserve soft tissues. The classic concept of Konservat-Lagerstätten defines a continuum between three end-member states in a ternary diagram (Seilacher *et al.* 1985): (1) Obrution deposits are fossil deposits that are characterised by the high quality preservation of fossils due to the rapid burial of organisms by sediment. Examples include the Burgess Shale (Cambrian, Canada; Butterfield 1990; Gaines 2014), the Eramosa Lagerstätte (Silurian, Canada; von Bitter *et al.* 2007) and the Hunsrück Slate (Devonian, Germany; Sutcliffe *et al.* 1999). (2) Stagnation deposits are localities with high-quality fossil preservation due to chemical, thermal and/or density-related stratification of the water body. The conditions in the lower layer of water (hypolimnion) in a stratified lake can be hostile to life (e.g., due to low oxygen levels); hostile conditions usually exclude the presence of benthos (e.g., bioturbators) and/or scavengers. The quality of preserved soft tissues depends on the rate of decay and the availability of mineral ions for soft tissue replication. Stagnation deposits include the Posidonienschiefer (Jurassic, Germany; Seilacher *et al.* 1985), Jehol (Cretaceous, China; Kielan-Jaworowska & Hurum 2006), Messel (Eocene, Germany; Tütken 2014) and Libros (Miocene, Spain; McNamara *et al.* 2009) deposits. (3) Bacterial sealing deposits are localities where carcasses adhere to biofilms of microbial colonies (i.e., microbial mats) or be entombed

within microbial mats. Microbial mats may provide mineral ions for soft tissue replication or form an external mould of the carcass. Examples are the Ediacara biota (Ediacaran; Gehling 1999; Janssen *et al.* 2022), Fezouata (Ordovician, Morocco; Roy *et al.* 2015), Crato (Cretaceous, Brazil; Varejão *et al.* 2019) and Las Hoyas (Cretaceous, Spain; Buscalioni & Fregenal-Martínez 2010) deposits.

The three Konservat-Lagerstätten states form a gradational series (Seilacher *et al.* 1985), e.g., the Mazon Creek Lagerstätte (Carboniferous, USA; Baird *et al.* 1986; Janssen *et al.* 2022) combines characteristics of bacterial sealing and obrution deposits, while the Solnhofen Lagerstätte (Jurassic, Germany; Kemp & Unwin 1997; Reisdorf & Wuttke 2012) combines characteristics of obrution, stagnation and bacterial sealing deposits. Seilacher *et al.* (1985) did not include conservation traps in their gradational series, e.g., tar seeps (e.g., Rancho La Brea, Pleistocene, USA; Stock 1930; DeSantis *et al.* 2019) and the preservation in amber (e.g., Myanmar, Cretaceous; Xing *et al.* 2016). Trap deposits can include remarkably preserved organisms and hence those deposits are defined as Konservat-Lagerstätten. Further, there are certain Lagerstätten that classify as both a Konzentrat-Lagerstätte (on account of the abundance of fossils) and a Konservat-Lagerstätte (on account of the preservation of nonmineralised materials), e.g., the Ruin Walsh Lagerstätte (Cambrian, USA; Webster *et al.* 2008) and the Quercy Phosphorites (Eocene, France; Tissier *et al.* 2017). The concept by Seilacher *et al.* (1985) is currently being revised with the aim to establish a site-based classification that is underlain by a fossil chemistry-based and facies classification (Kimmig & Schiffbauer 2023; Muscente *et al.* 2023). This classification system aims to make fossil compositions and mineralogies easily comparable between Lagerstätten and claims to be more open for the recognition of localised fossil deposits, that are distinct in time and depositional facies, but were historically termed as one geographically extensive Lagerstätte (Kimmig & Schiffbauer 2024).

Palaeogene (e.g., Enspel, Oligocene, Germany; Wedmann *et al.* 2000) and Neogene (e.g., Libros, Miocene, Spain; McNamara *et al.* 2009; McNamara *et al.* 2012a; McNamara *et al.* 2012b; McNamara

et al. 2016) Konservat-Lagerstätten usually show less complex diagenetic histories than their older counterparts and the physical and chemical characteristics of their depositional settings are more similar to modern settings (Hendy 2011). As a result, the preservation history of fossils is usually less obscured by syndepositional and postdepositional processes. As a result, taphonomic patterns are easier to identify.

For this thesis, fossils from the Palaeogene Geiseltal Konservat-Lagerstätte were studied (see Section 1.5).

1.3 Soft tissue preservation

Shells, bones and teeth are biomineralised tissues (i.e., "hard" tissues). Hard tissues dominate the fossil record. In contrast, many non-biomineralised tissues ("soft" tissues) including integument, muscle, internal organs and connective tissues, preserve less frequently in the fossil record. This is because soft tissues usually decay quickly *postmortem* and therefore the potential for preservation is lower than for hard tissues (Briggs *et al.* 1993; Orr *et al.* 2002; Briggs 2003; Purnell *et al.* 2018). Soft tissue preservation requires that fossilisation processes occur prior to the complete decomposition of the tissue. Controlling factors for the fidelity of preservation include the timing of specific fossilisation processes (see Section 1.3.1), which in turn are controlled by other taphonomic factors including climate, tissue chemistry, transport dynamics and environment. Certain environments can favour the preservation of soft tissues (Allison 2001; Briggs & McMahon 2016), e.g., those with low oxygen levels (Seilacher *et al.* 1985), those that are rich in clay (McMahon *et al.* 2016), those that are rich in metals (Petrovich 2001) and where organisms are entombed in microbial mats (Wilby *et al.* 1996) or resin (Jiang *et al.* 2022).

1.3.1 Modes of soft tissue preservation

Three basic modes of soft tissue preservation are identified (modified after Briggs 2003): (1) mineralisation, (2) organic preservation and (3) mouldic preservation.

(1) Mineralisation is the replacement of organic material by inorganic minerals. Mineralisation of soft tissues can occur due to three processes. These three processes are not mutually exclusive in a single fossil.

(1a) Authigenic replication is decay-driven mineralisation that replaces soft tissues up to cellular-level fidelity (Briggs *et al.* 1993). This replication reflects ion exchange between the environment (e.g., water and sediment) and the carcass. The ion exchange may occur exclusively within different regions of the decaying carcass. Minerals that can replicate soft tissues include calcium phosphate, calcium carbonate, pyrite, clay minerals, calcium sulfate, galena (Briggs 2001), silica (Yang *et al.* in review) and zeolites (Rossi *et al.* in preparation). The authigenic mineralization processes that are most relevant to this thesis are silicification (replication of soft tissues by silica) and phosphatisation (replication of soft tissues by calcium phosphate), which are discussed in detail in Sections 4.2, 4.3 and below.

(1b) Permineralisation is the infiltration and permeation of tissues by ion-rich fluids; the term is usually applied to the infiltration and permeation of tissues by silicic acid. Decay is not necessary to initiate or maintain this process, but decay can increase permeability and space to accommodate minerals and creates nucleation sites for organic ions and inorganic ions to bond (Carson 1991; Butts 2014; Mustoe 2023). The polymerisation process between organic and inorganic ions takes place via condensation reactions, thus promoting the precipitation of silica within and on tissue structures (Leo & Barghoorn 1976; Mustoe 2023). Permineralised fossils can preserve soft tissues with cellular-level fidelity. Numerous Lagerstätten include permineralised plant material (Trümper *et al.* 2018; Mustoe 2023), e.g., the Northern Tocantins Petrified Forest (Permian, Brazil; Trümper *et al.* 2020) and the “Petrified Forest” of Chemnitz

(Permian, Germany; Dietrich *et al.* 2013). The Rhynie Chert (Devonian, UK; Garwood *et al.* 2020) hosts a permineralised biota including plants, fungi and invertebrates.

(1c) Concretions are common in depositional settings with pore waters rich in key mineral ions, such as carbonate. Carbonate concretions (e.g., composed of siderite or calcite) can contain fossils that preserve soft tissues. Carbonate concretions can develop in organic-rich argillaceous sediments in shallow waters, where calcium carbonate forms a cocoon around a decaying carcass. It is notable that concretions do not have to nucleate on a carcass. The cocoon creates a largely self-contained system with limited diffusion of ions (Clements & Gabbott 2021). Within the developing concretion, the decay of the carcass slows down and preservation of tissues can take place (Clements & Gabbott 2021). The soft tissues within carbonate concretions can be preserved in a diversity of ways (McCoy *et al.* 2015): through replacement by mineralisation (see point 1a), as organic carbon (see point 2) or as moulds (see point 3). The rate of concretion growth can control the fidelity of preservation of the soft tissues inside the concretion (McCoy *et al.* 2015); experimental studies discovered that a low soft tissue fidelity is associated with a slow development of the concretion. The cementation of the concretion eventually ceases; different concretions are lithified to different extents. Siderite concretions from Mazon Creek (Carboniferous, USA; Cotroneo *et al.* 2016) reveal a diverse biota including invertebrates, vertebrates and plants.

(2) Organic preservation is the preservation of tissues as carbon-based (i.e., carbonaceous) remains due to the *in situ* polymerisation of organic compounds (primarily lipids) in soft tissues during decay and maturation (Evershed & Lockheart 2001; Gupta *et al.* 2006; Gupta *et al.* 2008a; Gupta *et al.* 2009). Organic preservation requires conditions that prevent scavenging and that facilitate incomplete soft tissue decay. The presence of organic residues is required to enable polymerisation processes. Organic preservation is promoted at elevated temperatures

but can start prior to deposition (Gupta *et al.* 2006; Gupta *et al.* 2009; Cody *et al.* 2011). One form of polymerisation is the incorporation of sulfur from sulfides and/or polysulfides into tissues during the polymerisation process. This polymerisation process is termed sulfurisation and results in extensive molecular crosslinking, which increases the resistance to degradation (Briggs 2001; Sinninghe Damsté *et al.* 2007; McNamara *et al.* 2016b). Lipids can survive up to billions of years (Cappellini *et al.* 2018). Polysaccharides can survive up to hundreds of millions of years, e.g., remnants of chitin in the cuticle of a 417 million-year-old eurypterid (Gupta *et al.* 2006; Cody *et al.* 2011). Protein remnants can survive for up to tens of millions of years (Slater *et al.* 2023a), whereas the evidence for nucleic acids (e.g., DNA) in sediment is limited to ca. 2 Ma (Kjær *et al.* 2022) and in fossils it is limited to ca. 1 Ma (van der Valk *et al.* 2021).

(3) Mouldic preservation is the preservation of soft tissues as an external mould (e.g., soft tissue moulds in ammonites from the Devonian of Morocco; Klug *et al.* 2008). Mouldic preservation is not considered further here as this thesis focuses on residues of soft tissues, not external moulds of soft tissues.

1.3.2 Melanosomes in the fossil record

Melanosomes are micron-sized cell organelles that synthesise and store melanin (Greek: melanos, black/very dark), which is a light-absorbing polymeric pigment (Riley 1997). Melanin is widespread in living organisms, but only vertebrate melanin is relevant in this thesis, i.e., only melanosomes and melanosomal melanin are considered further here. The abundances and anatomical distributions of melanosomes differ among extant vertebrates (i.e., amphibians, birds, fish, mammals and reptiles). Melanosomes typically occur in connective tissues, the eyes, integument (e.g., feathers, hair, skin) and internal organs (e.g., heart, kidneys, liver, lungs, spleen; D'Alba & Shawkey 2019; Rossi *et al.* 2019; McNamara *et al.* 2021; Guo *et al.* 2023). Current literature suggests that in many vertebrate groups (e.g., humans), skin melanosomes derive from melanocytes (Zuasti *et al.* 1998; Yamaguchi & Hearing

2014). In amphibians, reptiles and fish, skin melanosomes derive from melanocytes and melanophores (Yasutomi 1987; Zuasti *et al.* 1998; McNamara *et al.* 2021). Melanosomes can occur in internal tissues. The origin of melanosomes in the internal tissues of most vertebrates is poorly understood, but current research suggests that melanosomes in the internal organs of amphibians, reptiles and fish derive from melanin-rich phagocytes (melanomacrophages; Dang *et al.* 2019; Stosik *et al.* 2019). Melanin has many functions in vertebrates. The functions of melanin differ among organs, e.g., skin melanin plays a role in photoprotection, visual signalling and thermoregulation; in eyes, melanin plays a role in photoprotection and has antioxidant functions (McNamara *et al.* 2021).

Melanosomes can contain two forms of the pigment melanin: eumelanin and phaeomelanin. Eumelanin is associated with black, brown and grey colouration and phaeomelanin is associated with orange, rufous and grey colouration (Wakamatsu *et al.* 2002; Ito & Wakamatsu 2003; Ito *et al.* 2018; McNamara *et al.* 2021; Guo *et al.* 2023). Melanin can also generate structural colouration (Xiao *et al.* 2020; Jeon *et al.* 2021). The relative proportions of eumelanin and phaeomelanin in individual melanosomes vary among tissues, e.g., in extant amphibians, melanosomes are strongly eumelanin-dominated (Wolnicka-Glubisz *et al.* 2012; Rossi *et al.* 2019; Slater *et al.* 2023b).

Melanosomes can preserve on geological timescales (Vinther *et al.* 2008; Glass *et al.* 2012; Lindgren *et al.* 2012; McNamara *et al.* 2021). Fossil melanosomes occur as ovoid, rod-shaped and subspherical microbodies. Those microbodies were originally interpreted as fossilised decay bacteria (Wuttke 1983b; Liebig 2001; Toporski *et al.* 2002a). The geometry of fossil melanosomes is consistent with the geometry of both bacteria and melanosomes in modern animals (Liebig 2001; Moyer *et al.* 2014). Consideration of the spatial locations of such fossil microbodies in combination with their geometry can help constrain the interpretation of the fossil microbodies as melanosomes (Rossi *et al.* 2019; Rossi *et al.* 2020). Additional support for an interpretation as fossil melanosomes is the geochemical composition of these microbodies (Vinther 2016; Roy *et al.* 2020). Molecular signatures that are indicative of eumelanin and phaeomelanin can be acquired with time-of-flight secondary ion mass

spectrometry (ToF-SIMS) and alkaline hydrogen peroxide oxidation-high-performance liquid chromatography (AHPO-HPLC; Glass *et al.* 2012; Lindgren *et al.* 2012; Lindgren *et al.* 2018; Slater *et al.* 2020). Further, melanin in extant organisms chemically binds ions of metals (e.g., Na^{2+}, Mg^{2+}, Ca^{2+}, V^{2+}, $Fe^{2+/3+}$, Co^{2+}, Ni^{2+}, Cu^{2+}, Zn^{2+}, Cd^{2+}, Pb^{2+}) and non-metals (e.g., S^{-2}; Hong & Simon 2007; Di Mauro *et al.* 2017; Rossi *et al.* 2020; McNamara *et al.* 2021). It is intriguing to note that metal ions have been linked to melanin preservation in fossils. Whether these metal ions are bound to melanin is not known, except for Cu (Wogelius *et al.* 2011; Rossi *et al.* 2019; Rossi *et al.* 2020, 2021). Synchrotron-based analyses, such as synchrotron rapid scanning-X-ray fluorescence (SRS-XRF), X-ray absorption near-edge spectroscopy (XANES) and extended X-ray absorption fine structure analysis (EXAFS) can be used to study metals that are typically associated with eumelanin and phaeomelanin (SRS-XRF for quantitative data and XANES/EXAFS for evidence of the local chemical environment of chelated metals). Characterisation of these aspects of fossil melanosomes can constrain interpretations of melanin in fossils (Bergmann *et al.* 2012; Edwards *et al.* 2018; Manning *et al.* 2019).

Taphonomic experiments have demonstrated the survival of organic remains of melanosomes under various conditions comparable to those that exist during decay and diagenesis (McNamara 2013; Slater *et al.* 2020; Jarenmark *et al.* 2021; Rossi *et al.* 2021; Slater *et al.* 2023b).

Fossil melanosomes, however, are not always preserved as three-dimensional microbodies. Melanosomes can also be preserved as external moulds in amorphous organic matter (Zhang *et al.* 2010; Slater *et al.* 2020). Mouldic melanosomes indicate an unfavourable taphonomic scenario (e.g., strong oxidation rates and high pH) for the preservation of melanosomes as three-dimensional microbodies (Slater *et al.* 2020).

Melanosomes in fossil vertebrates are often the only preserved component of vertebrate soft tissues. Fossil melanosomes are abundant components in fossil soft tissues in Konservat-Lagerstätten, e.g., melanosomes define the skin and internal organs of amphibians from Saar-Nahe (Permian, Germany;

Rossi *et al.* 2020), define the isolated *Archaeopteryx* feather from Solnhofen (Jurassic, Germany; Carney *et al.* 2012), define the skin, internal organs and stomach contents of a fossil moonfish from Bolca (Eocene, Italy; Rossi *et al.* 2022) and define the eyespot, skin and internal organs of the frog *Pelophylax pueyoi* from Libros (Miocene, Spain; McNamara *et al.* 2009; McNamara *et al.* 2010; McNamara *et al.* 2016).

Melanosomes preserved in fossil vertebrates have been used to infer the integumentary colours of fossil vertebrates (Vinther 2015, 2020). Colours can infer behaviour and ecology of animals (Zhang *et al.* 2010; Manning *et al.* 2019; Vinther 2020; Cincotta *et al.* 2022; Rossi *et al.* 2022). Tissue-specific melanosome geometries in integumentary structures of pterosaurs (Cincotta *et al.* 2022) and dinosaurs, including extant birds (Rossi *et al.* 2019), indicate that the functions of feathers in visual communication originated in the early Mesozoic (Li *et al.* 2014; Cincotta *et al.* 2022). Further, melanosome geometry and chemistry can inform on internal soft tissue anatomy as these parameters vary significantly among tissues in extant vertebrates (Rossi *et al.* 2019). The abundances and anatomical distribution of melanosomes differ among extant vertebrate groups (i.e., amphibians, reptiles, mammals and birds; McNamara *et al.* 2021). Amphibian non-integumentary melanosomes greatly outnumber skin melanosomes (McNamara *et al.* 2018), whereas numbers of reptile melanosomes in integumentary and non-integumentary tissues are subequal (Rossi *et al.* 2019). Integumentary melanosomes are dominant in mammals and birds (Rossi *et al.* 2019). The abundances and anatomical distributions of melanosomes in fossil vertebrates may suggests potential shifts in the locations of synthesis and distribution of melanin (melanogenesis) from internal organs to the integument during the evolution of mammals and birds (McNamara *et al.* 2021). The spatial shift may be linked to endothermy and the evolution of the immune system (McNamara *et al.* 2021).

1.3.3 Vertebrate integument in the fossil record

The integument (Latin: integumentum, covering) is the organ system that surrounds the body of an organism. In extant vertebrates, the integument includes the skin and integumentary appendages, e.g., claws, feathers, horns, hair, scales and the shells of chelonians (turtles, terrapins and tortoises). Integuments have many functions, including mechanical support, visual signalling and the formation of a barrier against abrasion, chemical damage and pathogens (Alibardi 2003; Alesci *et al.* 2023; Terrill & Shultz 2023). In amphibians and fish, the integument supports thermoregulation, gas exchange and ion exchange between the organism and environment (Alibardi 2003; Alibardi *et al.* 2003).

Vertebrate integuments can be preserved in authigenic minerals, as thin layers of organic material, as impressions lacking soft tissue residues and as an inclusion (e.g., in amber). Carbonaceous and mineralised integumentary structures can co-occur in the same specimen (Benton *et al.* 2008). There have been several structural innovations in the vertebrate integument during vertebrate evolution. These integumentary innovations represent adaptations to the environment and/or promoted the evolution of new functional roles (Alibardi 2003; Alesci *et al.* 2023). Fossil integument can therefore inform on the evolution of locomotor modes, such as flight and also on ecology (e.g., animal behaviour, animal habitat; Alibardi 2003; Terril & Shultz 2023).

The fossil record of vertebrate integumentary structures is biased towards skin and feathers; hair is rarely fossilised (Eliason *et al.* 2017). This bias likely reflects variation in preservation potential of tissue types, different depositional environments and taphonomic processes (Kidwell 2001; Eliason *et al.* 2017). The following paragraph includes a few examples of fossil vertebrate skin.

Snakes and anurans of the Libros biota (Miocene, Spain; McNamara *et al.* 2009) preserve skin that is replaced by authigenic calcium phosphate with cellular-level fidelity. Features of the fossilised snake skin include layers of collagen fibres and melanosomes (McNamara *et al.* 2016a). The preserved

features closely resemble the skin layers of extant snakes. The fossilised skin of the anurans includes a layer of dermal collagen fibres that is interpreted as the preserved remains of the Eberth-Katschenko (E-K) layer in extant anurans (McNamara *et al.* 2009). Keratin remnants (amide and sulfur compounds) have been reported in organically preserved reptile scales (USA, Eocene; Edwards *et al.* 2011). The dorsal integument of the ankylosaur *Borealopelta* (Cretaceous, Canada; Brown *et al.* 2017) is defined as an organic film. Melanin was identified in the organic residues, but melanosomes were not discovered. Further, integumentary features such as horn sheaths and scales were reported (Brown *et al.* 2017). A specimen of the ceratopsian *Psittacosaurus* (Cretaceous, China; Bell *et al.* 2022) shows a variety of integumentary soft tissues including a cranial horn, scales and bristles (Bell *et al.* 2022); certain integumentary soft tissues, probably feathers, contain melanosomes (Zhang *et al.* 2010; Tahoun *et al.* 2022). The preserved features enable detailed anatomical reconstructions of the animal.

Fossil feathers are usually defined as a carbonaceous film (e.g., the feather of *Archaeopteryx*; Carney *et al.* 2012). The carbonaceous film may or may not preserve melanosomes. There are many cases of preserved feathers in basal avialans and non-avian dinosaurs (Zhang *et al.* 2010), e.g., *Anchiornis* (Jurassic, China; Cincotta *et al.* 2020; Lindgren *et al.* 2015), *Kulindadromeus* (Jurassic, Siberia; Godefroit *et al.* 2020) and *Beipiaosaurus* (Cretaceous, China; Xu *et al.* 2009). Further, integumentary structures in pterosaurs are also interpreted as feathers (Yang *et al.* 2019; Cincotta *et al.* 2022). This discovery is consistent with the hypothesis that feathers evolved in the early Mesozoic, probably in the Early Triassic (Benton *et al.* 2019) and therefore contributes greatly to our understanding of the evolution of flight.

Finally, soft tissues preserved in amber, e.g., fossil feathers from the Cretaceous (USA; Grimaldi *et al.* 2002) and lizard skin from the Cretaceous (Myanmar; Čerňanský *et al.* 2022), can reveal a high-quality preservation of integument but are always limited to small specimens or specimen fragments.

1.4 Fossil anurans

Anurans (ancient Greek: anura, without tail) are short-bodied, tailless amphibians (Fig. 1.1A). They are the most diverse group of extant amphibians and one of the most diverse groups of extant tetrapods (Vitt & Caldwell 2014; Feng *et al.* 2017; Scheele *et al.* 2019). Anuran populations are an important indicator of the health of modern ecosystems (Price *et al.* 2007; Dixon *et al.* 2011; Oda *et al.* 2016; Scheele *et al.* 2019). Extant anurans occupy a variety of habitats, including woodlands, swamps, meadows, tundra and deserts (Vitt & Caldwell 2014). Anurans usually reproduce in water and rarely on land (e.g., the midwife toad [Discoglossidae]; Márquez 1995). The life cycle of anurans includes the transformation from larva to adult frog (metamorphosis).

Anurans are divided informally in frogs and toads; these terms, however, do not represent real phylogenetic groupings (i.e., clades). The term “frog” is usually used to describe aquatic anurans that possess moist skin and long hindlimbs, whereas the term “toad” is typically applied to anurans that are more terrestrial and show a warty, dry skin and short hindlimbs. This thesis follows the above informal distinction between frogs and toads, using the predominant lifestyle and anatomy as discriminating characters. The distinction between frogs and toads is potentially useful when interpreting the taphonomy of fossil anurans, because terrestrial and aquatic anurans likely differ in taphonomy.

According to molecular phylogenetic analyses, crown-group frogs (Anura) originated over 200 Ma ago (Feng *et al.* 2017; Stocker *et al.* 2019). The terrestrial amphibamiforms from the Late Palaeozoic are considered to be the progenitors of modern amphibians (Schoch 2022; So et al. 2024). The earliest fossil record of anurans is represented by Early Triassic specimens that were assigned to the clade of Salientia (Evans & Borsuk-Białynick 2009; Ascarrunz *et al.* 2016). Additional salientians were discovered in sediments from the Late Triassic (Stocker *et al.* 2019) and the Early Jurassic (Jenkins Jr. & Shubin 1998). The salientian *Prosalirus bitis* (251–247 Ma, Early Jurassic, Kayenta Formation, USA; Ascarrunz *et al.* 2016) is thought to have the earliest Bauplan associated with leaping locomotion in salientians

(Jenkins Jr. & Shubin 1998; Reilly & Jorgensen 2011). Anurans are considered to have experienced a rapid diversification at the Cretaceous–Palaeogene boundary (Feng *et al.* 2017). The Cretaceous–Palaeogene extinction event may have facilitated explosive radiations of anurans through the creation of new ecological opportunities (Feng *et al.* 2017).

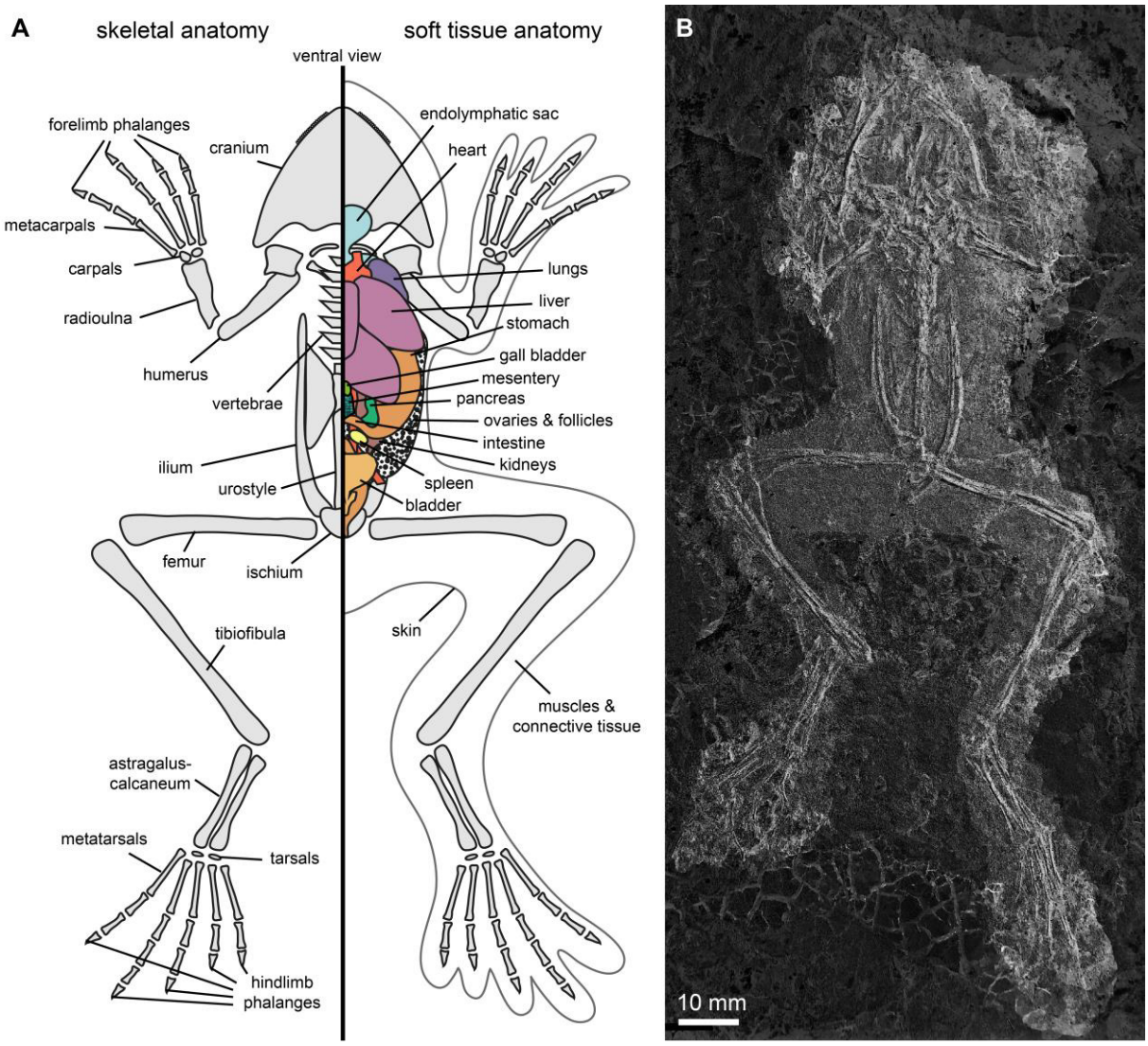


Figure 1.1: Anuran anatomy. A, Schematic of skeletal elements and soft tissues of the anuran body. B, Photograph in false colours of the skeleton of the largest anuran specimen (Pelobatidae; GMH Ce II-4949-1930) in the Geiseltal Collection. The skeleton of this specimen is near-complete and well-articulated. Photograph: D. Falk. Modified after Falk & Stache 2021.

Fossil anurans provide an ideal opportunity to understand taphonomic processes through space and time as the anuran Bauplan (Figs. 1.1A–B) and ecology have been retained since at least the Jurassic (Reilly & Jorgensen 2011; Roček 2013). Thus, variation in anuran preservation among fossil biotas is likely to relate primarily to environmental factors (e.g., temperature and habitat). By using a combination of information on the ecology and anatomy of extant anurans and taphonomic experiments, fossil anurans can provide insights into the evolution of anuran anatomy, ancient habitats and their depositional environments.

Fossil anurans are abundant components of many Lagerstätten and such have been studied from numerous Mesozoic, Palaeogene and Neogene Lagerstätten (Figs. 1.2A–D), including the Gold Spring Quarry (Early Jurassic, USA; Shubin & Jenkins 1995), Morrison Formation (Late Jurassic, USA; Henrici 1998), Las Hoyas (Early Cretaceous, Spain; Báez 2013), Niuweigang (Early Eocene, China; Wang *et al.* 2017), Messel (Middle Eocene, Germany; Wuttke 2018; Fig. 1.2C), Quercy (Middle to Late Eocene, France; Rage 2016; Georgalis *et al.* 2023), Rott (Late Oligocene, Germany; (Maus & Wuttke 2002), Enspel (Late Oligocene, Germany; Roček & Wuttke 2010), Bechlejovice (Early Oligocene, Czech Republic; Spinar 1972; Roček 2013; Fig. 1.2B), Libros (Late Miocene, Spain; McNamara *et al.* 2009; McNamara *et al.* 2012a; McNamara *et al.* 2016; Fig. 1.2D), Volchaya Balka and Gaverdovsky (Late Miocene, Russia; Syromyatnikova 2018), Langebaanweg (Early Pliocene, South Africa; Matthews *et al.* 2015) and Camp dels Ninots (Middle to Late Pliocene, Spain; Blain *et al.* 2023). Many fossil anuran specimens preserve soft tissues. Most fossil anuran studies to date have focussed on taxonomy. A few studies have investigated the lifestyle, geographic distribution and/or taphonomy of ancient anurans (Henrici & Fiorillo 1993; Du *et al.* 2000; Rage & Roček 2003; McNamara *et al.* 2009; Wuttke & Poschmann 2010; McNamara *et al.* 2012a; Wuttke *et al.* 2012; Gardner 2016; McNamara *et al.* 2016b; Talavera *et al.* 2019; Mörs *et al.* 2020; Blain *et al.* 2023).



Figure 1.2: Photographs of fossil anurans from several Palaeogene and Neogene biotas. A, Anuran from the Geiseltal biota (Eocene, Germany) conserved in nitrocellulose lacquer, Palaeobatrachidae, Natural Sciences Collections, Halle (Saale), Germany. B, Anuran from the Bechlejovice biota (Oligocene, Czech Republic) conserved in host sediment, Palaeobatrachidae, National Museum, Prague, Czech Republic. C, Anuran from the Messel biota (Eocene, Germany) conserved in resin, Pelobatidae, Natural History Museum, Brussels, Belgium. D, Anuran from the Libros biota (Miocene, Spain) conserved in host sediment, Ranidae, Natural History Museum, London, United Kingdom. Photographs: A, C, D. Falk. B, M. McNamara. D, V. Rossi.

1.5 The Geiseltal Konservat-Lagerstätte and Geiseltal Collection

The site that hosts the stagnation-type Eocene Geiseltal Konservat-Lagerstätte is located ca. 20 km southwest of Halle (Saale) in Saxony-Anhalt, central Germany. The biota is hosted in a ca. 120 m thick sedimentary succession that is dominated by repeated intervals (each 3–25 m thick) of claystones, siltstones and sandstones intercalated with lignite intervals (each ca. 10–50 m thick; Eissmann 2002; Blumenstengel 2004; Krutzsch 2011). The lignites were exploited commercially in a series of open cast mines from the late 19th century until 1993. The mines were flooded in 2003 and, therefore, the remaining fossiliferous outcrops are no longer accessible. The first fossil reported from the site was a single tapiromorph (Perissodactyla) bone recovered in 1908 (Barnes 1926; Hellmund 2018; Falk & Stache 2021). The bone was described by Ben E. Barnes (1903-1966) in 1926, who is credited with having pioneered the studies of the Geiseltal biota (Hellmund 2018). In the following years, a series of publications on excavation techniques, taphonomy, descriptions of the biota and reconstructions of the Eocene environment of the Geiseltal site were written by the director of the geological institute of the Halle University and the first excavation leader Johannes Walther (1860–1937). The publication series was continued by his successors Johannes Weigelt (1890–1948) and Erhard Voigt (1905–2004).

Fossil excavations took place from the mid-1920s to 2000 (excepting 1938–1949 and the mid-1980s–early 1990s; Haubold 1995; Hellmund 2018); excavations at several sites were concurrent with mining. Many specimens were lost due to the ongoing mining work, the forces of nature (e.g., weather) and the brittle nature of the fossil-bearing slabs (Krumbiegel *et al.* 1983). Slabs often broke once the host sediment dried out; in particular, slabs that contained small specimens (e.g., anurans, newts, reptiles and small mammals) were affected by the fragility. Voigt invented an excavation method to overcome this loss ("Lackfilm method"; Voigt 1933, 1988; Section 3.11.3). He exposed the upper surface of the fossils *in situ* and soaked it with a transfer medium. Voigt initially used paraffin wax as the transfer medium (Figs. 1.3A, E) but replaced the wax by a nitrocellulose lacquer (Figs. 1.2A, 1.3B) in subsequent years due to several benefits such as its low weight. Following hardening of the transfer medium, he

roughly exposed the reverse side of the fossil and removed the slab from the field. A preparator subsequently removed the remaining sediment cover on the specimen from the reverse side, yielding a fossil on a wax/lacquer support.

The Geiseltal fossil vertebrates were excavated from 35 discrete sites (Haubold & Hellmund 1998). Excavation sites were classified on the basis of sedimentology and fossil content as sinkholes, fluvial channel deposits and "dying fields" ("Leichenfelder"; Weigelt 1933; Krumbiegel 1962, 1975, 1977; Krumbiegel *et al.* 1983; Haubold & Krumbiegel 1984; Voigt 1988; Haubold & Hellmund 1998; Hellmund 2018). Each type of site has a different faunal composition (see Section 3.2 for more information).
Most Geiseltal fossils were excavated from lignite intervals. Vertebrate remains are relatively rare in the intercalating siltstones and sandstones ("Hauptmittel"; Haubold & Hellmund 1998). The geological sequence of the Geiseltal Lagerstätte includes six intervals, listed here from oldest to youngest: lower lower coal (LLC, "Untere Unterkohle"), lower middle coal (LMC, "Untere Mittelkohle"), upper middle coal (UMC, "Obere Mittelkohle"), upper sandstone/siltstone deposits (UHM, "Oberes Hauptmittel"), lower upper coal (LUC, "Untere Oberkohle") and middle upper coal (MUC, "Mittlere Oberkohle"; Lincke 1977; Haubold & Hellmund 1998).

The geological strata of the Geiseltal Konservat-Lagerstätte lack igneous components and other components that can be used for radiometric dating. Biostratigraphy was used to provide age estimates for the biota. The Middle Eocene Messel fauna (47 Ma; Mertz & Renne 2005) is similar to certain parts of the Geiseltal fauna. Mammal biochronology has been applied to correlate the lowermost lignite interval of the Geiseltal succession (Franzen & Haubold 1987; Aguilar *et al.* 1997) with the uppermost part of the succession hosting the Messel Lagerstätte. Hence, the Geiseltal strata are interpreted as Middle to Late Eocene in age. These mammal biochronology data are, however, controversial as diagnostic anatomical characters are difficult to verify in the Geiseltal mammals (Ring *et al.* 2020; Georgalis *et al.* 2021). Palynomorph biostratigraphy and estimates of sedimentation and compaction

rates suggest a late Early or Middle Eocene age. Collectively, these data indicate that the Geiseltal strata span up to the entire Lutetian Stage (Krutzsch *et al.* 1992; Krutzsch 2011; Georgalis *et al.* 2021). Further work is needed to fully resolve the exact age determination of the Geiseltal strata.

In the Eocene, the Geiseltal depositional environment was located a few kilometres west-southwest of the palaeo-North Sea (Küstermann *et al.* 2008; Krutzsch 2011; Hastings & Hellmund 2015a). The broad depositional environment of the Geiseltal strata has been described as a subtropical coastal bog; a halophile flora and fauna indicate elevated salinity in the water and soil (Krumbiegel *et al.* 1983). The region in the vicinity of lakes and ponds was dominated by swampy forests with dense vegetation, which were drained by meandering rivers with flood plains (Raupach 1948; Krumbiegel *et al.* 1983; Hastings & Hellmund 2015a).

Since 1934, most excavated specimens have been stored in the Geiseltal-Sammlung (Geiseltal Collection), which is located in the 16th century Allerheiligenkapelle (All Saints chapel) in Halle (Saale) and form part of the Natural Sciences Collections (ZNS) of the Martin-Luther-University Halle-Wittenberg in Halle (Saale). The collection was established by former excavation leaders Johannes Weigelt and Erhard Voigt. It includes ca. 50,000 specimens, more than 50% of which are vertebrates. Many plant fossils (Fig. 1.3D), a few sediment samples and a minority of vertebrate fossils of the Geiseltal Collection are located in several international institutions (e.g., Berlin [e.g., plants], Basel [e.g., birds], Coburg, Dessau-Rosslau [e.g., anurans], Dresden, Gottingen, Krefeld, Munich and Prague; Falk & Stache 2021). One anuran specimen from the Museum of Natural History Dessau-Rosslau (No. 11470) is included in this study. The Geiseltal Collection was recently awarded the status of “National wertvolles Kulturgut” (nationally valuable cultural heritage) in Germany.



Figure 1.3: Photographs of fossil specimens from the Geiseltal Collection. A, Alligatoroid crocodilian (Diplocynodon) in paraffin wax; the arrowhead indicates a cluster of gastroliths (stomach stones). B, Fish (Thaumaturus spannuthi) with soft tissue preservation in the eyespot and the body cavity; the specimen is conserved in nitrocellulose lacquer. C, Near-complete and articulated skeleton of the tapir-like ungulate

(Lophiodon); the specimen is conserved in gypsum. D, Angiosperm leaf with insect feeding traces on the lower left leaf margin; the specimen is conserved in the original sediment. E, Artiodactyl mammal (Amphirhagatherium) with preserved soft tissues in the body cavity; the specimen is conserved in paraffin wax; Photographs: A, O. Wings. B–E, D. Falk.

The Geiseltal biota includes amphibians (ca. five taxa; Figs. 1.1B, 1. 2A, 2.1A), fish (ca. four taxa; Fig. 1.3B), lizards (ca. 25 taxa), mammals (ca. 76 taxa; Fig. 1.3E) and birds (ca. 14 taxa). Among the mammals are bats, creodonts, marsupials, primates, rodents and many ungulates, including early equids and tapiromorphs (Fig. 1.3C). Invertebrates include bivalves, gastropods and a rich insect fauna (ca. 155 species; Krumbiegel *et al.* 1983). Plant fossils (Fig. 1.3D) are abundant and include cryptogams, gymnosperms and angiosperms (Rüffle *et al.* 1976; Krumbiegel *et al.* 1983; Wilde 1995; Rüffle & Litke 2000). The Geiseltal flora also includes rare fibrous laticifers termed “monkeyhair” (McCoy *et al.* 2021). Other components of the biota are crocodilian and avian eggs (Kohring & Hirsch 1996; Hastings & Hellmund 2015b; Mayr 2020), fossil resin (Simoneit *et al.* 2020) and trace fossils (Figs. 1.3A, D; Falk *et al.* 2019). Several insects show iridescent structural colours. Plants are reported to show green colour and the preservation of chlorophyll (Dilcher *et al.* 1970; Krumbiegel *et al.* 1983).

The biota includes abundant vertebrate specimens that are near-fully articulated, near-complete and/or preserve soft tissues, the latter including integument and stomach contents (Krumbiegel *et al.* 1983; Voigt 1988; Wilde & Hellmund 2010). The soft tissues of the Geiseltal fossil anurans have been described in detail; various soft tissues are reported to show cellular fidelity, including epidermis and dermis, collagen fibres, muscle tissue and blood vessels; bacteria are also reported (Voigt 1935, 1937). Voigt stated that the preserved tissues include a component of silicic acid (Voigt 1937) and suggested that preservation of all Geiseltal soft tissues results from a three-step process: (1) initial tanning of soft tissues by humic acid (from the lake/pore waters) followed by (2) impregnation and then (3) replacement by silicic acid (“molekularer Austausch” [molecular exchange], Voigt 1937, p. 19) during

diagenesis (Voigt 1937). Subsequent work suggested that tanning and silicification were mutually independent and apply to different tissues (Voigt 1988). The proposed source of silica is the host sediment, specifically diatoms, plant tissues rich in silica particles and silicates (Voigt 1937, 1988). The high fidelity preservation of vertebrate soft tissues by replication in authigenic silica is not known elsewhere in the fossil record.

Despite its taphonomic history and varied in fauna and flora, the Geiseltal biota was largely unstudied for almost 90 years. In 2018, a call by the Natural Sciences Collections (ZNS) in Halle (Saale) for international researchers sparked the initiation of a modern scientific investigation on the Geiseltal Collection. These recent studies are focused on the taxonomy of individual elements of the biota, e.g., the avifauna (Mayr 2020), mammals (Ring *et al.* 2020) and squamates (Georgalis *et al.* 2021) and rarely focus on taphonomy.

This thesis investigates the taphonomic history of the Geiseltal anurans using modern microbeam imaging and chemical analytical techniques.

1.6 Aims of this thesis

This thesis has three aims. The first aim of this study is to identify patterns in the skeletal taphonomy of the Geiseltal anurans using taphonomic metrics. The second aim is to assess the fidelity of soft tissue preservation and the historical taphonomic models (Voigt 1937, 1988) using modern techniques. The third aim of this thesis is to investigate the carbonaceous, melanosome-rich soft tissues that are associated with the Geiseltal anurans.

1.6.1 Identification of patterns in skeletal taphonomy

An objective of this thesis is to investigate the skeletal taphonomy of the fossil anurans from Geiseltal in order to assess for patterns in preservation. The study aims to develop a comparative approach using

skeletal element data from anurans to quantitative analysis of the skeletal taphonomy data from Geiseltal and other biotas (Chapter 3).

This study tests the hypotheses that:

(A) The fidelity of preservation is consistent for all skeletal elements.

(B) The fidelity of preservation is linked to excavation site and taxonomy.

(C) The cause of death is either desiccation or lake overturn.

(D) The preservation of anurans in lacustrine-hosted Palaeogene/Neogene settings shows taphonomic trends (e.g., recurring states of completeness and articulation in different fossil sites).

1.6.2 Testing the historic taphonomic models for soft tissue preservation

The study aims to analyse the Geiseltal anuran soft tissues and to test the evidence for a unique mode of preservation (Voigt 1937, 1988) using diverse microbeam imaging and chemical analytical techniques (Chapter 4).

This study tests the hypotheses that:

(A) Fossil anuran soft tissues are preserved.

(B) The fossil soft tissues include muscles, veins, pigment cells and integument, all preserved with sub-cellular fidelity.

(C) The anuran soft tissues, in particular the integument, are replicated in authigenic silica.

1.6.3 Investigating the anuran melanosomes

The study aims to investigate the carbonaceous, melanosome-rich soft tissues from the Geiseltal anurans (Chapter 5), if hypothesis 1.6.2 (A) is correct.

This study tests the hypotheses that:

(A) The melanosomes differ in geometry among body regions.

(B) The geometries of the melanosomes from Geiseltal anurans are similar to that of fossil anurans from selected Cenozoic biotas.

(C) Melanosome geometry is similar for the Geiseltal anurans and extant anurans and therefor informs on anuran biology.

2. Material and methods

This chapter describes the material and approaches used in this project, including a brief discussion of the basic principles, applications and limitations of each technique. This chapter also summarises the sample preparation protocols.

2.1 Fossil specimens

Early reports referred to ca. 200 anurans in the Geiseltal Collection (Kuhn 1941; Krumbiegel *et al.* 1983). Many specimens were reported as adult anurans and a few as tadpoles. Most of the specimens were excavated and prepared during the 1930s (Weigelt 1933; Kuhn 1941); the remainder, during the 1950s–1970s. Almost all specimens were prepared via the transfer method (i.e. "Lackfilm method"; Voigt 1933, 1988; see Section 3.11.3) and are conserved in paraffin wax or nitrocellulose lacquer; only one anuran specimen is hosted in-situ in sedimentary matrix.

Currently, 180 specimens in the Geiseltal Collection are assigned to Anura (including one specimen that is owned by the Museum of Natural History Dessau-Rosslau; Appendix 1); the location of the remaining 20 specimens is unknown. All 180 available specimens were investigated using a light microscope (Fig. 2.1A). All tadpoles (12 specimens) were then omitted from this study as they have a different Bauplan to adult anurans. The working dataset thus comprises 168 specimens (Appendix 3); 31 specimens of those are conserved in paraffin wax, 136 specimens are conserved in nitrocellulose lacquer and only one anuran specimen is hosted in-situ in sedimentary matrix and is conserved in water.

Most (n = 121) of the 168 studied specimens in this thesis were excavated from the "dying field" (Weigelt 1933; Hellmund 2018) deposits at the sites Cecilie II (Ce II) and Cecilie III (Ce III). Ce II exposes strata of the lignite interval lower upper coal (Haubold & Hellmund 1998) and Ce III exposes strata of

the lignite interval upper middle coal (Krumbiegel 1962a). Forty anurans are from sinkhole deposits (i.e., Cecilie I, Cecilie IV, Cecilie V, Cecilie VI, Leonhard III, Leonhard V and Neumark South XXXV; Haubold & Krumbiegel 1984). A single specimen is from riverbank and flood plain deposits, i.e., site XIV (Neumark West XIV in Haubold & Krumbiegel 1984) of interval lower lower coal (Krumbiegel 1962a; Haubold & Krumbiegel 1984). Stratigraphic data are not available for the remaining six specimens. A detailed description of the different deposit types is provided in Section 3.2: Geological Setting.

Most anuran specimens are of undetermined taxonomic affinity (n = 99). A sizeable minority have, however, been assigned previously to the (mainly terrestrial) Pelobatidae (n = 54) or (mainly aquatic) Palaeobatrachidae (n = 15) (Kuhn 1941; Roček & Rage 2000; Roček 2013; Roček *et al.* 2014). Certain specimens of the previously assigned specimens may represent Discoglossidae (Rage & Roček 2003; Roček 2013).

Many slabs retain small (< 10 mm) patches of dark, organic-rich sedimentary matrix; no distinctive sedimentary textures or fabrics are evident. Most slabs (n = 166) contain one specimen; the remaining two slabs each include two specimens. A single slab includes fish scales in addition to the anuran remains.

Completeness and articulation vary between specimens. Most specimens are well-articulated skeletons but show truncated skeletal elements at the edge of the slab. Specimens comprising disarticulated, scattered bones or isolated, articulated limbs are rare. Many Geiseltal anurans show a body outline that is characterised by patches of a dark brown homogenous material and/or patches of a beige to pale orange material with a honeycomb pattern. Early studies of the fossil anurans reported preservation of skin cells, glands, connective tissue, blood capillaries, melanophores and pale greenish coloration in certain specimens (Voigt 1935, 1937, 1988). Surprisingly, there has been no further investigation of these findings until the current study.

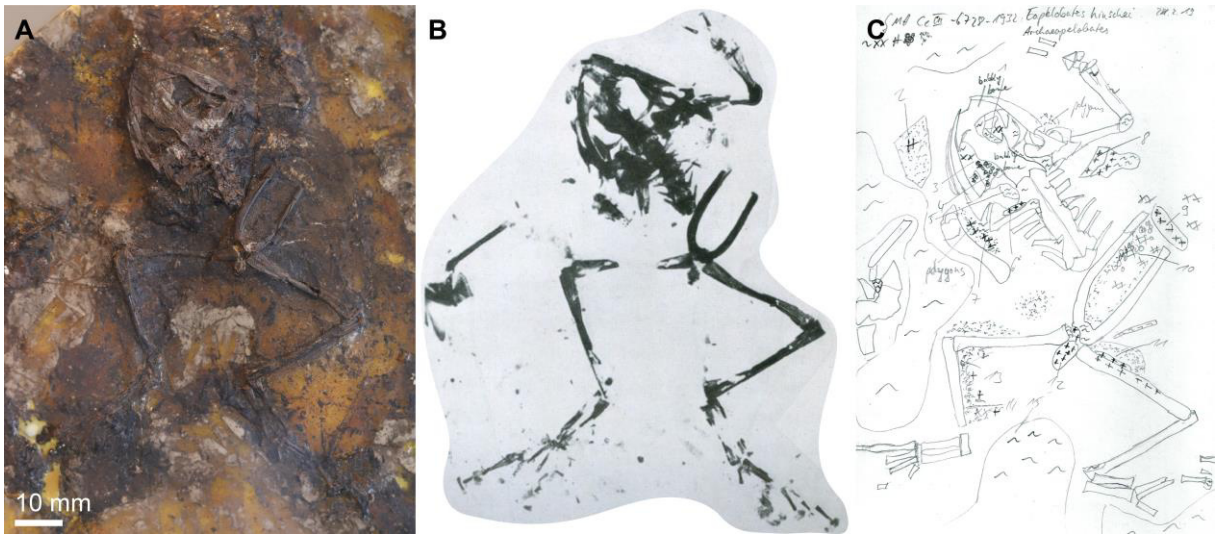


Figure 2.1: Photograph, X-ray image and hand drawing of an incomplete anuran from the Geiseltal Collection (Pelobatidae), GMH Ce III-6728-1932. A, Photograph showing the specimen conserved in nitrocellulose lacquer with dark body outline in the torso, abdomen and limbs. B, X-ray image of the specimen reveals the skeletal elements. C, Schematic hand drawing of the specimen skeleton with notes on the soft tissue textures and sediment patches that are present on the slab. Modified after Falk & Stache 2021. Photograph and drawing: D. Falk. X-ray image from Kuhn (1941).

2.2 Light microscopy

Prior to sampling, all 168 specimens were investigated using a Leica EZ4W microscope. Freehand sketches of all specimens include details of the macroscopic (e.g., skeleton) and microscopic features (e.g., microtextures) observed (Fig. 2.1C). It is noteworthy, that each specimen required a careful examination under the microscope to discriminate the specimen features (e.g., skeletal elements and soft tissues) from the surrounding embedding medium (i.e., lacquer and sediment; Figs. 2.1A–B). All samples of soft tissue and sediment were examined microscopically prior further analysis using a Leica EZ4W and/or a Leica DVM2500 high-power digital microscope with VZ700 C zoom lens.

2.3 Sampling and sample preparation

Sampling was necessary to investigate the chemistry of the anuran host sediment and several materials that indicated fossil soft tissues in anuran specimens to interpret the mode of soft tissue preservation. An investigation of complete specimens outside the Geiseltal Collection was not possible due to the national heritage status of the specimens. Sampling was performed using a sterile metal scalpel and sterile metal forceps (Fig. 2.2A). Samples of soft tissue and sediment samples are each ca. 0.5 x 0.5 mm in size (Appendix 1). Samples were mounted on aluminium stubs with carbon tape (Fig. 2.2B). Selected sediment samples were put in glass vials.

Four samples of soft tissue (4983-D3a1, 4983-D3b1, 6743-C8a and XXXV-11a-C2b1), each ca. 0.5 x 0.5 mm, were directly embedded in low viscosity resin (Spurr low viscosity test kit, Ted Pella Inc.). The embedded samples were then placed in a Memmert vacuum oven and held at 60°C for 30 minutes at low vacuum (35 mbar). The vacuum was then released over 15 seconds. This procedure (placing samples in vacuum oven) was repeated three times. Finally, the samples were polymerised at 60°C for 48 h. Due to incomplete polymerisation, two samples were polymerised for an additional 12–48 h at 70°C. Three samples were then cut using a Leica Ultracut UC7 RT ultramicrotome. Ultrathin sections were picked up on glass slides for subsequent analysis.

Low viscosity resin embedding protocol (Spurr low viscosity test kit, Ted Pella Inc.):

1. Mix resin following the manufacturer's recipe; stir slowly to avoid bubble formation.

2. Place samples in coffin moulds and fill coffin moulds carefully with resin.

3. Place samples in vacuum oven, set the temperature to 60°C and set pressure to 35 mbar (low vacuum). Leave sample for 30 minutes in oven, then release vacuum over 15 seconds. Repeat three times to promote infiltration of the resin into the sample.

4. Hold samples in oven at 60°C at low vacuum (35 mbar) for 48 h for polymerisation.

5. In case of incomplete polymerisation, polymerise samples in oven at 65–70°C at low vacuum (35 mbar) for an additional 12–48 h.

One sample (4936-a-A1, Appendix 1) of soft tissue was embedded in EpoThin low viscosity epoxy resin (Agar Scientific Ltd.) as follows. A plastic O-ring (ca. 26 mm diameter) was placed on Sellotape. The sample was put inside the O-ring and the O-ring filled carefully with epoxy resin. The sample embedded in epoxy resin was held at room temperature for 24h to allow the resin to polymerise. After further preparation of the sample, it was later used for SEM analysis, EPMA and μ-FTIR spectroscopy.

Resin embedding protocol for EpoThin low viscosity epoxy resin:

1. Dehydrate sample in vacuum oven for 24 h at 60°C.

2. Mix the resin and the hardener in a 2:1 ratio.

3. Place O-ring on sticky tape. Place sample in centre of O-ring using forceps.

4. Carefully fill O-ring with resin to envelope the sample in resin.

5. Hold sample in resin at room temperature for 24h to allow the resin to polymerise.

Sediment samples (Appendix 1) were collected from regions usually beyond the body outline. The samples usually contained brown to black, mm-sized sediment particles and/or pieces of up to ca. 3 x 3 mm that were sampled with forceps. Where sediment particles were too small for sampling with forceps, small regions of sediment on the slabs were scraped gently with a scalpel to collect sufficient fragmented sample material. The sediment samples that were analysed in this thesis are from 13 slabs; 11 slabs exclusively contain anuran bones and two slabs exclusively contain fish bones to compare the mineral content of anuran-hosting sediment with that of fish-hosting sediment. For each sample, a

small amount (0.1–2 g) of sediment was powdered manually with a sterile agate pestle and mortar (Fig. 2.2C). Powders were stored in sealed glass vials (Fig. 2.2D).

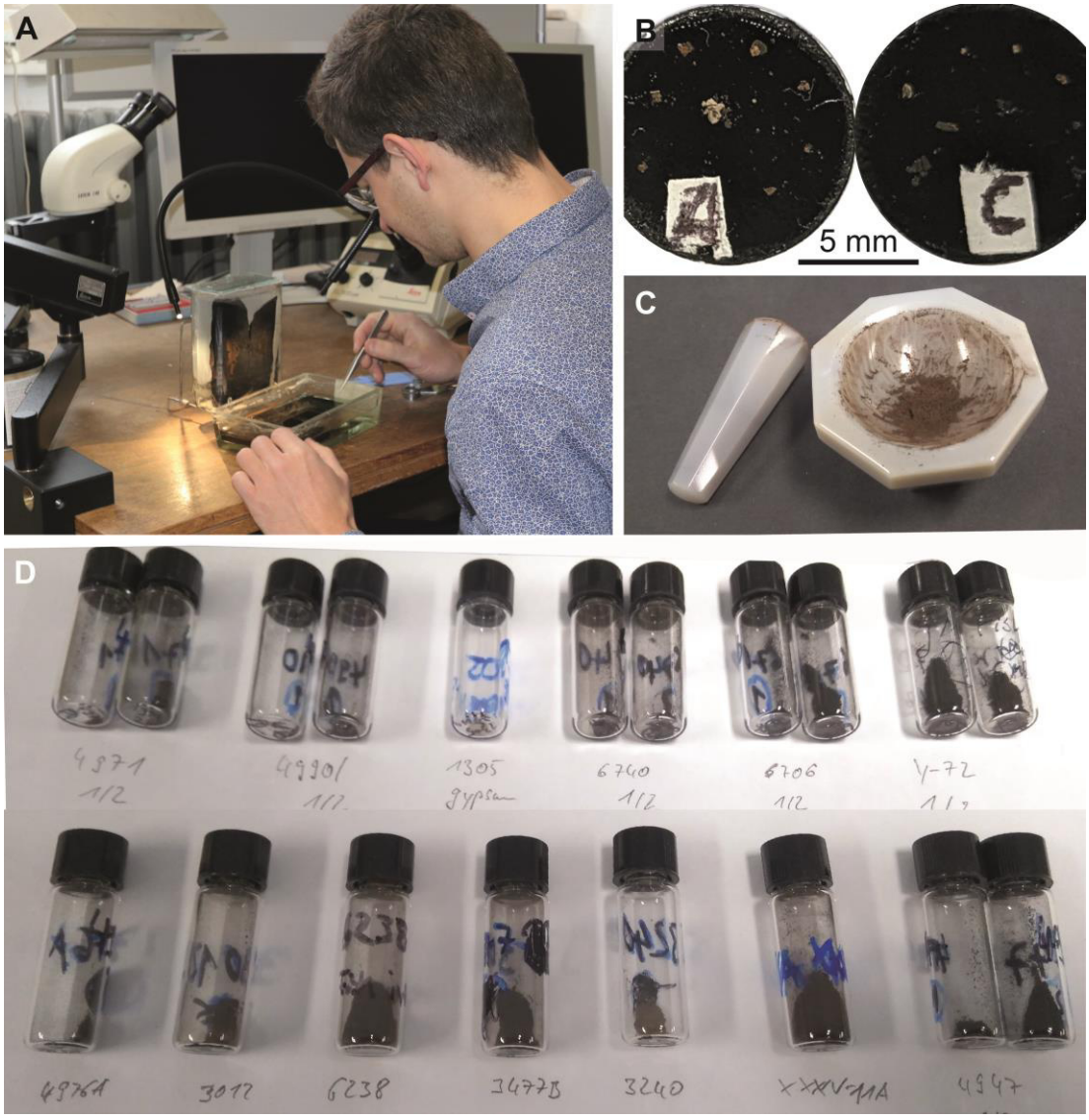


Figure 2.2: Photographs of the sampling of fossil soft tissues from the Geiseltal anurans, of the sediment sample preparation and of certain sediment and soft tissue samples. A, Sampling of fossil anuran soft tissues performed by D. Falk using sterile metal scalpels and forceps. B, Scanning electron microscope aluminium stubs with fossil soft tissue samples, each ca. 0.5 x 0.5 mm, on carbon sticky tape. C, Homogenisation of sediment samples with an agate pestle and mortar. D, Selected sediment samples in glass vials. Photographs: D. Falk.

Two sediment samples (XXXV-11_polished_01 and XXXV-11_polished_02; Appendix 1) were embedded in resin in coffin moulds using the protocol for the Spurr low viscosity resin (Ted Pella Inc). These two resin-embedded samples were too small to manually polish the sample surfaces using polishing plates. For easier handling, the two samples in resin were embedded in Clear Hard Type UV Resin (Let's Resin®, Apex Ce Specialists Ltd.). For this, two plastic O-rings (ca. 15 mm diameter) were placed on Sellotape. The two resin blocks containing the samples were then each placed in the centre of an O-ring. Each O-ring was filled with UV resin; the resin enveloped the sample. The resin was polymerised by the exposure to artificial UV light for 2 minutes. After polymerisation, samples were polished using a graded series of polishing plates (4,000 grit, 2,500 grit, and 1,200 grit, each for ca. 5–10 minutes, and finishing with 1 µm diamond paste on silk for ca. 20 minutes), mounted on Al stubs with carbon tape and sputter coated with Au.

Embedding protocol for Clear Hard Type UV Resin (Let's Resin®, Apex Ce Specialists Ltd.):

1. Place O-ring on sticky tape. Place sample in centre of O-ring.

2. Carefully fill O-ring with resin to envelop sample in resin.

3. Expose to artificial UV light for 2 minutes.

2.4 Scanning electron microscopy (SEM) and energy-dispersive X-ray spectroscopy (EDS)

Scanning electron microscopy (SEM) is a common imaging technique used in many fields of science including natural history sciences and material sciences. In palaeontology it is widely used for high-resolution imaging of micron-scale features including fossil soft tissues (McNamara *et al.* 2009; McNamara *et al.* 2016b; McNamara *et al.* 2018; Rossi *et al.* 2019; Slater *et al.* 2020; Cincotta *et al.* 2022).

A scanning electron microscope (Fig. 2.3A) contains an electron gun, an electron column, a specimen chamber and electron detectors (Abd Mutalib *et al.* 2017; Pan *et al.* 2018). The electron gun is located at the top of the electron column and produces an electron beam by passing an electric current across a tungsten filament in a vacuum. The emitted electron beam enters the electron column, where it passes through and is focussed by an anode (a metal disc with a hole in the centre) and a series of magnets, apertures and lenses. The focused beam enters the specimen chamber where it penetrates the sample surface and interacts with the uppermost few microns of the sample surface. This process generates secondary electrons, which are detected by a dedicated secondary electron detector that is located at an angle to the sample stage. The angular offset between the electron source and the detector induces a shadow effect that supports the conversion of electron counts into surface topography. Shadow effects can mask, however, features on sample surfaces with high topography and can create artefacts. The constructed secondary electron image of the sample surface can show features on the nanometre-scale.

Certain scanning electron microscopes can detect back-scattered electrons (BSE), which are of much higher energy than secondary electrons and are therefore emitted from deeper in the sample (Pan *et al.* 2018). A typical BSE detector is located directly above the sample and provides information on the elemental composition of a sample; heavier elements are associated with more backscatter events than lighter elements and therefore occur brighter in the backscatter electron image. Backscatter electron images are less impacted by the sample topography than secondary electron images.

The EDS detector detects X-rays that are generated by atoms that are penetrated by an electron beam. The electron beam interacts with atoms of the upper few microns of the sample surface (Abd Mutalib *et al.* 2017). When the electron beam interacts with an atom, an electron of an inner, low energy-level atom shell is knocked out and instantly replaced by an electron from an outer, high-energy level shell. This transition is associated with an energy imbalance that is resolved by the release of atom- and shell-

specific X-rays (i.e., X-rays that are diagnostic for certain atoms and energy levels). The detector counts the X-rays and differentiates them based on their energies. The qualitative chemical information from these X-rays can be visualised as X-ray spectra and elemental X-ray maps (Abd Mutalib *et al.* 2017). SEM and EDS are destructive techniques. Samples that are analysed by SEM or EDS can show irreversible micron-scale alterations (electron beam damage) in regions that are exposed to the electron beam for an extended period (e.g., during EDS element mapping).

The size of the specimen that can be accommodated in the scanning electron microscope sample chamber depends on the model of scanning electron microscope. Certain sample chambers are sufficiently large to accommodate samples that are several m^3 in size. The scanning electron microscope used in this thesis has a sample chamber that accommodates specimens up to ca. 0.1 m^3 (Fig. 2.3A). For specimens > 100 mm in width, certain regions of the specimens cannot be targeted by the electron beam because the movable sample stage in the sample chamber reaches its motion limits. In these cases, the regions of the specimen that are outside the free scope of the stage will need to be sampled.

Non-conductive samples are prone to charging during SEM analysis; consequently, images and chemical maps show artefacts such as poor focus, unstable surfaces, excessive contrast, brightness and saturation. To overcome charging problems, the sample can be sputter-coated with a 3–20 nm thick conductive layer of e.g., Au, Pd or C (Fig. 2.3B). Additional approaches to reduce sample charging include the reduction of the accelerating voltage, the reduction of the probe current, lowering the sample stage, lowering the working distance and/or the analysis of the sample in low vacuum. It is notable, that the scanning electron microscope used in this study has a variable pressure mode and cannot perform analyses on liquid or wet samples. In contrast, a scanning electron microscope with environmental mode can analyse liquid and wet samples.

In this project, a JEOL JSM IT100 VP-SEM (Fig. 2.3A) was used to image soft tissues of the Geiseltal anurans and the associated host sediment. Both secondary electron (SE) and backscatter electron (BSE) detectors were used for imaging. EDS was used to collect X-ray spectra and maps from soft tissues and associated sediment. Samples were usually ca. 0.5 x 0.5 mm in size and mounted on aluminium stubs using carbon tape (Fig. 2.2B); certain samples were sputter coated with Au. Samples were analysed at an accelerating voltage of 5–20 kV and a working distance of 6–10 mm for SEM and BSE images and at 10 kV and a working distance of 10 mm for EDS maps and spectra. Acquisition times of 30–45 min and a dwell time of 0.2 ms were used for EDS maps and an acquisition time of 120 s was used for EDS spectra.

Protocol for SEM, BSE and EDS operation:

1. Place sample on Al-stub on carbon sticky tape using sterile metal forceps.

2. Place sample in SEM specimen chamber. Close chamber and start process to create high vacuum in the chamber as per manufacturer's protocols.

3. Start imaging. Adjust focus, brightness and contrast. Adjust astigmatism and beam alignment (wobble) at magnification of ca. 6000x to get sample surface in focus.

4. Adjust focus, brightness and contrast as necessary during imaging.

5. Repeat adjustments of astigmatism and beam alignments each time the acceleration voltage, probe current, aperture or pressure is changed.

6. For EDS only: ensure working distance is 10 mm.

7. Switch to EDS user interface and ensure that analytical parameters are correct for the analysis type (e.g., single spot analysis, line mapping or spatial mapping).

8. Maintain count rate at ca. 3000–5000 counts per second by adjusting the probe current and/or accelerating voltage.



Figure 2.3: A selection of photographs of in-house techniques that were used for the analysis of the Geiseltal fossils in this thesis; Mary Ward Microbeam Laboratory, School of Biological, Earth and Environmental Sciences. A, Scanning Electron Microscope with BSE and EDS detector; JEOL JSM IT100 VP-SEM. B, Au sputter coater (left) and C sputter coater (right); both Agar Scientific SEM Sputter Coater with pumping system. C, Fourier-transform infrared spectrometer with attenuated total reflectance attachment; Perkin Elmer Spotlight 400i ATR-FTIR. D, Raman spectrometer; Renishaw InVia Qontor. Photographs: D. Falk.

2.5 Micro-Fourier-transform infrared spectroscopy (µ-FTIR)

Fourier-transform infrared spectroscopy (FTIR) has a wide range of applications for analysing the inorganic and organic chemistry of solids, powders and liquids. FTIR has common applications in food science, e.g., to detect traces of contaminants, and in cultural heritage studies, e.g., to analyse the chemical composition of paint and paintings. Geological applications include the detection of volatiles

in rock samples to infer magmatic processes. In palaeontology, FTIR is often used to analyse fossil soft tissues, e.g., to support the presence of chemical residues of collagen in fossils (Lee *et al.* 2017), to support the presence of eumelanin and phaeomelanin in fossils (McNamara *et al.* 2016b; Slater *et al.* 2023b) and to characterise taphonomic processes (Lebon *et al.* 2014; Slater *et al.* 2023b).

An FTIR spectrometer (Fig. 2.3C) consists of three basic components: (1) An infrared (IR) radiation source that emits radiation with wavelengths ranging from 10000–100 cm^{-1}, (2) an interferometer for the time-dependent modification of the spectral composition of the IR radiation and (3) a radiation intensity detector. FTIR spectra can be acquired by three basic techniques: reflectance, transmission and attenuated total reflectance (ATR). In reflectance mode, the IR radiation reaches the sample at a defined angle and a detector collects the radiation that is reflected at the same angle. In contrast, in transmission mode, the IR radiation that passes through the sample is collected by the detector. In ATR mode, the IR radiation passes through a crystal, which is in contact with the sample. The radiation is reflected at the crystal-sample interface and returns through the crystal to the detector. The sample penetration depth depends on the crystal material used. In all three techniques, some of the IR radiation that interacts with the surficial zone of the sample is absorbed by the sample.

FTIR analysis can provide information on the molecular composition of both inorganic and organic samples. Molecules of a sample interact with IR radiation that has a characteristic wavelength. The molecules respond by vibrating in one or more modes (stretching, bending, wagging, rocking and twisting of chemical bonds). The molecules will absorb IR radiation if the frequency is greater than or equal to the energy required to generate a vibrational mode in the molecule. The bonds in functional groups (e.g., amides) can also absorb IR radiation at characteristic frequencies. The absorbance of IR radiation by molecules and functional groups is recorded in an interferogram and then converted into a spectrum using a Fourier-transform. The spectrum in the mid-IR range (4000–400 cm^{-1}) shows two regions of interest: (1) 4000–1200 cm^{-1}; these wavenumbers are characteristic of functional groups

comprising mainly light atoms. (2) The fingerprint region between 1200–400 cm^{-1}; peaks here are characteristic of heavy atoms and can be diagnostic of a given compound. In general, peak height is linked to the concentration of the functional group.

FTIR analysis does not require a vacuum. The μ-FTIR system used for this thesis needed a manual supply of liquid nitrogen to cool the detector. The μ-FTIR analysis requires a flat sample surface, i.e. embedded samples require ultramicrotomy or extensive polishing prior to analysis. FTIR instruments can accommodate samples as large as the stage limits allow. Sample sizes typically range from 10 μm^3 to several cm^3. FTIR is an ostensibly non-destructive technique; that said, full quantification of chemical bonds requires destructive sample grinding in order to generate a powder. This powder is mixed with a known quantity of a different chemical powder ("spike"), that does not show any peak overlap with the sample.

An ATR-FTIR spectroscope (Perkin Elmer Spotlight 400i; Fig. 2.3C) was used in this study as it can analyse sample regions with an area of 100 x 100 μm rapidly for their chemical characterization and mineral phase determinations; the machine displays the chemistry in the form of a map. ATR analysis may not work correctly, if the crystal has problems making sufficient contact with a sample that is not of the correct hardness or flat enough. Indeed, the crystal may puncture a sample at the moment of contact. The IR radiation of the ATR penetrates typically around 5 μm into the sample; for organic samples, the penetration depth is only 1–2 μm.

In this thesis, an unknown mineral phase associated with the fossil anuran soft tissues was analysed using ATR μ-FTIR (Fig. 2.3C). The resin-embedded sample was polished manually for 15 minutes using diamond paste (1 μm grit) to remove the carbon coating and beam damage from prior electron microprobe analysis. The FTIR spectra were acquired from the freshly polished surface with a Perkin Elmer Spotlight 400i FTIR microscope system. An area of 100 x 100 μm was mapped using a spectral

resolution of 4 cm^{-1}, a spatial resolution of 1.56 μm^2 and 128 repeats. Spectra were processed post-acquisition using Perkin Elmer SpectrumIMAGE (v. R.1.11.2.0016) and Spectrum IR (v. 10.7.2) software as follows. An atmospheric correction was applied to the dataset and twenty spectra were extracted from a region of the skin and another twenty spectra extracted from a region of the embedding resin. A single averaged spectrum was generated for each sample type (skin and embedding resin, respectively); these averaged spectra were then baseline-corrected using a standard (non-interactive) algorithm and smoothed by a factor of 10. The resulting spectra were compared with similar spectra from the literature to determine the mineral phase.

Protocol for µ-FTIR ATR operation:

1. Cool detector with liquid nitrogen.

2. Measure background spectra.

3. Place sample in sample holder.

4. Select sample area to be analysed and perform measurements.

5. Perform atmospheric correction on acquired data using Perkin Elmer SpectrumIMAGE.

6. Perform additional post-acquisition processing of data (e.g. normalisation, averaging, base-line correction, smoothing) as required using external software (e.g., Perkin Elmer Spectrum IR).

2.6 Micro-Raman spectroscopy (µ-RS)

Raman spectroscopy has a wide range of applications, e.g., in the quality management of pharmaceutical industries, material sciences and biological sciences. It is a common way to identify gemstones and minerals. In palaeontology, Raman spectroscopy has provided supporting evidence for interpretations of fossil melanin (Rossi *et al.* 2022); more controversially (Alleon *et al.* 2021; Jurašeková *et al.* 2022; Wiemann & Briggs 2022), it has recently been used as a diagnostic tool to identify

degradation products of proteins and lipids in fossils (Wiemann *et al.* 2018; Fabbri *et al.* 2019; Wiemann & Briggs 2022).

A Raman spectrometer (Fig. 2.3D) uses a single wavelength, near-infrared laser that illuminates the sample. Most light is scattered from the sample without an energy change (i.e., Rayleigh scattering), but a minority of photons transfer energy to the molecules of the sample and return with an energy change (Raman scattering). The transfer of energy into molecules puts them into a vibrational mode (Smith & Dent 2019). Detectors collect the returned light and energies and convert the frequency shift (Raman shift) of the returned light into spectra. The scattered light passes through a series of filters that reduce and eliminate non-Raman-scattering and isolate the laser beam from scattered light.

The Raman shifts are commonly recorded for the wavelength range 250–4000 cm^{-1}. The range of 400–1500 cm^{-1} (fingerprint region) is considered to represent a combination of Raman shifts that is unique to the analysed chemical structure.

Raman scattering is stronger in molecules with homonuclear bonds (C-C or C=C) and weaker in polar bonds (C-O or O-H). Functional groups with symmetrical polar bonds (e.g., phosphates, sulfates), however, can also form strong bands (Smith & Dent 2019).

Raman spectroscopy does not require vacuum and usually does not require sample preparation (Pan *et al.* 2018). The approach can readily be applied to solids, powders and liquids. Raman spectroscopy can perform automated mapping of the chemistry of entire samples by acquiring spectra for each pixel in a raster. The size of a sample is limited to the scope of the movable sample stage. The machine used in this study can hold a sample of about ca. 150 mm x 150 mm x 50 mm (L x W x H) in size. Limitations in analysing samples using Raman spectroscopy relate to materials that are not Raman active, i.e., materials with no covalent bonds. Further, the sensitivity of Raman spectroscopy is limited by the

number of photons that show Raman scattering (ca. one photon for every 106 excitation photons). An additional limitation of Raman spectroscopy relates to the fluorescence of a sample. Fluorescence is an effect that is significantly more intense than the associated Raman scattering from a sample (Berry 2022). Fluorescence is caused by the absorption of light by an atom and the release of e.g., X-rays. The excitation of an electron results in its transition to a high-energy level. From this excited energy level, the molecule relaxes to the ground state by vibrational relaxation and the radiative transition can be associated with intense fluorescence emissions (especially where samples contain an amorphous mineral phase). Such emissions can obscure weak Raman peaks and bands and reduce the quality of spectra (Clarke & Oprysa 2004; Berry 2022). Fluorescence emissions can be reduced by changing the excitation wavelength, reducing the confocal pinhole diameter and photobleaching the sample (via exposure of the sample to laser irradiation prior to measurement).

Raman spectroscopy is usually non-destructive, but the laser beam can damage samples (beam damage) if the laser intensity is too high; this is particularly relevant during the analysis of organic matter. Beam damage is evident as an irreversible burn. In those cases, the acquired spectra of the measurements are invalid and further analysis of that same sampling point will yield artefacts due to thermal degradation.

In this study, μ-RS (Fig. 2.3D) was used to identify minerals in the sediment associated with the Geiseltal fossil anurans and to identify an unknown mineral phase present in the fossil anuran soft tissues. Samples of soft tissues and sediment were analysed using a Renishaw InVia Qontor confocal Raman microscope (Fig. 2.3D). Analyses used a 50 mW DPSS (diode-pumped, solid-state) 532 nm laser at 1%, 10% or 50% laser strength with a 50x or 100x objective, an exposure time of 1 s or 10 s and 10–100 accumulations per spectrum. For certain samples the region of interest was excited with a 30–60 s bleach prior to the acquisition of spectra in order to reduce the intensity of the fluorescent background.

Protocol for µ-RS operation:

1. Heat up the 532 nm laser.

2. Place sample on the sample stage in the Raman microscope.

3. Select the region of interest and collect the spectra. If required, expose the region of interest to laser irradiation prior to measurement for 30–60 s prior to the acquisition of spectra to reduce the intensity of the fluorescent background (bleaching).

4. Perform post-acquisition processing of data (e.g., baseline correction, smoothing, deconvolution) in an external software, if required. Choose parameters in post-acquisition processing carefully to ensure a stable spectrum across different polynomials and to prevent the generation of user-initiated artefacts.

2.7 Electron probe microanalysis (EPMA)

EPMA allows the quantitative and qualitative identification and mapping of chemical elements. It is widely used in material sciences and engineering, e.g., to characterise the chemical composition of materials. EPMA is used in several fields in the geosciences, such as petrology (e.g., to investigate meteorite composition), geochronology (e.g., for trace element identification) and palaeontology. In palaeontology EPMA is used to investigate fossilization processes (Zhang & Briggs 2007; Liesegang & Gee 2020; Muramiya *et al.* 2024).

SEM, EDS and the electron microprobe (EP) share a similar functional principle. An electron beam is emitted by a tungsten filament, lanthanum hexaboride crystal cathode or a field emission electron source. In vacuum conditions, the beam interacts with the sample atoms and causes certain electrons to vacate their shell, i.e., changing the energy level of the electrons. The replacement electrons from a higher energy level produce several effects of excitation, e.g., the emission of X-rays. EPs can operate in different ways: as wavelength-dispersive X-ray spectroscopy (WDS) and as energy-dispersive

spectroscopy (EDS, see Section 2.4). In EP wavelength-dispersive X-ray spectroscopy, the spectrometer consists of several bent analytical crystals that act as monochromators and an X-ray counter (Llovet *et al.* 2021; Yang *et al.* 2022). Each diffracting crystal is composed of a different material; typically, they are composed of lithium fluoride, pentaerythritol and thallium acid phthalate (Llovet *et al.* 2021; Yang *et al.* 2022). When X-rays encounter the analytical crystals at a specific angle, only those X-rays that satisfy Bragg's Law (i.e., the general relationship between the wavelength of the incident X-rays, angle of incidence and spacing between the crystal lattice planes of atoms) are reflected and a single wavelength is passed on to the counter. EPs are usually equipped with several spectrometers as WDS only allows the recording of one wavelength at a time (Batanova *et al.* 2018; Llovet *et al.* 2021). The principle of operation of WDS is slightly different from that of EDS, as an EDS detector detects X-rays and differentiates them on the basis of their energies and not on the basis of their wavelengths. The wavelengths detected by a WDS counter are diagnostic of specific elements and can be converted into spectra and maps. WDS analysis is ideally suited for the quantitative analysis of trace elements (Batanova *et al.* 2018); it has lower detection limits and a higher energy resolution than the EDS; overlaps between certain X-ray lines are less common (Llovet *et al.* 2021). As an EDS analysis usually requires shorter analysis times, it is often used as a preliminary analysis to determine major elements, followed by a WDS analysis to identify trace constituents (Llovet *et al.* 2021; Yang *et al.* 2022).

A limitation of WDS analyses is that an EP cannot identify any elements below atomic number three (e.g., H). Additionally, WDS analyses cannot identify element isotopes or to distinguish between different valence states of elements. For WDS analyses, a flat and highly polished (“mirror”) sample surface is needed. Furthermore, a thin conductive film (e.g., C or Au) needs to be sputter-coated to the surface of non-conductive samples to prevent charging effects (Yang *et al.* 2022). It is notable, that when using an EP, the electron beam can permanently alter or degrade the sample (electron beam damage).

In this thesis, EPMA was used to identify the mineral phase that is associated with the fossil anuran soft tissues. One sample of fossil anuran soft tissue was embedded in resin, polished, sputter coated with carbon and analysed with a field-emission CAMECA SX-5 FE electron microprobe at the Department of Earth Sciences, University of Oxford (UK). Certain measurements used a 5 nA beam with 10 µm spot size and a time correction applied to fluorine because of unstable count rates. All other measurements used a 2 nA beam with 10 µm spot size in order to minimise beam damage. A time-zero correction was applied to all elements to correct the measurements of X-ray intensities for elements whose signals were altered due to beam damage.

2.8 X-ray diffraction (XRD)

XRD analysis is commonly used in material sciences, environmental sciences, chemistry, forensic sciences. It investigates the physical properties (e.g., crystal structure and phase composition) of crystalline minerals. An XRD analysis provides data to answer analytical questions about the chemical and crystalline character of minerals. In palaeontology, XRD analysis is often used to investigate bone diagenesis (Piga *et al.* 2015; Grandi *et al.* 2023) and to identify mineral phases associated with fossil soft tissues (Anderson *et al.* 2020; Gueriau *et al.* 2020).

An X-ray diffractometer consists of three basic elements: an X-ray tube, a sample holder and an X-ray detector. In the X-ray tube, an electric current passes through a tungsten filament. The filament emits an electron beam that interacts with a target material that is typically composed of Cu (Bunaciu *et al.* 2015). As in an EDS analysis, the electrons from the beam dislodge electrons from low energy levels of atoms in the target material. When the electrons in the target material shift from the higher energy levels to the lower energy levels, they emit X-rays with wavelengths that are characteristic of the element the target material is composed of. The X-rays are filtered by a metal foil (composed of e.g., Ni) or a crystal monochromator (e.g., composed of pyrolytic graphite or silicon). The monochromatic

X-rays are collimated and directed onto a sample in the rotating sample stage. The X-rays are diffracted by the sample and enter the rotating detector, which measures the angle between incident and diffracted beam. Each mineral phase diffracts the X-rays differently, controlled by the atomic composition and crystal structure. The detector records and processes the X-ray photons (and angles) and converts the signal to a count rate, which then is visualised as a spectrum.

XRD is a powerful and rapid (< 20 min per sample) technique for the identification of unknown minerals (Bunaciu *et al.* 2015). Samples can be solid or liquid. X-ray powder diffraction requires destructive sampling and preparation of sample powders prior to analysis. For heterogenous samples, the detection limit for individual minerals is ca. 2% of the sample (Bunaciu *et al.* 2015). Certain minerals diffract X-rays at a similar angle, which can lead to superimposition of peaks of two or more different minerals in one spectrum.

In this thesis, XRD was used to investigate the mineralogy of the host sediment associated with the Geiseltal anurans and fish. Further, it was used to check for differences in the mineral composition in sediments between stratigraphic intervals. For each sample, a small amount (0.1–2 g) of sediment was powdered manually with a sterile agate pestle and mortar. XRD analysis was performed using a PANalytical Empyrean Series 2 microprobe with a Co X-ray tube, a PIXcel1D detector and a single crystal Si substrate in the Department of Earth Sciences, University of Oxford (UK).

The analysis of the host sediment associated with the Geiseltal anurans and fish revealed a limitation of this technique: mineral components can be identified by XRD analysis in contrast to amorphous organic material. The samples analysed have an organic composition; only a minority of samples include a mineral component. The concentration of this mineral content was close to the detection limit. As a result, the XRD analysis of the sediment samples returned qualitative data on mineralogy in certain samples but no quantitative data.

2.9 Synchrotron rapid scanning-X-ray fluorescence (SRS-XRF)

SRS-XRF is a rapid X-ray scanning technique to assess the spatial variation in element concentrations in materials. SRS-XRF is used in archaeology (e.g., to identify chemical elements in ink on historical parchments; Bergmann *et al.* 2012) and in plant sciences (e.g., to image chemical elements within plant tissues; Kopittke *et al.* 2018). In palaeontology, SRS-XRF has been used to investigate the chemistry of fossil tissues. The chemical composition of fossil tissues can be used to understand fossilisation processes (Bergmann *et al.* 2010; Gueriau *et al.* 2020; Rossi *et al.* 2020), to interpret the anatomy of organisms (Bergmann *et al.* 2010; Manning *et al.* 2019; Rossi *et al.* 2019), to provide insights into the phylogenetic affinities of fossils (Miyashita *et al.* 2019; Rogers *et al.* 2019) and to improve our understanding of colour preservation in fossils (Edwards *et al.* 2016).

SRS-XRF analysis is performed at a synchrotron facility (Lin *et al.* 2017; Edwards *et al.* 2018). Synchrotron facilities are technically sophisticated centres for operating particle accelerators, with their own specialised technical staff in place. SRS-XRF is not readily available to the public and operations need engineer assistance.

SRS-XRF analysis involves the following process: in the particle accelerator, electrons are accelerated to speeds that are ca. one third of the speed of light. They are forced to travel in a closed path by strong magnetic fields (Bergmann *et al.* 2012; Lin *et al.* 2017). Several physical effects lead to the emittance of X-rays by the moving electrons. The X-rays pass a monochromator and are focussed by several mirrors and pinholes. This focused X-ray beam raster-scans the sample. The beam interacts with the atoms of the sample, similar to XRD and EPMA techniques (Bergmann *et al.* 2012). Electrons are excited by the incident beam and electron transitions between energy levels lead to the emission of fluorescent X-rays (XRF). Fluorescent X-rays differ in their energy; the X-ray energy is diagnostic for different elements. A detector detects the X-rays for each measured element and a software converts the signal to a count rate, which then is visualised as a spectrum.

The elements of interest should be selected prior to XRF analysis in order to set the energy range of the analysed radiation (Edwards *et al.* 2018). This adjustment minimises the XRF signal from elements of no interest and therefore reduces noise in the spectra. The polarised and monochromatic characteristics of the synchrotron radiation minimises scattering of the emitted XRF. The high sensitivity of the XRF detector allows the detection of X-rays emitted by elements present even in trace amounts. SRS-XRF X-ray beams are intense (Lin *et al.* 2017; Edwards *et al.* 2018). The beams are polarised, monochromatic and collimated with a long focal length (Bergmann *et al.* 2012). A polished sample surface is not needed for micro- and macro-SRS-XRF; a microtomed surface is, however, essential for nano-SRS-XRF. SRS-XRF analysis does not require a vacuum for elements with high atomic number (K and heavier elements). SRS-XRF is a quantitative technique if calibrated standards are used.

In this thesis, the fossil specimen GMH CeIII-4967-1932 was selected for SRS-XRF analysis. The specimen was mounted directly on the sample stage. SRS-XRF data were collected at beam line 10-2 at the Stanford Synchrotron Radiation Lightsource (USA). The incident X-ray energy was set to 11 keV using a Si (111) double crystal monochromator with the storage ring containing 500 mA in top-off mode at 3.0 GeV. A micro-focused (2 × 2 µm) beam was provided by a Rh-coated Kirkpatrick-Baez mirror pair (pixel size 25 × 25 µm). Specimens were mounted at 45° to the incident X-ray beam and spatially rastered at 50 ms/pixel dwell time. The entire fluorescence spectrum was collected at each data point and the intensity of fluorescence lines for pre-selected elements (K, Ca, Ti, V, Cr, Mn, Fe, Co, Ni, Cu, Zn, AsPb, Cd, Sb and Hg) was monitored using a silicon drift Vortex detector. Element concentrations (µg/cm^2) were calibrated using NIST traceable thin film elemental standards. Data were processed using Sam's MicroAnalysis Toolkit software version 3.0.9 (Webb 2011). Data processing included edge removal and normalising to the time channel. Regions of interest (ROI) were selected for quantitative analysis. For each ROI, mean and standard deviation values were calculated for the concentration of each element.

Protocol for data processing in Sam's MicroAnalysis Toolkit (SMAK) 3.0.9:

1. Perform edge removal to remove dead pixels at the edge of the map.

2. Check data for variation in the incident flux using channel I0STRM.

3. If the I0STRM channel shows substantial variation, normalise fluorescence data to the I0STRM channel.

4. Check data for variation in the TIME channel.

5. If the TIME channel shows substantial variation, normalise fluorescence data to the TIME channel.

4. Check data for oversaturation of the detector (i.e., whether the deadtime is non-linear).

5. If the deadtime is non-linear, perform deadtime correction on fluorescence data.

6. Perform quantification on data, i.e., convert raw X-ray counts to concentrations by comparing the X-ray counts in the sample to X-ray counts in a standard of known concentration.

7. Perform multi-channel analysis to check for elements that were not identified when the data were collected at the beamline.

2.10 Quantitative taphonomy

Quantitative taphonomy involves the description of the taphonomy of a fossil using numerical parameters. Quantitative taphonomic studies facilitate the analysis of large datasets. Datasets are usually analysed using multivariate statistical methods (e.g., ANOVA, cluster analysis, linear and multiple regression analysis; Yesares-García & Aguirre 2004; Moore & Norman 2009). Quantitative taphonomy is commonly applied to palaeontological data, e.g., in the form of metrics, i.e., measures to express palaeontological features as numerical values (Mannion & Upchurch 2010; Brocklehurst *et al.* 2012; Cleary *et al.* 2015; Driscoll *et al.* 2019), and scores, i.e., the categorisation of non-numerical data to numerical variables (Dominici 2004; Fountaine *et al.* 2005).

This thesis uses quantitative analyses of skeletal taphonomy metrics to conduct a comparative analysis of the relationship between fossil preservation and palaeoenvironment for the Geiseltal fossil anurans (see Chapter 3). A modified form of the Skeletal Completeness Metric (SCM) proposed by Mannion & Upchurch (2010) was used to assess completeness and articulation at the level of individual skeletal elements and specimens in the Geiseltal anurans. Quantitative data were extracted from 140 anuran specimens on completeness, articulation and truncation. All data were explored statistically. Similar approaches have been used for the fossil anurans from Libros (Miocene, Spain; McNamara *et al.* 2009) and for anurans from Camp dels Ninots (Pliocene, Spain; Blain *et al.* 2023) to identify taphonomic patterns.

Quantitative approaches were also used in this thesis (Chapter 5). Data on the length, width and aspect ratio of a total of 6713 fossil and extant melanosomes were analysed. The data are used to characterise the geometry of melanosomes in the soft tissues of fossil and extant anurans.

2.11 Statistical analysis

Summary statistics were extracted for all datasets in this thesis; summary statistics typically include population size, mean, median, interquartile range and standard deviation. Statistical ranges are expressed as “mean ± standard deviation”.

Tests for statistical significance were performed on certain datasets to compare the means of two or more independent groups in order to determine whether means differ significantly in the dataset. All data were tested for normality and homoscedasticity prior to selecting a suitable significance test to compare the means of two or more independent groups (Table 2.1). Data were tested for normality using the Shapiro-Wilk test, histograms and Q-Q plots. Data were tested for homoscedasticity using Levene’s F-test, using boxplots and by comparing standard deviations between two or more

independent groups. For statistical testing, the null hypothesis was rejected when the p-value was below the threshold of significance (alpha level), i.e., $p < 0.05$.

Pearson's correlation test was used to assess the strength of the correlation between two variables. In this thesis, principal component analysis (PCA) and linear discriminant analysis (LDA) were used to reduce the dimensionality of certain datasets. PCA was used to reduce datasets with more than four variables to a few linear combinations, i.e., principal components, that explain the variability in the dataset. Linear discriminant analysis (LDA) was used to find a linear combination of variables that characterises or separates two or more classes in a particular dataset. Both PCA and LDA require datasets with one nominal category. PCA needs at least one data point in each group, whereas LDA requires at least two data points in each group to calculate mean values for the variance and covariance. PCA was applied to datasets that contain data on the geometry of melanosomes from different body regions in fossil and extant anurans (eight variables formed one data point for each group, i.e., the melanosome-containing body region of anuran specimens from a certain biota). PCA indicated which variables drove the variation in the dataset. LDA was applied to data on the chemistry of fossil soft tissues to determine which chemical elements drove the chemical variation in the dataset (the chemical data on several individual chemical elements for each analytical point in a specific body region of one anuran specimen formed the data points for each group, i.e., the analysed body region).

Standard statistical summary data and Pearson's correlation coefficients were calculated using Microsoft Excel. Significance tests were performed with PAST (PAleontological STatistics) v. 4.03, 4.15, 4.16c (Hammer *et al.* 2001) and Jasp 0.18.3 (Jasp Team 2024). PCA and LDA were performed with PAST 4.16c.

Table 2.1: Significance tests and assumptions for test validity.

Distribution	**Homoscedasticity**	**Number of sample groups**	**Significance test**	**Post-hoc test**
normal	Homoscedastic	2	Student t-test	not applicable
normal	Homoscedastic	>2	ANOVA	Tukey-Kramer (unequal sample size)
normal	Heteroscedastic	2	Student t-test for unequal variances	not applicable
normal	Heteroscedastic	>2	Welch	Dunn's
non-normal	Homoscedastic	2	Kolmogorov-Smirnov	not applicable
non-normal	Heteroscedastic	2	Mann-Whitney U	not applicable
non-normal	homoscedastic/heteroscedastic	>2	Kruskal-Wallis	Dunn's

2.12 Melanosome measurements

Melanosomes from fossil anurans were measured from SEM images using ImageJ v. 1.54g (Schneider *et al.* 2012). For each melanosome, length and width at an angle of 90 degrees between both variables were measured. Only melanosomes that were pristine (i.e., with no evidence for degradation) were measured. Further, only melanosomes that were consistent in brightness and thickness along their length were measured to ensure that the melanosomes were orthogonal to the line of sight. For each sample, at least 50 melanosomes were measured. The total dataset comprises measurements of 6713 melanosomes and incorporates datasets published by Rossi *et al.* (2019) and unpublished datasets provided by Valentina Rossi, Aaron Quigley and Beatriz Carazo del Hoyo (School of Biological, Earth and Environmental Sciences, University College Cork). The dataset published in Rossi *et al.* (2019) includes

measurements of 200 melanosomes from one anuran fossil (NHML-R4982; *Pelophylax pueyoi*) from the Libros biota (Miocene, Spain), measurements of in total 150 melanosomes from two specimens of the extant anuran *Hymenochirus boettgeri* (Congo dwarf clawed frog) and measurements of in total 850 melanosomes from three specimens of the extant anuran *Xenopus laevis*. Unpublished data were provided by Valentina Rossi and comprise measurements of 100 melanosomes from one anuran fossil (NHML-OR35814; *Palaeobatrachus luedecki*) of Bohemia (Rossi *et al.* 2020), probably of the Bechlejovice biota (Oligocene, Czech Republic). In addition, unpublished data were provided by Aaron Quigley and Beatriz Carazo del Hoyo and comprise measurements of in total 550 melanosomes from three specimens of the extant anuran *Bombina variegata* (yellow bellied toad) and measurements of in total 1000 melanosomes from three specimens of the extant anuran *Rhaebo guttatu*s (smooth-sided toad).

3. The skeletal taphonomy of anurans from the Eocene Geiseltal Konservat-Lagerstätte, Germany: insights into the controls on fossil anuran preservation

This chapter comprises the quantitative analysis of the skeletal taphonomy of the fossil anurans from the Geiseltal Lagerstätte and compares this to data from four additional Lagerstätten. The chapter comprises a paper that is published in the journal *Papers in Palaeontology* (Falk *et al.* 2022b), co-written by three authors. The chapter is organised as follows: Introduction, Geological setting, Material and method, Results, Discussion, Conclusion, Data archiving statement, Acknowledgements, Author contributions, References and Supporting information.

Falk, D., Wings, O. & McNamara, M. E. (2022). The skeletal taphonomy of anurans from the Eocene Geiseltal Konservat-Lagerstätte, Germany: insights into the controls on fossil anuran preservation. *Pap. Palaeontol.*, **8:** e1453. https://doi.org/10.1002/spp2.1453

Falk, D., Wings, O. & McNamara, M.E. (2022), Data from: The skeletal taphonomy of anurans from the Eocene Geiseltal Konservat-Lagerstätte, Germany: insights into the controls on fossil anuran preservation. *Dryad Digital Repository.* https://doi.org/10.5061/dryad.2bvq83brt

Candidate contribution to the study. DF contributed to the design of the study and performed a review of the literature. OW provided access to the Geiseltal Collection. DF obtained the taphonomic data for size, orientation, completeness, articulation and truncation for each of a total of 168 anuran fossil specimens. Based on this, DF identified taphonomic patterns and compared those with trends identified from skeletal completeness and articulation data from four additional Palaeogene and Neogene Lagerstätten. Data from those Lagerstätten were in parts previously obtained, interpreted and published by MMN (McNamara *et al.* 2012a); additional data were obtained by DF from a literature

review. DF performed the statistical analysis of the Geiseltal dataset and produced the figures. DF wrote the first draft of the paper and revised subsequent drafts in line with comments from the other authors. Following peer review, DF co-drafted the revisions to the paper with the other authors in accordance with comments from two reviewers.

Abstract. The Geiseltal biota is a lacustrine-hosted Konservat-Lagerstätte from the Eocene of central Germany. Despite its rich fauna and flora that is represented by at least 50,000 fossil vertebrates, insects and other invertebrates, plants and trace fossils, the taphonomy of the biota is still poorly understood. In particular, the anurans have not been the focus of taphonomic investigation. Here, we analysed the skeletal taphonomy of 168 anurans from Geiseltal and scored each specimen for orientation, completeness and articulation. Most specimens are partial skeletons that were truncated during preparation. This process introduces measurable artefacts into the taphonomic data and should be assessed in future taphonomic studies on fossil vertebrates. The Geiseltal anurans show several recurring taphonomic states, including disarticulation or loss of abdominal bones, loss of one or more limbs, extensive disarticulation and extensive loss of elements across the body. Relatively rare taphonomic states include loss of distal limb elements only, scattered bones and isolated, articulated limbs. These data are the basis of a new taphonomic model for the Geiseltal anurans. Comparative analysis of patterns in completeness and articulation in these specimens and in fossil anurans from other Cenozoic Lagerstätten reveals repeated taphonomic patterns in anuran preservation in lacustrine-hosted settings, such as proximal to distal trends in completeness, preferential loss of small peripheral bones, disarticulation of abdominal bones and reorientation of major body regions and limbs. The taphonomic controls in lacustrine systems are surface water temperature, lake depth, vegetation, exposure to bottom currents, transport mechanisms, extent of scavenging, decay regime, bone size and bone location in the skeleton. In turn, these are ultimately controlled by palaeoclimate, lake physiography and hydrology, and anuran anatomy. A universal approach to quantitative analysis of

skeletal taphonomy metrics will allow comparative testing of the relationship between preservation and palaeoenvironment for diverse fossil vertebrates.

3.1 Introduction

Konservat-Lagerstätten are fossil deposits that preserve unusually high-quality palaeontological information, characterised by high-fidelity preservation as (semi-)articulated skeletons and/or soft tissues (Seilacher *et al.* 1985; Muscente *et al.* 2017). These fossil remains can provide insights into the body plan and lifestyle of ancient organisms (Briggs 2014). In particular, an understanding of the skeletal taphonomy of fossil vertebrates can inform on physical and chemical characteristics of the depositional setting and on syn- and postdepositional processes. These processes include decay, transport and flotation (Beardmore *et al.* 2012; Briggs 2014), but also include biases related to sampling and taphonomy (Cleary *et al.* 2015; Dean *et al.* 2016). Skeletal taphonomy metrics (e.g., specimen completeness) have important applications in studies of palaeodiversity, phylogeny and historical palaeontology and allow biases in the fossil record to be assessed (Brocklehurst & Fröbisch 2014; Cashmore *et al.* 2020). Skeletal taphonomic data have been investigated systematically for various fossil vertebrates, such as the early tetrapod *Acanthostega* from the Devonian Aina Dal and Britta Dal Formations (Greenland; Coates 1996), the aquatic reptile *Serpianosaurus* from the Triassic Besano Formation (Switzerland; Beardmore *et al.* 2012; Beardmore and Furrer 2018), the bird *Archaeopteryx* and the dinosaur *Juravenator* from the Jurassic Solnhofen biota (Germany; Kemp and Unwin 1997; Reisdorf and Wuttke 2012*)*, rodent-like mammals (multituberculates) from the Cretaceous Jehol biota (China; Kielan-Jaworowska and Hurum 2006), the frog *Pelophylax pueyoi* from the Miocene Libros biota (Spain; McNamara et al. 2012*a*) and salamanders from the Miocene Rubielos de Mora biota (McNamara et al. 2012*b*).

The Middle Eocene Geiseltal biota includes >25,000 vertebrate specimens representing *c.* 125 taxa (Haubold & Krumbiegel 1984; Hellmund 2018). The biota includes specimens that are near-fully

articulated, near-complete and/or preserve soft tissues (Krumbiegel *et al.* 1983; Voigt 1988; Wilde & Hellmund 2010). Previous studies of the Geiseltal vertebrates focussed on systematic palaeontology, anatomy and evolution, applied to hippomorphs and tapiromorphs (Barnes 1926; Franzen 2003; Hellmund 2013; Ring *et al.* 2020), birds (Mayr 2020), fish (Jerzmanska 1977), reptiles (Hervet 2004; Smith 2009; Hastings & Hellmund 2015*a*) and anurans (Hinsche 1941; Kuhn 1941; Rage & Roček 2003). In contrast, there are few studies on the biostratinomy (Weigelt 1932; Krumbiegel 1977; Krumbiegel *et al.* 1983; Hellmund 1997; Hastings & Hellmund 2015*a*) and palaeoecology (Walter & Weigelt 1931; Krumbiegel *et al.* 1983) of the biota. In particular, the skeletal taphonomy of the Geiseltal vertebrates has not been investigated systematically. As a result, the palaeoecology, mode of death, biostratinomy and diagenesis of the fossil vertebrates are poorly understood and the biases affecting the biota are unknown.

As with many Cenozoic lacustrine-hosted Lagerstätten (e.g., Messel (Eocene, Germany), Enspel (Oligocene, Germany), Bechlejovice (Oligocene, Czech Republic) and Libros (Miocene, Spain)), anurans are abundant in the Geiseltal biota. These are potentially important index fossils for taphonomic studies because their general body plan and ecology has not changed markedly since the Lower Jurassic (Roček 2013) and thus variations in their preservation among biotas likely reflect primarily environmental factors. Fossil anurans therefore have the potential to provide unique insights into the palaeoenvironment of lacustrine-hosted Konservat-Lagerstätten, e.g. water depth, water temperature, presence/absence of bottom currents, etc. Here, we use systematic data on the skeletal taphonomy of the Geiseltal anurans (especially completeness and articulation) to test the following hypotheses: (1) that the fidelity of preservation is consistent for all skeletal elements, especially between homologous skeletal elements of the fore- and hind limbs and between the left and right sides of the body; (2) that the fidelity of preservation is linked to excavation site and taxonomy; (3) that specimens represent a series of repeating taphonomic states; (4) that the cause of death is desiccation or lake overturn; and (5) that comparative analysis of the taphonomy of anurans from Geiseltal and other important

Cenozoic biotas (i.e., Messel, Bechlejovice, Enspel and Libros) can identify broad taphonomic trends in anuran preservation in in lacustrine-hosted Cenozoic settings.

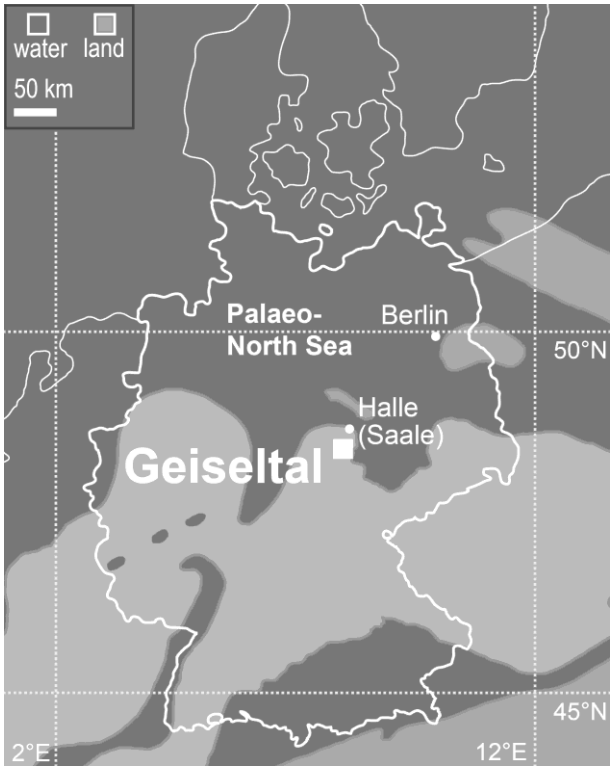


Fig. 3.1: Palaeogeography of the Eocene Geiseltal Lagerstätte (modified after Storch 1986; Hastings & Hellmund 2015b; Scotese 2016).

3.2 Geological setting

The Middle Eocene Geiseltal Lagerstätte is located approximately 20 km southwest of Halle (Saale) in Saxony-Anhalt, central Germany (Fig. 3.1) and has been of scientific interest for almost one hundred years (Barnes 1926). The biota is hosted within a *c.* 120-m thick succession of palustrine, limnic-palustrine and fluvial-terrestrial sediments that were deposited in the large (*c.* 75 km^2) WNW-ESE-trending Geiseltal inshore basin (Krumbiegel *et al.* 1983; Blumenstengel 2004; Hellmund & Hastings 2014). Basin formation was driven by a combination of three factors: (1) tectonics focussed in the North of the basin, (2) local halotectonics linked to the underlying Permian 'Zechstein' and Triassic 'Röt' deposits and (3) fluctuations in sea level of the Palaeo-North Sea located to the ENE (Küstermann *et al.*

2008; Krutzsch 2011; Fig. 3.1). The Geiseltal succession is dominated by repeated intervals (each 3–25 m thick) of claystones, siltstones and sandstones intercalated with lignite intervals (each *c.* 10–50 m thick; Eissmann 2002; Blumenstengel 2004; Krutzsch 2011). The lignites were exploited commercially in a series of open cast mines from the late 19th century until 1993. The mine region was flooded in 2003 and the remaining fossiliferous outcrops are no longer accessible.

Most Geiseltal vertebrates are hosted in lignite intervals. Vertebrate remains are relatively rare in the intercalating siltstones and sandstones ('Hauptmittel'; Haubold & Hellmund 1998). The succession includes six lignite intervals, listed here from oldest to youngest: lower lower coal (LLC, 'Untere Unterkohle'), lower middle coal (LMC, 'Untere Mittelkohle'), upper middle coal (UMC, 'Obere Mittelkohle'), upper sandstone/siltstone deposits (UHM, 'Oberes Hauptmittel'), lower upper coal (LUC, 'Untere Oberkohle') and middle upper coal (MUC, 'Mittlere Oberkohle'; Lincke 1977; Haubold & Hellmund 1998; Fig. 3.2). The Geiseltal succession lacks igneous components and thus cannot be dated radiometrically (Fig. 3.2). The LLC, LMC, UMC and UHM units are part of the Geiseltalian European Land Mammal Mega Zone (ELMMZ), which comprises the Mammal Paleogene Zones MP11 (LC) to MP 13 (UMC; Haubold & Hellmund 1998). The LLC corresponds to the uppermost part of the succession hosting the Middle Eocene Messel Lagerstätte (47 Ma; MP 11; Mertz and Renne 2005). The UMC corresponds to the sediments of the Middle Eocene Eckfeld Lagerstätte (44 Ma; MP 13; Mertz *et al.* 2000). The LUC and MUC are correlated with the lower Robiacian and MP 14 (Franzen & Haubold 1987; Aguilar *et al.* 1997). These mammal biochronology data are not universally accepted (see Ring *et al.* 2020) but a late early or middle Eocene age is most plausible. This is supported by palynomorph biostratigraphy, which indicates that the Geiseltal strata span up to the entire Lutetian (Krutzsch *et al.* 1992, Krutzsch 2011).

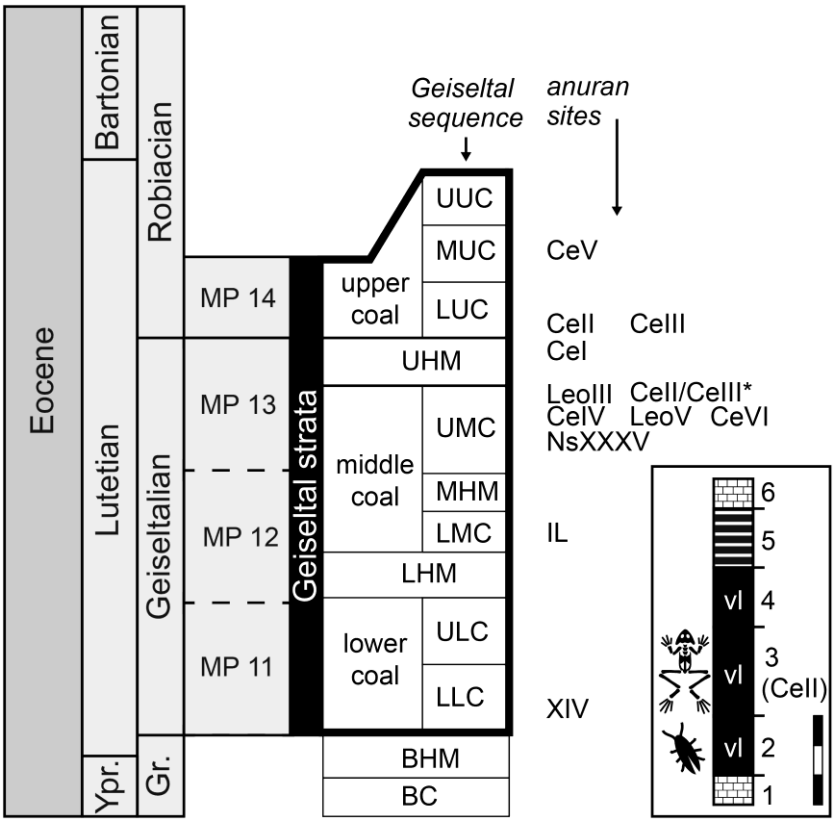


*Figure 3.2: Stratigraphy of the Geiseltal Lagerstätte (modified after Haubold & Hellmund 1998). Geiseltal sequence and anuran sites. Inset shows stratigraphic section of the interval containing site CeII ('dying field 1'), drawn using data from Raupach (1948). *Note that CeII/CeIII was originally assigned to UMC by Krumbiegel (1962a). Also note that the mammal biochronology data for the Geiseltal strata (MP) are not universally accepted (Ring et al. 2020). Abbreviations: BC, basal coal; BHM, basal 'Hauptmittel' ('Hauptmittel': intercalated sandy and silty successions); Ce, 'Cecilie' pit; Gr., Grauvian; IL, 'Geiselröhlitz' site; Leo, 'Leonhard' pit; LHM, lower 'Hauptmittel'; LLC, lower lower coal; LMC, lower middle coal; LUC, lower upper coal; MHM, middle 'Hauptmittel'; MUC, middle upper coal; Ns, 'Neumark-South' pit; Nw, 'Neumark-West' pit; UHM, upper 'Hauptmittel'; ULC, upper lower coal; UMC, upper middle coal; UUC, upper upper coal; v, varve-like; Ypr., Ypresian. 1; 6, carbonate bed; 2, dark lignites rich in insect fossils ('black coal'); 3, lignites rich in vertebrate fossils (site CeII, dying field 1); 4, lignites; 5, laminated lignites/dysodile coal ('Blätterkohle'). Scale bar in inset represents 0.3 m.*

Palaeoclimate was subtropical, usually frost-free (but see Grein *et al.* 2011) and humid (Krutzsch 2011) during deposition of the lignites, but semiarid and warm with seasonal precipitation during deposition of the clastic beds (Krutzsch 2011). Analyses of fossil leaves from clastic beds at the base of the Geiseltal

profile (most likely MP11 (supporting table 2 in Mosbrugger *et al.* 2005)) indicate mean annual temperatures of *c.* 23°C–25°C with cold month mean temperatures *c.* 17°C–21°C and mean annual precipitation *c.* 1,000 mm–1,600 mm (Mosbrugger *et al.* 2005).

The Geiseltal fossils were recovered during semi-continuous excavations from the mid-1920s to 2000, with breaks in excavation from 1938–1949 and the mid-1980s–early 1990s (Haubold 1995; Hellmund 2018). Vertebrate fossils were recovered from 36 sites in the mines 'Cecilie' (Ce), 'Leonhardt' (Leo), 'Neumark-West' (N_W), 'Neumark-South' (N_S), 'Mücheln-West' (M_W) and 'Mücheln-South' (M_S).
Excavation sites were usually <100 m² and classified as sinkholes (each *c.* 10–16 m wide and 3–8 m deep), fluvial channel deposits (up to 40 m wide and 15 m thick) or 'dying fields' ('Leichenfelder'; each with an area of *c.* 80 m x 100 m; Weigelt 1933; Krumbiegel 1962*a*, 1975, 1977; Krumbiegel et al. 1983; Haubold & Krumbiegel 1984; Weigelt 1989; Haubold & Hellmund 1998; Hellmund 2018).

The sinkholes are considered to have formed due to dissolution of underlying salt and gypsum deposits and subsequent subsidence; the resulting localised depressions were filled with carbonate-rich and saline waters derived from groundwater and surface water during wet periods (Weigelt 1934; Krumbiegel 1975, 1977; Krumbiegel *et al.* 1983). Sinkhole sediments are characterised by alternating layers of lacustrine chalk ('Seekreide') and dysodile lignites with rare diatomites (Weigelt 1934; Krumbiegel 1975, 1977; Krumbiegel *et al.* 1983). Biomarkers for chlorophyll (Dilcher *et al.* 1970) and the sapropelic character of the lignites suggest benthic dysoxia (Krumbiegel 1977). The best-preserved fossils in sinkhole excavation sites are considered to occur in the finely laminated lignites deposited in central parts of sinkholes (Krumbiegel *et al.* 1983); some fossils are considered to have been exposed subaerially before burial (Weigelt 1935).
Fluvial deposits have been attributed to meandering rivers with low current velocities and unstable banks (Krumbiegel 1977). Carbonate-rich sediments in certain sinkholes and dying fields have been linked to inputs of alkaline waters from inflowing rivers (Krumbiegel 1962*b*; Krumbiegel *et al.* 1983).

The river deposits include fossiliferous beds, that comprise white, cross-bedded sandstones and brown mudstone (Krumbiegel 1962*b*). Most fossils were recovered from the sandstones, whereas the mudstones preserve only occasional accumulations of bones (Krumbiegel 1962*b*). Fossil wood usually shows a N-S / NNE-SSW orientation; some fossil tree trunks and branches are associated with accumulations of vertebrate remains and are interpreted as fossil traps (Krumbiegel 1962*b*, 1977). The faunal composition of the river deposits differs from that of the sinkholes and dying fields, e.g., the river deposits are usually rich in crocodilian, palaeohippid, and turtle fossils (Krumbiegel 1962*b*; Krumbiegel *et al.* 1983). Floodplain sediments include halophile invertebrates (Krumbiegel 1977).

The dying fields comprise laterally restricted, laminated lignite seams, 0.2 m–0.8 m thick (Weigelt 1933; Raupach 1948; Krumbiegel *et al.* 1983), with particularly high densities of vertebrate fossils (e.g., *c.* 2,200 vertebrate specimens over a surface area of 914 m² at site Ce II (Weigelt 1940; Haubold 1995)). These deposits are localised to a geomorphological depression striking NE-SW within the central region of the Geiseltal basin (Weigelt 1933; Krumbiegel 1977). The dying field sediments are considered to have originated in shallow swampy troughs that formed during wet periods and persisted for tens to hundreds of years (Raupach 1948; Krumbiegel 1977). The lignite seams are usually under- and overlain by carbonate-rich beds interpreted as lake bank deposits (Raupach 1948), indicating temporal fluctuations in lake level and thus size (Raupach 1948).

The Geiseltal biota shares faunal elements with other important German Cenozoic Lagerstätten, especially Messel (Franzen 2005) and Eckfeld (Mertz *et al.* 2000). The Geiseltal vertebrate biota includes skeletal remains of mammals, amphibians, reptiles, fish and birds (Krumbiegel *et al.* 1983; Hellmund 2018) with rare crocodilian and avian eggs (Kohring & Hirsch 1996; Hastings & Hellmund 2015*a*; Mayr 2020). Invertebrates include bivalves, gastropods and diverse insects (*c.* 155 species (Krumbiegel *et al.* 1983)). Plant fossils are abundant and include cryptogams, gymnosperms and angiosperms (Rüffle *et al.* 1976; Krumbiegel *et al.* 1983; Wilde 1995; Rüffle & Litke 2000). The Geiseltal flora also includes rare fibrous laticifers termed ‘monkeyhair’ (McCoy *et al.* 2021). Fossil resin and trace

fossils are other common components of the Lagerstätte (Krumbiegel 1995; Falk *et al.* 2019; Simoneit *et al.* 2020). Preservation of the Geiseltal fossils has been linked to inputs of carbonate-rich waters (springs and rivers) derived from the Triassic Muschelkalk limestone plateau that outcrops to the S and SW (Krumbiegel *et al.* 1983). Preserved bacteria have been reported from coprolites, frog epidermis, beetle spiracles and fish eyes (Mrugowsky 1936), but these microbodies (at least those in the vertebrates) are likely to represent fossil melanosomes, which commonly define carbonaceous soft tissues of fossil vertebrates (Vinther *et al.* 2008; Rossi *et al.* 2019; Rossi *et al.* 2020).

The vast majority of the Geiseltal anurans were excavated and prepared during the 1930s (Weigelt 1933; Kuhn 1941); the remainder, during the 1950s–1970s (Supplementary Dataset 1, Falk *et al.* 2022). Almost all specimens were prepared via the transfer method (i.e. 'Lackfilm method' (Voigt 1933, 1988), Fig. S3.1); records indicate the loss of hundreds of specimens during the transfer process (Krumbiegel *et al.* 1983). Circa 200 anuran specimens were transferred successfully (Krumbiegel *et al.* 1983), but only 180 specimens (including tadpoles) are accounted for today; the location of the remaining 20 specimens is unknown. Early studies of the fossil anurans reported preservation of skin cells, glands, connective tissue, blood capillaries, melanophores and pale greenish coloration in some specimens (Voigt 1935, 1937, 1988).

3.3 Material and method

3.3.1 Fossil material

The Geiseltal Collection of the Natural Sciences Collections (ZNS) of the Martin Luther University Halle-Wittenberg in Halle (Saale) (Saxony-Anhalt, Germany) hosts at least 50,000 specimens from the Geiseltal Lagerstätte including *c.* 25,000 vertebrates. In this study, we examined 168 fossil anuran specimens from the collection. Most of the studied anurans (n = 121) were excavated from the dying field deposits at the sites Ce II (lignite interval LUC (Haubold & Hellmund 1998)) and Ce III (lignite interval UMC (Krumbiegel 1962*b*); Fig. 3.2). Forty anurans used in this study are from sinkhole deposits (i.e., Ce I, Ce IV, Ce V, Ce VI, Leo III, Leo V and N_sXXXV (Haubold & Krumbiegel 1984)). A single anuran

used in this study derives from river bank and flood plain deposits (site XIV (N_wXIV in Haubold & Krumbiegel 1984) of interval LLC (Krumbiegel 1962*b*; Haubold & Krumbiegel 1984); Fig. 3.2). Stratigraphic data are not available for the remaining six specimens.

Most of the fossil anurans (n = 99) are of undetermined affinity (Supplementary Dataset 1, Falk *et al.* 2022). Of the remainder, most have been previously assigned to the (mainly terrestrial) Pelobatidae (n = 54) and (mainly aquatic) Palaeobatrachidae (n = 15) (Kuhn 1941; Roček & Rage 2000; Roček 2013; Roček *et al.* 2014). Some specimens may represent Discoglossidae (Rage & Roček 2003; Roček 2013).

Completeness and articulation vary considerably. Most specimens are well-articulated skeletons (Fig. 3.3). Specimens comprising disarticulated and scattered bones or isolated, articulated limbs are rare. One specimen is conserved *in situ* in sedimentary matrix (with the slab conserved in water); most of the remaining specimens are conserved in nitrocellulose glue (Figs 3.3A, C–F, H–J) with a minority in paraffin wax (Figs 3.3B, G). Many slabs retain small (< 10 mm) patches of dark organic-rich sedimentary matrix; no distinctive sedimentary textures or fabrics are evident (Figs 3.3A–J). Most (n = 166) slabs hold one specimen; the remaining two slabs each include two specimens. A single slab includes fish scales.

The Geiseltal Collection includes tadpoles but these are excluded from the current study due to their poor preservation and markedly different Bauplan to the adult anurans. This study focusses exclusively on the anurans that represent post-tadpole developmental stages (n = 168). Unequivocal discrimination of adults, subadults and juveniles is not always possible.

Twenty-eight specimens were omitted from the study as poor preservation precluded confident identification of individual skeletal elements. The remaining 140 specimens comprise 54 pelobatids, 15 palaeobatrachids and 71 undetermined individuals. A total of 106 specimens are truncated either by the edge of the slab and/or the embedding medium.

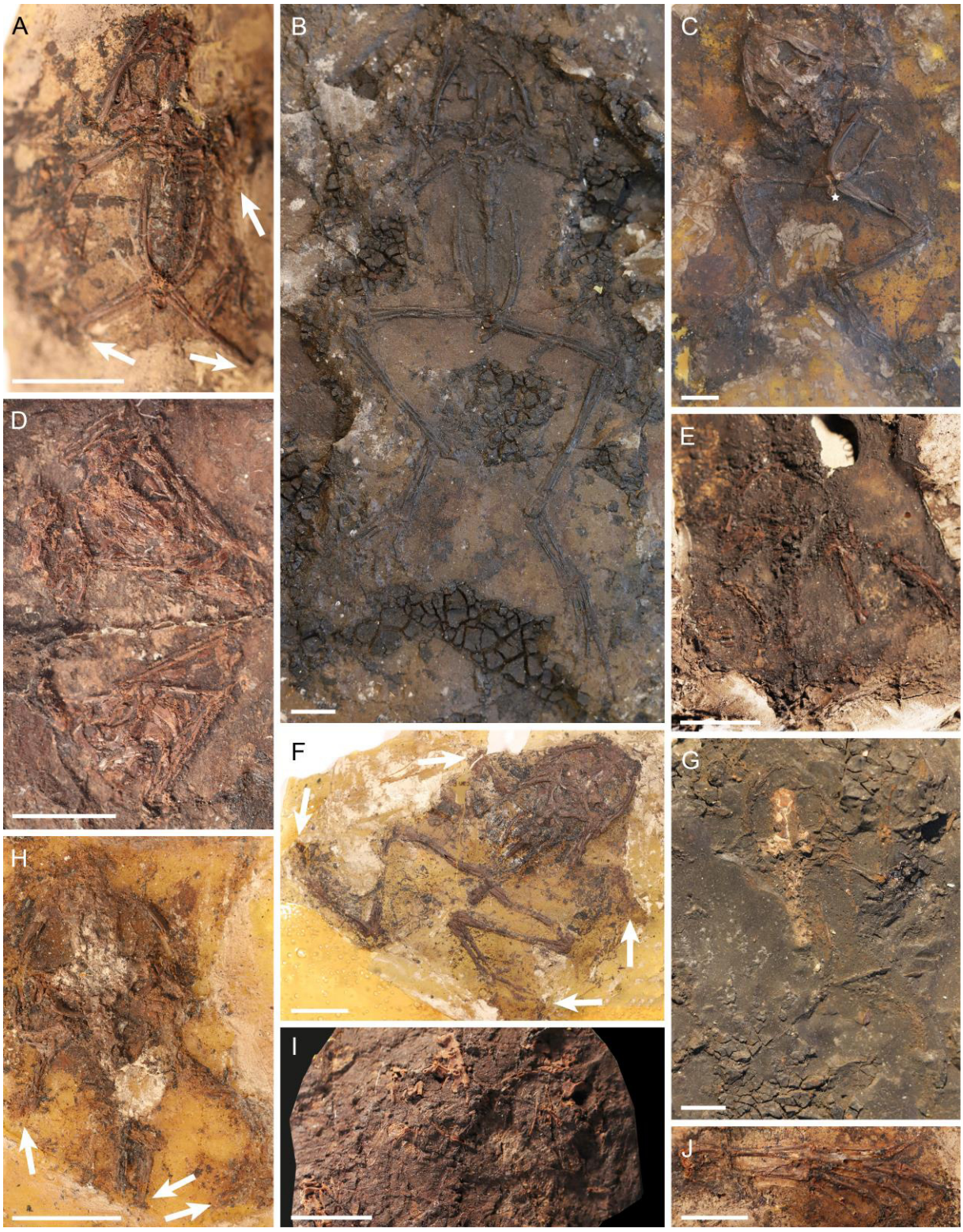


Figure 3.3: Variation in completeness and articulation among the Geiseltal anurans. Some specimens are truncated by the edge of the slab or embedding medium (arrows). Specimens belong to truncation categories T0–T4; untruncated specimens were assigned to a taphonomic state (for details see text). All slabs retain patches of dark organic-rich host sediment. Interpretative line drawings are shown in Fig. S3.2. A, Ce III-6735-1932; incomplete, near-fully-articulated, T2. B, Ce II-4949-1930; near-complete, near-fully articulated with patches of

sediment (apparent as dark polygons), T0, States 1, 9. C, Ce III-6728-1932; near-complete, partially articulated (the urostyle is shifted to the left), potential coprolite (star), T0, States 1, 7, 8. D, Ce IV-4953-1933; accumulation of mostly disarticulated bones, T0, States 4, 9. E, Ce III-6720-1932; incomplete, partially articulated anterior body, T0, States 3, 9. F, Ce III-6719-1932; near-complete, near-fully articulated, T2. G, Ce I-4947-1930; incomplete, lacking limbs, near-fully articulated, T0, States 2, 9. H, Ce III-6742-1932; incomplete, near-fully articulated, T4. I, IL 17A-1969; disarticulated and reorientated vertebrae and possible limb elements, T0, States 5, 9. J, Ce III-6737-1932; incomplete, near-fully-articulated foot showing digits I to V and several phalanges, States 6, 9. All scale bars represent 10 mm.

3.3.2 Skeletal anatomy

The skeleton of adult anurans comprises three major units: the cranium, axial skeleton and appendicular skeleton. The axial skeleton comprises the vertebral column (including eight pre-sacral vertebrae and the sacral vertebra), urostyle, ischium and ilia. The appendicular skeleton comprises the forelimbs (clavicle, coracoid, scapula, humerus, radioulna, carpals, metacarpals and phalanges) and hindlimbs (femur, tibiofibula, tibiale-fibulare, tarsals, metatarsals and phalanges). The torso here refers to the vertebrae, urostyle, ilia and ischium.

3.3.3 Size

The distance from the snout to the distal end of the urostyle (snout-urostyle length: SUL) is a proxy for specimen size (Gvoždík *et al.* 2008). SUL was measured from digital images of specimens (n = 28) using ImageJ v.1.53e (Schneider *et al.* 2012).

3.3.4 Orientation

Orientation was defined as (1) dorsal, ventral or dorso-ventral if the sagittal axis was perpendicular to the bedding on the slab, (2) oblique if it was inclined to bedding, or (3) lateral if it was parallel to bedding. Orientation was assessed for 121 specimens. The way up of specimens cannot be determined

unequivocally: the transfer process usually results in inverted way up relative to the presentation of specimens in the field (Fig. S3.1; Voigt 1933; Weigelt 1933), but whether this applies to all specimens is unclear. Orientation was assessed using the orientation of the scapula, pectoral girdle, teeth in the upper jaw and vertebrae. 'Left' and 'right' body sides of specimens were coded as per the presentation of the specimen on the transfer/slab.

3.3.5 Completeness

We used a modified form of the Skeletal Completeness Metric (SCM) proposed by Mannion & Upchurch (2010) to assess skeletal and specimen completeness in the Geiseltal anurans. The total number of skeletal elements in the body is estimated as 91 for the Geiseltal anurans. This value was derived from the number of bones in fully preserved body regions of different specimens and in the skeleton of the extant frog *Lithobates catesbeiana* (American bullfrog (Ranidae; De Iuliis & Pulerà 2011)); its skeletal configuration is near-identical to that of the Geiseltal anurans. Geiseltal specimens differ from *L. catesbeiana* in the shape and dimension of some skeletal elements (i.e. cranial elements, sacral vertebra) and by probably lacking prepollex and prehallux (neither element observed in Geiseltal specimens; prehallux usually absent in palaeobatrachids (Wuttke *et al.* 2012)). Further, *L. catesbeiana* includes partly fused tibiale and fibulare. These are fused in some adult pelobatids (Roček *et al.* 2014), but usually unfused in palaeobatrachids (Wuttke *et al.* 2012). The Geiseltal pelobatids and palaeobatrachids differ in cranial shape, metacarpal length and tibiofibula-femur length ratio. In addition, pelobatids (but not palaeobatrachids) show sculptured cranial bones and an ossified sternum (Roček *et al.* 2014); palaeobatrachids (but not pelobatids) commonly feature fused vertebrae (i.e. 'synsacrum'; Wuttke et al. 2012).

Completeness was not assessed for the following skeletal elements: (1) Individual elements of the cranium. These are usually superimposed and difficult to identify. The cranium is thus coded as present if at least one cranial bone is evident. (2) Individual elements of the pectoral girdle (clavicula, coracoid, scapula, sternum). These are often obscured by vertebrae or cranial elements. (3) Individual carpals

and tarsals. These are small, typically overlap and are coded as present if at least one carpal / tarsal is evident.

For most specimens, the margins of the slab or transfer are less than 50 mm from the bones in all directions. Some specimens comprise disarticulated associations of bones in which individual bones may be shifted from their original positions *in vivo* by several centimetres. Despite this, the associated bones clearly belong to a single specimen based on their size, anatomy and the presence of pairs of relevant elements. Bones were therefore coded as present if they are preserved < 50 mm from life position; complete specimens may thus be disarticulated. The presence / absence of all other skeletal elements was noted for each specimen. In most specimens, unequivocal identification of a limited number of bones (typically 3–4) was difficult due to superimposition, poor preservation and/or incomplete transfer. The assessment of the presence/absence of each skeletal element was therefore coded as 'confident' or 'not confident'. Only skeletal elements identified confidently were included in the study. Further, identification of small elements present as a set of three or more bones, e.g. individual vertebrae and phalanges, was often challenging and it was not always possible to determine the exact number of these elements present. For these bones, specimens were therefore assigned to one of the following completeness categories: vertebrae: 0, 1–3, 4–6 or 7–9 present; forelimb phalanges: 0, 1–3, 4–6, 7–9 or 10 present per hand; hindlimb phalanges: 0, 1–3, 4–6, 7–9, 10–12 or 13–14 present per foot.

Completeness data were assessed using two indices. *(1) Specimen completeness:* Percentage completeness was assessed for each specimen as follows. The total number of bones preserved in each specimen was expressed as a percentage of the total number of bones in a complete specimen, e.g., a specimen completeness value of 43% indicates that the specimen has 43% of the bones present *in vivo* (i.e., is 43% complete). Certain additional elements were excluded due to low confidence and/or truncation (see below). The calculation of specimen completeness may thus not use the *potential*

maximum number of 91 bones, e.g., for a specimen lacking a hand due to truncation, the maximum number of 91 bones was reduced (by the number of bones in the hand) to 77 bones. For elements present as a set (e.g., phalanges), the highest number for each completeness category was used in the calculation. For instance, in a specimen with left-hand phalanges assigned to category '1–3' and right-hand phalanges assigned to category '4–6', then the total number of phalanges is recorded as nine. The highest value and not the median value was chosen as the former may lead to an overestimation only, rather than an over- or underestimation when the median is used. Thus, the potential error in the dataset has only one polarity.

(2) S*keletal element completeness:* Presence / absence data were compiled for each element across the total dataset and expressed as a percentage of the number of specimens used in the calculation, e.g., 'urostyle – 39% (n = 138)' indicates that the urostyle is present in 39% of specimens in a dataset of 138. In this example, two specimens (out of a total dataset of 140 specimens) were omitted because identification of the urostyle was not confident and/or it was truncated. Bones present as a pair or as a set of three or more elements were considered complete if at least one bone from the pair / set is present. Since many skeletal elements are paired or present as a set, this index may artificially inflate completeness values.

A second measure of element completeness was therefore calculated as follows. First, the total number of bones was calculated for each element in the dataset. In the Geiseltal dataset, some elements and specimens were excluded due to low confidence and/or truncation, so the calculation may not use the *potential* maximum number of these elements in the dataset. For example, 140 specimens yield a potential maximum of 280 humeri, but our dataset includes a total of only 223 humeri. Presence / absence data for each element were expressed as a percentage of this maximum number of elements, e.g. 'humerus – 29%' indicates that 29% of all humeri in the dataset (i.e., 29% of 223) are present.

3.3.6 Truncation

Any analysis of the skeletal taphonomy of fossil vertebrates must consider how much of the specimen is present on the slab and to what extent this apparent completeness, and related apparent articulation, may be impacted by biases related to taphonomy and/or fossil preparation and conservation. If all skeletal elements are equally likely to be preserved, with similar fidelity, then taphonomic indices such as completeness and articulation should be independent of which bones are present on the slab. If, however, preservation potential varies among skeletal elements (e.g., due to biological factors linked to decay and anatomy), then values for completeness and articulation will vary among specimens depending on which bones are present. It is therefore essential to assess whether or not the skeletal taphonomy of specimens is impacted by fossil preparation. In particular, is apparent completeness equal to true completeness, or an artefact of preparation and / or conservation? This is a critical issue for the Geiseltal anurans, where variations in taphonomy have not been assessed and where the vast majority of specimens have been subject to invasive conservation via the transfer method. The primary risk during the transfer process is that part of the specimen – including some bones – may not transfer across to the new conserving material, generating a fossil that is "truncated". We therefore assessed the impact of truncation on skeletal taphonomy as follows.

Truncated bones are those where the edge of the slab or of the nitrocellulose glue/wax transfer passes through the bone, i.e. where part, but not all, of the bone is visible (Figs 3.3, 3.4). Most specimens included in the study (76%, n = 140) are truncated; depending on the position and orientation of the torso and limbs, truncation of a skeletal element may affect all elements that are more distal of it. For instance, a specimen with a truncated femur usually lacks the tibiofibula, tibiale-fibulare and foot of that limb. Where the truncated element is part of a set, e.g. metatarsals, both the element group itself and more distal elements may be truncated. For instance, the edge of the slab may pass through three metatarsals but lie proximal of the fourth and fifth metatarsal and of the phalanges (which are thus not present).

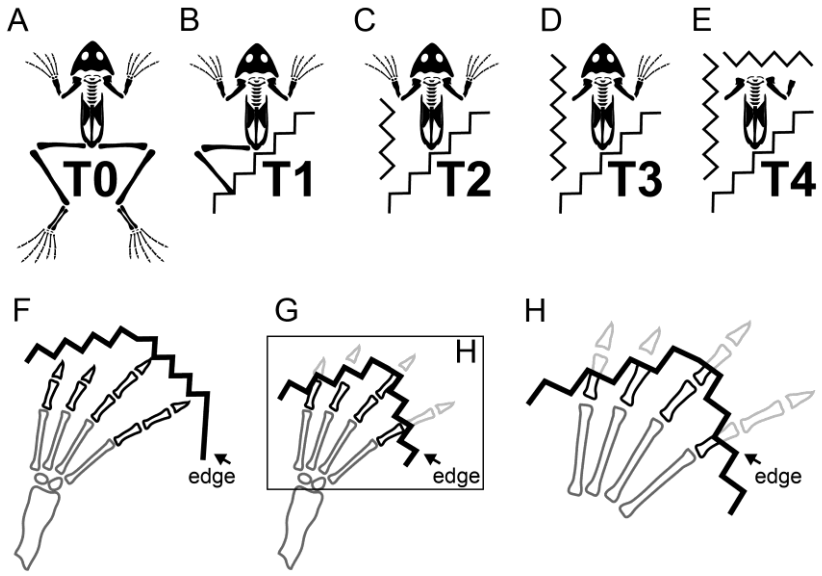


Figure 3.4: Truncation. A–E, Truncation categories for the Geiseltal anurans. A, T0: no bones truncated. B, T1: 0.1–24.9% of bones truncated. C, T2: 25–49.9% truncation. D, T3: 50–74.9% truncation. E, T4:75–100% truncation). F–H, Impact of truncation on completeness and articulation. F, hand is not truncated and includes ten phalanges (in black outline). G, H, hand is truncated by the edge of the slab (thick zigzag line). G, truncated hand lacks five phalanges, which are omitted from the study. The presence of five out of a measurable total of five phalanges thus results in a completeness value of 100%; this is the preferred approach for calculating completeness used in this study. The alternative approach is to include the bones truncated by the slab in the study but code them as 'absent' (Fig. S3), in which case the presence of five of ten phalanges yields a completeness value of 50%. This approach potentially biases specimen completeness to lower values and is rejected in this study. H, edge passes through three phalanges; these bones are coded as present, whereas bones beyond the edge are omitted.

Truncation was assessed for each skeletal element as it potentially impacts values for completeness and articulation (see below), depending on how the latter two indices are assessed (Fig. 3.4). This applies particularly to skeletal elements distal of truncated elements. For instance, in the case of a truncated femur with the anterior part of the bone on the slab, it is not possible to determine whether more distal skeletal elements are truly absent (i.e. disarticulated and lost) or were indeed preserved as part of the fossil, but subsequently lost during the transfer process. Two potential options for treating

this uncertainty are to: (1) omit skeletal elements distal to truncated elements from the analysis, or (2) code all skeletal elements distal to truncated elements as 'absent' (Fig. 3.4G). Both methods have the potential to bias values for specimen completeness. Method #1 is favoured herein as it does not incorporate assumptions regarding the presence / absence of bones distal of truncated elements (note that data are, however, provided for both methods; see Fig. S3.3). Using Method #1, truncated elements were coded as present. Elements distal of truncated elements were omitted from the study (Fig. 3.4H). In the assessment of specimen completeness, where at least one bone in an element set is truncated, the truncated element(s) was(were) coded as present. For instance, where three out of five truncated metatarsals are present and two are not visible but are potentially distal of the transfer edge, the latter two metatarsals are omitted from the study. Where at least one element in a set is truncated, the set was omitted from the analysis of completeness categories.

Truncation usually affects peripheral elements, i.e. phalanges; these elements are also the most numerous and thus make the greatest contribution to values for specimen percentage completeness and articulation. The values for percentage completeness and articulation of individual specimens may thus be impacted markedly by truncation. To assess this, the percentage of skeletal elements omitted from the study due to truncation was calculated for each specimen. Specimens were assigned to one of the following truncation categories (Figs 3.4A–E): T0 (no bones truncated), T1 (0.1–24.9% of bones truncated), T2 (25–49.9% truncation), T3 (50–74.9% truncation) and T4 (75–100% truncation).

3.3.7 Articulation

Articulation was assessed only for those joints that are present in the fossils, i.e. where all bones that form the joint are present. The total number of joints present in a complete specimen is 98. A joint was coded as articulated if the relevant bones are juxtaposed in life position. Herein, the term 'shoulder joint' refers to the articulation of the humerus and scapula and 'hip joint' refers to the articulation of the femur and ilium. For certain specimens, unequivocal identification of articulated joints is difficult

where bones are superimposed, poorly preserved or incompletely transferred. As with completeness, the assessment of the articulation state of each skeletal element was therefore coded as 'confident' or 'not confident'. Only joints for which articulation could be assessed confidently are included in the study. It was not always possible to determine the exact number of articulated joints between adjacent vertebrae, metacarpals, metatarsals, carpals, tarsals and phalanges. For these joints, specimens were therefore assigned to one of the following articulation categories: vertebrae: 0, 1–3, 4–6 or 7–8 joints articulated; metacarpals-carpals and metacarpals-phalanges: 0, 1–2, 3 or 4 articulated joints per hand; forelimb phalanges: 0, 1–2, 3–4 or 5–6 articulated joints per hand; metatarsals-tarsals and metatarsals-phalanges: 0, 1–2, 3–4 or 5 articulated joints per foot; hindlimb phalanges: 0, 1–3, 4–6 or 7–9 articulated joints per foot. Joint sets were coded as articulated if at least one joint is in life position. Where carpals and/or tarsals are absent or were omitted from the study, the articulation of the wrist and/or ankle joint was assessed using the preserved positions of the metacarpals and radioulna (0, 1–2, 3 or 4 articulated joints per hand), or tibiale-fibulare and metatarsals (0, 1–2, 3–4 or 5 articulated joints per foot), respectively.

As for completeness, articulation was assessed using two indices. *(1) Specimen articulation.* Percentage articulation was assessed for each specimen as follows. The total number of articulated joints in each specimen was expressed as a percentage of the total number of joints in a complete specimen, e.g., a specimen articulation value of 48% indicates that 48% of the joints in the specimen are articulated. For joint sets, the highest number for each articulation category was used in the calculation. *(2) Joint articulation.* Articulation / disarticulation data were compiled for each joint present across the total dataset and expressed as a percentage of the number of specimens used in the calculation, e.g. 'humerus-shoulder – 90% (n = 80)' indicates that the proximal humerus adjoins the shoulder in 90% of specimens in a dataset of 80. In this example, sixty specimens (out of a total dataset of 140 specimens) were omitted because either at least one adjoining skeletal element is absent, poorly preserved and/or truncated. Joints present as a pair or a set of three or more joints (e.g., phalanges) were considered

articulated if at least one bone from the pair / set is articulated. Since many joints are paired or present as a set, this index may artificially inflate completeness values.

Articulation data were therefore also expressed as a percentage of the number of joints across the total dataset. Firstly, the total number of each joint in the dataset was calculated. Some joints and specimens were excluded due to low confidence or absence. For instance, for paired joints, e.g. elbow (humerus-radioulna), the potential maximum number of 280 joints in the dataset (n = 140 specimens) is rarely achieved. Articulation data for each joint were then expressed as a percentage of this total number of joints, e.g. a joint articulation value of '87% (n = 119)' indicates that 87% of all elbow joints in a dataset of 119 joints are articulated.

Standard statistical summary data and Pearson's correlation coefficients were calculated using Microsoft Excel. Significance tests were performed with PAST (PAleontological STatistics) 4.03 (Hammer *et al.* 2001). For further details of our statistical approach, please see Supporting Information.

3.3.8 Comparative taphonomy

Data on the skeletal taphonomy of anurans from Libros were extracted from McNamara *et al.* 2012. Data for specimens from Lake Bechlejovice and Lake Messel were derived in part from published photographs and in part from study of hand specimens, and digital photographs of anurans in the collections of the National History Museum in Prague, Czech Republic (Bechlejovice) and Senckenberg Research Institute in Frankfurt/Main, Germany (Messel). Skeletal taphonomy data for specimens from Enspel were derived from published photographs only.

3.4 Results

3.4.1 Size

SUL data are normally distributed and range from 16–79 mm (41 mm ± 16 mm (n = 28)) (Supplementary Dataset 1; Falk *et al.* 2022). Differences in SUL between pelobatids (n = 15) and palaeobatrachids (n = 6) are not significant (two-sample t-test, unequal variance, p = 0.304).

3.4.2 Orientation

All specimens (n = 140) are orientated with the sagittal axis of the body parallel to bedding. It was not possible to determine orientation more precisely for 19 specimens (14% (n = 140)). Of the remaining 121 specimens, 23 (19%) are dorsal, 50 (41%) are ventral and 48 (40%), dorso-ventral (Fig. S3.4, Supplementary Dataset 1, Falk *et al.* 2022).

3.4.3 Completeness

Completeness data are presented in two ways: (1) for specimens; (2) for skeletal elements.

(1) Specimen completeness. Most specimens are incomplete, although there is substantial variation in the data (specimen completeness: 44% ± 28% (n = 140); Fig. 3.5A). Completeness increases when phalanges (64% ± 26% (n = 140); Fig. 3.5B) and entire hands and feet (75% ± 23% (n = 140); Fig. 3.5C) are omitted from the calculations. Differences in completeness values between these groups are significant (Kruskal-Wallis, p(same) = 3.92^{-14}).

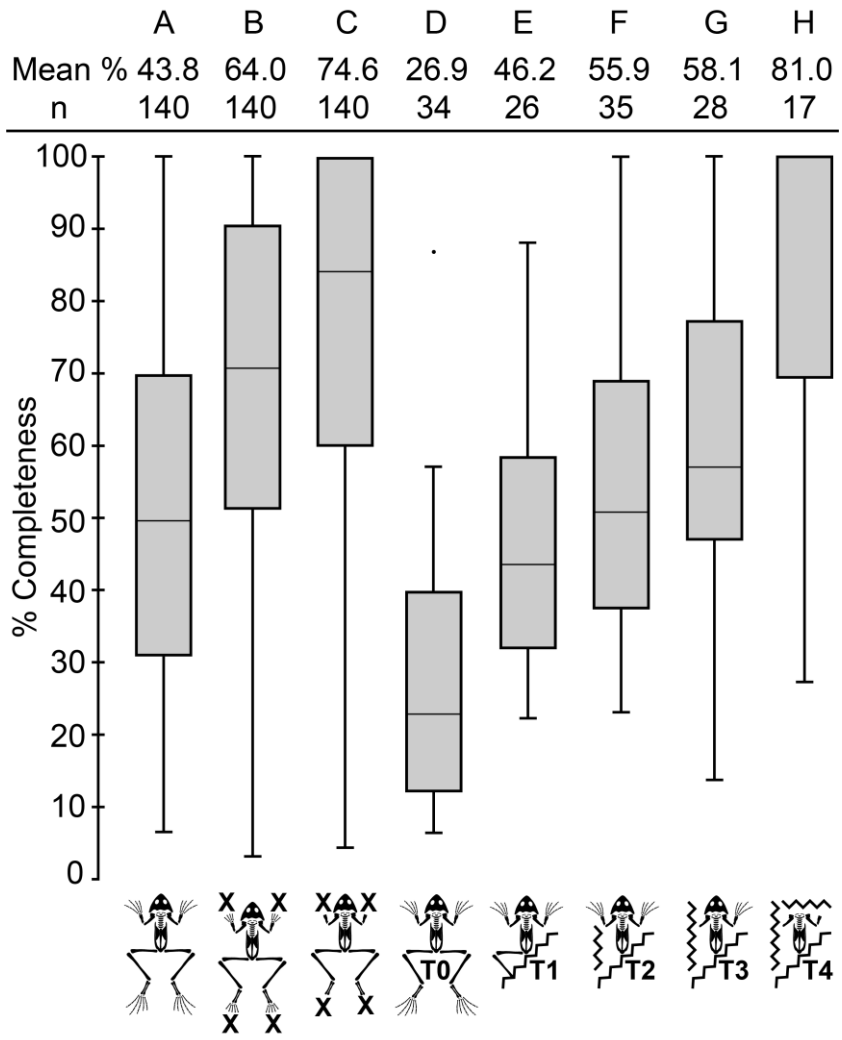


Figure 3.5: Impact of truncation on the percentage completeness of individual specimens. A–C, specimen completeness for the entire dataset; D–H, specimen completeness for truncation categories. A, no elements omitted from the dataset. B, phalanges omitted. C, entire hands and feet omitted. D, T0 (no truncation). E, T1 (0.1–24.9% truncation). F, T2 (25%–49.9% truncation). G, T3 (50%–74.9% truncation). H, T4 (75%–100% truncation). Horizontal lines in boxplots denote median value.

Fourteen specimens are complete, but all specimens classified as such are truncated (one specimen in category T2, three specimens in T3 and ten specimens in T4). Approximately one-third of specimens (34%, n = 126) lack at least one entire limb; this is not related to truncation. Further, twelve specimens comprise parts of articulated hindlimbs only. Ten of these show truncated proximal limb elements (one specimen in T2¸ three specimens in T3, six specimens in T4). The remaining two specimens are not

truncated and comprise, respectively, (1) the femur, tibiofibula and metatarsals articulated as a unit and (2) the tibiale-fibulare, metatarsals and phalanges articulated as a unit (Fig. 3.3J).

Most specimens (76% (n = 140)) are truncated by the edge of the slab or of the nitrocellulose glue / wax transfer (Fig. S3.5). Truncation of distal limb elements, i.e. forelimb phalanges and hindlimb phalanges, is common (65% (n = 105) and 94% (n = 106) of truncated specimens, respectively). Truncation of proximal limb elements, e.g. humerus and femur, is relatively rare (39% and 53% of truncated specimens, respectively (n = 106)) (Supplementary Dataset 1, Falk *et al.* 2022). Similar numbers of specimens are assigned to each of the truncation categories T0–T3 (Figs 3.5D–G, Fig. S3.5); few specimens are assigned to T4 (Fig. 3.5H). Specimen completeness increases progressively from T0 (27% ± 18% (n = 34)) to T1 (46% ± 18% (n = 26)), T2 (56% ± 21% (n = 35)), T3 (58% ± 24% (n = 28)) and T4 (81% ± 22% (n = 17); Figs 3.5D–H). These differences in completeness values are significant (ANOVA df = 4; F = 24.77; p(same) = $2.18e^{-15}$).

Differences between the specimen completeness values for palaeobatrachids (62% ± 6% (n = 15)) and pelobatids (50% ± 3% (n = 54)) are not significant (t-test (equal variance): t = 1.70, p(same mean) = 0.09). Further, there is no significant difference in the completeness of specimens from the upper coal (Ce II, Ce III, Ce V; 44% ± 28%; n = 111) and middle coal units (Ce IV, Ce VI, Leo III, Leo V, IL, NsXXXV; 46% ± 27%; n = 23; Mann-Whitney U-test: p(same median) = 0.64; see Supporting Information).

(2) Skeletal element completeness: Most skeletal elements are present in most specimens, although there is wide variation in the data (mean element completeness: 77% ± 20% (Figs 3.6, 3.7A)). The most complete skeletal elements are the cranium, femur and vertebrae (93%–98% of specimens (n = 108, 122 and 112, respectively)). Most specimens with vertebrae (63% (n = 102)) have a (near-)complete vertebral column (i.e., 7–9 vertebrae). Skeletal elements of the abdomen and distal limbs show lower completeness values. Most specimens include at least one (88% of specimens (n = 118)) or both (73%

(n = 118)) ilia and the urostyle (75% of specimens (n = 103)). Just over half of specimens include the ischium (62% of specimens (n = 76); Figs 3.6, 3.7A), carpals (53% of specimens (n = 93)) and forelimb phalanges (54% of specimens (n = 97)). The tarsals are the least complete elements (17% of specimens (n = 58); Figs 3.6, 3.7A).

There is a general trend for completeness to decrease progressively towards the distal parts of the forelimbs (humerus: 87% complete (n = 117); radioulna: 81% (n = 110); carpals (53% (n = 93); metacarpals: 70% (n = 96); forelimb phalanges (54% (n = 97)). Hindlimbs show a similar trend (femur: 93% (n = 122); tibiofibula: 88% (n = 112); tibiale-fibulare: 84% (n = 99); tarsals: 17% (n = 58); metatarsals: 76% (n = 82); hindlimb phalanges: 70% (n = 77); Figs 3.6, 3.7A). Hindlimb elements are usually more complete than homologous forelimb elements (Figs 3.6, 3.7A).

Completeness values for skeletal elements are generally lower (mean 62% ± 24%) when completeness is assessed relative to the total number of elements (not specimens; Fig. 3.7B), as many specimens contain only one element of a pair and few of a set. Trends in the data for skeletal elements, however, are similar to those described above for specimens (compare Figs 3.7A, B).

Phalanges are absent from 75% of hands (n = 171) and when present, are usually represented by three or fewer bones (mean 2.4 phalanges per specimen (n = 69)) (Fig. S3.7). Where forelimb phalanges are present in both hands, specimens show a mean of 7.0 phalanges (n = 24). No specimen has the full complement of ten forelimb phalanges in either hand. Similarly, phalanges are absent from 69% of feet (n = 106) (Fig. S3.7) and, where present, are usually represented by 1–3 phalanges (mean 2.8 phalanges per specimen (n = 36)). Where hindlimb phalanges are present on both feet, specimens show a mean of 7.9 phalanges (n = 13). No specimen has the full complement of 13–14 phalanges in a foot (Fig. S3.7).

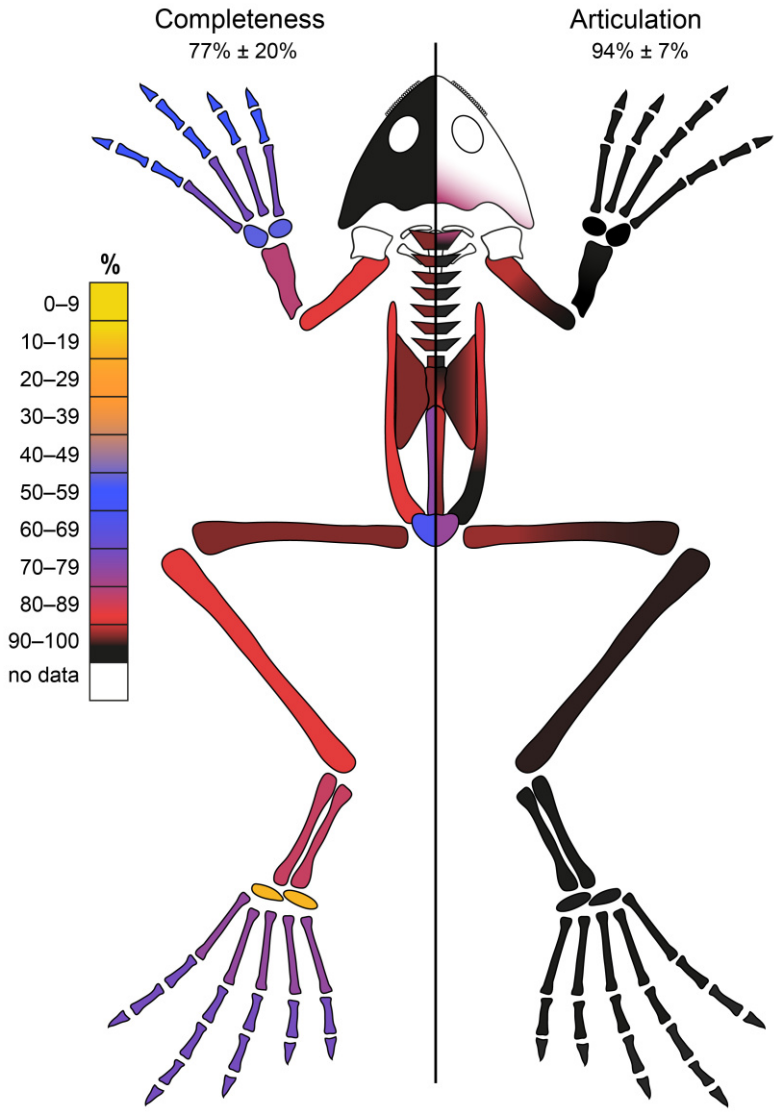


Figure 3.6: Schematic frog skeleton summarizing the percentage completeness and articulation values for each type of skeletal element in the Geiseltal anurans (n = 140); a black and white version of this figure is provided in the Supporting Information (Fig. S3.6).

Metacarpals are usually either absent (56% of hands (n = 187)) or complete (32% of hands); few specimens retain some, but not all, metacarpals. The mean number of metacarpals per specimen is 2.9 in the total dataset (n = 78) and 4.6 (n = 49) when specimens lacking metacarpals are excluded. Similarly, metatarsals are usually either absent (47% of feet (n = 142)) or complete (41% of feet); few specimens retain some, but not all, metatarsals (Fig. S3.7). The mean number of metatarsals per

specimen is 4.2 in the total dataset (n = 49) and 7.1 (n = 29) when specimens lacking metatarsals are excluded.

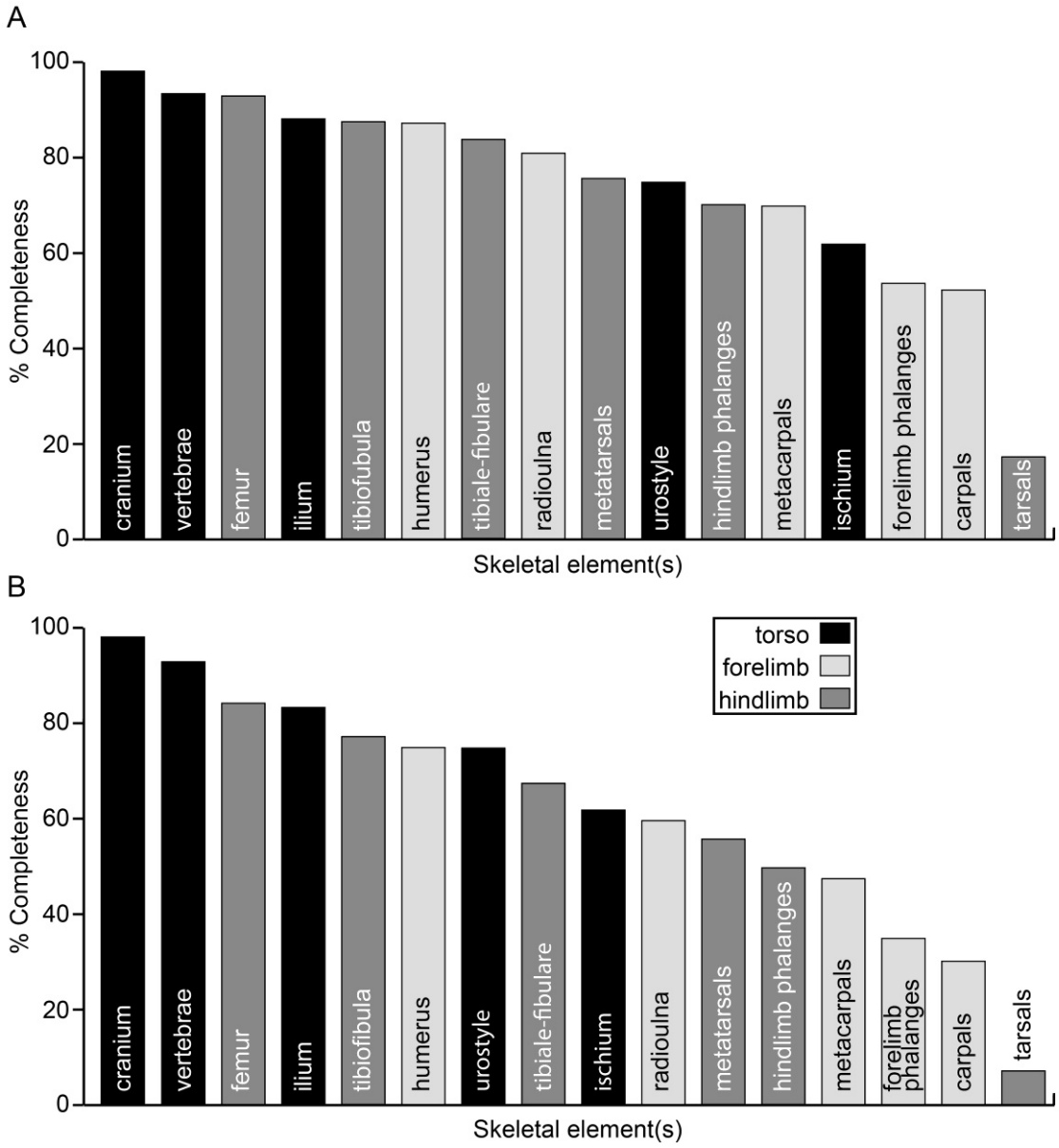


Figure 3.7: Percentage completeness of skeletal elements. A, percentage of specimens in the dataset for which each skeletal element is complete, i.e. represented by at least one element. For example, the completeness value for the femur is 93%; this indicates that 93% of specimens have at least one femur. B, percentage of skeletal elements present (i.e., complete), based on the total number of those elements in the dataset. For example, the completeness value for the femur is 84%; this indicates that 84% of all femura are present.

The tibiale-fibulare unit is present in 84% (n = 99) of specimens and is complete in 64% (n = 181) of all hindlimbs (Figs 3.7A, B, Fig. S3.7). The mean number of tibiale-fibulare bones per specimen is 2.6 in the total dataset (n = 72) and 3.3 (n = 56) when specimens lacking these elements are excluded.

In the total dataset, completeness values are positively correlated between the left and right sides of the body (Pearson's $r(10) = 0.99$, $p < 0.001$) and between homologous skeletal elements in the fore- and hindlimbs (Pearson's $r(3) = 0.89$, $p < 0.04$) (Figs 3.6, Fig. S3.8). Differences in completeness values between individual skeletal elements of palaeobatrachids and pelobatids are not significant (Mann-Whitney U-test: p(same median) = 0.097) (see Supporting Information).

3.4.4 Articulation

Articulation data are presented in two ways: (1) for individual specimens; (2) for individual skeletal elements.

(1) Specimen articulation: Most specimens are well articulated (specimen articulation 87% ± 19% (n = 140); Figs 3.8A, 3.9). Unlike completeness, articulation values do not vary significantly (Kruskal-Wallis; p(same) = 0.89) when phalanges (87% ± 21% (n = 140); Fig. 3.8B) and the entire pes and manus (86% ± 22% (n = 139); Fig. 3.8C) are omitted from the calculations.

Few specimens are fully articulated (21%, n = 140); most specimens classified as such are truncated (90%, n = 30) (Figs 3.8D–H, 3.9). Specimen articulation differs between the truncation categories: T0 (82% ± 22%, n = 34), T1 (87% ± 13%, n = 26), T2 (91% ± 11%, n = 35), T3 (87% ± 14%, n = 28) and T4 (87% ± 32%, n = 17) (Figs 3.8D–H). These differences are significant (Kruskal-Wallis; p(same) = 0.034). Only five specimens show articulation values <40%; two of these are fully disarticulated (Figs 3.8, 3.9).

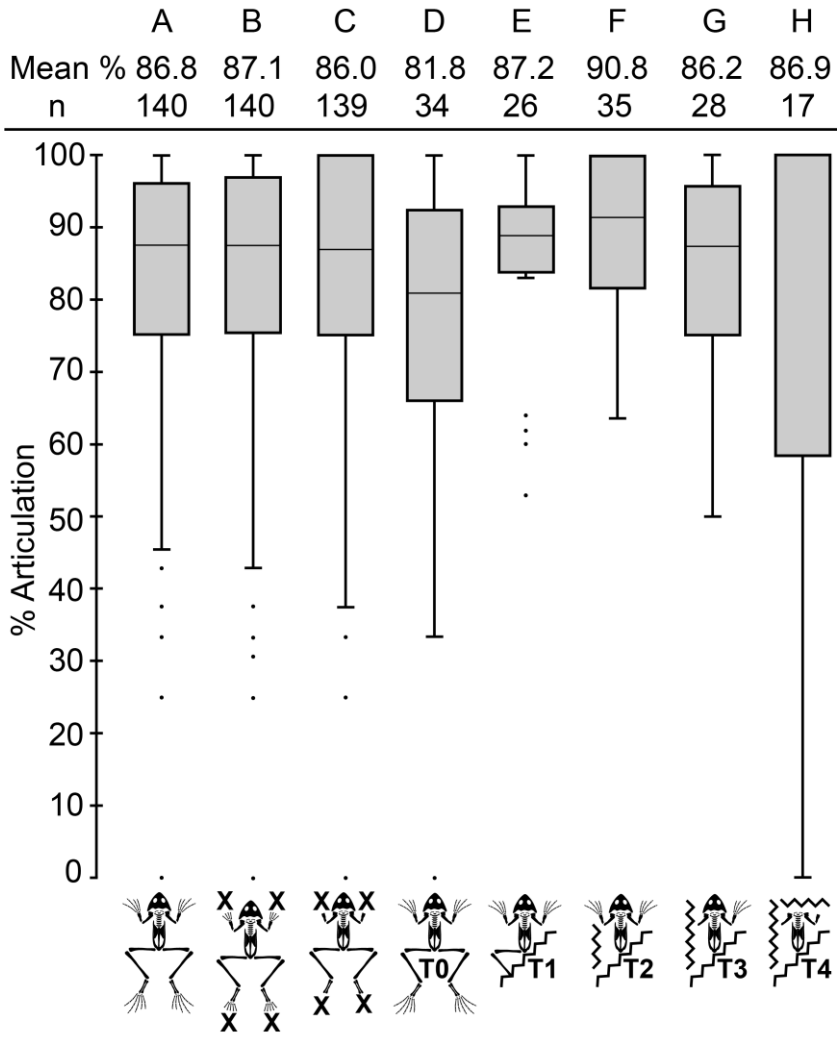


Figure 3.8: Impact of truncation on the percentage articulation of individual specimens. A–C, specimen articulation for the entire dataset; D–H, specimen articulation for truncation categories. A, no elements omitted from the dataset. B, phalanges omitted. C, entire hands and feet omitted. D–H, Specimens in truncation categories T0 (no truncation; D), T1 (0.1–24.9% truncation; E), T2 (25%–49.9% truncation; F), T3 (50%–74.9% truncation; G), T4 (75%–100% truncation; H). Horizontal lines in boxplots denote median value.

Differences between specimen articulation of palaeobatrachids (92% ± 9% (n = 15)) and pelobatids (84% ± 18% (n = 54)) are not significant (Mann-Whitney U-test: p(same median) = 0.053).

(2) Joint articulation: Overall, most joints present are well articulated (94% ± 7% of specimens; Figs 3.6, 3.10A). Where present, the joints of the fore- and hindlimb are articulated in >90% of specimens (Figs 3.6, 3.10A). Articulation values for distal limb joints are usually higher than for proximal limb joints (Fig.

3.6). Values are slightly lower (76%–90% of specimens) for many joints in the pelvic region (Figs 3.6, 3.10A). The vertebrae are usually well articulated (96% of specimens; n = 98; Figs 3.6, 3.10A).

Articulation values for skeletal elements are only slightly lower (mean articulation for the total dataset: 86% ± 8%) when articulation is assessed relative to the total number of joints (not specimens) present in the dataset (Fig. 3.10B). Most specimens, therefore, show articulation of both elements of a pair, or all elements of a set. When assessed in this way, articulation values for joints in the hip region, shoulder and limbs are usually only 10%–20% lower than when assessed per specimen (Fig. 3.10B). Unlike completeness, articulation values are high for the phalanges. Forelimb phalanges are articulated in all specimens (n = 31) and in 79% (n = 47) of hands. Hindlimb phalanges are articulated in all specimens (n = 34) and in 86% (n = 43) of feet (Figs 3.10A, B).

Even where carpals and tarsals are absent, the adjacent bones are *in situ* – and thus considered articulated – in most hands (85% (n = 33)) and feet (93% (n = 69); Fig. 3.10B).

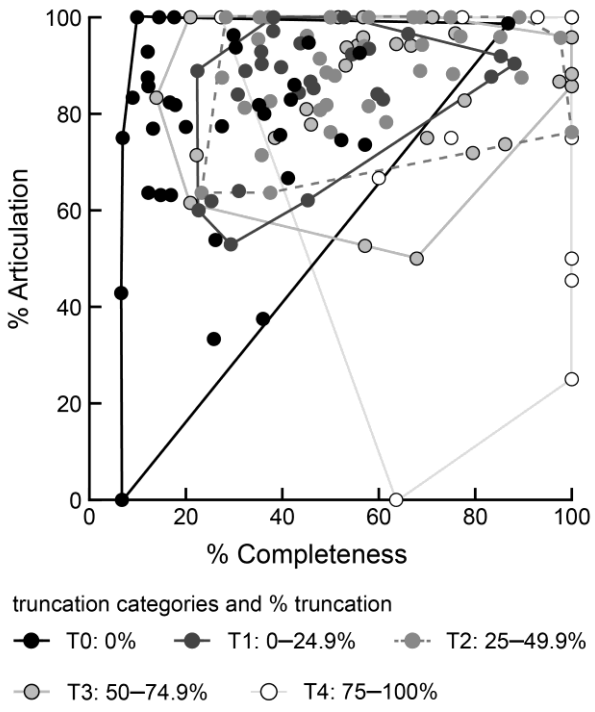


Figure 3.9: Percentage articulation versus percentage completeness for each specimen (n = 140).

For elements occurring as a set, the number of articulated elements present was considered. The vertebrae are usually well articulated: 56% of specimens show (near-)full articulation (7–8 joints articulated, n = 96). Less articulated states are relatively rare (Fig. S3.9). In contrast, most phalanges are poorly articulated. 76% of hands show two, or fewer, articulated phalangeal joints (n = 37; Fig. S3.9). Similarly, 72% of feet show two, or fewer, articulated phalangeal joints (n = 25; Fig. S3.9). Further, for joints between the phalanges and metacarpals, and phalanges and metatarsals, usually only 1–2 bones are articulated (41% of hands (n = 51) and 37% of feet (n = 54), respectively; Fig. S3.9). The metacarpal-carpal joints are fully articulated in 51% (n = 55) of hands (i.e., four joints articulated) and metatarsals-tarsals, in 75% (n = 12) of feet (i.e., five joints articulated); poorly articulated states are less common (Fig. S3.9).

Using the dataset for all joints, articulation values are positively correlated for the left and right sides of the body (Pearson's $r(16) = 0.897$, $p < 0.001$) and for homologous joints of the fore- and hindlimbs (Pearson's $r(5) = 0.773$, $p = 0.042$; Figs 3.6, Fig. S3.8). Differences in articulation values between individual skeletal elements of palaeobatrachids and pelobatids are significant (Mann-Whitney U-test: p(same) = 0.007; see Supporting Information).

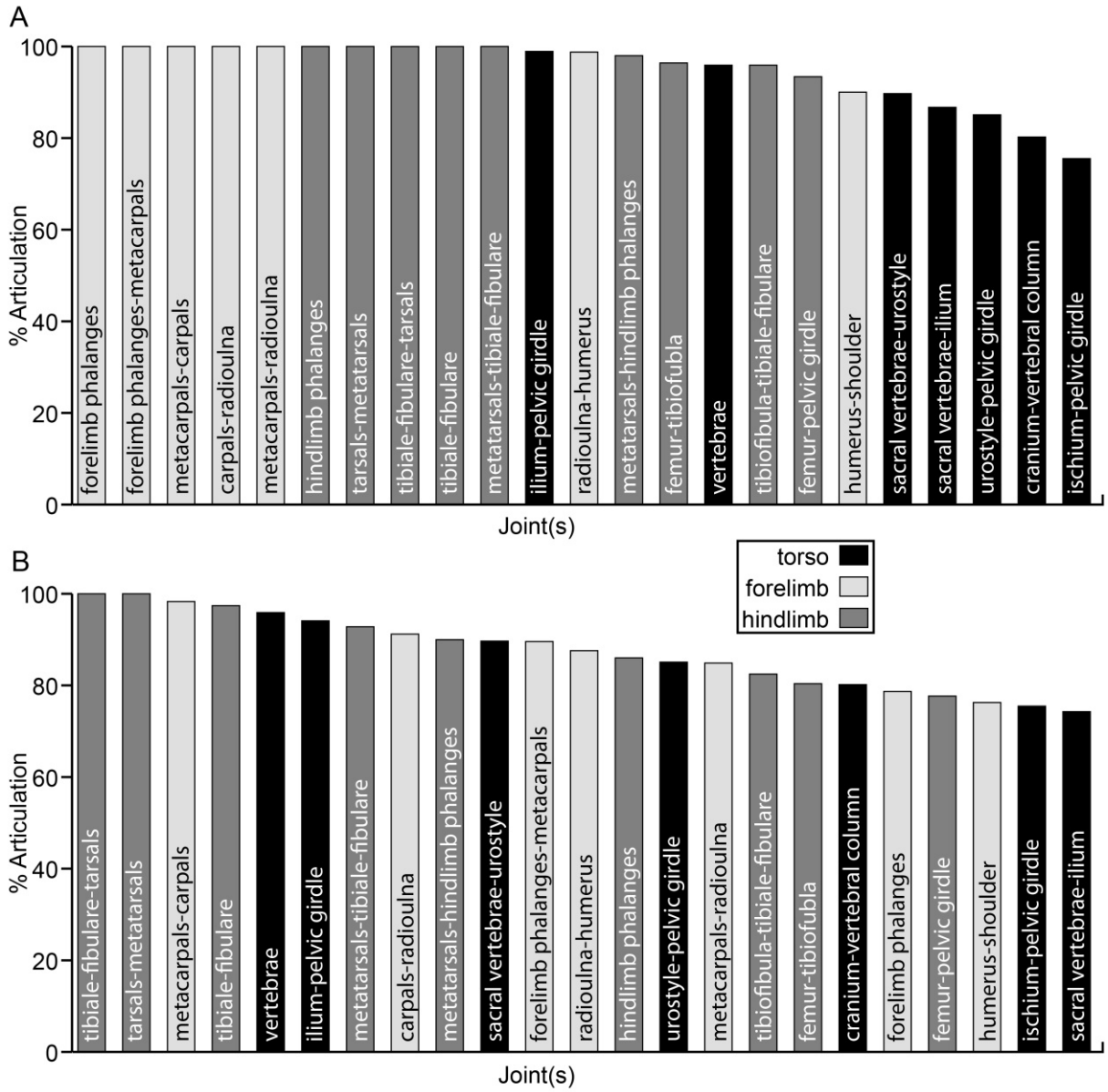


Figure 3.10: Percentage articulation of joints. A, percentage of specimens in the dataset for which each joint is articulated, i.e. represented by at least one articulated element. For example, the articulation value for the femur-tibiofibula (knee joint) is 96%; this indicates that at least one knee joint is articulated in 96% of specimens. B, percentage of articulated joints, based on the total number of those joints in the dataset. For example, the value for the femur-tibiofibula joint is 80%; this indicates that 80% of all knee joints in the dataset are articulated.

3.4.5 Relationship between completeness, articulation and truncation

Plotting articulation versus completeness shows that specimens show consistently high articulation values, albeit with a wider range in completeness values (Fig. 3.9). Six specimens do not fit this pattern

(with values 0%–42.9%, Figs 3.8A, 3.9). Four of these specimens belong to truncation category T0 (no truncation; Fig. 3.9) and two belong to truncation category T4 (highly truncated). The data fields for specimens belonging to truncation categories T1, T2 and T3 overlap almost completely, reflecting a similar range of values for completeness and articulation in each category (Fig. 3.9). Closer inspection of the articulation data does not show an obvious link with truncation. Thirty-five specimens plot below 75.2% articulation (outliers included), which is the lower quartile of the data (Q_1; Fig. 3.8A). Almost half of these specimens (n = 17) show little or no truncation (i.e., belong to T1 (n = 5) or T0 (n = 12)). Thirty-four specimens plot above the upper quartile (Q_3; Fig. 3.8A) and are thus > 96.3% articulated; almost half of these specimens (n = 16) are strongly affected by truncation (i.e., belong to T3 (n = 6) and T4 (n = 10)).

In contrast to articulation, the relative proportions of specimens in different truncation categories differs strongly for completeness. For instance, thirty-five specimens plot in the lower quartile for completeness (Q_1; <30.8% complete; Fig. 3.5A). Most of these specimens belong to T0 (n = 22; Fig. 3.5D). In contrast, many specimens in the upper quartile (Q_3; >69.7% complete (n = 35); Fig. 3.5A), belong to T4 (n = 13; Fig. 3.5H).

Distal limb bones (e.g. phalanges, carpals) are usually absent but, when present, are usually articulated (Fig. 3.6). In contrast, proximal limb elements (e.g. humerus, femur) are often complete but, when present, are less well articulated (with the torso, i.e. shoulder and hip joint, respectively). Vertebrae are nearly always present and usually form articulated units of two or more vertebrae (Figs 3.6, 3.10, Fig. S3.9). Bones adjacent to the vertebral column (e.g., urostyle, ilia), however, are less complete and joints where the vertebrae articulate with other elements (i.e., atlas vertebra–cranium, sacral vertebrae–urostyle, sacral vertebrae–ilium) are less articulated (Fig. 3.6). The ilium is usually present and articulated with the hip, but the urostyle and the ischium show lower values for both articulation and completeness (Fig. 3.6).

There is no significant difference in the completeness and articulation of specimens grouped in the following ways: (1) preserved at different sites (completeness: Kruskal-Wallis; p(same) = 0.84); articulation: Kruskal-Wallis; p(same) = 0.15; sinkholes: n = 25; dying field 1: n = 18; dying field 2: n = 92; Fig. S3.10). (2) Embedded in different materials (completeness (Kruskal-Wallis; p(same) = 0.90); articulation (Kruskal-Wallis; p(same) = 0.58); nitrocellulose glue: n = 104; nitrocellulose glue on gypsum: n = 6; paraffin wax: n = 29). (3) Determined (n = 69) and undetermined (n = 71) (Mann-Whitney U-test, completeness: p(same median) = 0.47; articulation: p(same median) = 0.13). (4) Percent truncation for different embedding materials (Kruskal-Wallis; p(same) = 0.28; Supporting Information).

3.5 Discussion

Our data reveal that the Geiseltal anurans vary markedly in their skeletal taphonomy. Some or all taphonomic features identified may relate, at least in part, to collector bias, study design, missing specimens and / or taxonomy. These potential biases are discussed at length in the Supporting Information. Alternatively, at least some of the data presented here could reflect taphonomic factors linked to the mode of death and biostratinomy of the fossils. These taphonomic factors are the focus of the discussion here, which is organised according to the key hypotheses that underpin this study.

Hypothesis (1): the fidelity of preservation is consistent for all skeletal elements, especially between homologous skeletal elements of the fore- and hind limbs and between the left and right sides of the body.

Our data reveal that this hypothesis is false: preservation varies among skeletal elements and is strongly linked to bone size and anatomical location.

The completeness values for individual specimens vary markedly depending on whether all, or a subset of skeletal elements (i.e., omitting phalanges or entire hands and feet) are used in the analysis (Figs 3.5A–C). Although the range of completeness values is similar for all three scenarios, mean values vary from 43.8% (no omissions) to 74.6% (omitting hands and feet; Figs 3.5A–C). This variation reflects much lower completeness values for peripheral, rather than proximal, skeletal elements; omitting the former elements clearly biases the data towards higher values (Figs 3.7A, B). Indeed, there is a strong proximal to distal trend in completeness, whereby both the fore- and hindlimb show progressively lower completeness values from proximal to distal bones (Fig. 3.6). Similar patterns have been reported from fossil vertebrates in marine (Beardmore *et al.* 2012) and lacustrine (McNamara et al. 2012*a, b*) settings.

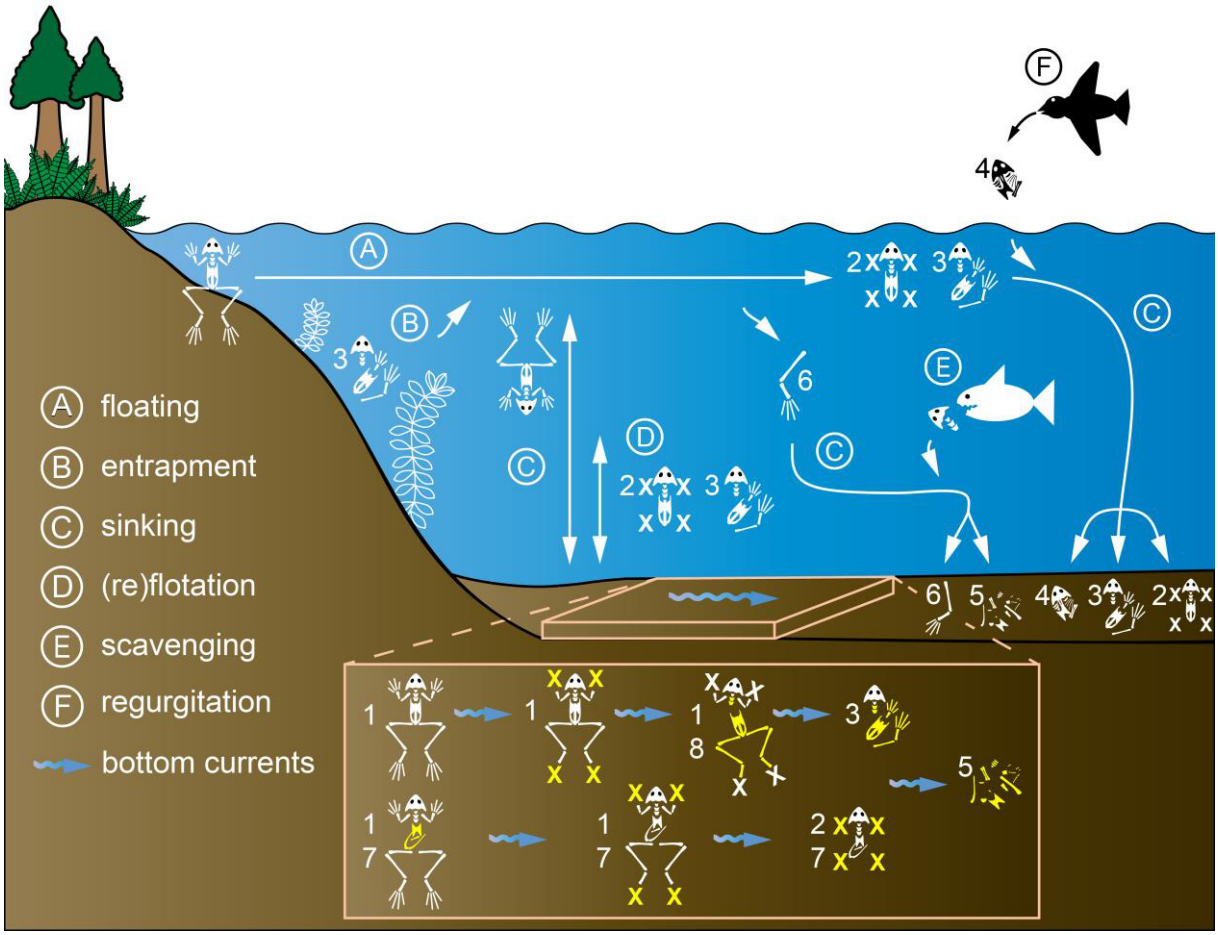


Figure 3.11: Distinct qualitative patterns in disarticulation and loss of skeletal elements in Geiseltal specimens reveal the controls on preservation and taphonomic pathways (A–E) in sinkhole and dying field deposits. See text for detailed characterisation of taphonomic states (1–9). States 1 to 3 form a genetically related sequence that

represents the progressive disarticulation and loss of elements from distal to proximal body regions with potential transitions to States 4, 5 and / or 6. States 7, 8 and 9 may be superimposed on any of the other taphonomic states.

Distal limb bones, e.g. phalanges, are usually absent; somewhat unexpectedly, distal bones that are present are better articulated than proximal elements (e.g. humerus), i.e. they are usually in life position (Figs 3.6, 3.10). This reflects loss of distal, small elements soon after disarticulation, likely by weak bottom currents (Dodson 1973; McNamara *et al.* 2012*a*), resulting in a scenario whereby distal elements are either complete and articulated, or absent. In contrast, proximal bones such as the humerus are larger and surrounded by more tissue, promoting their association with the carcass (and thus higher completeness values) even where they are disarticulated.

The low completeness values for carpals and tarsals (Figs 3.6, 3.7) may reflect difficulties in identification due to their small size (*c.* 1–4 mm) and one, or a combination, of associated factors. These include poor preservation, potential loss during preparation (Fig. S3.1), fusion *in vivo* to adjacent elements, reduction (Špinar 1972; Fabrezi 1993; Fabrezi & Alberch 1996) and/or incomplete ossification in juveniles (Špinar 1972; Fabrezi & Alberch 1996; Henrici & Haynes 2006; Roček *et al.* 2014). Preferred disarticulation and loss of carpals and tarsals during decay is less likely as the adjacent elements do not show similarly low completeness values or disarticulation (Fig. 3.10).

Similar completeness and articulation values for paired skeletal elements from opposite sides of the body indicate consistent broad taphonomic controls across the body. Except for carpals and tarsals, the completeness values for forelimb bones are usually lower than the homologous elements of the hindlimbs (Fig. 3.6). This feature has been discussed previously (Dodson 1973; McNamara *et al.* 2012a) and likely reflects the smaller size of most forelimb elements relative to hindlimb elements, facilitating removal of the former bones by weak bottom currents.

There is no link between either completeness or articulation and specimen orientation; the dorsal, ventral or dorso-ventral aspect of specimens reflects the most hydrodynamically stable orientation for anurans (McNamara *et al.* 2012*a*) and is independent of other skeletal taphonomy metrics.

Analysis of the data for specimen articulation, completeness and truncation reveals interesting results. Specimen articulation is independent of truncation (Fig. 3.8). This likely reflects the fact that articulation values do not show a single strong trend linked to anatomical location of bones in the body, but rather reflect several factors. In contrast, specimen completeness is strongly linked to truncation (Fig. 3.5), whereby less truncated specimens usually show lower percentage completeness values. This usually reflects the real absence of several, or many, phalanges. In such specimens, the apparent completeness is a close approximation of true completeness. In contrast, highly truncated specimens usually show higher completeness values. This is because many bones, typically numerous phalanges, are truncated and thus omitted from the completeness calculation (see Material and Method, Supporting Information). This highlights the critical importance of assessing truncation in studies of the skeletal taphonomy of fossil vertebrates.

Hypothesis (2): the fidelity of preservation is linked to excavation site and taxonomy.

Our data reveal that this hypothesis is false: preservation is independent of local variations in fossil locality and anuran group.

Similar completeness and articulation values for specimens from different types of fossil locality, e.g., sinkholes and dying fields, suggest similar taphonomic processes in operation across the Geiseltal basin. Similarly, completeness and articulation are broadly consistent among specimens from different stratigraphic levels at a single locality. The general suite of taphonomic processes and thus the controls on preservation are consistent through space and time and are not subject to short-term or spatially localised variations.

Similar completeness and articulation values for the Geiseltal pelobatids and palaeobatrachids (see Supporting Information) suggest that differences in absolute abundance of the two groups are not taphonomic in origin. The relatively paucity of palaeobatrachids is therefore likely to reflect a real biological signal, whereby they were simply less abundant members of the lake fauna. Pelobatids were numerically dominant (possibly due to behavioural factors – see Hypothesis 4 discussion below). The articulation values of individual skeletal elements in pelobatids and palaeobatrachids, however, differ significantly. Palaeobatrachids usually show higher articulation values for abdominal bones than pelobatids (see Supporting Information). The reasons for this difference are not clear but may relate to the relatively stable construction of the vertebral column and sacral body region due to fusion of vertebrae (forming a synsacrum) in palaeobatrachids. In addition, and/or alternatively, the differences in abdominal articulation may reflect differences in the activity of gut-derived decay bacteria linked to original gut flora and ultimately diet. There is no significant difference in preservation between specimens that were determined taxonomically and those that were not. The data suggest that the embedding material has no major impact on truncation, completeness and articulation values (see Supporting Information).

Hypothesis (3): specimens represent a series of repeating taphonomic states.

Our data confirm this hypothesis: the Geiseltal anurans represent a series of nine repeating taphonomic states (Fig. 3.11). These states were identified based on distinct qualitative patterns in disarticulation and loss of skeletal elements.

States 1 to 3 form a sequence that represents the progressive disarticulation and loss of elements from distal to proximal body regions with potential transitions to States 4, 5 and / or 6. Completeness and articulation values of States 1 to 6 overlap (Fig. S3.11) but differences are statistically significant (see

Supporting Information). States 7, 8 and 9 may be superimposed on any of the other taphonomic states (Fig. 3.11).

State 1 (18% of specimens (n = 34)): Specimens are generally well-articulated and complete except for peripheral and distal limb elements, which are disarticulated and/or lost (Figs 3.3B, C). This taphonomic pattern indicates preferred loss of smaller and lighter elements at the body margins and likely reflects one, or a combination, of the following factors. (a) Transport dynamics. Small/light bones are easier to transport than large/heavy bones (Dodson 1973). (b) Bottom currents. Peripheral elements are not protected by the body mass and are thus more susceptible to current-induced displacement while the carcass is residing on the floor of the water body prior to deposition of the next sedimentary layer. (c) Less soft tissue. Peripheral elements are associated with a low mass of soft tissues, i.e., muscles and connective tissue that promote the retention of articulation. Specimens belonging to State 1 reflect burial prior to substantial decay of soft tissues.

The relative timing of decay and deposition of vertebrate carcasses in aquatic environments is controlled, in large part, by ambient temperature (Wuttke 1983; Kidwell & Baumiller 1990; Carter & Tibbett 2006; Carter *et al.* 2008), which regulates microbial metabolism and abiotic reactions. Mean annual temperatures >20°C (Mosbrugger *et al.* 2005) during the Middle Eocene would likely be associated with lake surface temperatures >16°C (Elder & Smith 1988). These in turn would have promoted rapid decay of organic material and high rates of decay gas production, probably followed (in many cases) by (re)floating of carcasses after initial sinking (Wuttke 1983; Elder & Smith 1984; Elder & Smith 1988).

For State 1, although a brief period of (re)floating cannot be excluded, prolonged (re)floating is not plausible as it would generate widely dispersed skeletal elements and specimens missing part, or all, of limbs. State 1 specimens likely represent death and deposition during periods where (re)flotation is

inhibited by high water pressures (i.e., deposition in deep waters) or low temperatures (suppressing generation of decay gases), e.g., during a relatively cool and/or wet climatic regime. The proximate control is the exposure to bottom currents as these lead to disarticulation and loss of elements. Specimens were likely exposed for an extended period on the lake floor prior to burial by sediment. This is supported by the fine lamination of the host sediments (up to four laminae / mm in dying field 1 (Raupach 1948)), which is consistent with low sedimentation rates (Raupach 1948). Some laminae may reflect intermittent fine-grained debris flows and turbidites (Smith 1986) following collapse of riverbanks or sinkhole slopes (Krumbiegel *et al.* 1983). It is not possible, however, to test this hypothesis through examination of petrographic sections as almost all specimens are on transfers. Specimens in dying field 1 and 2 typically exhibit preferred orientations (Weigelt 1933), likely generated during transport and/or by bottom currents.

State 2 (29% of specimens (n = 34)): These specimens lack at least one entire limb but are otherwise well articulated (Fig. 3.3G). This state reflects more extensive decay of specimens than State 1 and probably some (re)flotation at the lake surface (or within the water column) prior to deposition. Such specimens likely represent deposition in relatively shallow and/or warm waters, i.e., where low water pressure was insufficient to prevent refloating and/or where warm temperatures enhanced the production of decay gas. Death and deposition therefore occurred during relatively warm and/or arid climatic regimes compared to those prevailing during deposition of State 1 specimens.

State 3 (29% of specimens (n = 34)): Largely incomplete and partially disarticulated specimens (Fig. 3.3E). These represent prolonged (re)floating of the carcass due to production of abundant decay gases and/or low water pressure (see above). This in turn reflects warmer and/or shallower waters than for State 2. Alternatively, State 3 specimens may represent a longer period of decay prior to transport, potentially due to entrapment of carcasses in littoral vegetation. Patterns of skeletal element loss are consistent with vertical settling from floating carcasses, with no evidence for directional scattering.

State 4 (9% of specimens (n = 34)): Clusters of densely packed bones including partly articulated elements (Fig. 3.3D). These may represent regurgitated digestive material / gastric pellets.

State 5 (9% of specimens (n = 34)): Widely disarticulated and reorientated skeletal elements (Fig. 3.3I). These represent either prolonged (re)floating favoured by warmer and/or shallower waters than in taphonomic States 2 and 3, or an extended period of pre-transport decay.

State 6 (6% of specimens (n = 34)): Isolated articulated limbs (Fig. 3.3J). These presumably are the missing skeletal elements of State 2 and State 3 specimens and comprise mostly articulated body units spatially separated from the (missing) remaining skeleton. Isolated limbs originate during decay of soft tissue at the shoulder joint and / or the hip joint. Weak bottom currents may disarticulate smaller limb elements (i.e., phalanges) after final deposition.

State 7 (21% of specimens (n = 34)): Specimens frequently showing disarticulation and / or loss of bones in the abdominal region (Fig. 3.3C), often despite the rest of the body being relatively well articulated and complete. This could reflect one, or both, of the following processes: (a) Abdominal collapse, i.e., decay-induced collapse of the prismatic configuration of the urostyle, ilia and sacral vertebra inside the abdominal skin sac (McNamara *et al.* 2012*a*). This is unlikely to be sufficiently violent to rupture the skin; in such cases, i.e., where the skin remains intact, no abdominal bones should be lost. (b) Abdominal rupture (Fig. 3.3C), i.e., violent eruption of decay gases from the abdomen (Wuttke 1983; McNamara et al. 2012*a*; Smith & Wuttke 2012). This likely reflects warm water temperatures (promoting production of decay gases); other factors include differences in diet among specimens (and thus variation in the composition of intestinal flora potentially impacting decay rate). Where abdominal rupture is accompanied by tearing of the skin, this may promote further disarticulation and loss of bones.

State 8 (18% of specimens (n = 34)): Reorientation of the lower body (Fig. 3.3C). The bones of the pelvic girdle (e.g., ischium, ilia) and usually hindlimbs are reorientated relative to the sagittal axis as defined by the head and vertebrae, typically with a single major disarticulation between the pelvic girdle and vertebrae. This represents disturbance of the carcass by either stronger bottom currents than those referred to in State 1 and/or disturbance of carcasses by weak currents at relatively advanced stages of decay prior to burial.

State 9: Articulated body units. Certain skeletal elements, e.g., the tibiale-fibulare, metatarsals, metacarpals and vertebrae, are usually either complete and articulated as a unit, or all elements in the group are absent (Fig. S3.7). This may reflect fusion of bones, as in the vertebrae of palaeobatrachids (Wuttke *et al.* 2012) and the tibiale-fibulare of anurans (Fabrezi 1993; Fabrezi *et al.* 2017) (although this may not be a feature of pelobatids (Roček *et al.* 2014) and palaeobatrachids (Wuttke *et al.* 2012)). Articulated units may also reflect differences in the resistance of soft tissues to decay within and external to the unit (Wuttke 1983).

Hypothesis (4): the cause of death is desiccation or lake overturn.

Our data reveal that this hypothesis is false. Previous studies have suggested that the Geiseltal anurans died during the desiccation of lakes and/or oxygen depletion of the water column during overturn of lake waters (Voigt 1934; Weigelt 1934). This, however, is unlikely as the anurans could presumably migrate to other water bodies during adverse conditions (Henrici & Fiorillo 1993; Todd *et al.* 2009). Further, the evidence for (re)flotation of carcasses is not consistent with desiccation.

Alternative modes of death for the Geiseltal anurans therefore must be considered. These include:

(1) Elevated salinity, as indicated by halophile ferns (Barthel & Rüffle 1970) and ostracods (Krumbiegel 1962*a*). As with the desiccation hypothesis, however, elevated salinity is unlikely to have killed many

anurans as the animals could have migrated during adverse conditions; further, some modern pelobatids tolerate brackish water (Stănescu *et al.* 2013).

(2) Starvation. This is not plausible as anurans typically migrate if food is scarce (Buchacher 1993; Todd *et al.* 2009). Further, certain Geiseltal anurans are associated with potential coprolites (e.g., Fig. 3.3C), suggesting death after a recent meal. Starvation during hibernation does not apply as the palaeoclimate was unlikely to have been sufficiently cold to promote enduring hibernation (Grein *et al.* 2011; Krutzsch 2011).

(3) Poisoning by algal blooms. Diatomite beds in some sinkhole deposits and records of abundant dinoflagellates (Krumbiegel *et al.* 1983) are direct evidence for algal blooms, which can be toxic to aquatic fauna (Carty & Parrow 2015; López-Cortés *et al.* 2015; Watson *et al.* 2015). The relative stratigraphic positions of the diatomite beds and the fossiliferous strata, however, are unclear. Further, extant pelobatids are terrestrial (Lizana *et al.* 1994) and therefore are unlikely to be affected by algal blooms (Henrici & Fiorillo 1993).

(4) Storm / flood events. Some specimens may have died due to high water turbulence during floods (Duellman & Trueb 1994; La Marca 2021); this may apply especially where specimens show a preferred orientation (Weigelt 1933), although the latter feature may originate *post mortem* (Henrici & Fiorillo 1993).

(5) Freezing. The Eocene greenhouse climate may have included rare weather events including temperatures below 0°C (Grein *et al.* 2011; Hu *et al.* 2018), which can be harmful to anurans. The Geiseltal water bodies, however, were probably sufficiently deep to remain ice-free at depth. This would have provided shelter (Manion & Brother Lawrence 1952; Voituron *et al.* 2009), which is important for tropical, mainly aquatic taxa with low cold tolerance (Brattstrom 1968; Costanzo *et al.* 2013), e.g., the Geiseltal palaeobatrachids. Terrestrial taxa, e.g. pelobatids, are unlikely to shelter in water bodies (Swanson & Graves 1995; Costanzo & Lee 2013), except during mating season (Lizana *et al.* 1994).

(6) Disease. Mass mortalities in extant anurans can result from disease, including chytridiomycosis (Lips 1999; Scheele *et al.* 2019) and *Ranavirus* (Price *et al.* 2017). Mass mortalities such as the dying fields at Geiseltal could therefore potentially reflect disease, but verification of this hypothesis is difficult because many diseases lack a physical expression that can be readily fossilised (Densmore & Green 2007).

(7) Predation / scavenging. A single fish specimen from Geiseltal contains anuran remains in the abdomen, presumably representing gut contents (see Voigt 1934: Tafel III, Fig. 1, No. A299). This, plus a limited number of specimens comprising accumulations of densely packed bones (Fig. 3.3D) or anterior/posterior body halves (Fig. 3.3E), represent limited evidence for predation / scavenging.

(8) Old age. The SUL data are normally distributed, confirming that the specimens represent a wide range of sizes and presumably ages (although there is no direct linear relationship between SUL and age (Liao *et al.* 2011)). Death by old age therefore cannot be excluded as a cause of death of at least some specimens.

(9) Mating-related. Mating-related mass mortality caused by drowning or exhaustion is common in extant anurans (Verrell & McCabe 1986; Trauth *et al.* 2000; Menin *et al.* 2006; Izzo *et al.* 2012) and has been invoked as the primary cause of death for some fossil anurans (McNamara *et al.* 2012*a*). Mating-related mortalities are plausible even for terrestrial anurans, e.g. pelobatids, as these return to the water to reproduce (Lizana *et al.* 1994).

Collectively, these data suggest that many Geiseltal anurans represent mating-related deaths, at least some of which may have occurred in mass mortalities. Evidence for recurring mass mortality events includes reports of tens to hundreds of specimens on individual bedding planes at many excavation sites (Haubold & Krumbiegel 1984; Hellmund & Hastings 2014). Further, the SUL data presented here (Supplementary Dataset 1, Falk *et al.* 2022) are consistent with a wide range of body sizes and presumably ages. The most plausible taphonomic scenario therefore involves a biological cause of death linked to anuran behaviour (homing instinct to return to the lake to breed) and subsequent

accumulation of carcasses via normal sedimentological processes (sinking, transport and deposition of carcasses in profundal lake regions). We cannot, however, exclude the possibility that some specimens (especially those preserved as isolated individuals) died due to freezing, disease or old age, but these three causes of death are difficult to verify.

Hypothesis (5): comparative taphonomic analysis of anurans from various Cenozoic biotas can identify broad taphonomic trends in anuran preservation.

Our data confirm this hypothesis: anurans preserved in the different biotas studied share common, repeated, taphonomic patterns. Irrespective of biota-specific taphonomic features (detailed below), this allows identification of the primary controls on the skeletal taphonomy of anurans from Cenozoic lacustrine-hosted Konservat-Lagerstätten.

Fossil anurans have been reported from several key Cenozoic Konservat-Lagerstätten, e.g. Messel (Middle Eocene, Germany; Wuttke 1983, 2018), Enspel (Late Oligocene, Germany; Roček & Wuttke 2010), Bechlejovice (Early Oligocene, Czech Republic; Špinar 1972; Roček 2013) and Libros (Late Miocene, Spain; McNamara *et al.* 2009; McNamara *et al.* 2012*a*). This provides an opportunity to conduct a comparative analysis of the taphonomy of anurans from different biotas to better understand the overarching controls upon preservation. Systematic data on skeletal taphonomy are available only for specimens from Libros, which are therefore the focus of this analysis.

Libros versus Geiseltal

The Libros frogs analysed by McNamara *et al.* (2012*a*) are monospecific (*Pelophylax pueyoi*) and hosted within deep-water laminated mudstones deposited in a perennial palaeolake (McNamara*, et al.* 2012*a*). The Libros anurans show higher completeness values for most skeletal elements (McNamara *et al.* 2012*a;* Table 3.1) than those from Geiseltal. This could be a real taphonomic signal or an artefact

of collection bias. If real, the higher completeness of the Libros frogs could reflect: (1) shorter residence time at the water surface due to cooler water temperatures (climate was cool during the Late Miocene relative to the mid-Eocene), enhancing sinking and mitigating against substantial decay and disarticulation prior to deposition; (2) the deep nature and high alkalinity of the Libros lake (at least several tens of metres deep; Ortí *et al.* 2003), thus preventing refloating; (3) the large area of the Libros lake and the deposition of the carcasses in central zones where bottom currents would have been weak and rare (McNamara *et al.* 2012*a*); (4) the absence of fish and other scavengers.

Table 3.1: Percentage of Libros specimens for which each skeletal element is complete or joint is articulated (data from McNamara et al. 2012a)

Skeletal element(s)	Completeness Libros (%)	Completeness Geiseltal (%)	Joint(s)	Articulation Libros (%)	Articulation Geiseltal (%)
Cranium	100	98.1	Cranium	100	n/a
Forelimb phalanges	25.0	53.6	Cranium-vertebrae	n/a	80.2
Metacarpals	n/a	69.8	Forelimb phalanges	21.0	100
Carpals	78.0	52.7	Forelimb phalanges-Metacarpals	n/a	100
Radioulna	95.6	80.9	Metacarpals-phalanges	n/a	100
Humerus	100	87.2	Phalanges-carpals	78.0	n/a
Vertebrae	98.1	92.9	Carpals-radioulna	89.1	100
Urostyle	100	74.8	Radioulna-humerus (elbow)	75.0	98.8
Ilium	100	88.1	Humerus-shoulder	95.3	90.0
Ischium	n/a	61.8	Vertebrae	84.4	95.9
Femur	100	93.4	Urostyle-sacral vertebra	71.9	89.7
Tibiofibula	100	87.5	Ilium-sacral vertebra	89.1	86.7
Astragalus-calcaneum	100	83.8	Urostyle-pelvic girdle	75	85.1
Metatarsals	n/a	17.2	Pelvic girdle-femur (hip)	82.8	93.4
Tarsals	81.0	75.6	Femur-tibiofibula	84.4	96.4
Hindlimb phalanges	28.0	70.1	Tibiale-fibulare	64.1	95.9
			Tibiale-fibulare-tarsals	66.8	100
			Tarsals-metatarsals	n/a	100
			Metatarsals-phalanges	n/a	98.0
			Hindlimb phalanges	27.5	100

It is possible that the differences in completeness between the anuran assemblages could reflect – at least in part – differences in the analytical approach in this study and in McNamara *et al.* 2012*a*. For

the Libros study, specimens comprising isolated anuran bones were omitted, but such specimens are included in the Geiseltal analysis. In addition, truncated specimens comprise a minority (35%) of the Libros dataset, but most (76%) of the Geiseltal dataset. Further, specimens showing moderate truncation (at least two truncated feet) were omitted from the Libros study but included herein.

Completeness values for the cranium, vertebrae and femura are similar for specimens in both sites; completeness shows a proximal-distal trend in both. This likely reflects a common taphonomic process, i.e., preferred loss of peripheral elements due to their small size and exposed position in the body (McNamara *et al.* 2012*a*). Both sites reveal similar articulation patterns for joints in the shoulder and hip region, which are less articulated than others. This reflects the similar anatomical configuration of the bones at these joints and similar taphonomic history, i.e., featuring decay-related collapse of the three-dimensional architecture of the hip bones and compaction during burial. In both sites few specimens show evidence for abdominal rupture; many Libros specimens show gut contents.

In contrast to the completeness data and general patterns of articulation, the articulation values for Geiseltal anurans are usually higher than those for Libros anurans (McNamara *et al.* 2012*a*; Table 3.1). This likely reflects the inclusion of truncated specimens in the Libros study. Other potential factors include collection bias or the strength of bottom currents (ultimately resulting in lower completeness, but higher articulation values).

A major biological (intrinsic) control on the skeletal taphonomy of the Libros anurans is the quality of preservation of the skin: better preserved skin is associated with higher values for completeness and articulation (McNamara *et al.* 2009). Future studies should assess any such taphonomic links for the Geiseltal anurans.

Other Cenozoic biotas

The skeletal taphonomy of anurans from Messel, Enspel and Bechlejovice has not been studied systematically. That said, some general qualitative statements are possible regarding the comparative taphonomy of these and the Geiseltal anurans (Table 3.2).

Anurans from all four Lagerstätten share a common proximal-distal trend in completeness (Table 3.2) (e.g. Fig. 3.3C, Fig. 3 in Köhler 2011, Fig. 6h in Roček & Wuttke 2010, Pl.102 No.608a in Špinar 1972, McNamara unpubl. data) that results from the preferred disarticulation of small and peripheral bones (probably linked to the low amount of surrounding soft tissue). Abdominal disarticulation is also common in all four biotas (Table 3.2) (Fig. 3.3C, Fig. 17.1 in McNamara 2007, Fig. 8a in Roček & Wuttke 2010, Pl.83 No.6210 in Špinar 1972, McNamara unpubl. data) and is probably linked to the collapse of the three-dimensional structure of the abdominal bones; loss of some of these elements in a limited number of specimens suggests rare abdominal rupture. Weak bottom currents, e.g., generated by inflowing streams, landslides, storm events or lake overturn, may reorientate anterior and posterior body halves and limbs (e.g. Fig. 8.4 in Wuttke 2018, Fig. 154 in Wuttke 1988, Fig. 4i in Roček & Wuttke 2010, Pl.76 No.35b in Špinar 1972, McNamara unpubl. data).

All specimens were deposited in profundal lake regions characterised by low sedimentation rates (Špinar 1972; Pirrung *et al.* 2001; Wuttke & Poschmann 2010). The palaeolakes differ, however, in key environmental parameters such as size, temperature, depth and the presence/absence of fish (Table 3.2) (Špinar 1972; Pirrung *et al.* 2001; Roček *et al.* 2006). Variations in lake characteristics can be directly related to taphonomic patterns (Fig. 3.12). Water temperature controls the rate of decay and decay gas production, i.e., lower temperatures inhibit (re)floating (Smith & Elder 1985). Surface water temperature is controlled by the broad palaeoclimatic setting. Deposition in deeper waters also inhibits refloating and abdominal rupture (Smith & Elder 1985) (e.g., Messel, Enspel).

Table 3.2: Comparative taphonomy of the anurans from Geiseltal, Messel (Eocene, Germany), Enspel (Oligocene, Germany), Bechlejovice (Oligocene, Czech Republic) and Libros (Miocene, Spain).

	Geiseltal lacustrine system	Lake Messel	Lake Bechlejovice	Lake Enspel	Lake Libros
Age/location	Eocene, *c.* 45 Ma, Germany	Eocene, *c.* 47 Ma, Germany	Oligocene, 26.8–25.5 Ma, Czech Republic	Oligocene, *c.* 24.7 Ma, Germany	Miocene, 11.2–8.7 Ma, Spain
Mean annual temperature	23–25°C (Mosbrugger *et al.* 2005)	16.8–23.9°C (Grein *et al.* 2011); 18 ± 2.5°C (Tütken 2014); surface water temperature: 25 ± 3°C (Tütken 2014)	Likely to be similar to Enspel: similar palaeolatitude	15–17°C	Unknown during deposition; 16–17°C reported for Vallesian sites Abezames (NW Spain) and Burgos (Central Spain)
Environment	Swamps, ponds, rivers	Volcanic maar	Thermal spring environment	Volcanic maar	Perennial bench-type lake
Size	Individual water bodies *c.* several hundreds of meters wide	*c.* 0.7 × 1.4 km	Several hundreds of metres wide	*c.* 2 km²	30–40 km²
Depth	Up to 15 m	200–300 m	50–60 m according to profile in Špinar (1972)	Several tens of metres to up to 240 m	Up to 100 m
Hydrology	Hydrologically open	Hydrologically closed	Hydrologically open	Hydrologically closed	Hydrologically open
Excavated facies	Swamps/ponds: littoral to profundal; rivers: channel & overbank deposits	Littoral to profundal	Profundal	Profundal	Littoral to profundal
Profundal sediments	Swamps/ponds: laminated, black lignites and dysodile coal (including varve-like couplets) with intercalated carbonate beds; rivers: white, cross-bedded sandstone & brown mudstone	Organic rich pelites ('oil shale') & fine laminated claystones/siltstones (with slumping structures, drainage structures); intercalated coarse-grained volcanoclastic turbiditic inclusions (increased for lake margins)	Laminated carbonaceous claystones, with intercalated volcaniclastics/pyroclastics	Black shales & coarse-grained volcaniclastics/ pyroclastics	Limestones (wackestones & packstones) & laminated mudstones (including oil shales and varves)
Bottom currents	Weak	Rare	No reference	Weak/absent	Weak/absent
Anuran taxonomy	Pelobatidae, Palaeobatrachidae & potentially Discoglossidae	Pelobatidae, Palaeobatrachidae & one unassigned species	Palaeobatrachidae, Discoglossidae, Pelobatidae, Ranidae	Pelobatidae, Palaeobatrachidae & Ranidae	Ranidae
Anuran abundance	Hundreds of adults & at least 12 tadpoles in swamps/ponds; few in fluvial deposits	n ≈ 250 adults & 2 tadpoles	n > 1000 adults & about 200 tadpoles	n = 8 adults & several hundred (mainly pelobatid) tadpoles	n > 73 adults & n > 79 tadpoles

(continued)

	Geiseltal lacustrine system	Lake Messel	Lake Bechlejovice	Lake Enspel	Lake Libros
Associated fish fauna	Swamps/ponds: abundant (up to four species); rivers: none	Abundant (eight genera & species)	Monospecific species *Umbra prochazkai* (Umbridae)	Monospecific species *Palaeorutilus enspelensis* (Cyprinidae)	None
Truncation	Many specimens	Many specimens	Many specimens	Many specimens	Many specimens
Completeness	Varying; few near-complete specimens (all lack phalanges)	Similarly complete to Geiseltal; few near-complete specimens (including near-complete phalanges)	More complete than Geiseltal; many near-complete specimens include peripheral & small elements (phalanges, carpals, tarsals)	More complete than Geiseltal; some near-complete specimens include near-complete phalanges & small elements such as carpals, tarsals	More complete than Geiseltal; some near-complete specimens include near-complete phalanges & small elements such as carpals, tarsals
Proximal-distal trend	Yes	Yes	Yes	Yes	Yes
Lack of distal elements	Common	Common	Rare; although missing elements commonly include peripheral elements	Common; mainly peripheral elements	Common; mainly peripheral elements
Lack of entire limbs	Common	Common	Rare	Common	Not reported
Articulation	High articulation for most elements present	Less articulated than Geiseltal	More articulated than Geiseltal; high articulation for most elements present	Similarly articulated to Geiseltal; high articulation for elements present (including distal limb elements)	Less articulated than Geiseltal; especially for limb elements
Disarticulation of limb elements or entire limbs	Occasional	Common	Occasional for phalanges and/or single limb joints (limb elements stay as unit)	Occasional	Common
Abdominal disarticulation	Common for the joints associated with the sacral vertebrae & ilia and/or the urostyle–hip joint	Common for the joints associated with the sacral vertebrae & ilia and/or the urostyle–hip joint	Common for the joints associated with the sacral vertebrae & ilia and/or the urostyle–hip joint	Common for the joints associated with the sacral vertebrae & ilia and/or the urostyle–hip joint	Common for the joints associated with the sacral vertebrae & ilia and/or the urostyle–hip joint
Reorientation of the lower body	Common	Common	Occasional; some posterior bodies slightly reorientated	Common	Not reported
Anterior and posterior body halves are independent units	Occasional; clearly separated anterior or posterior body halves	Common; separated anterior or posterior body halves often overlap; one body half can occur in isolation	rare	Occasional; clearly separated anterior or posterior body halves	Never

(continued)

	Geiseltal lacustrine system	Lake Messel	Lake Bechlejovice	Lake Enspel	Lake Libros
Other body regions are articulated units	Common: astragalus–calcaneum, metacarpals, metatarsals, vertebrae	Common: body halves, astragalus–calcaneum, metacarpals, metatarsals, vertebrae	Common: astragalus–calcaneum, metacarpals, metatarsals, vertebrae	Common: astragalus–calcaneum, metacarpals, metatarsals, vertebrae	Common: astragalus–calcaneum, metacarpals, metatarsals, vertebrae
Isolated limbs/parts of limbs	Rare	Rare	Rare	Not reported	Never
Extensively disarticulated skeletons or disarticulated bones	Rare	Rare	Rare in layers with abundant anurans; common in certain other layers (Špinar 1972)	Not reported	Rare (unidirectional scattered)
Other taphonomic characteristics	Specimen orientation always dorsoventral; specimens often show 'spread-eagled' attitude (term after Smith 1986); clusters of bones are rare	Common displacement of entire limbs (unnatural limb orientations especially at the shoulder & hip joint)	Not reported	Not reported	Joints can exhibit angles less than the minimum value possible *in vivo* (as a result of osmotic dehydration)
Geiseltal taphonomic state	States 2, 3, 9 > State 1 > States 7–8 > States 4, 5, 6	States 3, 9 > State 2 > States 6–8 > States 1, 4, 5	States 1, 9 > State 2 > State 7 > State 8 > States 4, 6	States 1, 2, 9 > States 7–8	States 1, 9 > State 2 > State 7 > States 3, 4, 5
References	Kuhn (1941); Raupach (1948); Weigelt (1933); Krumbiegel (1962*a*); Krumbiegel *et al.* (1983); Roček & Rage (2000); Rage & Roček (2003); Franzen (2005); Mosbrugger *et al.* (2005); Wuttke *et al.* (2012); Roček (2013); Roček *et al.* (2014)	Nix (2001); Pirrung *et al.* (2001); Franzen (2005); McNamara (2007); Grein *et al.* (2011); Gruber (2011); Tütken (2014); Smith & Lehmann (2014); Smith *et al.* (2018); Wuttke (2018)	Špinar (1972); Bellon *et al.* (1998); Roček (2003); Roček *et al.* (2006); Přikryl (2010); Gardner (2016); McNamara (2007, data)	Böhme (1996, 2000), Wedmann (2000); Pirrung *et al.* (2001); Maus & Wuttke (2002; 2004); Mertz *et al.* (2007); Roček & Wuttke (2010); Schindler & Wuttke (2010); Poschmann *et al.* (2010); Uhl & Herrmann (2010)	Anadòn *et al.* (1992); de las Heras *et al.* (2003); Ortí *et al.* (2003); Bruch *et al.* (2004); McNamara *et al.* (2006, 2009, 2012*a*)

Littoral vegetation can 'trap' carcasses (e.g., Enspel) (Wuttke & Poschmann 2010). This may prolong floating / decay and scavenging at or close to the water surface, delaying or preventing deposition in profundal regions (Wuttke & Poschmann 2010). This ultimately results in less complete specimens, isolated limbs and low numbers of specimens. Water depth, lake size, vegetation and presence/absence of scavengers are controlled by lake physiography and lake hydrology, which are both ultimately controlled by the climate. Larger lakes may yield a higher proportion of carcasses deposited soon after death, as the proportion of vegetated margins to lake area is lower than in a system with interconnected smaller water bodies (e.g., Geiseltal). Further, in larger lakes the profundal region is often deeper, inhibiting decay due to lower water temperatures and inhibiting generation of decay gases due to higher water pressure (Elder & Smith 1988). The extent of scavenging relates to the presence/absence of predators and scavengers (e.g., fish) in the lake. Where these are absent, specimens are more complete and articulated and scattered bones are rare (e.g., Enspel (Roček & Wuttke 2010), Bechlejovice (Špinar 1972)).

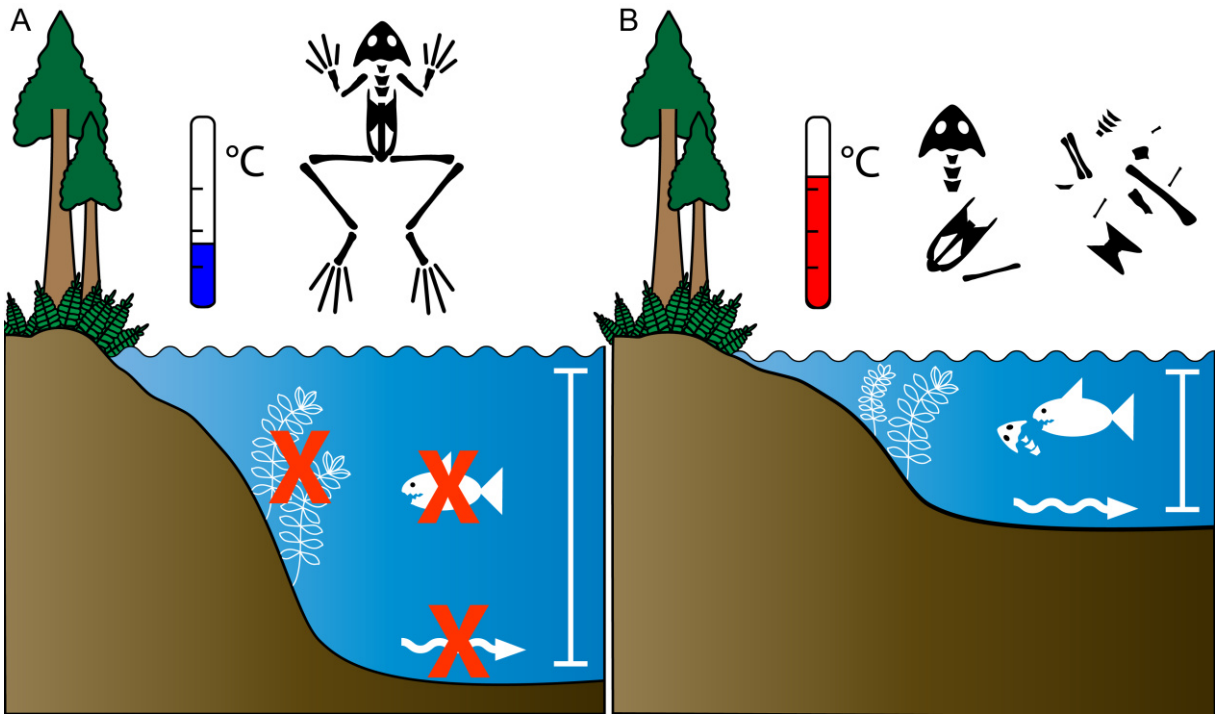


Figure 3.12: Controls on preservation for anurans in lacustrine-hosted Cenozoic biotas. A, fossils are more complete and articulated when carcasses were deposited during cooler climatic phases in deep, cool lakes, with

inhibited scavenging, bank vegetation and / or post-depositional disturbance. B, fossils are usually less complete and articulated when carcasses were deposited during warmer climatic phases in shallow, warm lakes, with scavengers present, pronounced bank vegetation and powerful post-depositional disturbance.

3.6 Conclusion

Most of the Geiseltal anurans likely died during or after mating. Most specimens are partially complete, partially articulated and truncated by the edge of the fossil slab / nitrocellulose glue transfer. Omitting truncated specimens in the taphonomic analysis introduces bias towards higher completeness values for truncated specimens. All specimens lack at least some phalanges; some specimens lack limb elements or entire limbs. Taphonomic extremes, such as near-complete, near-articulated specimens, isolated limbs and entirely disarticulated specimens are rare. Specimens show a proximal to distal trend in completeness and low completeness and articulation values for some abdominal bones. These data are the basis of a new taphonomic model for the Geiseltal anurans. Specimens represent nine taphonomic states based on distinct patterns in disarticulation and loss of skeletal elements. These states reflect different taphonomic pathways related to subtle variation in the depositional environment. The fidelity of preservation is consistent among stratigraphic levels and excavation sites. Potential biases in the dataset include collection history, truncation and taxonomy.

Comparative analysis of patterns in completeness and articulation in the Geiseltal specimens and in fossil anurans from other Lagerstätten reveals recurring taphonomic trends in anuran preservation in Cenozoic lake settings. These include proximal-distal trends for completeness in the limbs, abdominal disarticulation and/or the reorientation of the anterior or posterior body. The inter-biota skeletal taphonomy of Cenozoic anurans is ultimately controlled by climate (especially ambient temperature), lake physiography and anuran anatomy. Anurans are more complete and articulated in Lagerstätten from cooler climatic phases where decay, floating, scavenging and post-depositional disturbance of

carcasses were inhibited by deposition in relatively cool and / or deep lakes. These ultimate taphonomic controls are likely to apply to diverse vertebrates decaying in lacustrine settings.

3.7 Data archiving statement

Data for this study are available in the Dryad Digital Repository at https://doi.org/10.5061/dryad.2bvq83brt.

3.8 Acknowledgements

Thanks to the ZNS team, especially Frank Steinheimer and Michael Stache for access to the Geiseltal collections and databases and for useful historical information and to Bianca Bernstein for assistance. Thanks to all associates who performed documentation, preparation and curation of the Geiseltal specimens. Thanks also to Stephan Schaal and Elvira Braum for access to the Messel vertebrate collections, to Boris Ekrt for access to Bechlejovice specimens, Michael Wuttke and Markus Poschmann for access to the Enspel collections and to Luis Alcalá, Jordi Agustí and Ángel Galobart (Institut Català de Paleontologia Miquel Crusafont, Sabadell, Spain), Sebastà Calzada (Museu de Geologia del Seminari, Barcelona, Spain), Sandra Chapman (Natural History Museum, London, United Kingdom), Hermano Miguel Pérez (Museo del Colegio La Salle, Teruel, Spain), Eberhard Schindler (Senckenberg Research Institute, Frankfurt/Main, Germany), and Begoña Sánchez (Museo Nacional de Ciencias Naturales, Madrid, Spain) provided access to Libros specimens. The manuscript benefitted greatly from reviews by Josh Bonde, Christopher Dean and Sally Thomas. The research was funded by a Government of Ireland-Irish Research Council (IRC) Postgraduate Scholarship GOIPG/2018/3354 awarded to DF.

3.9 Author contributions

Conceptualization M. E. McNamara, O. Wings, D. Falk; Data curation D. Falk, M. E. McNamara; Formal analysis D. Falk, M. E. McNamara; Funding acquisition M. E. McNamara, D. Falk; Investigation D. Falk,

M. E. McNamara; Methodology M. E. McNamara, O. Wings, D. Falk; Project administration M. E. McNamara; Resources O. Wings, M. E. McNamara; Software D. Falk; Supervision M. E. McNamara, O. Wings; Validation M. E. McNamara, O. Wings, D. Falk; Visualization D. Falk; Writing – original draft – D. Falk, M. E. McNamara; Writing – review & editing – D. Falk, M. E. McNamara, O. Wings.

3.10 References

AGUILAR, J.-P., LEGENDRE, S. and MICHAUX, J. 1997. Actes du congres BiochroM'97. *Mémoires et travaux de l'Institut de Montpellier de l'École pratique des hautes études*, **21**, 1–818.

BARNES, B. 1926. Eine eozäne Wirbeltier-Fauna aus der Braunkohle des Geiseltales. *Jahrbuch des Halleschen Verbandes für die Erforschung der mitteldeutschen Bodenschätze*, **6**, 5–24.

BARTHEL, M. and RÜFFLE, L. 1970. Vegetationsbilder aus dem Alttertiär (Eozän) der Braunkohle des Geiseltales. *Wissenschaftliche Zeitschrift der Humboldt-Universität zu Berlin / Mathematisch-Naturwissenschaftliche Reihe*, **XIX**, 274–283.

BEARDMORE, S. R. and FURRER, H. 2018. Land or water: using taphonomic models to determine the lifestyle of the Triassic protorosaur *Tanystropheus* (Diapsida, Archosauromorpha). *Palaeobiodiversity and Palaeoenvironments*, **98**, 243–258.

BEARDMORE, S. R., ORR, P. J., MANZOCCHI, T., FURRER, H. and JOHNSON, C. 2012. Death, decay and disarticulation: modelling the skeletal taphonomy of marine reptiles demonstrated using *Serpianosaurus* (Reptilia; Sauropterygia). *Palaeogeography, Palaeoclimatology, Palaeoecology*, **337–338**, 1–13.

BELLON, H., BŮŽEK, Č., GAUDANT, J., KVAČEK, Z. and WALTER, H. 1998. The České Středohoří magmatic complex in Northern Bohemia ^{40}K-^{40}Ar ages for volcanism and biostratigraphy of the Cenozoic freshwater formations. *Newsletters on Stratigraphy*, **36**, 77–103.

BLUMENSTENGEL, H. 2004. 3.5 Tertiär. *In* WANSA, S. and RADZINSKI, K. (eds.). *Erläuterungen zur Geologischen Karte 1:25 000 von Sachsen-Anhalt (GK 25), Blatt Mücheln (Geiseltal), 4636*.

Landesamt für Geologie und Bergwesen Sachsen-Anhalt, Halle (Saale), Germany, Halle (Saale), 143 pp.

BÖHME, M. 1996. Revision der oligozänen und untermiozänen Vertreter der Gattung *Palaeoleuciscus* (Teleostei, Cyprinidae) Mitteleuropa. Unpublished PhD thesis, Universität Leipzig, Germany, 109 pp.

BÖHME, M. 2000. Die Cypriniden (Teleostei: Cypriniformes) des oberoligozänen Maares von Enspel nebst Bemerkungen zur Phylogenie und Biogeographie der Phoxininae. *Paläontologische Zeitschrift*, **74**, 99–112.

BRATTSTROM, B. H. 1968. Thermal acclimation in anuran amphibians as a function of latitude and altitude. *Comparative Biochemistry and Physiology*, **24**, 93–111.

BRIGGS, D. E. G. 2014. Konservat-Lagerstätten 40 years on: The exceptional becomes mainstream. *The Paleontological Society Papers*, **20**, 1–14.

BROCKLEHURST, N. and FRÖBISCH, J. 2014. Current and historical perspectives on the completeness of the fossil record of pelycosaurian-grade synapsids. *Palaeogeography, Palaeoclimatology, Palaeoecology*, **399**, 114–126.

BRUCH, A., UTESCHER, T., OLIVARES, C. A., DOLÁKOVÁ, N., IVANOV, D. and MOSBRUGGER, V. 2004. Middle and Late Miocene spatial temperature patterns and gradients in Europe-preliminary results based on palaeobotanical climate reconstructions. *Courier Forschungsinstitut Senckenberg*, **249**, 15–27

BUCHACHER, C. O. 1993. Field studies on the small Surinam toad, Pipa arrabali, near Manaus, Brazil. *Amphibia-Reptilia*, **14**, 59-69.

CARTER, D. O. and TIBBETT, M. 2006. Microbial decomposition of skeletal muscle tissue (*Ovis aries*) in a sandy loam soil at different temperatures. *Soil Biology and Biochemistry*, **38**, 1139–1145.

CARTER, D. O., YELLOWLEES, D. and TIBBETT, M. 2008. Temperature affects microbial decomposition of cadavers (*Rattus rattus*) in contrasting soils. *Applied Soil Ecology*, **40**, 129–137.

CARTY, S. and PARROW, M. W. 2015. Chapter 17 - Dinoflagellates. 773–807. *In* WEHR, J. D., SHEATH, R. G. and KOCIOLEK, J. P. (eds). *Freshwater Algae of North America*. Boston, Academic Press, 1066 pp.

CASHMORE, D. D., MANNION, P. D., UPCHURCH, P. and BUTLER, R. J. 2020. Ten more years of discovery: revisiting the quality of the sauropodomorph dinosaur fossil record. *Palaeontology*, **63**, 951–978.

CLEARY, T. J., MOON, B. C., DUNHILL, A. M. and BENTON, M. J. 2015. The fossil record of ichthyosaurs, completeness metrics and sampling biases. *Palaeontology*, **58**, 521–536.

COATES, M. 1996. The Devonian tetrapod *Acanthostega gunnari* Jarvik: postcranial anatomy, basal tetrapod interrelationships and patterns of skeletal evolution. *Transactions of The Royal Society of Edinburgh-Earth Sciences*, **87**, 363–421.

COSTANZO, J. P., DO AMARAL, M. C., ROSENDALE, A. J. and LEE, R. E., JR. 2013. Hibernation physiology, freezing adaptation and extreme freeze tolerance in a northern population of the wood frog. *Journal of Experimental Biology*, **216**, 3461–3473.

COSTANZO, J. P. and LEE, R. E., JR 2013. Avoidance and tolerance of freezing in ectothermic vertebrates. *Journal of Experimental Biology*, **216**, 1961–1967.

DE IULIIS, G. and PULERÀ, D. 2011. Chapter 6 - The frog. 127–145. *In* DE IULIIS, G. and PULERÀ, D. (eds). *The Dissection of Vertebrates*. Boston, Academic Press, 352 pp.

DEAN, C. D., MANNION, P. D. and BUTLER, R. J. 2016. Preservational bias controls the fossil record of pterosaurs. *Palaeontology*, **59**, 225–247.

DENSMORE, C. L. and GREEN, D. E. 2007. Diseases of amphibians. *Institute for Laboratory Animal Research Journal*, **48**, 235–254.

DILCHER, D. L., PAVLICK, R. J. and MITCHELL, J. 1970. Chlorophyll derivatives in Middle Eocene sediments. *Science*, **168**, 1447–1449.

DODSON, P. 1973. The significance of small bones in paleoecological interpretation. *Rocky Mountain Geology*, **12**, 15-19.

DUELLMAN, W. E. and TRUEB, L. 1994. Population Biology. 261–274. *In* DUELLMAN, W. E. and TRUEB, L. (eds). *Biology of amphibians*. John Hopkins University Press, Baltimore and London, 670 pp.

EISSMANN, L. 2002. Tertiary geology of the Saale-Elbe Region. *Quaternary Science Reviews*, **21**, 1245–1274.

ELDER, R. L. and SMITH, G. R. 1984. Fish taphonomy and paleoecology. *Geobios*, **17**, 287–291.

ELDER, R. L. and SMITH, G. R. 1988. Fish taphonomy and environmental inference in paleolimnology. *Palaeogeography, Palaeoclimatology, Palaeoecology*, **62**, 577–592.

FABREZI, M. 1993. The anuran tarsus. *Alytes*, **11**, 47–63.

FABREZI, M. and ALBERCH, P. 1996. The carpal elements of anurans. *Herpetologica*, **52**, 188–204.

FABREZI, M., GOLDBERG, J. and CHULIVER PEREYRA, M. 2017. Morphological variation in anuran limbs: constraints and novelties. *Journal of Experimental Zoology B: Molecular and Developmental Evolution*, **328**, 546–574.

FALK, D., MCCOY, V. and WINGS, O. 2019. Ichnofossils of the Eocene Fossillagerstätte Geiseltal (Saxony-Anhalt, Germany). *3rd International Conference of Continental Ichnology (ICCI 2019)*, *Abstract Volume & Field Trip Guide*, 15–18.

FALK, D., WINGS, O. and MCNAMARA, M. E. 2022. Data from: The skeletal taphonomy of anurans from the Eocene Geiseltal Konservat-Lagerstätte, Germany: insights into the controls on fossil anuran preservation. *Dryad Digital Repository. https://datadryad.org/stash/share/1zhwRX4fnutAapNPjRNqU7jAMPfgB8NFz0opSOnXTQU*

FRANZEN, J. L. 2003. Mammalian faunal turnover in the Eocene of central Europe. *Geological Society of America Special Papers*, **369**, 455–462.

FRANZEN, J. L. 2005. The implications of the numerical dating of the Messel fossil deposit (Eocene, Germany) for mammalian biochronology. *Annales de Paléontologie*, **91**, 329–335.

FRANZEN, J. L. and HAUBOLD, H. 1987. The biostratigraphic and palaeoecological significance of the Middle Eocene locality Geiseltal near Halle (German Democratic Republic). *Münchner Geowissenschaftliche Abhandlungen, Reihe A*, **10**, 93–100.

GARDNER, J. D. 2016. The fossil record of tadpoles. *Fossil Imprint*, **72**, 17–44.

GREIN, M., UTESCHER, T., WILDE, V. and ROTH-NEBELSICK, A. 2011. Reconstruction of the Middle Eocene climate of Messel using palaeobotanical data. *Neues Jahrbuch für Geologie und Paläontologie - Abhandlungen*, **260**, 305–318.

GRUBER, G. 2011. The fossil site and its importance - The Messel Maar. 23–28. *In* GRUBER, G. and MICHKLICH, N. (eds). *Messel, Treasures of the Eocene: The Book to the Exhibition Messel on Tour*. Hessisches Landesmuseum Darmstadt, 158 pp.

GVOŽDÍK, V., MORAVEC, J. and KRATOCHVÍL, L. 2008. Geographic morphological variation in parapatric Western Palearctic tree frogs, *Hyla arborea* and *Hyla savignyi*: are related species similarly affected by climatic conditions? *Biological Journal of the Linnean Society*, **95**, 539–556.

HAMMER, Ø., HARPER, D. A. T. and RYAN, P. D. 2001. PAST: Paleontological statistics software package for education and data analysis. *Palaeontologia Electronica*, **4**, 1–9.

HASTINGS, A. K. and HELLMUND, M. 2015*a*. Rare in situ preservation of adult crocodilian with eggs from the Middle Eocene of Geiseltal. *Palaios*, **30**, 446–461.

HASTINGS, A. K. and HELLMUND, M. 2015*b*. Gaining ground: horse-hunting crocodiles and giant birds; new research results on the Eocene world of Germany ca. 45 million years ago. Companion volume to the exhibition presented at the National Academy of Sciences Leopoldina from March 6th to May 29th, 2015 in Halle (Saale), Germany. Center for Natural Science Collections (ZNS), Halle (Saale), Germany, 120 pp.

HAUBOLD, H. 1995. Wirbeltiergrabung und -forschung im Geiseltaleozän. *Hallesches Jahrbuch für Geowissenschaften, Reihe B*, **17**, 1–18.

HAUBOLD, H. and HELLMUND, M. 1998. The Geiseltalmuseum of the Institute of Geological Sciences, University Halle-Wittenberg. - Epicontinental Triassic International Symposium - Excursions. *Hallesches Jahrbuch für Geowissenschaften, Reihe B*, **6**, 11–18.

HAUBOLD, H. and KRUMBIEGEL, G. 1984. Typenkatalog der Wirbeltiere aus dem Eozän des Geiseltals, 1934-1984 - 50 Jahre Geiseltalmuseum an der Martin-Luther-Univ. Halle-Wittenberg, Halle (Saale), 67 pp.

HELLMUND, M. 1997. Letzte Grabungsaktivitäten im südwestlichen Geiseltal bei Halle (Deutschland). *Hercynia, Neue Folge*, **30**, 163–176.

HELLMUND, M. 2013. Odontological and osteological investigations on propalaeotheriids (Mammalia, Equidae) from the Eocene Geiseltal Fossillagerstätte (Central Germany) - a full range of extraordinary phenomena. *Neues Jahrbuch für Geologie und Paläontologie - Abhandlungen*, **267**, 127–154.

HELLMUND, M. 2018. The former Geiseltal Museum (1934–2011), the Eocene Geiseltal Fossilagerstätte (Germany) and the scientific meaning of Ben Barnes as a pioneer of systematic quantitative vertebrate excavations in the Geiseltal lignites. *Anuário do Instituto de Geociências, Universidade Federal do Rio de Janeiro*, **41**, 108–119.

HELLMUND, M. and HASTINGS, A. K. 2014. Messel and Geiseltal: highlights from the Cenozoic; Excursion Guide, Part II - The Eocene Geiseltal Fossillagerstätte (Central Germany) and its Vertebrate Fossil Fauna with 13 figures and 1 table. 25–46. *In* SMITH, K. T., LEHMANN, T., HELLMUND, M. and HASTINGS, A. K. (eds). *SVP 2014*. Senckenberg Research Institute and Natural History Museum Frankfurt, Berlin, 46 pp.

HENRICI, A. C. and FIORILLO, A. R. 1993. Catastrophic death assemblage of *Chelomophrynus bayi* (Anura, Rhinophrynidae) from the middle Eocene Wagon Bed Formation of central Wyoming. *Journal of Paleontology*, **67**, 1016–1026.

HENRICI, A. C. and HAYNES, S. R. 2006. *Elkobatrachus brocki*, a new pelobatid (Amphibia: Anura) from the Eocene Elko Formation of Nevada. *Annals of Carnegie Museum*, **75**, 11–35.

HERVET, S. 2004. A new genus of 'Ptychogasteridae' (Chelonii, Testudinoidea) from the Geiseltal (Lutetian of Germany). *Comptes Rendus Palevol*, **3**, 125–132.

HINSCHE, G. 1941. Untersuchungen zum funktionellen Aufbau der Anuren mit besonderer Berücksichtigung der eozänen Geiseltalfunde. *Nova Acta Leopoldina, Neue Folge*, **10**, 313–343.

HU, Z., CRONIN, T. W. and TZIPERMAN, E. 2018. Suppression of cold weather events over high-latitude continents in warm climates. *Journal of Climate*, **31**, 9625–9640.

IZZO, T. J., RODRIGUES, D. J., MENIN, M., LIMA, A. P. and MAGNUSSON, W. E. 2012. Functional necrophilia: a profitable anuran reproductive strategy? *Journal of Natural History*, **46**, 2961–2967.

JERZMANSKA, A. 1977. The freshwater fishes from the Middle Eocene of Geiseltal. *Martin-Luther-Universität Halle-Wittenberg Wissenschaftliche Beiträge*, 41–65.

KEMP, R. A. and UNWIN, D. M. 1997. The skeletal taphonomy of *Archaeopteryx*: a quantitative approach. *Lethaia*, **30**, 229–238.

KIDWELL, S. M. and BAUMILLER, T. 1990. Experimental disintegration of regular echinoids: roles of temperature, oxygen, and decay thresholds. *Paleobiology*, **16**, 247–271.

KIELAN-JAWOROWSKA, Z. and HURUM, J. H. 2006. Limb posture in early mammals: sprawling or parasagittal. *Acta Palaeontologica Polonica*, **51**, 393–406.

KÖHLER, J. 2011. Habitat Lake Messel - Anuran Amphibians. 62–65. In GRUBER, G. and MICHKLICH, N. (eds). Messel, treasures of the Eocene: the book to the exhibition Messel on tour. Hessisches Landesmuseum Darmstadt, 158 pp.

KOHRING, R. and HIRSCH, K. F. 1996. Crocodilian and avian eggshells from the Middle Eocene of the Geiseltal, Eastern Germany. *Journal of Vertebrate Paleontology*, **16**, 67–80.

KRUMBIEGEL, G. 1962*a*. Die Fossilfundstellen der mitteleozänen Braunkohle des Geiseltales. *Wissenschaftliche Zeitschrift der Martin-Luther-Universität in Halle*, **11**, 173–208.

KRUMBIEGEL, G. 1962*b*. Ostracodenfunde im Tagebau Neumark-Süd (Geiseltal). *Geologie*, **11**, 334–353.

KRUMBIEGEL, G. 1975. Zur Palökologie der tertiären Fossilfundstellen des Geiseltales. *Hercynia, Neue Folge*, **12**, 400–417.

KRUMBIEGEL, G. 1977. Genese, Palökologie und Biostratigraphie der Fossilfundstellen im Eozän des Geiseltales. *Kongreß und Tagungsberichte der Martin-Luther-Universität Halle-Wittenberg, Wissenschaftliche Beiträge*, 113–138.

KRUMBIEGEL, G. 1995. Fossile Harze aus der Geiseltalbraunkohle und aus dem Tagebau Königsaue (Sachsen-Anhalt). *Hallesches Jahrbuch für Geowissenschaften, Reihe B*, **17**, 139–148.

KRUMBIEGEL, G., RÜFFLE, L. and HAUBOLD, H. 1983. Das eozäne Geiseltal: ein mitteleuropäisches Braunkohlenvorkommen und seine Pflanzen- und Tierwelt. A. Ziemsen Verlag, Die Neue Brehm-Bücherei, Wittenberg Lutherstadt, 227 pp.

KRUTZSCH, W., BLUMENSTENGEL, H., KIESEL, Y. and RÜFFLE, L. 1992. Paläobotanische Klimagliederung des Alttertiärs (Mitteleozän bis Oberoligozän) in Mitteldeutschland und das Problem der Verknüpfung mariner und kontinentaler Gliederungen. *Neues Jahrbuch für Geologie und Paläontologie - Abhandlungen,* **186**, 137–253.

KRUTZSCH, W. 2011. Stratigrafie und Klima des Palaogens im Mitteldeutschen Ästuar im Vergleich zur marinen nordlichen Umrahmung. *Zeitschrift der Deutschen Gesellschaft für Geowissenschaften*, **162**, 19–47.

KUHN, O. 1941. Die eozänen Anura aus dem Geiseltale nebst einer Übersicht über die fossilen Gattungen. *Nova Acta Leopoldina, Neue Folge*, **10**, 345–376.

KÜSTERMANN, W., RAPPSILBER, I. and THOMAE, M. 2008. Regionale und tektonische Voraussetzungen zur Bildung der Geiseltal-Senke. *Veröffentlichungen der Deutschen Gesellschaft für Geowissenschaften,* **235**, 12–21.

LA MARCA, E. 2021. Action Plan for *Atelopus oxyrhynchus*. 5 p.

LIAO, W. B., ZHOU, C. Q., LIU, Y. H. and MAO, M. 2011. Ecological traits in the Omei treefrog *Rhacophorus omeimontis* in a subtropical montane region. 107–122. *In* MURRAY, J. L. (ed.) *Frogs: biology, ecology and uses*. Nova Science Publishers, Incorporated, Hauppauge, United States, 186 pp.

LINCKE, L. 1977. Zur Geologie des Geiseltales. *Originalabhandlungen und Vorträge des Internationalen Kolloquiums vom 4.–5. November 1974 in Halle (Saale), Martin-Luther-Universität Halle-Wittenberg, Wissenschaftliche Beiträge 1977/2 (P5)*, 139–147.

LIPS, K. R. 1999. Mass mortality and population declines of anurans at an upland site in western Panama. *Conservation Biology*, **13**, 117–125.

LIZANA, M., MÁRQUEZ, R. and MARTÍN-SÁNCHEZ, R. 1994. Reproductive biology of *Pelobates cultripes* (anura: Pelobatidae) in Central Spain. *Journal of Herpetology*, **28**, 19–27.

LÓPEZ-CORTÉS, D. J., NÚÑEZ-VÁZQUEZ, E. J., BAND-SCHMIDT, C. J., GÁRATE-LIZÁRRAGA, I., HERNÁNDEZ-SANDOVAL, F. E. and BUSTILLOS-GUZMÁN, J. J. 2015. Mass fish die-off during a diatom bloom in the Bahía de La Paz, Gulf of California. *Hidrobiológica*, **25**, 39–48.

MANION, J. J. and BROTHER LAWRENCE, C. 1952. Winter kill of *Rana pipiens* in shallow ponds. *Herpetologica*, **8**, p. 32.

MANNION, P. D. and UPCHURCH, P. 2010. Completeness metrics and the quality of the sauropodomorph fossil record through geological and historical time. *Paleobiology*, **36**, 283–302.

MAUS, M. and WUTTKE, M. 2002. Comparative anatomical-morphological and taphonomical examination of the larvae of *Pelobates decheni* Troschel (1861) and *Eopelobates anthracinus* Parker (1929) (Anura: Pelobatidae) found at the Upper Oligocene sites at Enspel (Westerwald/Germany) and Rott (Siebengebirge/Germany). *Courier Forschungsinstitut Senckenberg*, **237**, 129–138.

MAUS, M. and WUTTKE, M. 2004. The ontogenetic development of *Pelobates cf. decheni* tadpoles from the Upper Oligocene of Enspel (Westerwald, Germany). *Neues Jahrbuch für Geologie und Paläontologie - Abhandlungen*, **232**, 215–230.

MAYR, G. 2020. An updated review of the Middle Eocene avifauna from the Geiseltal (Germany), with comments on the unusual taphonomy of some bird remains. *Geobios*, **62**, 45–59.

MCCOY, V. E., BOOM, A., WINGS, O., WAPPLER, T., LABANDEIRA, C. C. and GEE, C. T. 2021. Fossilisation of the Eocene "Monkeyhair" laticifer tree from Geiseltal, Germany: a deeper deeper understanding using micro-CT and pyrolysis GC/MS. *Palaios*, **36**, 1–14.

MCNAMARA, M. E. 2007. Comparative taphonomy of lacustrine-hosted exceptional faunas from the Miocene of NE Spain. Unpublished PhD thesis, University College Dublin, Ireland.

MCNAMARA, M. E., ORR, P. J., ALCALÁ, L., ANADÓN, P. and PEÑALVER, E. 2012*a*. What controls the taphonomy of exceptionally preserved taxa - environment or biology? A case study using frogs from the Miocene Libros Konservat-Lagerstätte (Teruel, Spain). *Palaios*, **27**, 63–77.

MCNAMARA, M. E., ORR, P. J., KEARNS, S. L., ALCALÁ, L., ANADÓN, P. and PENALVER MOLLA, E. 2009. Soft-tissue preservation in Miocene frogs from Libros, Spain: insights into the genesis of decay microenvironments. *Palaios*, **24**, 104–117.

MCNAMARA, M. E., ORR, P. J., MANZOCCHI, T., ALCALÁ, L., ANADÓN, P. and PEÑALVER, E. 2012*b*. Biological controls upon the physical taphonomy of exceptionally preserved salamanders from the Miocene of Rubielos de Mora, northeast Spain. *Lethaia*, **45**, 210–226.

MENIN, M., RODRIGUES, D. J. and LIMA, A. P. 2006. The tadpole of *Rhinella proboscidea* (Anura: Bufonidae) with notes on adult reproductive behavior. *Zootaxa*, **1258**, 47–56.

MERTZ, D. F. and RENNE, P. R. 2005. A numerical age for the Messel fossil deposit (UNESCO World Heritage Site) derived from $^{40}Ar/^{39}Ar$ dating on a basaltic rock fragment. *Courier Forschungsinstitut Senckenberg*, **255**, 67–75.

MERTZ, D. F., RENNE, P. R., WUTTKE, M. and MÖDDEN, C. 2007. A numerically calibrated reference level (MP28) for the terrestrial mammal-based biozonation of the European Upper Oligocene. *International Journal of Earth Sciences*, **96**, 353–361.

MERTZ, D. F., SWISHER, C. C., FRANZEN, J. L., NEUFFER, F. O. and LUTZ, H. 2000. Numerical dating of the Eckfeld maar fossil site, Eifel, Germany: a calibration mark for the Eocene time scale. *Naturwissenschaften*, **87**, 270–274.

MOSBRUGGER, V., UTESCHER, T. and DILCHER, D. L. 2005. Cenozoic continental climatic evolution of Central Europe. *Proceedings of the National Academy of Sciences USA*, **102**, 14964–14969.

MRUGOWSKY, J. 1936. Über fossile Bakterien aus dem Mitteleozän des Geiseltales. *Nova Acta Leopoldina, Neue Folge*, **3**, 597–603.

MUSCENTE, A. D., SCHIFFBAUER, J. D., BROCE, J., LAFLAMME, M., O'DONNELL, K., BOAG, T. H., MEYER, M., HAWKINS, A. D., HUNTLEY, J. W., MCNAMARA, M., MACKENZIE, L. A., STANLEY, G. D., HINMAN, N. W., HOFMANN, M. H. and XIAO, S. 2017. Exceptionally preserved fossil assemblages through geologic time and space. *Gondwana Research*, **48**, 164–188.

NIX, T. 2001. Räumliche Modellierung der geologischen und tektonischen Verhältnisse der Grube Messel. Unpublished report, *Berichte des Forschungsinstituts Senckenberg, Abteilung Messelforschung*, 1–47.

ORTÍ, F., ROSELL, L. and ANADÓN, P. 2003. Deep to shallow lacustrine evaporites in the Libros Gypsum (southern Teruel Basin, Miocene, NE Spain): an occurrence of pelletal gypsum rhythmites. *Sedimentology*, **50**, 361–386.

PIRRUNG, M., BUCHEL, G. and JACOBY, W. 2001. The tertiary volcanic basins of Eckfeld, Enspel and Messel (Germany). *Zeitschrift der Deutschen Geologischen Gesellschaft*, **152**, 27–60.

POSCHMANN, M., SCHINDLER, T. and UHL, D. 2010. Fossil-Lagerstätte Enspel - a short review of current knowledge, the fossil association, and a bibliography. *Palaeobiodiversity and Palaeoenvironments*, **90**, 3–20.

PRICE, S. J., ARIEL, E., MACLAINE, A., ROSA, G. M., GRAY, M. J., BRUNNER, J. L. and GARNER, T. W. J. 2017. From fish to frogs and beyond: impact and host range of emergent ranaviruses. *Virology*, **511**, 272–279.

PŘIKRYL, T. 2010. Paleogenní a neogenní rybí fauna vybraných lokalit na území České republiky (Research on Cenozoic fish fauna of the selected localities of the Czech Republic). Unpublished PhD thesis (in Czech with an English abstract), Charles University, Czech Republic, 1 p.

RAGE, J.-C. and ROČEK, Z. 2003. Evolution of anuran assemblages in the Tertiary and Quaternary of Europe, in the context of palaeoclimate and palaeogeography. *Amphibia-Reptilia*, **24**, 133–167.

RAUPACH, F. V. 1948. Beitrag zur Geiseltalforschung. *In* LANGE, P. D. E. (ed.) *Abhandlungen der Geologischen Landesanstalt Berlin, Neue Folge,* Akademie-Verlag GmbH Berlin, **Heft 214**, Berlin, 3–18.

REISDORF, A. G. and WUTTKE, M. 2012. Re-evaluating Moodie's opisthotonic-posture hypothesis in fossil vertebrates Part I: Reptiles—the taphonomy of the bipedal dinosaurs *Compsognathus longipes* and *Juravenator starki* from the Solnhofen Archipelago (Jurassic, Germany). *Palaeobiodiversity and Palaeoenvironments*, **92**, 119–168.

RING, S. J., BOCHERENS, H., WINGS, O. and RABI, M. 2020. Divergent mammalian body size in a stable Eocene greenhouse climate. *Scientific Reports*, **10**, 3987.

ROČEK, Z. 2003. Larval development in Oligocene palaeobatrachid frogs. *Acta Palaeontologica Polonica*, **48**, 595–607.

ROČEK, Z. 2013. Mesozoic and Tertiary Anura of Laurasia. *Palaeobiodiversity and Palaeoenvironments*, **93**, 397–439.

ROČEK, Z., BÖTTCHER, R. and WASSERSUG, R. 2006. Gigantism in tadpoles of the Neogene frog *Palaeobatrachus*. *Paleobiology*, **32**, 666–675.

ROČEK, Z. and RAGE, J. 2000. Tertiary Anura of Europe, Africa, Asia, North America, and Australia. *Amphibian Biology*, **4**, 1332–1387.

ROČEK, Z. and WUTTKE, M. 2010. Amphibia of Enspel (Late Oligocene, Germany). *Palaeobiodiversity and Palaeoenvironments*, **90**, 321–340.

ROČEK, Z., WUTTKE, M., GARDNER, J. D. and SINGH BHULLAR, B.-A. 2014. The Euro-American genus *Eopelobates*, and a re-definition of the family Pelobatidae (Amphibia, Anura). *Palaeobiodiversity and Palaeoenvironments*, **94**, 529–567.

ROSSI, V., MCNAMARA, M. E., WEBB, S. M., ITO, S. and WAKAMATSU, K. 2019. Tissue-specific geometry and chemistry of modern and fossilized melanosomes reveal internal anatomy of extinct vertebrates. *Proceedings of the National Academy of Sciences*, **116**, 17880–17889.

ROSSI, V., WEBB, S. M. and MCNAMARA, M. E. 2020. Hierarchical biota-level and taxonomic controls on the chemistry of fossil melanosomes revealed using synchrotron X-ray fluorescence. *Scientific Reports*, **10**, 8970.

RÜFFLE, L. and LITKE, R. 2000. Ergänzungen zur Eozän-Flora des Geiseltales, Deutschland, und einiger weiterer Eozän-Fundstätten. *Feddes Repertorium*, **111**, 449–463.

RÜFFLE, L., MÜLLER-STOLL, W. and LITKE, R. 1976. Eozäne Floren des Geiseltales. *Abhandlungen des Zentralen Geologischen Institutes, Berlin*, **26**, 199–238.

SCHEELE, B. C., PASMANS, F., SKERRATT, L. F., BERGER, L., MARTEL, A., BEUKEMA, W., ACEVEDO, A. A., BURROWES, P. A., CARVALHO, T., CATENAZZI, A., DE LA RIVA, I., FISHER, M. C., FLECHAS, S. V., FOSTER, C. N., FRÍAS-ÁLVAREZ, P., GARNER, T. W. J., GRATWICKE, B., GUAYASAMIN, J. M., HIRSCHFELD, M., KOLBY, J. E., KOSCH, T. A., LA MARCA, E., LINDENMAYER, D. B., LIPS, K. R., LONGO, A. V., MANEYRO, R., MCDONALD, C. A., MENDELSON, J., PALACIOS-RODRIGUEZ, P., PARRA-OLEA, G., RICHARDS-ZAWACKI, C. L., RÖDEL, M.-O., ROVITO, S. M., SOTO-AZAT, C., TOLEDO, L. F., VOYLES, J., WELDON, C., WHITFIELD, S. M., WILKINSON, M., ZAMUDIO, K. R. and CANESSA, S. 2019. Amphibian fungal panzootic causes catastrophic and ongoing loss of biodiversity. *Science*, **363**, 1459–1463.

SCHINDLER, T. and WUTTKE, M. 2010. Geology and limnology of the Enspel Formation (Chattian, Oligocene; Westerwald, Germany). *Palaeobiodiversity and Palaeoenvironments*, **90**, 21–27.

SCHNEIDER, C. A., RASBAND, W. S. and ELICEIRI, K. W. 2012. NIH Image to ImageJ: 25 years of image analysis. *Nature Methods*, **9**, 671–675.

SCOTESE, C. R. 2016. PALEOMAP PaleoAtlas for GPlates and the PaleoData Plotter Program, PALEOMAP Project, http://www.earthbyte.org/paleomap-paleoatlas-for-gplates/

SEILACHER, A., REIF, W.-E., WESTPHAL, F., RIDING, R., CLARKSON, E. N. K., WHITTINGTON, H. B., WHITTINGTON, H. B. and MORRIS, S. C. 1985. Sedimentological, ecological and temporal patterns of fossil Lagerstätten. *Philosophical Transactions of the Royal Society of London B: Biological Sciences*, **311**, 5–24.

SIMONEIT, B. R. T., OTTO, A., MENOR-SÁLVAN, C., OROS, D. R., WILDE, V. and RIEGEL, W. 2020. Composition of resinites from the Eocene Geiseltal brown coal basin, Saxony-Anhalt, Germany and comparison to their possible botanical analogues. *Organic Geochemistry*, **152**, 104138.

SMITH, G. R. and ELDER, R. L. 1985. Environmental interpretation of burial and preservation of Clarkia fishes. 85–94. *In* SMILEY, C. J. (ed.) *Late Cenozoic History of the Pacific North West*. American Association for the Advancement of Science Pacific Division, San Francisco, 417 pp.

SMITH, K. T. 2009. Eocene Lizards of the Clade *Geiseltaliellus* from Messel and Geiseltal, Germany, and the Early Radiation of Iguanidae (Reptilia: Squamata). *Bulletin of the Peabody Museum of Natural History*, **50**, 219–306.

SMITH, K. T. and LEHMANN, T. 2014. Messel and Geiseltal: highlights from the Cenozoic. Excursion Guide, Part I - The Messel-Pit Fossil Site: A window into the Eocene World. 25–46. *In* SMITH, K. T., LEHMANN, T., HELLMUND, M. and HASTINGS, A. K. (eds). *SVP 2014*. Senckenberg Research Institute and Natural History Museum Frankfurt, Berlin, 46 pp.

SMITH, K. T., SCHAAL, S. F. and HABERSETZER, J. 2018. *Messel - an ancient greenhouse ecosystem*. Schweizerbart Science Publishers, Stuttgart, Germany, Senckenberg Gesellschaft für Naturfoschung, Frankfurt am Main, 355 pp.

SMITH, K. T. and WUTTKE, M. 2012. From tree to shining sea: taphonomy of the arboreal lizard *Geiseltaliellus maarius* from Messel, Germany. *Palaeobiodiversity and Palaeoenvironments*, **92**, 45–65.

SMITH, R. M. H. 1986. Sedimentation and palaeoenvironments of Late Cretaceous crater-lake deposits in Bushmanland, South Africa. *Sedimentology*, **33**, 369–386.

ŠPINAR, Z. V. 1972. *Tertiary frogs from central Europe*. Dr. W. Junk N. V. Publishers The Hague & Czechoslovak Academy of Sciences Prague, 286 pp.

STĂNESCU, F., IOSIF, R., SZÉKELY, D., SZÉKELY, P., ROŞIORU, D. and COGĂLNICEANU, D. 2013. Salinity tolerance in *Pelobates fuscus* (Laurenti, 1768) tadpoles (Amphibia: Pelobatidae). *Travaux du Muséum National d'Histoire Naturelle "Grigore Antipa"*, **56**, 103–108.

STORCH, G. 1986. Die Säuger von Messel: Wurzeln auf vielen Kontinenten. *Spektrum der Wissenschaften*, **6**, 48–65.

SWANSON, D. L. and GRAVES, B. M. 1995. Supercooling and freeze intolerance in overwintering juvenile spadefoot toads (*Scaphiopus bombifrons*). *Journal of Herpetology*, **29**, 280–285.

TODD, B. D., LUHRING, T. M., ROTHERMEL, B. B. and GIBBONS, J. W. 2009. Effects of forest removal on amphibian migrations: implications for habitat and landscape connectivity. *Journal of Applied Ecology*, **46**, 554-561.

TRAUTH, S. E., MCCALLUM, M. L. and CARTWRIGHT, M. E. 2000. Breeding mortality in the wood frog, *Rana sylvatica* (Anura: Ranidae), from Northcentral Arkansas. *Journal of the Arkansas Academy of Science*, **54**, 154–156.

TÜTKEN, T. 2014. Isotope compositions (C, O, Sr, Nd) of vertebrate fossils from the Middle Eocene oil shale of Messel, Germany: implications for their taphonomy and palaeoenvironment. *Palaeogeography, Palaeoclimatology, Palaeoecology*, **416**, 92–109.

UHL, D. and HERRMANN, M. 2010. Palaeoclimate estimates for the Late Oligocene taphoflora of Enspel (Westerwald, West Germany) based on palaeobotanical proxies. *Palaeobiodiversity and Palaeoenvironments*, **90**, 39–47.

VERRELL, P. A. and MCCABE, N. 1986. Mating balls in the common toad, Bufo bufo. *British Herpetological Society Bulletin*, **16**, 28–29.

VINTHER, J., BRIGGS, D. E., PRUM, R. O. and SARANATHAN, V. 2008. The colour of fossil feathers. *Biology Letters*, **4**, 522–525.

VOIGT, E. 1933. Die Übertragung fossiler Wirbeltierleichen auf Zellulose-Filme, eine neue Bergungsmethode für Wirbeltiere aus der Braunkohle. *Palaeontologische Zeitschrift*, **15**, 72–78.

VOIGT, E. 1934. Die Fische aus der mitteleozänen Braunkohle des Geiseltales mit besonderer Berücksichtigung der Weichteile. *Nova Acta Leopoldina, Neue Folge*, **2**, 21–146.

VOIGT, E. 1935. Die Erhaltung von Epithelzellen mit Zellkernen, von Chromatophoren und Corium in fossiler Froschhaut aus der mitteleozänen Braunkohle des Geiseltales. *Nova Acta Leopoldina, Neue Folge*, **3**, 339–360.

VOIGT, E. 1937. Weichteile an Fischen, Amphibien und Reptilien aus der eozänen Braunkohle des Geiseltales. *Nova Acta Leopoldina, Neue Folge,* **5**, 116–142.

VOIGT, E. 1988. Preservation of soft tissues in the Eocene lignite of the Geiseltal near Halle (Saale). *Courier Forschungsinstitut Senckenberg*, **107**, 325–343.

VOITURON, Y., BARRÉ, H., RAMLØV, H. and DOUADY, C. J. 2009. Freeze tolerance evolution among anurans: frequency and timing of appearance. *Cryobiology*, **58**, 241–247.

WALTER, J. and WEIGELT, J. 1931. Die eozäne Lebewelt in der Braunkohle des Geiseltals. *Nova Acta Leopoldina, Neue Folge,* **1**, 1–27.

WATSON, S. B., WHITTON, B. A., HIGGINS, S. N., PAERL, H. W., BROOKS, B. W. and WEHR, J. D. 2015. Harmful Algal Blooms. 873–920. *In* WEHR, J. D., SHEATH, R. G. and KOCIOLEK, J. P. (eds). *Freshwater Algae of North America*. Academic Press, Boston, 1066 pp.

WEDMANN, S. 2000. Die Insekten der oberoligozänen Fossillagerstätte Enspel (Westerwald, Deutschland): Systematik, Biostratinomie und Paläoökologie. PhD thesis, Georg-August-Universität zu Göttingen, Germany. Naturhistorisches Museum Mainz, Landessammlung für Naturkunde Rheinland-Pfalz, Mainzer Naturwissenschaftliches Archiv, **Beiheft 23**, 154 pp.

WEIGELT, J. 1932. Das Lebensbild zur Bildungszeit der mitteleozänen Braunkohlen des Geiseltals. *Paläontologische Zeitschrift*, **14**, 4–24.

WEIGELT, J.1933. Die Biostratonomie der 1932 auf der Grube Cecilie im mittleren Geiseltal ausgegrabenen Leichenfelder. *Nova Acta Leopoldina, Neue Folge,* **1**, 157–174.

WEIGELT, J.1934. Die Geiseltalgrabungen des Jahres 1933 und die Biostratonomie der Fundschichten. *Nova Acta Leopoldina, Neue Folge***, 1**, 552–660.

WEIGELT, J.1935. *Lophiodon* in der oberen Kohle des Geiseltales. *Nova Acta Leopoldina, Neue Folge,* **3**, 369–402.

WEIGELT, J.1940. Der heutige Stand der Geiseltalforschung. *Naturwissenschaften*, **28**, 343–350.

WEIGELT, J. 1989. *Recent vertebrate carcasses and their paleobiological implications*. University of Chicago Press, Chicago, 188 pp.

WILDE, V. 1995. Die Makroflora aus dem Mitteleozän des Geiseltalgebietes, kurze Übersicht und Vergleiche. *Hallesches Jahrbuch für Geowissenschaften, Reihe B*, **17**, 121–138.

WILDE, V. and HELLMUND, M. 2010. First record of gut contents from a Middle Eocene equid from the Geiseltal near Halle (Saale), Sachsen-Anhalt, Central Germany. *Palaeobiodiversity and Palaeoenvironments*, **90**, 153–162.

WUTTKE, M. 1983. Aktuopaläontologische Studien über den Zerfall von Wirbeltieren. Teil I: Anura. *Senckenbergiana Lethaea*, **64**, 529–560.

WUTTKE, M. 1988. Amphibien am Messelsee - Salamander und Frösche. 95–99. In KELLER, T., SCHAAL, S., SCHAAL, S. and ZIEGLER, W. (eds). Messel - Ein Schaufenster in die Geschichte der Erde und des Lebens. Verlag Waldemar Kramer, Frankfurt am Main, 315 pp.

WUTTKE, M. 2018. Chapter 9 – Amphibians in Messel - in the Water and on Land. 113–119. *In* SMITH, K. T., SCHAAL, S. F. and HABERSETZER, J. (eds). *Messel - an ancient greenhouse ecosystem*. Schweizerbart Science Publishers, Stuttgart, Germany, Senckenberg Gesellschaft für Naturfoschung, Frankfurt am Main, 355 pp.

WUTTKE, M. and POSCHMANN, M. 2010. First finding of fish in the diet of a water-dwelling extinct frog *Palaeobatrachus* from the Upper Oligocene Fossil-Lagerstätte Enspel (Westerwald Mountains, Western Germany). *Palaeobiodiversity and Palaeoenvironments*, **90**, 59–64.

WUTTKE, M., PŘIKRYL, T., RATNIKOV, V. Y., DVOŘÁK, Z. and ROČEK, Z. 2012. Generic diversity and distributional dynamics of the Palaeobatrachidae (Amphibia: Anura). *Palaeobiodiversity and Palaeoenvironments*, **92**, 367–395.

3.11 Supporting information

The Supporting information can be found online at https://doi.org/10.1002/spp2.1453.

3.11.1 Limitations of this study

Our study of the Geiseltal anurans has certain limitations relating to the historical background of the site, our approach and anuran taxonomy.

Historical background. Most of the Geiseltal anurans are partially complete skeletons with high articulation values. It is likely that as with other historical fossil collections, these features of the Geiseltal anuran collection reflect a collection bias towards specimens that are considered better preserved. A further potential collection bias relates to peri- or post-collection damage. Indeed, hundreds of specimens are known to have been discarded due to damage induced during excavation (Krumbiegel *et al.* 1983). The process of conservation has also impacted the composition of the anuran collections: certain weather conditions and sediment types hindered fossil recovery via the transfer process (Krumbiegel 1962). Further, fossils excavated in the 1930s were subject to trials with different embedding materials such as paraffin wax, clay, gypsum and nitrocellulose glue; in some cases, these trials resulted in damage or loss of fossils (Voigt 1933, 1988). The collections are thus likely to show a temporal bias caused by changes in the use of embedding materials and other conservation practices over time.

Historical records refer to 32 discrete sites within the basin where fossil vertebrates were recovered (Haubold & Hellmund 1998). Our dataset, however, represents a potential maximum of 15 sites only

(12 sites supported by records plus three specimens of unknown provenance). Further, most specimens (n = 102) in our study are from a single site; certain sites are represented by only a single specimen. These features indicate that the Geiseltal anuran collection may be biased towards certain fossil sites within the Geiseltal basin. In turn, this likely reflects inconsistency in the approach to the field excavations over time. Most anurans were excavated from the two dying field sites Ce II and Ce III (119 specimens) and two sinkhole sites Ce I and Ce IV (32 specimens). These were excavated between 1930 and 1933. In subsequent years, the focus of excavation moved to other sites, but few specimens were excavated (six specimens in 1934, five specimens after 1950; no data on collection date are available for an additional six specimens). Historical records indicate that certain excavations, especially those conducted in the 1950s and 1970s, were performed under considerable time pressure and/or were not completely excavated due to ongoing lignite mining, flooding, rockfalls/landslides and/or coal seam fires (Krumbiegel 1962; Haubold & Krumbiegel 1984). Further, certain excavations are widely regarded to have prioritised bigger vertebrates (pers. Comm. Michael Stache, ZNS, Halle (Saale)) and / or to have discarded poorly preserved specimens (Krumbiegel 1962). As a result, many anurans, especially poorly preserved specimens, were not recovered and incorporated into the collections. This may explain, at least in part, the low number of anuran specimens (n = 6) recovered between 1934 and 1970.

A confounding factor (in the temporal variation in the recovery of fossil anurans) is stratigraphy. Excavation sites in strata of younger stratigraphic age, e.g. in the upper coal (Fig. 3.2), are reported to have more abundant fossil vertebrates and greater vertebrate diversity than stratigraphically older deposits (Hastings & Hellmund 2015). It is therefore possible that the bias in our dataset towards Ce II and Ce III is not entirely due to collection methods, but could reflect real, biological, variation in the absolute abundance and/or fidelity of preservation of anurans through time. This is supported by our analysis of completeness data: there is no significant difference in the fidelity of preservation (represented by completeness values) between specimens from the stratigraphic intervals middle coal and upper coal. Interpretations of the impact of stratigraphy on preservation must, however, also

consider reports that stratigraphic data for at least some specimens and/or sites may be inaccurate or erroneous (Ring *et al.* 2020, Krutzsch 2011).

A further potential bias in the anuran collection may relate to palaeoenvironmental setting. Fossil specimens are not evenly distributed among different settings: most are from dying fields (121 specimens from two sites), with relatively few from sinkholes (43 specimens from seven sites) and only one specimen from fluvial channel deposits (one site). This has been considered to reflect, at least in part, a biological signal linked to ecology (Krumbiegel 1962). This variation may, of course, also reflect taphonomic processes, whereby preservation of relatively complete skeletons was favoured in certain settings. Our analysis, however, of completeness values for specimens from sinkholes and dying fields failed to yield significant differences. This suggests that taphonomic factors are not the primary cause of the variation in fossil abundance among different palaeoenvironments.

There are additional uncertainties in the data available for certain fossil anuran specimens. It is unclear which specimens, if any, derive from mass mortality events as historical records do not include data on the number and distribution of anurans on single bedding planes. Secondly, excavation lists of fossil specimens indicate that many specimens are missing and are not included in the current collections.

Our approach. It is possible that certain aspects of our analytical approach have introduced bias to our data. Twenty-eight specimens were omitted from the study as poor preservation precluded confident identification of individual skeletal elements. The omission of these specimens may have resulted in the underrepresentation of taphonomic state 5 (disarticulated and reorientated skeletal elements) in our dataset.

In our approach we omitted elements from the skeletal taphonomic analysis that are distal to truncated bones as it is not possible to determine whether these (more distal) bones are truly absent (i.e.,

disarticulated and lost) or were indeed preserved as part of the fossil, but subsequently lost during the transfer process. Given that truncation usually affects distal bones and that distal bones have lower completeness values than proximal bones, our method of scoring completeness for truncated specimens (using only those bones that are present on the fossil slab) may therefore have artificially inflated completeness values. The alternatives, however, are to score all bones distal of truncated bones as either present or absent, neither approach is satisfactory as both incorporate assumptions regarding the presence / absence of bones distal of truncated elements. We consider our approach, although imperfect, to be the most appropriate and accurate solution to this problem.

Completeness and articulation were not assessed for individual elements of the following skeletal elements: (1) Cranium: bones are usually superimposed and difficult to identify. (2) Pectoral girdle (clavicula, coracoid, scapula, sternum): these are often obscured by vertebrae or cranial elements. (3) Carpals and tarsals: these are small and typically overlap For each of these three categories, the relevant skeletal unit is coded as present if at least one of the constituent bones is evident. Categories (1) to (3) therefore do not provide taphonomic information on the individual elements of the cranium, pectoral girdle and carpals/tarsals. Our approach here may thus have the potential to bias values for specimen completeness and articulation.

The same approach is applied to all specimens; any impact will be consistent across the dataset.

Anuran taxonomy. Finally, our dataset includes different anuran groups: rare aquatic palaeobatrachids and abundant terrestrial pelobatids. It is thus possible that our data incorporate a taxonomic bias related to factors such as ecology, skeletal structure and/or tissue composition. Indeed, skeletal anatomy (Fabrezi *et al.* 2017) and skin composition (Elkan 1968; Ponssa *et al.* 2017) differ between extant aquatic and terrestrial anurans, and these factors are known to impact preservation patterns in fossil anurans (McNamara *et al.* 2009; McNamara *et al.* 2012; Wuttke & Reisdorf 2012). Our data reveal, however, that the pelobatids and palaeobatrachids from Geiseltal show similar completeness and

articulation values. This suggests that differences in absolute abundance of the two groups in our dataset are not taphonomic in origin. The relatively paucity of palaeobatrachids therefore probably reflects a real biological signal, whereby they were simply less abundant members of the lake fauna.

3.11.2 Statistical testing

We tested all data for normality using the Shapiro-Wilk test and Q-Q plots prior to selecting a suitable significance test (Table 3.2 and Table 3.3).

Table 3.2: Significance tests on skeletal completeness data.

test groups	**population (n)**	**normality of data**	**differences between groups**
specimen completeness values vs. specimen completeness values (phalanges omitted) vs. specimen completeness values (hands omitted)	n = 140 for each group	non-normal (significant Shapiro-Wilk test)	significant (Kruskal Wallis test)
specimen completeness values vs. truncation groups	T0: n = 34, T1: n = 26, T2: n = 35, T3: n = 28, T4: n = 17	normal (non-significant Shapiro-Wilk test)	significant (one-way ANOVA test)
completeness values pelobatids vs. palaeobatrachids	pelobatids: n = 54, palaeobatrachids: n = 15	normal (non-significant Shapiro-Wilk test)	non-significant (t-test, equal variance)
completeness values of individual skeletal elements of pelobatids vs. palaeobatrachids	n = 16 for each group	non-normal (significant Shapiro-Wilk test)	non-significant (Mann-Whitney U-test)

specimen completeness values of excavation sites	sinkholes: n = 25; dying field 1: n = 18; dying field 2: n = 92; [the single fluvial channel specimen was omitted from this analysis]	non-normal (significant Shapiro-Wilk test)	non-significant (Kruskal-Wallis test)
specimen completeness values of determined vs. undetermined specimens	determined: n = 69, undetermined: n = 71	non-normal (significant Shapiro-Wilk test)	non-significant (Mann-Whitney U-test)
specimen completeness values of taphonomic states 1 to 6	state 1: n = 6, state 2: n = 10, state 3: n = 10, state 4: n = 3, state 5: n = 3, state 6: n = 2	non-normal (significant Shapiro-Wilk test)	significant (Kruskal-Wallis test)
specimen completeness values of embedding materials	nitrocellulose glue: n = 104, nitrocellulose glue on gypsum: n = 6, paraffin wax: n = 29	non-normal (significant Shapiro-Wilk test)	non-significant (Kruskal-Wallis test)
specimen completeness values of excavation sites of stratigraphic levels	upper coal (Ce II, Ce III, Ce V): n = 111, middle coal (Ce IV, Ce VI, Leo III, Leo V, IL, NsXXXV): n = 23 [the single site of the lower coal interval holds only one specimen and was omitted from this analysis]	non-normal data (significant Shapiro-Wilk test)	non-significant (Mann-Whitney U-test)
specimen truncation values of embedding materials	nitrocellulose glue: n = 104, nitrocellulose glue on gypsum: n = 6, paraffin wax: n = 29	non-normal (significant Shapiro-Wilk test)	non-significant (Kruskal-Wallis test)

Pearson's correlation test was used to assess any correlations in completeness values for all skeletal elements on the left and right sides of the body and for homologous elements of the fore- and hindlimbs.

Table 3.3: Significance tests on specimen articulation data.

test groups	**population (n)**	**normality of data**	**differences between groups**
specimen articulation values vs. specimen completeness values (phalanges omitted) vs. specimen completeness values (hands omitted)	specimen articulation values: n = 140, specimen completeness values (phalanges omitted): n = 140, specimen completeness values (hands omitted): n = 139	non-normal (significant Shapiro-Wilk test)	non-significant (Kruskal Wallis test)
specimen articulation values vs. truncation groups	T0: n = 34, T1: n = 26, T2: n = 35, T3: n = 28, T4: n = 17	non-normal (significant Shapiro-Wilk test)	significant (Kruskal-Wallis test)
articulation values pelobatids vs. palaeobatrachids	pelobatids: n = 54, palaeobatrachids: n = 15	non-normal (significant Shapiro-Wilk test)	non-significant (Mann-Whitney U-test)
articulation values of individual skeletal elements of pelobatids vs. palaeobatrachids	n = 23 for each group	non-normal (significant Shapiro-Wilk test)	significant (Mann-Whitney U-test)
specimen articulation values of excavation sites	sinkholes: n = 25; dying field 1: n = 18; dying field 2: n = 92; [the single fluvial channel specimen was omitted from this analysis]	non-normal (significant Shapiro-Wilk test)	non-significant (Kruskal-Wallis test)
specimen articulation values of determined vs. undetermined specimens	determined: n = 69, undetermined: n = 71	non-normal (significant Shapiro-Wilk test)	non-significant (Mann-Whitney U-test)

specimen articulation values of taphonomic states 1 to 6	state 1: n = 6, state 2: n = 10, state 3: n = 10, state 4: n = 3, state 5: n = 3, state 6: n = 2	non-normal (significant Shapiro-Wilk test)	significant (Kruskal-Wallis test)
specimen articulation values of embedding materials	nitrocellulose glue: n = 104, nitrocellulose glue on gypsum: n = 6, paraffin wax: n = 29	non-normal (significant Shapiro-Wilk test)	non-significant (Kruskal-Wallis test)

Pearson's correlation test was used to assess any correlations in articulation values for all joints on the left and right sides of the body and for homologous joints of the fore- and hindlimbs.

3.11.3 Supporting figures and tables

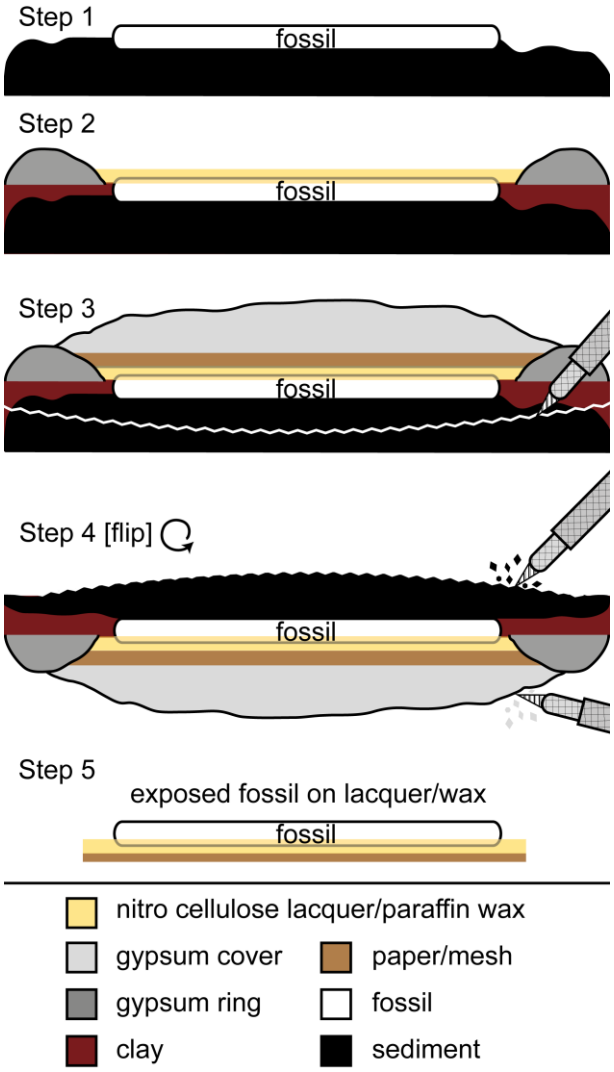


Fig. S3.1. Schematic illustration of the resin transfer method ('Lackfilm' method (after Voigt 1933)). For some specimens, the fossil was removed after step 2 by peeling away the lacquer and the attached fossil (Krumbiegel et al. 1983). Step 1: Exposure of fossil. Step 2: Application of clay and gypsum ring followed by nitrocellulose lacquer or paraffin wax. Step 3: Application of paper or mesh and gypsum cover. Step 4: Exposure of fossil from reverse side and removal of sediment cover, gypsum and clay. Step 5: Fossil is exposed on a lacquer/wax backing; lower surface of the fossil is now exposed on top.

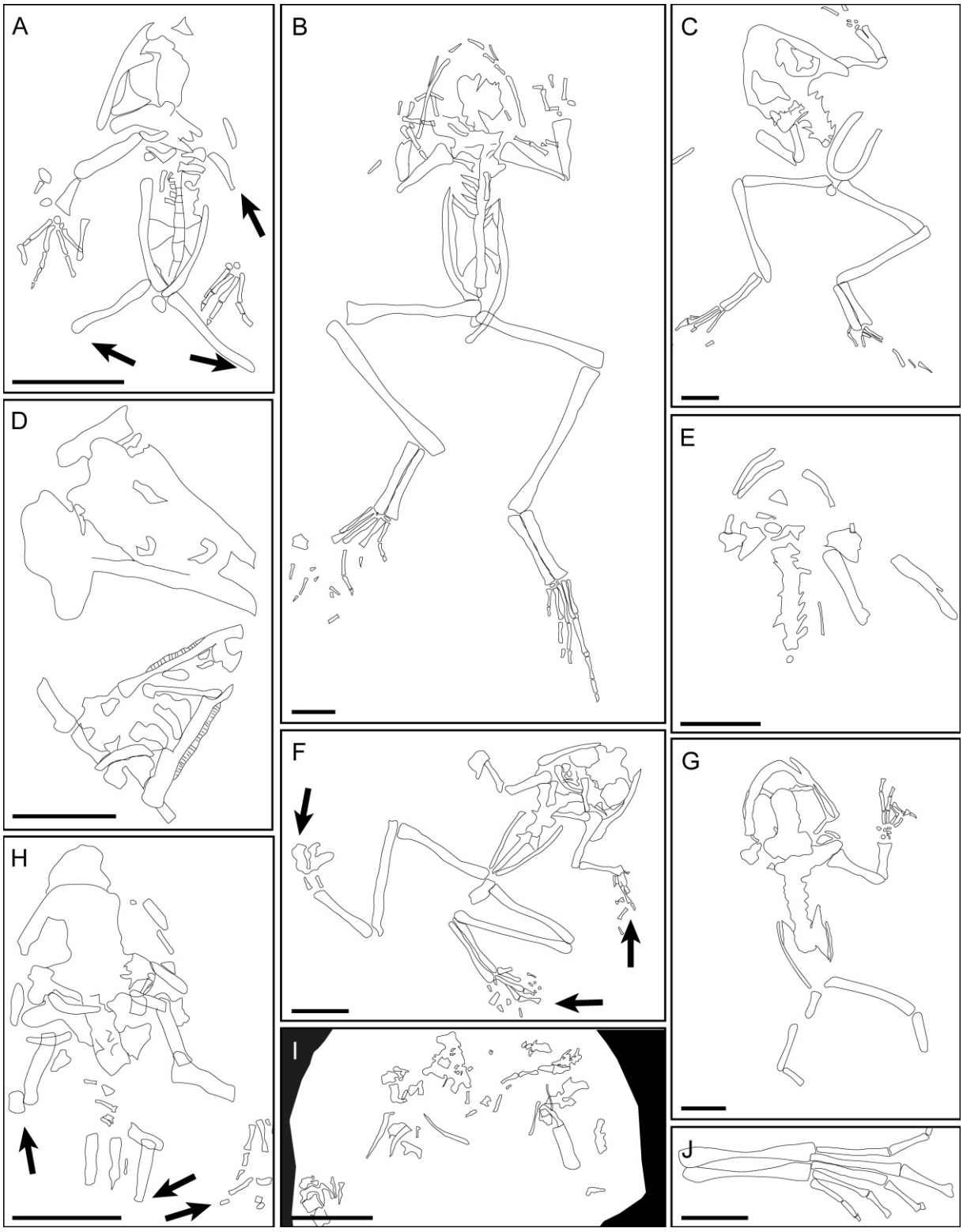


Fig. S3.2. Line drawings for specimens shown in Fig. 3.3. A, Ce III-6735-1932. B, Ce II-4949-1930. C, Ce III-6728-1932. D, Ce IV-4953-1933. E, Ce III-6720-1932. F, Ce III-6719-1932. G, Ce I-4947-1930. H, Ce III-6742-1932. I, IL 17A-1969. J, Ce III-6737-1932. All scale bars represent 10 mm.

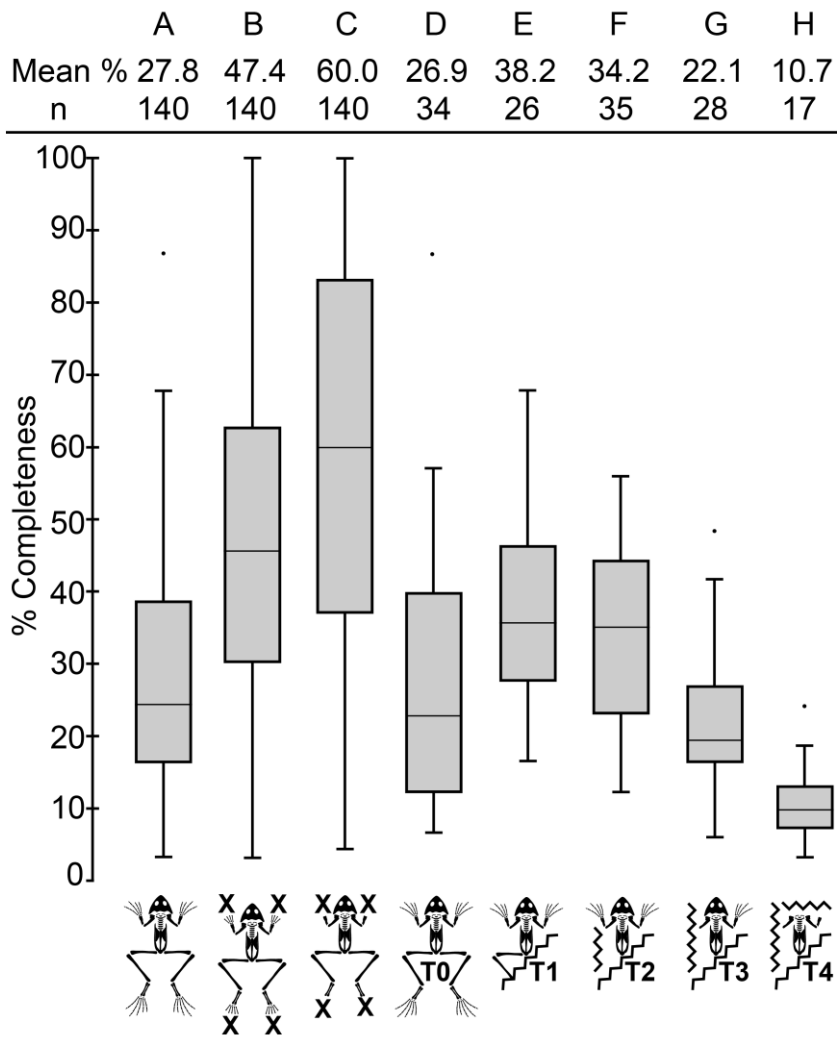


Fig. S3.3. Trends in completeness for Geiseltal anurans where elements distal to truncated elements are coded as 'absent' (rather than being omitted). A–C, specimen completeness for the entire dataset; D–H, specimen completeness for truncation categories. A, no elements omitted from the dataset. B, phalanges omitted. C, entire hands and feet omitted. D–H, specimens in truncation categories T0–T4. D, no truncation. E, truncation group T1 (0.1–24.9% truncation). F, truncation group T2 (25%–49.9% truncation). G, truncation group T3 (50%–74.9% truncation). H, truncation group T4 (75%–100% truncation). The horizontal line in each boxplot denotes median value for each category.

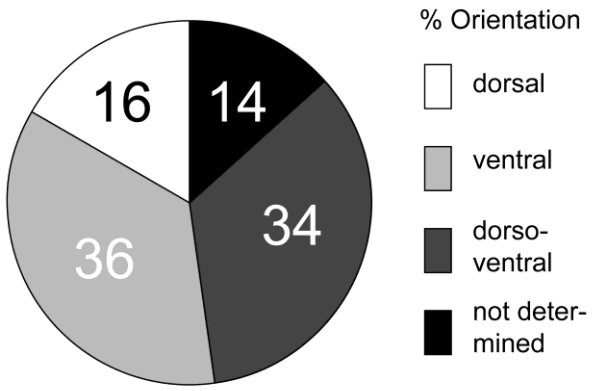


Fig. S3.4. Specimen orientation (n = 140).

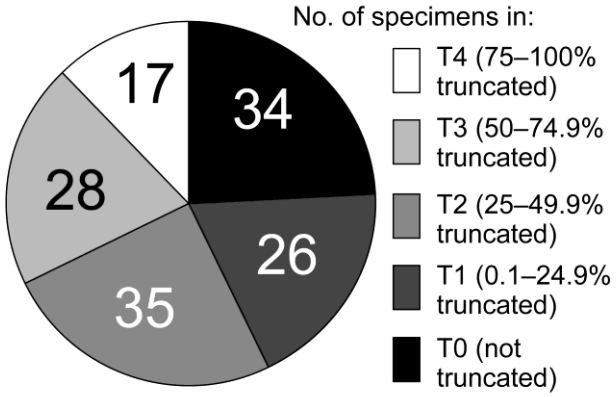


Fig. S3.5. Distribution of specimens among truncation categories T0–T4 (n = 140).

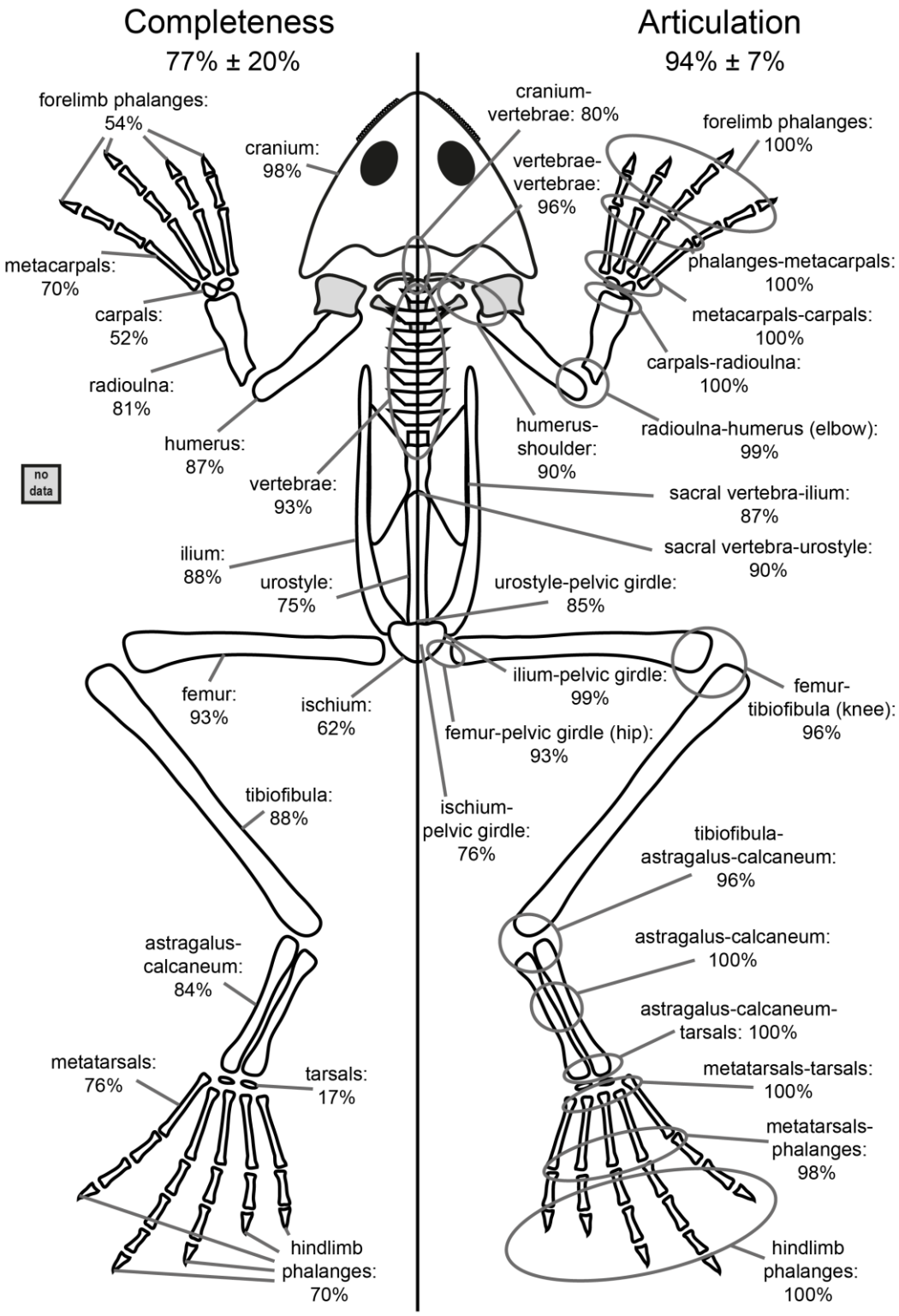


Fig. S3.6. Schematic frog skeleton summarizing the percentage completeness and articulation values for each type of skeletal element in the Geiseltal anurans (n = 140). Percentage values indicate the percentage of specimens that show the skeletal element or the articulated joint; for paired elements or elements in a set, at least one element of the pair or set must be visible in order to be coded as present.

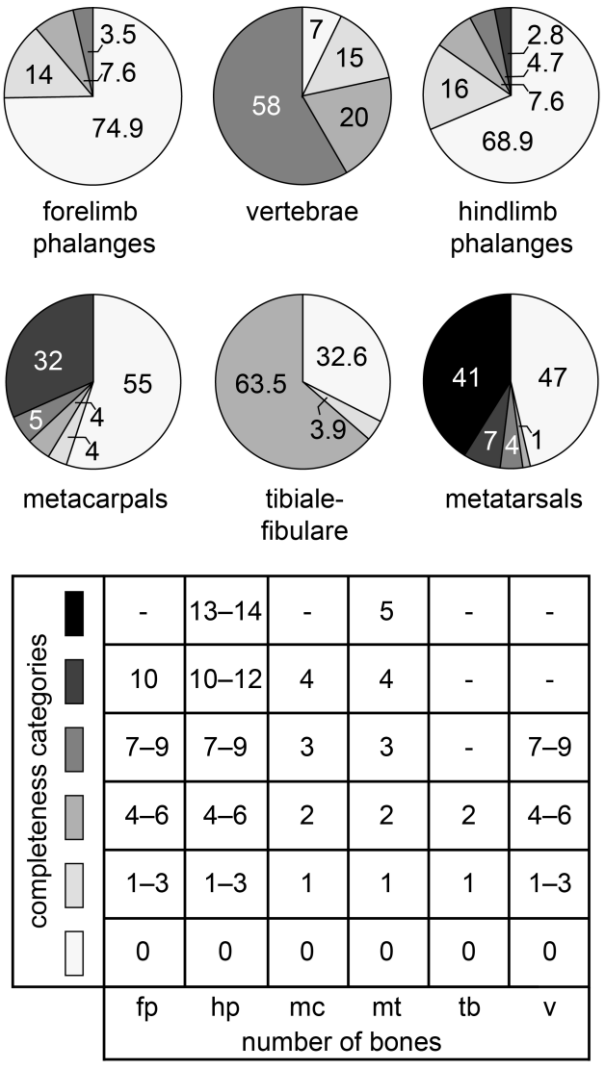


Fig. S3.7. Distribution of skeletal elements among completeness groups. Values in the plots are percentages. Numbers in the key refer to the number of skeletal elements that are present in the hands, feet or torso. Grey tones denote different completeness groups or truncation categories, respectively. For instance, the phalanges are absent in 74.9% of hands and the vertebral column shows 7–9 vertebrae in 58% of specimens. Abbreviations: fp, forelimb phalanges; hp, hindlimb phalanges; mc, metacarpals; mt, metatarsals; tb, tibiale-fibulare; v, vertebrae.

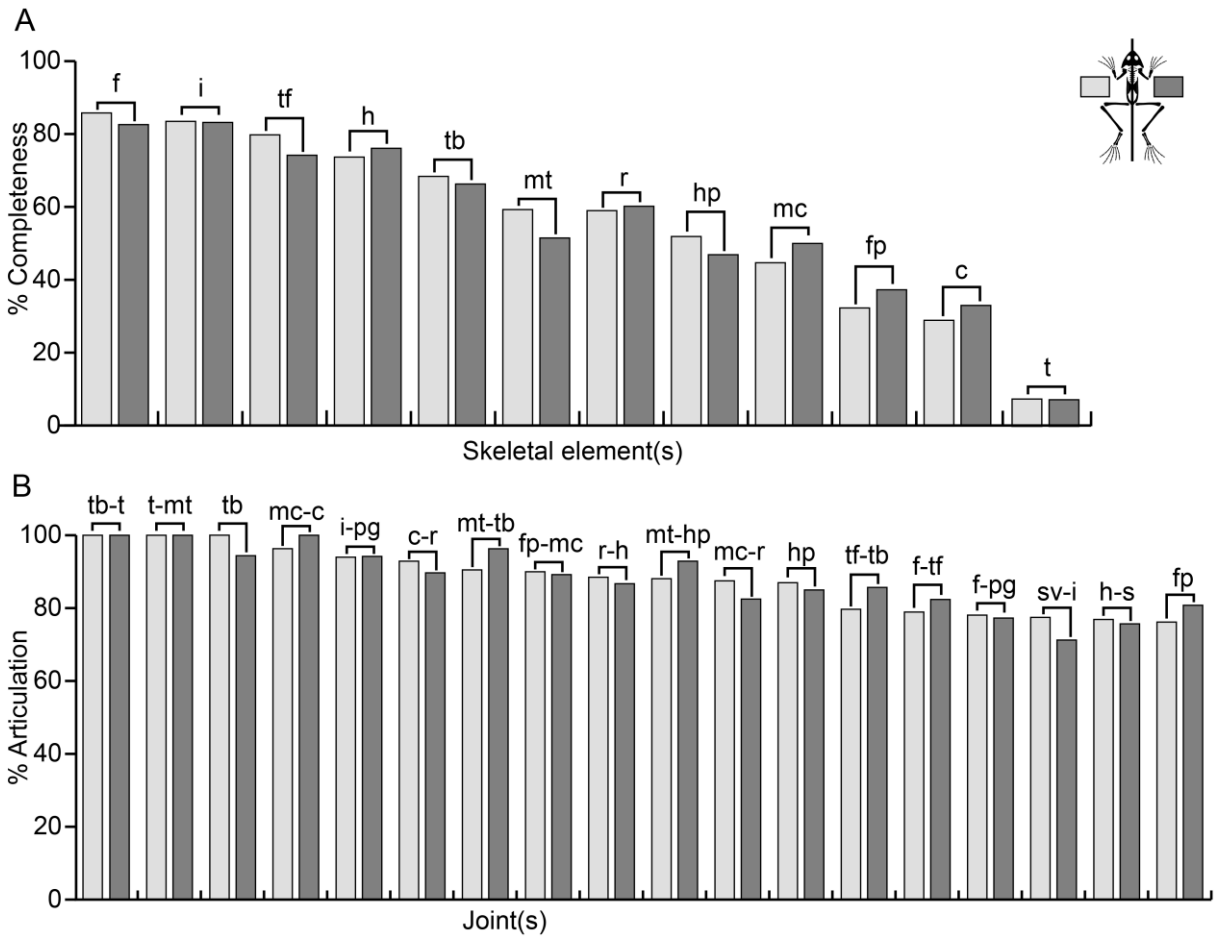


Fig. S3.8. Percentage completeness for each element and percentage articulation for each joint, on the left and right sides of the body. "Left" and "right" are as presented in hand specimen, with the cranium at top. Light grey shading denotes data for the left-hand side of the body, and dark grey shading denotes data for the right-hand side of the body. Elements present as a pair or as a group are coded as complete if at least one of the elements is present. Joints present as a pair or as a group are coded as articulated if at least one of the joints is in life position. A, percentage completeness for each element. B, percentage articulation for each joint. Abbreviations: c, cranium; f, femur; fp, forelimb phalanges; hp, hindlimb phalanges; h, humerus; i, ischium; mc, metacarpals; mt, metatarsals; pg, pelvic girdle; s, shoulder; sv, sacral vertebrae; r, radioulna; t, tarsals; tb, tibiale-fibulare; tf, tibiofibula; v, vertebrae.

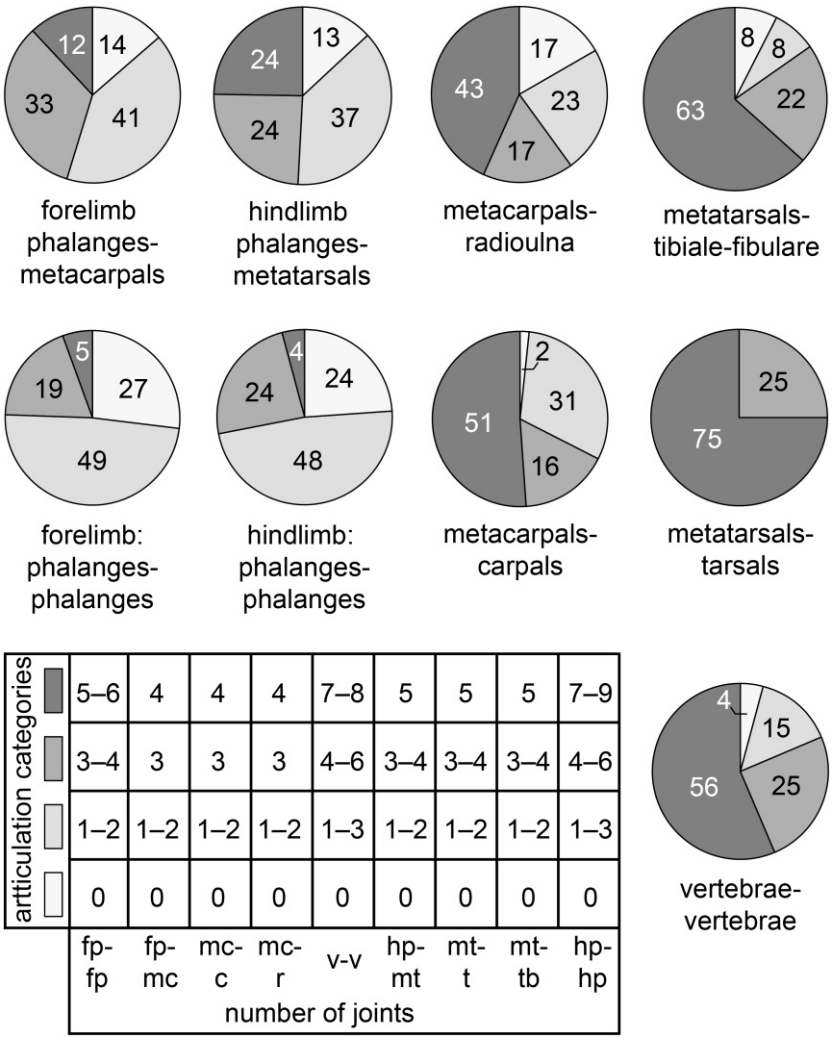


Fig. S3.9. Distribution of joints among articulation groups. Pie chart values are percentages. Numbers in the key refer to the number of joints that are articulated in a given hand, foot or torso, respectively. Grey tones denote different articulation groups. For instance, 27% of hands show no articulated phalanges and 48% of hands reveal 1–2 articulated joints.

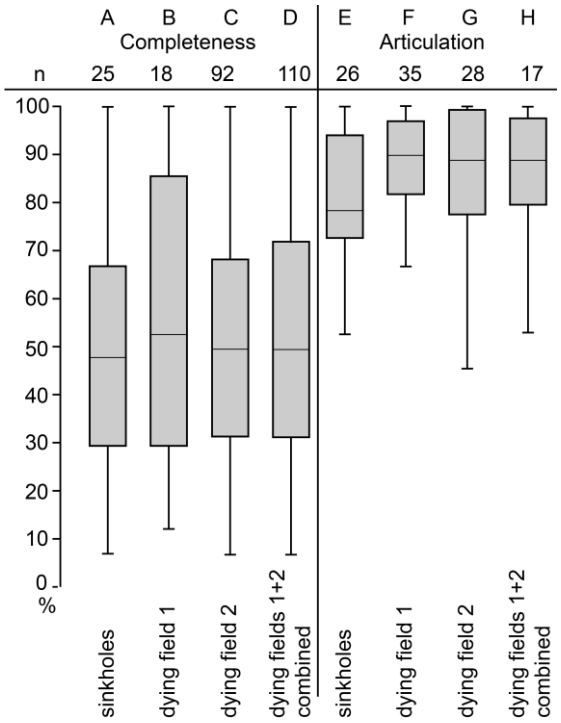


Fig. S3.10. Trends in completeness (A–D) and articulation (E–H) for Geiseltal anurans among excavation sites. A & E, sinkholes (i.e. Ce I, Ce IV, Ce V, Ce VI, Leo III, Leo V and NsXXXV). B & F, dying field 1 (Ce II), C & G, dying field 2 (Ce III). D & H, combined data for dying field 1 (Ce II) and 2 (Ce III). The horizontal line in each boxplot denotes median value for each site.

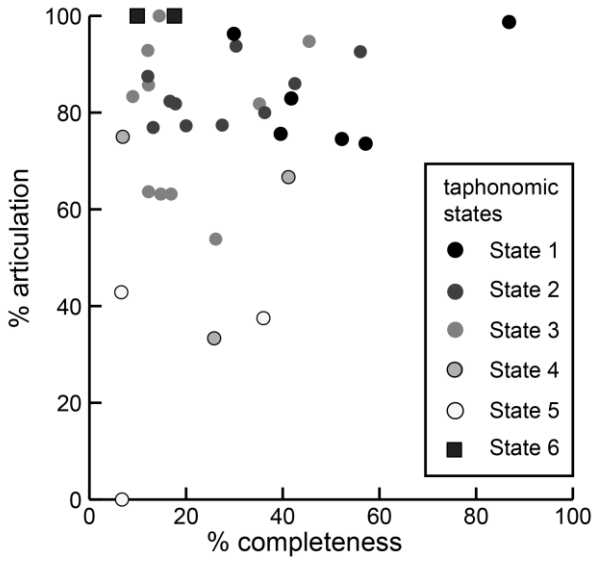


Fig. S3.11. Percentage articulation versus percentage completeness for truncated specimens that are not truncated (n = 34).

SUPPORTING TABLE 3.1. Percentage completeness (A) and articulation (B) per skeletal element and joint.

Data are provided as a percentage of total specimens, total elements (for completeness) and total joints (for articulation). For instance, the forelimb phalanges are present in 53.6% of specimens, but only 34.9% of the theoretical maximum number of forelimb phalanges are present.

(A)

Completeness	% completeness	
	specimens (i.e. % specimens for which the element is present)	**elements** (i.e. % of elements present out of element maximum number)
cranium	98.1	98.1
forelimb phalanges	53.6	34.9
metacarpals	69.8	47.4
carpals	52.7	31.0
radioulna	80.9	59.6
humerus	87.2	74.9
vertebrae	92.9	92.9
urostyle	74.8	74.8
ischium	61.8	61.8
ilium	88.1	83.3
femur	93.4	84.2
tibiofibula	87.5	77.2
tibiale-fibulare	83.8	67.4
tarsals	17.2	7.2
metatarsals	75.6	55.7
hindlimb phalanges	70.1	49.7
mean completeness	77.1	61.9

(B)

Articulation	% articulation	
	specimens (i.e. % specimens for which the element is articulated)	**joints** (i.e. % joints articulated out of joint maximum number)
metacarpals-radioulna (no carpals)	100.0	84.8
forelimb phalanges	100.0	78.7
phalanges-metacarpals	100.0	89.6
metacarpals-carpals	100.0	98.3
carpals-radioulna	100.0	91.2
radioulna-humerus (=elbow)	98.8	87.6
humerus-shoulder	90.0	76.3
cranium-vertebrae	80.2	80.2
vertebrae	95.9	95.9
sacral vertebrae-urostyle	89.7	89.7
sacral vertebrae-ilium	86.7	74.3
ischium-pelvic girdle	75.5	75.5
ilium-pelvic girdle	98.9	94.1
urostyle-pelvic girdle	85.1	85.1
pelvic girdle-femur (hip)	93.4	77.7
femur-tibiofibula (knee)	96.4	80.4
tibiofibula-tibiale-fibulare	95.9	82.5
tibiale-fibulare	100.0	97.4
tibiale-fibulare-tarsals	100.0	100.0
tarsals-metatarsals	100.0	100.0
metatarsals-phalanges	98.0	90.0
hindlimb phalanges	100.0	86.0
metatarsals-tibiale-fibulare (no tarsals)	100.0	92.8
mean articulation	94.0	85.7

SUPPORTING TABLE 3.2. Percentage completeness (A) and articulation (B) per skeletal element and joint, respectively, in pelobatids and palaeobatrachids. For instance, the forelimb phalanges are present in 62.8% of specimens of pelobatids.

(A)

Completeness	% specimens for which the element is present	
	Pelobatidae	**Palaeobatrachidae**
cranium	100.0	100.0
forelimb phalanges	62.8	63.6
metacarpals	85.0	76.9
carpals	65.1	63.6
radioulna	91.3	78.6
humerus	94.1	86.7
vertebrae	98.0	100.0
urostyle	80.9	100.0
ischium	69.7	85.7
ilium	94.1	93.3
femur	94.0	100.0
tibiofibula	85.0	100.0
tibiale-fibulare	80.6	100.0
tarsals	25.0	42.9
metatarsals	67.7	100.0
hindlimb phalanges	65.5	100.0
mean completeness	82.2	88.7

(B)

Articulation	% specimens for which the element is articulated	
	Pelobatidae	**Palaeobatrachidae**
metacarpals-radioulna (no carpals)	100.0	100.0
forelimb phalanges	100.0	100.0
phalanges-metacarpals	100.0	100.0
metacarpals-carpals	100.0	100.0
carpals-radioulna	100.0	100.0
radioulna-humerus (=elbow)	97.2	100.0
humerus-shoulder	89.7	100.0
cranium-vertebrae	81.8	91.7
vertebrae	97.8	100.0
sacral vertebrae-urostyle	85.7	100.0
sacral vertebrae-ilium	92.5	100.0
ischium-pelvic girdle	86.4	71.4
ilium-pelvic girdle	100.0	100.0
urostyle-pelvic girdle	81.3	100.0
pelvic girdle-femur (hip)	97.2	100.0
femur-tibiofibula (knee)	100.0	100.0
tibiofibula-tibiale-fibulare	96.2	100.0
tibiale-fibulare	100.0	100.0
tibiale-fibulare-tarsals	100.0	100.0
tarsals-metatarsals	100.0	100.0
metatarsals-phalanges	94.4	100.0
hindlimb phalanges	100.0	100.0
metatarsals-tibiale-fibulare (no tarsals)	100.0	100.0
mean articulation	94.5	98.6

3.11.4 Supporting references

ELKAN, E. 1968. Mucopolysaccharides in the anuran defence against desiccation. *Journal of Zoology*, **155**, 19–53.

FABREZI, M., GOLDBERG, J. and CHULIVER PEREYRA, M. 2017. Morphological variation in anuran limbs: constraints and novelties. *Journal of Experimental Zoology B: Molecular and Developmental Evolution*, **328**, 546–574.

HASTINGS, A. K. and HELLMUND, M. 2015. Gaining ground: horse-hunting crocodiles and giant birds; new research results on the Eocene world of Germany ca. 45 million years ago. Companion volume to the exhibition presented at the National Academy of Sciences Leopoldina from

March 6th to May 29th, 2015 in Halle (Saale), Germany. Center for Natural Science Collections (ZNS), Halle (Saale), Germany, 120 pp.

HAUBOLD, H. and HELLMUND, M. 1998. The Geiseltalmuseum of the Institute of Geological Sciences, University Halle-Wittenberg. - Epicontinental Triassic International Symposium - Excursions. *Hallesches Jahrbuch für Geowissenschaften, Reihe B*, **6**, 11–18.

HAUBOLD, H. and KRUMBIEGEL, G. 1984. Typenkatalog der Wirbeltiere aus dem Eozän des Geiseltals, 1934-1984 - 50 Jahre Geiseltalmuseum an der Martin-Luther-Univ. Halle-Wittenberg, Halle (Saale), 67 pp.

KRUMBIEGEL, G. 1962. Die Fossilfundstellen der mitteleozänen Braunkohle des Geiseltales. *Wissenschaftliche Zeitschrift der Martin-Luther-Universität in Halle*, **11**, 173–208.

KRUMBIEGEL, G., RÜFFLE, L. and HAUBOLD, H. 1983. *Das eozäne Geiseltal: ein mitteleuropäisches Braunkohlenvorkommen und seine Pflanzen- und Tierwelt*. A. Ziemsen Verlag, Die Neue Brehm-Bücherei, Wittenberg Lutherstadt, 227 pp.

MCNAMARA, M. E., ORR, P. J., ALCALÁ, L., ANADÓN, P. and PEÑALVER, E. 2012. What controls the taphonomy of exceptionally preserved taxa - environment or biology? A case study using frogs from the Miocene Libros Konservat-Lagerstätte (Teruel, Spain). *Palaios*, **27**, 63–77.

MCNAMARA, M. E., ORR, P. J., KEARNS, S. L., ALCALÁ, L., ANADÓN, P. and PENALVER MOLLA, E. 2009. Soft-tissue preservation in Miocene frogs from Libros, Spain: insights into the genesis of decay microenvironments. *Palaios*, **24**, 104–117.

PONSSA, M. L., BARRIONUEVO, J. S., PUCCI ALCAIDE, F. and PUCCI ALCAIDE, A. 2017. Morphometric variations in the skin layers of frogs: an exploration into their relation with ecological parameters in *Leptodactylus* (Anura, Leptodactylidae), with an emphasis on the Eberth-Kastschenko layer. *The Anatomical Record*, **300**, 1895–1909.

RING, S. J., BOCHERENS, H., WINGS, O. and RABI, M. 2020. Divergent mammalian body size in a stable Eocene greenhouse climate. *Scientific Reports*, **10**, 3987.

VOIGT, E. 1933. Die Übertragung fossiler Wirbeltierleichen auf Zellulose-Filme, eine neue Bergungsmethode für Wirbeltiere aus der Braunkohle. *Palaeontologische Zeitschrift*, **15**, 72–78.

VOIGT, E. 1988. Preservation of soft tissues in the Eocene lignite of the Geiseltal near Halle (Saale). *Courier Forschungsinstitut Senckenberg*, **107**, 325–343.

WUTTKE, M. and REISDORF, A. G. 2012. Taphonomic processes in terrestrial and marine environments. *Palaeobiodiversity and Palaeoenvironments*, **92**, 1–3.

4. Fossilized anuran soft tissues reveal a new taphonomic model for the Eocene Geiseltal Konservat-Lagerstätte, Germany

This chapter represents the quantitative and qualitative analysis of the fossil soft tissues of the Geiseltal anurans and elucidates a new taphonomic model for the Geiseltal Lagerstätte. The chapter comprises a paper that is published in the journal *Scientific Reports* (Falk *et al.* 2024) and is co-written by five authors. The chapter is organised as follows: Introduction, Results, Discussion, Methods, Data availability statement, References, Acknowledgements, Author contributions, Competing interests and Supplementary Information.

Falk, D., Wings, O., Unitt, R., Wade, J. & McNamara, M. E. (2024). Fossilized anuran soft tissues reveal a new taphonomic model for the Eocene Geiseltal Konservat-Lagerstätte, Germany. *Sci. Rep.*, **14**, 1–14. https://doi.org/10.1038/s41598-024-55822-y.

Candidate contribution to the study. DF contributed to the design of the study and performed a literature review on the soft tissue features of the Geiseltal anurans. OW provided access to the Geiseltal Collection and sampling permission. Using a microscope, DF investigated 168 anuran specimens from the Geiseltal Collection and identified and documented soft tissue features. Both DF and MMN collected the samples for the following techniques: EDS, EPMA, micro-FTIR, micro-Raman spectroscopy and SEM. DF collected the samples for the XRD analysis. DF prepared the samples as follows: polishing, homogenisation and sputter-coating. DF performed the following analyses: SEM and EDS. Resin-embedding and micro-FTIR were carried out by DF with assistance from MMN and technical staff. JW performed the EPMA analysis, RU performed micro-Raman spectroscopy with assistance of DF and MMN performed the micro-SRS-XRF analysis. XRD analysis was performed at the University of Oxford by local staff. DF performed the statistical analysis of the dataset. DF wrote the first draft of the paper, produced the figures and revised subsequent drafts in line with comments from the other

authors. Following peer review, DF co-drafted the revisions to the paper with the other authors in accordance with comments from two reviewers.

Abstract. The Eocene Geiseltal Konservat-Lagerstätte (Germany) is famous for reports of three dimensionally preserved soft tissues with sub-cellular detail. The proposed mode of preservation, direct replication in silica, is not known in other fossils and has not been verified using modern approaches. Here, we investigated the taphonomy of the Geiseltal anurans using diverse microbeam imaging and chemical analytical techniques. Our analyses confirm the preservation of soft tissues in all body regions but fail to yield evidence for silicified soft tissues. Instead, the anuran soft tissues are preserved as two layers that differ in microstructure and composition. Layer 1 comprises sulfur-rich carbonaceous microbodies interpreted as melanosomes. Layer 2 comprises the mid-dermal Eberth-Katschenko layer, preserved in calcium phosphate. In addition, patches of original aragonite crystals define the former position of the endolymphatic sac. The primary modes of soft tissue preservation are therefore sulfurization of melanosomes and phosphatization of more labile soft tissues, i.e., skin. This is consistent with the taphonomy of vertebrates in many other Konservat-Lagerstätten. These findings emphasize an emerging model for pervasive preservation of vertebrate soft tissues via melanosome films, particularly in stagnation-type deposits, with phosphatization of more labile tissues where tissue biochemistry is favorable.

4.1 Introduction

Konservat-Lagerstätten are characterized by high fidelity preservation of fossils as articulated skeletons and/or with soft tissues[1,2]. Such fossils provide critical insights into the evolution of extant plants and animals[2,3]. Konservat-Lagerstätten from the Paleogene and Neogene are of particular interest as they typically have experienced less complex diagenetic histories[4], including less thermal maturation, than their geologically older counterparts. As a result, the pathways leading to preservation are usually not completely obscured by chemical alteration and/or deformation. Further, fossils from Paleogene and

Neogene Konservat-Lagerstätten are usually anatomically similar to extant analogues[4]. Models for preservation developed using such fossils can therefore be applied to fossils from older Konservat-Lagerstätten in order to inform interpretations of preserved anatomy, chemistry, and the controls on preservational fidelity.

Notable Paleogene Konservat-Lagerstätten include the Geiseltal biota of central Germany (late early to middle Eocene[5,6]), which is the subject of renewed interest due to the recent reopening of the collections for scientific access[7]. The biota is represented by ca. 50,000 specimens, more than half of which are vertebrates, including amphibians, fish, lizards, mammals, and birds[7,8]. Many vertebrates preserve soft tissues, evident in hand specimens as pale- to brown-toned body outlines[8-11]. The preserved soft tissues were first investigated in the 1930s[12-16] (reviewed in Voigt[10]). These studies reported the preservation of muscle tissue (in artiodactyls, bats, fish, frogs, lizards and palaeohippids), cartilage (in bats, newts, palaeohippids and reptiles), blood vessels with erythrocytes (in frogs and lizards), integument (bat- and frog skin, lizard scales, feathers and hair of artiodactyls, marsupials, and palaeohippids), connective tissue (in bats, crocodiles, fish, frogs, lizards) and calcium carbonate crystals of the endolymphatic sac (in frogs). Pigment cells were reported in bats (skin), fish (eyes and skin), newts (skin) and frogs (skin)[10,16]; “Melaninkörnchen” [melanin granules] (Voigt[16], p. 9; Voigt[10], p. 328) and/or “Pigmentkörnchen” [pigment granules] (Voigt[16], p. 5; Voigt[10], p. 336) were reported in fish (eyes and skin), frogs (skin) and marsupials (hair; Voigt[10], p. 328). Fossil bacteria were reported in fish, frogs and the coprolites of crocodiles[10,17]. In addition, certain specimens of artiodactyls and perissodactyls preserve stomach contents[10,11,14]. Collectively, these reports of subcellular anatomical details for various soft tissues in different vertebrate groups describe a fidelity of preservation that is among the highest known for any Lagerstätte. Ultrastructural preservation of soft tissues with comparable fidelity is known for other fossil vertebrates from Neogene[18,19] and Cretaceous biotas[20], but is often restricted to a limited number of taxa.

The proposed mode of preservation of the Geiseltal fossils, i.e., direct three-dimensional replication in silica[10,16], is not known elsewhere in the fossil record. The evidence for this mode of preservation therefore warrants consideration and validation. The fidelity of anatomical preservation of soft tissues in Geiseltal fossils was originally assessed using transmitted light microscopy of whole tissue samples (i.e., not tissue sections)[10,12-14,16]. These studies also investigated the chemistry of the soft tissues by combustion of tissue samples and analysis of the residues using refractometry[16]. Based on these tests, the soft tissues were interpreted as inorganic in composition[16]. Reaction of post-combustion tissue residues with hydrofluoric acid and “Kalisalz" [potassium salt] (Voigt[16], p. 19) yielded potassium fluorosilicate crystals; this was interpreted as evidence that the preserved tissue includes a component of silicic acid[16]. Voigt suggested that preservation of the soft tissues resulted from a three-step process: (1) initial tanning of integument by humic acid (from the lake / pore waters) followed by (2) impregnation and then (3) replacement by silicic acid (“molekularer Austausch” [molecular exchange], Voigt[16], p. 19) during diagenesis[16]. Subsequent work suggested that tanning and silicification were mutually independent and apply to different tissues[10]. The proposed source of silica is the host sediment, specifically diatoms, plant tissues rich in silica particles, and silicates[10,16].

Voigt’s interpretation that the Geiseltal fossils are preserved, at least in part, via silicification is intriguing: this mode of soft tissue preservation usually applies to microbes, plants and arthropods[21] but rarely to vertebrates (but see Channing, et al.[22]). Aside from the direct replacement model proposed for the Geiseltal fossils, silicification is usually considered to occur via permineralization or encrustation[21,23,24]. In each of these three mechanisms of silicification, the source of silica is universally considered to be the external environment, i.e., host sediment rich in ash and/or silica-saturated porewaters.

In sum, due to the reported high fidelity preservation coupled with replication of vertebrate soft tissues in silica, the Geiseltal biota is considered to have a unique taphonomic history. Despite this, the soft

tissue taphonomy of the Geiseltal vertebrates has not been investigated in recent years. This is particularly surprising given the proposed preservation of fossil bacteria (other instances of which have been widely reinterpreted as preserved melanosomes[19,25-27]). Here, we address this issue by investigating the mode of preservation of the Geiseltal anurans using various chemical- and imaging techniques. The anurans are of particular interest because they are abundant and are reported to preserve various soft tissues with cellular-level fidelity (Supplementary Table S4.2)[9,10,13,28]. These include: (1) the stratum corneum and stratum germinativum of the epidermis[10,13] plus associated bacteria[17], (2) the stratum spongiosum and stratum compactum of the dermis, including collagen fibers[10,13], (3) pigment cells of the stratum vasculare[10,13]; (4) muscle tissue with subcellular banding[10,13,29], (5) connective tissue with banding[13] and (5) statoliths of the endolymphatic sac[16].

In this study, we assess the evidence for high fidelity preservation of the soft tissues reported by Voigt via direct replacement in authigenic silica. Our study failed to recover evidence for this mode of preservation and for preservation of most of the tissues reported originally. Claims of a unique taphonomic history and a remarkably high fidelity of preservation for the Geiseltal fossils are therefore unsupported.

4.2 Results

For this study, we examined 168 fossil anuran specimens from the Geiseltal Collection (Natural Sciences Collections of the Martin Luther University Halle-Wittenberg; Supplementary Table S4.1) using light microscopy, scanning electron microscopy (SEM), energy-dispersive X-ray spectroscopy (EDS), micro-Raman spectroscopy, micro-Fourier transform infrared spectroscopy (FTIR) and electron microprobe analysis (EMPA) in order to better characterize the fidelity and mode of preservation (see Methods). One specimen is conserved on the original host sediment in water. Most of the remaining specimens are conserved on resin slabs (Supplementary Table S4.1)[8], with a minority on slabs of gypsum or

paraffin wax; small patches of sediment are often retained on the slabs. We analyzed 57 samples of the anuran soft tissues and 22 samples of sediment.

Light microscopy and SEM imaging reveal that the soft tissues of the Geiseltal anurans are preserved as three materials that differ in their spatial distribution, color, texture, thickness, and chemical characteristics (Fig. 4.1). Two materials are layered and are referred to here as Layers 1 and 2. Due to variations in the plane of splitting among and within individual specimens, each layer may not be visible over the full extent of the soft tissues in each specimen (Figs. 4.1, 4.2, 4.3a,b,c); the third material occurs only in the posterior of the cranium and along the vertebral column (Fig. 4.1a,f).

Layer 1 occurs in 90% (total n = 168) of specimens (100% of palaeobatrachids (total n = 15) and 93% of pelobatids (total n = 54)). Within an individual specimen, it can occur in some, or all, of the following body regions: eyespots, torso, abdomen and limbs (Fig. 4.1a,b,c,d,e). The layer is usually black to brown in color, with a microgranular texture and polygonal cracking (Figs. 4.1e, 4.2a, 4.3a; Supplementary Fig. S4.1). It can extend over an area of several square centimeters and is over- and underlain by Layer 2 (Figs. 4.1e, 4.2a). Layer 1 usually comprises two sublayers. The outermost sublayer (1a) is amorphous and ca. 10–20 µm thick (Fig. 4.2b; Supplementary Fig.S4.1). This outer amorphous sublayer transitions gradually to an inner sublayer (1b) rich in microbodies, each ca. 0.5–3 µm long (Fig. 4.3m; Supplementary Fig. S4.1c,d,g). Sublayer 1b comprises several bands of densely packed microbodies that alternate with bands dominated by amorphous matrix (and with few microbodies; Fig. 4.3h,l; Supplementary Fig. S4.1). In several samples, Layer 1 lacks Sublayer 1a, comprising densely packed microbodies (Sublayer 1b) only. The microbodies lack a preferred orientation.

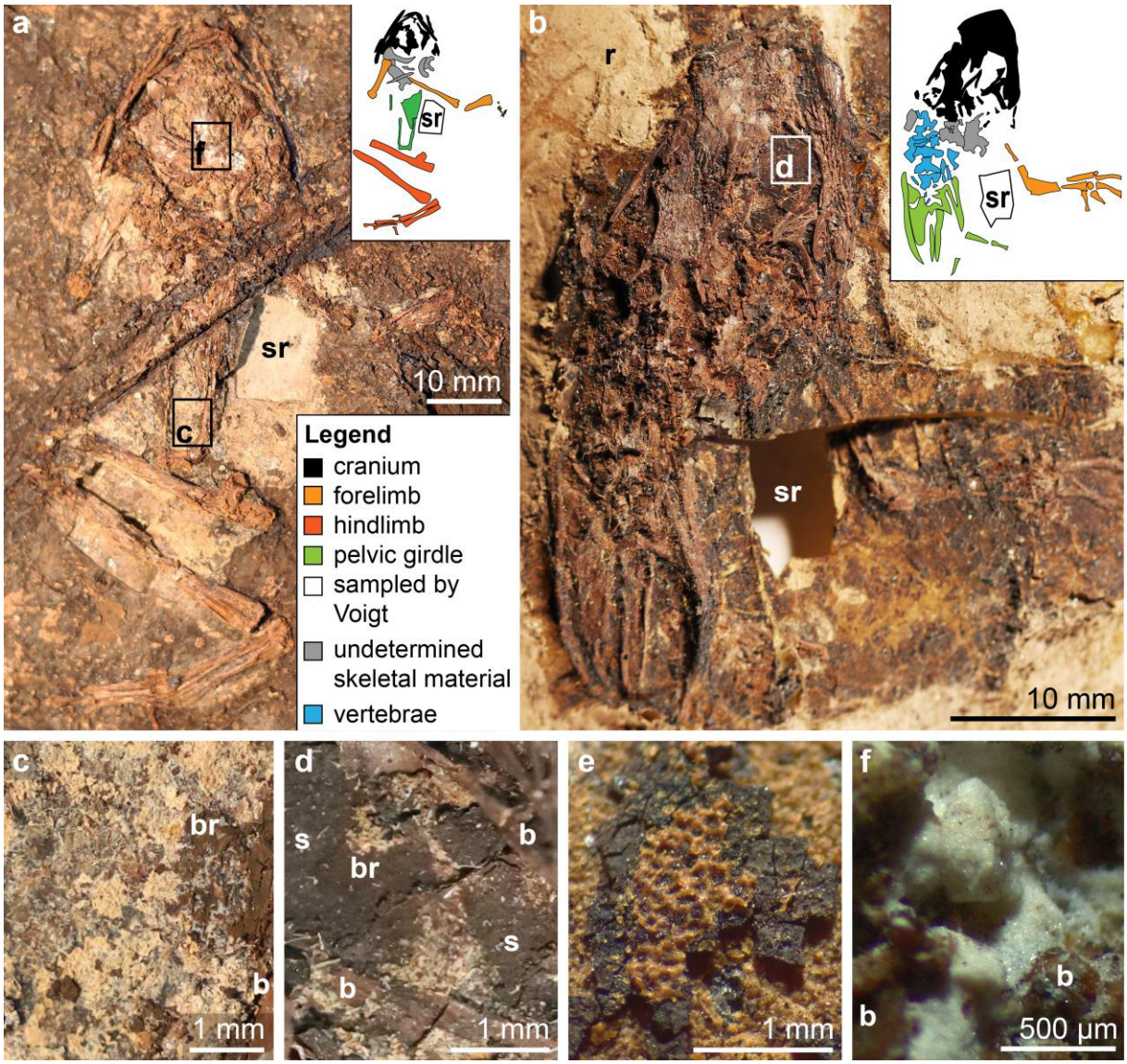


Figure 4.1: Soft tissue preservation in anurans from the Eocene Geiseltal biota. (a–b) Photographs of specimens showing extensive soft tissues, visible as a cream-colored friable material and/or a dark brown material. Boxes indicate regions shown in (c), (d) and (f). Insets show color-coded line drawings of the bones; Legend in (a) also applies to (b). (a) GMH CeIII-6698-1932 (Pelobatidae). The two parallel linear features crossing the torso are preparation artefacts. (b) GMH CeIII-6743-1932 (Pelobatidae). (c–f) Light micrographs showing details of the soft tissues. (c) Cream-colored, friable material overlain by thin brown material. (d) Dark grey-brown sediment (s) overlain by brown material and, in turn, the cream-colored material. Sediment and brown material are superficially similar in hand specimen but are readily distinguished using light microscopy and especially SEM. (e) GMH CeIII-4936a-1932 (Pelobatidae). Orange material with a striking honeycomb texture occurs in two layers, separated by a thick, blocky, dark brown material. (f) Pale, homogenous material in the cranium. b, bone, br, brown material, r, resin, s, sediment, sr, region sampled by Voigt.

EDS spectra of Layer 1 show peaks for carbon, oxygen and sulfur (Supplementary Figs. 4.1, 4.3). EPMA reveals a composition that includes sulfur, calcium and traces of oxygen, phosphorus, fluorine, and chlorine (Supplementary Table S4.3); these data confirm that Layer 1 is organic in character.

Layer 2 occurs in 70% of specimens (67% of palaeobatrachids and 83% of pelobatids). Within an individual specimen, it can occur in some, or all, of the following body regions: cranium (including eyespots), torso, abdomen and hindlimbs. It is 20–30 µm thick (Fig. 4.3h; Supplementary Fig. S4.2) and its preservation shows a spectrum between two end-member states. In 11% of specimens, Layer 2 is exclusively yellow to orange in color (Fig. 4.1b), cohesive, continuous and brittle, with a striking honeycomb texture (Fig. 4.1e); it can extend over an area of up to several square centimeters. The honeycomb texture includes both depressions in the surface of the layer plus perforations that expose the underlying Layer 1 (Fig. 4.1e; Supplementary Fig. S4.2). In 30% of specimens, Layer 2 is exclusively pale yellow, friable and discontinuous, with an amorphous texture (Figs. 4.1a,b,c,d, 4.3c; Supplementary Fig. S4.2). In 29% (n = 168) of specimens, both states of Layer 2 are present (Fig. 4.1a,b).

Where Layer 2 shows a cohesive texture, SEM analysis reveals three sublayers that can be discriminated on the basis of their texture. The outermost sublayer (2a) shows a pattern of perforations that expose the underlying Layer 1; the perforations are oval to irregular in shape and ca. 10–30 µm wide, with a spacing of 100–200 µm (Fig. 4.3a). High-magnification images of the external-facing surface of the layer reveal a network of oval to irregular-shaped microdepressions, each ca. 0.5 µm wide (Fig. 4.3e,i). The outer surface of the layer often shows clusters of spheroidal to ovoid microbodies, each ca. 0.5 µm long (Fig. 4.3e). The inner-facing surface of Layer 2 reveals Sublayers 2b and 2c (Fig. 4.3b,f,g). Sublayer 2b comprises densely packed fibers (each ca. 5–10 µm long and 2–3 µm wide) that are orientated (sub-)parallel to the layer surface (Figs. 4.2a, 4.3b,g,j; Supplementary Figs. S4.1, S4.2); some fibers are curved to sinuous (Fig. 4.3b,f), especially adjacent to the perforations that penetrate the layer. Each fiber comprises a chain of juxtaposed, poorly defined, globules each ca. 2–3 µm long (Figs. 4.2a, 4.3f,j);

each globule has a distinctive surficial microfabric formed by aligned ridges and grooves (Fig. 4.3j). This microfabric usually shows a consistent orientation in adjacent globules within a single fiber (Fig. 4.3j). Sublayer 2b transitions gradually to Sublayer 2c, the innermost sublayer (Figs. 4.2a, 4.3a,f,k). The latter is characterized by dispersed globules similar in shape, size and texture to those in Sublayer 2b (Figs. 4.3k, 4.4b). Where the plane of splitting removes the globules into the counterpart, the surface of the underlying Layer 1 shows external molds of the globules (Fig. 4.4b).

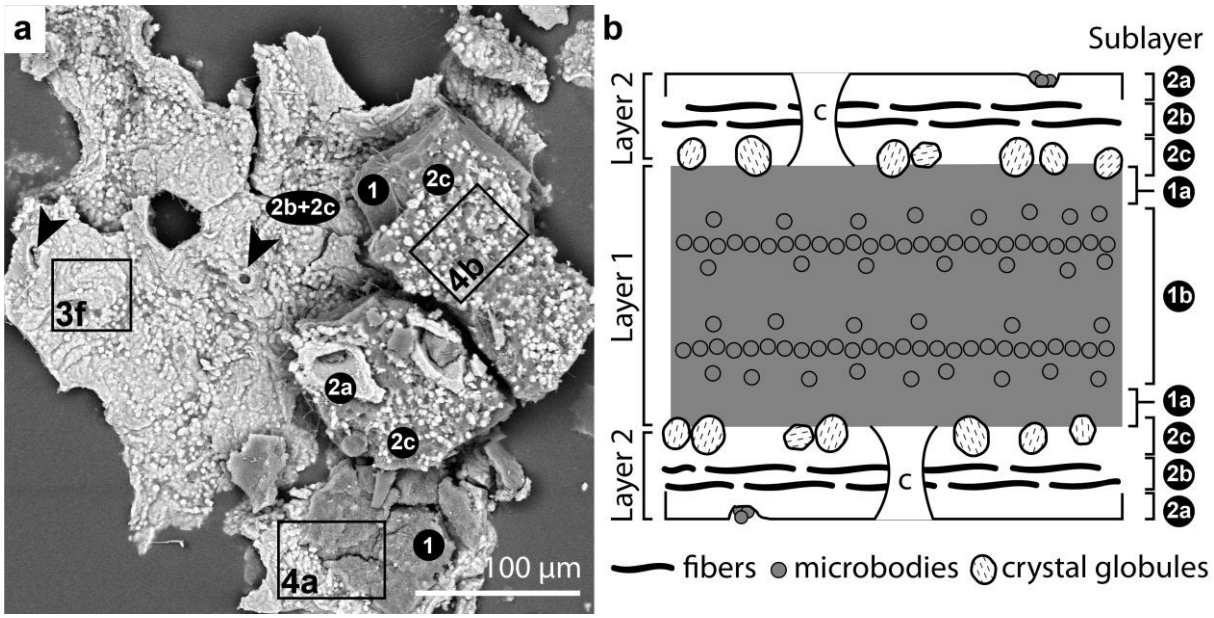


Figure 4.2: Succession of soft tissue layers in the Geiseltal anurans. (a) CeIII-4967-1932 (Pelobatidae). Backscatter electron image of a fractured sample of soft tissue. Not all soft tissue layers are continuous across the entire area of the sample. Bright-toned region in left center of image shows Layer 2 in ventral aspect, overlain by dark-toned Layer 1 (in right of image), which, in turn, is overlain by Layer 2. (b) Schematic vertical section of soft tissues. Layer 1 is sandwiched between two layers of Layer 2. Layer 2 comprises a thin, outer, amorphous sublayer (2a) underlain by a thicker fibrous sublayer (2b) and, in turn, an innermost sublayer defined by closely spaced crystal globules (2c). Layer 1 comprises an outer amorphous sublayer (1a) and an inner sublayer with zones of densely packed microbodies alternating with zones with rare microbodies (1b). c, position of centrifugal fibers.

EDS spectra from Layer 2 show peaks for calcium, phosphorus, oxygen and fluorine (Supplementary Figs. 4.1, 4.3); the composition of the layer is thus interpreted as calcium phosphate, with a likely (albeit

minor) component of fluorapatite. This composition is supported by EPMA (Supplementary Table S4.3), which reveals that Layer 2 has a composition consistent with apatite. In samples where Layer 1 and Layer 2 co-occur, EDS maps confirm the contrasting composition of Layer 1 and Layer 2 (Fig. 4.4a,b; Supplementary Fig. S4.1). FTIR spectra reveal peaks centered at 963 cm^{-1} (v_1PO_4), 1012 cm^{-1} (v_3PO_4) and 1456 cm^{-1} (v_3CO_3), consistent with carbonated hydroxyapatite (Fig. 4.5; Supplementary Table S4.4)[30-32]. Other peaks centered at 864 cm^{-1} (v_2CO_3), 1092 cm^{-1} (v_3PO_4), 1436 cm^{-1} and 1456 cm^{-1} (v_3CO_3; Fig. S4.5; Supplementary Table S4.4) are characteristic of carbonated fluorapatite (francolite)[30-32]. The material preserving Layer 2 therefore probably represents a mixture of both mineral phases. Notably, the v_2CO_3 band indicates a carbonate ion substitution for the phosphate tetrahedron (B-type substitution)[30], which suggests a biological apatite[30].

In 42% of specimens (47% of palaeobatrachids and 63% of pelobatids), a white material occurs in the posterior part of the cranium and along the vertebral column (Fig. 4.1a,f). SEM analysis reveals densely packed, short euhedral crystals (Fig. 4.3n; Supplementary Fig. S4.3). Individual crystals are ca. 1–30 µm long; some show evidence for multiple phases of growth (Supplementary Fig. S4.3). EDS spectra reveal peaks for calcium, oxygen, and carbon, consistent with calcium carbonate (Supplementary Fig. S4.3). This composition is supported by Raman spectra, which reveal a major peak at 1084 cm^{-1} ($v_1CO_3^{2-}$) and minor peaks at 152 cm^{-1}, 179 cm^{-1}, 205 cm^{-1} and 704 cm^{-1} ($v_4CO_3^{2-}$; Supplementary Fig. S4.3); this spectrum is characteristic of aragonite[33].

Differences between taxonomic groups in the number of specimens that show Layer 1, Layer 2 and the white material are not statistically significant (independent samples t-test, $p = 0.664$) and may reflect differences in sample size.

The vast majority of fossil-bearing sediments at Geiseltal have been previously characterized as “Weichbraunkohle” [soft brown coal] (Pickel and Wolf[34], p. 482). Our SEM, EDS, Raman and XRD data (for the sediment associated with the anurans) confirm a composition dominated by organic matter

with almost no detrital minerals such silicates or clays (Supplementary Note; Supplementary Fig. S4.5, Supplementary Table S4.5).

4.3 Discussion

The microstructures preserved in the soft tissues of the Geiseltal anurans can be interpreted in the context of soft tissue microstructures preserved in fossil vertebrates from other Konservat-Lagerstätten. The microbodies of Layer 1 resemble microstructures associated with other fossil vertebrates that were initially interpreted as fossil bacteria[17,35-37]. In recent years, however, microbodies with a similar geometry and spatial distribution associated with diverse fossil vertebrates have been interpreted as fossil melanosomes[19,38-42]; these interpretations are supported by extensive chemical evidence for fossil melanin[18,26,38,42,43]. Even though the melanosome hypothesis is now widely accepted, it is nonetheless important to investigate new fossil reports from first principles[44], as in the text that follows here.

The size and geometry of the fossil microbodies in the Geiseltal anurans (ca. 0.6 ± 0.4 µm long; Fig. 4.3e,m; Supplementary Fig. S4.1) are consistent with those of melanosomes preserved in other fossil anurans (ca. 0.6 µm long[42]; ca. 0.4–1.2 µm long[19,40]) and in extant anurans (ca. 0.2–1.5 µm long[42]), but also with modern bacteria (0.2–5 µm[45]). Interpretations of the nature of the fossil microbodies should therefore consider additional attributes, such as the spatial distribution of the microbodies, as follows. In decaying carcasses, bacteria can form external biofilms (derived from the integument and / or sediment) and internal biofilms (derived from the gut flora) that degrade soft tissues[46,47]. The external surface of Layer 2a (the outermost of the preserved soft tissue layers in the fossils), however, preserves only rare microbodies (Fig. 4.3e); most of the fossil microbodies are sandwiched between the two layers of Layer 2. This distribution of microbodies is not consistent with bacterial overgrowth of carcasses.

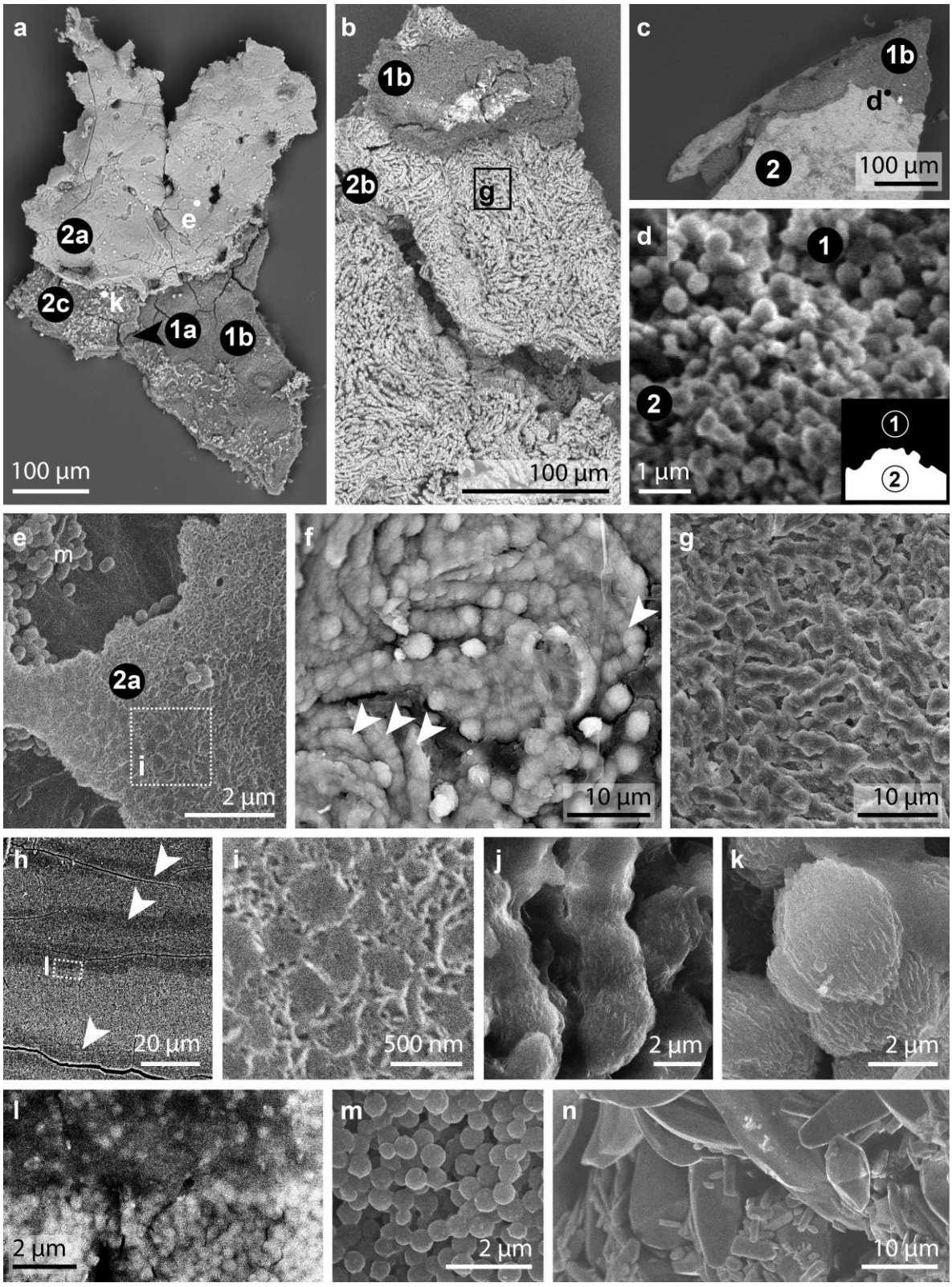


Figure 4.3: Electron micrographs of soft tissues in the Geiseltal anurans. (a–c), Backscatter electron images showing Layer 1 (dark tones) and Layer 2 (bright tones). (d–n), Secondary electron images (d,e,i,j,k,m,n) and backscatter electron images (f,g,h,l) showing microstructures. (a) Successive layers showing continuous amorphous outer surface of Layer 2 (Sublayer 2a) underlain by Sublayer 1a, in turn underlain by Sublayer 1b;

Sublayers 1a and 1b show polygonal cracking. The plane of splitting has exposed Sublayer 2c locally where Sublayers 2a and 2b separated into the counterpart. (b) Inner surface of Layer 2 showing curved to sinuous fibers of Sublayer 2b, overlain by Sublayer 1b (top of image). (c) Layer 2 underlain by Layer 1. (d) Detail of region indicated in c showing Layer 2 underlain by Layer 1. Layer 2 comprises small irregular granules that are often juxtaposed or conjoined. Layer 1 comprises round microbodies. (e) Detail of region indicated in (a), showing outer surface of Layer 2 with distinctive dimpled texture; see (i) for detail. Microbodies occur on the layer surface and in surface cavities. (f) Sinuous fibers of Layer 2 (Sublayer 2b) crudely defined by irregular globules of calcium phosphate (see j and k). (g) Detail of region indicated in (b). (h) Backscatter electron micrograph showing alternating microbody-poor (arrows) and microbody-rich sublayers in Layer 1 in the torso. (i) Detail of region indicated in e showing dimpled outer surface of Layer 2. (j) Detail of the fibers in Sublayer 2b showing closely spaced to juxtaposed, irregular, poorly defined globules with similar nanotexture to those in Sublayer 2c. (k) Close-up of individual globule from Sublayer 2c showing irregular surface and margins, with a poorly defined fibrillar nanotexture. (l), Detail of (h). Transition of microbody-rich to -poor sublayer in Layer 1. (m) Microbodies from Layer 1 in the torso. (n) Densely packed euhedral crystals comprising pale material in cranium. (a,e,f,i,k,m) GMH CeIII-4967-1932; (c,b,d,g,n) GMH CeIII-6698-1932; (h,j,l), GMH CeIII-4936a-1932.

Further, the stacking of successive microbody layers in Layer 1, where microbodies have size-specific geometries in each layer (Supplementary Fig. S4.1), is difficult to explain as a bacterially generated structure. Instead, this feature is consistent with a melanosome origin[20,44]: melanosomes in extant and fossil vertebrates have tissue-specific geometries[42]. Given that melanosomes are resistant to degradation[20,48], collapse of the soft tissues during decay and extended degradation of body tissues would therefore ultimately yield melanosome-rich tissue residues[20]. Size-specific layering can be generated where melanosomes from different tissues are superimposed, and where carcasses are not disturbed by bottom currents during exposure on the sediment surface[20]. In the Geiseltal anurans, the layering of microbodies from different populations (defined by geometry) is consistent with decay-induced layering of melanosomes derived from different tissues[42].

Collectively, these data indicate that the fossil microbodies are extremely unlikely to represent fossil bacteria; the microbodies are most parsimoniously interpreted as fossil melanosomes.

Several notable features of the Geiseltal melanosomes are treated briefly here. The melanosomes lack distinctive surface nanotextures, as reported in some modern melanosomes[19,37,49] and melanosomes from the Libros biota (Miocene, Spain)[18,19]. This may reflect a taxonomic and/or tissue-specific signal, enrichment in pheomelanin[37] or a low fidelity of preservation (taphonomic bias). Unlike the Libros anuran melanosomes, some of which are partially replaced in calcium phosphate[19], those in the Geiseltal anurans show no calcium phosphate mineralization. This likely reflects taphonomic differences between the two biotas, e.g., the availability of phosphate ions and the timing of phosphatization (see below). The layers of amorphous, melanosome-poor material that separate layers of melanosomes in the soft tissues (Fig. 4.3h,l; Supplementary Figure S4.1) are difficult to interpret conclusively. The amorphous layers may represent residues of tissues that had limited, or no, melanin *in vivo.* Alternatively, they may represent remains of degraded melanosomes[50].

The melanosomes of Layer 1 are rich in sulfur; this is consistent with the chemistry of melanosomes from other fossil biotas including Libros (Miocene, Spain[19]), Bolca (Eocene, Italy[39]) and Messel (Eocene, Germany[51]) and suggests preservation via sulfurization[19]. This process involves diagenetic incorporation of bacterially- or decay-generated sulfides (and / or polysulfides) into organic matter under anoxic conditions[52]. Sulfurized tissues are highly cross-linked and thus resistant to bacterial degradation[53]. Sulfurization is common in dysoxic to euxinic, organic-rich sediments deposited in restricted basins with a stratified water column and abundant bacterial sulfate reduction in the upper part of the sediment column[19]. In such settings, the source of sulfur is considered to be the organic-rich host sediment[19]. Preservation of the Geiseltal melanosomes via sulfurization is supported by the preservation of fossil latex (monkeyhair laticifers) in the laminated sediments[54]; this material is formed by natural low-temperature sulfurization of plant tissue at diagenetic temperatures of <100°C[55].

Layer 2 is interpreted as the mid-dermal Eberth-Katschenko (E-K) layer of anuran skin. In extant anurans, the E-K layer comprises collagen fibers, glycosaminoglycans, proteoglycans and calcium phosphate granules[56-59]. The layer is situated between the stratum spongiosum (of the outer dermis) and stratum compactum (of the inner dermis; Fig. 4.6). Centrifugal fibers perforate and traverse the E-K layer vertically, connecting the overlying stratum spongiosum with the underlying stratum compactum and hypodermis[56,57]. The columns form a regular pattern (spaced ca. 100–500 µm apart)[56,57,60]. As a result, the E-K layer in extant anurans shows a honeycomb pattern in plan view.

Layer 2 is interpreted as the preserved remains of the E-K layer based on the following features: (1) both the fossil layer and the E-K layer have a sharp, well-defined outer surface; (2) the irregular, poorly-defined inner surface of the fossil layer is consistent with the E-K layer in extant anurans, where collagen fibers of the layer interweave with those of the underlying stratum compactum[56,57]; (3) the fossil layer is ca. 3–30 µm thick (Fig. 4.3h); this range of thicknesses is consistent with that of the E-K layer in extant anurans (1–30 µm[57,58,61]); (4) The presence of two successive layers of Layer 2 in the fossils (Fig. 4.2a) is consistent with the superposition of the E-K layer from the dorsal and ventral skin during decay and collapse of the carcass; and (5) the size of the perforations and the perforation pattern (Fig. 4.1e; Supplementary Fig. S4.2) that form the honeycomb texture in the fossils are consistent with those of the centrifugal fibers in extant anurans (3–4 per 100 µm^2 and 10–50 µm in diameter in extant anurans)[56,57,60].

All of the above features also characterize the preserved E-K layer in fossil anurans from the Libros biota[18]; in addition, the collagen fibers preserved in fossils from both localities are usually sinuous where continuous. There are, however, a number of notable differences between the preserved features of the E-K layer in the Geiseltal anurans, those preserved in the Libros frogs and those described in extant anurans.

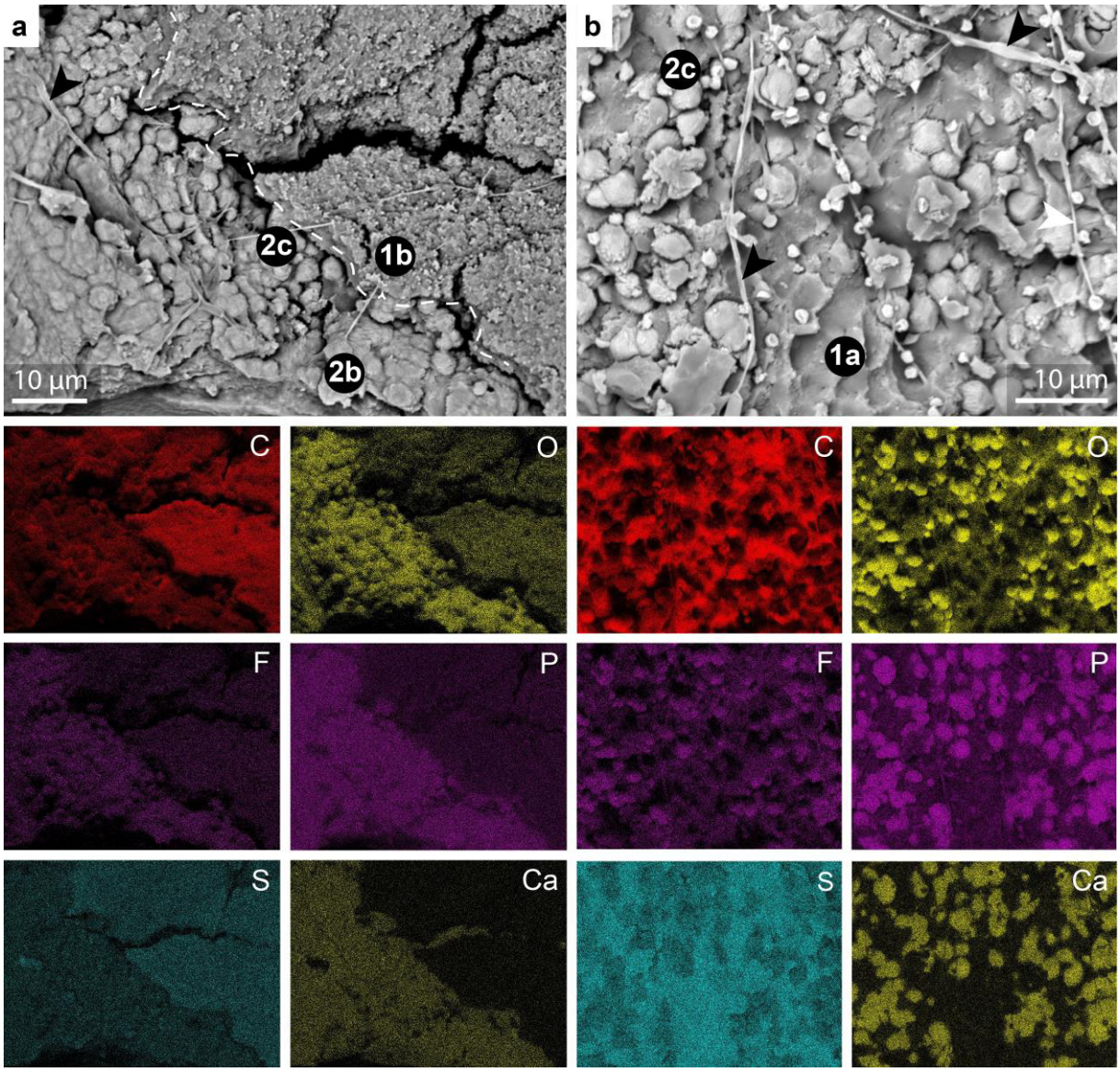


Figure 4.4: Chemical mapping of the soft tissues of GMH CeIII-4967-1932; see Methods for analytical parameters. (a–b) Backscatter electron images showing Layers 1 and 2. (a) shows Sublayers 1b, 2b and 2c. (b) shows Sublayers 1a and 2c. Elongate features on the sample surface are interpreted as fungal contaminants (arrowheads). (a) Sublayers 2b and 2c are enriched in Ca, P and O and, to a lesser extent, F. Sublayer 1b is enriched in C and S. (b) Irregular globules of Sublayer 2c (see also Fig. 4.3k) are enriched in Ca, P and O and, to a lesser extent, F. Sublayer 1a is enriched in C and S.

First, the constituent fibers of the E-K layer are thicker (ca. 2–4 µm thick; Fig. 4.3f,g,j) in the Geiseltal anurans than in the Libros and extant frogs. In extant frogs, the collagen fibers of the E-K layer are each ca. 0.1–2 µm thick[56,57,60]; the fibers in the Libros frogs are ca. 1–2 µm thick[18] and were thus interpreted

as preserved individual collagen fibers. The fibers in the Geiseltal anurans are shorter (ca. 10–20 µm; Fig. 4.3b,g) than those in the Libros frogs (ca. 20–100 µm[18]). Despite these differences, the Geiseltal fibers are considered to be best interpreted as individual collagen fibers and not fiber bundles; the latter would be expected to vary more in width than the preserved fibers.

The preserved E-K layer is replicated in calcium phosphate (Fig. 4.4a); no other soft tissues in the Geiseltal anurans share this mode of preservation. Phosphatization of soft tissues is controlled, at least in part, by the availability of phosphate ions (PO_4^{3-})[62-64] and thus the source(s) of phosphate ions must be considered. Selective preservation of the skin, the most surficial tissue of the body, would be consistent with (a) sedimentary source(s) of phosphate ions, e.g., sedimentary organic matter, biogenic apatite, benthic microbial mats and redox cycling of phosphorus by iron oxyhydroxides[65]. The mode of conservation of the specimens renders it difficult to completely exclude these potential sedimentary sources, as only limited volumes of sediment are available for analysis. Based on the sediment analyzed in this study, however, there is no evidence for sedimentary apatite, benthic microbial mats, iron minerals or abundant phosphate minerals (Supplementary Fig. S4.5, Supplementary Table S4.5); there is thus no obvious sedimentary source of phosphate.

The fine lamination of the sediment (Supplementary Fig. S4.4) suggests low sedimentation rates and extended exposure (weeks to months) of the specimens on the lake floor without being completely covered by sediment. If sedimentary organic matter were the primary phosphate source[66], specimens might therefore be expected to show preferential phosphatization of skin on only one side of the body (i.e., the surface in contact with the sediment)[65]. Further, this phosphate source might also be expected to result in the preservation of the epidermis and upper dermis (assuming that the outer skin layers have a similar propensity to bind calcium as the E-K layer collagen). Neither of these features, however, are present in the Geiseltal anurans.

In sum, the preservation of both the ventral and dorsal E-K layer, the restriction of phosphatization to this specific component of the skin and the lack of evidence for sedimentary phosphate are inconsistent with a sedimentary source of phosphate and instead collectively indicate an internal phosphate source, i.e., from inside the decaying carcass. Bones are an obvious phosphate source but show no evidence for dissolution; the phosphate must therefore have derived from the soft tissues.

Collagen is decay-resistant and readily promotes nucleation of calcium phosphate[18,62,67]. The E-K layer is rich in calcium phosphate granules *in vivo*[56,57,68] and thus contains a local phosphate source for the replication of the collagen fibers of the E-K layer (Fig. 4.6). The decreasing fidelity of fiber preservation from the external part of the E-K layer towards more internal zones is consistent with higher concentrations of calcium phosphate granules in the outer regions of the E-K layer, as in extant anurans[57,68]. The absence of other preserved soft tissues may reflect a lack of internal phosphate sources and/or the complete degradation of other tissues prior to phosphatization (possibly due to proximity to the source of decay bacteria). The skeletal taphonomy of the Geiseltal anurans indicates prolonged transport in surface waters and/or prolonged exposure on the lake floor[8]. This, plus warm surface water temperatures[8] may have facilitated (partial) decay of soft tissues, including connective tissues and internal organs, prior to deposition. The skin, however, is likely to have retained cohesion until late decay[69].

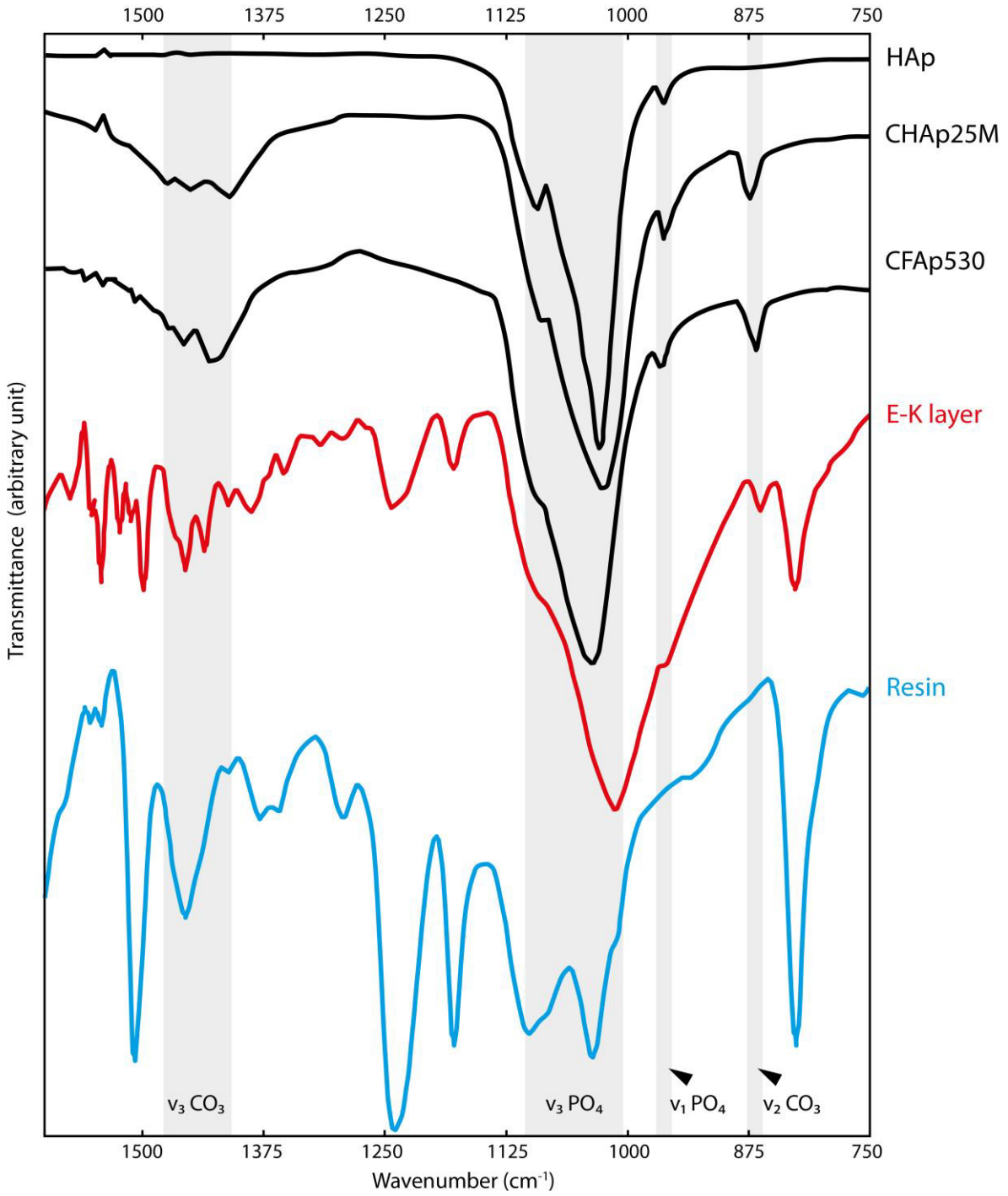


Figure 4.5: FTIR spectroscopy of the mineral phase that replicates the E-K Layer (GMH CeIII-4936a-1932; Pelobatidae). The FTIR spectrum of the E-K layer (red) shares several bands with spectra of carbonated hydroxyapatite (CHAp25M) and carbonated fluorhydroxyapatite (CFAp530). The peaks at 1509 cm^{-1}, 1242 cm^{-1}, 1180 cm^{-1}, and 828 cm^{-1} probably derive from the embedding resin (modified from Antonakos et al.[30]).

In our taphonomic model (Fig. 4.6), calcium and phosphate ions originated from the dissolution of E-K layer calcium phosphate granules during late decay[18]. This required pH <4[70,71]. Such conditions may exist, even in a highly localized fashion (i.e., as microenvironments[18]), in a carcass following the liberation of acidic byproducts of decay[72]. Rapid dissolution of the granules would have generated local high concentrations of phosphate. Reprecipitation of calcium phosphate (i.e., apatite) on collagen fibers of the E-K layer likely required a slightly higher pH value, but < pH 6.38 (i.e., below the carbonic acid dissociation constant) and where concentrations of dissolved phosphate in the tissue were sufficiently high to inhibit calcium carbonate precipitation[73]. The large crystals of calcium phosphate and associated low fidelity of preservation of the collagen fibers (Fig. 4.3j,k) likely reflects two factors: extended decay of the collagen fibers (yielding a low density of suitable nucleation points for calcium phosphate but generates space between nucleation points for increased crystal sizes) and local high phosphate concentrations, thus favoring crystal growth over nucleation. Continued growth and ultimately merging of adjacent crystals would have crudely replicated the (sinuous) morphology of the original fibers (Fig. 4.3f). Individual globules and short lengths of merged globules (Fig. 4.3k) in the lower E-K layer (Sublayer 2c) likely reflect lower concentrations, or later availability, of calcium phosphate during decay, precluding replication of entire fibers. Aligned nanotextures in adjacent globules (Fig. 4.3k) may reflect an underlying biomolecular/stereochemical template.

The epidermis, the upper dermis, and the centrifugal fibers (Fig. 4.2b) of the skin are not preserved. This suggests that the various cellular and non-cellular components of those soft tissues have a lower capacity to bind calcium than the E-K layer fibers and/or decayed completely before the tissue entered the phosphatization window.

In summary, our model for phosphatization of the E-K layer of the Geiseltal anurans comprises the following steps (Fig. 4.6): (1) extensive decay of the carcasses led to liquefaction of internal tissues, but only partial decay of collagen in the E-K layer. Other skin components may have been present. (2) The

release of acidic decay products locally lowered pH to <4 and dissolved the granules of the E-K layer. (3) Calcium and phosphate ions diffused the short distance to the E-K layer collagen fibers. (4) Calcium phosphate precipitated where pH <6.38 and the affinity of the collagen to bind calcium ions was high. (5) Any other remaining skin components decayed completely because they had a lower affinity for phosphate and/or the available phosphate was consumed by replication of the E-K layer collagen.

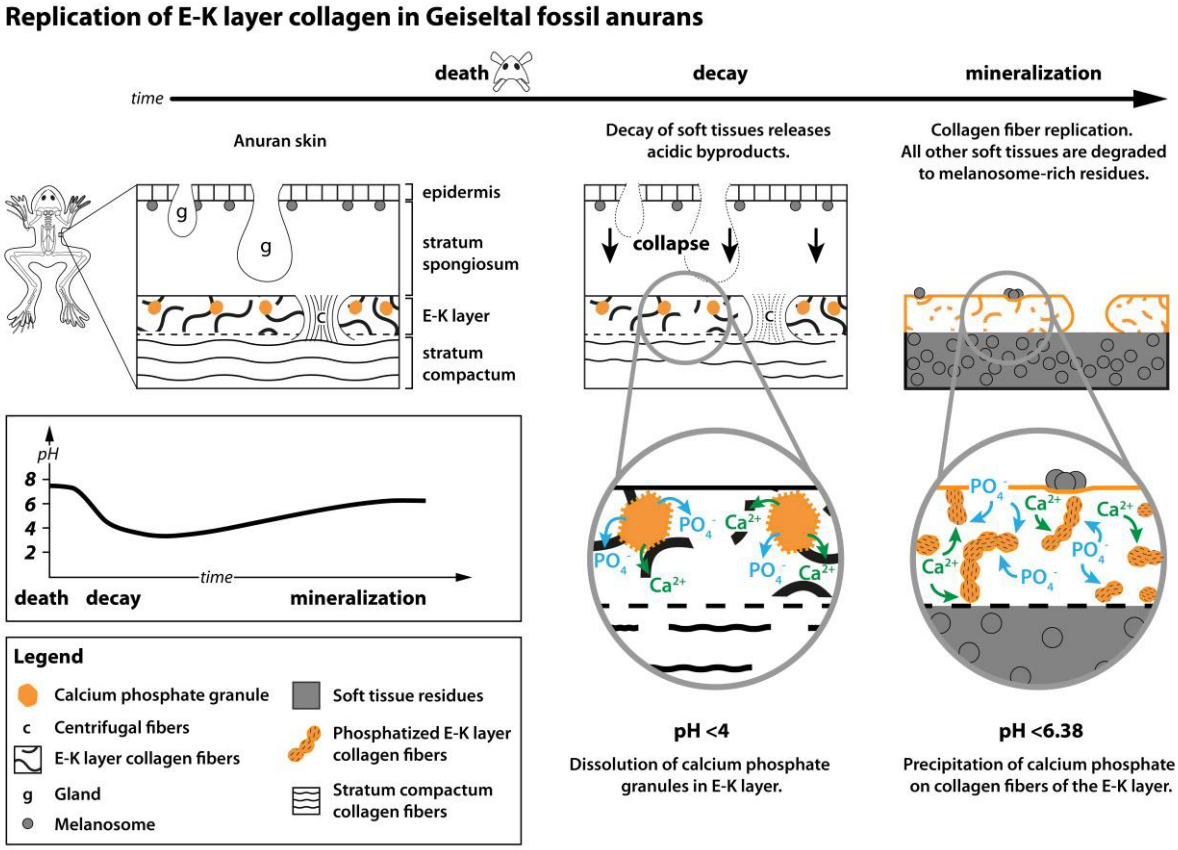


Figure 4.6: Taphonomic model for the preservation of the E-K layer in the Geiseltal anurans.

The location and size of the aragonite crystals in the cranium and along the vertebral column are consistent with those of crystals of the endolymphatic sac. In extant anurans, this organ encircles the hindbrain and forms cysts between each pair of successive vertebrae[74,75]; it stores and mobilizes calcium for skeletal development[74-76]. The sac contains several generations of aragonite crystals[74,76] that are similar in size (1–10 µm) and habit (euhedral, oval or elongated with broad peaks on both sides;

Fig. 4.3n)[74,76] to the crystals in the Geiseltal anurans (Fig. 4.3n). The masses of aragonite in the Geiseltal anurans are therefore likely to represent original crystals of the endolymphatic sac. This suggests local pH values > 6.38 for the duration of decay[72,73]. This decay microenvironment may have been promoted by the presence of bounding membranes during the early stages of decay (when most organic acids are liberated). In extant anurans the size of the endolymphatic reserves varies among families[77] and, within a single species (e.g., metamorphosing tadpoles of *Rana temporaria*), larger endolymphatic reserves are associated with high environmental calcium concentrations[75]. This suggests that Geiseltal anurans with particularly large volumes of aragonite crystals lived during periods where the lake waters were relatively rich in calcium.

Our analysis of the proportions of specimens that show the melanosome layer, the E-K layer and aragonite crystals – in particular, the absence of significant differences between palaeobatrachids and pelobatids – suggests that taxonomy does not impact preservation.

In both the Libros and Geiseltal anurans, the E-K-layer is replicated in calcium phosphate and envelopes melanosome-rich carbonaceous layers that are preserved via sulfurization. The fidelity of preservation of the E-K layer, however, is higher for Libros specimens; further, the melanosomes of Libros specimens are partially mineralized[19]. The higher fidelity of the Libros E-K layer collagen fibers relative to the Geiseltal specimens may reflect less decay prior to mineralization as (1) more intact collagen fibers would have more nucleation sites, thus limiting crystal growth and (2) lower concentrations of decay acids. For the Libros anurans, both elements would have constrained the growth of calcium phosphate crystals, facilitating finer replication of fibers than at Geiseltal. By the time the skin of the Geiseltal anurans entered the phosphatization window, it may not have been sufficiently intact to allow high fidelity replication.

Another contributing factor to this taphonomic variation may be the amount of phosphate ions present in the E-K layer *in vivo*: the layer varies in thickness and lateral extent among extant anurans[57,61].

In conclusion, our reinvestigation of the fossilized soft tissues of the Geiseltal anurans failed to find evidence for many tissue components reported formerly, i.e., bacteria, blood vessels, cellular details of the epidermis, collagen of the stratum spongiosum and stratum compactum, muscles, and pigment cells. Compounding this, there is no evidence for the preservation of soft tissues via silicification. We can, however, confirm the preservation of certain tissue- and ultrastructural features: melanosomes (preserved via sulfurization), collagen fibers of the mid-dermal E-K layer (replicated in calcium phosphate) and the aragonite crystals of the endolymphatic sac. Claims of a unique taphonomic history and an unusually high fidelity of preservation for the Geiseltal fossils are therefore unsupported, requiring reevaluation of the capacity of the fossil record to preserve labile vertebrate soft tissues as three-dimensional silica replacements. Instead, the Geiseltal biota highlights an emerging taphonomic pattern for fossil vertebrates in lacustrine ecosystems, i.e., body outlines defined (in whole or part) as melanosome films and localized mineralization of tissues in calcium phosphate, where microenvironments rich in phosphate develop during decay and where tissues have a high potential for phosphatization. This taphonomic pattern applies to biotas such as Las Hoyas (Cretaceous, Spain)[78,79], Ribesalbes (Miocene, Spain)[80], Libros (Miocene, Spain)[18,19] and Bechlejovice (Oligocene, Czech Republic)[80]. Our results highlight the importance of the reevaluation of historic fossil collections using modern techniques in order to unveil incorrect interpretations and scrutinize established scientific paradigms.

4.4 Methods

4.4.1 Fossil material

The middle Eocene Geiseltal locality is located ca. 20 km southwest of Halle (Saale) in Saxony-Anhalt, Germany. The geology of the site is reviewed in detail in Falk, et al.[8] and a summary is provided here.

In brief, the vast majority of Geiseltal fossil vertebrates are hosted within lignites, which occur at various intervals in a ca. 120 m thick succession of palustrine, limnic-palustrine and fluvial sediments[9,81,82]. The lignites were commercially exploited in a series of open cast mines for ca. 100 years and most anuran specimens were recovered during the 1930s[28,83]. The mines were flooded in 2003 and the fossiliferous sites are no longer accessible.

The Geiseltal Collection is housed in the Natural Sciences Collections (ZNS) of the Martin Luther University Halle-Wittenberg in Halle (Saale; Saxony-Anhalt, Germany). Most of the fossil anurans are conserved via the transfer method, whereby the bones and soft tissues (and sometimes patches of associated host sediment) were transferred to nitrocellulose glue or wax in order to facilitate long-term storage (see Falk, et al.[8] for details).

For this study, we examined 168 fossil anuran specimens from the Geiseltal Collection. The dataset (Supplementary Table S4.1) is identical as that used in Falk, et al.[8], comprising Pelobatidae (n = 54; which are predominantly terrestrial), Palaeobatrachidae (n = 15; which are predominantly aquatic) and anurans of undetermined affinity (n = 99). Some specimens may represent Discoglossidae[84,85]. All specimens represent post-tadpole developmental stages, but discrimination of adults, subadults and juveniles was not possible.

Specimens are usually well-articulated but vary in completeness[8]. Most specimens are conserved in nitrocellulose glue (Fig. 4.1a,b), with a minority in paraffin wax. One specimen is *in situ* in the original sedimentary matrix; the slab is conserved in water. Many specimens are associated with patches of dark organic-rich sediment (Fig. 4.1d). The distinction between this sedimentary matrix and potential soft tissue, however, is not always clear; it was not, therefore, assumed *a priori* that patches of dark material adjacent to the bones represent preserved soft tissue. Most slabs show residues of pale grey

clay at and close to the slab margins; these residues derive from the resin transfer process[8,86]. Some specimens are associated with plant remains (n = 33).

4.4.2 Scanning electron microscopy (SEM) and energy-dispersive X-ray spectroscopy (EDS) analysis

Small (1–2 mm^2) fragments of soft tissues were dissected from six specimens using sterile tools. Samples of sediment (dark material from regions beyond the body outline) were dissected from four specimens. Samples were mounted on aluminum stubs with carbon tape. Four samples of soft tissue were embedded in a low viscosity resin (Ted Pella Inc.) in a Memmert vacuum oven at 60–70°C until the desired hardness was achieved (48h–96h). Two sediment samples were dehydrated in the same vacuum oven at 60°C for 24 h, embedded in the above resin at 60°C for 72h, polished using a graded series of polishing plates (finishing with 1 µm diamond paste on silk) and mounted on Al stubs with carbon tape. Selected soft tissue and sediment samples were sputter coated with Au. Samples were analyzed using a JEOL IT100 VP-SEM at an accelerating voltage of 5–20 kV and a working distance of 6–10 mm for SEM images and at 10 kV and a working distance of 10 mm for EDS maps and spectra. Acquisition times of 30–45 min and a dwell time of 0.2 ms were used for EDS maps and an acquisition time of 120 s was used for EDS spectra.

4.4.3 X-ray diffraction (XRD) analysis

16 samples of sediment were selected for analysis. These samples are all dark in color and were distinguished from the soft tissues as they were collected from regions usually beyond the body outline. The samples are from 11 resin slabs, representing four stratigraphic intervals (nine anuran sites). For each sample, a small amount (0.1–2 g) of sediment was powdered manually with a sterile agate pestle and mortar. XRD analysis was performed using a PANalytical Empyrean Series 2 microprobe with a Co X-ray tube, a PIXcel1D detector and a single crystal Si substrate.

4.4.4 Electron microprobe analysis (EPMA)

One sample of soft tissues from the torso of specimen GMH CeIII-4936a-1932 was embedded in EpoThin 2 epoxy resin (Agar Scientific Ltd.), polished, carbon coated and analyzed with a CAMECA SX-5 FE electron microprobe. Certain measurements used a 5 nA beam with 10 µm spot size and a time-correction applied to Fluorine because of unstable count rates. All other measurements used a 2 nA beam and 10 µm spot size in order to minimize beam damage and a time-zero correction applied to all elements.

4.4.5 Micro-Fourier transform infrared spectroscopy (FTIR)

The sample for EPMA was used subsequently for FTIR analysis. The resin-embedded sample was polished using diamond paste (1 µm grit) to remove the carbon coating and EPMA beam damage. FTIR spectra were acquired from the freshly polished surface with a Perkin Elmer Spotlight 400i FTIR microscope system. An area of 100 x 100 µm was mapped using a spectral resolution of 4 cm^{-1}, a spatial resolution of 1.56 μm^2 and 128 repeats. Spectra were processed post-acquisition using Perkin Elmer SpectrumIMAGE (v. R.1.11.2.0016) and Spectrum IR (v. 10.7.2) software as follows. An atmospheric correction was applied to the dataset and twenty spectra were extracted from a region of the skin and from a region of the embedding resin. A single averaged spectrum was generated for each sample type (skin and embedding resin, respectively); these average spectra were then baseline-corrected using a standard (non-interactive) algorithm and smoothed by a factor of 10.

4.4.6 Micro-Raman spectroscopy

Samples of soft tissues and sediment were analyzed using a Renishaw InVia Qontor confocal Raman microscope. Analyses used a 50 mW DPSS (diode-pumped, solid-state) 532 nm laser at 1%, 10% or 50% laser strength with a 50x or 100x objective, an exposure time of 1 s or 10 s and 10–100 accumulations per spectrum. For some samples the analytical area was excited with a 30–60 s bleach prior to the acquisition of spectra in order to reduce the fluorescent background.

4.4.7 Statistical analysis

Standard statistical summary data were calculated using Microsoft Excel. The number of specimens with preserved soft tissues was expressed as a percentage of the total number of specimens (n = 168). Significance tests were performed with PAST (PAleontological STatistics) 4.15[87] using the independent samples t-test (α level = 0.05). Data were tested for normality and homogeneity prior to conducting the t-test.

4.5 Data availability

The datasets used during this study are part of the Supplementary Files. Additional data can be requested from the corresponding author.

4.6 References

1. Briggs, D. E. G. Konservat-Lagerstätten 40 years on: the exceptional becomes mainstream. *Paleontol. Soc. Pap.* **20**, 1–14, https://doi.org/10.1017/S1089332600002771 (2014).
2. Seilacher, A. *et al.* Sedimentological, ecological and temporal patterns of fossil Lagerstätten. *Phil. Trans. R. Soc. Lond. B* **311**, 5–24, https://doi.org/10.1098/rstb.1985.0134 (1985).
3. Muscente, A. D. *et al.* Exceptionally preserved fossil assemblages through geologic time and space. *Gondwana Res.* **48**, 164–188, https://doi.org/10.1016/j.gr.2017.04.020 (2017).
4. Hendy, A. J. W. Taphonomic overprints on Phanerozoic trends in biodiversity: lithification and other secular megabiases. In *Taphonomy* (eds. Allison, P. A. & Bottjer, D. J.) 19–77 (Springer, 2011).
5. Ring, S. J., Bocherens, H., Wings, O. & Rabi, M. Divergent mammalian body size in a stable Eocene greenhouse climate. *Sci. Rep.* **10**, 3987, https://doi.org/10.1038/s41598-020-60379-7 (2020).

6. Georgalis, G. L., Rabi, M. & Smith, K. T. Taxonomic revision of the snakes of the genera *Palaeopython* and *Paleryx* (Serpentes, Constrictores) from the Paleogene of Europe. *Swiss J. Palaeontol.* **18**, 1–140, https://doi.org/10.1186/s13358-021-00224-0 (2021).

7. Hellmund, M. The former Geiseltal Museum (1934–2011), the Eocene Geiseltal Fossilagerstätte (Germany) and the scientific meaning of Ben Barnes as a pioneer of systematic quantitative vertebrate excavations in the Geiseltal lignites. *Anu. do Inst. de Geocienc.* **41**, 108–119, https://dx.doi.org/10.11137/2018_1_108_119 (2018).

8. Falk, D., Wings, O. & McNamara, M. E. The skeletal taphonomy of anurans from the Eocene Geiseltal Konservat-Lagerstätte, Germany: insights into the controls on fossil anuran preservation. *Pap. Palaeontol.* **8,** 1–34, https://doi.org/10.1002/spp2.1453 (2022).

9. Krumbiegel, G., Rüffle, L. & Haubold, H. *Das eozäne Geiseltal: ein mitteleuropäisches Braunkohlenvorkommen und seine Pflanzen- und Tierwelt*. 227 pp. (A. Ziemsen Verlag, 1983).

10. Voigt, E. Preservation of soft tissues in the Eocene lignite of the Geiseltal near Halle (Saale). *Cour. Forschungsinst. Senckenberg* **107**, 325–343 (1988).

11. Wilde, V. & Hellmund, M. First record of gut contents from a middle Eocene equid from the Geiseltal near Halle (Saale), Sachsen-Anhalt, Central Germany. *Palaeobiodivers. Palaeoenviron.* **90**, 153–162, https://doi.org/10.1007/s12549-010-0028-ymc (2010).

12. Voigt, E. Die Fische aus der mitteleozänen Braunkohle des Geiseltales mit besonderer Berücksichtigung der Weichteile. *Nova Acta Leopold. NF* **2**, 21–146 (1934).

13. Voigt, E. Die Erhaltung von Epithelzellen mit Zellkernen, von Chromatophoren und Corium in fossiler Froschhaut aus der mitteleozänen Braunkohle des Geiseltales. *Nova Acta Leopold. NF* **3**, 339–360 (1935).

14. Voigt, E. Weichteile an Säugetieren aus der eozänen Braunkohle des Geiseltales. *Nova Acta Leopold. NF* **4**, 301–310 (1936).

15. Voigt, E. Über das Haarkleid einiger Säugetiere aus der mitteleozänen Braunkohle des Geiseltales. *Nova Acta Leopold. NF* **4**, 317–335 (1936).

16. Voigt, E. Weichteile an Fischen, Amphibien und Reptilien aus der eozänen Braunkohle des Geiseltales. *Nova Acta Leopold. NF* **5**, 116–142 (1937).

17. Mrugowsky, J. Über fossile Bakterien aus dem Mitteleozän des Geiseltales. *Nova Acta Leopold. NF* **3**, 597–603 (1936).

18. McNamara, M. E. *et al.* Soft-tissue preservation in Miocene frogs from Libros, Spain: insights into the genesis of decay microenvironments. *Palaios* **24**, 104–117, https://doi.org/10.2110/palo.2008.p08-017r (2009).

19. McNamara, M. E., van Dongen, B. E., Lockyer, N. P., Bull, I. D. & Orr, P. J. Fossilization of melanosomes via sulfurization. *Palaeontology* **59**, 337–350, https://doi.org/10.1111/pala.12238 (2016).

20. McNamara, M. E. *et al.* Fossilized skin reveals coevolution with feathers and metabolism in feathered dinosaurs and early birds. *Nat. Commun.* **9**, 2072, https://doi.org/10.1038/s41467-018-04443-x (2018).

21. Butts, S. H. Silicification. *Paleontol. Soc. Pap.* **20**, 15–34, https://doi.org/10.1017/S1089332600002783 (2014).

22. Channing, A., Schweitzer, M. H., Horner, J. R. & McEneaney, T. A silicified bird from Quaternary hot spring deposits. *Proc. R. Soc. B* **272**, 905–911, https://doi.org/10.1098/rspb.2004.2989 (2005).

23. Butts, S. H. & Briggs, D. E. Silicification through time. In *Taphonomy* (eds. Allison, P. A. & Bottjer, D. J.) 411–434 (Springer, 2011).

24. Zhao, T., Hu, L. & Pan, Y. Silicification of feathers in a modern hot spring in New Zealand. *Earth Environ. Sci. Trans. R. Soc. Edinburgh* **113**, 119–125, https://doi.org/10.1017/S1755691022000068 (2022).

25. Glass, K. *et al.* Direct chemical evidence for eumelanin pigment from the Jurassic period. *Proc. Natl. Acad. Sci.* **109**, 10218–10223, http://doi.org/10.1073/pnas.1118448109 (2012).

26. Lindgren, J. *et al.* Molecular preservation of the pigment melanin in fossil melanosomes. *Nat. Commun.* **3**, 1–7, http://dx.doi.org/10.1038/ncomms1819 (2012).

27. Vinther, J., Briggs, D. E., Prum, R. O. & Saranathan, V. The colour of fossil feathers. *Biol. Lett.* **4**, 522–525, https://doi.org/10.1098/rsbl.2008.0302 (2008).

28. Kuhn, O. Die eozänen Anura aus dem Geiseltale nebst einer Übersicht über die fossilen Gattungen. *Nova Acta Leopold. NF* **10**, 345–376 (1941).

29. Brenner, H. Paläophysiologische Untersuchungen an der fossilen Muskulatur aus der eozänen Braunkohle des Geiseltales bei Halle (Saale). *Nova Acta Leopold. NF* **7**, 95–118 (1939).

30. Antonakos, A., Liarokapis, E. & Leventouri, T. Micro-Raman and FTIR studies of synthetic and natural apatites. *Biomaterials* **28**, 3043–3054, https://doi.org/10.1016/j.biomaterials.2007.02.028 (2007).

31. Regnier, P., Lasaga, A., Berner, R., Han, O. & Zilm, K. Mechanism of CO_3^{2-} substitution in carbonate-fluorapatite: evidence from FTIR spectroscopy, ^{13}C NMR, and quantum mechanical calculations. *Am. Mineral.* **79**, 809–818, https://doi.org/10.2138/am-1996-3-425 (1994).

32. Vandeginste, V., Cowan, C., Gomes, R. L., Hassan, T. & Titman, J. Natural fluorapatite dissolution kinetics and Mn^{2+} and Cr^{3+} metal removal from sulfate fluids at 35 °C. *J. Hazard. Mater.* **389**, 1–14, https://doi.org/10.1016/j.jhazmat.2020.122150 (2020).

33. Urmos, J., Sharma, S. K. & Mackenzie, F. T. Characterization of some biogenic carbonates with Raman spectroscopy. *Am. Mineral.* **76**, 641–646, http://www.minsocam.org/ammin/AM76/AM76_641.pdf (1991).

34. Pickel, W. & Wolf, M. Kohlenpetrographische und geochemische Charakterisierung von Braunkohlen aus dem Geiseltal (DDR). *Erdöl, Kohle, Erdgas, Petrochem.* **42**, 481–484 (1989).

35. Lindgren, J. *et al.* Biochemistry and adaptive colouration of an exceptionally preserved juvenile fossil sea turtle. *Sci. Rep.* **7**, 1–13, https://doi.org/10.1038/s41598-017-13187-5 (2017).

36. Toporski, J. K. W. *et al.* Morphologic and spectral investigation of exceptionally well-preserved bacterial biofilms from the Oligocene Enspel formation, Germany. *Geochim. Cosmochim. Acta* **66**, 1773–1791, https://doi.org/10.1016/S0016-7037(01)00870-5 (2002).

37. Moyer, A. E. *et al.* Melanosomes or microbes: testing an alternative hypothesis for the origin of microbodies in fossil feathers. *Sci. Rep.* **4**, 1–9, https://doi.org/10.1038/srep04233 (2014).

38. McNamara, M. *et al.* Decoding the evolution of melanin in vertebrates. *Trends Ecol. Evol.* **36**, 430–443, https://doi.org/10.1016/j.tree.2020.12.012 (2021).

39. Rossi, V., Unitt, R., McNamara, M., Zorzin, R. & Carnevale, G. Skin patterning and internal anatomy in a fossil moonfish from the Eocene Bolca Lagerstätte illuminate the ecology of ancient reef fish communities. *Palaeontology* **65**, 1–11, https://doi.org/10.1111/pala.12600 (2022).

40. Zhang, F. *et al.* Fossilized melanosomes and the colour of Cretaceous dinosaurs and birds. *Nature* **463**, 1075–1078, https://doi.org/10.1038/nature08740 (2010).

41. McNamara, M. E. *et al.* Non-integumentary melanosomes can bias reconstructions of the colours of fossil vertebrates. *Nat. Commun.* **9**, 1–9, https://doi.org/10.1038/s41467-018-05148-x (2018).

42. Rossi, V., McNamara, M. E., Webb, S. M., Ito, S. & Wakamatsu, K. Tissue-specific geometry and chemistry of modern and fossilized melanosomes reveal internal anatomy of extinct vertebrates. *Proc. Natl. Acad. Sci.* **116**, 17880–17889, https://doi.org/10.1073/pnas.1820285116 (2019).

43. Vinther, J. Fossil melanosomes or bacteria? A wealth of findings favours melanosomes. *Bioessays* **38**, 220–225, https://doi.org/10.1002/bies.201500168 (2016).

44. Lindgren, J. *et al.* Interpreting melanin-based coloration through deep time: a critical review. *Proc. R. Soc. B* **282**, 20150614, https://doi.org/10.1098/rspb.2015.0614 (2015).

45. Marshall, W. F. *et al.* What determines cell size? *BMC Biol.* **10**, 1–22, https://doi.org/10.1186/1741-7007-10-101 (2012).

46. Iniesto, M., Villalba, I., Buscalioni, A., Guerrero, M. & López-Archilla, A. The effect of microbial mats in the decay of anurans with implications for understanding taphonomic processes in the fossil record. *Sci. Rep.* **564**, 1–18, https://doi.org/10.1038/srep45160 (2017).

47. Butler, A. D., Cunningham, J. A., Budd, G. E. & Donoghue, P. C. J. Experimental taphonomy of *Artemia* reveals the role of endogenous microbes in mediating decay and fossilization. *Proc. R. Soc. B* **282**, 1–10, https://doi.org/doi:10.1098/rspb.2015.0476 (2015).

48. McNamara, M. E. The taphonomy of colour in fossil insects and feathers. *Palaeontology* **56**, 557–575, https://doi.org/10.1111/pala.12044 (2013).

49. Akazaki, S. *et al.* Three-dimensional analysis of melanosomes isolated from B16 melanoma cells by using ultra high voltage electron microscopy. *Microscopy Res.* **2**, 1–8, http://dx.doi.org/10.4236/mr.2014.21001 (2014).

50. Slater, T. S., Edwards, N. P., Webb, S. M., Zhang, F. & McNamara, M. E. Preservation of corneous β-proteins in Mesozoic feathers. *Nat. Ecol. Evol.* **7**, 1706–1713, https://doi.org/10.1038/s41559-023-02177-8 (2023).

51. Rossi, V., Webb, S. M. & McNamara, M. E. Hierarchical biota-level and taxonomic controls on the chemistry of fossil melanosomes revealed using synchrotron X-ray fluorescence. *Sci. Rep.* **10**, 1–10, https://doi.org/10.1038/s41598-020-65868-3 (2020).

52. Sinninghe Damsté, J. S., Kok, M. D., Köster, J. & Schouten, S. Sulfurized carbohydrates: an important sedimentary sink for organic carbon? *Earth Planet. Sci. Lett.* **164**, 7–13, https://doi.org/10.1016/S0012-821X(98)00234-9 (1998).

53. Goldstein, G. *et al.* Bacterial degradation of black and white feathers. *Auk* **121**, 656–659, https://doi.org/10.1093/auk/121.3.656 (2004).

54. McCoy, V. E. *et al.* Fossilisation of the Eocene "monkeyhair" laticifer tree from Geiseltal, Germany: a deeper understanding using micro-CT and pyrolysis GC/MS. *Palaios* **36**, 1–14, https://doi.org/10.2110/palo.2020.052 (2021).

55. Lönartz, M. I., McCoy, V. E., Gee, C. T. & Geisler, T. Palaeoenvironmental conditions for the natural vulcanization of the Eocene “monkeyhair” laticifers from Geiseltal, Germany, as elucidated by Raman spectroscopy. *Palaeobiodivers. Palaeoenviron.*, 1–13, https://doi.org/10.1007/s12549-022-00566-8 (2023).

56. Elkan, E. Mucopolysaccharides in the anuran defence against desiccation. *J. Zool.* **155**, 19–53, https://doi.org/10.1111/j.1469-7998.1968.tb03028.x (1968).

57. Ponssa, M. L., Barrionuevo, J. S., Pucci Alcaide, F. & Pucci Alcaide, A. Morphometric variations in the skin layers of frogs: an exploration into their relation with ecological parameters in *Leptodactylus* (Anura, Leptodactylidae), with an emphasis on the Eberth-Kastschenko layer. *Anat. Rec.* **300**, 1895–1909, https://doi.org/10.1002/ar.23640 (2017).

58. Azevedo, R. A. *et al.* Structural aspects of the Eberth-Katschenko layer of *Bufo ictericus* integument: histochemical characterization and biochemical analysis of the cutaneous calcium (Amphibian, Bufonidae). *Micron* **36**, 61–65, https://doi.org/10.1016/j.micron.2004.06.004 (2005).

59. Elkan, E. Ground substance: an anuran defense against desiccation. *Physiology of the Amphibia* **3**, 101–110 (1976).

60. Zanger, K., Schwinger, G. & Greven, H. Mechanical properties of the skin of *Rana esculenta* (Anura, Amphibia) with some notes on structures related to them. *Ann. Anat.* **177**, 509–514, https://doi.org/10.1016/S0940-9602(11)80082-8 (1995).

61. Mangione, S., Garcia, G. & Cardozo, O. M. The Eberth–Katschenko layer in three species of ceratophryines anurans (Anura: Ceratophrydae). *Acta Zool.* **92**, 21–26, https://doi.org/10.1111/j.1463-6395.2009.00442.x (2011).

62. Briggs, D. E. G., Kear, A. J., Martill, D. M. & Wilby, P. R. Phosphatization of soft-tissue in experiments and fossils. *J. Geol. Soc.* **150**, 1035–1038, https://doi.org/10.1144/gsjgs.150.6.1035 (1993).

63. Sagemann, J., Bale, S. J., Briggs, D. E. G. & Parkes, R. J. Controls on the formation of authigenic minerals in association with decaying organic matter: an experimental approach. *Geochim. Cosmochim. Acta* **63**, 1083–1095, https://doi.org/10.1016/S0016-7037(99)00087-3 (1999).

64. Derek, E. G. B. & Kear, A. J. Decay and mineralization of shrimps. *Palaios* **9**, 431–456, https://doi.org/10.2307/3515135 (1994).

65. Wilby, P. R., Briggs, D. E. G., Bernier, P. & Gaillard, C. Role of microbial mats in the fossilization of soft tissues. *Geology* **24**, 787–790, http://dx.doi.org/10.1130/0091-7613(1996)024<0787:ROMMIT>2.3.CO;2 (1996).

66. Lucas, J. & Prévôt, L. The synthesis of apatite by bacterial activity: mechanism. *Sci. Geol. Met.* **77**, 83–92 (1985).

67. Nudelman, F., Lausch, A. J., Sommerdijk, N. A. J. M. & Sone, E. D. In vitro models of collagen biomineralization. *J. Struct. Biol.* **183**, 258–269, https://doi.org/10.1016/j.jsb.2013.04.003 (2013).

68. Katchburian, E. *et al.* Mineralized dermal layer of the Brazilian tree-frog *Corythomantis greeningi*. *J. Morphol.* **248**, 56–63, https://doi.org/10.1pi002/jmor.1020 (2001).

69. Wuttke, M. Aktuopaläontologische Studien über den Zerfall von Wirbeltieren. Teil I: Anura. *Senckenbergiana Lethaea* **64**, 529–560 (1983).

70. Kootstra, A. M. J., Brilman, D. W. F. & Kersten, S. R. A. Dissolution of phosphate from pig manure ash using organic and mineral acids. *Waste Manage.* **88**, 141–146, https://doi.org/10.1016/j.wasman.2019.03.038 (2019).

71. Smith, E. A., Mayfield, C. I. & Wong, P. T. S. Physical and chemical characterization of selected natural apatites in synthetic and natural aqueous solutions. *Water Air Soil Pollut.* **8**, 401–415, https://doi.org/10.1007/BF00228655 (1977).

72. Briggs, D. E. & Wilby, P. R. The role of the calcium carbonate-calcium phosphate switch in the mineralization of soft-bodied fossils. *J. Geol. Soc.* **153**, 665–668, https://doi.org/10.1144/gsjgs.153.5.0665 (1996).

73. Briggs, D. E. G. The role of decay and mineralization in the preservation of soft-bodied fossils. *Annu. Rev. Earth Planet. Sci.* **31**, 275–301, https://doi.org/10.1146/annurev.earth.31.100901.144746 (2003).

74. Pich, A. A. & Sanchez, C. R. Clinical challenge: the endolymphatic system in the Denny's tree frog (*Polypedates dennysi*). *J. Zoo Wildl. Med.* **48**, 602–606, https://doi.org/10.1638/2016-0110.1 (2017).

75. Pilkington, J. & Simkiss, K. The mobilization of the calcium carbonate deposits in the endolymphatic sacs of metamorphosing frogs. *J. Exp. Biol.* **45**, 329–341, https://doi.org/10.1242/jeb.45.2.329 (1966).

76. Kawamata, S. Growth aspects of calcium carbonate crystals of the endolymphatic sac in the tree frog (*Hyla arborea japonica*): A pulse-chase study. *Microscopy* **36**, 392–397, https://doi.org/10.1093/oxfordjournals.jmicro.a050646 (1987).

77. Coleman, R. Ultrastructural observations on the parathyroid glands of *Xenopus laevis* Daudin. *Z. Zellforsch.* **100,** 201–214, https://doi.org/10.1007/BF00343880 (1969).

78. Navalón, G., Marugán-Lobón, J., Chiappe, L. M., Luis Sanz, J. & Buscalioni, Á. D. Soft-tissue and dermal arrangement in the wing of an Early Cretaceous bird: Implications for the evolution of avian flight. *Sci. Rep.* **5**, 1–7, https://doi.org/10.1038/srep14864 (2015).

79. Gupta, N. S. *et al.* Molecular taphonomy of macrofossils from the Cretaceous Las Hoyas Formation, Spain. *Cretac. Res.* **29**, 1–8, https://doi.org/10.1016/j.cretres.2006.12.009 (2008).

80. McNamara, M. E. *Comparative taphonomy of lacustrine-hosted exceptional faunas from the Miocene of NE Spain*, PhD thesis, University College Dublin, (2007).

81. Blumenstengel, H. 3.5 Tertiär. In *Erläuterungen zur Geologischen Karte 1:25 000 von Sachsen-Anhalt (GK 25), Blatt Mücheln (Geiseltal)* (eds Wansa S. & Radzinski, K.), 143 pp. (Landesamt für Geologie und Bergwesen Sachsen-Anhalt, Halle (Saale), Germany, 2004).

82. Hellmund, M. & Hastings, A. K. Part II - The Eocene Geiseltal Fossillagerstätte (Central Germany) and its vertebrate fossil fauna with 13 figures and 1 table. In *Messel and Geiseltal:*

Highlights from the Cenozoic; Excursion Guide SVP 2014 (eds Smith, K. T., Lehmann T., Hellmund, M. & Hastings, A. K.) 25–46 (Senckenberg Research Institute and Natural History Museum Frankfurt, 2014).

83. Weigelt, J. Die Biostratonomie der 1932 auf der Grube Cecilie im mittleren Geiseltal ausgegrabenen Leichenfelder. *Nova Acta Leopold. NF* **1**, 157–174 (1933).

84. Rage, J.-C. & Roček, Z. Evolution of anuran assemblages in the tertiary and quaternary of europe, in the context of palaeoclimate and palaeogeography. *Amphibia-Reptilia* **24**, 133–167, https://doi.org/10.1163/156853803322390408 (2003).

85. Roček, Z. Mesozoic and Tertiary anura of Laurasia. *Palaeobiodivers. Palaeoenviron.* **93**, 397–439, https://doi.org/10.1007/s12549-013-0131-y (2013).

86. Voigt, E. Die Übertragung fossiler Wirbeltierleichen auf Zellulose-Filme, eine neue Bergungsmethode für Wirbeltiere aus der Braunkohle. *PalZ* **15**, 72–78, https://doi.org/10.1007/bf03041642 (1933).

87. Hammer, Ø., Harper, D. A. T. & Ryan, P. D. PAST: Paleontological statistics software package for education and data analysis. *Palaeontologia Electronica* **4**, 1–9, https://www.nhm.uio.no/english/research/resources/past/ (2001).

4.7 Acknowledgements

We thank the Natural Sciences Collections team in Halle (Saale, Germany), especially Frank Steinheimer and Michael Stache, for access to the Geiseltal collections and databases and for useful historical information; Bianca Bernstein (Museum Weißenfels, Germany) and Naomi O'Reilly (University College Cork, Ireland) for assistance and advice; Peter Chung, Valentina Rossi (both University College Cork, Ireland) and Ninon Robin (French National Centre for Scientific Research, France) for assistance, advice and training; Katherine Clayton for X-Ray Diffraction analysis and Andrew Matzen for EPMA (both University of Oxford, UK). The research was funded by a Government of Ireland-Irish Research Council

(IRC) Postgraduate Scholarship GOIPG/2018/3354 and an International Association of Sedimentologists (IAS) Postgraduate Research Grant, both awarded to DF; MMN was funded by European Research Council Consolidator Grant ERC-COG-2020-1010003293-PALAEOCHEM.

4.8 Author contributions

Conceptualization MMN, OW, DF; Data curation DF, MMN; Formal analysis DF, RU, MMN, JW; Funding acquisition MMN, DF; Investigation DF, MMN, RU, JW; Methodology MMN, OW, DF; Project administration MMN; Resources OW, MMN, RU, JW; Software DF, MMN, RU; Supervision MMN, OW; Validation MMN, OW, DF, RU, JW; Visualization DF, MMN; Writing – original draft – DF, MMN; Writing – review & editing –MMN, DF, OW, RU, JW.

4.9 Competing interests

The authors declare no competing interests.

4.10 Supplementary information

The Supplementary information can be found online at https://doi.org/10.1038/s41598-024-55822-y.

4.10.1 Sediment analysis

Most of the Geiseltal anurans are conserved on resin slabs, where original sedimentary matrix is usually preserved as patches of a dark brown to black homogenous material; these patches are usually a few square millimeters wide and 1–2 mm thick (Fig. 4.1d). Sediment patches are usually more abundant, larger (a few square centimeters wide) and thicker (a few millimeters thick) where specimens are

conserved on gypsum and in paraffin wax. The sediment is brittle and shows polygonal cracking, where fragments can show a vitreous, coal-like fracture surface.

Specimen GMH XXXV-11-1970 is conserved in a slab of host sediment (approximately 10 x 10 cm) and stored in water. The sediment is homogeneous, dark brown to black, fine grained, and shows mm-scale lamination (Supplementary Fig. S4.5). Laminae are planar and continuous. The splitting surface reveals several macroscopic plant remains (i.e., leaves) adjacent to the specimen, but there is no preferential orientation of the plant material and no sedimentary clasts or grains are visible; there is, therefore, no evidence for substantial sediment input or water flow.

Raman spectroscopy of powdered sediment samples of GMH XXXV-11-1970 and GMH CeI-4947-1930 failed to identify minerals; the sediment samples showed evidence of thermal damage even at extremely low laser power, which is consistent with a sediment composition dominated by organic matter. EDS spectra of five powdered samples show major peaks for oxygen and sulfur; some spectra also show a minor peak for calcium. XRD analysis of 16 samples failed to yield quantitative mineralogical data, most likely due to the organic-rich nature of the sediment, but detected quartz, aragonite, calcite, hydroxyapatite, gypsum and illite/smectite in various samples at concentrations close to detection limits (Supplementary Table S4.5). The minor quantities of quartz present may reflect minor sediment input; calcite and aragonite may derive from precipitation and hydroxyapatite may derive from phosphate minerals in the sediment or bone fragments. Gypsum and illite/smectite probably represent contamination during conservation. Although the sediment samples are from anuran specimens that represent five fossil excavation sites and four stratigraphic intervals, there are no major differences in composition among the samples (as evidenced by SEM, EDS, XRD and microscopic analysis).

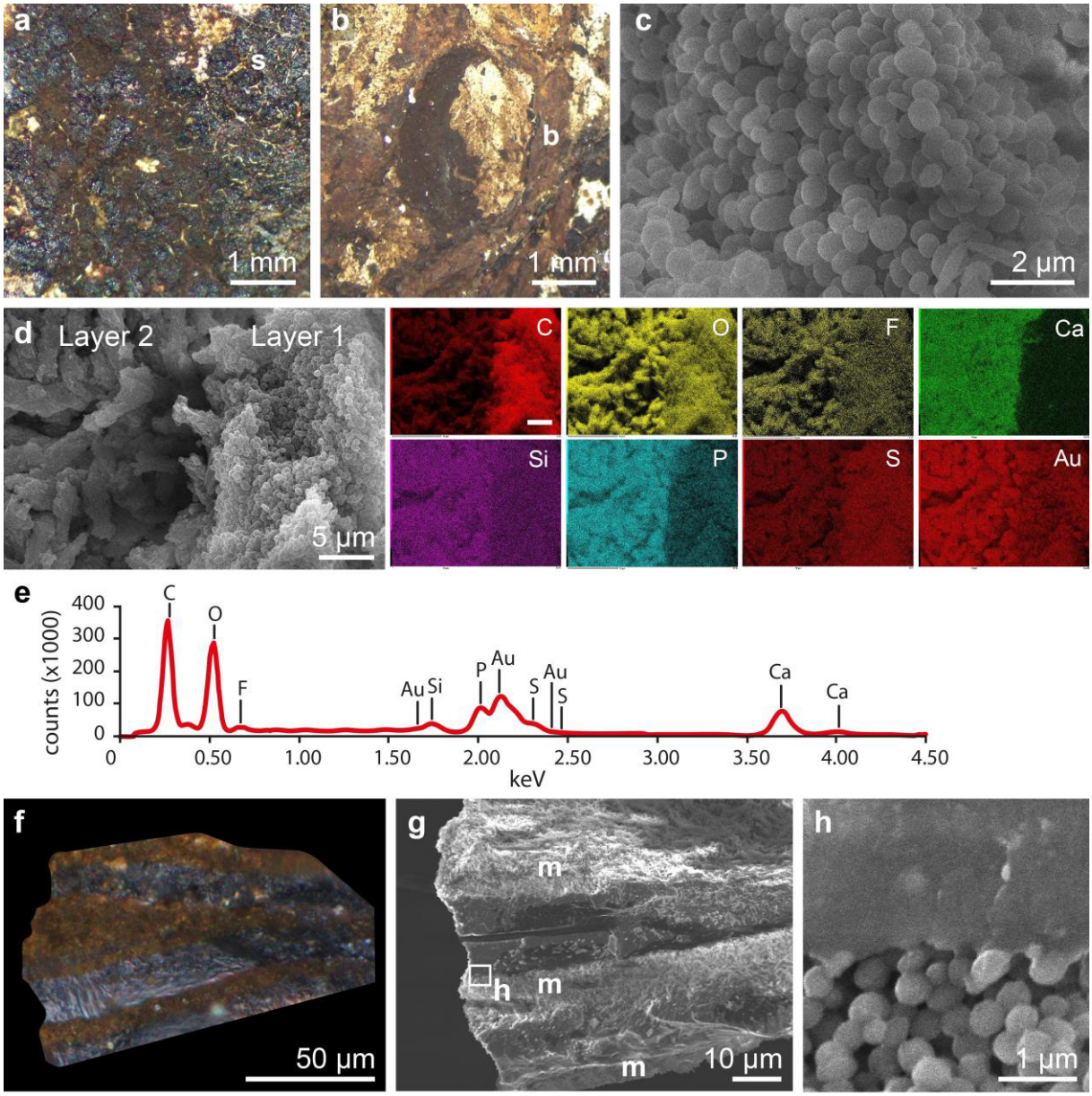
SEM analysis of sediment samples from GMH XXXV-11-1970 reveals micron-scale lamination. Individual laminae are highly anastomosing and laterally discontinuous, with alternating microlaminae that vary in tone in backscatter electron images. These variations in tone correspond to variations in oxygen and calcium in EDS maps (Supplementary Fig. S4.5), suggesting variation in the content of calcium carbonate. The sediment hosts irregularly dispersed, irregular to oval structures 10–150 µm long, that deform the surrounding laminae. The structures show a porous texture and are enriched in sulfur.

The fossil-bearing sediments at Geiseltal have been characterized as “Weichbraunkohle” [soft brown coal] (Pickel and Wolf[1], p. 482) rich in huminite (52–82%) with a mineral-bituminous groundmass (6–31%) and minor mineral content (<4%). This previous study reported a mineral-bituminous groundmass with a high organic content, a calcium carbonate bearing mineral-bituminous groundmass and low mineral content[1], as in our analysis of GMH XXXV-11-1970. Clearly, during deposition, input of organic debris was higher than for siliciclastic sediment, suggesting deposition in a low-energy regime characterized by low pH and sedimentary anoxia[1], with episodic variation in environmental conditions, thus forming fine macro-lamination. The highly anastomosing, discontinuous, micron-scale lamination (Supplementary Fig. S4.5) resembles liptinite macerals in coals, that derive from algae (lamalganite)[2,3]. The oval porous structures likely represent coal macerals, i.e., sclerotinites[1,4] and/or liptinites[1,2].

4.10.2 Influence of calcium- and carbonate-rich waters on soft tissue preservation

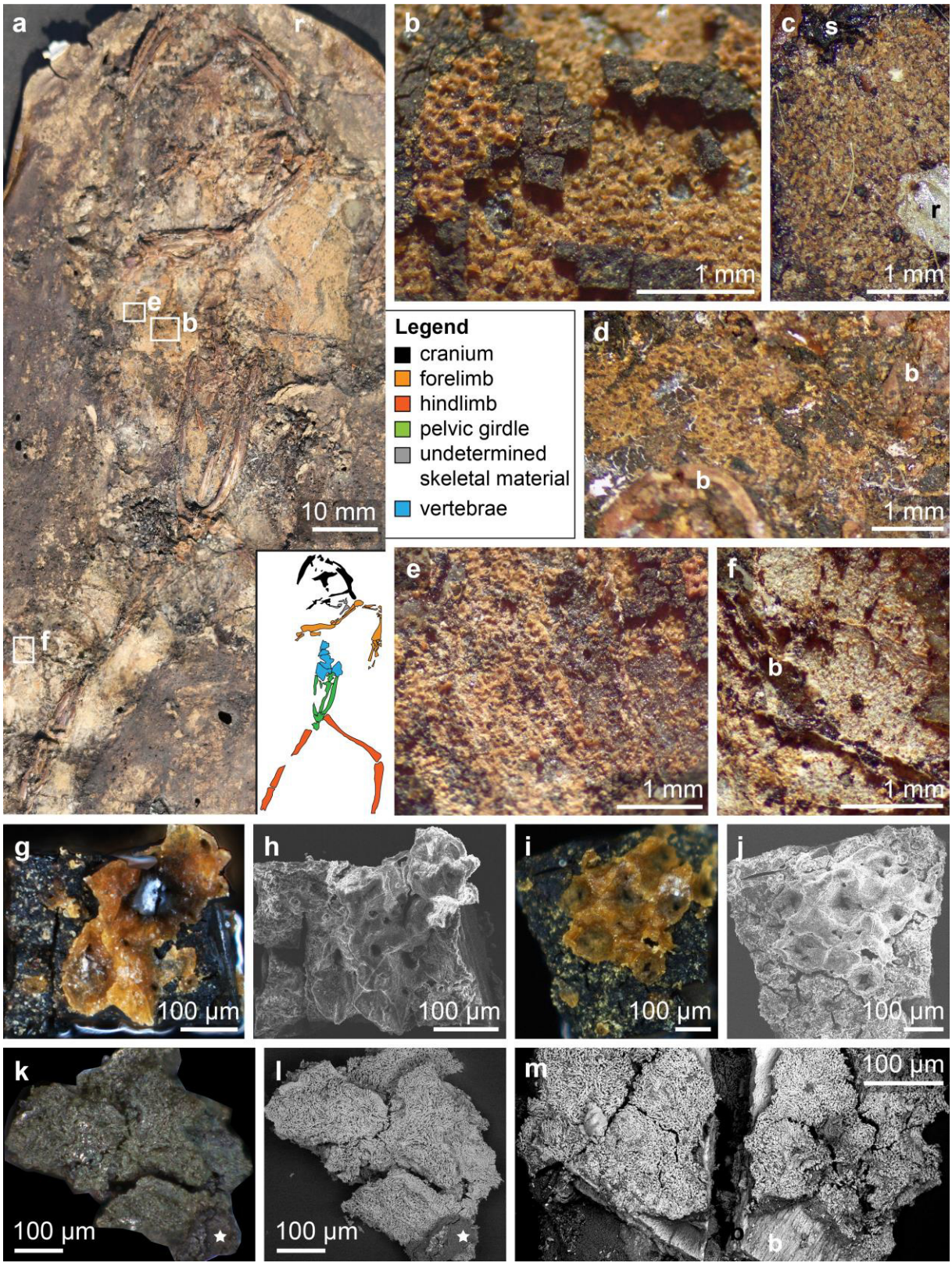
Preservation of the Geiseltal anurans has been previously linked to an influx of calcium- and carbonate-rich waters derived from Triassic sediments at the southern border of the Geiseltal basin[5]. These fluvial waters are considered to have raised the pH of the Geiseltal lakes, promoting preservation of both the skeletons and soft tissues of the fossil vertebrates[5–7]. There is, however, no evidence for calcium carbonate precipitates in association with the anuran soft tissues. The anuran E-K layer is replicated in calcium phosphate. Our study shows that the phosphate source and precipitation were localized to the anuran skin and were therefore independent of environmental influences.

4.10.3 Supplementary figures and tables



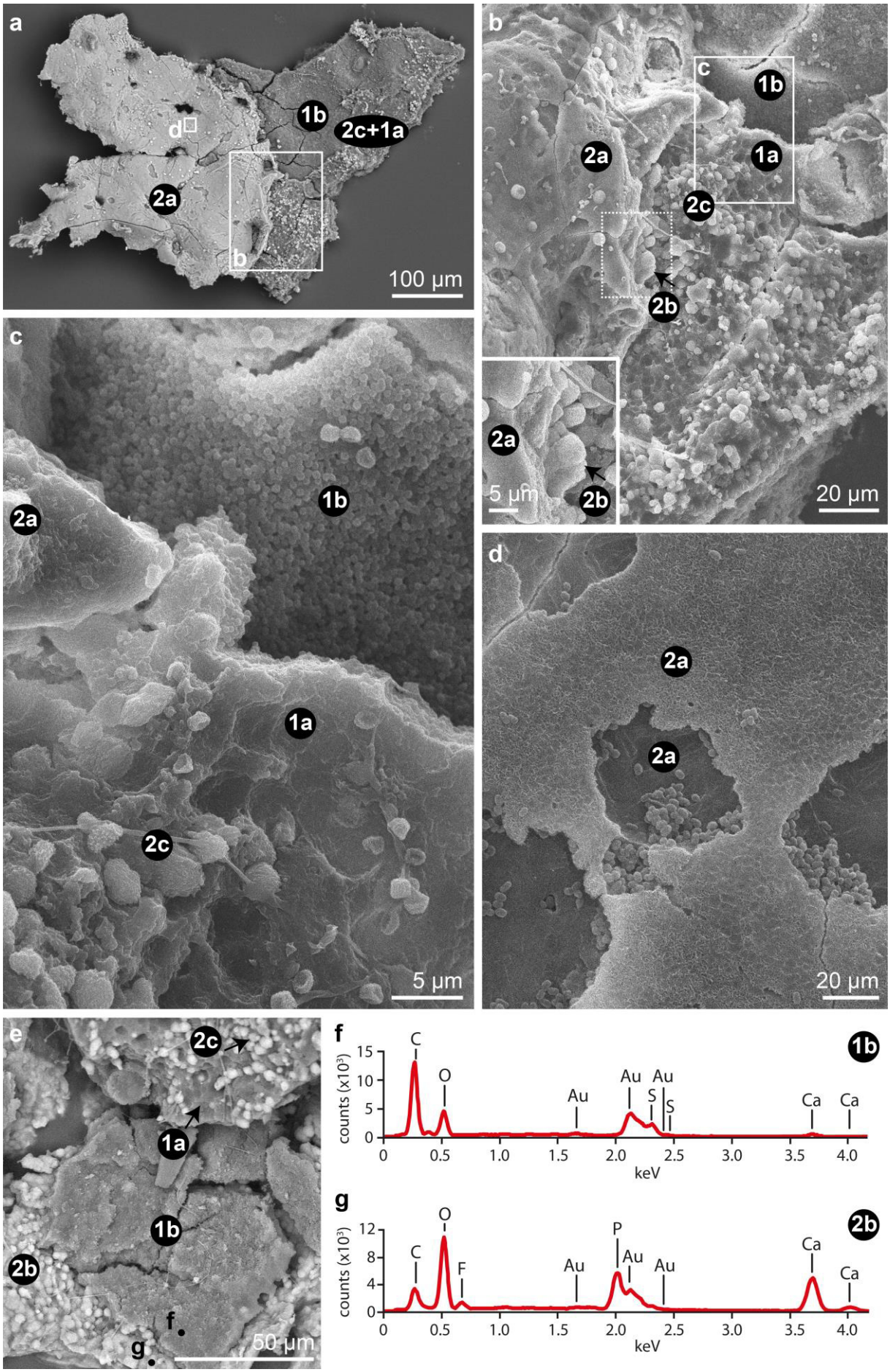
Supplementary Figure S4.1: Layer 1, interpreted as a carbonaceous layer that contains melanosomes. (a–b) Light micrographs of the dark brown material of Layer 1. (a) Region shown reveals (dark brown) Layer 1 next to (black) sediment and is from the inner thigh of GMH CeIII-6748-1932 (Anura indet.). (b) Eyespot of GMH CeIII-6733-1932 (Anura indet.). (c) Scanning electron micrograph showing melanosomes of Layer 1 in the torso of GMH CeIII-6698-1932 (Pelobatidae). (d) Secondary electron micrograph and EDS maps of the junction between Layers 1 and 2 in GMH CeIII-6698-1932, where the melanosome-rich Layer 1 overlaps fibers of Sublayer 2b. Layer 1 is enriched in C and, to a lesser extent, S; Layer 2 is enriched in P, Ca and, to a lesser extent, F. Si possibly represents sediment underneath Layer 2; scale bar is 5 µm. (e) EDS spectrum of region shown in (d); see Methods for analytical

parameters. (f) Light micrograph of a vertical cross-section of Layer 1, showing melanosome-rich bands (brown) and melanosome-poor bands (black). Sample is from the torso of GMH CeIII-6698-1932. (g–h) Secondary electron micrographs of sample in (f). (g) Bands rich in melanosomes and bands with few melanosomes. (h) Detail of inset in g, showing junction between zones where melanosomes are abundant (lower half of image) and rare (upper half of image). b, bone, m, melanosomes, s, sediment.

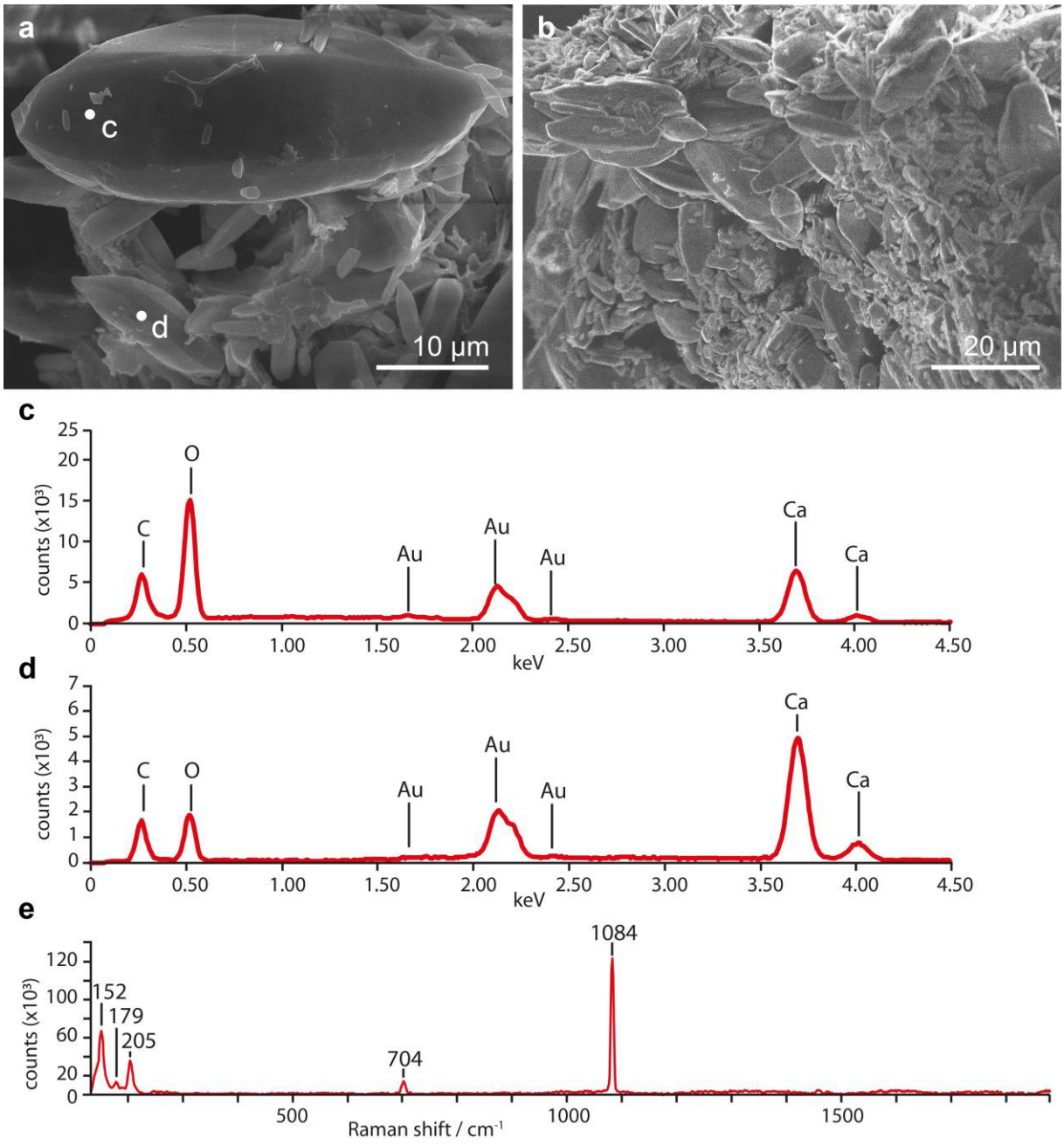


Supplementary Figure S4.2. Layer 2, interpreted as the mid-dermal Eberth-Katschenko (E-K) layer. (a) Photograph of specimen GMH CeIII-4936a-1932 (Pelobatidae) showing extensive pale yellow- to orange-colored patches of Layer 2 in the cranium, torso, abdomen and limbs. Insets show color-coded line drawings of the bones. (b) Detail

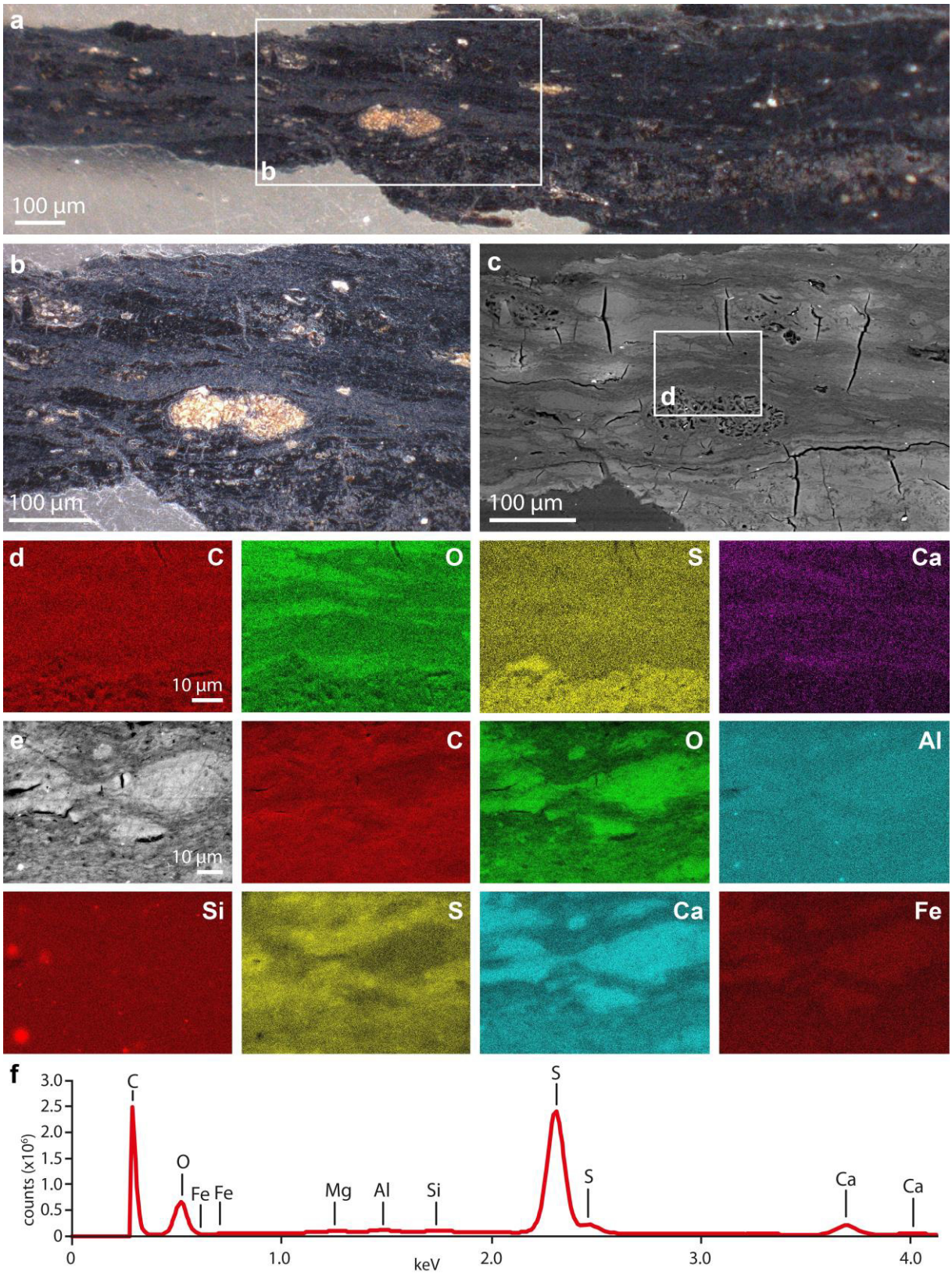
of region in (a) showing perforations in Layer 2. Layer 2 occurs in two layers, separated by a thick, blocky, dark brown material (Layer 1). (c) Perforations in Layer 2, in the abdomen of GMH CeIII-4990-1932 (Pelobatidae). (d) Perforations in Layer 2, in the torso of GMH CeIII-6738-1932 (Anura indet.). (e) Detail of region in a, showing different taphonomic states of Layer 2: orange with perforations (well-preserved E-K layer) and pale and structureless (poorly preserved E-K layer). (f) Detail of a, showing pale structureless Layer 2 (poorly preserved E-K layer). (g) Light micrograph shows patches of orange Sublayer 2a on black Layer 1 of specimen GMH CeIII-4936a-1932. (h) Secondary electron micrograph of (g). (i) Light micrograph showing patches of orange Sublayer 2a with honeycomb texture, overlying black Layer 1 of specimen GMH CeIII-4936a-1932. (j) Secondary electron micrograph of (i). (k) Light micrograph of GMH CeIII-6698-1932 (Pelobatidae) showing a small patch of Layer 1 (star) and extensive Layer 2 (Sublayer 2b) in ventral aspect. (l), Backscatter electron micrograph of (k) shows Layer 1 (star) on Sublayer 2b. (m) Backscatter electron micrograph of succession of preserved soft tissues and bone in GMH CeIII-6698-1932 from top to bottom of the sample: Layer 2 (Sublayer 2b), Layer 1, bone, Layer 1, Layer 2 (Sublayer 2b). b, bone, r, resin, s, sediment.


a
1b
2c+1a
d
2a
b
100 µm
b
c
1b
2a
1a
2c
2b
2a
5 µm
2b
20 µm
c
2a
1b
1a
2c
5 µm
d
2a
2a
20 µm
e
2c
1a
1b
2b
f
g
50 µm
f
1b
counts (x10³)
C
O
Au
Au
Au
S
S
Ca
Ca
keV
g
2b
counts (x10³)
C
O
F
Au
P
Au
Au
Ca
Ca
keV

Supplementary Figure S4.3. Succession of soft tissue layers in the Geiseltal anurans. (a–d), Electron micrographs of GMH CeIII-4967-1932-B6 (Pelobatidae) show soft tissue Sublayer 1b (melanosome-rich), Sublayer 1a (melanosome-poor), Sublayer 2c (globules, that form molds in Sublayer 1a), Sublayer 2b (fibrous) and Sublayer 2a (amorphous). Not all soft tissue layers are continuous across the entire area of the sample. (a) Backscatter electron image showing soft tissue layers. (b) Secondary electron image of region indicated in (a), showing successive preserved skin layers. Close-up in bottom left corner shows fibers of Sublayer 2b overlain by amorphous Sublayer 2a. (c) Secondary electron image of region indicated in (b). Sublayer 1b is separated by Sublayer 1a from Sublayer 2c. (d) Secondary electron image of region indicated in (a). Dimpled outer, amorphous surface of Sublayer 2a with local clusters of ovoid microbodies. (e–g) Backscatter electron image of a region in CeIII-4967-1932-B6 and EDS point spectra of regions (f) and (g) in (e); Au peaks are from the gold sputter coat; see Methods for analytical parameters. (e) Successive layers showing irregular globules of Sublayer 2c underlain by homogenous Sublayer 1a, melanosome-rich Sublayer 1b, and in turn fibrous Sublayer 2b. (f) EDS spectrum of Sublayer 1b Ca peak reflects X-ray signal from the underlying Sublayer 2b. (g) EDS spectrum of Sublayer 2c.



Supplementary Figure S4.4. Aragonite crystals in the cranium. (a), Secondary electron image of euhedral, micron-scale crystals in the white material in GMH CeIII-4967-1932 (Pelobatidae). (b) Secondary electron image of white material in the cranium of GMH CeIII-6698-1932 (Pelobatidae). Points in (a) indicate the locations where the EDS point spectra in (c) and (d) were collected. (c–d), EDS point spectra from points indicated in (a). Sample is Au coated. (e) Raman spectrum for sample shown in (b) with a major peak at 1084 cm^{-1} ($v_1CO_3^{2-}$) and minor peaks at 152 cm^{-1}, 179 cm^{-1}, 205 cm^{-1} and 704 cm^{-1} ($v_4CO_3^{2-}$). This spectrum is characteristic of aragonite[8].



Supplementary Figure S4.5. Analysis of the host sediment associated with GMH XXXV-11-1970 (Anura indet.); see Methods for analytical parameters. (a–b) Light micrographs of a vertical polished section through the sediment. (c) Backscatter electron image of (b) showing alternating dark and bright, laterally discontinuous laminae

(probably liptinite coal macerals) surrounding porous structures interpreted as isolated sclerotinite coal macerals. (d) EDS maps of the region shown in (c). (e) Secondary electron micrograph and EDS maps. Bright areas in the micrograph are enriched in O, Ca and to a lesser extent, Fe; dark areas are enriched in S and to a lesser extent, C; localized hotspots of Si likely reflect contamination during polishing. (f) EDS spectrum from area shown in (e).

Supplementary Table S4.1. Master dataset with soft tissue data for the Geiseltal anurans. Data are shown for each of 168 specimens used in the study. Hyphen (-) indicates an unknown date of specimen collection (column D) and/or lacking stratigraphic data (column L). Abbreviations in columns G and H indicate the anatomical region where Layers 1 and 2 occur. "mold" refers to an external mold of E-K layer tissue texture in resin or wax. "skeleton" refers to a specimen comprising articulated bones from most or all of the cranium, torso, abdomen and/or limbs. "disarticulated bones" refer to skeletal elements that are not in their original relative body positions in vivo. "x" denotes where Layer 1 and/or Layer 2 is/are present but lack anatomical data (e.g., due to the unconfident determination of skeletal elements). "#" denotes where a feature is present. "?" indicates uncertainty regarding the presence/absence of a feature.

Abbreviations. Ce, 'Cecilie' pit; IL, 'Geiselröhlitz' site; GMH, Geiseltalmuseum Halle; indet., indeterminate; Leo, 'Leonhard' pit; LMC, Lower Middle Coal; LUC, Lower Upper Coal; MC, Middle Coal; MUC, Middle Upper Coal; Nw, 'Neumark-West' pit; N/A, not applicable; UHM, Upper 'Hauptmittel' ('Hauptmittel': intercalated sandy and silty successions); UMC, Upper Middle Coal; XXXV, Neumark-Süd pit (NsXXXV). Anatomical region: cr, cranium; eye, eyespot; ext, beyond the body margin; fl, forelimbs; fp, forelimb phalanges; hl, hindlimbs; hp, hindlimb phalanges; pel, pelvic girdle; tor, torso; vc, vertebral column.

museum prefix	site prefix	specimen number	year of collection	anuran family	short description	Layer 1 (melanosome layer)	Layer 2 (E-K layer)	white material (aragonite crystals)	sediment on slab	plant remains	stratigraphic interval	embedding material
GMH	CeII	6709	1930	Pelobatidae	skeleton	x	hl, hp	#	#		LUC	paraffin wax (gypsum frame)
GMH	CeIII	6687	1932	Palaeobatrachidae	skeleton	fl, tor, vc, pel, hl			#		LUC	nitrocellulose glue
GMH	CeIV	2893	1933	Anura indet.	disarticulated bones	hl, pel, ext	hl, pel		#		UMC	nitrocellulose glue
GMH	CeIII	4939	1932	Pelobatidae	skeleton	x	cr, vc		#		LUC	paraffin wax (gypsum frame)
GMH	CeIII	4126	1932	?Pelobatidae	skeleton	cr, vc, tor	tor, vc, pel, ext		#	#	LUC	nitrocellulose glue
GMH	Ce	9002	-	Pelobatidae	skeleton						-	paraffin wax
GMH	CeIII	4935	1931	Pelobatidae	skeleton	eye, cr, tor, ext	vc, tor, pel, hl, ext	#	#		LUC	paraffin wax (gypsum frame)
GMH	CeII	6703	1930	Palaeobatrachidae	skeleton	x			#		LUC	paraffin wax (gypsum frame)
GMH	CeII	4950	1930	Palaeobatrachidae	skeleton	x			#		LUC	paraffin wax (gypsum frame)
GMH	CeII	6700	1930	?Pelobatidae	skeleton	fl	mold: fl, vc, pel, hl	#	#		LUC	paraffin wax (gypsum frame)
GMH	IL	17A	1969	Anura indet.	disarticulated bones	x	x	#	#		LMC	nitrocellulose glue
GMH	IL	17C	1969	Anura indet.	disarticulated bones				#		LMC	nitrocellulose glue
GMH	CeIII	6727	1932	Anura indet.	disarticulated bones				#		LUC	nitrocellulose glue on gypsum
GMH	CeII	6704	1930	Anura indet.	disarticulated bones	x	hl, ext	#	#		LUC	paraffin wax (gypsum frame)
GMH	CeIII	6762	1933	Pelobatidae	skeleton	eye	tor, pel, hl	#	#		LUC	nitrocellulose glue
GMH	CeIII	6718	1932	Pelobatidae	skeleton	x			#		LUC	nitrocellulose glue
GMH	CeIII	4956	1932	Pelobatidae	skeleton	x	eye, cr, fl, pel, hl, ext	#	#		LUC	nitrocellulose glue
GMH	CeII	6708	1930	?Pelobatidae	skeleton		mold: fl, tor	#			LUC	paraffin wax (gypsum frame)
GMH	CeI	4947	1930	Pelobatidae	skeleton	eye, tor, pel	mold: fl, tor, pel, hl	#	#		UHM	paraffin wax (gypsum frame)
GMH	CeIII	4975	1932	Pelobatidae	skeleton	fl, tor	tor, hl, ext		#	?	LUC	nitrocellulose glue
GMH	CeII	4940	1931	Anura indet.	disarticulated bones	x	x		#		LUC	paraffin wax
GMH	CeIII	6725	1932	Anura indet.	skeleton (hindlimb only)	hl, ext	hp, hl	#	#	#	LUC	nitrocellulose glue on gypsum
GMH	CeII	4944	1930	Pelobatidae	disarticulated bones	x	cr, hl, tor + mold tor	#	#		LUC	paraffin wax
GMH	CeIII	6720	1932	Anura indet.	skeleton (cranium+upper body)	x	vc		#		LUC	nitrocellulose glue on gypsum
GMH	CeVI	4976B	1934	Anura indet.	skeleton (hindlimbs only)	x			#		?UMC/?LUC	nitrocellulose glue
GMH	CeIII	4968	1932	?Pelobatidae	skeleton	x		#	#	?	LUC	nitrocellulose glue
GMH	CeIII	4989	1932	Anura indet.	skeleton	x		#	#		LUC	nitrocellulose glue
GMH	CeIV	4953	1933	Pelobatidae	disarticulated bones	x	x	#	#	?	UMC	nitrocellulose glue
GMH	CeIII	4958	1933	?Pelobatidae	skeleton	cr, tor, hl, ext	cr, tor, hl, hp, ext	#	#		LUC	nitrocellulose glue
GMH	CeIV	4960	1933	Pelobatidae	disarticulated bones	x		#	#	#	UMC	nitrocellulose glue
GMH	CeIV	4955	1933	Anura indet.	skeleton	ext	pel, hl	#	#	?	UMC	nitrocellulose glue
GMH	CeIV	4957	1933	?Palaeobatrachidae	skeleton	fl, hl, hp, ext	fp, ext		#		UMC	nitrocellulose glue
GMH	CeIII	4967	1932	Pelobatidae	skeleton	tor	cr, fl, tor, pel, hl	#	#		LUC	nitrocellulose glue
GMH	CeIII	6729	1932	Anura indet.	skeleton	cr, fl, tor	eye, fl, tor, hl		#		LUC	nitrocellulose glue
GMH	CeIII	6761	1932	?Pelobatidae	skeleton	ext		#	#		LUC	nitrocellulose glue
GMH	CeIV	2895	1933	Anura indet.	disarticulated bones	x			#	#	UMC	nitrocellulose glue
GMH	CeIII	1305	1933	Anura indet.	skeleton (hindlimbs only)	x	hl, fp		#		LUC	nitrocellulose glue
GMH	CeIII	6748	1932	Anura indet.	skeleton	fl, pel, hl, ext	tor, pel, hl		#		LUC	nitrocellulose glue
GMH	CeIII	6747	1932	Anura indet.	skeleton	x	fl, hl, fp, ext		#	#	LUC	nitrocellulose glue
GMH	CeIII	1307	1933	Anura indet.	disarticulated bones	x	fl, fp, tor, pel, hl, ext	#	#		LUC	nitrocellulose glue
GMH	CeIII	4988	1932	Anura indet.	skeleton (hindlimbs only)	x		#	#		LUC	nitrocellulose glue
GMH	CeIII	6740	1933	Anura indet.	skeleton (lower body only)	pel, hl, hp, ext	pel, hl, ext		#		LUC	nitrocellulose glue
GMH	CeIII	6743	1932	Pelobatidae	skeleton	eye, pel, ext	cr, fl, fp, vc, tor, pel, ext	#	#		LUC	nitrocellulose glue
GMH	CeIII	6754A	1933	Pelobatidae	skeleton	tor, pel	cr, vc, fl, tor, pel, hl	#	#		LUC	nitrocellulose glue
GMH	CeIII	4990	1932	Pelobatidae	skeleton	eye, tor, pel, hl	cr, tor, vc, pel, hl	#	#		UMC	nitrocellulose glue
GMH	CeIII	6745	1932	Pelobatidae	skeleton	eye, pel	fl, tor, pel, hl		#		LUC	nitrocellulose glue
GMH	CeIII	6754B	1933	?Discoglossidae/?Palaeoatrachidae	skeleton	eye, vc, tor, pel, hl, ext	cr, tor, pel, hl		#		LUC	nitrocellulose glue
GMH	NwXIV/?CeXIV	1275	1954	Anura indet.	skeleton						-	nitrocellulose glue
GMH	CeIII	6759	1932	Pelobatidae	skeleton	tor, vc	fl, tor, pel, hl	#	#		LUC	nitrocellulose glue
GMH	CeIII	4978	1932	Pelobatidae	skeleton	eye, tor, ext	cr, fl, tor	#	#		LUC	nitrocellulose glue
GMH	CeIII	6757	1932	Pelobatidae	skeleton	eye, fl, tor, pel	eye, cr, fl, tor, vc, pel, ext	#	#		LUC	nitrocellulose glue
GMH	CeIII	6693	1933	Anura indet.	disarticulated bones	x	hl, pel		#		LUC	nitrocellulose glue
GMH	CeIII	6749	1932	?Palaeobatrachidae	skeleton	x	cr, fl, tor, hl, ext	#	#		LUC	nitrocellulose glue
GMH	CeI	4951	1930	Pelobatidae	skeleton	x			#		UHM	paraffin wax
GMH	CeII	7130	1931	?Palaeobatrachidae	skeleton (single hindlimb only)						LUC	paraffin wax
GMH	Ce	7197	-	Anura indet.	skeleton (cranium+spine)				#		-	paraffin wax
GMH	CeIII	6750A	1933	?Pelobatidae	skeleton (big anuran)	x	cr, fl, tor, pel, hl	#	#		LUC	nitrocellulose glue
GMH	CeIV	4980	1933	Pelobatidae	disarticulated bones	x	x		#	#	UMC	nitrocellulose glue
GMH	CeIII	4983	1932	?Pelobatidae	skeleton	eye, cr	eye, cr, fl, fp, tor, pel, hl	#	#	#	LUC	nitrocellulose glue
GMH	CeIII	4991	1932	Pelobatidae	skeleton	x	vc, tor, pel, hl	#	#	?	LUC	nitrocellulose glue
GMH	CeIII	4987	1933	Anura indet.	skeleton	x	tor		#		LUC	nitrocellulose glue
GMH	CeV	3012	1934	Anura indet.	skeleton	fl, tor, ext	cr, fl, pel, ext	#	#	#	MUC	nitrocellulose glue
GMH	LeoV	3477A	1934	Pelobatidae	skeleton	cr, vc, tor, pel, hl, ext	cr, fp, fl, tor		#	#	MC	nitrocellulose glue

GMH	CeIII	4993	1932	Anura indet.	skeleton (cranium only)	eye, cr	eye, cr, tor		#		LUC	nitrocellulose glue
GMH	CeIII	6751	1932	?Palaeobatrachidae	skeleton	cr, vc, tor	vc, tor, pel, hl, ext	#			LUC	nitrocellulose glue
GMH	CeIII	6739	1932	Anura indet.	skeleton	x	x	#	#	#	LUC	nitrocellulose glue
GMH	CeIII	6733	1932	Pelobatidae	skeleton	eye, tor	cr, ext		#	#	LUC	nitrocellulose glue
GMH	CeIII	6711	1933	Anura indet.	skeleton	x	pel	#	#		LUC	nitrocellulose glue
GMH	CeIII	6738	1932	Anura indet.	skeleton (upper body only)	fl, tor	cr, fl, tor		#		LUC	nitrocellulose glue
GMH	CeIII	6736	1932	Anura indet.	skeleton (single lower hindlimb only)	x	hl		#		LUC	nitrocellulose glue
GMH	CeIII	6737	1932	Anura indet.	skeleton (single lower hindlimb only)	x	hl		#		LUC	nitrocellulose glue
GMH	CeIII	4998	1932	Anura indet.	skeleton (single hindlimb without foot)	x			#		LUC	nitrocellulose glue
GMH	CeIII	6717	1933	Anura indet.	disarticulated bones	x	x		#		LUC	nitrocellulose glue
GMH	CeIII	6731	1932	Anura indet.	skeleton	eye	ext		#		LUC	nitrocellulose glue
GMH	CeIII	6735	1932	Pelobatidae	skeleton	eye, tor, vc, pel	fl, tor, fp, pel, hl	#	#		LUC	nitrocellulose glue
GMH	CeIII	4997	1932	Pelobatidae	skeleton		cr, vc, tor, pel				LUC	nitrocellulose glue
GMH	CeIII	4996	1932	Anura indet.	skeleton	x	tor, pel, hl	#	#	?	LUC	nitrocellulose glue
GMH	CeIII	6732	1932	?Palaeobatrachidae	skeleton	vc, pel	hl, hp	#	#		LUC	nitrocellulose glue
GMH	CeIII	4999	1932	Anura indet.	disarticulated bones	x			#	#	LUC	nitrocellulose glue
GMH	CeIII	4994	1932	Anura indet.	skeleton	pel	pel		#		LUC	nitrocellulose glue
GMH	CeIV	6688	1933	?Palaeobatrachidae	skeleton	fp, ext	fl, hl		#	#	UMC	nitrocellulose glue
GMH	CeIII	6716	1932	?Palaeobatrachidae	skeleton (lower body only)	x	pel		#		LUC	nitrocellulose glue
GMH	CeIII	4992	1932	Pelobatidae	skeleton	cr, fl, pel, hl	fl, pel, hl		#	#	LUC	nitrocellulose glue
GMH	CeIII	6723(1)	1932	Anura indet.	skeleton	x	fl, pel, ext		#		LUC	nitrocellulose glue
GMH	CeIII	6760	1932	?Discoglossidae/?Pelobatidae	skeleton	x	fl, tor, pel	#	#		LUC	nitrocellulose glue
GMH	CeIII	4995	1932	?Discoglossidae/?Pelobatidae	skeleton	x	cr, vc	#	#		LUC	nitrocellulose glue
GMH	CeIII	4962	1932	Palaeobatrachidae	skeleton	x	fl, tor, pel, hl	#	#		LUC	nitrocellulose glue
GMH	CeII	4942	1930	?Palaeobatrachidae	skeleton	tor, pel	cr, fl, vc, tor, pel		#		LUC	paraffin wax (gypsum frame)
GMH	CeIV	6699	1933	?Palaeobatrachidae	skeleton	x	cr, vc, tor, pel, hl		#	#	UMC	nitrocellulose glue
GMH	CeIII	4959	1932	Anura indet.	skeleton (hindlimbs only)	hl	hl		#	#	LUC	nitrocellulose glue
GMH	CeIV	4961	1933	?Pelobatidae	skeleton	x	pel		#	#	UMC	nitrocellulose glue
GMH	CeIV	6696	1933	Pelobatidae	skeleton	x	fl, tor		#		UMC	nitrocellulose glue
GMH	CeIII	4936a	1932	Pelobatidae	skeleton	eye	cr, vc, fl, tor, pel, hl		#		LUC	nitrocellulose glue
GMH	XXXV	11A	1970	Anura indet.	skeleton	eye, cr	cr, fl, tor, pel, hl		#	#	UMC	sediment
GMH	LeoV	3477B	1934	Pelobatidae	skeleton	eye, cr, fl, tor, pel, hl, ext	cr, fl, fp, vc, pel, hl, ext		#	#	MC	nitrocellulose glue
GMH	CeIII	1301	1932	Pelobatidae	skeleton	x			#		LUC	nitrocellulose glue
GMH	CeIII	1302	1933	?Pelobatidae	skeleton	x		#	#		LUC	nitrocellulose glue
GMH	CeIII	1312	1932	Pelobatidae	skeleton	hl	tor, pel, hl	#	#		-	nitrocellulose glue
GMH	CeIII	1537	1932	Pelobatidae	skeleton	pel	cr, tor, pel	#	#	#	LUC	nitrocellulose glue
GMH	CeI	4608	1931	Pelobatidae	skeleton	x	x	#	#		UHM	paraffin wax
GMH	CeIV	4665	1933	Pelobatidae	disarticulated bones	x			#	#	UMC	nitrocellulose glue
GMH	CeII	4934	1930	Pelobatidae	skeleton	x		#	#		LUC	paraffin wax (gypsum frame)
GMH	CeIII	4936	1932	Palaeobatrachidae	skeleton	x		#	#		LUC	paraffin wax (gypsum frame)
GMH	CeIII	4941	1931	Pelobatidae	skeleton	x	cr	#	#		LUC	paraffin wax (gypsum frame)
GMH	CeII	4943	1930	Pelobatidae	skeleton	x	vc, hl, cr, fl, ext	#	#		LUC	paraffin wax (gypsum frame)
GMH	CeII	4946	1930	Pelobatidae	skeleton	x	ext	#	#	#	LUC	paraffin wax (gypsum frame)
GMH	CeII	4948	1930	Palaeobatrachidae	skeleton	x	cr, fl, tor, pel, ext	#	#		LUC	paraffin wax (gypsum frame)
GMH	CeII	4949	1930	Pelobatidae	skeleton	x			#		LUC	paraffin wax (gypsum frame)
GMH	CeIII	4965	1932	Pelobatidae	skeleton	eye	eye, tor, hl	#	#		LUC	nitrocellulose glue
GMH	CeIV	4971	1933	Pelobatidae	skeleton	eye	cr, vc, fl, tor, pel, hl, hp	#	#		UMC	nitrocellulose glue
GMH	CeIII	4972	1932	?Pelobatidae	skeleton	fl	cr, vc, tor, pel, hl	#	#		LUC	nitrocellulose glue
GMH	CeIII	4973	1931	Pelobatidae	skeleton	eye, pel, ext	cr, tor, pel	#	#		LUC	nitrocellulose glue
GMH	CeIII	4977	1932	Pelobatidae	skeleton	x			#		LUC	nitrocellulose glue
GMH	CeIII	4979	1931	?Pelobatidae	skeleton	x			#		LUC	nitrocellulose glue
GMH	CeIII	4981	1932	Palaeobatrachidae	skeleton	x	cr, fl, tor, vc, hl, ext		#	?	LUC	nitrocellulose glue
GMH	CeIII	4984	1933	Palaeobatrachidae	skeleton	x	pel, hl	#	#		LUC	nitrocellulose glue
GMH	CeIII	4985	1932	Palaeobatrachidae	skeleton	x	fl, pel	#	#		LUC	nitrocellulose glue
GMH	CeIV	6685	1933	Palaeobatrachidae	skeleton	x	x		#	#	UMC	nitrocellulose glue
GMH	CeIII	6686	1932	Anura indet.	skeleton	x		#	#	?	LUC	nitrocellulose glue
GMH	CeIII	6689	1933	?Pelobatidae	skeleton	x			#		LUC	nitrocellulose glue
GMH	CeIV	6691	1933	Palaeobatrachidae	skeleton	eye, cr	cr, vc, fp, fl, tor, pel		#		UMC	nitrocellulose glue
GMH	CeIV	6692	1933	Pelobatidae	skeleton	eye, cr, fp, tor, ext	eye, cr, fl, vc	#	#		UMC	nitrocellulose glue
GMH	CeIV	6697	1933	Pelobatidae	skeleton (upper body only)	eye, tor, pel, hl	eye, cr, vc, tor, pel, hl		#		UMC	nitrocellulose glue
GMH	CeIII	6698	1932	Pelobatidae	skeleton	hl, ext	cr, pel, hl, ext	#	#	#	LUC	nitrocellulose glue
GMH	CeIII	6701	1930	Pelobatidae	skeleton (single lower hindlimb only)		fp		#		LUC	paraffin wax (gypsum frame)
GMH	CeII	6706	1930	Pelobatidae	skeleton	eye, fl, tor	tor, vc, pel	#	#		LUC	paraffin wax (gypsum frame)
GMH	CeII	6707	1930	Pelobatidae	skeleton	eye, fl, tor, ext	eye, fl, tor	#	#	#	LUC	paraffin wax (gypsum frame)
GMH	CeIII	6715	1932	?Pelobatidae	skeleton	cr	cr, fl, tor, pel		#	#	LUC	nitrocellulose glue
GMH	CeIII	6719	1932	?Pelobatidae	skeleton	eye, hp		#	#	#	LUC	nitrocellulose glue

GMH	CeIII	6721	1932	?Palaeobatrachidae	skeleton (hindlimb only)	hl	hl		#		LUC	nitrocellulose glue on gypsum
GMH	CeIII	6722	1932	Anura indet.	skeleton	ext	pel, hl		#		LUC	nitrocellulose glue on gypsum
GMH	CeIII	6726	1932	Palaeobatrachidae	skeleton	x			#		LUC	nitrocellulose glue on gypsum
GMH	CeIII	6728	1932	Pelobatidae	skeleton	eye, tor, pel, hl	eye, cr, pel, tor, fl, hl	#	#		LUC	nitrocellulose glue
GMH	CeIII	6742	1932	Palaeobatrachidae	skeleton (upper body only)	eye, fl, tor	fl, tor	#	#	#	LUC	nitrocellulose glue
GMH	CeIII	6744	1932	?Pelobatidae	skeleton	x	fl, tor, fp, hl		#		LUC	nitrocellulose glue
GMH	CeIII	6755	1932	Palaeobatrachidae	skeleton	tor, hl, ext	pel, hl		#		LUC	nitrocellulose glue
GMH	CeIII	6756	1933	Palaeobatrachidae	skeleton	eye, tor	cr, fl, tor, pel, ext	#	#		LUC	nitrocellulose glue
GMH	CeIII	6834	1932	Pelobatidae	skeleton	fl, tor, pel	eye, fl, tor, pel, hl	#	#		LUC	nitrocellulose glue
GMH	CeII	7136	1930	Pelobatidae	skeleton		ext	#	#		LUC	paraffin wax (gypsum frame)
GMH	CeIII	7189	-	Anura indet.	skeleton (hindlimb only)	x		#	#		-	paraffin wax (gypsum frame)
GMH	CeIII	4664	1933	?Pelobatidae	disarticulated bones	x	x	#	#		LUC	nitrocellulose glue
GMH	-	4432A	-	Anura indet.	disarticulated bones	x	x		#	#	-	nitrocellulose glue
GMH	CeIV	4121	1932	Anura indet.	disarticulated bones	x	x	#	#	?	UMC	nitrocellulose glue
GMH	CeIV	4661	1933	Anura indet.	disarticulated bones	x			#		UMC	nitrocellulose glue
GMH	CeIV	4660	-	Anura indet.	disarticulated bones		fl, tor		#		UMC	nitrocellulose glue
GMH	CeIV	4669	1933	Anura indet.	disarticulated bones		fp, fl		#		UMC	nitrocellulose glue
GMH	CeIV	4656	1933	Anura indet.	disarticulated bones		x		#		UMC	nitrocellulose glue
GMH	IL	178	1969	Anura indet.	disarticulated bones				#		LMC	nitrocellulose glue
GMH	CeII	6710	1930	Anura indet.	isolated tibiofibula	hl			#		LUC	paraffin wax (gypsum frame)
GMH	CeIII	6724	1932	Anura indet.	disarticulated bones	x			#	#	LUC	nitrocellulose glue on gypsum
GMH	CeIII	1311	1931	Anura indet.	disarticulated bones		x		#		LUC	nitrocellulose glue on gypsum
GMH	CeVI	4976A	1934	Anura indet.	single hindlimb and ?humerus (corner)	x			#		?UMC/?LUC	nitrocellulose glue
GMH	CeIII	6723	1932	Anura indet.	disarticulated bones				#		LUC	nitrocellulose glue on gypsum
GMH	CeIV	4657	1933	?Palaeobatrachidae	disarticulated bones	x	x		#	?	UMC	nitrocellulose glue
GMH	CeIV	4952	1933	?Pelobatidae	cranium only	eye, cr	cr		#	?	UMC	nitrocellulose glue
GMH	CeIV	4954	1933	Anura indet.	disarticulated bones	x	x	#	#		UMC	nitrocellulose glue
GMH	CeIII	1308	1932	Anura indet.	disarticulated bones	x			#		LUC	nitrocellulose glue
GMH	CeIV	4663	1933	Anura indet.	disarticulated bones	x			#		UMC	nitrocellulose glue
GMH	CeIV	1303	1933	Anura indet.	disarticulated bones	fl	fl		#		UMC	nitrocellulose glue
GMH	CeIII	1306	-	Anura indet.	disarticulated bones	x			#		LUC	nitrocellulose glue
GMH	CeIV	1304	1933	Anura indet.	disarticulated bones	x	x		#		UMC	nitrocellulose glue
GMH	CeIII	6752	1933	Anura indet.	disarticulated bones	x	x		#		LUC	nitrocellulose glue
GMH	CeIII	4986	1933	Anura indet.	disarticulated bones	x			#	#	LUC	nitrocellulose glue
GMH	CeIII	4982	1932	Anura indet.	disarticulated bones	x			#		LUC	nitrocellulose glue
GMH	LeoIII	3240	1934	Anura indet.	disarticulated bones	x	x		#		UMC	nitrocellulose glue
GMH	CeIV	6712	1932	Anura indet.	skeleton (poorly preserved)	x			#		UMC	nitrocellulose glue
GMH	CeIII	4974	1932	?Palaeobatrachidae	disarticulated bones	x	x		#	?	LUC	nitrocellulose glue
GMH	CeI	6702	1930	Anura indet.	single femur and tibiofibula	ext			#		UHM	paraffin wax (gypsum frame)

Supplementary Table S4.2. Historical description, interpretation, and mode of preservation of the soft tissue features of the Geiseltal anurans.

Historical Description/Observation	Historical Interpretation	Reference(s)	Notes
uppermost layer of many superimposed skin layers, transparent (Voigt 1935); clear or slightly yellowish (Voigt 1935); brittle and chippy (Voigt 1935); appears as homogenous, featureless layer or as layer with cell borders visible (Voigt 1935); visible in many specimens (but in different states of preservation) (Voigt 1935)	epidermis	Voigt 1935, p. 6–7; Voigt 1988, p. 328–329, 340	
large, flat, polygonal nucleated cells (usually hexagonal, 25–30 µm in diameter, grainy surface) (Voigt 1935, 1988); extension over wide areas of some anuran specimens (Voigt 1935); bottle cell openings between cell margins (Voigt 1935)	stratum corneum of the epidermis	Voigt 1935, p. 6–7; Voigt 1988, p. 328–329, 340	
thicker than stratum corneum and layered (Voigt 1935, 1988); merged with stratum corneum (Voigt 1935); hosts numerous nucleated cells, that are smaller (9–15 µm diameter) than those in layer above (stratum corneum) (Voigt 1935); hosts elongated cells (Voigt 1935)	stratum germinativum (with bottle cells) of the epidermis	Voigt 1935, p. 7–8; Voigt 1988, p. 328–329, 340	
epithelial cells that show nuclei within (Voigt 1935, 1988); large mucous glands (Voigt 1988); ca. 40 µm long cornificated hooks (isolated or connected with each other) (Voigt 1935, 1988); epidermis merged with corium due to diagenesis (Voigt 1935)	features of the epidermis	Voigt 1935, p. 6–7, 12; Voigt 1988, p. 326, 329, 328, 340	The term corium is now referred to as dermis.
lumpy, mesh-like surface made of woven fibers (fibers are 2–3 µm thick, individual fibers are formed by a sequence of spherical or bubble-shaped structures, but those structures can also appear individually; spherical or bubble-shaped structures are bigger where the fibrous sequence structure is lost) (Voigt 1935); surface shows round-oval and polygonal pits (0.07–0.15 mm) (Voigt 1935)	dermis (corium after Voigt) with two layers of stratum spongiosum: (1) upper layer = stratum vasculare with numerous large mucous glands and characteristic connective tissue collagen fibers (include globular structures) penetrated by a net of blood vessels; contains pigment cells; natural splitting surface; (2) lower layer = stratum glandulare with intersecting connective tissue collagen fibers and embedded blood vessels (15-20 µm in diameter and with 10 µm thick walls)	Voigt 1935,p. 8–10, 24; Voigt 1988, p. 329	In modern nomenclature, the terms stratum vasculare and stratum glandulare are no longer in use and represent the stratum spongiosum.
underneath corium as pale (almost white), homogenous, flaky layer (Voigt 1935, Voigt 1988); fine grained with regular distribution of holes (Voigt 1935); in some cases made up of intersected microscopic fibers (Voigt 1935)	stratum compactum of the dermis	Voigt 1935, p. 11–12, 24; Voigt 1988, p. 329	
swollen collagen fibers in connective tissue of the corium with blood vessels containing brownish matter (Voigt 1935, Voigt 1988)	collagen fibers in dermis with potential blood capillaries	Voigt 1935, p. 14, 24; Voigt 1988, p. 326	
visible as holes/cavities in fibrous connective tissue of corium (Voigt 1935); upper part of glands as part of the epidermis usually missing (due to preparation process/removal of sediment) (Voigt 1935); ca. 60 gland holes per mm^2 (Voigt 1935, 1988); longitudal axis: 100–170 µm (Voigt 1935); upper parts of glands in stratum corneum (if preserved) are visible as Y-shaped cleft in the centre of oval, slightly curved discs altogether forming papilla (20–30 µm in diameter) (Voigt 1935)	glands	Voigt 1935, p. 9, 12, 13; Voigt 1988, p. 329	
numerous small channels (5–20 µm thick with 10 µm thick walls) in fibrous connective tissue that is between glands (Voigt 1935); in crosscut sections with tear drop shaped openings or as longitudal section (channels) (Voigt 1935); diverse orientations of channels (Voigt 1935); filled with very dark, almost red brown, homogenous or flaky material (Voigt 1935, Voigt 1988)	blood or lymph vessels	Voigt 1935, p. 10, 14; Voigt 1988, p. 326	
dark, star-like shaped structures (0.05–0.1 mm in diameter) with long, branched, arm-like processes with dark granules (Voigt 1935, 1988); state of pigment expansion (Voigt 1935)	melanophores with melanin granules	Voigt 1988, p. 329; Voigt 1935, p.15	
oval cells, 20–30 µm in diameter (Voigt 1935); sometimes filled with highly refractive granules (Voigt 1935); oval cells enclose star-like structures (which are interpreted as melanophores) (Voigt 1935, 1988)	xantholeucophores	Voigt 1935, p. 16; Voigt 1988, p. 329	
n/a	well-preserved melanophores in stratum vasculare	Voigt 1935, p. 9	No observation given.
(...) filled with dark melanine granules (Voigt 1988)	melanin granules in skin	Voigt 1988, p. 329; Voigt 1935, p. 8	
n/a	"Melaninkörnchen" [melanin granules]	Voigt 1937, p. 9–10; Voigt 1988, p. 328–329, 336	No observation given.
n/a	pigment granules in skin	Voigt 1937, p.9; Voigt 1988, p.336	No observation given.
n/a	"Pigmentkörnchen" [pigment granules]	Voigt 1937, p. 5, 9–10; Voigt 1988, p. 336	No observation given.
n/a	pigment granules in stratum germinativum	Voigt 1935, p. 8	No observation given.
n/a	epidermis and pigment cells of the skin	Voigt 1988, p. 326	No observation given.

well-preserved, striated, silicified with “occasionally, brittle fibrils broken into tiny prismatic rodlets” (Voigt 1988); show double refraction under microscope; fibers with A and I bands (Brenner 1939)	muscle	Brenner 1939, p. 110–111; Voigt 1988, p. 326; Voigt 1937, p. 10	
short and roundish or ovoid microbodies; slim rods that differ in length and show slightly rounded edges; short rods with rounded edges	bacteria	Mrugowsky 1936, p. 7–8	
white material in central cranium and along vertebral column are accumulations of microscopic crystals; refractometry, optical features and dissolution with hydrochloric acid point to aragonite crystals (statoliths); distribution of aragonite in the fossil skeletons is similar to location of statoliths in modern anurans	statoliths of the endolymphatic sac	Voigt 1937, p. 10–12	
Methods			
statolith description, chemical analysis and refractometry	n/a	Voigt 1937, p. 10–12	
combustion of fossil skin samples and refractometry	n/a	Voigt 1937, p. 18	
chemical analysis of fossil skin combustion remains	n/a	Voigt 1937, p. 19	
Mode of preservation			
soft tissues as direct 3D replication in silica	n/a	Voigt 1937, p. 19; Voigt 1988	
soft tissue preservation process: tanning by humic acids, followed by impregnation and "molekularer Austausch" [molecular exchange] (Voigt 1937) of soft tissues by silicic acid	n/a	Voigt 1937, p. 19–20	
soft tissue preservation process linked to diagenesis (metasomatism)	n/a	Voigt 1937, p. 19, p. 23, p. 27	
tanning and silicification processes are mutually independent	n/a	Voigt 1988, p. 331	
host sediment as source of silica	n/a	Voigt 1937, p. 20; Voigt 1988, p. 331	

Supplementary Table S4.3. Raw data for EPMA of sample GMH CeIII-4936a-1932-A1 (in resin).

1) Calculation of Oxygen by Stoichiometry

		durango_ap	4936-1-A1_	4936-1-A1_	4936-1-A1_2na	4936-1-A1_5na_again	4936-1-A1_organic	4936-1-A1_	durango
	Beam current (nA)	5.0	5.0	5.0	2.0	5.0	5.0	5.0	5.0
Weight %	F	3.73	2.63	3.08	2.78	3.08	0.11	2.83	3.70
	P	17.77	11.31	12.05	11.26	11.29	0.18	10.65	17.59
	Cl	0.40	0.15	0.10	0.19	0.14	0.01	0.16	0.39
	Ca	38.24	30.43	31.85	30.52	30.91	1.49	27.33	38.52
	S	0.15	1.02	1.12	1.27	1.15	9.21	0.95	0.13
	O	38.22	26.76	28.28	26.72	26.91	0.82	24.67	38.10
	Total	98.52	72.30	76.49	72.73	73.48	11.81	66.58	98.43
Atomic %	F	4.7598	4.6612	5.1462	4.8965	5.3681	1.4650	5.4131	4.7282
	P	13.8950	12.2932	12.3494	12.1706	12.0683	1.4589	12.5036	13.7862
	Cl	0.2757	0.1424	0.0875	0.1788	0.1323	0.0910	0.1592	0.2698
	Ca	23.1084	25.5499	25.2165	25.5023	25.5358	9.5803	24.7923	23.3246
	S	0.1153	1.0703	1.1103	1.3230	1.1890	74.1771	1.0804	0.1013
	O	57.8458	56.2830	56.0901	55.9288	55.7065	13.2276	56.0514	57.7900
	Total	100	100	100	100	100	100	100	100
Oxide %	F	3.7339	2.6314	3.0811	2.7776	3.0797	0.1078	2.8284	3.7010
	P_2O_5	40.7200	25.9259	27.6220	25.7914	25.8647	0.4010	24.4071	40.3131
	Cl	0.4036	0.1500	0.0977	0.1893	0.1416	0.0125	0.1552	0.3941
	CaO	53.5094	42.5764	44.5660	42.7025	43.2437	2.0804	38.2390	53.8925
	S	0.1526	1.0197	1.1218	1.2665	1.1511	9.2087	0.9527	0.1338
	Total	98.5195	72.3033	76.4887	72.7272	73.4808	11.8104	66.5824	98.4344
	X	-17659	13694	13514	13685	13685	13751	13514	-17724
	Y	-32551	-472	-581	-478	-478	-764	-601	-32513
	Z	233	79	78	78	85	67	77	236
	Point #	1	2	3	4	5	6	7	8
	Date	Wednesday, April 26, 2023 3:44:19 PM	Wednesday, April 26, 2023 3:52:43 PM	Wednesday, April 26, 2023 4:25:17 PM	Wednesday, April 26, 2023 5:19:56 PM	Wednesday, April 26, 2023 5:27:46 PM	Wednesday, April 26, 2023 5:31:32 PM	Wednesday, April 26, 2023 5:35:26 PM	Wednesday, April 26, 2023 5:39:15 PM

2) Measuring Oxygen

	Beam current (nA)	4.9775
Weight %	F	2.8767
	O	32.0139
	P	12.2025
	Cl	0.1009
	Ca	31.8193
	S	1.2162
	Total	80.2294
Atomic %	F	4.4785
	O	59.1813
	P	11.6525
	Cl	0.0841
	Ca	23.4816
	S	1.122
	Total	100
	X	13516
	Y	-580
	Z	78
	Point #	1
	Date	Wednesday, April 26, 2023 4:38:40 PM

Supplementary Table S4.4. FTIR peak assignments for the calcium phosphate mineral phase analyzed in a sample of the E-K layer from specimen GMH CeIII-4936a-1932.

	wavelength (cm^{-1})	
	peak	**shoulder**
v_2CO_3	864	
v_1PO_4	963	
v_3PO_4	1012	1092
v_3CO_3	1436, 1456	

Supplementary Table S4.5. Raw data for X-ray diffraction bulk mineralogy analysis of sediment associated with Geiseltal anurans. Sample 1305-S1 represents a conservation material comprising mainly illite/smectite and muscovite with a minor composition of quartz, chlorite, feldspar and gypsum.

Sample	Quartz	K-feldspar	Calcite	Aragonite	Gypsum	Hydroxylapatite	Muscovite	Illite/Smectite	Chlorite	Clay Subtotal	Total	Description	Site Prefix	Stratigraphic Intervall	Specimen Number
1305-S1	10	3			1		33	49	4	86	100	grey contaminant on slab	CeIII	LUC/UMC	CeIII-1305-1933
3012-S1	X			X						0	0	black/brown sediment	CeV	MUC	CeV-3012-1934
3240-S1	X				X	X		X		0	0	black/brown sediment	LeoIII	UMC	LeoIII-3240-1934
4947-S1						X				0	0	black/brown sediment	CeI	UHM	CeI-4947-1930
4947-S2					X					0	0	black/brown sediment	CeI	UHM	CeI-4947-1930
4976A-S1	X				X					0	0	black/brown sediment	CeVI	UMC	CeVI-4976A-1934
6706-S1					X					0	0	black/brown sediment	CeII	LUC/UMC	CeII-6706-1930
6706-S2					X					0	0	black/brown sediment	CeII	LUC/UMC	CeII-6706-1930

4.10.4 Supplementary references

1. Pickel, W. & Wolf, M. Kohlenpetrographische und geochemische Charakterisierung von Braunkohlen aus dem Geiseltal (DDR). *Erdöl, Kohle, Erdgas, Petrochem.* **42**, 481–484 (1989).
2. Pickel, W. *et al.* Classification of liptinite – ICCP System 1994. *Int. J. Coal Geol.* **169**, 40–61, http://dx.doi.org/10.1016/j.coal.2016.11.004 (2017).
3. Gallwitz, H. Kalk, Kieselsäure und Schwefeleisen in der Braunkohle des Geiseltales und ihre Bedeutung für die Fossilisation. *PalZ* **29**, 33–37 (1955).
4. Taylor, G. H. & Cook, A. C. Sclerotinite in Coal - its Petrology and Classification. *Geol. Mag.* **99**, 41–52, https://doi.org/10.1017/S0016756800057113 (1962).

5. Krumbiegel, G., Rüffle, L. & Haubold, H. *Das eozäne Geiseltal: ein mitteleuropäisches Braunkohlenvorkommen und seine Pflanzen- und Tierwelt*. 227 pp. (A. Ziemsen Verlag, 1983).

6. Haubold, H. & Thomae, M. Stratigraphische Revision der Wirbeltierfundstellen des Geiseltaleozäns. *Hallesches Jb. Geowiss.* **15**, 3–20 (1990).

7. Voigt, E. Weichteile an Fischen, Amphibien und Reptilien aus der eozänen Braunkohle des Geiseltales. *Nova Acta Leopold. NF* **5**, 116–142 (1937).

8. Urmos, J., Sharma, S. K. & Mackenzie, F. T. Characterization of some biogenic carbonates with Raman spectroscopy. *Am. Mineral.* **76**, 641–646, http://www.minsocam.org/ammin/AM76/AM76_641.pdf (1991).

5. Evolutionary constraints on anuran melanin for 45 million years

This chapter presents a quantitative analysis of the fossil soft tissues of the soft tissue metal chemistry and the geometry of fossil microbodies (i.e., melanosomes) preserved in the Geiseltal anurans. Geometry data for melanosomes from the Geiseltal anurans is combined with data from anurans from two additional fossil localities and from extant anurans in order to shed light on the evolution of melanin in anurans. The chapter comprises a manuscript that has been submitted to the journal *iScience* and is co-written by seven authors. The chapter is organised as follows: Summary, Introduction, Results, Discussion, Limitations of the study, Acknowledgements, Author contributions, Declaration of interests, References, Star Methods and Supplemental Information.

Candidate contribution to the study. DF contributed to the design of the study and performed a literature review on the soft tissue features of the Geiseltal anurans. OW provided access to the Geiseltal Collection and sampling permission. Both DF and MMN collected soft tissue samples for SEM imaging. VR provided SEM images and measurement data of melanosomes from certain extant specimens and from fossil specimens that are not from Geiseltal. MMN provided SEM images on a fossil specimen that is not from Geiseltal. AQ and BCH provided certain SEM images and measurement data on melanosomes from extant specimens. DF performed the SEM analysis on the Geiseltal samples and certain extant samples. MMN collected the micro-SRS-XRF data. DF performed the measurements of melanosomes from the Geiseltal dataset and from certain Libros samples. DF performed the statistical analysis of all fossil and extant data. DF processed the SRS-XRF data with assistance from MMN and SW. DF wrote the first draft of the paper, produced the figures and revised subsequent drafts in line with comments from the other authors.

Abstract. Fossil evidence of melanin is a remarkable palaeobiological resource but the evolution of melanin through deep time is poorly resolved, partly because few studies have integrated data from

fossils and their extant relatives. Here, we use data on melanin-rich organelles – melanosomes – in extant and fossil anurans to show that evolution of melanin in the skin during the last ca. 45 million years is decoupled from that in the eyes and internal tissues. Melanosomes from the skin differ in geometry between extant and fossil species. In contrast, melanosomes from the eyes and internal tissues show strongly conserved geometries in all fossil and extant species. These tissue-level trends in melanosome evolution are probably controlled by physiological constraints on melanosome function that have been in place at least since the Eocene. The liberation of skin melanosomes from such constraints on geometry may reflect evolutionary tradeoffs linked to diversification of integumentary coloration and/or habitat.

5.1 Introduction

Melanin is a light-absorbing polymeric pigment[1-3] that is widespread in living organisms and serves critical physiological roles in photoprotection, visual signaling, thermoregulation, metal regulation and as an antioxidant. [4] In vertebrates, melanin is packaged as membrane-bound organelles – melanosomes – that typically occur in connective tissues, the eyes, integument (e.g., feathers, hair and skin) and internal organs (e.g., heart, kidneys, liver, lungs and spleen).[1-5]

Fossil evidence of melanin can inform on the original colors[6-14], physiology[5,15], internal anatomy[5,16,17] and phylogenetic position[18] of fossils and on physical and chemical taphonomic processes.[19-26] Few studies, however, have addressed the evolution of melanin in a particular vertebrate group.[4,7,12,15] Given the diverse biological functions of melanin, especially of non-integumentary melanins[5,27,28], comparative analysis of melanin in extant and fossil representatives of related taxa has the potential to shed light on the evolution of vertebrate physiology[15] and ecology.[7] Here, we use anurans as a case study: we combine data on the geometry of melanosomes extracted from various tissues in extant anurans (Table 5.1 in Star Methods) with data from fossil specimens from various localities, in order to shed light on the evolution of melanosomes in anurans over geological timescales.

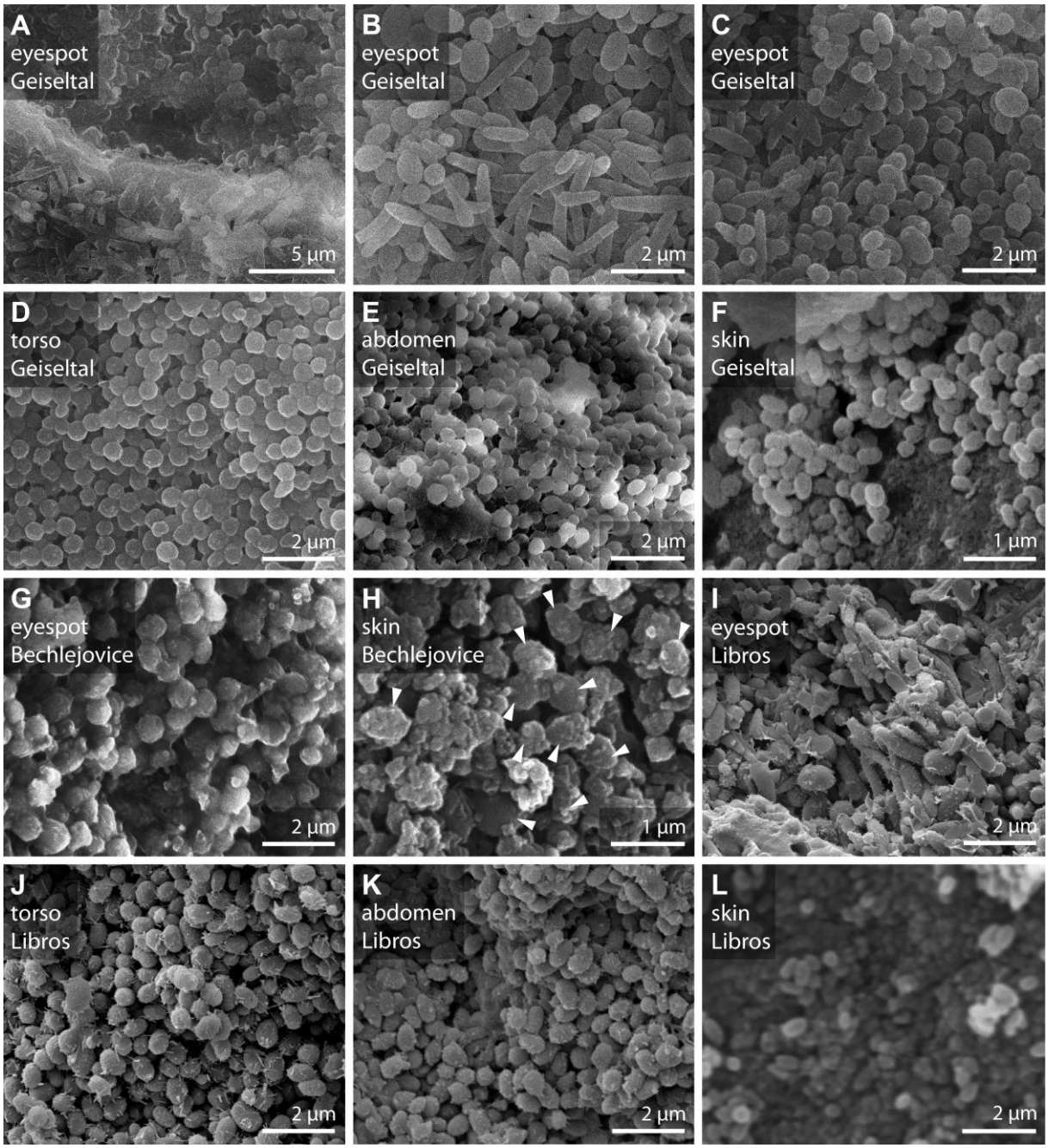


Figure 5.1: Electron micrographs of melanosomes preserved in fossil anuran soft tissues. (A–L) Fossil melanosomes from different body regions of specimens from Geiseltal (Eocene, Germany, A–F), Bechlejovice (Oligocene, Czech Republic, G–H) and Libros (Miocene, Spain, I–L). (A–C, G, I) Fossil melanosomes from the eyespots. (D, J) Fossil melanosomes from the torso. (E, K) Fossil melanosomes from the abdomen. (F, H, L) Fossil melanosomes from the skin. (A) Layer of ovoid melanosomes overlain by a layer of rod-shaped melanosomes, GMH CeIII-4983-1932. (B) Rod-shaped melanosomes and ovoid melanosomes, GMH CeIII-4983-1932. (C) Ovoid melanosomes, GMH CeIII-6698-1932. (D) Spheroidal melanosomes, GMH CeIII-4967-1932. (E) Spheroidal and ovoid melanosomes, GMH CeIII-4967-1932. (F) Ovoid melanosomes, GMH CeIII-4967-1932. (G) Ovoid melanosomes, NHML-OR35184. (H)

Ovoid melanosomes (arrowheads), NHML-OR35184. (I) Rod-shaped melanosomes and ovoid melanosomes, NHML-R4982. (J) Ovoid melanosomes, NHML-R4982. (K) Ovoid melanosomes, NHML-R4982. (L) Ovoid melanosomes, MNCN 63798.

The fossil anurans used in this study are from the Konservat-Lagerstätten of Geiseltal (Middle Eocene, Germany), Bechlejovice (Early Oligocene, Czech Republic) and Libros (Late Miocene, Spain). Specimens from all three biotas preserve soft tissues that are defined, in part, by dark carbonaceous films of melanosomes[17,29-31] (Figures 5.1 and 5.2). Our dataset spans ca. 45 million years and thus provides an excellent opportunity to investigate evolutionary trends in melanosome geometry. This requires, however, that the tissue of origin is known for melanosomes preserved in different body regions of fossils. While melanosomes in the eyespots of fossils can reasonably be interpreted as derived primarily from the eye (i.e., iris, choroid and/or retinal pigmented epithelium), fossil melanosomes from the body outline have many potential origins.[5,27] The fossil anurans used in this study all preserve the E-K layer of the mid-dermis in calcium phosphate.[17,29,30] Fossil melanosomes located external to this layer derive from the skin (i.e., the upper dermis and/or epidermis).[16,29,30] Melanosomes preserved medial to the mineralized skin most plausibly derive from one, or more, of the internal organs. In extant anurans, melanosomes show tissue-specific variation in geometry and chemistry[5]; these attributes may therefore constrain interpretations of the tissue of origin. Prior to using preserved melanosome attributes for evolutionary studies, the impact of diagenesis on these attributes must be considered. The elemental[17,22,23] and organic chemistry[10,24,26,32] of fossil melanosomes are subject to strong diagenetic alteration and thus vary among biotas.[17] In contrast, changes in melanosome geometry during fossilization are controlled primarily by temperature[33]; maximum burial temperatures are inferred to be similar for all three of the biotas studied here (see Methods) and thus geometry is the key melanosome attribute examined in this study.

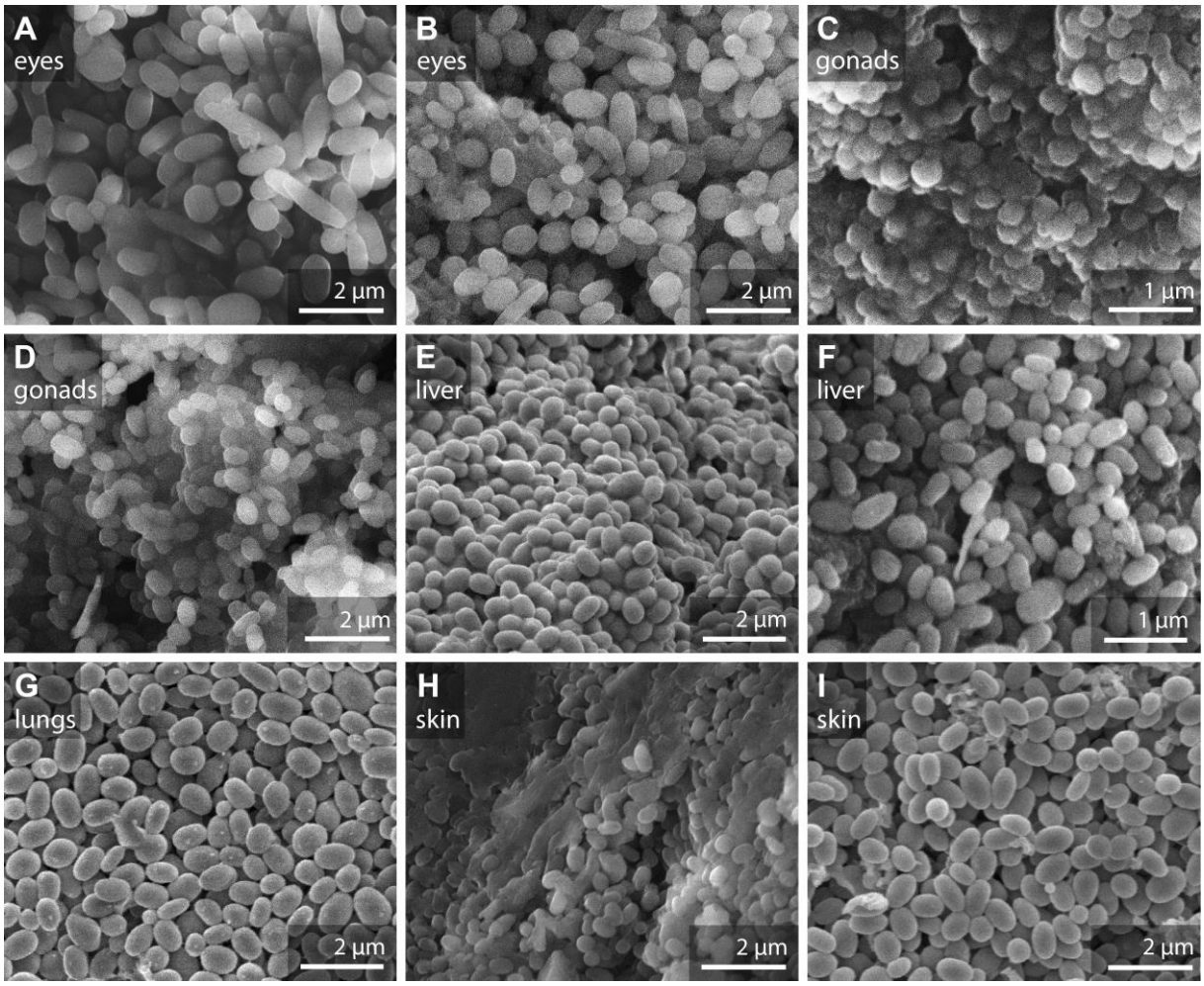


Figure 5.2: Melanosomes from soft tissues of extant anurans. (A) Eye, Bombina variegata. (B) Eye, Rhaebo guttatus. (C) Gonads, Bombina variegata. (D) Gonads, Rhaebo guttatus. (E) Liver, Xenopus laevis. (F) Liver, Rhaebo guttatus. (G) Lungs, Xenopus laevis. (H) Skin, Rhaebo guttatus. (I) Skin, Xenopus laevis.

Spheroidal and ovoid melanosomes were previously identified from integumentary and non-integumentary fossil soft tissues in the Geiseltal specimens.[29] Melanosomes were previously identified from the skin and eyespot of a specimen from Bechlejovice.[17] Previous reports of melanosomes preserved in the fossil anuran specimen NHML-R4982 from Libros include data on melanosome geometry and chemistry[5], summarized as follows. Melanosomes are spheroids, ovoids and rods in the eyespot; in contrast, melanosomes from both the torso and abdomen are spheroids and ovoids. In the abdomen, these melanosomes are separated spatially into two populations (interpreted as skin and liver melanosomes, respectively). In specimen NHML-R4982, Cu and Zn are enriched in the torso and

pelvis; Zn is enriched in the eyespot and the body outline (interpreted as skin melanosomes[5]). Comparable data have not been reported previously for anurans from Geiseltal and Bechlejovice.

5.2 Results

5.2.1 Melanosome geometry

Scanning electron microscopy confirms the preservation of melanosomes in all studied samples of fossil anuran soft tissues (Figure 5.1); all enzymatic tissue extracts from extant anurans comprise primarily melanosomes (Figure 5.2).

The morphospace (area and data distribution on a width/length scatterplot) for melanosomes from extant anurans and for anurans from Geiseltal and Libros is broadly similar, albeit with some longer melanosomes in the Libros anurans and larger spheroidal forms in the Geiseltal anurans (Figure 5.3A). The morphospace for melanosomes from the Bechlejovice anurans is markedly smaller than that for the other biotas, but this probably reflects the smaller sample size (Figures 5.3A and S5.7A; Pearson's $r(2) = 0.9085$, $p = 0.0915$ where the morphospace is defined by convex hulls and Pearson's $r(2) = 0.3224$, $p = 0.6776$ where the morphospace is defined by 95% confidence ellipses).

Melanosomes from extant and fossil anurans vary in length (extant: 693 ± 244 nm; fossil: 651 ± 321 nm; Figures 5.1, 5.2, S5.9, S5.11, S5.13, S5.15) and aspect ratio (extant: 0.672 ± 0.17; fossil: 0.820 ± 0.18; Figures 5.1, 5.2, S5.10, S5.12, S5.14, S5.16). As in other extant anurans[5,27], melanosomes from the extant species studied here show tissue-specific geometry (Figures 5.2, S5.9–S5.16); melanosomes from a given tissue, however, vary somewhat in geometry among species (Figures 5.2, S5.9–S5.16). As expected, melanosomes from fossil specimens show different geometries among body regions, i.e., abdomen, eyespots, skin, and torso (Figure 5.3; Figures S5.9–S5.16). The morphospace of the total dataset largely corresponds to the morphospace of melanosomes from the eyespots of fossil specimens and eyes of extant specimens, indicating that the eye melanosomes are responsible for

most of the observed melanosome diversity (Figures 5.3A and 5.3B, S5.3). The morphospace for melanosomes from a particular body region / tissue is independent of sample size (Pearson's $r(14) = 0.117$, $p = 0.666$ if morphospace were defined by 95% confidence ellipses).

Eyes and eyespots. Melanosomes from the eyes of extant anurans and from the eyespots of Libros and Geiseltal specimens show populations of spheroids, ovoids and rods (Figures 5.1A–C, 5.1I, 5.2A–B); each dataset (i.e., one dataset per fossil biota and the dataset comprising all extant anurans studied) occupies a large region of morphospace (Figures 5.3B and S5.3). Populations of rods are usually mixed with ovoids and spheroids (Figure 5.2B), but rods can also form spatially separated clusters and layers (Figures 5.1A–C, 5.1I; 5.2A). Melanosomes from the eyespots of the Bechlejovice anurans show only ovoid geometries (Figure 5.1G) that define a small morphospace (Figure 5.3B). Accordingly, boxplots of melanosome length (Figure S5.9) and aspect ratio (Figure S5.10) show that except for Bechlejovice, eye melanosomes from each dataset show similar variation in aspect ratio and length. Melanosomes from the four datasets are similar in length (differences are not significant; Welch test, $p = 0.210$; Table S5.1) and melanosomes from the Libros specimens and extant anurans are similar in aspect ratio (differences are not significant; Dunn's post hoc test, $p = 0.646$; Table S5.2). Melanosomes from the Geiseltal and Bechlejovice specimens, however, differ significantly in aspect ratio from extant anuran melanosomes (Table S5.2); this reflects, at least in part, the presence of large spheroidal melanosomes in the Geiseltal dataset and the absence of rod-shaped melanosomes in the Bechlejovice dataset.

Skin. SEM images of melanosomes from the skin of extant and fossil anurans show intermingled spheroids and ovoids (Figures 5.1F, 5.1H, 5.1L, 5.2H, 5.2I). Each of the four datasets occupies a similar region of morphospace (Figure 5.3C). Melanosomes from the Bechlejovice, Libros and extant specimens are similar in length (Figure S5.11; differences are not significant, Table S5.2), but melanosomes from Geiseltal are significantly smaller than all others (Figure S5.11; Table S5.4).

Melanosomes from all fossil skin samples show similar aspect ratios; those aspect ratios are higher than in extant anurans (Figure S5.12; differences are significant, Table S5.2).

Abdomen (fossil specimens) / Internal tissues (extant specimens). SEM images show predominantly spheroids in the Geiseltal specimens (Figure 5.1E) and ovoids in the Libros specimen (Figure 5.1K) and in extant anurans (Figures 5.2C–G).

Melanosomes from the abdomen of fossils from Libros and Geiseltal show little overlap in morphospace (Figures 5.3E and 5.3F) and differ significantly in geometry (Table S5.2), suggesting that they originate from different tissues. The morphospace for the Geiseltal abdominal melanosomes shows little overlap with that of connective tissue (Figures S5.6C and S5.8C) or the spleen (Figures S5.6D and S5.8D) in extant anurans and is much smaller than that for the lungs (Figures S5.6E and S5.8E) and liver (Figures 5.3E and S5.4C). Instead, the morphospace of the Geiseltal abdominal melanosomes most closely resembles that of the gonads of extant anurans (Figure 5.3F). Indeed, the aspect ratio of the fossil melanosomes strongly resembles that of the gonads of *Bombina* (Figure S5.14; Kolmogorov-Smirnov test, $p = 0.7829$). Except for these data on *Bombina*, the melanosomes from all internal organs of extant anurans differ in geometry to those from the abdomen of Geiseltal specimens (Figures S5.13 and S5.14). The gonads are thus the most plausible source for the abdominal melanosomes in the Geiseltal anurans.

Melanosomes from population 1 from the abdomen of the Libros specimen occupy a similar morphospace to that of melanosomes from the liver (Figure 5.3E), gonads (Figure 5.3F) and lungs (Figures S5.4C and S5.8E) but show little overlap in morphospace with that of connective tissue (Figures S5.6C and S5.8C) and the spleen (Figures S5.6D and S5.8D). The morphospace for the Libros abdominal melanosomes is, however, greater than that for the gonads (Figure 5.3F) and lungs (Figures S5.6E and S5.8E); given the smaller sample size for the Libros melanosomes than for these extant tissues, it is thus unlikely that the fossil melanosomes represent a subset of, and derive from, these tissues. Statistical analysis of the geometry data reveals that the Libros melanosomes of population 1 do not differ significantly in geometry to those from the connective tissue (Figures S5.6C and S5.8C) or from

the lungs (Figures S5.6E and S5.8E) of extant anurans. The spleen, however, can be excluded as a likely source of the fossil melanosomes because of their dissimilar morphospace relative to that of the fossil melanosome morphospace (see above). The lungs can be excluded as a likely source because the morphospace of the liver (Figure 5.3E) shows a better overlap with that from population 1; the aspect ratio of population 1 is also more similar to that from the liver than for that from the lungs (Table S5.2). Further, melanosomes are much more abundant in the liver of anurans relative to other internal tissues.[5,27] Collectively, these data indicate that the melanosomes of population 1 are most parsimoniously interpreted as from the liver of extant anurans (Table S5.2), and not as skin melanosomes as reported by Rossi *et al.*[5]. This interpretation is supported by statistical analyses: the geometry of melanosomes from population 1 (in specimen NHML-R4982) differs from that of unequivocal skin melanosomes (in specimen MNCN 63798; aspect ratio: two-sample t-test, $p = 0.001$; length: two-sample t-test, $p = 1.189*10^{-4}$). Further, melanosomes from population 1 are significantly larger than melanosomes from the skin of extant specimens (two-sample t-test, $p = 3.231*10^{-8}$; Table S5.1).

Melanosomes from abdomen population 2 occupy a similar morphospace to the liver and gonads of extant anurans. The former differ significantly in size from all melanosome populations in extant specimens and have similar aspect ratios to those from connective tissue (Figures S5.6C and S5.8C), the liver (Figure 5.3F), lungs (Figures S5.6E and S5.8E) and the spleen (Table S5.2). The fossil melanosomes, however, are unlikely to derive from connective tissue (due to low abundance of melanosomes *in vivo*), the lungs (little overlap in morphospace) or spleen (due to the small size of the tissue *in vivo*); liver and gonads are more likely potential sources.

Torso (fossil specimens) / Internal tissues (extant specimens). SEM images show that melanosomes are spheroids and ovoids in the Geiseltal specimens (Figure 5.1D) and ovoids in the Libros specimen (Figure 5.1J). Melanosomes from the torso of specimens from Libros and Geiseltal overlap considerably in morphospace (Figure 5.3D) but differ significantly in size (Table S5.2), suggesting different tissue origins for each specimen.

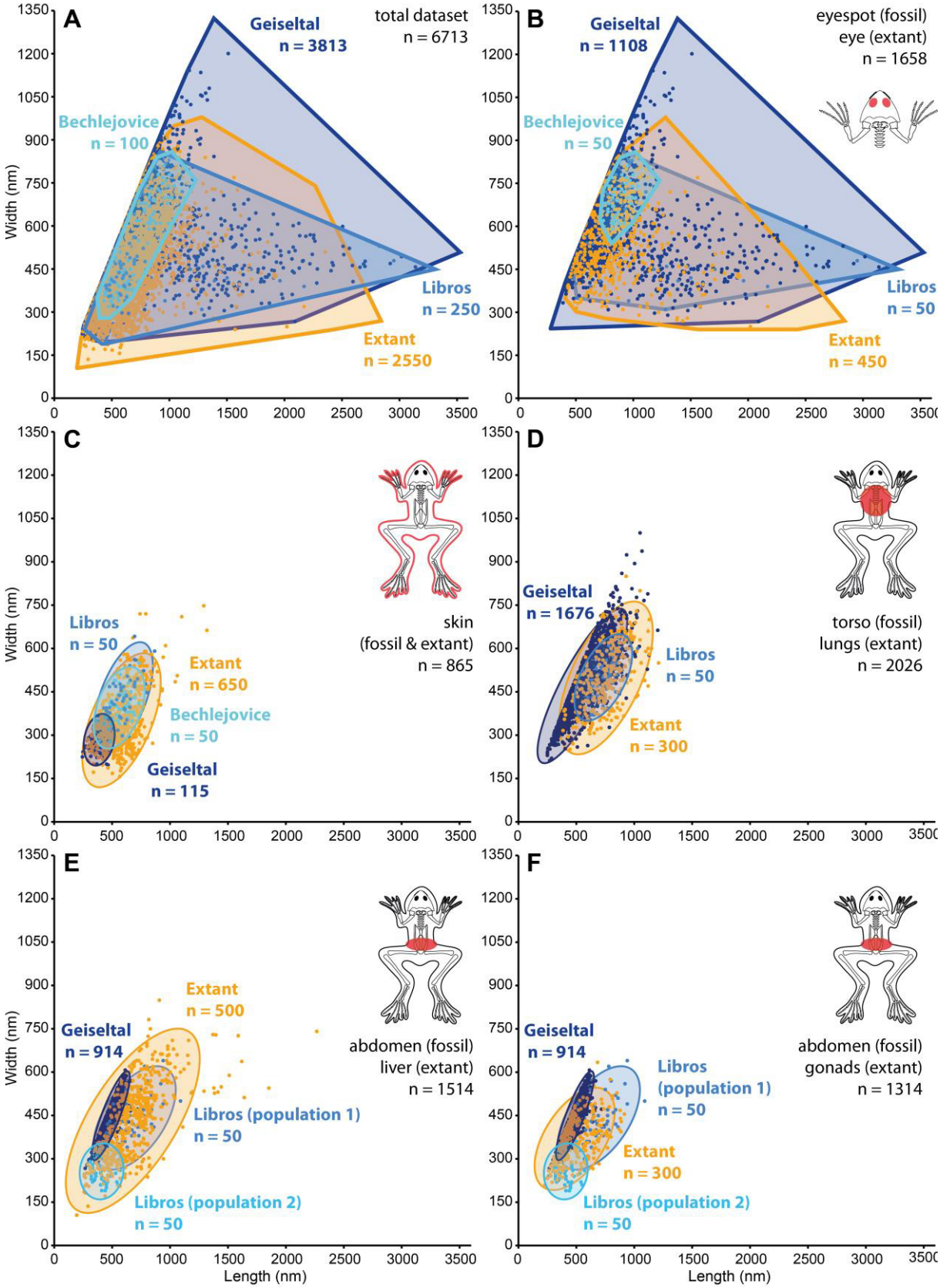


Figure 5.3: Scatterplots showing the morphospace for melanosomes from fossil and extant anurans. Fossil data are for various body regions of fossil anurans from the Geiseltal, Bechlejovice and Libros biotas; extant data are for various organs. (A–B) Convex hulls are used to visualise the morphospace for the total dataset and for the

eyes/eyespots. (C–F) 95% confidence ellipses are used to visualise the morphospace for each tissue / body region. Schematic frog skeleton indicates the sampling region for melanosomes from fossil anurans. (A) Morphospace of the total dataset. (B) Morphospace of melanosomes from the eyespots of fossil specimens and eyes of extant specimens. (C) Morphospace of melanosomes from fossil skin and skin from extant anurans. (D) Morphospace of melanosomes from the torso of fossil specimens and from the lungs of extant specimens. (E) Morphospace of melanosomes from the abdomen of fossil specimens and from the liver of extant specimens. (F) Morphospace of melanosomes from the abdomen of fossil specimens and from the gonads of extant specimens.

The morphospace for melanosomes from the torso of the Libros specimen shows extensive overlap with that for several tissues in extant anurans, i.e., the heart (Figures S5.6A and S5.8A), lungs (Figures 5.3D and S5.4B), liver (Figures S5.5B and S5.7D), connective tissue (Figures S5.5C and S5.7E) and the spleen (Figures S5D and S5.7F). Melanosomes from the liver and spleen of extant specimens can be excluded as a likely source for the fossil torso melanosomes as melanosomes from these tissues each differ significantly in length from the fossil melanosomes. Of the remaining tissues, the lungs are the most plausible source for the fossil melanosomes; indeed, statistical analysis of the geometry data reveals no significant differences between these and the melanosomes from the torso of the Libros specimen (Table S5.2). The lungs are thus the most likely source for the torso melanosomes of the Libros specimen.

The morphospace for torso melanosomes from Geiseltal specimens is much larger than that for connective tissue (Figures S5.5C and S5.7E), the spleen (Figures S5.5D and S5.5F) and the gonads (Figures S5.6B and S5.8B) in extant anurans; these tissues are thus unlikely to represent the source of the fossil melanosomes. The morphospace for the Geiseltal torso melanosomes is, however, smaller than (and could potentially represent a subset of) that for the heart (Figures S5.6A and S5.8A) and liver (Figures S5.5E and S5.7D). The heart is an unlikely source because it contains few melanosomes in extant anurans[5], but the liver, which contains abundant melanosomes *in vivo*[5,27], is a more plausible source. Notably, the morphospace of the Geiseltal torso melanosomes closely resembles that of

melanosomes from the lungs of extant anurans (Figures 5.3D and S5.4B); both melanosome length and aspect ratio, however, differ significantly between these two datasets (Figures S5.15 and S5.16, Table S5.2). The Geiseltal torso melanosomes are therefore difficult to assign confidently to a particular tissue based on these basic geometry data.

Collectively, these data demonstrate that interpretation of the tissue origins of the fossil melanosomes in the torso of anurans from Geiseltal is equivocal using basic geometric parameters (i.e., length and aspect ratio). Exploration of the data using additional parameters (mean length, mean aspect ratio, kurtosis for length and aspect ratio, skew for length and aspect ratio and interquartile range for length and aspect ratio) is therefore necessary in order to identify the tissue source of the melanosomes.

Principal component analysis (PCA) of the geometry data for the total dataset successfully resolves major patterns in melanosome geometry; the first and second principal components (PC1 and PC2) combined explain nearly 100% of the variation in the raw dataset (Figure 5.4A). The PCA plot reveals a strong signal for different tissues and body regions (Figures 5.4A and 5.4B). The differences between groups primarily reflect variation in PC1, which in turn primarily reflects melanosome length (more specifically: mean length and interquartile range for length; Figure 5.4A). Data for all fossil eyespots and eyes of extant specimens form a distinct group in the far right of the plot; the data for skin melanosomes from all fossil and extant specimens form a tight cluster in the far left of the plot. Between these two groups lie the data for the lungs, liver and gonads of extant specimens and for the torso and abdomen of Geiseltal and Libros specimens. For all of these samples (liver, lungs, gonads for extant specimens); torso and abdomen for fossil specimens), the position of the relevant datapoints along the PC1 axis is most critical as this PC is responsible for most of the variation in the dataset. As expected, Libros abdomen population 1 plots close to the extant liver along the PC1 axis; population 2, however, plots in the far left of the morphospace, close to the gonads. This suggests that the abdomen of the Libros anuran includes both liver and gonad melanosomes. The Libros torso

melanosomes plot closest to the lungs; this is consistent with both the morphospace plots and statistical analyses.

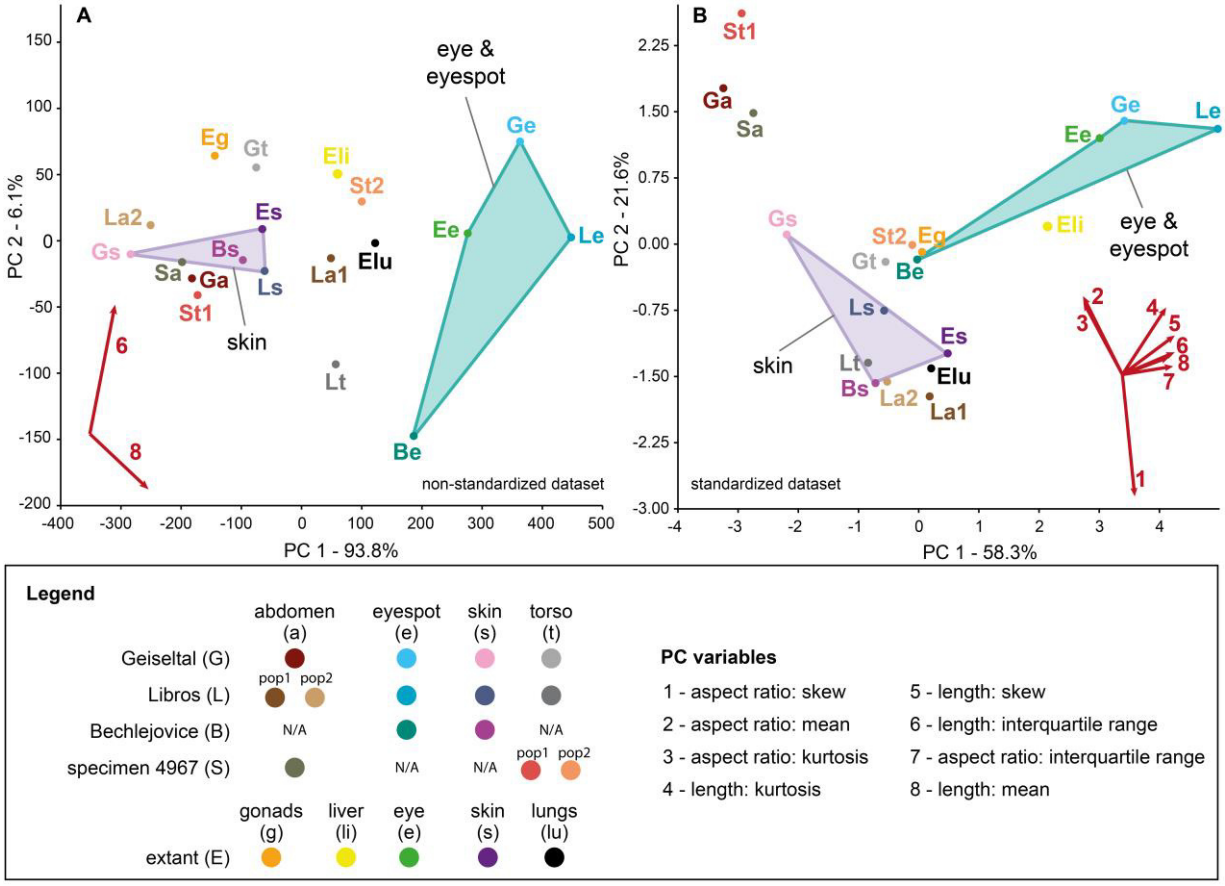


Figure 5.4: Principal Components Analysis (PCA) of geometry data for melanosomes from different body regions of fossil and extant anurans. Data point labels use upper case to denote biota and lower case, body region as indicated in (C), e.g., Ge denotes Geiseltal eyespot. pop1, population 1; pop2, population 2. Data for specimen GMH CeIII-4967-1932 are included in the Geiseltal data and are shown separately. (A) Non-standardised dataset; the biplot in the bottom of the morphospace plot shows that most of the morphological variation is driven by the mean and interquartile range of melanosome length. The vectors for the variables 1, 2, 3, 4, 5 and 7 are too small to be displayed at this scale. (B) Standardised dataset; the biplot in the bottom of the morphospace plot shows that most of the morphological variation is driven by the skew, mean and kurtosis of melanosome aspect ratio. Most data points plot closely to each other and the morphospace of abdomen, skin and torso show an extensive overlap. Discrimination between skin and non-integumentary tissues is only possible for eye tissues / eyespots. This PCA does not yield meaningful results.

As expected, the Geiseltal abdominal melanosomes plot close to the gonads. The torso melanosomes plot between the gonads (to the left of the morphospace) and the liver and lungs (to the right), albeit more closely to the gonads, suggesting a common source with the abdominal melanosomes. The proximity of the torso melanosomes to the liver and lungs, however, suggests that the torso of certain Geiseltal anurans may also include melanosomes from those two sources. This is supported by the data from three sampling points (torso sample 1, torso sample 2 and abdomen sample) from the Geiseltal specimen GMH CeIII 4967-1932 (Figure 5.4A). Torso sample 1 plots close to the abdomen sample and not far from the gonads, whereas torso sample 2 plots between the liver and lungs (Figure 5.4A).

These interpretations of the Geiseltal torso melanosomes can be tested using the preserved chemistry of the melanosomes: in extant vertebrates, melanosomes show tissue-specific chemistry.[5]

5.2.2 SRS-XRF analysis constrains interpretations of fossil soft tissues

Chemical mapping using synchrotron rapid scanning-X-ray fluorescence analysis (SRS-XRF) can reveal cryptic tissue-specific variation in the chemistry of fossil melanosome films, even if the preserved chemistry has been impacted by diagenesis.[5,17] Previous SRS-XRF analyses of the adult anuran specimen from Libros reveal a relatively homogeneous metal chemistry for the internal melanosomes..[5] The PCA results reported here, however, indicate the lungs as the source of the torso melanosomes, the liver as the source of melanosomes from abdominal population 1 and the gonads, for melanosomes from abdominal population 2. This shows that variation in the geometry of fossil melanosomes is not always accompanied by variation in melanosome chemistry, as in extant anurans.[5] The homogenous chemistry of the internal melanosomes in the Libros anurans may be an original biological feature (i.e., whereby melanosome geometry and chemistry are independent in certain taxa) or may reflect overprinting of original chemical variation during diagenesis. Chemical data have not been reported previously for specimens from Geiseltal. We therefore used SRS-XRF to test our

interpretation of a single tissue source for the preserved melanosome films from the torso and abdomen of GMH CeIII 4967-1932 (Figures 5.5A–I, S5.1F, S5.19A–C). Principal component analysis (PCA) of the SRS-XRF element maps (Figures 5.5D–H, S5.18) yields various components that, in conjunction with the element maps (Figure 5.6), facilitate the identification of 13 regions of interest (ROI) selected for further analysis (Figures S5.19–S5.23, S5.24A). To aid visualization of chemical variation among ROI, the data were $\log_{10}$-transformed and combined to form six groups (Figures 5.7 and S5.24B): Groups I–IV collectively represent all soft tissue samples and are characteristically enriched in Ca and Ni (and, to a lesser extent, Cu, Ti, Co, V, Mn and Cr) relative to Groups V and VI, which collectively represent sedimentary matrix and embedding resin. Groups I and II (from the torso and abdomen, respectively) are enriched in Zn, with slightly more Ni and/or Ca in Group II. In contrast, Groups III and IV (from the hindlimbs) are depleted in Zn and (especially for Group III) enriched in Ca (Figure 5.7, Table S5.3).

These differences in metal concentrations are significant for many elements (Tables S5.6, S5.7A–B). Ca, Cu and Zn are of particular relevance as Ca is a major component of the mineralized skin in the Geiseltal anurans[29] and Cu and Zn are often associated with melanosome films in fossil vertebrates.[17,34,35] Ca and Ni concentrations differ significantly among all groups (Tables S5.7A–B). Differences in element concentrations between Group I and Group II are significant only for Ca and Ni, but not Zn (or other elements). Groups I and II differ from Groups III and IV in their Ni, Cu and Zn concentrations. Variation in Ca among groups most likely reflects differences in the relative thickness and/or continuity of the E-K layer (which is replicated in calcium phosphate) in these sample regions; Ni shows similar spatial variation to Ca and is thus probably associated primarily with the mineralized E-K layer. Variation in Cu and Zn primarily reflect variation in the composition of the melanosome films.

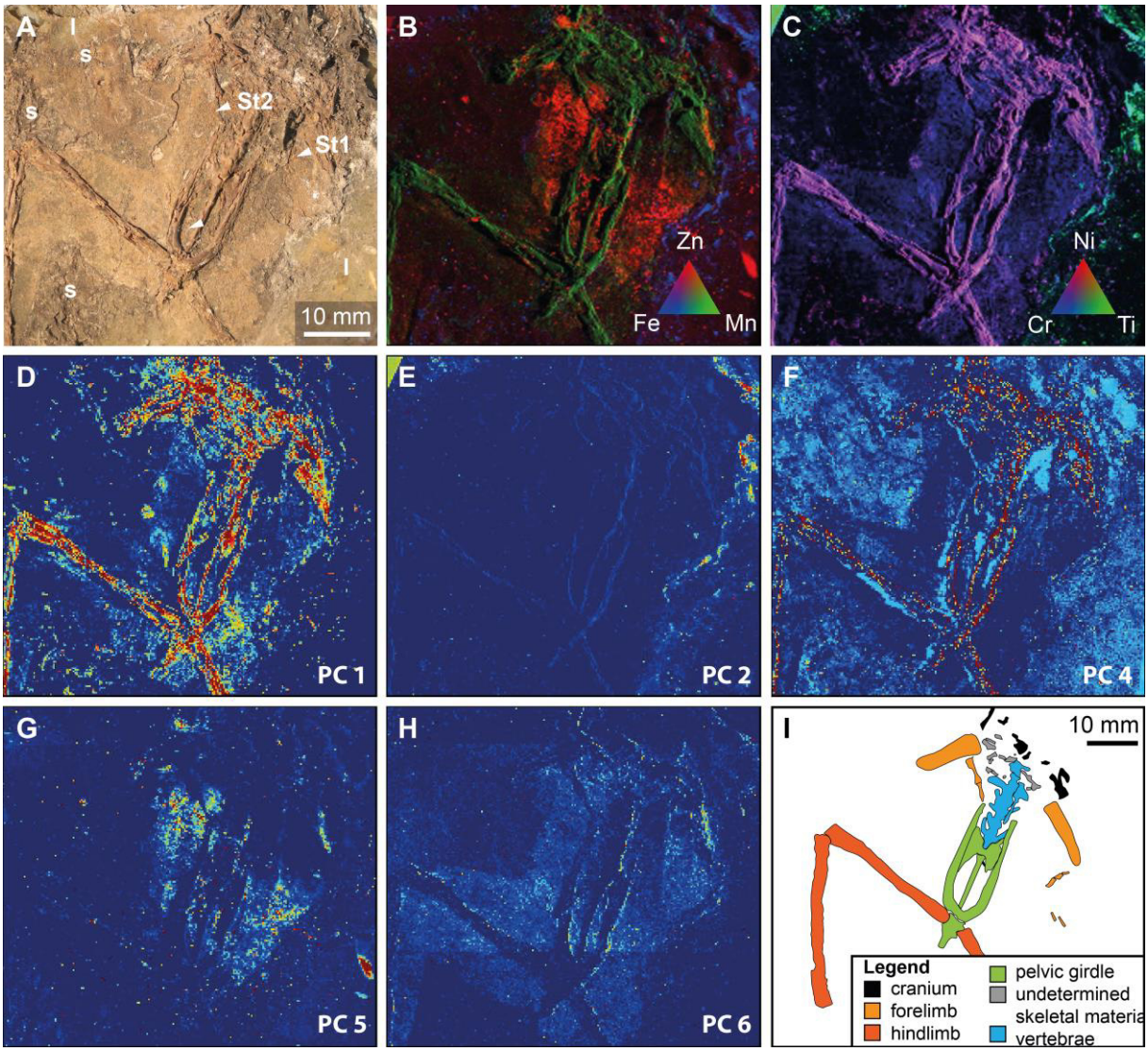


Figure 5.5: Synchrotron rapid scanning-X-ray fluorescence (SRS-XRF) analysis of GMH CeIII-4967-1932 from the Eocene Geiseltal biota. (A) Truncated photograph of the specimen showing extensive soft tissues, visible as a beige-coloured material and/or a dark brown material in the torso and around the hindlimbs. Arrowheads indicate sample locations; s, sediment, St1, sampling location 1 in torso, St2 sampling location 2 in torso, l, lacquer. Scale in (A) also applies to (B–H). (B, C) SRS-XRF tricolour maps of the region shown in (A). (D–H) Maps for selected principal components (PCs) identified during principal component analysis of the SRS-XRF data (see Methods). PC 1 corresponds primarily to Ca, Ni and Sb. PC 2 corresponds primarily to Fe. PC 4 corresponds to Co and Cu. PC 5 corresponds primarily to Zn. PC 6 corresponds primarily to Ti, V, Cr and Mn. The map in (H) shows horizontal bands that differ in tone; these features are artefacts generated during data acquisition. (I) Line drawing of the skeleton.

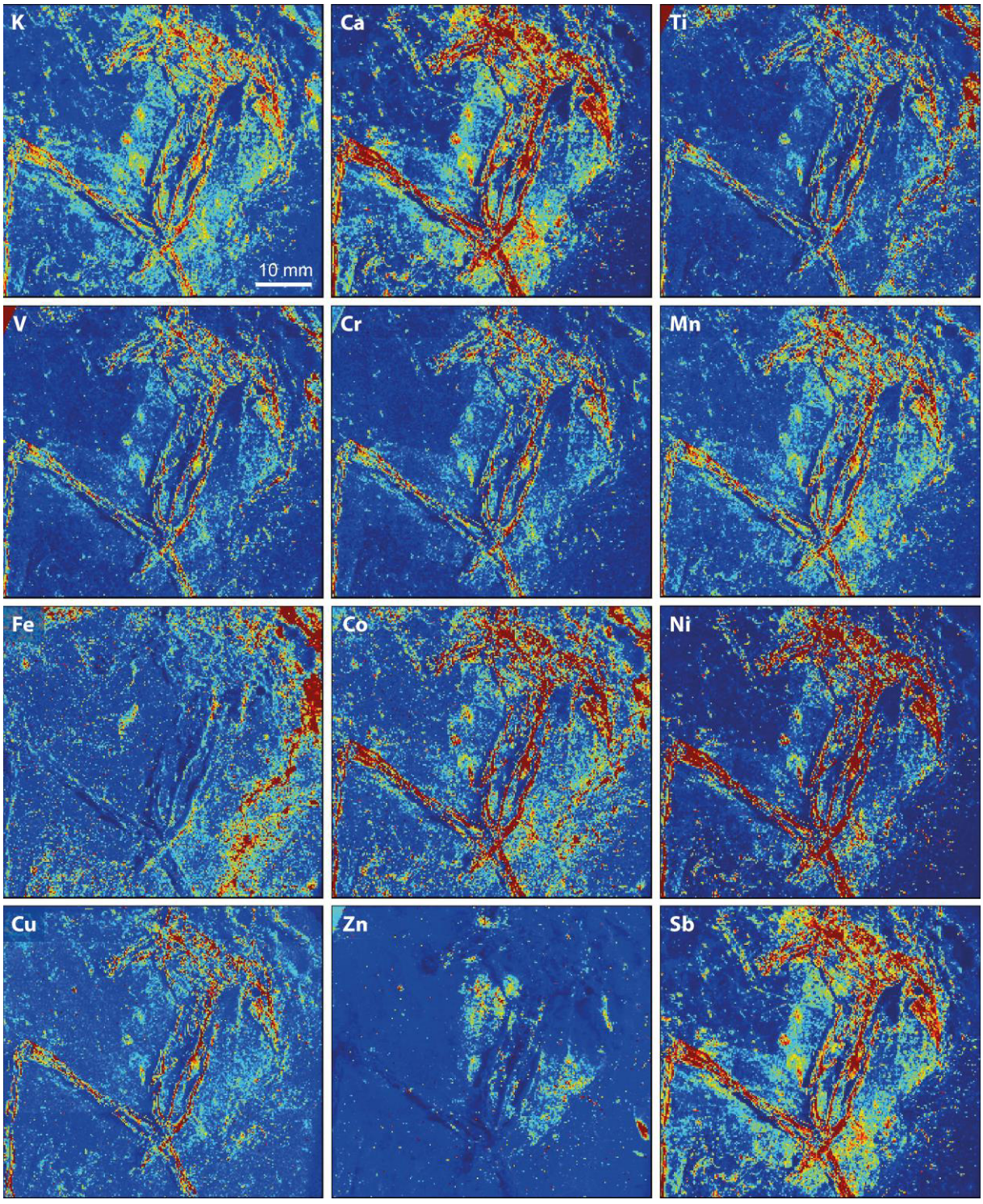


Figure 5.6: SRS-XRF maps of GMH CeIII-4967-1932. Bones are enriched in K, Ca, Mn, Co, Ni, Cu and Sb relative to the host sediment and embedding lacquer. The soft tissues in the torso are enriched in Zn relative to the bones, host sediment and lacquer. K, Ca, Mn, Co, Ni, and Sb are associated with soft tissues in the torso, in the abdomen and in the hindlimbs. The map for Cu shows horizontal bands that differ in tone; these features are artefacts generated during data acquisition. Scale in map for K applies to all figure parts.

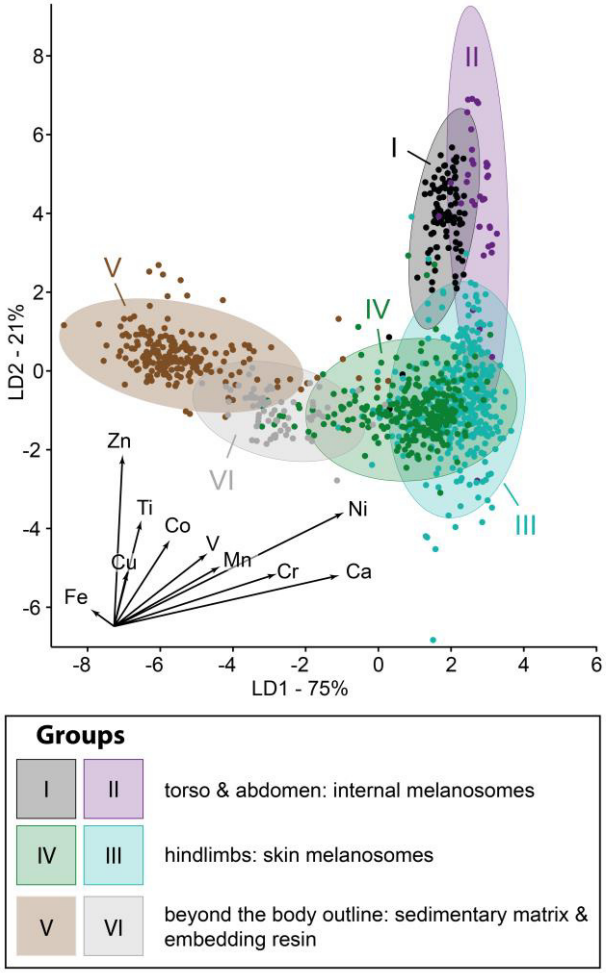


Figure 5.7: Linear discriminant analysis (LDA) of the metal chemistry of selected regions of interest (ROI) in SRS-XRF maps of GMH CeIII-4967-1932 (Figure S5.19). The chemospace for each ROI is represented by 95% confidence ellipses. The biplot in the bottom left of the chemospace plot shows that most of the chemical variation in the dataset is driven by Ca, Ni, and Zn.

These data indicate that Groups I (torso) and II (abdomen) likely represent melanosomes from a common source. This supports the PCA of the melanosome geometry parameters, which indicates that melanosomes from the torso and the abdomen derive primarily from the gonads. There is no evidence from the SRS-XRF data for additional melanosome sources in the torso (i.e., liver and / or lungs); this is not fully consistent with the PCA plot, which shows that the melanosome geometry data from St2 plot closest to, and between, the liver and lungs. The sample St2 may therefore represent a very localized region of melanosomes from the liver / lungs that is too small to be identified in the SRS-XRF maps. Alternatively, the melanosomes from the gonads, liver and/or lungs and gonads do not differ in chemistry in this fossil taxon; as with the Libros anuran (see above), this could be explained as a real biological feature or as a diagenetic artefact. Groups III and IV likely represent melanosomes from a different source to Groups I and II; the location of these samples and the lack of evidence for redistribution of internal melanosomes into the limbs (as would be evidenced by elevated Zn

concentrations in the melanosomes from the hindlimbs), suggests that Groups III and IV represent skin melanosomes. The chemical differences between Groups III and IV may reflect a greater contribution of preserved E-K layer to the signal for Group III and/or a greater contribution of host matrix to the signal for Group IV.

5.3 Discussion

This study shows that the melanosomes from various body regions of fossil anurans from the Miocene and Eocene are similar in geometry to melanosomes from corresponding body regions in extant anurans. The tissue of origin of the fossil melanosomes is tightly constrained for those in the eyespots and skin of the fossil anurans, based on the anatomical location of samples (for the fossil eyespot melanosomes) and position of analyzed melanosomes external to the mineralized fossil dermis (for the fossil skin melanosomes).

Preserved melanosomes from the torso and abdomen of the fossil specimens cannot be confidently attributed to specific internal tissues using anatomical location alone. Basic geometry data (length and aspect ratio) eliminate certain potential candidate tissues but do not identify a single tissue of origin. Consideration of melanosome morphospace, the relative size of tissues *in vivo* and the relative abundance of melanosomes in different tissues *in vivo* eliminates additional candidate tissues. Multivariate analysis of a broad suite of melanosome geometric parameters provides additional constraints on interpretations. By placing these results in the context of the metal chemistry of the fossil melanosomes, it is possible to successfully determine whether the fossil melanosomes represent one, or more, tissues. With one exception (see below), all of the fossil melanosomes can be confidently ascribed to a single tissue origin, respectively the lungs, liver, or gonads. The only exception are the melanosomes from sample St2 from the torso of one Geiseltal specimen. These melanosomes are similar in geometry to the liver and lungs, but do not differ in chemistry from melanosomes from the

other torso sample and from the abdomen, which collectively are interpreted as gonad melanosomes based on their geometry. Given the limited sample size, it is not possible to determine whether the disparity between the chemical and geometric data is an original biological signal or an artefact of fossilization. Given the consistent preservation of tissue-specific chemical differences between melanosomes from the eyes, skin and internal organs (the latter considered collectively), diagenetic overprinting seems unlikely. Decoupling of geometry from chemistry in the internal melanosomes of fossil anurans also seems unlikely as it has implications for the physiological functions of those melanosomes in metal homeostasis.[4] The discrepancy between the chemical and geometric data may be most plausibly interpreted as a function of the small size of the SEM sample used for analysis of melanosome geometry. Testing this is beyond the scope of this study; more extensive sampling of fossil melanosome films could benefit future studies but may not always be feasible.

5.3.1 Conservation of anatomy implies conservation of function

The anuran Bauplan has been conserved since the Late Triassic[36-38] and is largely decoupled from habitat[37,39]: extant anurans that occupy different habitats (including woodlands, swamps, meadows, tundra and deserts) retain a similar Bauplan.[39] The fossil anurans from Geiseltal and Bechlejovice (Pelobatidae and Palaeobatrachidae) and Libros (Ranidae) closely resemble extant anurans in skeletal anatomy and skin structure.[29,30,40,41] The habitats and lifestyles of the fossil anurans from each locality and the extant specimens are broadly comparable. It is therefore reasonable to infer broad similarities in organ function among the anurans in our dataset; it is unlikely that minor differences in habitat (e.g., lake physiography / water depth / water chemistry) and anuran lifestyle (e.g., predominantly aquatic or terrestrial) would impact organ function. The functional roles of melanin in the anuran eye, skin and internal organs (e.g., lungs, liver and gonads) were therefore probably established by the Late Triassic. Notwithstanding this, the skin of extant anurans shows marked interspecific variation, in terms of coloration, presence / absence of a lateral line system and adaptations to particular habitats.

5.3.2 Conservation of melanosome geometry

Our data show that the geometry of melanosomes in the eyespots of fossil anurans from the Miocene and Eocene is similar to that of ocular melanosomes in extant anurans. Data for the Libros frogs is fully consistent with that for extant anurans; excepting some large spheroidal melanosomes, the Geiseltal eye melanosomes are also consistent with extant examples. Differences between the Bechlejovice eye melanosomes and all others can be explained by sampling of only one eye tissue (and thus only one melanosome population) in the fossil. Collectively, these data indicate that eye melanosome geometry has been conserved in anurans since the Middle Eocene, i.e. for ca. 45 million years. This, in turn, strongly suggests that the functions of ocular melanins in anurans have been conserved over this period. The internal melanosomes of the studied fossil anurans can be assigned to the liver, lungs and gonads using a combination of data on melanosome geometry and chemistry; thus, the preserved attributes of melanosomes from internal tissues are also consistent with evolutionary conservatism since the Middle Eocene.

Conservation of anatomy implies conservation of function. The functional implications of melanosome geometry in vertebrates are not fully understood; the former is hypothesized to relate to melanosome monomer chemistry and, in turn, metal chemistry, UV absorption capacity, oxidative properties and antioxidant properties[4], but this hypothesis has not been tested. More superficial links between melanosome geometry and tissue function have been characterized for feathers and hair[13], whereby melanosome geometry is linked to visible color. The controls on melanosome geometry in other tissues have not been investigated, but potential functions can be discussed in the context of existing literature. In the vertebrate eye, melanosomes are considered to function primarily in photoprotection and in regulation of oxidative tissue damage[18,42,43]; it is reasonable to assume such functions apply to anuran eye melanosomes. The visual system is highly conserved in anurans: they typically see in color[44], with high spatial resolution and broad spectral sensitivity, including low ambient illumination.[45-47] Like most anurans[48-50], all of the extant anurans studied are adapted to nocturnal

vision. It is therefore not unreasonable to consider that strong conservatism in the anuran visual system may be reflected in conserved melanosome geometries in the group. Interspecific variation in eye melanosome geometry may relate to plastic characters of the eye[47,51-54] such as iris color, pupil shape, ecology and/or activity period.

Similarly, there are no definitive data on the specific controls on the geometry of melanosomes in internal organs, although these melanosomes are linked to functional roles in metal homeostasis and antioxidant functions.[4,5] Irrespective of the precise physiological functions of melanosomes in the eyes and internal tissues of anurans, the similar geometry of these melanosomes in the fossil and extant anurans strongly implies that the most important functional constraints have not changed since the Middle Eocene.

Notably, our data on melanosome geometry and chemistry provide strong support for the preservation of gonad melanosomes in the torso and abdomen of the anuran specimen GMH CeIII-4967-1932 from Geiseltal. The extent of these melanosomes in the torso could be explained by mobilization of melanosomes following liquefaction of the gonads during decay. Non-integumentary melanosomes can redistribute through parts of the body if carcasses are disturbed by currents[27]. The gonads are, however, small organs, with relatively little melanin (compared to e.g., the liver[5,27]). Alternatively, the fossil melanosomes may derive from internal oocytes[55,56], which in gravid female anurans can occupy a large proportion of the volume of the torso. The geometry of melanosomes from oocytes, however, has not been investigated, so it is unknown at what stage during oocyte and/or tadpole development the melanosomes from the gonads and oocytes can be discriminated. If oocytes are indeed the source of the fossil melanosomes, the specimen would be a gravid female. This is consistent with other evidence[29,40] that the Geiseltal anurans visited the depositional environment to breed. These data therefore represent tentative evidence for the sex of fossil anurans, with potential applications to other vertebrates.

The geometry of the skin melanosomes in all fossil anurans studied differs to that in the extant anurans in our dataset, indicating that skin melanosomes are not subject to the same functional constraints as melanosomes from other tissues. Potential links between melanosome geometry and skin color have not been investigated for extant anurans, but previous work on reptiles has shown that melanosome geometry is independent of skin color in the group.[15] A similar relationship may also apply to amphibians, but our dataset, is not sufficiently large to allow definitive assessment of the nature of any links between the geometry of skin melanosomes in anurans to skin color.

Irrespective of the above interspecific differences in skin melanosome geometry, our dataset reveals some notable shared features. Skin melanosomes are smaller than most or all non-integumentary melanosomes in a given taxon and are similar in different body regions (dorsal / ventral). These features suggest the presence of large-scale functional controls that are, yet, unknown.

In conclusion, our study provides strong evidence for tissue-specific trends in the evolution of melanin in anurans over the last ca. 45 million years, whereby evolution of melanosomes in the skin is decoupled from that in the eyes and internal tissues. We report that specific melanosome geometries in the eyes and internal body tissues (lungs, liver and gonads) have been evolutionarily conserved since the Middle Eocene, but skin melanosomes in fossil and extant anurans differ in geometry. These patterns most likely reflect disparate physiological constraints on melanosome function in these tissues since the Middle Eocene. Liberation of skin melanosomes from such constraints may reflect evolutionary tradeoffs linked to diversification of integumentary coloration, activity period, the presence / absence of a lateral line system and/or habitat. Combination of multivariate analysis of a comprehensive suite of melanosome geometry attributes, plus chemical data using SRS-XRF, is a much more powerful tool to constrain the origins of fossil melanosomes than basic geometric attributes alone. Broader application of this approach has the potential to reveal novel aspects of the evolution of anatomy, physiology and behavior in other vertebrate groups.

5.4 Limitations of the study

The limitations of this study relate mainly to sample size, i.e. the number of fossil and extant taxa and the number of fossil samples used. Only six specimens of the Geiseltal anurans were available for destructive sampling of soft tissues for SEM analysis; one specimen was available for the SRS-XRF analysis. In particular, the destructive sampling of the soft tissues was limited to a maximum of five sample locations per specimen. Such limitations on sampling of fossils from Konservat-Lagerstätten are typical for this fossil type; in the case of the Geiseltal anurans, the collection has National Heritage status, which places additional constraints on sampling and international loans of specimens.

Only four extant taxa were used in our dataset. Sampling of additional extant taxa would have exceeded the financial and temporal limitations of this study.

Finally, although the impact of diagenesis on melanosomes is well characterised[23-25,33,57,58], we cannot completely exclude the possibility that unknown taphonomic factors may impact preserved melanosome geometries.

5.5 Acknowledgements

We thank the ZNS team, especially Frank Steinheimer and Michael Stache for access to the Geiseltal collections and databases and for useful historical information. Thanks to all associates who performed documentation, preparation and curation of the Geiseltal specimens. Thanks to Bianca Bernstein (Museum Weißenfels, Germany) and Naomi O'Reilly (University College Cork, Ireland) for assistance and advice; Peter Chung and Tiffany Slater (both University College Cork) for assistance, advice and training. Sandra Chapman (Natural History Museum, London, United Kingdom) and Begoña Sánchez (Museo Nacional de Ciencias Naturales, Madrid, Spain) provided access to fossil specimens. The research was funded by a Government of Ireland-Irish Research Council (IRC) Postgraduate Scholarship

GOIPG/2018/3354 awarded to DF; MMN, BCH and VR were funded by European Research Council Consolidator Grant ERC-COG-2020-1010003293-PALAEOCHEM awarded to MMN; MMN and AQ were funded by a Science Foundation Ireland Frontiers for the Future grant 20/FFP-P/8871 awarded to MMN.

5.6 Author contributions

Conceptualization M. E. McNamara, O. Wings, D. Falk; Data curation D. Falk, M. E. McNamara, A. Quigley, V. Rossi; Formal analysis D. Falk, M. E. McNamara; Funding acquisition M. E. McNamara, D. Falk; Investigation D. Falk, M. E. McNamara; Methodology M. E. McNamara, D. Falk, O. Wings; Project administration M. E. McNamara; Resources O. Wings, M. E. McNamara, A. Quigley, V. Rossi, B. Carazo del Hoyo; Software S. M. Webb; Supervision M. E. McNamara, O. Wings; Validation M. E. McNamara, O. Wings, D. Falk, S. Webb, V. Rossi, A. Quigley, B. Carazo del Hoyo; Visualization D. Falk, M. E. McNamara; Writing – original draft – D. Falk, M. E. McNamara; Writing – review & editing – M. E. McNamara, D. Falk, O. Wings, V. Rossi, A. Quigley, B. Carazo del Hoyo, S. M. Webb.

5.7 Declaration of interests

The authors declare no competing interests.

5.8 References

1. D'Alba, L., and Shawkey, M.D. (2019). Melanosomes: biogenesis, properties, and evolution of an ancient organelle. Physiol. Rev. *99*, 1–19. https://doi.org/10.1152/physrev.00059.2017.

2. Guo, L., Li, W., Gu, Z., Wang, L., Guo, L., Ma, S., Li, C., Sun, J., Han, B., and Chang, J. (2023). Recent advances and progress on melanin: from source to application. Int. J. Mol. Sci. *24*, 1–26, 4360. https://doi.org/10.3390/ijms24054360.

3. Riley, P.A. (1997). Melanin. Int. J. Biochem. Cell Biol. *29*, 1235–1239. https://doi.org/10.1016/S1357-2725(97)00013-7.

4. McNamara, M.E., Rossi, V., Slater, T.S., Rogers, C.S., Ducrest, A.-L., Dubey, S., and Roulin, A. (2021). Decoding the evolution of melanin in vertebrates. Trends Ecol. Evol. *36*, 430–443. https://doi.org/10.1016/j.tree.2020.12.012.

5. Rossi, V., McNamara, M.E., Webb, S.M., Ito, S., and Wakamatsu, K. (2019). Tissue-specific geometry and chemistry of modern and fossilized melanosomes reveal internal anatomy of extinct vertebrates. Proc. Natl. Acad. Sci. USA *116*, 17880–17889. https://doi.org/10.1073/pnas.1820285116.

6. Lindgren, J., Sjövall, P., Carney, R.M., Cincotta, A., Uvdal, P., Hutcheson, S.W., Gustafsson, O., Lefèvre, U., Escuillié, F., Heimdal, J., et al. (2015). Molecular composition and ultrastructure of Jurassic paravian feathers. Sci. Rep. *5*, 1–13, 13520. https://doi.org/10.1038/srep13520.

7. Rossi, V., Unitt, R., McNamara, M., Zorzin, R., and Carnevale, G. (2022). Skin patterning and internal anatomy in a fossil moonfish from the Eocene Bolca Lagerstätte illuminate the ecology of ancient reef fish communities. Palaeontology *65*, 1–11, e12600. https://doi.org/10.1111/pala.12600.

8. Vinther, J. (2020). Reconstructing vertebrate paleocolor. Annu. Rev. Earth Planet. Sci. *48*, 345–375. https://doi.org/10.1146/annurev-earth-073019-045641.

9. Zhang, F., Kearns, S.L., Orr, P.J., Benton, M.J., Zhou, Z., Johnson, D., Xu, X., and Wang, X. (2010). Fossilized melanosomes and the colour of Cretaceous dinosaurs and birds. Nature *463*, 1075–1078. https://doi.org/10.1038/nature08740.

10. McNamara, M.E., Orr, P.J., Kearns, S.L., Alcalá, L., Anadón, P., and Peñalver, E. (2016). Reconstructing carotenoid-based and structural coloration in fossil skin. Curr. Biol. *26*, 1075–1082. https://doi.org/10.1016/j.cub.2016.02.038.

11. Lindgren, J., Kuriyama, T., Madsen, H., Sjövall, P., Zheng, W., Uvdal, P., Engdahl, A., Moyer, A.E., Gren, J.A., and Kamezaki, N. (2017). Biochemistry and adaptive colouration of an exceptionally preserved juvenile fossil sea turtle. Sci. Rep. *7*, 1–13. https://doi.org/10.1038/s41598-017-13187-5.

12. Cincotta, A., Nicolaï, M., Campos, H.B.N., McNamara, M.E., D'Alba, L., Shawkey, M.D., Kischlat, E.-E., Yans, J., Carleer, R., Escuillié, F., and Godefroit, P. (2022). Pterosaur melanosomes support signalling functions for early feathers. Nature *604*, 684–688. https://doi.org/10.1038/s41586-022-04622-3.

13. Li, Q., Gao, K.-Q., Vinther, J., Shawkey, M.D., Clarke, J.A., D'Alba, L., Meng, Q., Briggs, D.E.G., and Prum, R.O. (2010). Plumage color patterns of an extinct dinosaur. Science *327*, 1369–1372. https://doi.org/10.1126/science.1186290.

14. Babarović, F., Puttick, M.N., Zaher, M., Learmonth, E., Gallimore, E.-J., Smithwick, F.M., Mayr, G., and Vinther, J. (2019). Characterization of melanosomes involved in the production of non-iridescent structural feather colours and their detection in the fossil record. J. R. Soc. Interface *16*, 1–9, 20180921. https://doi.org/10.1098/rsif.2018.0921.

15. Li, Q., Clarke, J.A., Gao, K.Q., Zhou, C.F., Meng, Q., Li, D., D'Alba, L., and Shawkey, M.D. (2014). Melanosome evolution indicates a key physiological shift within feathered dinosaurs. Nature *507*, 350–364. https://doi.org/10.1038/nature12973.

16. McNamara, M.E., Zhang, F., Kearns, S.L., Orr, P.J., Toulouse, A., Foley, T., Hone, D.W.E., Rogers, C.S., Benton, M.J., Johnson, D., et al. (2018). Fossilized skin reveals coevolution with feathers and metabolism in feathered dinosaurs and early birds. Nat. Commun. *9*, 1–7, 2072. https://doi.org/10.1038/s41467-018-04443-x.

17. Rossi, V., Webb, S.M., and McNamara, M.E. (2020). Hierarchical biota-level and taxonomic controls on the chemistry of fossil melanosomes revealed using synchrotron X-ray fluorescence. Sci. Rep. *10*, 1–10, 8970. https://doi.org/10.1038/s41598-020-65868-3.

18. Rogers, C.S., Astrop, T.I., Webb, S.M., Ito, S., Wakamatsu, K., and McNamara, M.E. (2019). Synchrotron X-ray absorption spectroscopy of melanosomes in vertebrates and cephalopods: implications for the affinity of *Tullimonstrum*. Proc. R. Soc. B. *286*, 1–8, 20191649. https://doi.org/10.1098/rspb.2019.1649.

19. Lindgren, J., Nilsson, D.-E., Sjövall, P., Jarenmark, M., Ito, S., Wakamatsu, K., Kear, B.P., Schultz, B.P., Sylvestersen, R.L., Madsen, H., et al. (2019). Fossil insect eyes shed light on trilobite optics and the arthropod pigment screen. Nature *573*, 122–125. https://doi.org/10.1038/s41586-019-1473-z.

20. Jarenmark, M., Sjövall, P., Ito, S., Wakamatsu, K., and Lindgren, J. (2021). Chemical evaluation of eumelanin maturation by ToF-SIMS and alkaline peroxide oxidation HPLC analysis. Int. J. Mol. Sci. *22*, 1–16, 161. https://doi.org/10.3390/ijms22010161.

21. Lindgren, J., Uvdal, P., Sjövall, P., Nilsson, D.E., Engdahl, A., Schultz, B.P., and Thiel, V. (2012). Molecular preservation of the pigment melanin in fossil melanosomes. Nat. Commun. *3*, 1–7. http://dx.doi.org/10.1038/ncomms1819.

22. Rogers, C.S., Webb, S.M., and McNamara, M.E. (2021). Synchrotron x-ray fluorescence analysis reveals diagenetic alteration of fossil melanosome trace metal chemistry. Palaeontology *64*, 63–73. https://doi.org/10.1111/pala.12506.

23. Rossi, V., Webb, S.M., and McNamara, M.E. (2021). Maturation experiments reveal bias in the chemistry of fossil melanosomes. Geology *49*, 784–788. https://doi.org/10.1130/G48696.1.

24. Slater, T.S., Ito, S., Wakamatsu, K., Zhang, F., Sjövall, P., Jarenmark, M., Lindgren, J., and McNamara, M.E. (2023). Taphonomic experiments reveal authentic molecular signals for fossil melanins and verify preservation of phaeomelanin in fossils. Nat. Commun. *14*, 1–15, 5651. https://doi.org/10.1038/s41467-023-40570-w.

25. Slater, T.S., McNamara, M.E., Orr, P.J., Foley, T.B., Ito, S., and Wakamatsu, K. (2020). Taphonomic experiments resolve controls on the preservation of melanosomes and keratinous tissues in feathers. Palaeontology *63*, 103–115. https://doi.org/10.1111/pala.12445.

26. Slater, T.S., Edwards, N.P., Webb, S.M., Zhang, F., and McNamara, M.E. (2023). Preservation of corneous β-proteins in Mesozoic feathers. Nat. Ecol. Evol. *7*, 1706–1713. https://doi.org/10.1038/s41559-023-02177-8.

27. McNamara, M.E., Kaye, J.S., Benton, M.J., Orr, P.J., Rossi, V., Ito, S., and Wakamatsu, K. (2018). Non-integumentary melanosomes can bias reconstructions of the colours of fossil vertebrates. Nat. Commun. *9*, 1–9. https://doi.org/10.1038/s41467-018-05148-x.

28. Dubey, S., and Roulin, A. (2014). Evolutionary and biomedical consequences of internal melanins. Pigment Cell & Melanoma Research *27*, 327–338. https://doi.org/10.1111/pcmr.12231.

29. Falk, D., Wings, O., Unitt, R., Wade, J., and McNamara, M.E. (2024). Fossilized anuran soft tissues reveal a new taphonomic model for the Eocene Geiseltal Konservat-Lagerstätte, Germany. Sci. Rep. *14*, 1–14, 7876. https://doi.org/10.1038/s41598-024-55822-y.

30. McNamara, M.E., Orr, P.J., Kearns, S.L., Alcalá, L., Anadón, P., and Penalver Molla, E. (2009). Soft-tissue preservation in Miocene frogs from Libros, Spain: insights into the genesis of decay microenvironments. Palaios *24*, 104–117. https://doi.org/10.2110/palo.2008.p08-017r.

31. McNamara, M.E., van Dongen, B.E., Lockyer, N.P., Bull, I.D., and Orr, P.J. (2016). Fossilization of melanosomes via sulfurization. Palaeontology *59*, 337–350. https://doi.org/10.1111/pala.12238.

32. Colleary, C., Dolocan, A., Gardner, J., Singh, S., Wuttke, M., Rabenstein, R., Habersetzer, J., Schaal, S., Feseha, M., Clemens, M., et al. (2015). Chemical, experimental, and morphological evidence for diagenetically altered melanin in exceptionally preserved fossils. Proc. Natl. Acad. Sci. USA *112*, 12592–12597. https://doi.org/10.1073/pnas.1509831112.

33. McNamara, M.E. (2013). The taphonomy of colour in fossil insects and feathers. Palaeontology *56*, 557–575. https://doi.org/10.1111/pala.12044.

34. Wogelius, R.A., Manning, P.L., Barden, H.E., Edwards, N.P., Webb, S.M., Sellers, W.I., Taylor, K.G., Larson, P.L., Dodson, P., You, H., et al. (2011). Trace metals as biomarkers for eumelanin pigment in the fossil record. Science *333*, 1622–1626. https://doi.org/10.1126/science.1205748.

35. Manning, P.L., Edwards, N.P., Bergmann, U., Anné, J., Sellers, W.I., van Veelen, A., Sokaras, D., Egerton, V.M., Alonso-Mori, R., Ignatyev, K., et al. (2019). Pheomelanin pigment remnants mapped in fossils of an extinct mammal. Nat. Commun. *10*, 1–13, 2250. https://doi.org/10.1038/s41467-019-10087-2.

36. Feng, Y.-J., Blackburn, D.C., Liang, D., Hillis, D.M., Wake, D.B., Cannatella, D.C., and Zhang, P. (2017). Phylogenomics reveals rapid, simultaneous diversification of three major clades of Gondwanan frogs at the Cretaceous–Paleogene boundary. Proc. Natl. Acad. Sci. USA *114*, 5864–5870. https://doi.org/10.1073/pnas.1704632114.

37. Reilly, S.M., and Jorgensen, M.E. (2011). The evolution of jumping in frogs: morphological evidence for the basal anuran locomotor condition and the radiation of locomotor systems in crown group anurans. J. Morphol. *272*, 149–168. https://doi.org/10.1002/jmor.10902.

38. Stocker, M.R., Nesbitt, S.J., Kligman, B.T., Paluh, D.J., Marsh, A.D., Blackburn, D.C., and Parker, W.G. (2019). The earliest equatorial record of frogs from the Late Triassic of Arizona. Biol. Lett. *15*, 1–5, 20180922. https://doi.org/10.1098/rsbl.2018.0922.

39. Vitt, L.J., and Caldwell, J.P. (2014). Chapter 17 - Frogs. In Herpetology, 4th edition, L.J. Vitt, and J.P. Caldwell, eds. (Academic Press), pp. 471–522. https://doi.org/10.1016/B978-0-12-386919-7.00017-4.

40. Falk, D., Wings, O., and McNamara, M.E. (2022). The skeletal taphonomy of anurans from the Eocene Geiseltal Konservat-Lagerstätte, Germany: insights into the controls on fossil anuran preservation. Pap. Palaeontol. *8*, 1–34, e1453. https://doi.org/10.1002/spp2.1453.

41. McNamara, M.E., Orr, P.J., Alcalá, L., Anadón, P., and Peñalver, E. (2012). What controls the taphonomy of exceptionally preserved taxa - environment or biology? A case study using frogs from the Miocene Libros Konservat-Lagerstätte (Teruel, Spain). Palaios *27*, 63–77. https://doi.org/10.2110/palo.2010.p10-126r.

42. Hu, D.-N., Simon, J.D., and Sarna, T. (2008). Role of ocular melanin in ophthalmic physiology and pathology. Photochem. Photobiol. *84*, 639–644. https://doi.org/10.1111/j.1751-1097.2008.00316.x.

43. Sitiwin, E., Madigan, M.C., Gratton, E., Cherepanoff, S., Conway, R.M., Whan, R., and Macmillan, A. (2019). Shedding light on melanins within *in situ* human eye melanocytes using 2-photon microscopy profiling techniques. Sci. Rep. *9*, 1–18, 18585. https://doi.org/10.1038/s41598-019-54871-y.

44. Yovanovich, C.A.M., Koskela, S.M., Nevala, N., Kondrashev, S.L., Kelber, A., and Donner, K. (2017). The dual rod system of amphibians supports colour discrimination at the absolute visual threshold. Phil. Trans. R. Soc. Lond. B *372*, 1–10, 20160066. http://dx.doi.org/10.1098/rstb.2016.0066.

45. Buchanan, B.W. (1993). Effects of enhanced lighting on the behaviour of nocturnal frogs. Animal behaviour *45*, 893–899. https://doi.org/10.1006/anbe.1993.1109.

46. Buchanan, B.W. (2006). Observed and potential effects of artificial night lighting on anuran amphibians. In Ecological Consequences of Artificial Night Lighting, C. Rich, and T. Longcore, eds. (Island Press), pp. 192–220.

47. Yovanovich, C.A.M., Grant, T., and Kelber, A. (2019). Differences in ocular media transmittance in classical frog and toad model species and its impact on visual sensitivity. J. Exp. Biol. *222*, 1–5. https://doi.org/10.1242/jeb.204271.

48. Anderson, S.R., and Wiens, J.J. (2017). Out of the dark: 350 million years of conservatism and evolution in diel activity patterns in vertebrates. Evolution *71*, 1944–1959. https://doi.org/10.1111/evo.13284.

49. Duellman, W.E., and Trueb, L. (1994). Biology of Amphibians (John Hopkins University Press). https://doi.org/10.1126/science.232.4747.271.a.

50. Mohun, S.M., and Davies, W.I.L. (2019). The evolution of amphibian photoreception. Front. Ecol. Evol. *7*, 1–12, 321. https://doi.org/10.3389/fevo.2019.00321.

51. Wiens, John J., Graham, Catherine H., Moen, Daniel S., Smith, Sarah A., and Reeder, Tod W. (2006). Evolutionary and ecological causes of the latitudinal diversity gradient in hylid frogs: treefrog trees unearth the roots of high tropical diversity. Am. Nat. *168*, 579–596. https://doi.org/10.1086/507882.

52. Moen, D.S., Irschick, D.J., and Wiens, J.J. (2013). Evolutionary conservatism and convergence both lead to striking similarity in ecology, morphology and performance across continents in frogs. Proc. R. Soc. B. *280*, 1–9, 20132156. https://doi.org/10.1098/rspb.2013.2156.

53. Schott, R.K., Fujita, M.K., Streicher, J.W., Gower, D.J., Thomas, K.N., Loew, E.R., Bamba Kaya, A.G., Bittencourt-Silva, G.B., Guillherme Becker, C., Cisneros-Heredia, D., et al. (2024). Diversity and evolution of frog visual opsins: spectral tuning and adaptation to distinct light environments. Mol. Biol. Evol. *41*, 1–23. https://doi.org/10.1093/molbev/msae049.

54. Thomas, K.N., Gower, D.J., Streicher, J.W., Bell, R.C., Fujita, M.K., Schott, R.K., Liedtke, H.C., Haddad, C.F.B., Becker, C.G., Cox, C.L., et al. (2022). Ecology drives patterns of spectral transmission in the ocular lenses of frogs and salamanders. Functional Ecology *36*, 850–864. https://doi.org/10.1111/1365-2435.14018.

55. Méndez-Tepepa, M., Morales-Cruz, C., García-Nieto, E., and Anaya-Hernández, A. (2023). A review of the reproductive system in anuran amphibians. Zool. Lett. *9*, 1–17. https://doi.org/10.1186/s40851-023-00201-0.

56. Wake, M.H., and Dickie, R. (1998). Oviduct structure and function and reproductive modes in amphibians. J. Exp. Zool. *282*, 477–506. https://doi.org/10.1002/(SICI)1097-010X(199811/12)282:4/5<477::AID-JEZ6>3.0.CO;2-#.

57. Korytowski, W., and Sarna, T. (1990). Bleaching of melanin pigments. Role of copper ions and hydrogen peroxide in autooxidation and photooxidation of synthetic dopa-melanin. J. Biol. Chem. *265*, 12410–12416. https://doi.org/10.1016/S0021-9258(19)38362-0.

58. McNamara, M.E., Briggs, D.E.G., Orr, P.J., Field, D.J., and Wang, Z. (2013). Experimental maturation of feathers: implications for reconstructions of fossil feather colour. Biol. Lett. 9, 1–6, 20130184. https://doi.org/10.1098/rsbl.2013.0184.

59. Lönartz, M.I., McCoy, V.E., Gee, C.T., and Geisler, T. (2023). Palaeoenvironmental conditions for the natural vulcanization of the Eocene “monkeyhair” laticifers from Geiseltal, Germany, as elucidated by Raman spectroscopy. Palaeobiodivers. Palaeoenviron., 1–13. https://doi.org/10.1007/s12549-022-00566-8.

60. Falk, D., and Stache, M. (2021). Die eozänen Froschlurche der Geiseltal-Sammlung, Interdisziplinäre Zugänge zum Rätsel der Fossilerhaltung. In Eine Frage der Perspektive, Objekte als Vermittler von Wissenschaft, E. Seidl, F. Steinheimer, and C. Weber, eds. (Gesellschaft für Universitätssammlungen e.V.), pp. 39–47. http://dx.doi.org/10.18452/23915.

61. Krumbiegel, G., Rüffle, L., and Haubold, H. (1983). Das eozäne Geiseltal: ein mitteleuropäisches Braunkohlenvorkommen und seine Pflanzen- und Tierwelt (A. Ziemsen Verlag).

62. Kuhn, O. (1941). Die eozänen Anura aus dem Geiseltale nebst einer Übersicht über die fossilen Gattungen. Nova Acta Leopold. NF *10*, 345–376.

63. Roček, Z. (2013). Mesozoic and Tertiary anura of Laurasia. Palaeobiodivers. Palaeoenviron. *93*, 397–439. https://doi.org/10.1007/s12549-013-0131-y.

64. Roček, Z., and Rage, J. (2000). Tertiary anura of Europe, Africa, Asia, North America, and Australia. Amphibian Biology *4*, 1332–1387. http://rocek.gli.cas.cz/Publications/Ro%C4%8Dek%20and%20Rage%202000-.pdf.

65. Roček, Z., Wuttke, M., Gardner, J.D., and Singh Bhullar, B.-A. (2014). The Euro-American genus *Eopelobates*, and a re-definition of the family Pelobatidae (Amphibia, Anura). Palaeobiodivers. Palaeoenviron. *94*, 529–567. https://doi.org/10.1007/s12549-014-0169-5.

66. Roček, Z., Rage, J.-C., and Venczel, M. (2021). Fossil frogs of the genus *Palaeobatrachus* (Amphibia: Anura) (Schweizerbart Science Publishers).

67. Rage, J.-C., and Roček, Z. (2003). Evolution of anuran assemblages in the Tertiary and Quaternary of Europe, in the context of palaeoclimate and palaeogeography. Amphibia-Reptilia *24*, 133–167. https://doi.org/10.1163/156853803322390408.

68. Voigt, E. (1935). Die Erhaltung von Epithelzellen mit Zellkernen, von Chromatophoren und Corium in fossiler Froschhaut aus der mitteleozänen Braunkohle des Geiseltales. Nova Acta Leopold. NF *3*, 339–360.

69. Voigt, E. (1937). Weichteile an Fischen, Amphibien und Reptilien aus der eozänen Braunkohle des Geiseltales. Nova Acta Leopold. NF *5*, 116–142.

70. Voigt, E. (1988). Preservation of soft tissues in the Eocene lignite of the Geiseltal near Halle (Saale). Cour. Forschungsinst. Senckenberg *107*, 325–343.

71. Pickel, W., and Wolf, M. (1989). Kohlenpetrographische und geochemische Charakterisierung von Braunkohlen aus dem Geiseltal (DDR). Erdöl, Kohle, Erdgas, Petrochem. *42*, 481–484.

72. Gardner, J.D. (2016). The fossil record of tadpoles. Foss. Imp. *72*, 17–44. http://dx.doi.org/10.14446/FI.2016.17.

73. Přikryl, T. (2010). Paleogenní a neogenní rybí fauna vybraných lokalit na území České republiky (Research on Cenozoic fish fauna of the selected localities of the Czech Republic). PhD thesis (Univerzita Karlova).

74. Roček, Z. (2003). Larval development in Oligocene palaeobatrachid frogs. Acta Palaeontol. Pol. *48*, 595–607. https://www.app.pan.pl/article/item/app48-595.html.

75. Roček, Z., Böttcher, R., and Wassersug, R. (2006). Gigantism in tadpoles of the Neogene frog *Palaeobatrachus*. Paleobiology *32*, 666–675.

76. Špinar, Z.V. (1972). Tertiary frogs from central Europe (The Hague & Czechoslovak Academy of Sciences Prague). https://doi.org/10.1007/978-94-010-2932-2.

77. McNamara, M.E., Orr, P.J., Manzocchi, T., Alcalá, L., Anadón, P., and Peñalver, E. (2012). Biological controls upon the physical taphonomy of exceptionally preserved salamanders from the Miocene of Rubielos de Mora, northeast Spain. Lethaia *45*, 210–226. https://doi.org/10.1111/j.1502-3931.2011.00274.x.

78. Peñalver, E. (1996). Los yacimientos con insectos fósiles de Aragón (España). PaleoEntomología *16*, 139–146.

79. McNamara, M.E., Orr, P.J., Kearns, S.L., Alcalá, L., Anadón, P., and Peñalver-Mollá, E. (2010). Exceptionally preserved tadpoles from the Miocene of Libros, Spain: ecomorphological reconstruction and the impact of ontogeny upon taphonomy. Lethaia *43*, 290–306. https://doi.org/10.1111/j.1502-3931.2009.00192.x.

80. Schneider, C.A., Rasband, W.S., and Eliceiri, K.W. (2012). NIH Image to ImageJ: 25 years of image analysis. Nat. Methods *9*, 671–675. https://doi.org/10.1038/nmeth.2089.

81. Hammer, Ø., Harper, D.A.T., and Ryan, P.D. (2001). PAST: Paleontological statistics software package for education and data analysis. Palaeontol. Electron. *4*, 1–9.

82. Webb, S.M. (2011). The MicroAnalysis Toolkit: X-ray Fluorescence Image Processing Software. AIP Conference Proceedings *1365*, 196–199. https://doi.org/10.1063/1.3625338.

5.9 Star Methods

5.9.1 Fossil material

In this study, we examined fossil anuran specimens from three stagnation-type Konservat-Lagerstätten (Table 5.1): Geiseltal (Eocene, Germany), Bechlejovice (Oligocene, Czech Republic) and Libros (Miocene, Spain). All studied specimens represent adults.

The Eocene Geiseltal biota includes amphibians, reptiles, mammals, birds and insects. Circa 50,000 specimens from the biota are hosted in the Geiseltal Collection of the Natural Sciences Collections (ZNS) of Martin Luther University Halle-Wittenberg, Halle (Saale), Germany. Many specimens of fossil vertebrates show evidence for preserved soft tissues, such as (part or all of) the body outline. The

preservation of Geiseltal fossil latex (monkeyhair laticifers) indicates diagenetic temperatures of max. 100 °C.[59] Previous experiments revealed little to no impact on melanin chemistry at maturation temperatures of 100 °C[24], and thus changes in geometry at these temperatures should be minimal. Anurans are abundant, represented by at least 180 specimens, with reports of hundreds of specimens lost during excavations.[60,61] The anurans include representatives of Pelobatidae, Palaeobatrachidae[62-66] and probably Discoglossidae.[63,67] Specimens vary in their taphonomy but are usually well-articulated skeletons.[40] Many Geiseltal anurans preserve soft tissues[29,68-70], i.e., fossil skin, melanosomes and aragonite crystals of the endolymphatic sac.[29] Here, we examine the fossil melanosomes from various body regions (i.e., eyespot, skin, torso, abdomen and limbs) of six Geiseltal anuran specimens. Four of the studied specimens were previously assigned to the Pelobatidae[62-65], which are predominantly terrestrial; two specimens are of undetermined affinity (Figure S5.1). Five specimens are conserved in nitrocellulose glue and one specimen is preserved *in situ* in sedimentary matrix (i.e., brown coal[29,71]); the slab is conserved in water. All slabs retain small (< 10 mm^2) patches of dark organic-rich sedimentary matrix; no distinctive sedimentary textures or fabrics are evident.

The Oligocene Bechlejovice biota includes anurans, caudates, reptiles and fish.[72-76] The Lagerstätte was formed in a large, permanent lake surrounded by temporarily active volcanoes. [75] Adult anurans are abundant (> 1,000 specimens) and are often near-complete and well-articulated[40,76]; many specimens show patches of dark brown (1–3 cm^2) carbonaceous soft tissues in the cranium and torso. Here, we examine the soft tissues from the eyespot and torso in one specimen (*Palaeobatrachus luedecki* (Anura: Palaeobatrachidae), NHML-OR35814, Natural History Museum London) from Bohemia. The specimen is conserved in laminated mudstone (Figure S5.1). The state of preservation of the specimen and microscopic study results of the sediment are consistent with specimens from Bechlejovice (M. E. McNamara pers. obs.). There are no other known Konservat-Lagerstätten from Bohemia (Czech Republic) that preserve articulated anurans of this taxon with soft tissues and thus the specimen is most plausibly interpreted as from the Bechlejovice locality.

The Miocene Libros Konservat-Lagerstätte includes amphibians, birds, snakes, and insects[10,30,33,77,78] with adult anurans being the most abundant faunal element (n > 73).[30] Several vertebrate groups preserve soft tissues.[10,16,27,30,41,77,79] The maximum burial temperature for Libros is estimated at < 40 °C.[33] Anurans are usually (near-)complete and well-articulated and often preserve skin and melanosomes; many specimens also preserve stomach contents[30,41] and aragonite crystals of the endolymphatic sac.[30] Here, we study soft tissues from two frog specimens (*Pelophylax pueyoi* (Anura: Ranidae), NHML-R4982 and MNCN 63798). Both NHML-R4982 (Natural History Museum London, UK) and MNCN 63798 (Museo Nacional de Ciencias Naturales, Madrid, Spain) are hosted in laminated mudstone. Both specimens preserve soft tissues of the body outline as a combination of dark carbonaceous material rich in melanosomes[5,30,41] and a pale material that represents the preserved Eberth-Katschenko layer of the skin.[30] The data presented here represent an excerpt of the dataset in Rossi *et al.* [5] and unpublished data provided by VR.

5.9.2 Extant material

Tissue samples from eleven adult specimens of four extant anuran species were analyzed (Table 5.1): *Bombina variegata* (yellow bellied toad; Anura: Bombinatoridae; n = 3), *Hymenochirus boettgeri* (Congo dwarf clawed frog; Anura: Pipidae; n = 2), *Rhaebo guttatus* (smooth-sided toad; Anura: Bufonidae; n = 3) and *Xenopus laevis* (African clawed frog; Anura: Pipidae; n = 3). Tissue samples were dissected using clean dissection needles, scalpels and forceps. Most dissections were performed under a Leica EZ4W stereo microscope. Melanosomes were extracted from tissues using a modified version of the enzymatic digestion protocol in Rossi *et al.* [5], described in detail in Cirtina *et al.* (in prep.). In brief, over the course of ten days, the tissue samples were washed with acetone and deionized water and treated with daily cycles of a solution of phosphate buffer, Proteinase-K and dithiothreitol (DTT) and incubated at 37.5 °C overnight. Samples were then washed once more as above, placed in HCl for 24 h and then in heptane for 24 h. Finally, the samples were pelletized in acetone and air-dried inside a fume cupboard.

Table 5.1: Soft tissue samples from extant and fossil anurans used in this study.

Family / species	Predominant lifestyle	Sampling region for soft tissues	Origin	n	Specimen number	Data source
Bombina variegata (yellow bellied toad)	terrestrial	eye, gonads, liver, skin (ventral & dorsal)	extant	3	YBT1, YBT2, YBT3	A. Quigley (measurement data & SEM images)
Hymenochirus boettgeri (Congo dwarf clawed frog)	aquatic	eye, liver	extant	2	Hym_Frog_1, Hym_Frog_3	Rossi *et al.* [5] (measurement data), V. Rossi (SEM images)
Rhaebo guttatus (smooth-sided toad)	terrestrial	eye, heart, gonads, lung, liver, skin (ventral & dorsal)	extant	3	SST1–SST3	A. Quigley (measurement data & SEM images)
Xenopus laevis (African clawed frog)	aquatic	connective tissue, eye, heart, liver, lungs, skin (dorsal), spleen	extant	3	Xeno_Frog_1, Xeno_Frog_2, Xeno_Frog_3	Rossi *et al.* [5] (measurement data), V. Rossi (SEM images)
Palaeobatrachus luedecki	aquatic	eyespot, skin	Bohemia / Bechlejovice (Oligocene, Czech Republic)	1	NHML-OR35814	Rossi *et al.* [17] (samples), V. Rossi (measurement data, SEM images & photographs)
Pelobatidae and Anura indet.	terrestrial	eyespot, abdomen, limbs, skin, torso	Geiseltal (Eocene, Germany)	6	GMH CeIII 4936a-1932, GMH CeIII 4967-1932, GMH CeIII 4983-1932, GMH CeIII 6698-1932, GMH CeIII 6743-1932, GMH XXXV-11a-1970	D. Falk (measurement data, SEM images & photographs)
Pelophylax pueyoi	terrestrial	eyespot, abdomen, skin, torso	Libros (Miocene, Spain)	2	NHML-R4982; MNCN 63798	Rossi *et al.* [5] (R4982: measurement data & photographs); M. McNamara (63798: SEM images)

5.9.3 Scanning electron microscopy (SEM)

Six specimens from the Geiseltal biota were sampled (Table 5.1). Small (1–2 mm^2) fragments of fossil soft tissues were dissected from several body regions including the eyespot, torso, abdomen and limbs using scalpel and forceps. Soft tissue samples were mounted on aluminum stubs with carbon tape for subsequent analysis. Selected soft tissue samples were sputter coated with Au. Samples were analyzed using a JEOL JSM IT100 VP-SEM at an accelerating voltage of 5–20 kV and a working distance of 6–10 mm for SEM images. High resolution images were obtained using a high resolution aperture with the microscope in high resolution mode and with probe currents of 14–37 A.U. Brightness and contrast were adjusted for selected SEM images in Figures 5.1 and 5.2 using Adobe Photoshop CC 2019.

5.9.4 Measurements

Melanosomes were measured from SEM images using ImageJ v. 1.54g.[80] Melanosomes selected for analysis lack evidence for degradation and are consistent in tone and thickness along their length (and are thus orthogonal to the line of sight). Length and width were measured from at least 50 melanosomes per sample; the total dataset comprises 6713 melanosomes (including fossil and extant melanosomes).

5.9.5 Analysis of melanosome geometry data

Fossil samples from the abdomen are located posterior to the joint between the sacral vertebra and last free vertebra; samples anterior to this joint are from the thorax. Melanosome geometry was assessed for each tissue region (Table 5.1) as follows. Data were first calculated for eight melanosome parameters: mean length, mean aspect ratio, kurtosis (for length and, separately, aspect ratio), skew (for length and, separately, aspect ratio) and interquartile range (for length and, separately, aspect ratio). These data were analyzed using Principal Components Analysis in PAST (Palaeontological Statistics) v. 4.16c[81] (Figure S5.17A). A second PCA was performed using the same dataset as for the first PCA, but the melanosome parameters from above were added for three samples from GMH CeIII

4967-1932 (two samples from the torso and one sample from the abdomen; Figure 5.4A) to interpret the tissue of origin for each of those melanosome populations. A third and fourth PCA (Figures S5.4B and S5.17B) were performed using standardized datasets of the above PCA due to the dominance of certain PC variables in the first PCA. Data were standardized using the following data transformation: $(x - \mu) / \sigma$ (where μ denotes the mean, x denotes the value to be transformed, σ denotes the standard deviation). These PCAs did not yield meaningful results (Figures S5.4B and S5.17B).

Data from each body region (in fossils) and tissue (in extant anurans) were tested for normality and homoscedasticity prior to further analysis. Differences in melanosome geometry among the samples were explored using various significance tests, i.e., the independent t-test, the Kolmogorov-Smirnov test, ANOVA, Welch test and Kruskal-Wallis test. The data were then investigated further using the Tukey or Dunn post-hoc test. The significance and post-hoc test used for a particular analysis was dependent on sample size, homogeneity of variance in the data and normality of the data.

The relationship between the number of data points for each sample and the area of the corresponding PCA morphospace was assessed using Pearson's correlation test in Microsoft Excel.

5.9.6 Synchrotron rapid scanning-X-ray fluorescence analysis (SRS-XRF)

Specimen GMH CeIII-4967-1932 was mounted directly on the sample stage. SRS-XRF data were collected at beam line 10-2 at the Stanford Synchrotron Radiation Lightsource (USA). The incident X-ray energy was set to 11 keV using a Si (111) double crystal monochromator with the storage ring containing 500 mA in top-off mode at 3.0 GeV. A micro-focused (2 × 2 µm) beam was provided by a Rh-coated Kirkpatrick-Baez mirror pair (pixel size 25 × 25 µm). Specimens were mounted at 45° to the incident X-ray beam and spatially rastered at 50 ms / pixel dwell time. The entire fluorescence spectrum was collected at each data point and the intensity of fluorescence lines for pre-selected elements (K, Ca, Ti, V, Cr, Mn, Fe, Co, Ni, Cu, Zn, AsPb, Cd, Sb, and Hg) was monitored using a silicon

drift Vortex detector. Element concentrations (μg/cm^2) were calibrated using NIST traceable thin film elemental standards. Data were processed using Sam's MicroAnalysis Toolkit (SMAK) software version 3.0.9.[82]

5.9.7 Analysis of SRS-XRF data

Initial data processing included edge removal and normalization to the time channel. Preliminary data analysis in SMAK used a built-in image analysis function to analyze chemical variation in maps for Ca, Ti, V, Cr, Mn, Fe, Co, Ni, Cu and Zn using principal components analysis (PCA), with the output comprising a map for each component. Thirteen regions of interest (ROI) were selected for further analysis using these component maps (Figures 5.5 and S5.18) and the original SRS-XRF element maps (Figure 5.6). SRS-XRF spectra were produced using the PyMCA algorithm in SMAK. Peaks were usually fitted using the following parameters: spectrometer zero, spectrometer gain, detector width and a fixed PileUp factor of $1.0*10^{-8} \pm 1*10^{-8}$. Selected spectra were fitted using an adjusted pileup factor of $3.0*10^{-6}$–$4.5*10^{-6} \pm 1*10^{-8}$ in order to remove pile up peaks for Ca (Figures S5.19–S5.23).

All subsequent analyses were performed in PAST (Palaeontological Statistics) v. 4.16c.[81] PCA was used to assess chemical variation among the ROI analyzed. Differences in elemental concentrations among ROI were visualized using Linear Discriminant Analysis (LDA). Due to the high abundance of Ca relative to other elements, the data were $\log_{10}$-transformed (with zero values replaced by 10^{-11} prior to data transformation). One datapoint belonging to ROI 6 was identified as an outlier and omitted. Based on the LDA results, the 13 ROI were used to form into six groups for further analysis (Figures 5.7, S5.19, S5.24). The data for these groups are visualized using 95% confidence ellipses in order to show the chemospace that will contain the mean in 95% of cases where the data distribution is subsampled. Chemical differences among the ROI were assessed for statistical significance using the Welch test or the Kruskal-Wallis test (depending on the characteristics of the data, i.e., normality and homoscedasticity) and Dunn's post-hoc test.

The relationship between the number of data points for each ROI and the area of the corresponding LDA chemospace was assessed using Pearson's correlation test in Microsoft Excel.

5.10 Supplemental information

5.10.1 Principal components analysis (PCA) of the geometry data

Two Principal components analyses (PCA) of the geometry data were performed in PAST (Palaeontological Statistics) v. 4.16c[1] to resolve major patterns in melanosome geometry (Figure 5.4). Data were first calculated for eight melanosome parameters (see Star Methods, Figures 5.4 and S5.17) using the raw dataset A second PCA was performed using the same dataset as for the first PCA, but the melanosome parameters from above were added for three samples from GMH CeIII 4967-1932 (two samples from the torso and one sample from the abdomen; Figure 5.4A) to interpret the tissue of origin for each of those melanosome populations. A third and fourth PCA (Figures S5.4B and S5.17B) were performed using standardized datasets of the above PCAs due to the dominance of certain PC variables in the first PCA. Data were standardized using the following data transformation: $(x – \mu) / \sigma$ (where μ denotes the mean, x denotes the value to be transformed, σ denotes the standard deviation). The first and second principal components (PC 1 and PC 2) collectively explain 76% and 80%, respectively, of the variation in the standardised datasets (Figures 5.4B and S5.17B). Most variation in the data is driven by the skew, the kurtosis and mean of the aspect ratio data and the skew of the length data. The PCA using standardised datasets did not yield meaningful results; most data points plot closely to each other and the morphospace of abdomen, skin and torso show an extensive overlap. Discrimination between skin and non-integumentary tissues is only possible for eye tissues / eyespots.

5.10.2 Principal components analysis (PCA) of SRS-XRF data

The maps for the principal components are based on the PCA of the SRS-XRF data and represent the regions in the specimen that differ most from each other in their mapped elemental composition. The

map for PC 1 (Figure 5.5D) identifies the skeleton of the specimen and patches in the torso and in the limbs as the map regions with the most chemical variance. PC 1 corresponds primarily to Ca, Ni and Sb (Figure 5.6). The map for PC 2 (Figure 5.5E) depicts regions that are consistent with preparation artefacts (e.g., cracks that are close to the edges of the slab; Figures 5.5A and 5.5C). PC 2 corresponds primarily to Fe (Figure 5.6). PC 3 (Figure S5.18A) lacks a strong signal for the soft tissues, skeletal elements, sediment and/or nitrocellulose lacquer. PC 3 corresponds primarily to Fe (Figure 5.6). The map for PC 4 (Figure 5.5F) highlights the embedding material and the skeleton. PC 4 corresponds primarily to Co and Cu (Figures 5.5F and 5.6). The map for PC 5 (Figure 5.5G) highlights regions in the torso and in the abdomen between the urostyle and ilia. PC 5 corresponds primarily to Zn (Figures 5.5B and 5.6); the patches in PC 5 show a similar spatial extent to those in the Zn element map (Figure 5.6). The map for PC 6 (Figure 5.5H) corresponds to the soft tissues in the torso, abdomen and in the limbs and highlights the body outline. The map shows horizontal bands that differ in tone; these features are artefacts generated during data acquisition. PC 6 corresponds to primarily to Ti, V, Cr and Mn (Figures 5.5C and 5.6). PC 7–10 (Figures S5.18B–E) lack a strong signal for the soft tissues, skeletal elements, sediment and/or nitrocellulose lacquer.

5.10.3 SRS-XRF analysis constrains interpretations of fossil soft tissues

The extent and tissue of origin of melanosome films in the Geiseltal anurans can be difficult to determine in hand specimen, as the colour and texture of the soft tissues often resemble those of the surrounding embedding medium. Chemical mapping using synchrotron rapid scanning-X-ray fluorescence analysis (SRS-XRF) can discriminate fossil soft tissues from the host sediment and can reveal cryptic tissue-specific variation in the chemistry of melanosome films, even if the preserved chemistry has been impacted by diagenesis.[2-4] We therefore used this approach to assess the chemistry of the melanosome films in an anuran specimen from Geiseltal (GMH CeIII 4967-1932; Figures 5.5A–I, S5.1F, S5.18A). Principal component analysis (PCA) of the SRS-XRF element maps (Figures 5.5D–H, S5.18) yielded various components (see Section 5.10.2) that, in conjunction with the element maps

(Figure 5.6), facilitated the identification of 13 regions of interest (ROI) for further analysis (Figures S5.19–S5.23). Most of these ROI differ significantly in chemistry (Tables S5.3–S5.5). The LDA chemospace reveals that for many individual ROI, the data are tightly clustered, but overlap with the data for other ROI (Figure S5.24A). To aid visualisation of chemical variation among ROI, the data were $\log_{10}$-transformed and combined to form the following six groups (Figures 5.7 and S5.24B): Group I (ROI 1–3; soft tissues in the torso and abdomen), Group II (ROI 4; soft tissues in the torso), Group III (ROI 5–7 and 10; soft tissues in the hindlimbs), Group IV (ROI 8 and 9; soft tissues in the hindlimbs), Group V (ROI 11 and 13; embedding lacquer), Group VI (ROI 12; sediment). These groups occupy distinct regions of chemospace. Groups I–IV collectively represent all soft tissue samples and are characteristically enriched in Ca and Ni (and, to a lesser extent, Cu, Ti, Co, V, Mn and Cr) relative to Groups V and VI, which collectively represent sedimentary matrix and embedding lacquer; Groups V and VI are enriched in Fe relative to the soft tissues. Among the soft tissue data, Groups I and II (from the torso and abdomen) are enriched in Zn, with slightly more Ni and/or Ca in Group II. In contrast, Groups III and IV (from the hindlimbs) are depleted in Zn and (especially for Group III) enriched in Ca (Figure 5.7, Table S5.3).

These differences in metal concentrations are significant for many elements (Tables S5.6, S5.7A–B). Ca, Cu and Zn are of particular relevance as Ca is a major component of the mineralised skin in the Geiseltal anurans[5] and Cu and Zn are often associated with melanosome films in fossil vertebrates.[3,6,7] These elements are thus the focus of the text below. Ca and Ni concentrations differ significantly among all groups (Tables S5.7A–B). Differences in element concentrations between Group I and Group II are significant only for Ca and Ni, but not Zn (or other elements).

Groups I and II differ from Groups III and IV in their Ni, Cu and Zn concentrations; Group IV shows significantly lower Ca and Ni concentrations compared to Groups I–IV (Tables S5.3, S5.7A–B). Among all groups, Ca and Ni concentrations are lowest for Groups V and VI, whereas Cu and Zn concentrations are similar to concentrations in Group III and IV (Tables S5.3).

The area of chemospace for individual groups shows a significant, positive, correlation with the number of data points in that group (Pearson's r(4) = 0.968, p = 0.002 where chemospace is defined by convex hulls; Pearson's r(4) = 0.863, p = 0.027 where chemospace is defined by 95% ellipses). There is thus a link between the extent to which the data are distributed in chemospace and sample size.

Collectively, these data indicate that Groups I and II likely represent melanosomes from a common source, i.e., a single tissue or multiple tissues with similar melanosome chemistry. Groups III and IV likely represent melanosomes from a different source to Groups I and II; the chemical differences between Groups III and IV may reflect a greater contribution of preserved E-K layer to the signal for Group III and/or a greater contribution of host matrix to the signal for Group IV.

5.10.4 Supplemental references

1. Hammer, Ø., Harper, D.A.T., and Ryan, P.D. (2001). PAST: Paleontological statistics software package for education and data analysis. Palaeontol. Electron. *4*, 1–9.
2. Rossi, V., McNamara, M.E., Webb, S.M., Ito, S., and Wakamatsu, K. (2019). Tissue-specific geometry and chemistry of modern and fossilized melanosomes reveal internal anatomy of extinct vertebrates. Proc. Natl. Acad. Sci. USA, *116*, 17880–17889. https://doi.org/10.1073/pnas.1820285116.
3. Rossi, V., Webb, S.M., and McNamara, M.E. (2020). Hierarchical biota-level and taxonomic controls on the chemistry of fossil melanosomes revealed using synchrotron X-ray fluorescence. Sci. Rep. *10*, 1–10, 8970. https://doi.org/10.1038/s41598-020-65868-3.
4. Rossi, V., Webb, S.M., and McNamara, M.E. (2021). Maturation experiments reveal bias in the chemistry of fossil melanosomes. Geology *49*, 784–788. https://doi.org/10.1130/G48696.1.

5. Falk, D., Wings, O., Unitt, R., Wade, J., and McNamara, M.E. (2024). Fossilized anuran soft tissues reveal a new taphonomic model for the Eocene Geiseltal Konservat-Lagerstätte, Germany. Sci. Rep. *14*, 1–14, 7876. https://doi.org/10.1038/s41598-024-55822-y.

6. Manning, P.L., Edwards, N.P., Bergmann, U., Anné, J., Sellers, W.I., van Veelen, A., Sokaras, D., Egerton, V.M., Alonso-Mori, R., Ignatyev, K., et al. (2019). Pheomelanin pigment remnants mapped in fossils of an extinct mammal. Nat. Commun. *10*, 1–13, 2250. https://doi.org/10.1038/s41467-019-10087-2.

7. Wogelius, R.A., Manning, P.L., Barden, H.E., Edwards, N.P., Webb, S.M., Sellers, W.I., Taylor, K.G., Larson, P.L., Dodson, P., You, H., et al. (2011). Trace metals as biomarkers for eumelanin pigment in the fossil record. Science *333*, 1622–1626. https://doi.org/10.1126/science.1205748.

5.10.5 Supplementary figures and tables

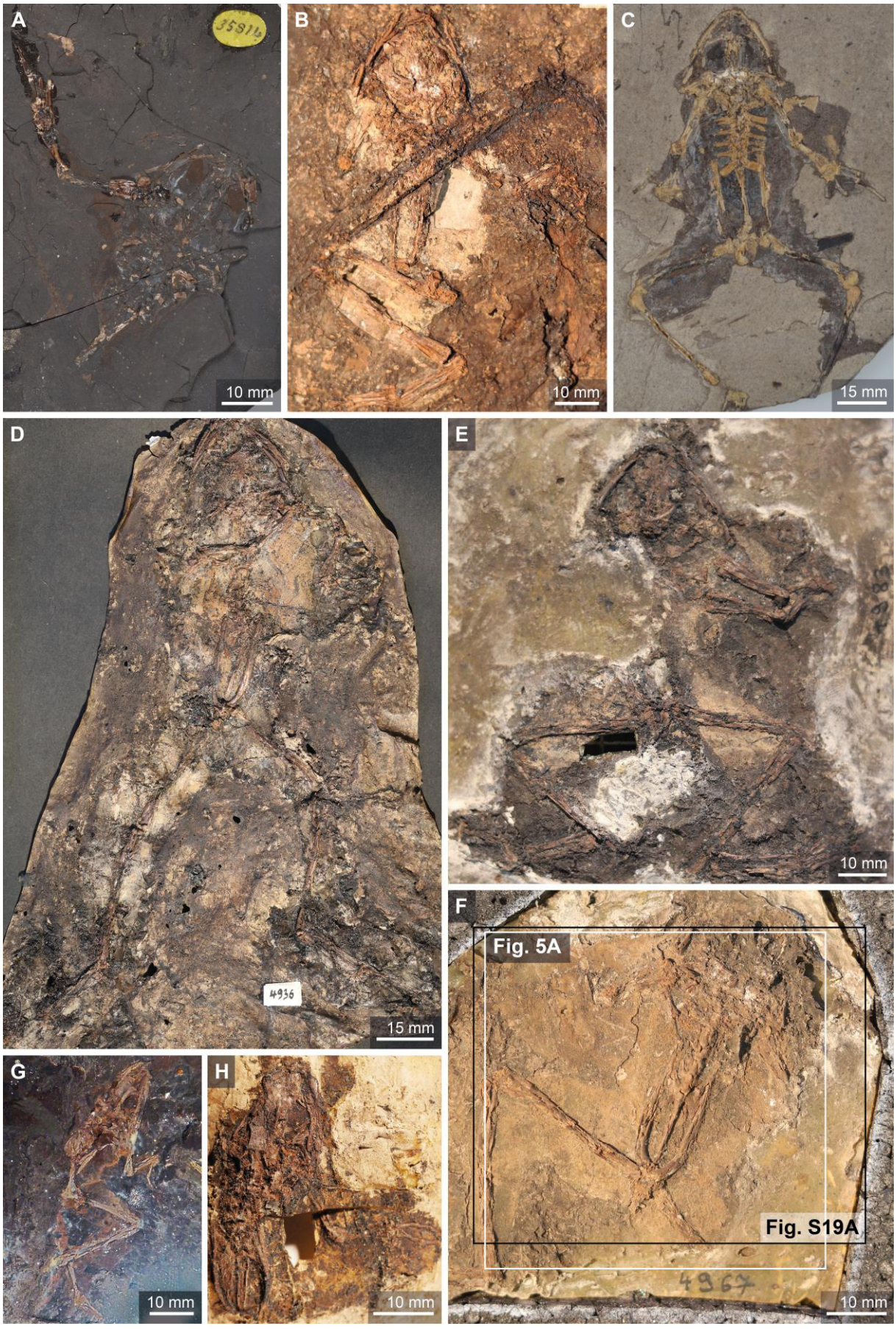


Figure S5.1 (page before): Photographs of fossil anuran specimens from Geiseltal (Germany), Libros (Miocene, Spain) and Bechlejovice (Oligocene, Czech Republic). Soft tissues are visible as a matte cream-coloured material and/or a dark brown material. (A) NHML-OR35814 (Bohemia / Bechlejovice). (B) GMH CeIII-6698-1932 (Geiseltal). (C) NHML-R4982 (Libros). (D) GMH CeIII-4936a-1932 (Geiseltal). (E) GMH CeIII-4983-1932 (Geiseltal). (F) GMH CeIII-4967-1932 (Geiseltal). (G) GMH XXXV-11A-1970 (Geiseltal). (H) GMH CeIII-6743-1932 (Geiseltal). Photographs: (A, V). Rossi; (B, D–F) D. Falk; (C) M. McNamara.

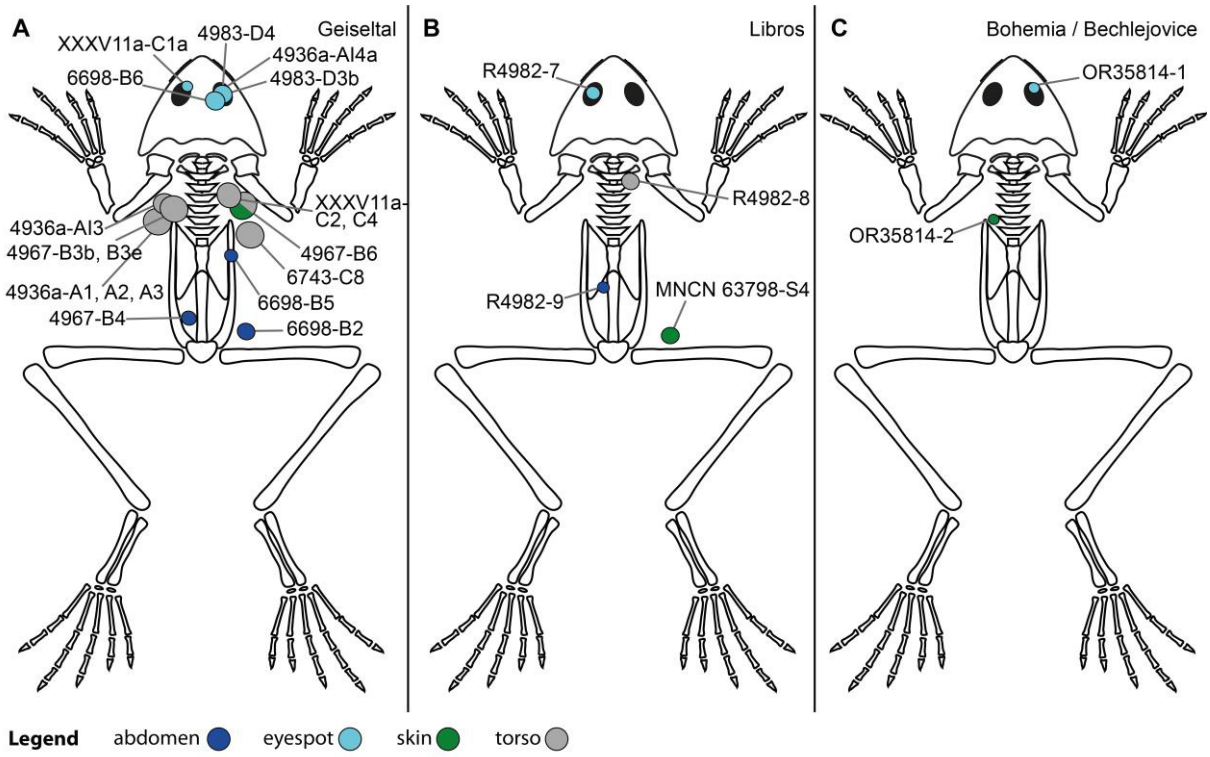


Figure S5.2: Schematic frog skeletons showing sample locations of soft tissue samples. Samples were taken from the abdomen, eyespot, skin and torso. Locations on the left- and right sides of the body are shown as presented in hand specimen. (A) GMH CeIII-6698-1932, GMH CeIII-4983-1932, GMH CeIII-4936a-1932, GMH CeIII-4967-1932, GMH CeIII-6743-1932, GMH XXXV-11A-1970. (B) MNCN 63798, NHML-R4982. (C) NHML-OR35814.

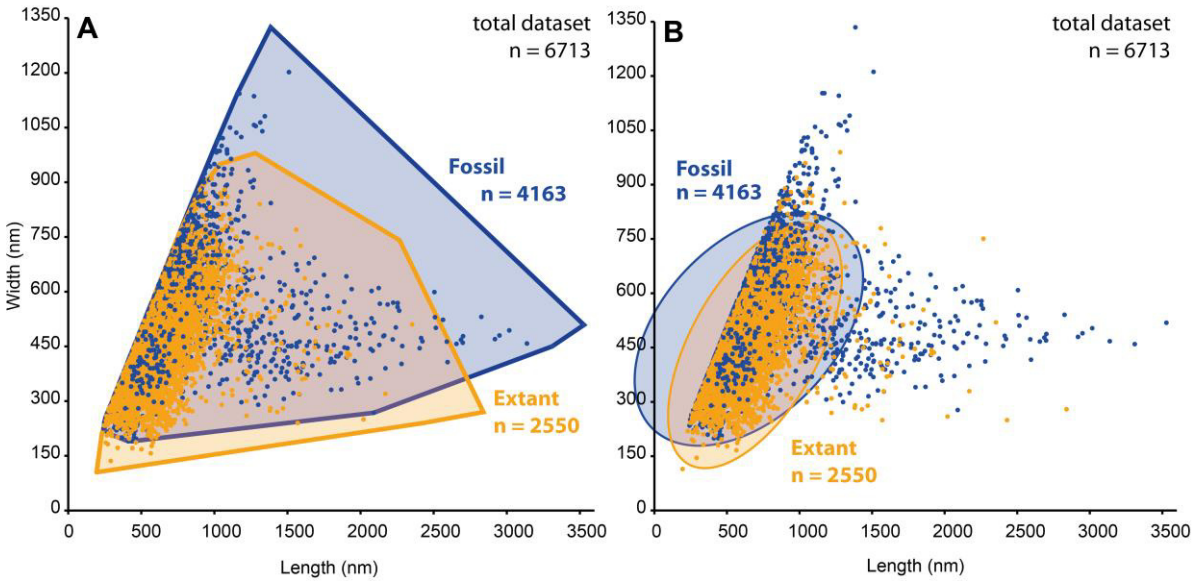


Figure S5.3: Scatterplots showing the morphospace occupied by melanosomes from fossil anurans and extant specimens. (A) Melanosomal morphospace represented by convex hulls. (B) Melanosomal morphospace represented by 95% confidence ellipses.

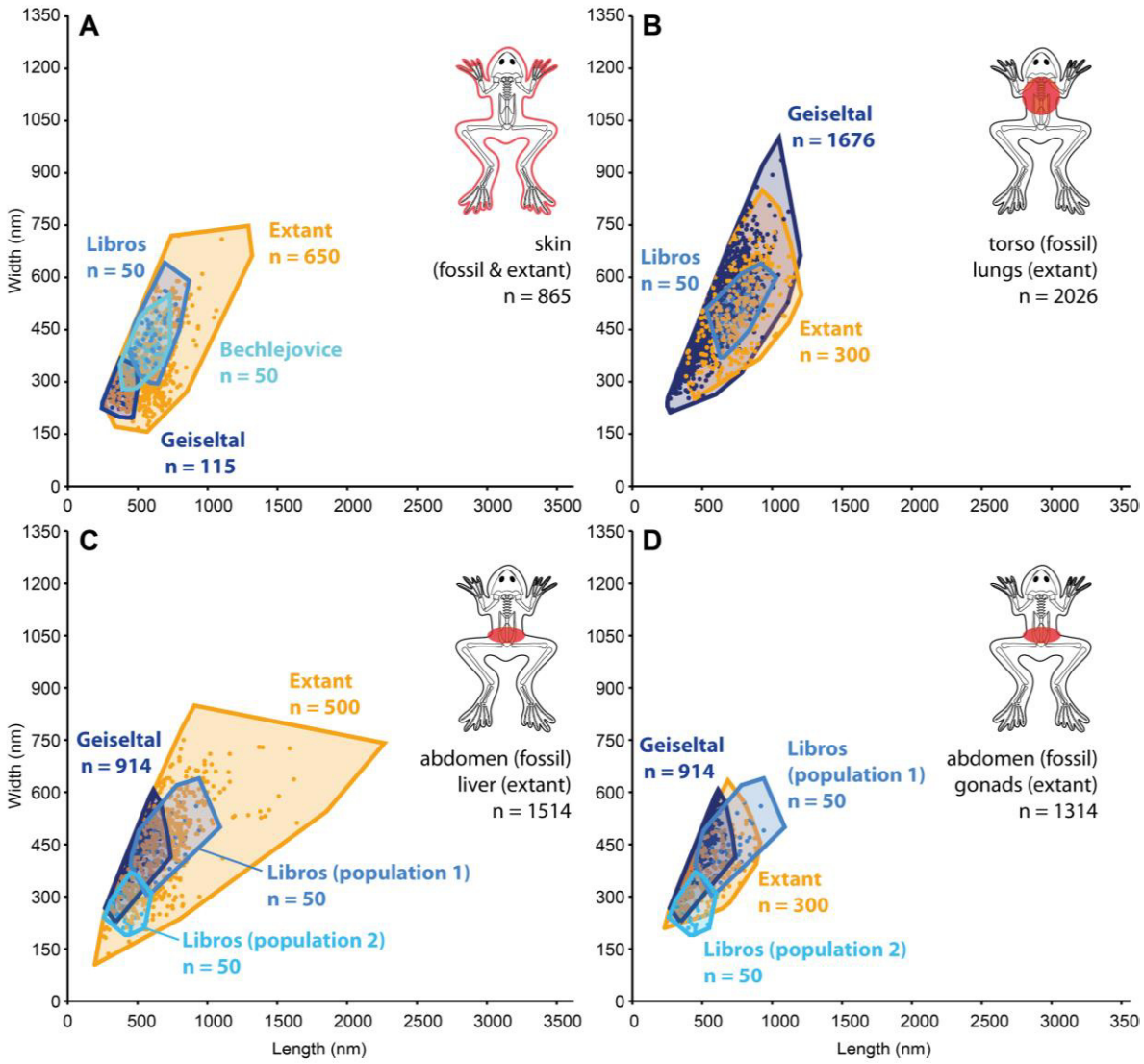


Figure S5.4: Scatterplots showing the melanosomal morphospace for different body regions of fossil anurans from the Geiseltal, Bechlejovice and Libros biotas and for specific soft tissues from extant anurans. Convex hulls are used to visualise morphospace. Schematic frog skeleton indicates the sample region for melanosomes from fossil anurans. (A) Morphospace of melanosomes from fossil skin and skin from extant anurans. (B) Morphospace of melanosomes from the torso of fossil specimens and from the lungs of extant specimens. (C) Morphospace of melanosomes from the abdomen of fossil specimens and from the liver of extant specimens. (D) Morphospace of melanosomes from the abdomen of fossil specimens and from the gonads of extant specimens.

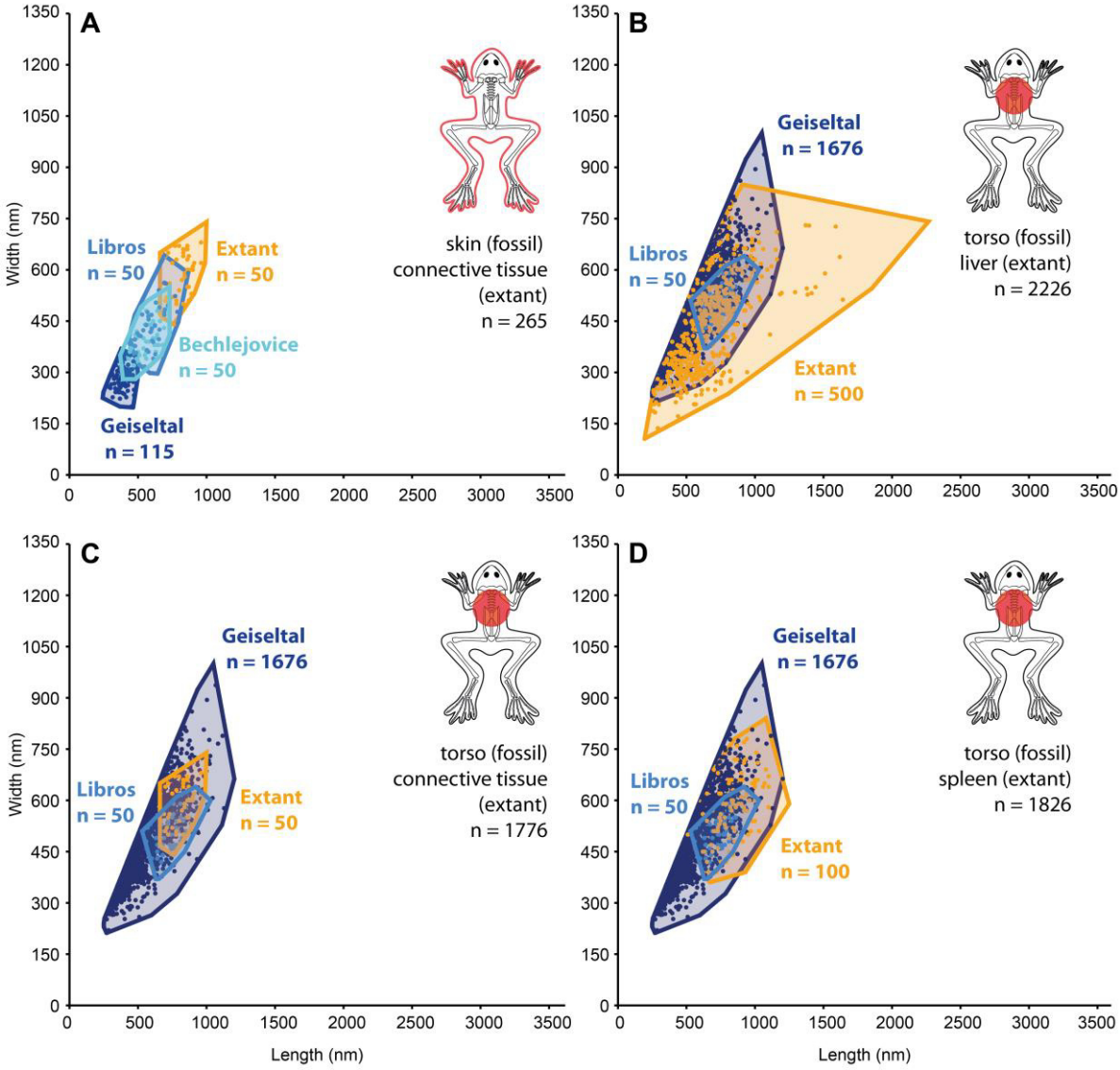


Figure S5.5: Scatterplots showing the melanosomal morphospace for different body regions of fossil anurans from the Geiseltal, Bechlejovice and Libros biotas and for specific soft tissues from extant anurans. Convex hulls are used to visualise morphospace. Schematic frog skeleton indicates the sample region for melanosomes from fossil anurans. (A) Melanosomal morphospace for the skin of fossils and the connective tissue of extant anurans. (B) Melanosomal morphospace for the torso of fossils and the liver of extant anurans. (C) Melanosomal morphospace for the torso of fossils and for the connective tissue of extant anurans. (D) Melanosomal morphospace for the torso of fossils and for the spleen of extant anurans.

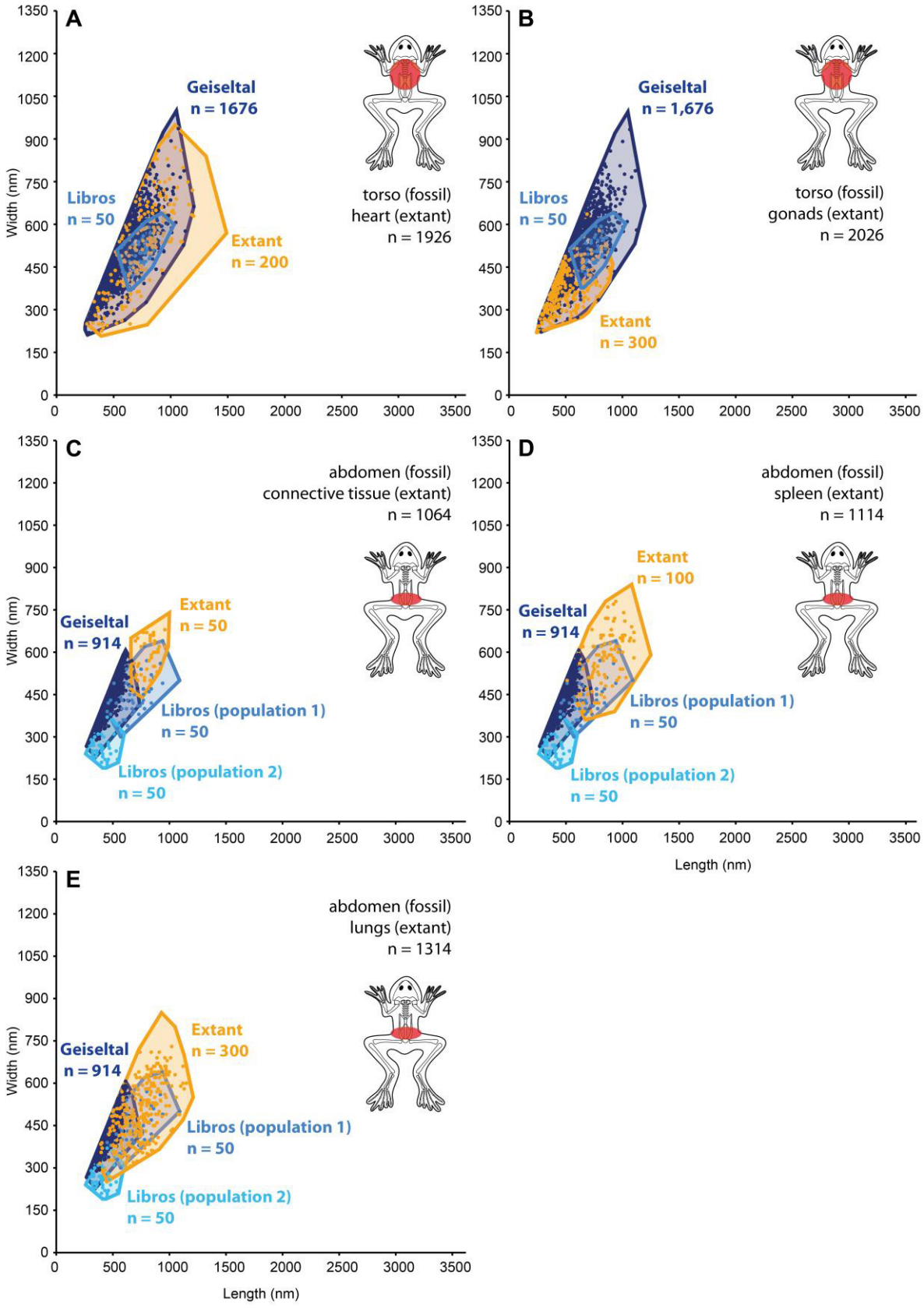


Figure S5.6: Scatterplots showing the melanosomal morphospace for different body regions of fossil anurans from the Geiseltal, Bechlejovice and Libros biotas and for specific soft tissues in extant anurans. Convex hulls are used

to visualise morphospace. Schematic frog skeleton indicates the sample region for melanosomes from fossil anurans. (A) Melanosomal morphospace for the torso of fossils and the heart of extant anurans. (B) Melanosomal morphospace for the torso of fossils and the gonads of extant anurans. (C) Melanosomal morphospace for the abdomen of fossils and for connective tissue of extant anurans. (D) Melanosomal morphospace for the abdomen of fossils and for the spleen of extant anurans. (E) Melanosomal morphospace for the abdomen of fossils and for the lungs of extant anurans.

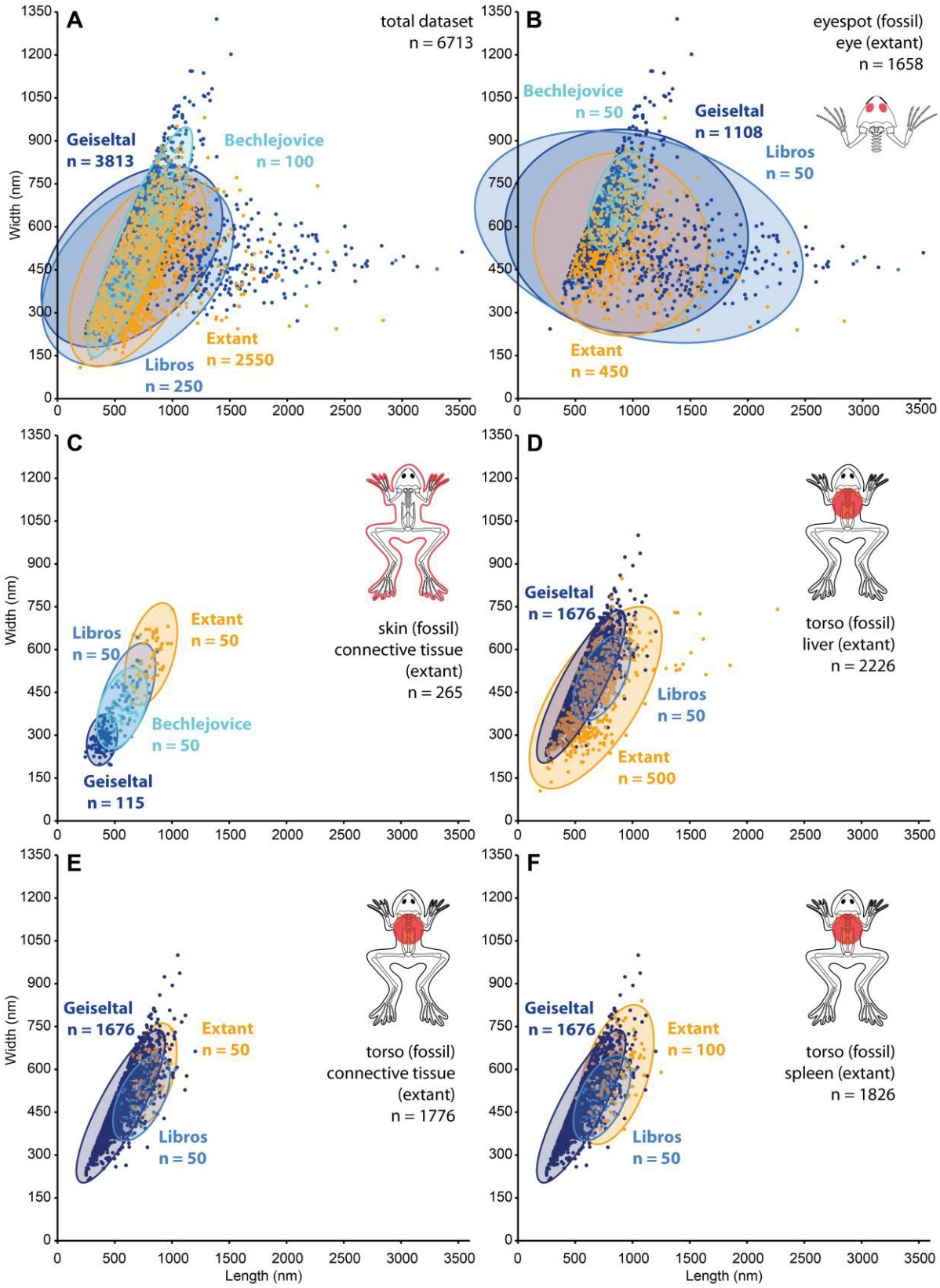


Figure S5.7: Scatterplots showing the morphospace for melanosomes from fossil and extant anurans. Fossil data are for various body regions of fossil anurans from the Geiseltal, Bechlejovice and Libros biotas; extant data are for various organs. 95% confidence ellipses are used to visualise the morphospace for each tissue / body region.

Schematic frog skeleton indicates the sample region for melanosomes from fossil anurans. (A, B) Morphospace of the total dataset (A) and for the eyespots of fossil specimens and eyes of extant specimens (B); note that the confidence ellipses cover large regions in the plot area that lack data points and include negative values. (C) Melanosomal morphospace for the skin of fossils and the connective tissue of extant anurans. (D) Melanosomal morphospace for the torso of fossils and the liver of extant anurans. (E) Melanosomal morphospace for the torso of fossils and for the connective tissue of extant anurans. (F) Melanosomal morphospace for the torso of fossils and for the spleen of extant anurans.

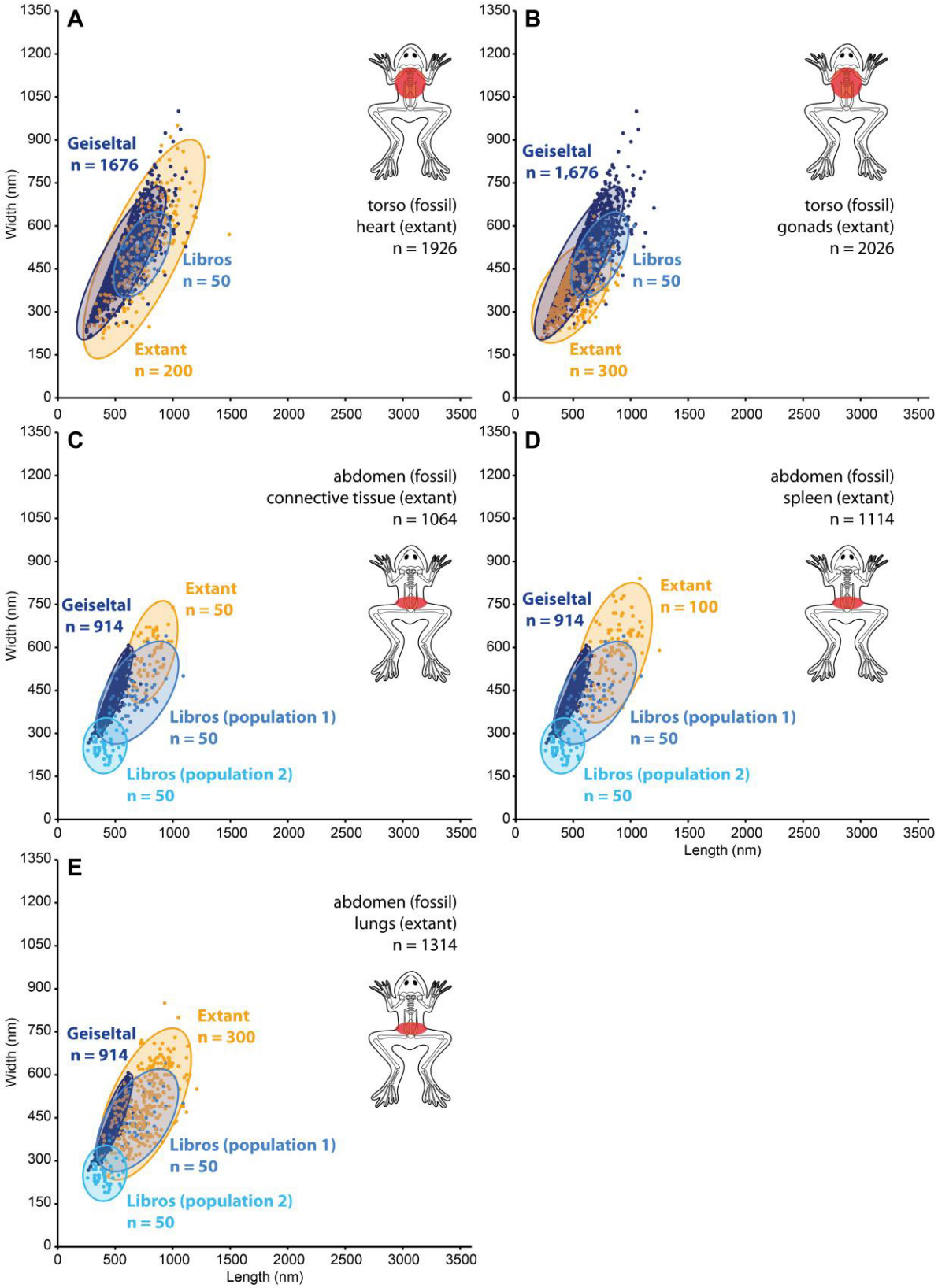


Figure S5.8: Scatterplots showing the melanosomal morphospace for different body regions of fossil anurans from the Geiseltal, Bechlejovice and Libros biotas and for specific soft tissues in extant anurans. 95% confidence ellipses are used to visualise morphospace. Schematic frog skeleton indicates the sample region for melanosomes from

fossil anurans. (A) Melanosomal morphospace for the torso of fossils and the heart of extant anurans. (B) Melanosomal morphospace for the torso of fossils and the gonads of extant anurans. (C) Melanosomal morphospace for the abdomen of fossils and for the connective tissue of extant anurans. (D) Melanosomal morphospace for the abdomen of fossils and for the spleen of extant anurans.(E) Melanosomal morphospace for the abdomen of fossils and for the lungs of extant anurans.

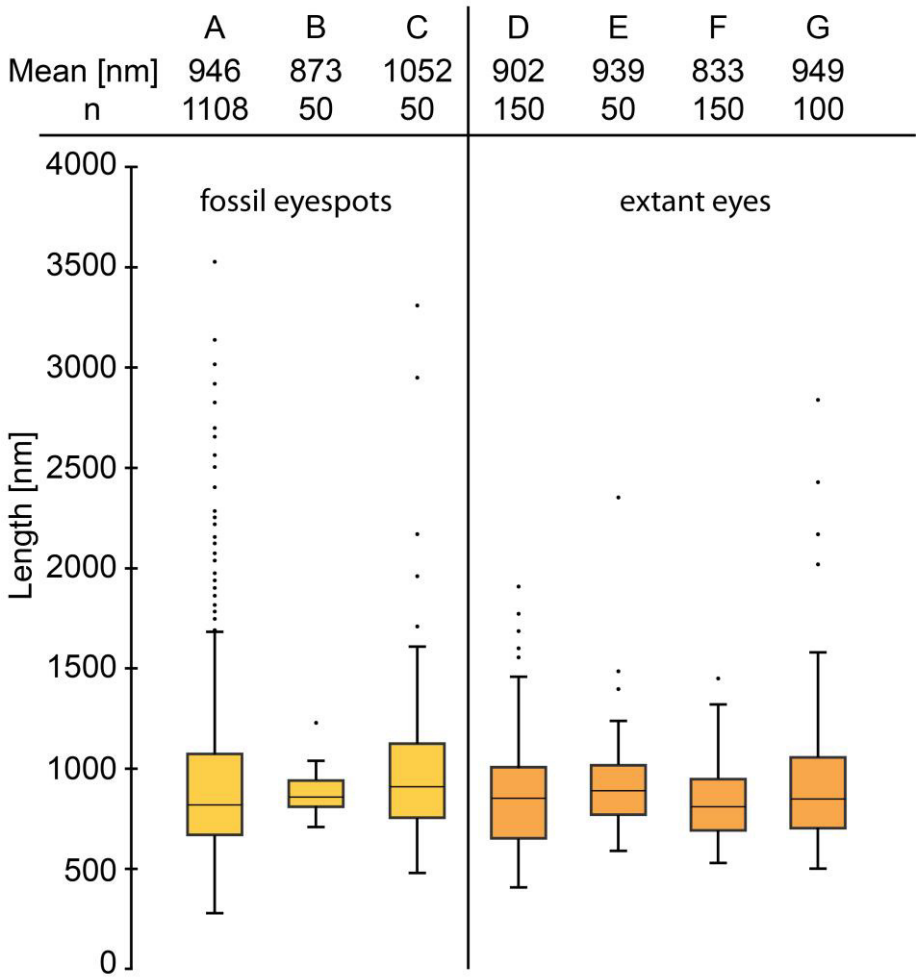


Figure S5.9: Boxplots showing length of melanosomes from the eyespots in fossil anuran specimens and from the eyes in extant anurans. Horizontal bars in boxplots denote the median value. (A) Eyespots in the Geiseltal specimens (n = 3). (B) Eyespots in the Bechlejovice specimen. (C) Eyespots in the Libros specimen. (D) Eyes of Rhaebo guttatus. (E) Eyes of Bombina variegata. (F) Eyes of Xenopus laevis. (G) Eyes of Hymenochirus boettgeri.

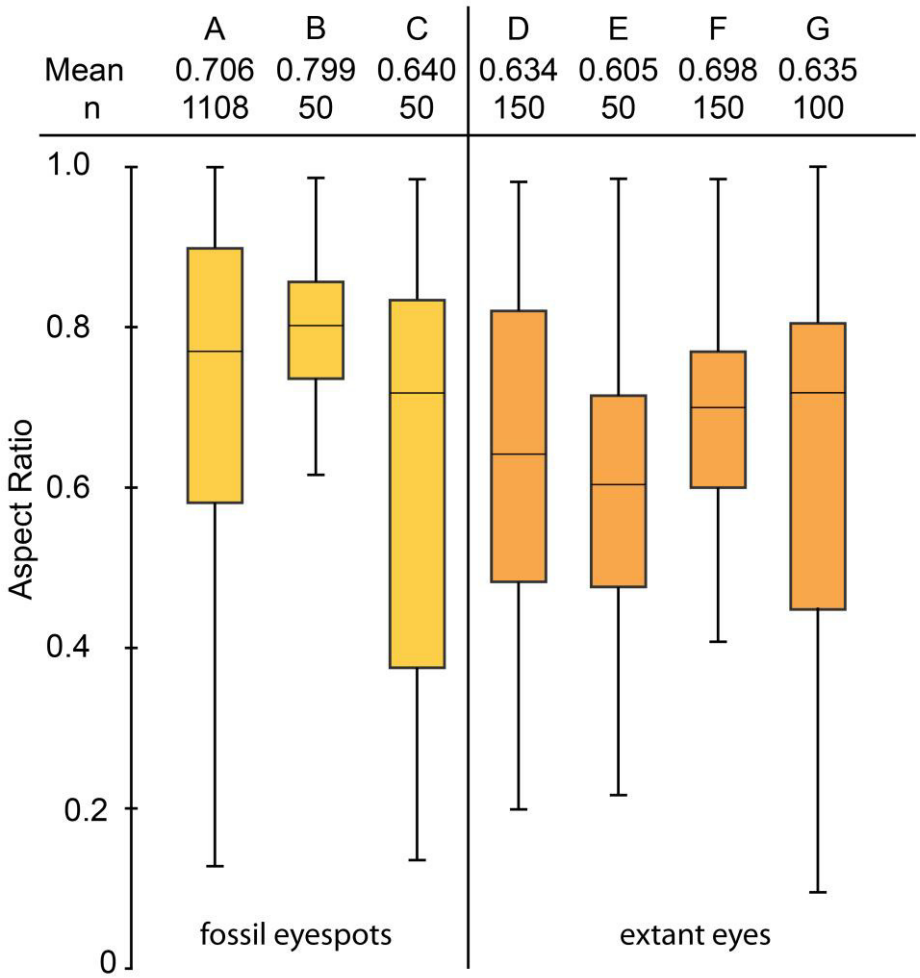


Figure S5.10: Boxplots showing aspect ratio of melanosomes from the eyespots in fossil anuran specimens and from the eyes in extant anurans. Horizontal bars in boxplots denote the median value. (A) Eyespots in the Geiseltal specimens (n = 3). (B) Eyespots in the Bechlejovice specimen. (C) Eyespots in the Libros specimen. (D) Eyes of Rhaebo guttatus. (E) Eyes of Bombina variegata. (F) Eyes of Xenopus laevis. (G) Eyes of Hymenochirus boettgeri.

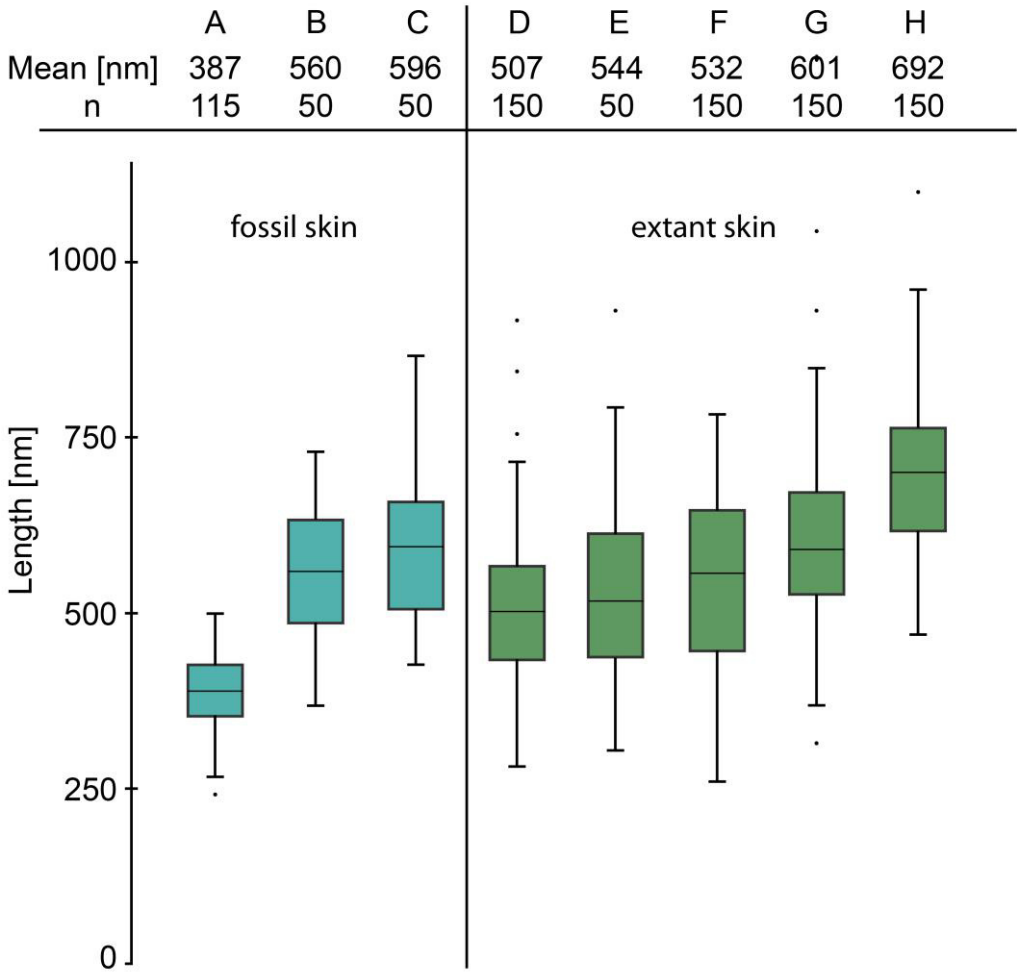


Figure S5.11: Boxplots showing length of melanosomes from the skin in fossil anuran specimens and from the skin of extant anurans. Horizontal bars in boxplots denote the median values. (A) Skin in the Geiseltal specimen. (B) Skin in the Bechlejovice specimen. (C) Skin in the Libros specimen. (D) Dorsal skin of Rhaebo guttatus. (E) Ventral skin of Rhaebo guttatus. (F) Dorsal skin of Bombina variegata. (G) Ventral skin of Bombina variegata. (H) Dorsal skin of Xenopus laevis.

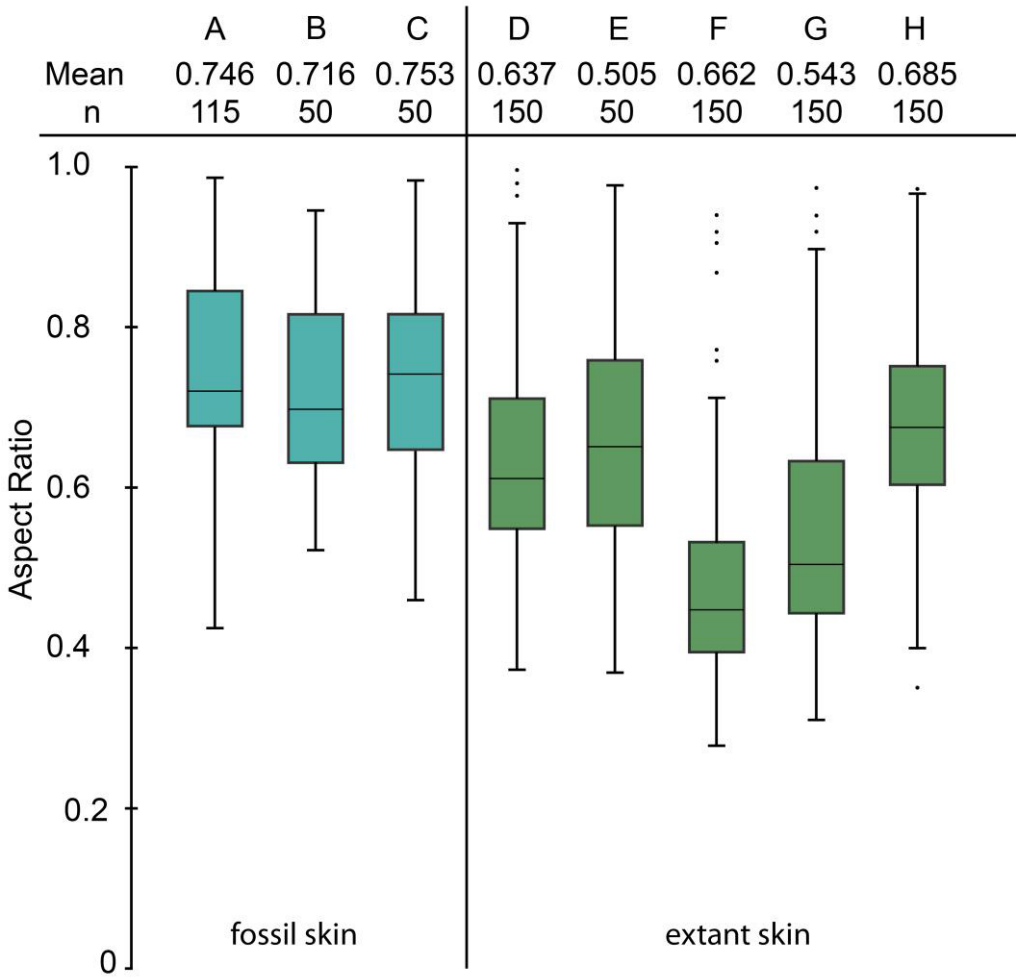


Figure S5.12: Boxplots showing aspect ratio of melanosomes from the skin in fossil anuran specimens and from the skin of extant anurans. Horizontal bars in boxplots denote the median value. (A) Skin in the Geiseltal specimen. (B) Skin in the Bechlejovice specimen. (C) Skin in the Libros specimen. (D) Dorsal skin of Rhaebo guttatus. (E) Ventral skin of Rhaebo guttatus. (F) Dorsal skin of Bombina variegata. (G) Ventral skin of Bombina variegata. (H) Dorsal skin of Xenopus laevis.

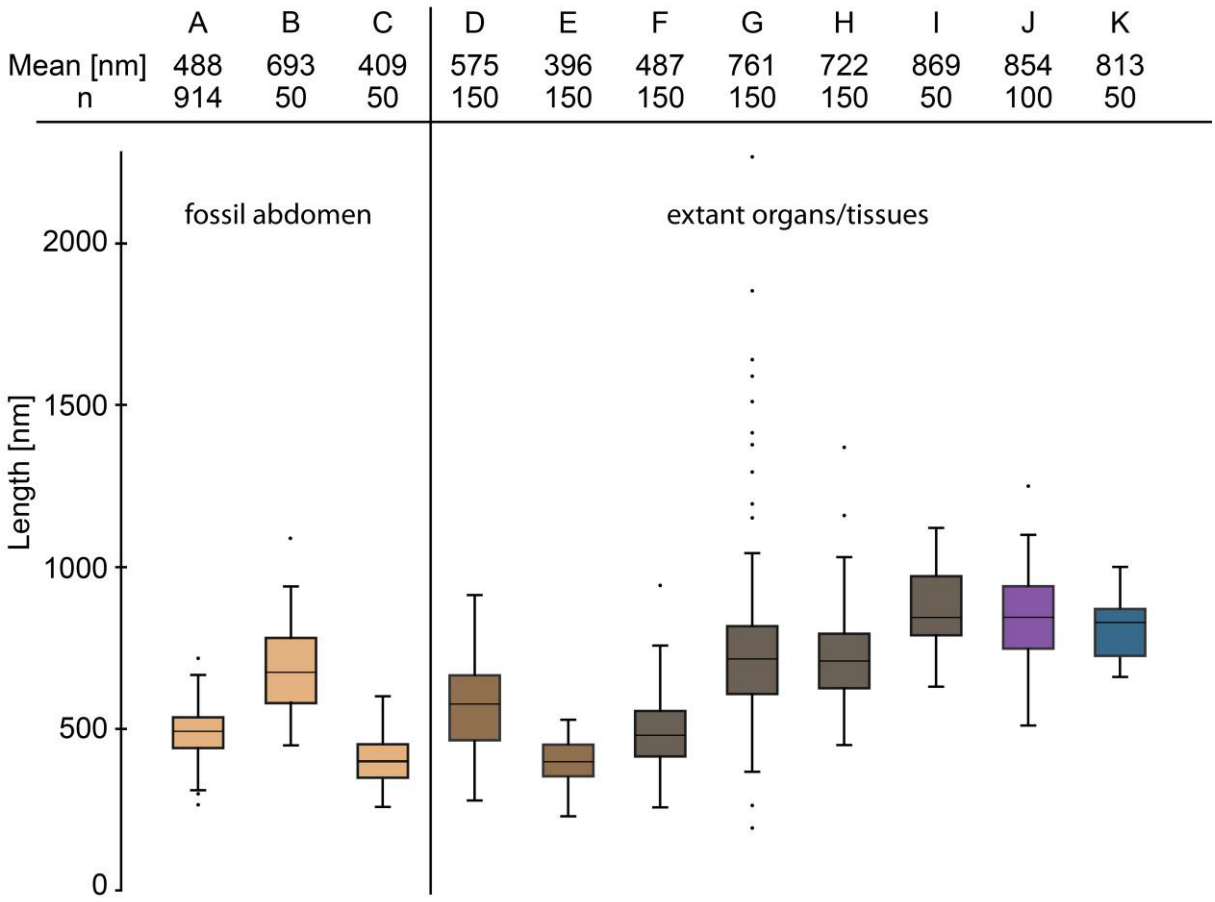


Figure S5.13: Boxplots showing length of melanosomes from the abdomen in fossil anuran specimens and from non-integumentary soft tissues of extant anurans. Horizontal bars in boxplots denote the median value. (A) Abdomen of the Geiseltal specimens (n = 2). (B) Abdomen of the Libros specimen, population 1. (C) Abdomen of the Libros specimen, population 2. (D) Gonads of Rhaebo guttatus. (E) Gonads of Bombina variegata. (F) Liver of Rhaebo guttatus. (G) Liver of Bombina variegata. (H) Liver of Xenopus laevis. (I) Liver of Hymenochirus boettgeri. (J) Spleen of Xenopus laevis. (K) Connective tissue of Xenopus laevis.

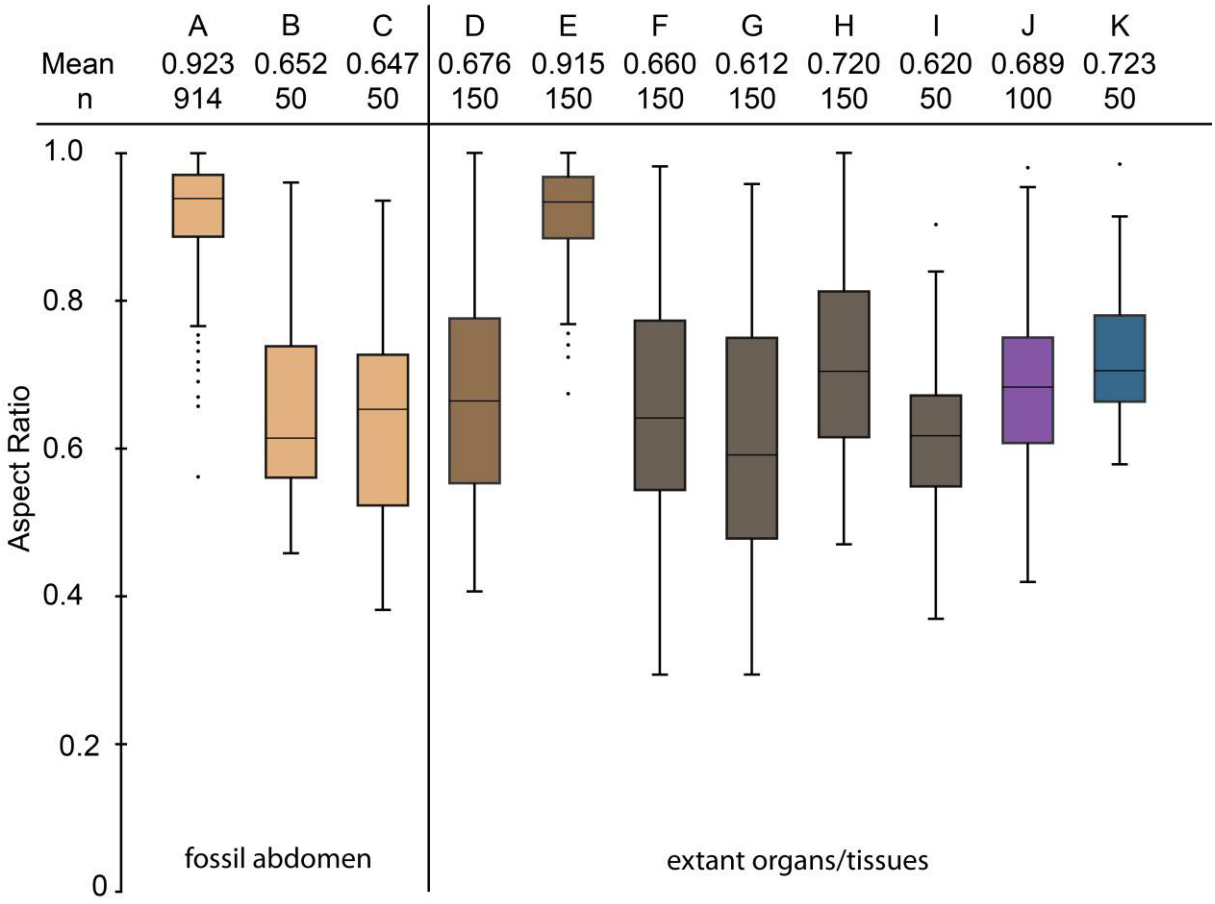


Figure S5.14: Boxplots showing aspect ratio of melanosomes from the abdomen of fossil anuran specimens and from non-integumentary soft tissues of extant anurans. Horizontal bars in boxplots denote the median value. (A) Abdomen of the Geiseltal specimens (n = 2). (B) Abdomen of the Libros specimen, population 1. (C) Abdomen of the Libros specimen, population 2. (D) Gonads of Rhaebo guttatus. (E) Gonads of Bombina variegata. (F) Liver of Rhaebo guttatus. (G) Liver of Bombina variegata. (H) Liver of Xenopus laevis. (I) Liver of Hymenochirus boettgeri. (J) Spleen of Xenopus laevis. (K) Connective tissue of Xenopus laevis.

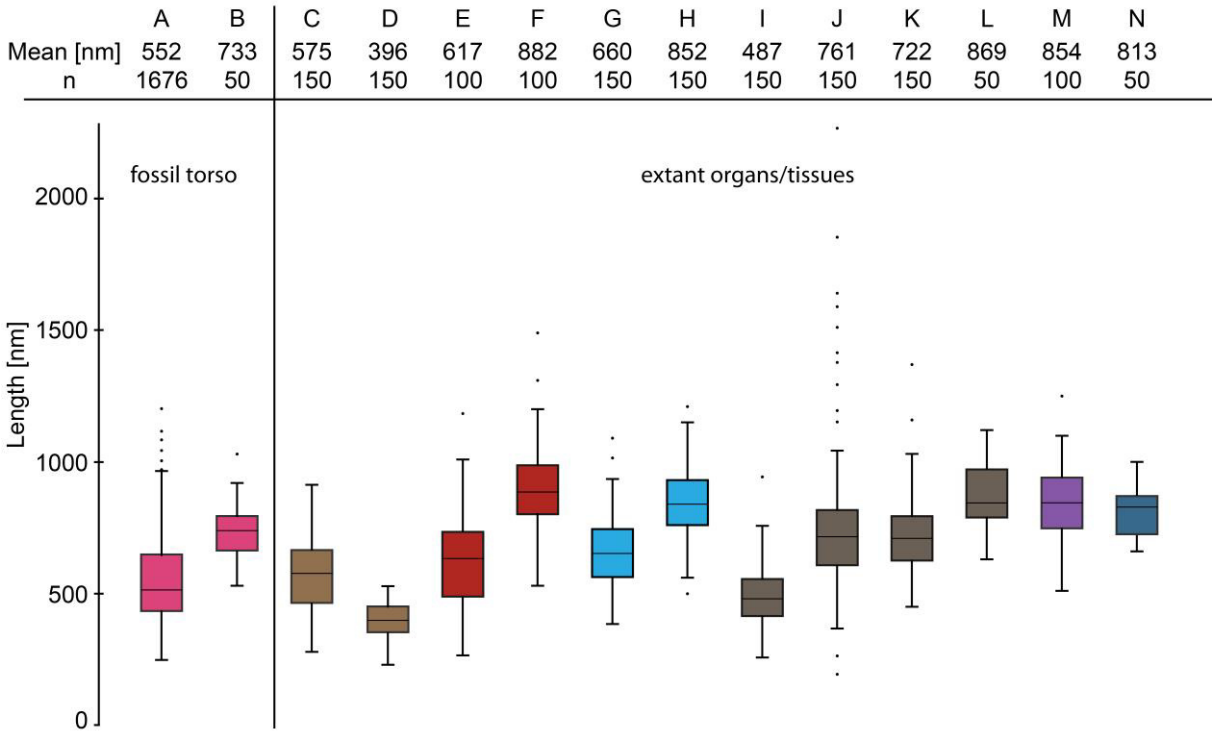


Figure S5.15: Boxplots showing length of melanosomes from the torso in fossil anuran specimens and from non-integumentary soft tissues of extant anurans. Horizontal bars in boxplots denote the median values. (A) Torso of the Geiseltal specimens (n = 4). (B) Torso of the Libros specimen. (C) Gonads of Rhaebo guttatus. (D) Gonads of Bombina variegata. (E) Heart of Rhaebo guttatus. (F) Heart of Xenopus laevis. (G) Lungs of Rhaebo guttatus. (H) Lungs of Xenopus laevis. (I) Liver of Rhaebo guttatus. (J) Liver of Bombina variegata. (K) Liver of Xenopus laevis. (L) Liver of Hymenochirus boettgeri. (M) Spleen of Xenopus laevis. (N) Connective tissue of Xenopus laevis.

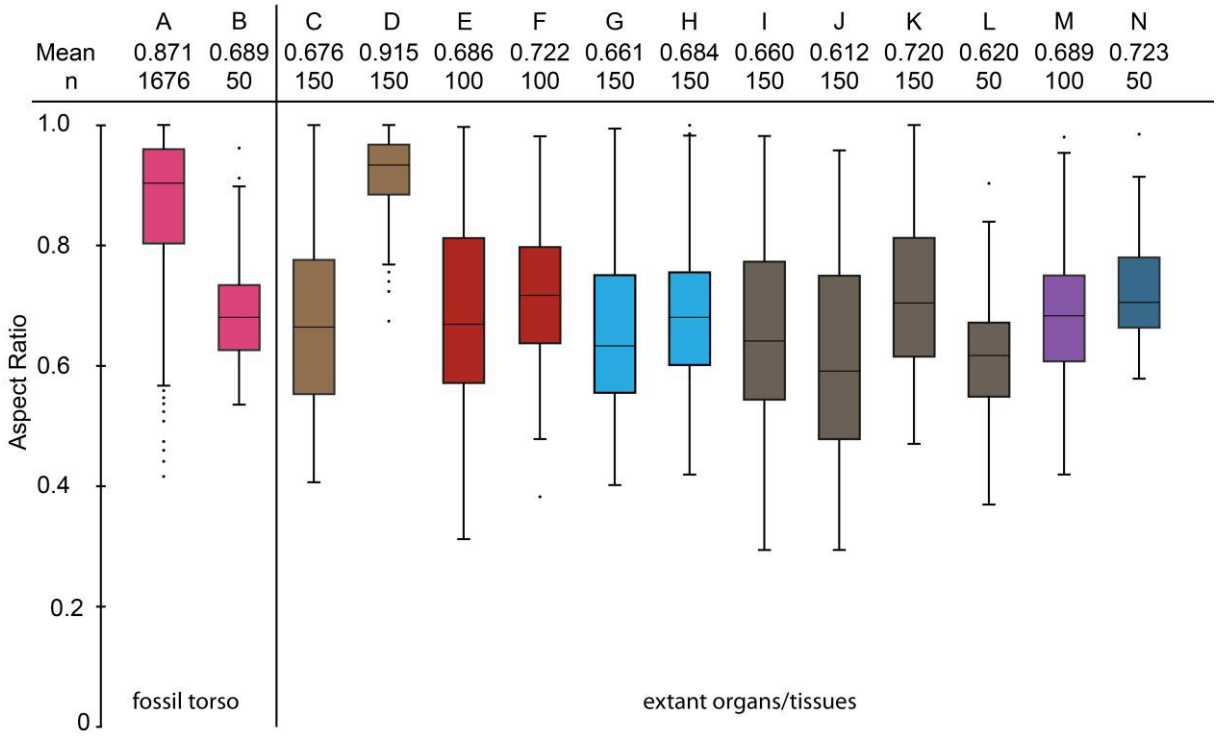


Figure S5.16: Boxplots showing aspect ratio of melanosomes from the torso in fossil anuran specimens and from non-integumentary soft tissues of extant anurans. Horizontal bars in boxplots denote the median values. (A) Torso of the Geiseltal specimens (n = 4). (B) Torso of the Libros specimen. (C) Gonads of Rhaebo guttatus. (D) Gonads of Bombina variegata. (E) Heart of Rhaebo guttatus. (F) Heart of Xenopus laevis. (G) Lungs of Rhaebo guttatus. (H) Lungs of Xenopus laevis. (I) Liver of Rhaebo guttatus. (J) Liver of Bombina variegata. (K) Liver of Xenopus laevis. (L) Liver of Hymenochirus boettgeri. (M) Spleen of Xenopus laevis. (N) Connective tissue of Xenopus laevis.

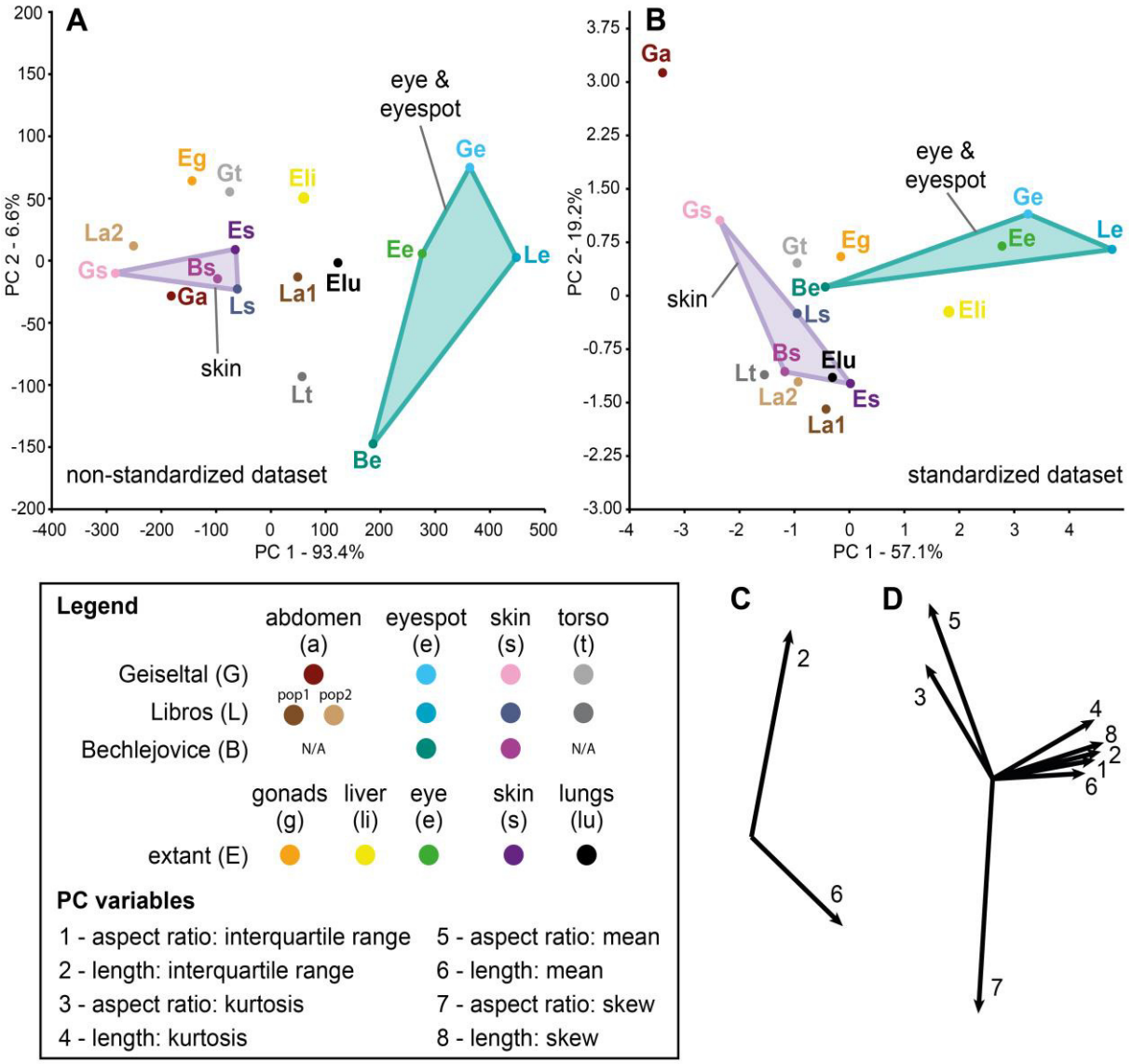


Figure S5.17: Principal Components Analysis (PCA) of geometry data for melanosomes from different body regions of fossil and extant anurans. Data point labels use upper case to denote biota and lower case, body region, e.g., Ge denotes Geiseltal eyespot. pop1, population 1; pop2, population 2. Specimen GMH CeIII-4967-1932 is included in the Geiseltal dataset, but not shown separately. (A) PCA of the raw dataset. (B) PCA of the standardized dataset. (C) Biplot for (A). The vectors for the variables 1, 3, 4, 5, 7 and 8 are too small to be displayed at this scale. (D) Biplot for (B).

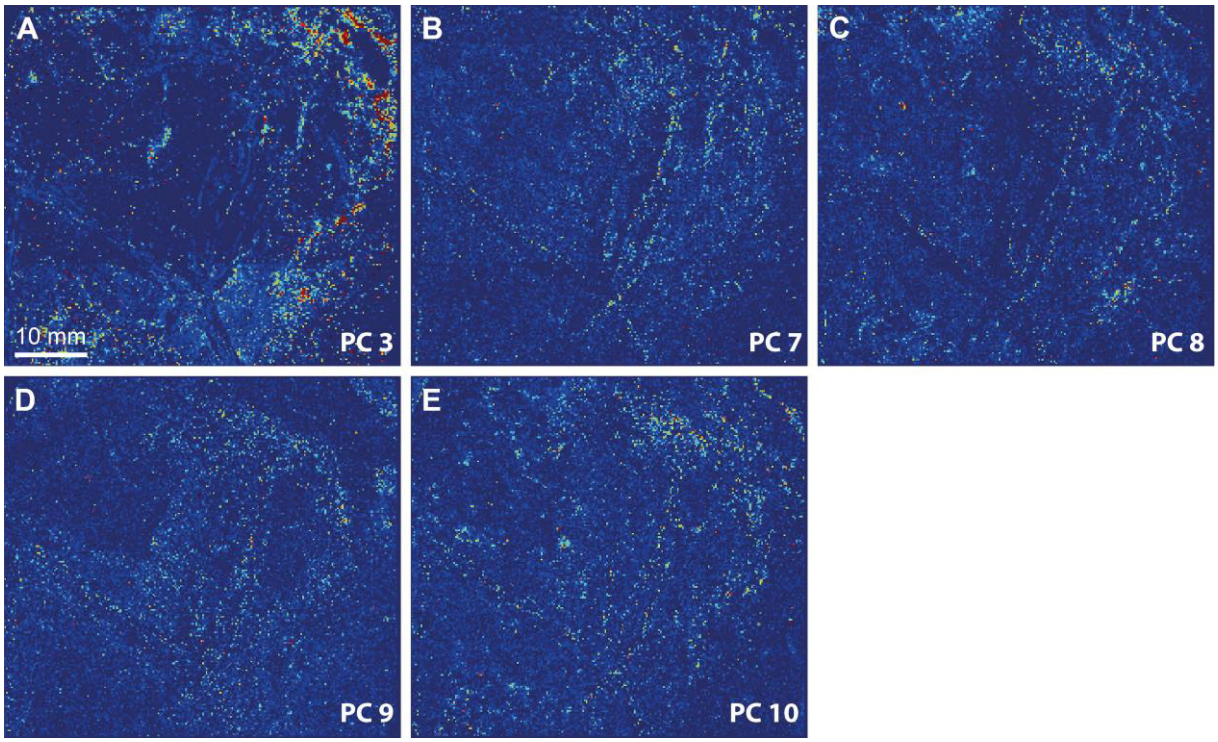


Figure S5.18: Maps for selected principal components based on principal component analysis of SRS-XRF data from GMH CeIII-4967-1932 (see Star Methods). These principal components lack a strong signal for the soft tissues, skeletal elements, sediment and/or nitrocellulose lacquer. The maps of PC 1, PC 2, PC 4, PC 5 and PC 6 are displayed in Figure 5.5. (A) PC 3. (B) PC 7. (C) PC 8. (D) PC 9. (E) PC 10. Scale in (A) applies to all maps.

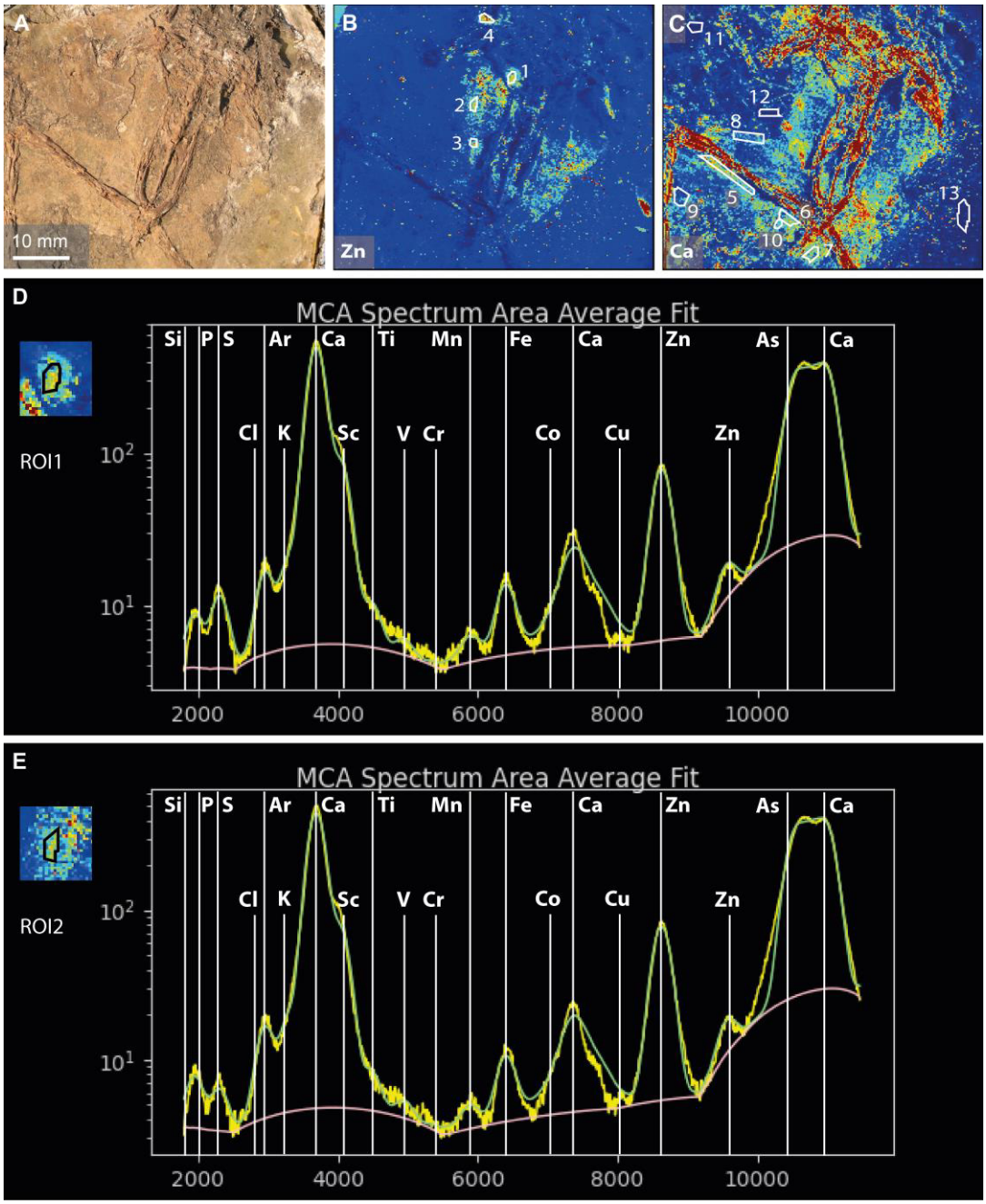


Figure S5.19: Multi channel analysis (MCA) for regions of interest (ROI) in GMH CeIII-4967-1932. MCA spectra for ROI 3–13 are shown in Figures S5.20–S5.23. (A) Photograph of region shown in Figure S5.1F. (B) Zn SRS-XRF element map with insets indicating ROI 1–4. (C) Ca SRS-XRF element map with insets indicating ROI 5–13. (D) MCA for ROI 1; Ni was not included as the Ni-kα and kβ peaks could not be identified. (E) MCA for ROI 2; Ni was not included as the Ni-kα and kβ peaks could not be identified.

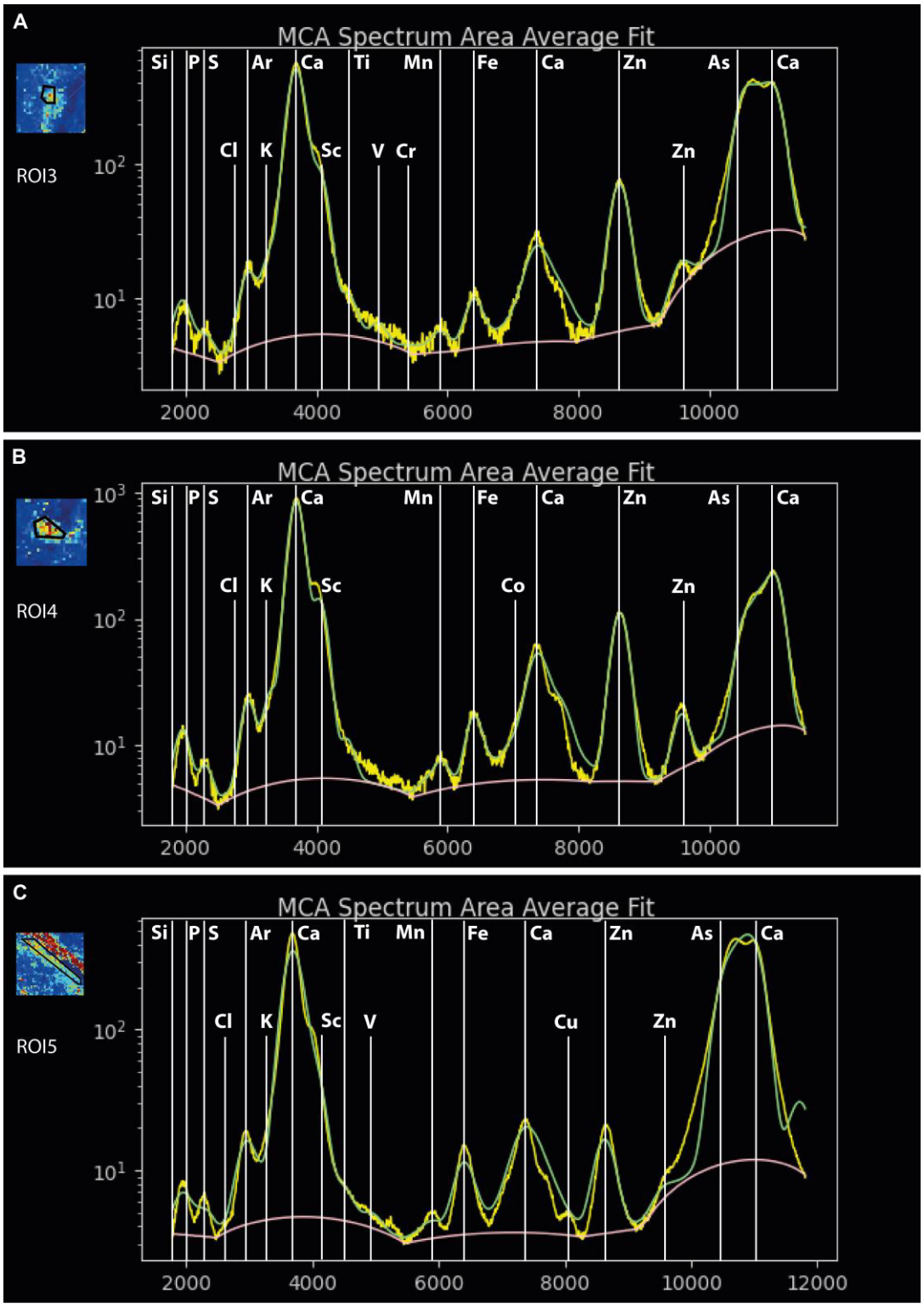


Figure S5.20: MCA for ROI 3–5 (see Figures S5.19B and S5.19C) in GMH CeIII-4967-1932. (A) MCA for ROI 3; Ni and Cu were not included as the kα and kβ peaks for Ni and Cu could not be identified. (B) MCA for ROI 4; Ti, V, Cr, Co and Ni were not included as the kα and kβ peaks for these elements could not be identified. (C) MCA for ROI 5; Cr, Co and Ni were not included as the kα and kβ peaks for these elements could not be identified.

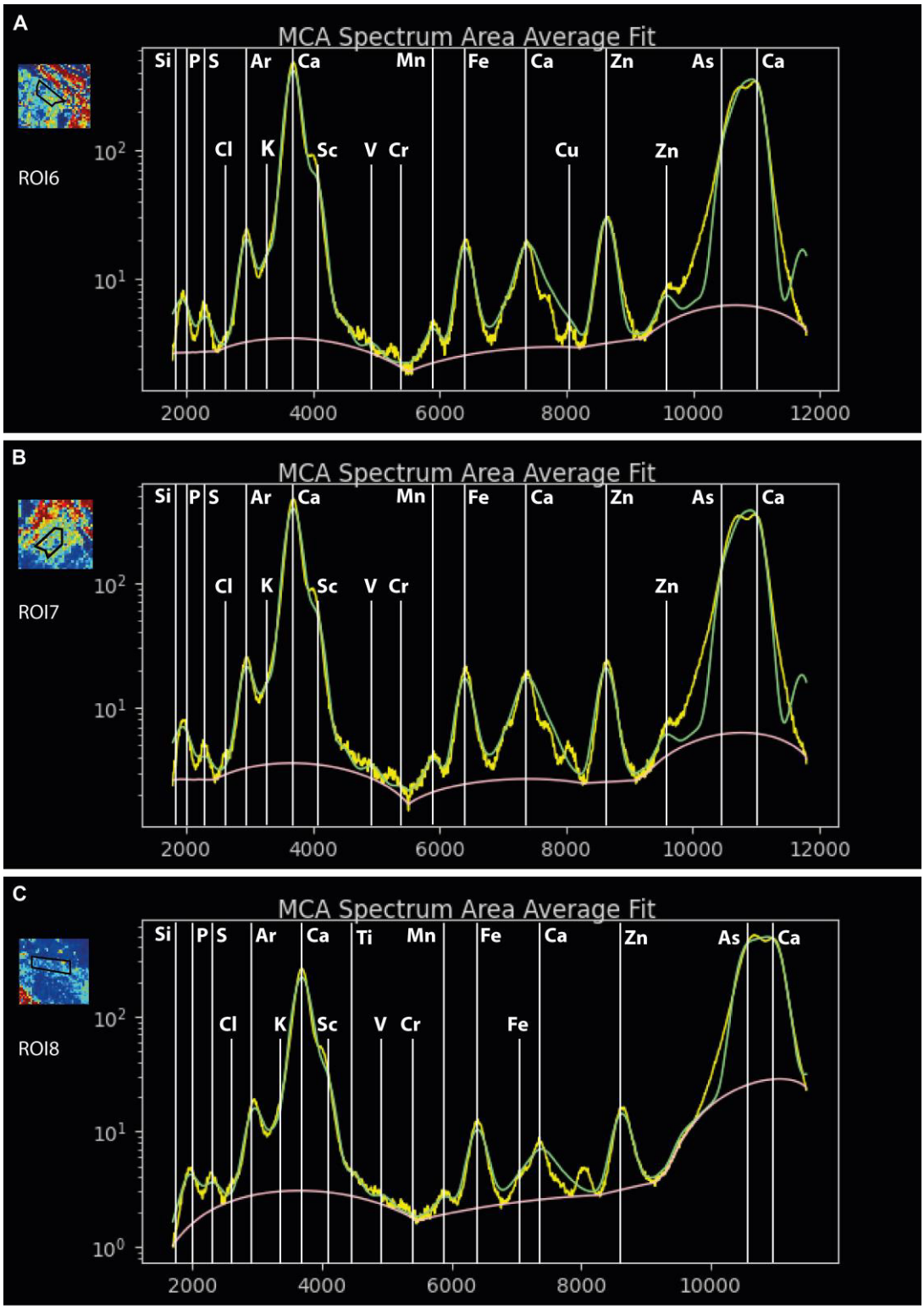


Figure S5.21: MCA for ROI 6–8 (see Figure S5.19C) in GMH CeIII-4967-1932. (A) MCA for ROI 6; Ti, Co and Ni were not included as the kα and kβ peaks for these elements could not be identified. (B) MCA for ROI 7; Ti, Co, Ni and Cu were not included as the kα and kβ peaks for these elements could not be identified. (C) MCA for ROI 8; Co, Ni and Cu were not included as the kα and kβ peaks for these elements could not be identified.

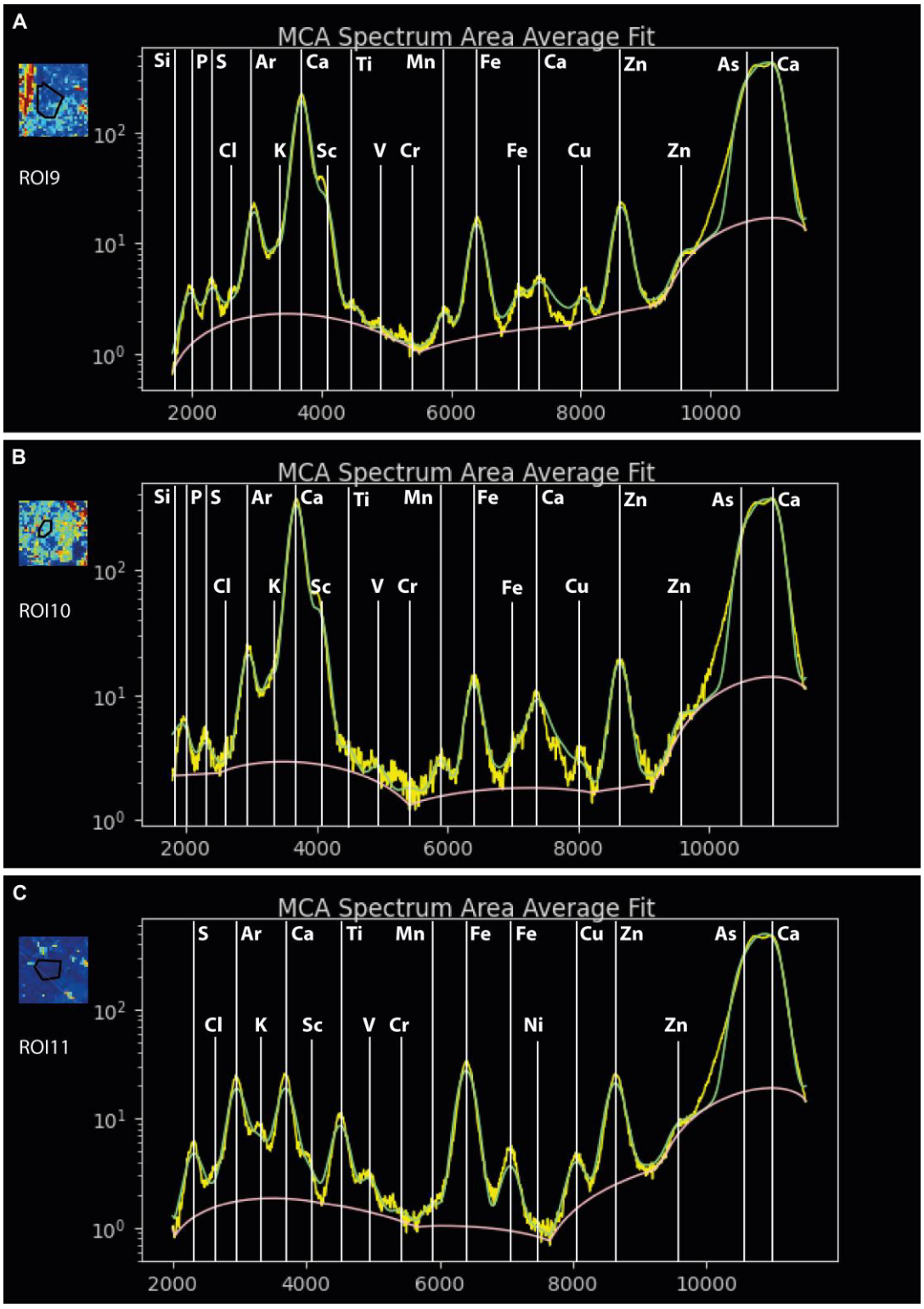


Figure S5.22: MCA for ROI 9–11 (see Figure S5.19C) in GMH CeIII-4967-1932. (A) MCA for ROI 9; Co and Ni were not included as the kα and kβ peaks for these elements could not be identified. (B) MCA for ROI 10; Co and Ni were not included as the kα and kβ peaks for these elements could not be identified. (C) MCA for ROI 11; Co was not included as the Co-kα and kβ peaks could not be identified.

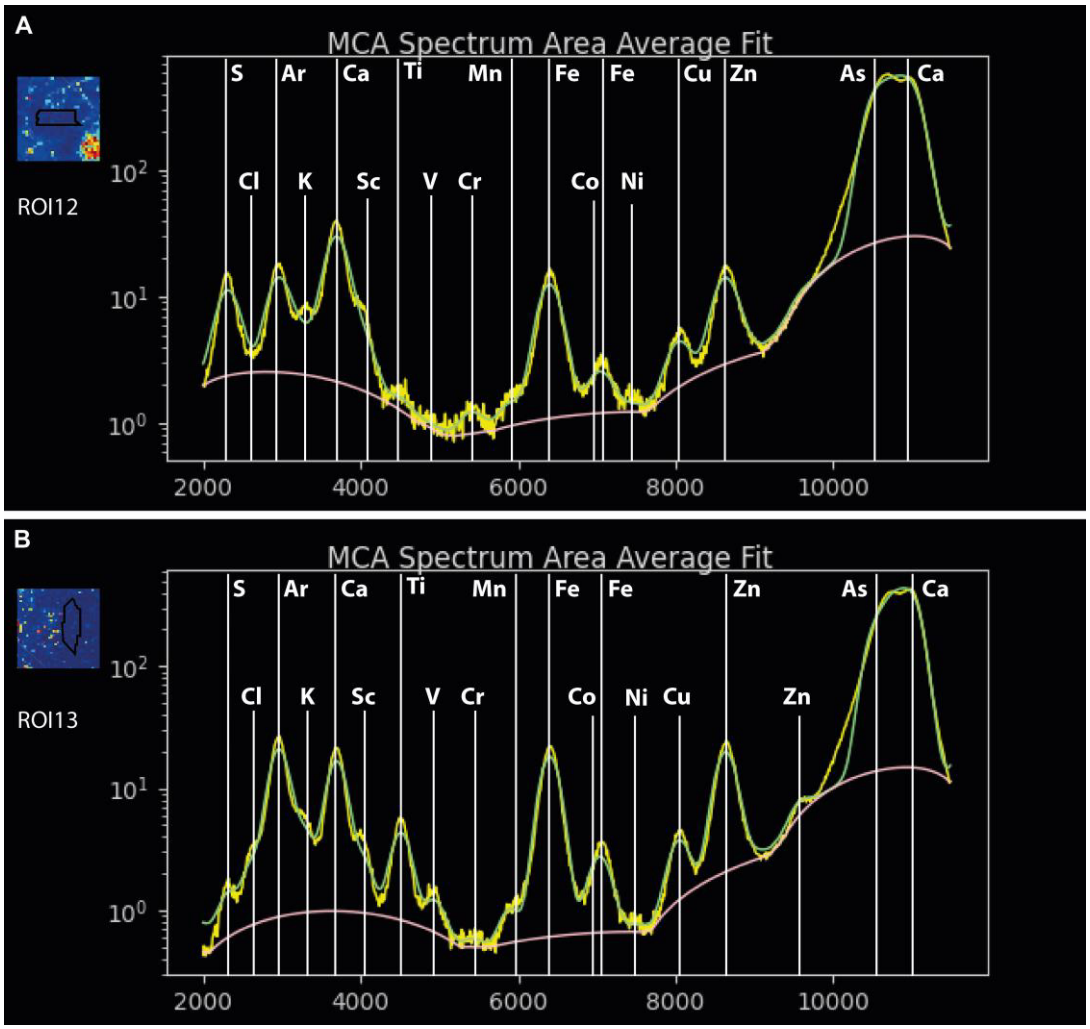


Figure S5.23: MCA for ROI 12–13 (see Figure S5.19C) in GMH CeIII-4967-1932. (A) MCA for ROI 12. (B) MCA for ROI 13.

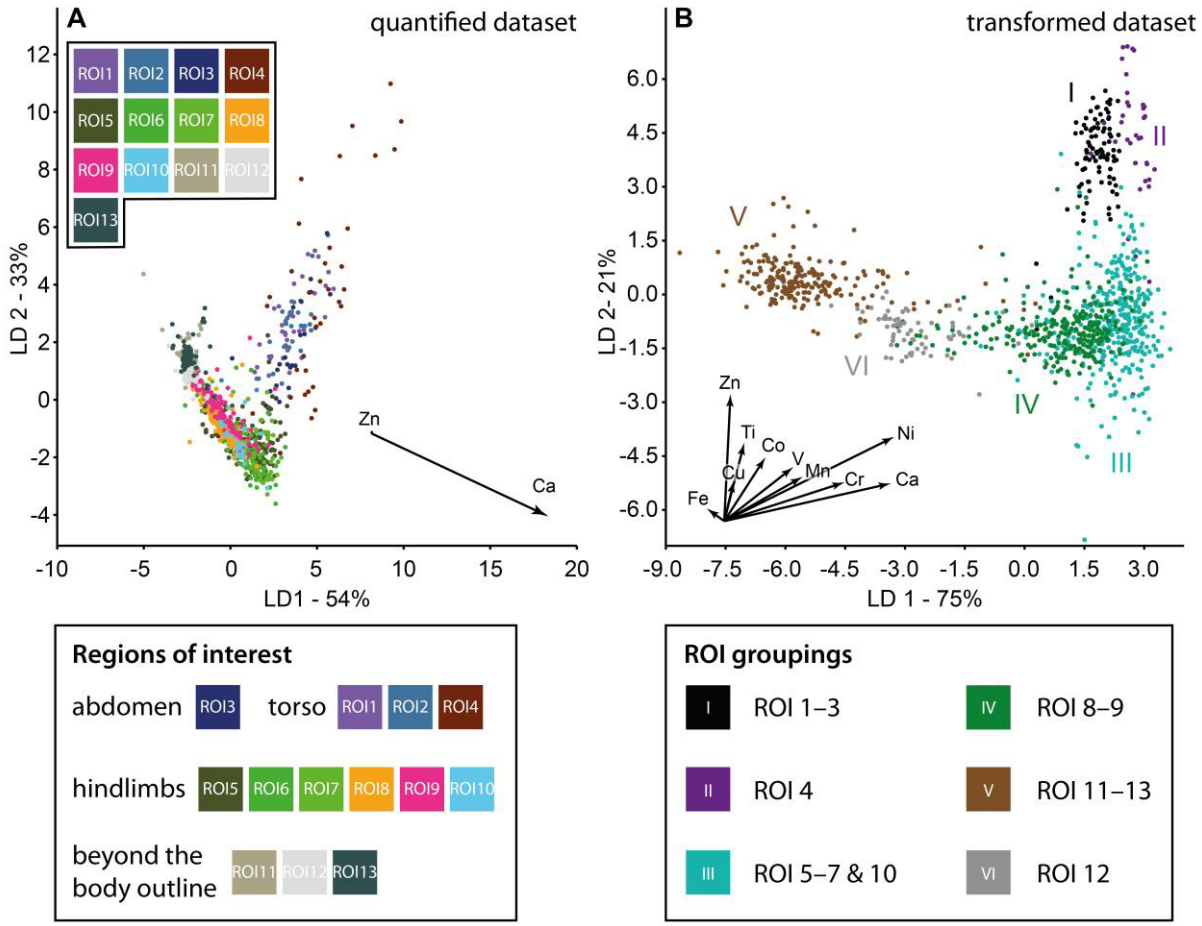


Figure S5.24: Linear discriminant analysis (LDA) of the SRS-XRF data from regions of interest (ROI) in GMH CeIII-4967-1932. (A) LDA of the SRS-XRF metal chemistry data from 13 ROI (Figures S5.19B–C); data were quantified but not processed further. Certain clusters of data points show extensive overlap. Most chemical variation in the data is driven by Ca; the vectors for Fe, Cu, Ti, Co, V, Mn, Ni and Cr are too small to be visible at this scale. (B) LDA of the log_{10}-transformed metal chemistry data from six ROI groupings; numbers in parentheses indicate constituent ROI in each group. Most chemical variation is driven by Ca, Ni, and Zn.

*Table S5.1. Significance tests on melanosome geometry data. Post-hoc test results are provided in Table S5.2. * Denotes cases where the highest standard deviation among groups was less than twice the lowest standard deviation and the data were treated as homoscedastic even if Levene's test revealed a significant p-value.*

Fossil melanosome dataset	Extant melanosome dataset	Data transformation	Normality	Homoscedasticity of variance	Test	p-value	Post-hoc test
total dataset length	total dataset length	log_{10}	normal	homoscedastic*	t-test	4.790E-22	N/A
total dataset aspect ratio	total dataset aspect ratio	none	non-normal	homoscedastic*	Kolmogorov-Smirnov	9.172E-272	N/A
total length dataset split into Geiseltal, Libros and Bechlejovice subsets	total dataset length	log_{10}	normal	homoscedastic*	ANOVA	3.519E-26	Tukey's
total aspect ratiio dataset split into Geiseltal, Libros and Bechlejovice subsets	total dataset aspect ratio	none	non-normal	homoscedastic*	Kruskal-Wallis	0	Dunn's
eyespot melanosome length	eyes aspect length	log_{10}	normal	heteroscedastic	Welch	0.210	N/A
eyespot melanosome aspect ratio	eyes aspect ratio	none	non-normal	heteroscedastic	Kruskal-Wallis	4.007E-11	Dunn's
torso length	connective tissue length	log_{10}	normal	heteroscedastic	Welch	1.463E-42	Dunn's
torso aspect ratio	connective tissue aspect ratio	none	non-normal	homoscedastic	Kruskal-Wallis	4.356E-33	Dunn's
torso length	gonads length	log_{10}	normal	heteroscedastic	Welch	1.810E-37	Dunn's
torso aspect ratio	gonads aspect ratio	none	non-normal	homoscedastic*	Kruskal-Wallis	1.250E-26	Dunn's
torso length	heart length	none	normal	heteroscedastic	Welch	3.160E-33	Dunn's
torso aspect ratio	heart aspect ratio	none	non-normal	homoscedastic*	Kruskal-Wallis	1.717E-64	Dunn's
torso length	liver length	none	normal	heteroscedastic	Welch	2.324E-32	Dunn's
torso aspect ratio	liver aspect ratio	none	non-normal	homoscedastic*	Kruskal-Wallis	1.764E-145	Dunn's
torso length	lungs length	none	normal	heteroscedastic	Welch	1.102E-45	Dunn's
torso aspect ratio	lungs aspect ratio	none	non-normal	homoscedastic*	Kruskal-Wallis	1.363E-101	Dunn's
torso length	spleen length	log_{10}	normal	heteroscedastic	Welch	6.068E-53	Dunn's
torso aspect ratio	spleen aspect ratio	none	non-normal	homoscedastic	Kruskal-Wallis	5.918E-50	Dunn's
abdomen length	connective tissue length	none	normal	heteroscedastic	Welch	2.165E-43	Dunn's
abdomen aspect ratio	connective tissue aspect ratio	none	non-normal	heteroscedastic	Kruskal-Wallis	7.975E-70	Dunn's
abdomen length	gonads length	none	normal	heteroscedastic	Welch	2.588E-22	Dunn's
abdomen aspect ratio	gonads aspect ratio	none	non-normal	heteroscedastic	Kruskal-Wallis	1.812E-68	Dunn's
abdomen length	liver length	none	normal	heteroscedastic	Welch	3.625E-42	Dunn's
abdomen aspect ratio	liver aspect ratio	none	non-normal	heteroscedastic	Kruskal-Wallis	6.536E-186	Dunn's
abdomen length	lungs length	none	normal	heteroscedastic	Welch	5.139E-56	Dunn's
abdomen aspect ratio	lungs aspect ratio	none	non-normal	heteroscedastic	Kruskal-Wallis	2.094E-142	Dunn's
abdomen length	spleen length	none	normal	heteroscedastic	Welch	8.093E-51	Dunn's
abdomen aspect ratio	spleen aspect ratio	none	non-normal	heteroscedastic	Kruskal-Wallis	3.535E-88	Dunn's
skin length	skin length	none	normal	heteroscedastic	Welch	1.145E-54	Dunn's
skin aspect ratio	skin aspect ratio	none	normal	homoscedastic*	ANOVA	2.566E-21	Tukey's
skin length	connective tissue length	none	normal	homoscedastic*	ANOVA	8.390E-93	Tukey's
skin aspect ratio	connective tissue aspect ratio	none	normal	homoscedastic	ANOVA	0.389	N/A
Libros abdomen population 1 aspect ratio	skin aspect ratio	none	normal	homoscedastic	t-test	0.165	N/A
Libros abdomen population 1 length	skin length	none	normal	homoscedastic	t-test	3.231E-08	N/A

Table S5.2. Summary of post-hoc test results on melanosome geometry data. Pop, population.

** Denotes that the dataset was log_{10}-transformed prior to testing.*

Datasets	Melanosome length				Melanosome aspect ratio			
all fossil melanosomes (three localities) & all extant melanosomes	*Tukey's test*	Libros*	Bechlejovice*	Extant*	*Dunn's test*	Libros	Bechlejovice	Extant
	Geiseltal*	0.003	1.725E-04	1.905E-12	Geiseltal	2.524E-51	2.153E-09	4.688E-314
	Libros*		0.346	0.928	Libros		0.001	0.824
	Bechlejovice*			0.421	Bechlejovice			3.730E-04
eyespot (fossil v extant)	*n/a*	Libros*	Bechlejovice*	Extant*	*Dunn's test*	Libros	Bechlejovice	Extant
	Geiseltal*				Geiseltal	0.043	0.041	1.066E-10
	Libros*		n/a		Libros		0.003	0.646
	Bechlejovice*				Bechlejovice			1.049E-05
torso (fossil) & connective tissue (extant)	*Dunn's test*	Libros*	Extant*	n/a	*Dunn's test*	Libros	Extant	n/a
	Geiseltal*	2.364E-15	3.760E-23	n/a	Geiseltal	1.716E-20	2.434E-16	n/a
	Libros*		0.153	n/a	Libros		0.438	n/a
torso (fossil) & gonads (extant)	*Dunn's test*	Libros*	Extant*	n/a	*Dunn's test*	Libros	Extant	n/a
	Geiseltal*	4.517E-15	1.463E-12	n/a	Geiseltal	2.115E-19	1.369E-11	n/a
	Libros*		9.581E-25	n/a	Libros		1.288E-08	n/a
torso (fossil) & heart (extant)	*Dunn's test*	Libros	Extant	n/a	*Dunn's test*	Libros	Extant	n/a
	Geiseltal	6.486E-15	9.871E-37	n/a	Geiseltal	5.267E-20	7.738E-51	n/a
	Libros		0.278	n/a	Libros		0.224	n/a
torso (fossil) & liver (extant)	*Dunn's test*	Libros	Extant	n/a	*Dunn's test*	Libros	Extant	n/a
	Geiseltal	2.374E-15	1.196E-34	n/a	Geiseltal	1.501E-18	5.397E-137	n/a
	Libros		5.705E-04	n/a	Libros		0.957	n/a
torso (fossil) & lungs (extant)	*Dunn's test*	Libros	Extant	n/a	*Dunn's test*	Libros	Extant	n/a
	Geiseltal	6.253E-15	6.370E-69	n/a	Geiseltal	2.630E-19	3.066E-90	n/a
	Libros		0.900	n/a	Libros		0.863	n/a
torso (fossil) & spleen (extant)	*Dunn's test*	Libros*	Extant*	n/a	*Dunn's test*	Libros	Extant	n/a
	Geiseltal*	6.908E-15	9.246E-46	n/a	Geiseltal	3.234E-20	1.267E-34	n/a
	Libros*		0.047	n/a	Libros		0.735	n/a
abdomen (fossil) & connective tissue (extant)	*Dunn's test*	Libros pop1	Libros pop2	Extant	*Dunn's test*	Libros pop1	Libros pop2	Extant
	Geiseltal	2.498E-21	2.313E-10	4.283E-32	Geiseltal	4.547E-29	5.224E-29	4.789E-25
	Libros pop1		1.500E-30	0.093	Libros pop1		0.993	0.536
	Libros pop2			1.365E-39	Libros pop2			0.541
abdomen (fossil) & gonads (extant)	*Dunn's test*	Libros pop1	Libros pop2	Extant	*Dunn's test*	Libros pop1	Libros pop2	Extant
	Geiseltal	2.017E-19	1.506E-10	3.903E-04	Geiseltal	3.071E-28	1.970E-28	1.145E-30
	Libros pop1		4.278E-29	4.795E-24	Libros pop1		0.977	4.685E-08
	Libros pop2			5.499E-06	Libros pop2			3.780E-08
abdomen (fossil) & liver (extant)	*Dunn's test*	Libros pop1	Libros pop2	Extant	*Dunn's test*	Libros pop1	Libros pop2	Extant
	Geiseltal	2.489E-20	1.910E-07	3.881E-75	Geiseltal	3.199E-28	2.662E-28	5.511E-166
	Libros pop1		9.487E-26	0.030	Libros pop1		0.990	0.625
	Libros pop2			4.642E-33	Libros pop2			0.613
abdomen (fossil) & lungs (extant)	*Dunn's test*	Libros pop1	Libros pop2	Extant	*Dunn's test*	Libros pop1	Libros pop2	Extant
	Geiseltal	3.714E-20	8.155E-08	1.260E-109	Geiseltal	8.109E-29	8.585E-29	4.036E-114
	Libros pop1		3.970E-26	0.344	Libros pop1		0.997	0.483
	Libros pop2			1.706E-49	Libros pop2			0.486
abdomen (fossil) & spleen (extant)	*Dunn's test*	Libros pop1	Libros pop2	Extant	*Dunn's test*	Libros pop1	Libros pop2	Extant
	Geiseltal	2.679E-20	1.346E-09	6.650E-59	Geiseltal	4.937E-29	5.830E-29	8.307E-48
	Libros pop1		1.179E-28	0.036	Libros pop1		0.991	0.587
	Libros pop2			2.295E-50	Libros pop2			0.595
skin (fossil v extant)	*Dunn's test*	Libros	Bechlejovice	Extant	*Tukey's test*	Libros	Bechlejovice	Extant
	Geiseltal	1.765E-21	1.940E-15	1.729E-46	Geiseltal	0.964	0.602	0.000E+00
	Libros		0.183	0.264	Libros		0.917	6.455E-07
	Bechlejovice			0.485	Bechlejovice			5.038E-05
skin (fossil) & connective tissue (extant)	*Tukey's test*	Libros	Bechlejovice	Extant	*n/a*	Libros	Bechlejovice	Extant
	Geiseltal	0.000E+00	0.000E+00	0.000E+00	Geiseltal			
	Libros		0.091	0.000E+00	Libros		n/a	
	Bechlejovice			0.000E+00	Bechlejovice			

Table S5.3. SRS-XRF element concentration mean data (µg/cm^2) from regions of interest (ROI) and grouped ROI in GMH CeIII-4967-1932. Data were normalised to the time channel prior to quantification. (A) ROI 1–13. (B) Groups I–VI (grouped ROI).

(A)

	Element									
ROI	Ca	Ti	V	Cr	Mn	Fe	Co	Ni	Cu	Zn
1	39574.0	445.6	185.5	111.4	127.7	236.0	118.8	300.2	36.5	476.4
2	36597.6	377.2	171.2	103.0	98.5	189.9	100.9	247.3	33.5	457.7
3	42011.0	451.0	196.4	107.6	110.4	177.6	104.6	296.4	33.8	445.7
4	64050.6	503.9	198.4	129.9	149.1	277.0	181.7	654.7	45.0	594.3
5	36158.9	348.0	153.4	87.4	93.0	230.5	88.5	231.0	26.8	114.6
6	32999.8	186.3	90.7	53.8	72.3	280.1	65.7	169.0	20.6	155.0
7	35318.6	221.2	108.0	60.0	76.3	293.5	80.4	194.7	26.3	128.7
8	19236.0	214.5	95.2	56.3	57.2	183.8	50.4	85.3	25.0	91.1
9	16077.9	111.0	55.4	32.3	43.7	230.4	38.1	49.8	17.8	122.5
10	27327.1	158.8	81.5	45.3	52.6	195.3	45.4	105.3	17.0	104.5
11	2168.5	442.9	104.7	41.0	34.9	494.8	57.2	12.3	22.2	148.5
12	2993.6	76.1	31.6	32.2	31.9	229.7	36.0	18.7	25.7	98.7
13	1762.6	215.1	40.2	12.4	18.3	318.4	36.1	9.4	20.1	134.8

(B)

	Element									
ROI	Ca	Ti	V	Cr	Mn	Fe	Co	Ni	Cu	Zn
I	39098.8	422.4	183.0	107.5	113.1	205.4	108.9	280.3	34.8	462.3
II	64050.6	503.9	198.4	129.9	149.1	277.0	181.7	654.7	45.0	594.3
III	34706.7	274.2	125.6	71.7	82.5	251.9	78.9	201.7	24.6	126.1
IV	17919.1	171.3	78.6	46.3	51.6	203.2	45.3	70.5	22.0	104.2
V	1887.1	285.0	60.0	21.2	23.4	372.5	42.6	10.3	20.7	139.0
VI	2993.6	76.1	31.6	32.2	31.9	229.7	36.0	18.7	25.7	98.7

Table S5.4. Summary of the results of significance testing on SRS-XRF data from regions of interest (ROI) and grouped ROI in GMH CeIII-4967-1932. Post-hoc test results are shown in Table S5.5.

Dataset	Normality	Homoscedasticity of variance	Test	p-value	Post-hoc test
ROI 1–13	non-normal	heteroscedastic	Kruskal-Wallis	1.658E-277	Dunn's
ROI I–VI	non-normal	heteroscedastic	Kruskal-Wallis	1.615E-258	Dunn's

Table S5.5. Results of Dunn's post-hoc test on the SRS-XRF data from regions of interest (ROI) and grouped ROI in GMH CeIII-4967-1932. Red font denotes statistically non-significant p-values. (A) ROI 1–13. (B) Groups I–VI (grouped ROI).

(A)

Dunn's test	ROI2	ROI3	ROI4	ROI5	ROI6	ROI7	ROI8	ROI9	ROI10	ROI11	ROI12	ROI13
ROI1	**0.190**	**0.891**	**0.165**	1.071E-07	2.153E-21	1.818E-11	3.769E-32	4.167E-51	1.704E-17	2.472E-38	4.380E-72	4.173E-74
ROI2		**0.312**	0.008	6.634E-04	3.185E-14	6.221E-07	4.689E-22	8.611E-38	7.802E-13	2.767E-28	1.812E-56	3.636E-56
ROI3			**0.179**	3.971E-05	1.264E-14	4.484E-08	5.016E-21	3.369E-34	7.292E-14	6.075E-27	2.647E-50	2.117E-48
ROI4				1.865E-12	2.195E-28	1.590E-16	4.310E-41	1.105E-61	3.283E-22	5.670E-47	1.283E-83	6.316E-87
ROI5					1.911E-12	0.003	1.259E-28	2.096E-56	3.406E-09	1.191E-32	3.859E-82	4.502E-105
ROI6						0.002	0.022	2.579E-12	**0.096**	7.286E-07	4.818E-29	2.606E-28
ROI7							2.180E-08	7.039E-23	1.995E-04	2.543E-14	4.199E-42	4.516E-43
ROI8								3.622E-08	**0.725**	7.221E-04	1.620E-24	4.683E-24
ROI9									0.006	**0.220**	2.875E-07	1.624E-04
ROI10										**0.076**	2.851E-09	6.604E-07
ROI11											1.274E-08	6.738E-06
ROI12												0.032

(B)

Dunn's test	ROI II (4)	ROI III (5–7, 10)	ROI IV (8–9)	ROI V (11, 13)	ROI VI (12)
ROI I (1–3)	0.023	3.335E-25	8.528E-83	1.702E-129	5.857E-109
ROI II (4)		3.065E-21	2.866E-55	1.495E-82	1.283E-83
ROI III (5–7, 10)			2.231E-44	2.528E-98	2.176E-70
ROI IV (8–9)				2.663E-13	1.096E-18
ROI V (11, 13)					1.834E-04

Table S5.6. Summary of the results of significance testing on SRS-XRF data from regions of interest (ROI) and grouped ROI in GMH CeIII-4967-1932. Post-hoc test results are shown in Table S5.7. (A) ROI 1–13. (B) Groups I–VI (grouped ROI).

(A)

Metal	Normality	Homoscedasticity of variance	Test	p-value	Post-hoc test
Cu	non-normal	heteroscedastic	Kruskal-Wallis	2.136E-56	Dunn's
Ti	normal	heteroscedastic	Welch	7.129E-74	Dunn's
V	normal	heteroscedastic	Welch	2.280E-90	Dunn's
Cr	normal	heteroscedastic	Welch	3.035E-105	Dunn's
Mn	normal	heteroscedastic	Welch	2.947E-103	Dunn's
Fe	normal	heteroscedastic	Welch	2.181E-15	Dunn's
Co	non-normal	heteroscedastic	Kruskal-Wallis	1.310E-96	Dunn's
Ni	normal	heteroscedastic	Welch	8.020E-88	Dunn's
Zn	non-normal	heteroscedastic	Kruskal-Wallis	4.332E-113	Dunn's
Ca	normal	heteroscedastic	Welch	2.505E-147	Dunn's

(B)

Metal	Normality	Homoscedasticity of variance	Test	p-value	Post-hoc test
Cu	normal	heteroscedastic	Welch	1.58E-24	Dunn's
Ti	non-normal	heteroscedastic	Kruskal-Wallis	7.30E-72	Dunn's
V	normal	heteroscedastic	Welch	1.04E-89	Dunn's
Cr	normal	heteroscedastic	Welch	5.09E-42	Dunn's
Mn	normal	heteroscedastic	Welch	1.12E-65	Dunn's
Fe	non-normal	heteroscedastic	Kruskal-Wallis	7.21E-33	Dunn's
Co	normal	heteroscedastic	Welch	1.51E-41	Dunn's
Ni	normal	heteroscedastic	Welch	2.87E-80	Dunn's
Zn	normal	heteroscedastic	Welch	4.79E-75	Dunn's
Ca	normal	heteroscedastic	Welch	1.68E-141	Dunn's

Table S5.7. Results of Dunn's post-hoc test on the SRS-XRF data from regions of interest (ROI) and grouped ROI in GMH CeIII-4967-1932. Red font denotes statistically non-significant p-values. (A) ROI 1–13. (B) Groups I–VI (grouped ROI).

(A)

Ca	ROI 2	ROI 3	ROI 4	ROI 5	ROI 6	ROI 7	ROI 8	ROI 9	ROI 10	ROI 11	ROI 12	ROI 13
ROI 1	0.618	0.580	0.018	0.288	0.080	0.227	5.649E-09	9.758E-11	0.022	1.354E-25	2.393E-22	1.779E-37
ROI 2		0.329	0.005	0.704	0.273	0.550	7.370E-07	2.045E-08	0.072	1.514E-21	1.217E-18	3.395E-31
ROI 3			0.134	0.129	0.038	0.105	7.557E-08	2.668E-09	0.011	5.244E-21	1.866E-18	2.596E-28
ROI 4				4.326E-05	6.136E-06	9.758E-05	2.470E-18	1.940E-20	1.337E-05	1.024E-38	7.776E-35	5.398E-55
ROI 5					0.237	0.696	9.164E-16	6.591E-18	0.059	3.318E-42	6.181E-37	7.671E-86
ROI 6						0.539	6.689E-08	6.432E-10	0.261	2.458E-28	2.981E-24	5.444E-50
ROI 7							1.052E-08	1.054E-10	0.132	1.197E-28	1.082E-24	4.237E-48
ROI 8								0.196	0.036	3.688E-13	4.373E-10	5.492E-28
ROI 9									0.006	5.582E-09	1.391E-06	2.310E-18
ROI 10										1.173E-10	7.868E-09	3.675E-15
ROI 11											0.322	0.196
ROI 12												0.013

Co	ROI 2	ROI 3	ROI 4	ROI 5	ROI 6	ROI 7	ROI 8	ROI 9	ROI 10	ROI 11	ROI 12	ROI 13
ROI 1	0.540	0.982	0.358	0.048	3.087E-07	0.005	8.716E-12	3.444E-19	1.822E-07	4.302E-09	2.466E-23	4.800E-25
ROI 2		0.577	0.133	0.270	2.674E-05	0.046	8.221E-09	4.110E-15	5.145E-06	6.303E-07	5.383E-19	7.208E-20
ROI 3			0.437	0.107	2.014E-05	0.018	2.674E-08	1.587E-13	2.845E-06	6.798E-07	5.531E-17	3.902E-17
ROI 4				0.002	7.351E-10	1.294E-04	2.528E-15	1.847E-23	1.969E-09	7.149E-12	1.037E-27	5.079E-30
ROI 5					4.799E-07	0.125	2.010E-16	4.869E-29	2.955E-06	2.872E-09	1.647E-32	7.518E-45
ROI 6						0.006	0.062	9.841E-07	0.107	0.199	1.812E-10	2.792E-11
ROI 7							1.907E-06	9.318E-14	6.714E-04	1.780E-04	5.657E-18	2.765E-20
ROI 8								3.574E-04	0.581	0.789	1.097E-07	2.972E-08
ROI 9									0.145	0.002	0.037	0.129
ROI 10										0.500	0.006	0.018
ROI 11											2.682E-06	4.678E-06
ROI 12												0.376

Cr	ROI 2	ROI 3	ROI 4	ROI 5	ROI 6	ROI 7	ROI 8	ROI 9	ROI 10	ROI 11	ROI 12	ROI 13
ROI 1	0.739	0.869	0.990	0.070	1.153E-07	2.345E-05	3.869E-07	7.844E-18	8.673E-06	3.189E-23	1.449E-23	5.736E-42
ROI 2		0.651	0.732	0.192	2.560E-06	2.194E-04	9.088E-06	4.156E-15	5.019E-05	3.397E-20	1.858E-20	3.208E-36
ROI 3			0.878	0.098	4.757E-06	1.993E-04	1.636E-05	4.039E-13	3.733E-05	1.410E-17	9.913E-18	3.637E-29
ROI 4				0.071	1.398E-07	2.598E-05	4.736E-07	1.440E-17	9.185E-06	6.414E-23	3.000E-23	3.270E-41
ROI 5					3.094E-08	1.279E-04	2.906E-08	1.631E-27	1.050E-04	8.646E-33	5.578E-34	1.513E-86
ROI 6						0.255	0.433	2.884E-05	0.559	7.593E-10	4.902E-10	3.668E-27
ROI 7							0.598	2.987E-07	0.182	4.341E-12	2.582E-12	7.982E-30
ROI 8								2.622E-08	0.278	8.972E-14	3.732E-14	9.109E-41
ROI 9									0.040	0.010	0.010	2.242E-11
ROI 10										2.819E-04	2.781E-04	2.640E-09
ROI 11											0.973	0.003
ROI 12												0.002

Cu	ROI 2	ROI 3	ROI 4	ROI 5	ROI 6	ROI 7	ROI 8	ROI 9	ROI 10	ROI 11	ROI 12	ROI 13
ROI 1	0.913	0.645	0.789	1.936E-05	9.469E-16	3.015E-05	2.629E-09	3.566E-21	5.333E-14	2.285E-07	3.452E-12	2.612E-15
ROI 2		0.585	0.879	8.233E-05	3.127E-14	9.780E-05	2.754E-08	4.336E-19	3.830E-13	1.109E-06	4.532E-11	1.106E-13
ROI 3			0.489	6.685E-05	7.358E-13	6.356E-05	7.848E-08	1.163E-16	9.362E-13	1.193E-06	2.251E-10	3.385E-12
ROI 4				1.050E-04	2.154E-14	1.288E-04	2.820E-08	1.774E-19	4.227E-13	1.364E-06	4.279E-11	7.005E-14
ROI 5					3.699E-10	0.571	0.003	1.164E-17	2.516E-08	0.036	3.535E-06	3.858E-10
ROI 6						4.917E-06	3.746E-04	0.111	0.076	0.002	0.353	0.390
ROI 7							0.085	4.142E-10	1.670E-06	0.193	6.723E-04	2.419E-05
ROI 8								2.667E-08	6.072E-05	0.873	0.025	0.002
ROI 9									0.425	3.903E-06	0.015	0.007
ROI 10										1.514E-04	0.019	0.018
ROI 11											0.044	0.010
ROI 12												0.818

Fe	ROI 2	ROI 3	ROI 4	ROI 5	ROI 6	ROI 7	ROI 8	ROI 9	ROI 10	ROI 11	ROI 12	ROI 13
ROI 1	0.042	0.017	**0.186**	**0.232**	**0.492**	**0.053**	1.804E-04	**0.125**	0.029	8.892E-07	0.001	**0.083**
ROI 2		**0.579**	9.357E-04	**0.148**	**0.084**	2.904E-05	**0.294**	**0.332**	**0.742**	2.358E-12	**0.382**	2.884E-05
ROI 3			4.236E-04	**0.058**	0.033	2.073E-05	**0.825**	**0.138**	**0.832**	1.650E-11	**0.889**	2.469E-05
ROI 4				0.004	0.025	**0.685**	7.783E-08	0.002	8.533E-04	7.027E-04	1.956E-06	**0.958**
ROI 5					**0.536**	1.218E-05	1.513E-05	**0.515**	**0.099**	1.960E-17	0.001	1.315E-06
ROI 6						9.469E-04	4.043E-05	**0.273**	**0.058**	2.894E-12	9.112E-04	8.041E-04
ROI 7							7.019E-14	7.811E-06	4.848E-05	3.043E-04	3.801E-10	**0.614**
ROI 8								0.002	**0.612**	7.690E-30	**0.913**	8.756E-18
ROI 9									**0.217**	1.749E-16	0.015	1.796E-06
ROI 10										4.674E-11	**0.687**	5.957E-05
ROI 11											5.110E-22	3.850E-06
ROI 12												1.940E-11

Mn	ROI 2	ROI 3	ROI 4	ROI 5	ROI 6	ROI 7	ROI 8	ROI 9	ROI 10	ROI 11	ROI 12	ROI 13
ROI 1	**0.172**	**0.704**	**0.750**	0.013	2.798E-06	1.805E-04	1.754E-11	1.688E-17	4.632E-07	2.034E-25	1.074E-23	6.739E-43
ROI 2		**0.411**	**0.096**	**0.524**	0.004	0.040	2.228E-06	6.741E-11	1.986E-04	1.473E-17	4.090E-16	2.770E-30
ROI 3			**0.512**	**0.122**	5.608E-04	0.007	5.595E-07	5.548E-11	3.175E-05	6.497E-17	1.219E-15	1.070E-26
ROI 4				0.004	5.216E-07	4.565E-05	1.726E-12	1.185E-18	1.186E-07	1.151E-26	6.376E-25	1.927E-44
ROI 5					2.524E-04	0.024	5.610E-13	2.239E-22	5.329E-05	4.253E-32	8.301E-30	1.630E-79
ROI 6						**0.318**	0.018	9.575E-07	**0.076**	6.263E-14	2.488E-12	1.238E-32
ROI 7							9.427E-04	1.570E-08	0.016	6.311E-16	2.709E-14	2.473E-34
ROI 8								0.002	**0.669**	9.693E-10	2.847E-08	2.726E-28
ROI 9									**0.197**	8.869E-04	0.006	1.856E-12
ROI 10										6.622E-04	0.003	7.486E-08
ROI 11											**0.561**	0.013
ROI 12												0.001

Ni	ROI 2	ROI 3	ROI 4	ROI 5	ROI 6	ROI 7	ROI 8	ROI 9	ROI 10	ROI 11	ROI 12	ROI 13
ROI 1	**0.584**	**0.642**	**0.081**	**0.143**	0.003	0.019	2.328E-09	7.550E-15	0.001	1.601E-26	3.699E-23	4.088E-39
ROI 2		**0.350**	0.025	**0.484**	0.028	**0.103**	4.928E-07	1.052E-11	0.008	3.977E-22	3.948E-19	2.671E-32
ROI 3			**0.291**	**0.083**	0.003	0.013	6.956E-08	4.486E-12	9.652E-04	2.610E-21	1.078E-18	5.942E-29
ROI 4				2.165E-04	5.984E-07	1.582E-05	5.141E-16	9.664E-23	2.093E-06	5.351E-36	3.647E-32	9.109E-52
ROI 5					0.014	**0.128**	2.465E-14	6.718E-24	0.007	5.933E-41	1.255E-35	2.158E-84
ROI 6						**0.511**	1.188E-04	3.608E-10	**0.242**	6.240E-23	3.841E-19	1.203E-41
ROI 7							1.545E-05	4.392E-11	**0.114**	1.266E-23	6.331E-20	1.019E-40
ROI 8								0.002	**0.267**	1.791E-13	2.630E-10	4.390E-29
ROI 9									0.006	6.109E-06	5.073E-04	5.344E-13
ROI 10										2.212E-08	9.390E-07	2.580E-12
ROI 11											**0.314**	**0.170**
ROI 12												0.009

Ti	ROI 2	ROI 3	ROI 4	ROI 5	ROI 6	ROI 7	ROI 8	ROI 9	ROI 10	ROI 11	ROI 12	ROI 13
ROI 1	**0.531**	**0.602**	**0.962**	0.029	2.919E-12	7.551E-08	6.082E-10	2.579E-27	3.773E-09	0.002	3.459E-32	7.311E-14
ROI 2		**0.289**	**0.503**	**0.200**	2.316E-09	7.908E-06	2.801E-07	5.914E-22	1.902E-07	0.020	1.270E-26	1.805E-10
ROI 3			**0.633**	0.017	1.876E-10	3.865E-07	1.762E-08	2.253E-21	9.515E-09	0.001	1.048E-25	2.270E-11
ROI 4				0.027	3.102E-12	7.227E-08	6.286E-10	4.365E-27	3.512E-09	0.002	6.048E-32	8.426E-14
ROI 5					3.412E-14	4.823E-07	9.460E-12	1.662E-43	1.025E-07	**0.076**	2.345E-46	3.517E-19
ROI 6						**0.081**	**0.088**	1.272E-06	**0.418**	1.276E-05	9.860E-11	**0.935**
ROI 7							**0.740**	1.800E-10	**0.050**	0.011	6.064E-15	0.046
ROI 8								3.062E-13	**0.060**	0.001	3.640E-18	0.040
ROI 9									0.025	4.292E-19	0.026	7.941E-08
ROI 10										1.746E-04	3.399E-04	**0.426**
ROI 11											5.619E-24	1.280E-06
ROI 12												2.249E-12

V	ROI 2	ROI 3	ROI 4	ROI 5	ROI 6	ROI 7	ROI 8	ROI 9	ROI 10	ROI 11	ROI 12	ROI 13
ROI 1	**0.764**	**0.533**	**0.680**	**0.134**	2.194E-08	6.151E-05	1.799E-08	7.410E-20	8.389E-06	1.371E-14	3.689E-30	7.461E-32
ROI 2		**0.383**	**0.918**	**0.294**	5.013E-07	4.332E-04	5.453E-07	4.931E-17	4.294E-05	1.309E-12	1.517E-26	1.794E-27
ROI 3			**0.328**	**0.051**	9.403E-08	5.338E-05	1.155E-07	2.243E-16	5.499E-06	8.158E-13	1.095E-24	9.997E-25
ROI 4				**0.341**	4.291E-07	4.659E-04	4.393E-07	1.445E-17	4.735E-05	7.419E-13	2.103E-27	1.211E-28
ROI 5					1.369E-10	9.257E-05	2.762E-12	5.834E-34	3.429E-05	6.698E-20	3.895E-48	4.288E-66
ROI 6						**0.074**	**0.648**	7.857E-06	**0.731**	0.003	2.167E-14	3.233E-15
ROI 7							**0.122**	1.323E-09	**0.126**	6.214E-06	3.392E-19	1.055E-20
ROI 8								2.967E-08	**0.525**	2.074E-04	1.034E-18	6.058E-22
ROI 9									0.013	**0.345**	1.483E-04	9.996E-04
ROI 10										**0.086**	1.396E-06	9.304E-06
ROI 11											2.232E-05	1.476E-04
ROI 12												**0.251**

Zn	ROI 2	ROI 3	ROI 4	ROI 5	ROI 6	ROI 7	ROI 8	ROI 9	ROI 10	ROI 11	ROI 12	ROI 13
ROI 1	**0.825**	**0.927**	**0.868**	2.502E-24	9.693E-26	1.803E-13	1.661E-40	6.386E-15	1.453E-15	5.522E-04	1.904E-26	7.445E-09
ROI 2		**0.918**	**0.953**	4.167E-21	9.164E-23	7.835E-12	1.172E-35	5.528E-13	2.761E-14	0.002	1.374E-23	1.494E-07
ROI 3			**0.958**	6.872E-16	9.416E-18	1.383E-09	1.071E-26	3.035E-10	1.817E-12	0.005	1.071E-18	4.588E-06
ROI 4				6.848E-23	2.096E-24	1.176E-12	1.713E-38	5.558E-14	6.533E-15	0.001	3.685E-25	3.566E-08
ROI 5					**0.076**	0.016	1.294E-08	0.005	**0.199**	1.652E-14	0.013	5.478E-12
ROI 6						4.113E-04	0.003	9.037E-05	**0.822**	4.181E-16	**0.451**	2.846E-13
ROI 7							3.295E-11	**0.988**	0.010	6.791E-06	5.531E-05	0.003
ROI 8								5.423E-14	**0.125**	7.655E-31	**0.065**	4.285E-32
ROI 9									0.007	1.095E-06	1.044E-05	9.603E-04
ROI 10										8.465E-09	**0.771**	2.961E-06
ROI 11											6.462E-17	0.020
ROI 12												5.364E-14

(B)

Ca	ROI II	ROI III	ROI IV	ROI V	ROI VI
ROI I	0.004	0.028	1.090E-20	5.257E-75	3.528E-35
ROI II		3.031E-06	2.057E-21	3.515E-56	7.776E-35
ROI III			4.544E-27	4.967E-122	7.175E-39
ROI IV				4.956E-35	5.957E-10
ROI V					0.028

Co	ROI II	ROI III	ROI IV	ROI V	ROI VI
ROI I	**0.175**	1.422E-06	1.810E-30	2.079E-39	2.886E-35
ROI II		2.169E-06	1.102E-20	3.793E-26	1.037E-27
ROI III			1.275E-24	7.913E-36	5.040E-27
ROI IV				0.008	1.628E-05
ROI V					0.015

Cr	ROI II	ROI III	ROI IV	ROI V	ROI VI
ROI I	**0.916**	6.045E-08	2.055E-23	1.481E-78	9.091E-37
ROI II		1.952E-04	4.485E-12	2.609E-39	3.000E-23
ROI III			8.497E-13	1.976E-87	3.902E-26
ROI IV				1.040E-33	2.508E-09
ROI V					0.024

Cu	ROI II	ROI III	ROI IV	ROI V	ROI VI
ROI I	**0.671**	3.611E-20	3.524E-31	1.587E-27	1.979E-19
ROI II		1.642E-08	8.771E-14	1.531E-12	4.279E-11
ROI III			2.501E-05	7.613E-04	0.004
ROI IV				**0.583**	**0.808**
ROI V					**0.546**

Fe	ROI II	ROI III	ROI IV	ROI V	ROI VI
ROI I	0.001	**0.052**	**0.109**	5.472E-12	0.032
ROI II		0.018	2.845E-06	**0.215**	1.956E-06
ROI III			2.382E-07	2.125E-13	1.715E-05
ROI IV				1.906E-29	**0.279**
ROI V					8.890E-18

Mn	ROI II	ROI III	ROI IV	ROI V	ROI VI
ROI I	**0.271**	4.925E-06	4.165E-25	6.785E-74	7.997E-33
ROI II		1.870E-05	1.256E-16	2.599E-43	6.376E-25
ROI III			4.239E-19	4.692E-90	1.776E-25
ROI IV				2.303E-27	1.862E-06
ROI V					0.010

Ni	ROI II	ROI III	ROI IV	ROI V	ROI VI
ROI I	0.030	6.243E-04	1.468E-24	1.440E-77	3.771E-36
ROI II		2.404E-06	7.247E-21	1.118E-52	3.647E-32
ROI III			2.918E-25	2.383E-110	3.562E-34
ROI IV				3.912E-31	2.133E-08
ROI V					0.023

Ti	ROI II	ROI III	ROI IV	ROI V	ROI VI
ROI I	**0.874**	3.848E-12	2.801E-35	1.101E-19	1.354E-50
ROI II		1.586E-06	5.934E-18	1.024E-10	6.048E-32
ROI III			8.293E-18	1.435E-04	3.073E-33
ROI IV				7.824E-05	8.473E-11
ROI V					2.587E-19

V	ROI II	ROI III	ROI IV	ROI V	ROI VI
ROI I	**0.571**	3.923E-08	1.785E-28	8.406E-58	1.082E-48
ROI II		0.003	4.222E-12	9.668E-26	2.103E-27
ROI III			3.907E-18	5.277E-56	3.248E-38
ROI IV				2.080E-12	2.439E-13
ROI V					0.014

Zn	ROI II	ROI III	ROI IV	ROI V	ROI VI
ROI I	**0.944**	8.893E-55	2.515E-62	8.625E-14	3.742E-41
ROI II		7.315E-25	1.422E-29	3.529E-07	3.685E-25
ROI III			0.008	5.004E-24	0.010
ROI IV				2.822E-31	**0.350**
ROI V					3.708E-18

6. Discussion

This thesis has generated five major findings, which are discussed in the following sections: (1) patterns in the skeletal taphonomy of the Geiseltal anurans recur in anurans from other Cenozoic biotas (Section 6.1), (2) the cause of death of the Geiseltal anurans was likely mating-related (Section 6.2), (3) the soft tissues of the Geiseltal anurans are sulfurised and replicated in calcium phosphate (Section 6.3), (4) the melanosomes from the Geiseltal anurans show tissue-specific geometries (Section 6.4) and (5) anuran melanosomes have strongly conserved geometries since the Middle Eocene (Section 6.5).

In Section 6.6, these findings are compared with data that have been published for the Libros anurans to assess similarities and differences in the skeletal taphonomy, the soft tissue preservation and the geometry of preserved melanosomes. This comparative analysis shows that the model for the preservation of the Geiseltal anurans can be applied to other biotas and that preserved melanosomes in anurans from both biotas show tissue-specific geometries.

The data and interpretations presented here are not without limitations; the latter are discussed in Section 6.7.

6.1 Recurring taphonomic trends in anuran preservation

The Geiseltal anurans reveal nine taphonomic patterns (see Section 3.5). Some of these patterns were also identified in fossil anurans from several Cenozoic Konservat-Lagerstätten, that represent lake environments, e.g. Messel (Middle Eocene, Germany; Wuttke 1988, 2018), Enspel (Late Oligocene, Germany; Roček & Wuttke 2010), Bechlejovice (Early Oligocene, Czech Republic; Špinar 1972; Roček 2013) and Libros (Late Miocene, Spain; McNamara *et al.* 2009; McNamara *et al.* 2012a). Recurring trends in anuran preservation in these biotas include proximal-distal trends for completeness in the limbs, abdominal disarticulation and/or the reorientation of the anterior or posterior body. These

trends in anurans between biotas are subject to three ultimate controls: (1) climate, (2) lake physiography and (3) anuran anatomy.

(1) Climate controls the ambient temperature including the water temperature. The relative timing of decay and deposition of vertebrate carcasses in aquatic environments is controlled, in large part, by ambient temperature (Wuttke 1983a; Kidwell & Baumiller 1990; Carter & Tibbett 2006; Carter *et al.* 2008), which regulates microbial metabolism and abiotic reactions. Warm water temperatures promote bacterial decay and the production of decay gases. The latter can lead to increased transportation times (e.g., by re-floating of the carcass after initial sinking, Wuttke 1983b) or initialise abdominal rupture, resulting in disarticulation and loss of skeletal elements.

(2) The lake physiography and hydrology controls water depth, lake size, vegetation and presence or absence of scavengers. Deposition in deeper waters inhibits refloating and abdominal rupture (Smith & Elder 1985; e.g., Messel and Enspel). Littoral vegetation can trap carcasses (e.g., Enspel; Wuttke & Poschmann 2010), which may prolong floating/decay and scavenging at or close to the water surface. Vegetation can also delay or prevent the deposition of the carcass in profundal regions (Wuttke & Poschmann 2010). Larger lakes may yield a higher proportion of carcasses deposited soon after death, given that the proportion of vegetated margins to lake area is lower than in a system with interconnected smaller water bodies (e.g. Geiseltal). Furthermore, in larger lakes the profundal region is often deeper, inhibiting decay due to lower water temperatures and inhibiting generation of decay gases due to higher water pressure (Elder & Smith 1988). Specimens are more complete and articulated and scattered bones are rare, when predators and scavengers (e.g. fish) are absent in the lake.

(3) Anuran anatomy controls the frequent disarticulation and/or loss of bones in the abdominal region, induced by either abdominal collapse (McNamara *et al.* 2012a) or abdominal rupture (Wuttke 1983a; Smith & Wuttke 2012). In addition, it is notable that small skeletal elements (e.g., phalanges and skeletal elements from taxa with small body sizes) are easier to transport

than large and/or heavy bones (Dodson 1973). Further, the quality of preservation of the anuran skin impacts the skeletal taphonomy, whereby better preserved skin is associated with higher values for completeness and articulation (McNamara *et al.* 2009).

6.2 The death of the Geiseltal anurans was likely mating-related

Previous studies have suggested that the Geiseltal anurans died during the desiccation of lakes and/or oxygen depletion of the water column during overturn of lake waters (Voigt 1934; Weigelt 1934). This, however, is unlikely because the anurans could presumably migrate to other water bodies during adverse conditions (Henrici & Fiorillo 1993; Todd *et al.* 2009). Furthermore, the evidence for (re)flotation of carcasses is not consistent with desiccation.

Nine alternative modes of death for the Geiseltal anurans are discussed in detail in Section 3.5, whereby death by disease, death by old age and death due to mating behaviour are the most likely scenarios. Mass mortalities in extant anurans can result from disease (Scheele *et al.* 2019). Many diseases lack physical expressions that can fossilise; the verification of a disease-related death on the skeletal elements is therefore not possible. Death by natural causes including old age is another possible scenario as the fossil anurans represent a wide range of body sizes. The normal distributed anuran body sizes suggest that: 1) few specimens in the population died as young adults, 2) many specimens died at a certain adult age with a specific body size and 3) few specimens exceeded the average age/body size and died at a later age). Reports of tens to hundreds of specimens on individual bedding planes at many excavation sites (Haubold & Krumbiegel 1984; Hellmund & Hastings 2014) suggest recurring mass mortality events. It is unlikely that the death of numerous specimens in a relative short time is linked to age and other natural causes. The most likely scenario are mating-related deaths.



Figure 6.1: Mating Geiseltal anurans form a mating ball. Drawing: A. Pieri.

Mating-related mass mortality caused by drowning or exhaustion is common in extant anurans (Verrell & McCabe 1986; Trauth *et al.* 2000; Menin *et al.* 2006; Izzo *et al.* 2012) and can be fatal for whole populations (Falk *et al.* 2022a). Mating-related mortalities also affect terrestrial anurans, e.g., the pelobatids (which are more abundant than the aquatic palaeobatrachids in the Geiseltal), as they return to the water to reproduce (Lizana *et al.* 1994). Further, the fossil soft tissues of the Geiseltal

anurans indicate that certain specimens were females: melanosomes in the torso and abdomen of specimen GMH CeIII-4967-1932 (Pelobatidae) likely derive from the gonads; this shows, that the specimen was a gravid female and supports the hypothesis, that the anurans returned to the water to breed (Fig. 6.1). The anurans from the Libros biota (Miocene, Spain) are also thought to represent mating-related mortalities (McNamara *et al.* 2012a).

6.3 The soft tissues from the Geiseltal anurans are sulfurised and replicated in calcium phosphate

The Geiseltal anuran soft tissues were previously reported to be preserved in authigenic silica (Voigt 1937, 1988) – a mode of soft tissue preservation that usually applies to microbes, plants and arthropods (Butts 2014) but rarely to vertebrates (but see Channing *et al.* 2005; Yang *et al.* 2024). A suite of modern electron beam and spectroscopic techniques were used to analyse the soft tissues and sediments of the Geiseltal anurans. Scanning electron microscopy (SEM) was used as it is a standard technique for high-resolution, high-magnification imaging in research. Energy-dispersive X-ray spectroscopy (EDS) is coupled with SEM and was therefore chosen as a time and cost-effective way to analyse the chemistry of the fossil soft tissues. µ-Raman spectroscopy was chosen as a readily available, in-house technique for mineral determinations of potential mineral grains in homogenised sediment samples; the sediment samples visibly lacked mineral grains. Therefore, X-ray diffraction (XRD) was chosen as (a standardised) technique to identify mineral components (> 4%) in homogenised sediment samples. µ- Raman spectroscopy was chosen for the mineral phase determination of two mineralised anuran soft tissues; the analysis was inconclusive for the calcium phosphate phase (Layer 2) due to strong fluorescence. Electron probe microanalysis (EPMA) is not affected by fluorescence and more precise than EDS. EPMA was therefore chosen to investigate the calcium phosphate mineral phase; the analytical results were inconclusive due to a sample preparation issue. In the meantime, an in-house µ-Fourier transform infrared spectrometer was set up and readily available for the acquisition of

spectra, that revealed the calcium phosphate mineral phase of Layer 2 and confirmed a biological origin of the mineral.

The diverse microbeam imaging and chemical analytical analyses of soft tissues from the Geiseltal anurans (see Chapter 4) confirm the preservation of soft tissues in all anuran body regions but fail to yield evidence for silicified soft tissues. Instead, the anuran soft tissues are preserved as two layers that differ in microstructure and composition. Layer 1 comprises sulfur-rich carbonaceous microbodies interpreted as melanosomes. Layer 2 comprises the mid-dermal Eberth-Katschenko (E-K) layer, preserved in calcium phosphate (more specifically a mixture of biological carbonated hydroxyapatite and carbonated fluorapatite, Fig. 4.5). In addition, patches of original aragonite crystals define the former position of the endolymphatic sac. This study found no evidence for additional fossil soft tissues preserved with sub-cellular fidelity, e.g., muscles, veins, pigment cells and additional layers of the anuran integument. The primary modes of soft tissue preservation are therefore sulfurisation of melanosomes and phosphatisation of more labile soft tissues, i.e., skin.

The fossil soft tissues of the Geiseltal anurans contain micron-sized microbodies that were interpreted as melanosomes instead of bacteria (see Section 4.3 for discussion). In short, the distribution of those microbodies and their geometries indicate that they are melanosomes. Further, the layering of microbodies from different populations (defined by geometry) is consistent with decay-induced layering of melanosomes derived from different tissues (Rossi *et al.* 2019).

The melanosomes in the Geiseltal anurans are rich in sulfur; this is consistent with the chemistry of melanosomes from other fossil biotas (Section 1.3.2) including Libros (Miocene, Spain), Bolca (Eocene, Italy) and Messel (Eocene, Germany) and suggests preservation via sulfurization (Section 1.3.1; McNamara *et al.* 2016b). Sulfurised tissues are highly cross-linked and thus resistant to bacterial degradation (Goldstein *et al.* 2004). Sulfurisation is common in dysoxic to euxinic, organic-rich sediments deposited in restricted basins with a stratified water column and abundant bacterial sulfate

reduction in the upper part of the sediment column (McNamara *et al.* 2016b). In such settings, the source of sulfur is considered to be the organic-rich host sediment (McNamara *et al.* 2016b). The Geiseltal environment has been characterised as series of swampy water bodies (mainly ponds and lakes and rarely rivers). The sediments of those lakes and ponds diagenetically turned into lignites (i.e., brown coals, Pickel & Wolf 1989), which host most of the Geiseltal biota. The lignites reveal high organic and only minor inorganic contents (Section 4.10.1). The sediments of the Geiseltal ponds and lakes were therefore organic rich (Fig. 6.2) and an ideal source of sulfur. Preservation of the Geiseltal melanosomes via sulfurisation is also supported by the preservation of fossil latex (monkeyhair laticifers), i.e., sulfurised plant material, in the laminated sediments (Lönartz *et al.* 2023). Sulfurisation as mode of preservation of organic matter has been reported from various marine and non-marine biotas (Sinninghe Damsté *et al.* 1993); examples include the biotas from Holzmaden (Posidonia shale, Jurassic, Germany; Lindgren *et al.* 2018), Bolca (Eocene, Italy; Rossi *et al.* 2022), Messel (Eocene, Germany; Rossi *et al.* 2019), Bechlejovice (Oligocene, Czech Republic; Roček 2003; Rossi *et al.* 2020) and Libros (Miocene, Spain; McNamara *et al.* 2016b).

In extant anurans, the skin comprises several layers including the epidermis, which is the outermost layer, the stratum spongiosum, the mid-dermal Eberth-Katschenko (E-K) layer, the stratum compactum and the hypodermis, which is the bottom layer of the skin (Fig. 4.6). The Geiseltal anurans preserve the E-K layer. In extant anurans, the E-K layer comprises collagen fibres, glycosaminoglycans, proteoglycans and calcium phosphate granules (Elkan 1968; Elkan 1976; Ponssa *et al.* 2017). Centrifugal fibres perforate and traverse the E-K layer vertically, connecting the overlying stratum spongiosum with the underlying stratum compactum and the hypodermis (Elkan 1968; Ponssa *et al.* 2017). The columns form a regular pattern (Zanger *et al.* 1995). As a result, the E-K layer in extant anurans shows a honeycomb pattern in plan view. The E-K layer is rich in calcium phosphate granules *in vivo* (Elkan 1968; Elkan 1976; Ponssa *et al.* 2017). The functions of the E-K layer in extant anurans are not completely resolved; a role in controlling evaporative water loss is assumed (Ponssa *et al.* 2017).



Figure 6.2: A dead Geiseltal frog with disarticulated bones in arms and legs on the bottom of a pond. Most of the skin is still intact. Drawing: A. Pieri.

The preserved E-K layer in the Geiseltal anurans is replicated in calcium phosphate (more specifically a mixture of biological carbonated hydroxyapatite and carbonated fluorapatite, Fig. 4.5) as a result of phosphatisation processes (Section 1.3.1). The main control for the replication of soft tissues in calcium phosphate is the availability of phosphate ions. The Geiseltal sediments likely did not act as phosphate sources as there are no indicators for a sedimentary phosphate content (Sections 4.10.1 and 4.10.3). Further, the fine lamination of the sediment suggests low sedimentation rates and extended exposure

(weeks to months) of the specimens on the lake floor without being completely covered by sediment. If sedimentary organic matter were the primary phosphate source, specimens might therefore be expected to show preferential phosphatisation of skin on only one side of the body (i.e., the surface in contact with the sediment; Wilby *et al.* 1996). The lack of preservation of the epidermis and the preservation of both dorsal and ventral E-K layer suggest, that the phosphate source was inside the decaying carcass. Bones can be omitted as phosphate source as they do not show evidence for dissolution. The phosphate therefore derived from the soft tissues – most likely the collagen from the skin. Collagen is decay-resistant and readily promotes nucleation of calcium phosphate (Briggs *et al.* 1993; McNamara *et al.* 2009; Nudelman *et al.* 2013). Dissolved calcium phosphate granules in the E-K layer acted as local phosphate source for the replication of the collagen fibres of the E-K layer (Fig. 4.6). Calcium phosphate dissolution requires a microenvironment of pH <4 (Smith *et al.* 1977; Kootstra *et al.* 2019), which was facilitated following the liberation of acidic byproducts of decay (Briggs & Wilby 1996). The generation of local high concentrations of phosphate inhibited calcium carbonate precipitation (Briggs 2003). In those local microenvironments the phosphate reprecipitated as calcium phosphate (i.e., apatite) on collagen fibres of the E-K layer when pH values < 6.38 (i.e., below the carbonic acid dissociation constant). The phosphate availability decreases towards the internal layers of the skin, which results in a decreasing fidelity of fibre preservation. The absence of other preserved soft tissues may reflect a lack of internal phosphate sources. Alternatively (or in addition), it reflects the complete degradation of other tissues prior to phosphatisation, e.g. due to proximity to the source of decay bacteria, prolonged transport of the carcass in warm surface waters and/or prolonged exposure of the carcass on the lake floor (Section 6.1). The epidermis, the upper dermis and the centrifugal fibres of the skin are not preserved. This suggests that the various cellular and non-cellular components of those soft tissues have a lower capacity to bind calcium than the E-K layer fibres and/or decayed completely before the tissue entered the phosphatisation window.

The phosphatisation window likely opened soon after death, when the calcium phosphate granules in the E-K layer started to dissolve and significant quantities of phosphate became mobile. The decay of

internal tissues started directly with the anuran death. Coherent patches of the mineralised E-K layer in the torso in several specimens suggest a collapse of the body cavity while the E-K layer was not completely mineralised and to some extent flexible.

Mineralisation of vertebrate soft tissues is known from numerous marine and non-marine biotas through time and space (Dornbos 2011; Muscente *et al.* 2017) including biotas from the Gogo Formation (Devonian, Australia; Trinajstic *et al.* 2007), Solnhofen (Jurassic, Germany; Delsett *et al.* 2022, the Santana Formation (Cretaceous, Brazil; Martill 1988) and Libros (Miocene, Spain; McNamara *et al.* 2009).

In extant anurans, aragonite crystals are stored in the endolymphatic sac (i.e., the endolymphatic organ) to mobilise calcium for the skeletal development (Pilkington & Simkiss 1966; Pich & Sanchez 2017). The endolymphatic organ encircles the hindbrain and form cysts between each pair of successive vertebrae (Pilkington & Simkiss 1966; Pich & Sanchez 2017). The location, size and crystal habit of the aragonite crystals in the cranium and along the vertebral column of the Geiseltal anurans are consistent with those of crystals of the endolymphatic sac. The preservation of those aragonite crystals suggests the creation of a local microenvironment during early stages of decay (e.g., enclosed by bounding membranes) with pH values > 6.38 for the duration of decay. Larger endolymphatic aragonite reserves are associated with high environmental calcium concentrations (Pilkington & Simkiss 1966). This suggests that Geiseltal anurans with particularly large volumes of aragonite crystals lived during periods where the lake waters were relatively rich in calcium. Indeed, the Geiseltal environment may have been under influx of calcium- and carbonate-rich waters (Section 4.10.2) derived from Triassic sediments at the southern border of the Geiseltal basin (Krumbiegel *et al.* 1983). These waters, however, did not influence the modes of preservation (i.e., phosphatisation and sulfurisation) of the anuran fossil soft tissues.

The investigated anuran host-sediments and mineralised soft tissues don't show considerable amounts of silica. There is no evidence for silicified soft tissues in the Geiseltal anurans as proposed by Voigt

(1937) and Voigt (1988). Further, there is no evidence for a source of silica in the sediments associated with the fossil anurans.

The preservation of the Geiseltal anurans follow a taphonomic pattern for fossil vertebrates in lacustrine ecosystems, i.e., body outlines defined (in whole or part) as melanosome films and the localised phosphatisation of tissues. This taphonomic pattern applies to various lacustrine-hosted biotas including Las Hoyas (Cretaceous, Spain; Gupta *et al.* 2008a), Bechlejovice (Oligocene, Czech Republic; McNamara 2007), Ribesalbes (Miocene, Spain; McNamara *et al.* 2010a) and Libros (Miocene, Spain; McNamara *et al.* 2009; McNamara *et al.* 2016b). It is notable, that the replication of tissues in authigenic calcium phosphate is bound to the development of phosphate-rich microenvironments during decay and also to tissues that have a high potential for phosphatisation (e.g., collagen).

6.4 Melanosomes from the Geiseltal anurans show tissue-specific geometries

Melanosomes were discovered in the fossil anuran soft tissues from Geiseltal (Fig. 6.3). The melanosomes from several body regions (i.e., eyespot, torso, abdomen and skin) differ in their geometry. The combination and analysis of the melanosome geometry data from Geiseltal and geometry data from extant anurans reveal potential tissues of origin for the fossil melanosomes of different body regions. The anatomical location of the samples for fossil eyespot melanosomes and the position of analysed skin melanosomes external to the mineralised E-K layer constrain the tissue of origin of those fossil melanosomes. Preserved melanosomes from the torso and abdomen of the fossil specimens cannot be confidently attributed to specific internal tissues using anatomical location alone. The combination of melanosome morphospace, the relative size of tissues *in vivo*, the relative abundance of melanosomes in certain tissues *in vivo*, multivariate analysis of a broad suite of melanosome geometric parameters and data on the metal chemistry of the fossil melanosomes can constrain the tissue of origin of fossil melanosomes from the torso and abdomen.

The morphospace for melanosomes from extant anurans and for anurans from Geiseltal is broadly similar (Fig. 5.3A). Melanosomes from the eyes of extant anurans and from the eyespots of Geiseltal specimens show populations of spheroids, ovoids and rods. Populations of rods are usually mixed with ovoids and spheroids, but rods can also form spatially separated clusters and layers. Fossil skin melanosomes were sampled from the surface of the preserved E-K layer. Melanosomes from the skin of extant and fossil anurans show intermingled spheroids and ovoids; aspect ratios from fossil skin samples are higher than in extant anurans. Skin melanosomes from the Geiseltal specimens are the smallest melanosomes among all body regions in fossil specimens and all tissues in extant specimens. Melanosomes from the abdomen of Geiseltal specimens are predominantly spheroids. The morphospace of the Geiseltal abdominal melanosomes most closely resembles that of the gonads of extant anurans (Fig. 5.3F). Melanosomes from the torso of Geiseltal specimens are spheroids and ovoids. The Geiseltal torso melanosomes are difficult to assign confidently to a particular tissue based on these basic geometry data. The morphospace of the Geiseltal torso melanosomes closely resembles that of melanosomes from the lungs of extant anurans (Fig. 5.3D); melanosome length and aspect ratio, however, differ significantly between these two datasets. The morphospace for the Geiseltal torso melanosomes is smaller than that for the heart and liver and could potentially represent a subset of heart and liver. The heart is, however, an unlikely source because it contains few melanosomes in extant anurans (Rossi et al. 2019), but the liver is a plausible source as melanosomes are much more abundant in the liver of anurans relative to other internal tissues (McNamara *et al.* 2018; Rossi *et al.* 2019).

Principal component analysis (PCA) of the geometry data for the melanosome data from Geiseltal anurans, Bechlejovice anurans (Oligocene, Czech Republic), Libros anurans (Miocene, Spain) and extant anurans resolves major patterns in melanosome geometry. The PCA plot reveals a strong signal for different tissues and body regions. Data for all fossil eyespots and eyes of extant specimens form a distinct group (Figs. 5.4 and S5.17). Similarly, the data for skin melanosomes from all fossil and extant specimens form a tight cluster. Data for the lungs, liver and gonads of extant specimens and for the

torso and abdomen of Geiseltal specimens lie between the eyespot group and the skin cluster. Geiseltal abdominal melanosomes plot close to the skin cluster and gonads. The abdominal melanosomes were analysed from underneath the E-K layer and thus, cannot represent skin melanosomes. According to the data, the gonads are the most plausible source of melanosomes in the abdomen of the Geiseltal specimens. Geiseltal torso melanosomes plot close to the gonads, but also the liver. The data from two melanosome samples from the torso of GMH CeIII 4967-1932 plot close to the abdomen of the same specimen and between the lungs and the liver of extant specimens, respectively. This suggests that this specimen has two sources of melanosomes in the torso (i.e., gonads and/or lungs or liver); one of the two samples shows a similar geometry to the abdominal melanosomes in specimen GMH CeIII 4967- 1932 and originate likely from the same tissue.

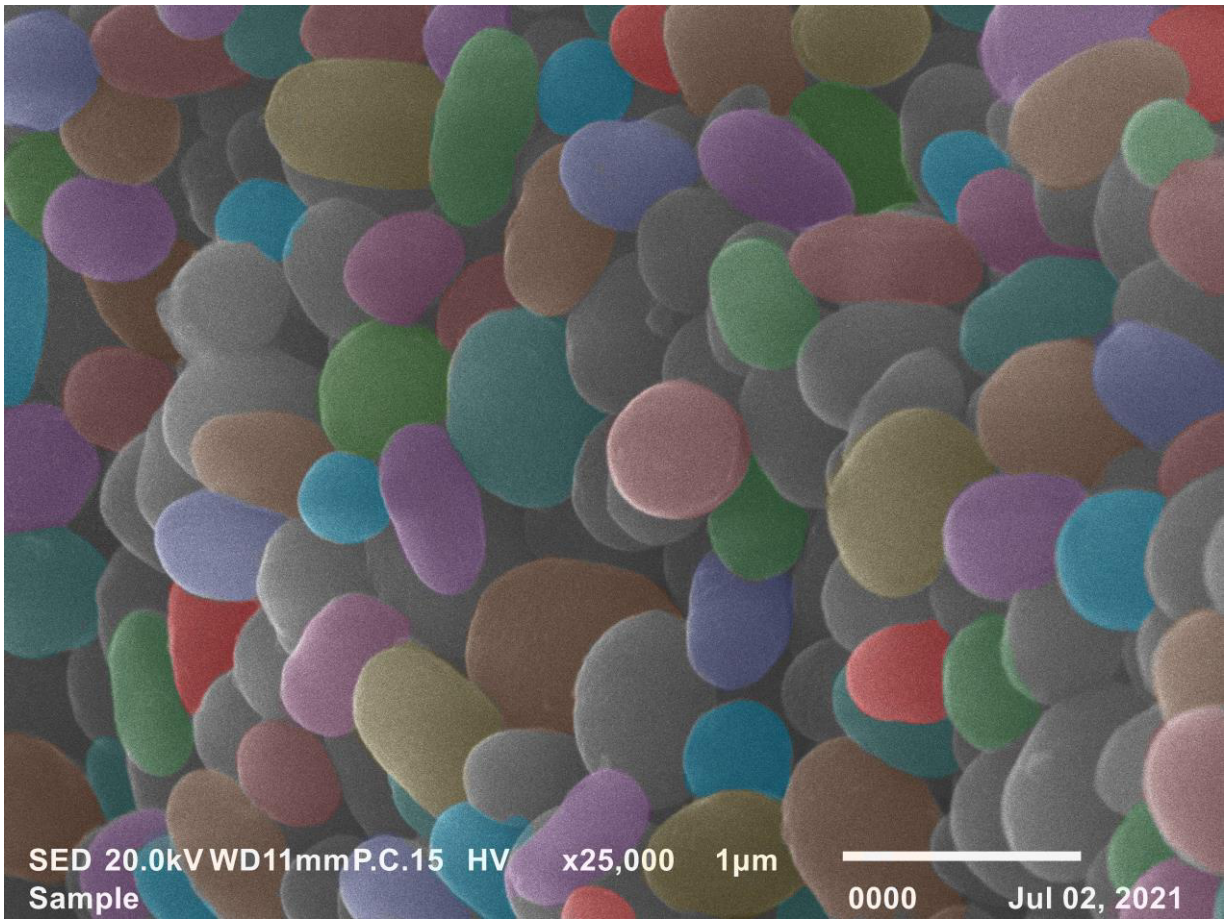


Figure 6.3: SEM image of fossil melanosomes (coloured) from an anuran eyespot. Image: D. Falk

Synchrotron rapid scanning-X-ray fluorescence (SRS-XRF) was chosen as technique to investigate the melanosome chemistry, as it is a cutting-edge technology that allows the detection of X-rays emitted by elements present even in trace amounts. Chemical mapping using SRS-XRF analysis indicate that the preserved melanosome films from the torso and abdomen of GMH CeIII 4967-1932 likely represent melanosomes from a common source. There is no evidence from the SRS-XRF data for additional melanosome sources in the torso (i.e., liver and/or lungs); this is not fully consistent with the PCA plot, which shows that the melanosome geometry data from one sample of GMH CeIII 4967-1932 plot closest to, and between, the liver and lungs (Fig. 5.4B). This sample may therefore represent a very localised region of melanosomes from the liver/lungs that is too small to be identified in the XRF maps. Alternatively, the melanosomes from the gonads, liver and/or lungs and gonads do not differ in chemistry; as with the Libros anuran (Rossi *et al.* 2019; Rossi *et al.* 2020), this could be explained as a real biological feature or as a diagenetic artefact. The PCA of the melanosome geometry parameters indicates that melanosomes from both the torso and abdomen derive primarily from the gonads, which in extant anurans are small organs, with relatively little melanin (compared to e.g., the liver; McNamara *et al.* 2013). The extent of these melanosomes in the torso could be explained by mobilisation of melanosomes following liquefaction of those tissues during decay. Non-integumentary melanosomes can redistribute through parts of the body if carcasses are disturbed by e.g., currents (McNamara *et al.* 2018). Alternatively, the fossil melanosomes may derive from oocytes inside the gonads (Wake & Dickie 1998; Méndez-Tepepa *et al.* 2023), which in gravid female anurans can occupy a large proportion of the volume of the torso. The geometry of melanosomes from oocytes has not been investigated and it is therefore at what stage during oocyte and/or tadpole development the melanosomes from the gonads and oocytes can be discriminated. Melanosome films in the limbs likely represent melanosomes from a different source. The location of these samples and the lack of evidence for redistribution of internal melanosomes into the limbs, as it would be evidenced by e.g., elevated Zn concentrations, suggests that melanosomes in the limbs represent skin melanosomes. Chemical variations between

regions of interest of the same body region (e.g., torso, abdomen and limbs) can also reflect a chemical contribution of preserved E-K layer and host matrix.

In summary, the melanosomes from Geiseltal specimens likely derive from the eyes, the skin, the gonads and the liver or lungs. According to the melanosome data, the specimen GMH CeIII 4967-1932 may represent a gravid female.

6.5 Melanosomes show evolutionarily conserved geometries

Melanosomes from various body regions of fossil anurans from the Eocene, Oligocene and Miocene are similar in geometry to melanosomes from corresponding body regions in extant anurans. This is not surprising, as the Bauplan has been conserved since the Late Triassic (Feng *et al.* 2017; Stocker *et al.* 2019). The fossil anurans from Geiseltal and Bechlejovice (Pelobatidae and Palaeobatrachidae) and Libros (Ranidae) closely resemble extant anurans in skeletal anatomy and skin structure. Further, the habitats and lifestyles of the fossil anurans from each locality and the extant specimens are broadly comparable. Conservation of anatomy implies conservation of function. It is reasonable to assume that organ functions among the anuran taxa that were used for the study in Chapter 5 are overall similar. It is unlikely that minor differences in habitat (e.g., lake physiography/water depth/water chemistry) and anuran lifestyle (e.g., predominantly aquatic or terrestrial) would impact organ function. The functional roles of melanin in the anuran eye, skin and internal organs (e.g., lungs, liver and gonads) were therefore probably established by at least the Eocene. Furthermore, the widely unchanged anuran Bauplan and amphibious lifestyle since the Mesozoic suggest similar functional roles of melanin in up to Late Triassic anurans (although this is up to now not scientifically verified).

The geometry of melanosomes in the eyespots of fossil anurans from the Miocene and Eocene is similar to that of ocular melanosomes in extant anurans, which indicates that eye melanosome geometry has been conserved in anurans since the Middle Eocene. This suggests that the function of ocular melanin in anurans has been conserved over ca. 45 million years. In the vertebrate eye, melanosomes play a

role in photoprotection and in regulation of oxidative tissue damage (Hu *et al.* 2008; Rogers *et al.* 2019; Sitiwin *et al.* 2019). The visual system in anurans is highly conserved. Anurans typically see in colour (Yovanovich *et al.* 2017), with high spatial resolution and broad spectral sensitivity, including low ambient illumination (Buchanan 1993; Anderson & Wiens 2017; Yovanovich *et al.* 2019). Like most anurans (Duellman & Trueb 1994; Anderson & Wiens 2017; Mohun & Davies 2019), all of the extant anurans studied are adapted to nocturnal vision. The strong conservatism in the anuran visual system is likely to be reflected in conserved melanosome geometries.

Further, the internal melanosomes of the studied fossil anurans can be assigned to tissues of extant specimens; the preserved attributes of melanosomes from internal tissues are also consistent with evolutionary conservatism since the Middle Eocene. Functional roles of melanosomes in internal organs of extant anurans include metal homeostasis and antioxidant functions (Rossi *et al.* 2019; McNamara *et al.* 2021) and likely did not change since the Middle Eocene, probably earlier.

Differences in the geometry of the skin melanosomes between fossil and extant anurans indicate the functional constraints of skin melanosomes differ from those of melanosomes from other tissues. Functions of melanosomes geometry cannot be confidently linked with skin colour (Li *et al.* 2014). Shared skin melanosome features among fossil and extant anurans occur: skin melanosomes are smaller than most or all non-integumentary melanosomes in a given taxon and skin melanosomes show similar geometries in different body regions (i.e., dorsal/ventral). The large-scale functional controls for the geometry of skin melanosomes are unknown. The liberation of skin melanosomes from functional constraints as in the eyespots and internal organs may reflect evolutionary tradeoffs linked to diversification of integumentary coloration, activity period, the presence/absence of a lateral line system and/or habitat. It is unlikely that differences in the melanosome geometries among soft tissues are related to tissue-specific taphonomic pathways. The geometry of melanosomes has been reported to be altered by the effects of pressure and temperature (McNamara *et al.* 2018) but not by tissue chemistry. Diagenetic alteration of melanosomes in Geiseltal is unlikely as the preservation of Geiseltal fossil latex (monkeyhair laticifers) indicates diagenetic temperatures of max. 100 °C (Lönartz *et al.*

2023), which are much lower than the reported experimental temperatures (>200 °C) to induce diagenetic melanosome shrinkage (McNamara *et al.* 2013; Slater *et al.* 2020; Slater *et al.* 2023b). It is notable, that the fossil latex were excavated from slightly older stratigraphic levels than the anurans.

6.6 Comparative taphonomy of anurans from Geiseltal and Libros

The ultimate taphonomic controls on preservation (Section 6.1) are likely to apply to diverse vertebrates decaying in lacustrine settings. Here they are used in the context of anuran preservation in other biotas, in particular the Libros biota (Miocene, Spain)

Anurans are more complete and articulated in Lagerstätten from cooler climatic phases where decay, floating, scavenging and post-depositional disturbance of carcasses were inhibited by deposition in relatively cool and/or deep lakes. The completeness values of the Libros anurans are higher for most skeletal elements (McNamara *et al.* 2012a, Table 3.1). For the Middle Eocene, the mean annual temperatures for the Geiseltal are calculated with >20°C (Mosbrugger *et al.* 2005), which can be associated with lake surface temperatures of >16°C (Elder & Smith 1988). In the Miocene the mean annual temperatures were considerably cooler (Mosbrugger *et al.* 2005); mean annual temperatures of 16–17°C (Bruch *et al.* 2004) are reported for the Vallesian sites Abezames (NW Spain) and Burgos (Central Spain; Table 3.2). Further, the Libros lake was considerably deeper than the Geiseltal ponds and lakes (Table 3.2), thus preventing refloating of carcasses. Fossil fish are reported from Geiseltal (Voigt 1934, 1937; Jerzmanska 1977), suggesting that scavengers were present and likely fed on anuran carcasses. In contrast, in the Libro lake, fish and other scavengers were absent (McNamara *et al.* 2012a). Finally, the anurans from the Libros Lagerstätte derive from the central zones of the Libros lake, where bottom currents would be rare and weak. The area of the Libros lake was much larger than the individual Geiseltal ponds and lakes. Although, bottom currents in the small Geiseltal water bodies were also generally weak, the frequent absence of small skeletal elements in the Geiseltal anurans

(Fig. 6.2) and reports of preferred orientations of skeletons (Weigelt 1933) suggest more frequent or stronger bottom currents than in the Libros lake.

The anuran taxa from the Libros biota (Ranidae) followed a primarily aquatic lifestyle, whereas the pelobatids from the Geiseltal biota followed a primarily terrestrial lifestyle and the palaeobatrachids a primarily aquatic lifestyle. All anurans retained a similar overall Bauplan since the Late Triassic (Feng *et al.* 2017; Stocker *et al.* 2019), which is overall independent of the living habitat (Reilly & Jorgensen 2011; Vitt & Caldwell 2014). Indeed, the skeletons of the fossil anurans from Libros (McNamara *et al.* 2012a) and Geiseltal (Sections 3.3.2, 3.4.3 and 3.5) are very similar in their elements. Further, anurans from both biotas preserve similar soft tissues, including the mid-dermal E-K layer, replicated in calcium phosphate, that envelops melanosome-rich carbonaceous layers preserved via sulfurisation (McNamara *et al.* 2009; McNamara *et al.* 2012a; McNamara *et al.* 2016b; Sections 4.2 and 4.3). Although the modes of soft tissue preservation in both biotas are the same, the fidelity of preservation of the E-K layer collagen fibres is higher for Libros specimens.

The higher fidelity of the Libros E-K layer collagen fibres relative to the Geiseltal specimens may reflect less decay prior to mineralisation as (1) more intact collagen fibres would have more nucleation sites, thus limiting crystal growth and (2) lower concentrations of decay acids. For the Libros anurans, both elements would have constrained the growth of calcium phosphate crystals, facilitating finer replication of fibres than at Geiseltal. By the time the skin of the Geiseltal anurans entered the phosphatisation window, it may not have been sufficiently intact to allow high fidelity replication. Higher ambient temperatures for the Geiseltal water bodies (resulting in promoted decay of tissues) compared to the Libros lake and prolonged transport of Geiseltal specimens (Section 6.1) support the hypothesis from above (i.e., decay of skin prevented high fidelity preservation). Taphonomic variation between biotas is also controlled by the amount of phosphate ions present in the E-K layer *in vivo*. In extant anurans, the E-K layer varies in thickness and lateral extent among extant anurans (Mangione *et al.* 2011; Ponssa *et al.* 2017). The phosphate supply for the replication of collagen fibres may have differed between specimens from both biotas. Collectively, the phosphate availability was higher for Libros specimens,

as the high fidelity preservation of collagen fibres is accompanied with certain melanosomes that are also phosphatised (McNamara *et al.* 2009). It is notable, that here is no evidence for a major phosphate supply from the embedding sediments in any of the two biotas.

Anurans from Libros and Geiseltal show sulfurised melanosomes from the eyespots, skin and internal tissues (i.e., from the liver and/or gonads in Geiseltal specimens and from lungs, liver and/or gonads in Libros specimens). The geometries of melanosome from the eyespot are similar for both biotas. This is probably linked to retained functional roles in metal homeostasis and antioxidant functions (Rossi *et al.* 2019; McNamara *et al.* 2021; Section 5.1).

Skin melanosomes from both biotas show the same shapes (i.e., intermingled spheroids and ovoids; Section 5.2.1); skin melanosomes from the Geiseltal specimen are, however, significantly smaller compared to those from the Libros specimen. The size difference may be related to diagenetic shrinkage, linked to integumentary coloration, the presence/absence of a lateral line system and/or the habitat. Diagenetic alteration of melanosomes in Geiseltal is unlikely as the preservation of Geiseltal fossil latex (monkeyhair laticifers) indicates diagenetic temperatures of max. 100 °C (Lönartz *et al.* 2023), which are much lower than the reported experimental temperatures (>200 °C) to induce diagenetic melanosome shrinkage (McNamara *et al.* 2013; Slater *et al.* 2020; Slater *et al.* 2023b). It is notable, that is the fossil latex were excavated from slightly older stratigraphic levels than the anurans. Potential links between melanosome geometry and skin colour have not been investigated for extant anurans, but previous work on reptiles has shown that melanosome geometry is independent of skin colour in the group (Li *et al.* 2014), which may also apply to amphibians. Limited geometry data from the extant anuran taxa *Bombina* (yellow bellied toad; Figs. S5.11, S5.12), however, imply a link between melanosome geometry and skin colour. More data is needed to confirm this link. Lateral line systems in the skin of certain anurans (e.g., the aquatic *Xenopus*) have been reported to contain melanosomes for non-visual light detection. There is no data on the geometries of melanosome from lateral line systems in anurans; most of the Geiseltal anurans were mainly terrestrial and likely did not have a lateral line system that could have been the source for the sampled skin melanosomes. The small skin

melanosomes from the Geiseltal specimen may be related to unknown functional constraints related to slight differences in the habitat (e.g., lake physiography, climate and lifestyle). It is notable, that similar to extant specimens, the skin melanosomes from Libros and Geiseltal specimens are smaller than most or all non-integumentary melanosomes in a given taxon (Section 5.2.1).

The soft tissues from Geiseltal and Libros specimens are comparable in their overall chemical composition. Ca, Cu and Zn are of particular relevance as Ca is a major component of the mineralised skin (i.e., the E-K layer) in the Geiseltal (Section 4.2) and Libros anurans (Rossi *et al.* 2019; Rossi *et al.* 2020). Ca and is thus probably associated primarily with the mineralised E-K layer. Cu and Zn are often associated with melanosome films in fossil vertebrates (Wogelius *et al.* 2011; Manning *et al.* 2019; Rossi *et al.* 2020). Variation in Cu and Zn primarily reflect variation in the composition of the melanosome films which may be related to tissue chemistry (Rossi *et al.* 2019) and/or diagenetic alteration (in particular Cu; Rossi *et al.* 2021).

In summary, the preservation of the Geiseltal and Libros anurans is generally similar. Libros and Geiseltal anurans show mineralised skin layers and carbonaceous melanosome-rich films (originating from eyes, skin and internal organs). The higher skeletal element completeness and higher fidelity of preservation of soft tissues in Libros specimens compared to Geiseltal specimens is related to inhibited decay due to a cooler climate and a deep lake with no bottom currents and the absence of predators and scavengers. In result, the Libros specimens reached the taphonomic window for soft tissue preservation in a state, where tissues were still intact enough, so that phosphates could replicate those tissues. In contrast, Geiseltal specimens experienced warmer climate, prolonged transport and potential scavenging; this all decreased the possibilities to preserve complete specimens and the same fidelity of preservation of soft tissues as in Libros.

6.7 Limitations and biases

Although the study aims of this thesis (Section1.6) were achieved, this study has limitations that are mainly related to the historical background of the Geiseltal Collection, anuran taxonomy and the analytical approaches.

6.7.1 Historical background

Fossil collections may be subject to biases that cannot easily be identified from historical reports (e.g., field documentations, inventory registers, loan agreements and newspapers) and other forms of documentation (e.g., personal communications and the objects themselves). For the Geiseltal site, Krumbiegel 1962a and Krumbiegel *et al.* 1983 reported the loss of hundreds of anuran specimens during the excavation process. Damage on fossils and loss of fossils during fossil recovery are primarily related to weather (e.g., rain, storm, coal fires and landslides) and lithology (e.g., fossils and host material were fragile once the host material dried out). Further, during the excavations some fossils were used in trials of different embedding materials, which, in some cases, resulted in unidentifiable damage or loss of fossils (Voigt 1933, 1988). The collection may be therefore biased towards specimens that were considered better preserved (i.e., specimens that show more complete and more articulated skeletal elements) and/or were not damaged during excavation. Specimens that were not considered valuable for research, preparation, exhibition or storage may have not been collected (collector bias). Only a few anuran specimens in the Geiseltal Collection represent disarticulated or single skeletal element specimens; data on skeletal completeness for additional vertebrate groups do not exist, but a recent viewing of fish and mammalian specimens suggest a similar pattern for those groups (i.e., lack of widely disarticulated specimens). The collection may also be biased towards specimens that are not complete due to post-collection events (although those specimens were complete following the excavation), such as specimen preparation and specimen storage. The specimens are stored in historical drawers and were exposed to uncontrolled climate conditions for decades, which may have caused degradation of fossil soft and hard tissues. The impact of damage during preparation and of the

storage conditions on the fossils is, compared to the biases introduced by excavation processes, considered to be minor. Collectively, these issues indicate, that the Geiseltal Collection may be biased towards more complete and/or more articulated specimens. Without biases, the fossil anurans from the Geiseltal site are likely to include more specimens that are less complete and/or less articulated (i.e., specimens of taphonomic states 4–6, Section 3.5).

The Geiseltal fossil vertebrates were excavated from 35 discrete sites within the Geiseltal basin (Haubold & Hellmund 1998). The dataset in Chapter 3 (i.e., the 168 assessed anuran specimens), however, comprises fossils from a potential maximum of 15 sites only. Twelve out of 15 sites are supported by records in the Geiseltal Collection inventory register and three additional sites relate to three specimens of unknown provenance. Further, most specimens (n = 102) in this study are from a single site; certain other sites are represented by only a single specimen. Most specimens were excavated between 1930 and 1933 and only some specimens were excavated between 1934 and the 1970s. The low number of excavated anuran specimens after 1934 may relate to excavation leaders prioritising the excavation of larger vertebrates (personal communication Michael Stache, preparator Natural Sciences Collections) and/or a considerable time pressure due to ongoing lignite mining, flooding, rockfalls and landslides and/or coal seam fires (Krumbiegel 1962b; Haubold & Krumbiegel 1984). The number of anuran specimens in the Geiseltal Collection does not represent the real number of findings per excavation site, but rather is biased towards excavation sites exploited earlier in the history of the mines (e.g., Cecilie I–III, which are exploited from 1930–1933). Excavation sites in younger strata (the upper coal), which include the sites Cecilie I-III, are reported to preserve more abundant fossil vertebrates and a greater vertebrate diversity than stratigraphically older deposits (Hastings & Hellmund 2015a, b). This may reflect a real, biological variation in the absolute abundance (i.e., population size) and/or variation in taphonomy of anurans through time. Further, note that stratigraphic data for at least some specimens and/or sites may be inaccurate (Krutzsch 2011; Ring *et al.* 2020).

Fossil specimens are not evenly distributed through depositional settings whereby most are excavated from dying field sediments, that have originated in shallow swampy troughs that formed during wet periods (121 specimens from two sites). Relatively few specimens (43 specimens from seven sites) are from sinkhole sediments. Those sediments originated in small and deep lakes with saline waters. Only one specimen is from fluvial channel deposits (one site). This may reflect, at least in part, a biological signal linked to ecology (e.g., shallow ponds and lakes are preferred anuran habitats; Krumbiegel 1962a) and/or a taphonomic signal (e.g., prolonged transport of carcasses). The biological signal is also supported by the relative abundance of depositional settings of the fossil sites. Most fossil sites in the Geiseltal basin represent sinkhole deposits, that are spread in the centre and west of the basin (Krumbiegel *et al.* 1983). In contrast, only few fossil sites are dying field deposits; these are clustered in the northern centre of the Geiseltal basin. Fossil sites in fluvial deposits are rarer than in the other two depositional settings and without a preferential location in the basin. There is no statistical difference in the skeletal taphonomy data between specimens from dying field deposits and the sinkhole deposits (Section 3.4.5). This is additional support that the abundance of specimens represents a biological signal.

There are uncertainties in the data available for certain fossil anuran specimens. It is unclear which specimens derive from mass mortality events as historical records usually do not include data on the number and distribution of anurans on single bedding planes (but see Weigelt 1933 and Weigelt 1934 for sketches, that reveal the distribution of certain specimens). Further, excavation lists of fossil specimens (Kuhn 1941) indicate that many specimens are missing and are not included in the current collections. A collection material request for Geiseltal specimens to 64 international institutions (Appendix I) revealed the location of several specimens; the majority of specimens are not anurans.

Voigt (1935), Voigt (1937) and Voigt (1988) reported and photographed numerous subcellular soft tissue features for the Geiseltal anurans that he based on his taphonomic model (i.e., silicification). He

sampled several specimens destructively (patches of ca. 10 cm^2; Figs. 4.1A–B), embedded the samples in resin and investigated the samples using a Pan-Phot microscope from Leitz-Wetzlar (Voigt 1935). The samples (“micro samples” [Mikropräparate/Lackpräparate]) are stored with the Geiseltal Collection, but many of the sampled specimens are lost. It was impossible to match the existing specimens, that show obvious sampling regions, with the existing “micro samples”. Certain “micro samples” are lost. Sampling from the “micro samples” was not permitted. This study found no evidence for the proposed mode of preservation and for most of the subcellular details that Voigt reported in the available microsamples and sampled specimens (e.g., Figs. 4.1A–B). It is therefore unlikely, that the lost anuran specimens reveal soft tissues that are not analysed in this thesis.

It is unlikely, that other vertebrates from Geiseltal are silicified for the following reasons: (1) none of the sediment samples from anuran slabs from four stratigraphic levels and nine sites indicated a considerable silica content; there is no evidence that the sediment acted as silica source; (2) none of the additionally examined amphibians (newts), mammals (bats and artiodactyls) and fish from the Geiseltal Collection showed indicators for a preservation different to that of the anurans; (3) fish contain melanosome layers, that are sulfurised, and mineralised soft tissues that contain large quantities of calcium and phosphorus (Falk *et al.* in prep), suggesting similar taphonomic conditions as for the anurans; (4) the dissolution of large amounts of silica requires highly alkaline conditions (ca. pH > 8); these conditions would likely prevent the phosphatisation process, which requires acidic conditions for the dissolution (pH < 4) and mineralisation (pH < 6.38) of calcium phosphate in anuran soft tissues.

Other Geiseltal fossils may also preserve ultrastructural details replicated in calcium phosphate, if a phosphate source was available and the tissue had a high potential for phosphatisation (e.g., collagen).

6.7.2 Anuran taxonomy

Aquatic palaeobatrachids are rare in the dataset, whereas terrestrial pelobatids are abundant. Due to the national heritage status of the Geiseltal Collection, sampling permission was granted for six specimens only. These specimens were chosen primarily by their soft tissue features. Soft tissues were sampled from pelobatid and specimens of undetermined affinity. Sampled specimens revealed soft tissue features in high fidelity preservation in sufficient quantity for destructive sampling; there were no palaeobatrachids that fulfilled these criteria. The fossil soft tissues in palaeobatrachids have been assessed quantitatively. The lack of palaeobatrachids in the sample set, however, reveals a taxonomic bias that indirectly creates biases related to e.g., ecology, skeletal structure and/or tissue composition. Indeed, skeletal anatomy (Fabrezi *et al.* 2017) and skin composition (Elkan 1968; Ponssa *et al.* 2017) differ between extant aquatic and terrestrial anurans, but also among extant taxa from the same group. Anuran anatomy and skin composition are known to impact preservation patterns in fossil anurans (McNamara *et al.* 2009; McNamara *et al.* 2012a; Wuttke & Reisdorf 2012). This thesis reveals, however, that the pelobatids and palaeobatrachids from Geiseltal show similar completeness and articulation values (see Chapter 3) and similar soft tissue features (see Chapter 4). Both similarities suggest that taxonomy of the Geiseltal anurans does not impact anuran preservation. The relative paucity of palaeobatrachids therefore probably reflects a real biological signal, whereby they were simply less abundant members of the lake fauna. Alternatively, the number of palaeobatrachid specimens in the collection reflect a sampling bias (see Section 6.7.1), e.g., if palaeobatrachids were discarded due to failed wax- or resin-transfers or if they were most abundant in the sites excavated later than the 1940s when excavators prioritised the excavation of larger-sized vertebrates to the “small” palaeobatrachids. These hypotheses are challenging to test on a family-level and with the historical documentation available.

6.7.3 Analytical approaches

It is possible that certain aspects of the analytical approaches in this study have introduced biases to the data. Twenty-eight specimens were omitted from the study in Chapter 3 (assessment of the skeletal element completeness and articulation) as poor preservation precluded confident identification of individual skeletal elements. These specimens are single bone fragments and clusters of bone fragments. The omission of these specimens may have resulted in the underrepresentation of taphonomic state 5 (disarticulated and reorientated skeletal elements) in the dataset.

In the taphonomic metric approach (see Chapter 3), skeletal elements that are distal to truncated bones were omitted as it was not possible to determine whether these (more distal) bones were truly absent (i.e., disarticulated and lost prior to burial) or were indeed preserved as part of the fossil, but subsequently lost during the transfer process (i.e., the excavation method, see Fig. S3.1). Given that truncation (i.e., when the edge of the slab passes through a bone) usually affects distal bones and that distal bones have lower completeness values than proximal bones, the used method here of scoring completeness for truncated specimens (using only those bones that are present on the fossil slab, Section 3.3.6) may therefore have artificially inflated completeness values. The alternatives, however, are to score all bones distal of truncated bones as either present or absent; neither approach is satisfactory as both options incorporate assumptions regarding the presence/absence of bones distal of truncated elements. The applied approach herein is, although imperfect, considered to be the most appropriate solution to this problem.

Completeness and articulation were not assessed for individual elements of the cranium, the pectoral girdle and the carpals and tarsals. The individual elements of those skeletal units are usually superimposed, obscured by other skeletal elements and/or too small to be confidently identified. The relevant skeletal unit is coded as present if at least one of the constituent bones is evident. This approach does not provide taphonomic information on the individual elements of the cranium,

pectoral girdle and carpals/tarsals. Our approach here may thus have the potential to bias values for specimen completeness and articulation. The same approach is applied to all specimens; any impact will be consistent across the dataset.

Anuran specimens that were omitted from the skeletal taphonomy analysis (n = 28) comprise unidentifiable skeletal remains. Those specimens should be considered to represent a 10^{th} taphonomic state. If those specimens are in fact anuran skeletal remains (and not e.g., reptile remains) and do not represent artefacts of historical biases (see 6.7.1), then the taphonomic pathways of the omitted specimens were probably very versatile resulting in skeletal disarticulation and loss of characteristic skeletal element features. Taphonomic state 10 can be seen as a cryptic taphonomic state.

The limitations of the studies in Chapters 4 and 5 relate primarily to sample size, i.e. the number of fossil and extant taxa and the number of fossil samples used. Six Geiseltal anurans were sampled destructively for fossil soft tissues; for each specimen, a maximum of five areas were sampled. Only one specimen was available for SRS-XRF analysis. Such limitations on sampling of fossils from Konservat-Lagerstätten are typical for this fossil type; in the case of the Geiseltal anurans, the collection has National Heritage status, which places additional constraints on sampling and international loans of specimens. To ensure that the six selected specimens represent the entire dataset the following hierarchical criteria were applied to each specimens (starting with the most important criteria): (1) the specimen shows among the best preservational states of fossil soft tissues apparent in the entire dataset; (2) the specimen shows as many preservational states of soft tissues that are reported in the dataset as possible; (3) the specimen shows as many soft tissues as possible, regardless of their preservational states; (4) the specimen is complete and articulated to determine the spatial distribution of the fossil soft tissues in the skeleton; (5) the specimen shows fossil soft tissues and is embedded in host sediment. All selected specimens showed fossilised skin and melanosome films in different areas of the body; one specimen is hosted in sediment (i.e., the only

anuran specimen in the collection). It is likely that specimens that were not sampled preserve melanosome films in other body areas. Many melanosome films may also be covered by the fossilised skin and are not visible without analytical techniques (e.g., XRF-SRS).

For the combination of melanosome geometry and chemistry data from fossil and extant specimens in the study in Chapter 5, data from only four extant anuran taxa were provided. The study depended on the provided data from extant anurans. The anurans were dissected by Aaron Quigley, Beatriz Carazo del Hoyo and Valentina Rossi (University College Cork, Ireland). The dissected 11 individuals represent three anuran families (i.e., *Bombinatoridae*, *Bufonidae* and *Pipidae*) out of 49 anuran families worldwide (Vitt & Caldwell 2014) and include species that follow a primarily aquatic (two taxa) and terrestrial lifestyles (two taxa). Extant anurans occupy a variety of habitats, including woodlands, swamps, meadows, tundra and deserts; anurans usually reproduce in water. Individuals of different families and taxa within those families may differ in their ecology, e.g., their lifestyles (e.g., burrowing), their habitats, their diet, behaviour (e.g., reproduction and colour display) and anatomy (i.e., presence/absence of a lateral line system). The evolutionary indications made by the analysis of the melanosome data from fossil and extant anurans (Chapter 5) are based on a generalisation of anuran lifestyles (i.e., in this study: aquatic and terrestrial), habitats (i.e., all taxa live in pond and lake environments or the vicinity of these), diets (i.e., the assumption of a comparable diet among taxa), behaviours (e.g., all taxa show similar behaviours such as nocturnal adaptation and mating in water) and assumes the same age of the dissected adult specimens. For the four studied taxa, data on ecology, diet, behaviour and anatomy is similar (Vitt & Caldwell 2014). The age of the studied individuals is not known and the data on the melanosome distribution in the anuran body has only been reported for *Xenopus* (Provencio *et al.* 1998; Zuasti *et al.* 1998). Slight differences in ecology and anatomy among those taxa are not likely to have impacted the major study results. It is notable, that the relation between colour display (i.e., skin pigmentation) and the geometries of melanosome in those tissues remains unclear.

The impact of diagenesis on melanosomes is well characterised (Korytowski & Sarna 1990; McNamara 2013; McNamara *et al.* 2013; Colleary *et al.* 2015; Slater *et al.* 2020; Rossi *et al.* 2021; Slater *et al.* 2023a; Slater *et al.* 2023b). Heat (250 °C) and pressure (250 bar) experiments on melanosomes from feathers revealed a shrinkage of ca. 20% in length and width (not aspect ratio) of melanosomes (McNamara *et al.* 2013). Estimates of shrinkage of melanosomes calculated from fossils confirm these experimental results (Hu *et al.* 2018; Norden *et al.* 2019). It therefore unlikely that unknown taphonomic factors have impacted the geometries of preserved melanosomes.

Most anuran specimens from Geiseltal do not contain much embedding sediment on the slab. Only limited volumes of sediment were available for analysis. One anuran specimen is hosted in-situ in sedimentary matrix and is conserved in water (GMH XXXV-11-1970). This specimen has been excavated from an older stratigraphic level than most of the other specimens in this thesis. The sediment associated with GMH XXXV-11A-1970 may not be representative for the depositional setting of most Geiseltal anurans. The information from the sediment on the depositional setting of the Geiseltal anurans is therefore very limited. The lack of sediment associated with the Geiseltal anurans is frustrating as the Geiseltal site represents a depositional setting (i.e., small and shallow lakes and ponds) that differs strongly from that of the deep maar lakes of many important lacustrine Cenozoic biotas (e.g., Messel, Enspel and Eckfelder Maar). Thus, a comparison of sedimentary patterns and sediment chemistries between Geiseltal and other biotas is lacking. Such a comparison could reveal the role of the embedding sediment for the preservation of anurans and their soft tissues in lacustrine depositional settings. Bigger quantities of Geiseltal sediment from the stratigraphic levels that hosted the fossil anurans could include the investigation of grain sizes, grading and sedimentary structures such as bedding and bed forms to inform on flow regimes and the associated transport of carcasses. Carcass transport impacts the skeletal completeness and articulation (Section 6.1). The precise sedimentary context could also inform on sedimentary controls on the preservation of the anuran skin, such as the sediment acidity and the organic content in the sediment and reveal if the sediment acted

as an ion source for the mineralisation of tissues. The chemistry of Geiseltal melanosomes may be biased due to diagenetic overprinting of the original melanosome chemistry (Rossi *et al.* 2021). The chemistry of the sediment associated with the Geiseltal anurans would clarify if the sediment acted as a source for an enrichment of the soft tissues by metal elements, in particular Cu.

Significance tests (e.g., the independent t-test and ANOVA) are performed in Chapter 5 to statistically explore the differences in melanosome geometries among fossil and extant anuran specimens. It is notable that in this study, the significance tests (e.g., ANOVA; Section 5.2.1 and the supplementary tables in Section 5.10.5) on datasets with hundreds of entries tend to give conservative results (i.e., p-values that are lower than the alpha level of 0.05). This statistical issue relates to large sample sizes (Lin *et al.* 2013) and may bias the results of the comparison of melanosome geometries among fossil and extant anurans towards differences among datasets (instead of similarities). The probability for those Type 1 errors (false positives) can be reduced by the application of a Bonferroni-style correction and/or the use of the Nemenyi post-hoc test for nonparametric multiple comparisons. In Chapter 5, the statistical results are usually accompanied with different forms of data visualisation (e.g., scatter plots); thus, the p-value is not the only parameter that is considered for the interpretation of statistical results. In conclusion, statistical conservatism is likely not an issue for the interpretation of the melanosome geometry data among fossil and extant anurans.

7. Concluding remarks

This chapter summarises the major conclusions of this thesis and proposes several new directions for future studies on the taphonomy of the Geiseltal Konservat-Lagerstätte.

7.1 Conclusions

The conclusions relate to the taphonomy of the Geiseltal anurans, which has comprehensive implications for the controls on preservation of skeletal elements of anurans and anuran soft tissues in lacustrine-hosted environments. Additional conclusions relate to the modes of preservation of the Geiseltal anuran soft tissues. Further, the distribution, geometry and chemistry of melanosomes in fossil and modern anurans infer on the evolution of melanin.

1) The skeletons of the Geiseltal anurans vary in completeness but are usually well-articulated. The completeness and articulation differ among anuran skeletal elements. Distal limb bones (e.g. phalanges, carpals) are usually absent but, when present, are usually articulated with adjoining bones. Proximal limb elements (e.g. humerus, femur) are often complete but, when present, are less well articulated with adjoining bones. The completeness and articulation of preservation of skeletal elements is independent of excavation site and taxonomy.

2) The cause of death of the Geiseltal anurans is primarily mating-related (i.e., death by exhaustion and/or drowning). Certain specimens may have died as a result of old age and/or disease.

3) The preservation of anurans in lacustrine-hosted Palaeogene/Neogene settings shows taphonomic trends including proximal to distal trends in completeness, preferential loss of small peripheral bones, disarticulation of abdominal bones and reorientation of major body regions. Taphonomic controls in lacustrine systems include surface water temperature, lake

depth, vegetation, exposure to bottom currents, transport mechanisms, scavenging, decay regime, bone size and location in the skeleton. These are ultimately controlled by palaeoclimate, lake physiography and hydrology and anuran anatomy.

4) Fossil soft tissues of the Geiseltal anurans include the mid-dermal Eberth-Katschenko (E-K) layer, which is replicated in calcium phosphate (more specifically a mixture of biological carbonated hydroxyapatite and carbonated fluorapatite) and carbonaceous layers that contain sulfur-rich carbonaceous microbodies interpreted as melanosomes. Euhedral aragonite crystals from the endolymphatic organ in anurans are preserved. The primary modes of soft tissue preservation are therefore sulfurisation and phosphatisation. There is no evidence for silicified soft tissues or the preservation of other preserved soft tissues such as muscles, veins, cells or additional integument layers.

   The fidelity of preservation of soft tissues of the Geiseltal anurans is independent of anuran taxonomy or any influx of calcium- and carbonate-rich waters.

5) The preservation of the Geiseltal anurans is consistent with the taphonomy of vertebrates in many other Konservat-Lagerstätten. This is the basis of a model for pervasive preservation of vertebrate soft tissues via melanosome films, particularly in stagnation-type deposits, with phosphatisation of more labile tissues, where microenvironments rich in phosphate develop during decay, and where tissues have a high potential for phosphatisation.

6) The fossil melanosomes from different body locations of the Geiseltal anurans derive from several tissues, i.e., internal organs (for melanosomes from the torso and abdomen – probably the gonads and lungs and/or the liver), the eyes (for melanosomes from the eyespots) and the skin (for melanosomes from the external surface of mineralised skin). The melanosomes show tissue-specific geometries and chemistries.

7) The melanosomes from the Geiseltal anurans, from anurans from other Cenozoic biotas and from extant anurans reveal that evolution of melanin in the skin has been decoupled from that in the eyes and internal tissues during the last ca. 45 million years. Melanosomes from the skin differ in geometry in extant and fossil species, but melanosomes from the eyes and internal tissues show strongly conserved geometries. These trends in melanosome evolution are probably controlled by physiological constraints on melanosome function that have been in place at least since the Middle Eocene. The geometry of skin melanosomes may reflect evolutionary tradeoffs linked to diversification of integumentary coloration and/or habitat.

8) This thesis highlights the justification for museum fossil collections and their accessibility to researchers. This thesis also emphasises the importance of the re-evaluation of fossil collections using modern techniques in order to reassess historical interpretations.

7.2 Future perspectives

This section proposes several new directions for future study of the taphonomy of the Geiseltal Konservat-Lagerstätte that arise from the findings of this thesis.

7.2.1 Comparative taphonomy – an approach to identify patterns in skeletal taphonomy

Patterns in skeletal taphonomy can shed light on the controls of fossil preservation. Comparative approaches are useful to elucidate patterns in preservation among Konservat-Lagerstätten. It is therefore important to place taphonomic data (e.g., on skeletal taphonomy and mode of preservation) in the context of taphonomic data from Konservat-Lagerstätten that were formed in similar environmental settings. This thesis suggests the following parameters that may be useful for future comparison of lacustrine-hosted Konservat-Lagerstätten: age/location of the Lagerstätte, mean annual palaeotemperature, broad geological setting (e.g., fault-bounded lake and maar lake), environmental

parameters (lake size, lake depth, hydrologically open/closed, bottom currents, stratification permanent/intermittent/absent), excavated facies (marginal or central lake facies etc.), sediment characteristics (laminated, bedded, grading, grain size, mineralogy etc.), taxonomy, abundance of fossils, presence/absence of predators and/or scavengers (e.g., the associated fish fauna), truncation of specimens, skeletal taphonomy metrics (completeness, articulation and orientation), soft tissues present/absent and which soft tissues are preserved, the mode(s) of (soft tissue) preservation and major trends in skeletal taphonomy (e.g., the presence/absence of a proximal-distal trend in the skeletal element completeness, the lack of entire limbs, the disarticulation of entire limbs, the presence of isolated limbs, abdominal disarticulation and the presence of extensively disarticulated specimens). Future studies on the taphonomy of Konservat-Lagerstätten should provide data on these parameters to facilitate comparative analyses of data from several Konservat-Lagerstätten.

7.2.2 Testing the taphonomic model for the preservation of anuran soft tissues using other Geiseltal vertebrates

Soft tissues have been reported in many vertebrate groups in the Geiseltal Konservat-Lagerstätte (Voigt 1988). Future studies should test the taphonomic model for the preservation of anuran soft tissues presented in this thesis using other Geiseltal vertebrates (e.g., artiodactyls, bats, fish and newts). These studies have the potential to identify similarities and differences in preservation among vertebrates. The results will illuminate the ultimate controls on the formation of the Geiseltal Konservat-Lagerstätte.

7.2.3 Extending the melanosome geometry and chemistry dataset

This thesis developed datasets of geometry and chemical data for melanosomes from extant and fossil anurans. Future studies should include data from more fossil and extant taxa to provide additional confidence in the analytical results, which, in turn, will facilitate the identification of the source tissue(s) of fossil melanosomes. More specifically, additional samples of melanosomes from anurans that show

obvious skin pigmentation may clarify why anuran skin melanosomes vary among extant taxa. Then, the data from extant taxa should be compared with that from fossil taxa.

7.2.4 Investigating the functions of melanin

Future studies should investigate the functions of melanin in different tissues (especially internal tissues) and whether functions for a particular tissue type differ among vertebrate groups or among species in a given vertebrate group.

7.2.5 Testing the evolutionary conservatism model for melanosomes

The known functions of melanin for vision in anuran eyes imply a conservatism of eye melanosome geometries in anurans and other vertebrate groups. Future studies should test whether melanosomes from the eyes of other vertebrates (e.g., additional amphibians, bird, fish, mammals and reptiles) show conserved geometries over geological time. It should be tested whether the concept of conserved melanosome geometries applies to tissues other than the eyes.

7.3 Closing words: Long live the frog king!

(English version below)

Anuren, also Frösche und Kröten, oft nur als „Frösche“ zusammengefasst bezeichnet, sind außerordentlich faszinierende Kreaturen. Während ich diese Arbeit schrieb, habe ich diese verrückten Amphibien mehr und mehr liebgewonnen. Nicht umsonst ist der Froschkönig in dem gleichnamigen Märchen ein verwunschener Prinz...

Einerseits sehen Frösche freundlich, fast tollpatschig aus, aber andererseits sind sie Jäger mit spitzen Zähnen (obwohl sie diese nur im Oberkiefer aufweisen – mit Ausnahme von *Gastrotheca guentheri*, der in beiden Kiefern Zähne hat). Die Metamorphose, also die Veränderung des gesamten Körperbaus von Kaulquappe zu erwachsenenem Frosch, muss schlimmer sein als jede menschliche Pubertät, und doch stehen sie dies durch. Frösche leben buchstäblich überall. Sie brauchen das Wasser, können aber auch außerhalb des Wassers leben. Sie können gefrieren und wieder auftauen, sie können die Hitze in Wüsten überleben, sie leben sogar auf Bäumen und in Pflanzen. Ihr „Quaaak“ ist eines der bekanntesten Geräusche von Mutter Natur, aber es gibt auch Frösche, die wie quietschendes Spielzeug oder aggressive, fauchende Katzen klingen (*Breviceps*). Frösche sehen Farben! Manche Frösche sind nur wenige Millimeter klein (z. B. *Paedophryne amanuensis*), andere sind mehrere Dezimeter groß (z. B. *Conraua goliath*). Diese Geschöpfe sind weit mehr als nur grüne, hüpfende Kreaturen, die sich und ihre Weibchen bei der Paarung töten können oder sich versehentlich mit Fischen oder Holzstöcken paaren; einige von ihnen tragen atemberaubende Farben, andere sind giftig oder haben durchscheinende Bäuche, die die Organe offenbaren („Glasfrösche“). Wiederum andere nehmen Vaterschaftsurlaub und tragen die Eier des Partners auf ihrem Rücken (*Alytes obstetricans*) oder können sogar „fliegen“ (*Rhacophorus nigropalmatus*). Frösche dienen als wichtige Indikatoren für den Zustand moderner Ökosysteme. Diese eigentümlichen Tiere sind es wert, ernster genommen zu warden – sei es als Fossilien oder lebende Objekte.

Frösche sind noch vor den Dinosauriern entstanden. Sie sind seit ca. 200 Millionen Jahren auf der Erde, lebten mit T-Rex Seite an Seite und überlebten mehrere Massenaussterben und Eiszeiten. In den letzten Jahren wurden die Frösche mit einer schrecklichen Pilzpandemie konfrontiert (Chytridiomykose), die zum Teil durch den menschlichen Handel verbreitet wird. Einige Froschpopulationen sind glücklicherweise zäh genug und zeigen bereits eine gewisse Resistenz gegen diese Krankheit. Meiner Meinung nach, werden Frösche eine der Tiergruppen sein, die neben Ratten und Kakerlaken uns Menschen überleben.

Lang lebe der Froschkönig!



Figure 7.1: Lang lebe der Froschkönig/long live the frog king! Photograph: P. Chung, modified.

(English version)

Anurans, that are frogs and toads, usually called “frogs”, are fascinating amphibians. While writing this thesis I fell in love with them more and more. There is a reason, why the “frog king” in a (German) fairytale is a bewitched prince…

On one hand, frogs look friendly, almost clumsy, but on the other hand, they are hunters with teeth (although, they all have them in the upper jaw only – except for *Gastrotheca guentheri*, who has teeth in both jaws). Going through metamorphosis, to change the complete body structure, must be worse than any human puberty and yet, they do it. Frogs live literally everywhere. They need water but can survive inside and outside of it. They can freeze and defrost, survive the heat in deserts and even live in plants and on trees. Their “ribbit” is one of the most recognisable sounds of mother nature, but there are also frogs that sound like squeaking toys or hissing cats (*Breviceps*). Frogs can see colours! Certain frogs are tiny, a few millimetres in size (e.g., *Paedophryne amanuensis*), others are large, several decimetres long (e.g., *Conraua goliath*). Those creatures are far more than just green, jumping beings, that potentially kill their females during mating or accidently mate with fish or wooden sticks; some of them reveal awesome skin colouring, others are poisonous or have translucent bellies (“glass frogs”). And yet others take paternity leave and carry their partner’s eggs with them (*Alytes obstetricans*) or can “fly” (*Rhacophorus nigropalmatus*). Frogs serve as important indicators of the health of modern ecosystems. Those peculiar animals are worth taking more seriously as both fossils and living objects.

Frogs originated before the dinosaurs and have been on earth for ca. 200 million years. They lived side by side with T-rex and survived several mass extinctions and ice ages. In recent years, frogs are facing a fungus-related pandemic (chytridiomycosis, in parts spread by human trade). Luckily some frog populations are tough enough and already show some resistance against this disease. In my opinion, frogs will become one of the animal groups that will outlive us humans and share the world with rats and cockroaches.

Long live the frog king!

8. References

Abd Mutalib, M., Rahman, M. A., Othman, M. H. D., Ismail, A. F. & Jaafar, J. (2017). Chapter 9 - Scanning Electron Microscopy (SEM) and Energy-Dispersive X-Ray (EDX) Spectroscopy. 161–179. *In* Hilal, N., Ismail, A. F., Matsuura, T. & Oatley-Radcliffe, D. (eds). *Membrane Characterization*. Elsevier, 458 pp., https://doi.org/10.1016/B978-0-444-63776-5.00009-7.

Aguilar, J.-P., Legendre, S. & Michaux, J. (1997). Actes du congres BiochroM'97. *Mémoires et travaux de l'Institut de Montpellier de l'École pratique des hautes études*, **21**, 1–818.

Alesci, A., Pergolizzi, S., Mokhtar, D. M., Fumia, A., Aragona, M., Lombardo, G. P., Messina, E., D'Angelo, R., Lo Cascio, P., Sayed, R. K. A., Albano, M., Capillo, G. & Lauriano, E. R. (2023). Morpho-structural adaptations of the integument in different aquatic organisms. *Acta Histochem.*, **125**, 1–11, 152031, https://doi.org/10.1016/j.acthis.2023.152031.

Alibardi, L. (2003). Adaptation to the land: the skin of reptiles in comparison to that of amphibians and endotherm amniotes. *J. Exp. Zool. B*, **298B**, 12–41, https://doi.org/10.1002/jez.b.24.

Alibardi, L., Spisni, E. & Toni, M. (2003). Presence of putative histidine-rich proteins in the amphibian epidermis. *J. Exp. Zool. A*, **297**, 105–117, https://doi.org/10.1002/jez.a.10232.

Alleon, J., Montagnac, G., Reynard, B., Brulé, T., Thoury, M. & Gueriau, P. (2021). Pushing Raman spectroscopy over the edge: purported signatures of organic molecules in fossil animals are instrumental artefacts. *BioEssays*, **43**, 1–7, 2000295, https://doi.org/10.1002/bies.202000295.

Allison, P. A. (1988). Konservat-Lagerstätten: cause and classification. *Paleobiology*, **14**, 331–344, https://doi.org/10.1017/S0094837300012082.

Allison, P. A. & Briggs, D. E. (1993). Exceptional fossil record: distribution of soft-tissue preservation through the Phanerozoic. *Geology*, **21**, 527–530, https://doi.org/10.1130/0091-7613(1993)021%3C0527:EFRDOS%3E2.3.CO;2.

Allison, P. A. (2001). Chapter 3.2.1 - Decay. 270–273. *In* Briggs, D. E. G. & Crowther, P. R. (eds). *Palaeobiology II*. Blackwell Science Ltd., 608 pp., https://doi.org/10.1002/9780470999295.ch60.

Anderson, L. C. (2001). Chapter 3.2.6 - Transport and spatial fidelity. 289–292. *In* Briggs, D. E. G. & Crowther, P. R. (eds). *Palaeobiology II*. Blackwell Science Ltd., 608 pp., https://doi.org/10.1002/9780470999295.ch65.

Anderson, R. P., Tosca, N. J., Saupe, E. E., Wade, J. & Briggs, D. E. G. (2020). Early formation and taphonomic significance of kaolinite associated with Burgess Shale fossils. *Geology*, **49**, 355–359, https://doi.org/10.1130/G48067.1.

Anderson, S. R. & Wiens, J. J. (2017). Out of the dark: 350 million years of conservatism and evolution in diel activity patterns in vertebrates. *Evolution*, **71**, 1944–1959, https://doi.org/10.1111/evo.13284.

Ascarrunz, E., Rage, J.-C., Legreneur, P. & Laurin, M. (2016). *Triadobatrachus massinoti*, the earliest known lissamphibian (Vertebrata: Tetrapoda) re-examined by µCT scan, and the evolution of trunk length in batrachians. *Contrib. Zool.*, **85**, 201–234, https://repository.naturalis.nl/pub/610011.

Aturaliya, S. & Lukasewycz, A. (1999). Experimental forensic and bioanthropological aspects of soft tissue taphonomy: 1. factors influencing postmortem tissue desiccation rate. *J. Forensic Sci.*, **44**, 893–896, https://doi.org/10.1520/JFS12011J.

Báez, A. M. (2013). Anurans from the Early Cretaceous Lagerstätte of Las Hoyas, Spain: new evidence on the Mesozoic diversification of crown-clade Anura. *Cretac. Res.*, **41**, 90–106, https://doi.org/10.1016/j.cretres.2012.11.002.

Baird, G. C., Sroka, S. D., Shabica, C. W. & Kuecher, G. J. (1986). Taphonomy of Middle Pennsylvanian Mazon Creek area fossil localities, Northeast Illinois: significance of exceptional fossil preservation in syngenetic concretions. *Palaios*, **1**, 271–285, https://doi.org/10.2307/3514690.

Barnes, B. (1926). Eine eozäne Wirbeltier-Fauna aus der Braunkohle des Geiseltales. *Jahrbuch des Halleschen Verbandes für die Erforschung der mitteldeutschen Bodenschätze*, **6**, 5–24.

Batanova, V. G., Sobolev, A. V. & Magnin, V. (2018). Trace element analysis by EPMA in geosciences: detection limit, precision and accuracy. *IOP Conference Series: Materials Science and Engineering*, **304**, 1–17, 012001, https://dx.doi.org/10.1088/1757-899X/304/1/012001.

Baumjohann, K. & Benecke, M. (2022). Mind your decompositional assumptions. *Forensic Sci.*, **2**, 725–740, https://doi.org/10.3390/forensicsci2040054.

Beardmore, S. R., Orr, P. J., Manzocchi, T., Furrer, H. & Johnson, C. (2012). Death, decay and disarticulation: modelling the skeletal taphonomy of marine reptiles demonstrated using *Serpianosaurus* (Reptilia; Sauropterygia). *Palaeogeogr. Palaeoclimatol. Palaeoecol.*, **337–338**, 1–13, https://doi.org/10.1016/j.palaeo.2012.03.018.

Beardmore, S. R. & Furrer, H. (2018). Land or water: using taphonomic models to determine the lifestyle of the Triassic protorosaur *Tanystropheus* (Diapsida, Archosauromorpha). *Palaeobiodivers. Palaeoenviron.*, **98**, 243–258, https://doi.org/10.1007/s12549-017-0299-7.

Bell, P. R., Hendrickx, C., Pittman, M., Kaye, T. G. & Mayr, G. (2022). The exquisitely preserved integument of *Psittacosaurus* and the scaly skin of ceratopsian dinosaurs. *Commun. Biol.*, **5**, 809, https://doi.org/10.1038/s42003-022-03749-3.

Benton, M. J. (2008). How to find a dinosaur, and the role of synonymy in biodiversity studies. *Paleobiology*, **34**, 516–533, https://doi.org/10.1666/06077.1.

Benton, M. J., Zhonghe, Z., Orr, P. J., Fucheng, Z. & Kearns, S. L. (2008). The remarkable fossils from the Early Cretaceous Jehol Biota of China and how they have changed our knowledge of Mesozoic life: presidential address, delivered 2nd May 2008. *Proc. Geol. Assoc.*, **119**, 209–228, https://doi.org/10.1016/S0016-7878(08)80302-1.

Benton, M. J., Dhouailly, D., Jiang, B. & McNamara, M. E. (2019). The early origin of feathers. *Trends Ecol. Evol.*, **34**, 856–869, https://doi.org/10.1016/j.tree.2019.04.018.

Bergmann, U., Morton, R. W., Manning, P. L., Sellers, W. I., Farrar, S., Huntley, K. G., Wogelius, R. A. & Larson, P. (2010). *Archaeopteryx* feathers and bone chemistry fully revealed via synchrotron imaging. *Proc. Natl. Acad. Sci.*, **107**, 9060–9065, https://doi.org/10.1073/pnas.1001569107.

Bergmann, U., Manning, P. L. & Wogelius, R. A. (2012). Chemical mapping of paleontological and archeological artifacts with synchrotron X-rays. *Annu. Rev. Anal. Chem.*, **5**, 361–389, https://doi.org/10.1146/annurev-anchem-062011-143019.

Bernard, E. L., Ruta, M., Tarver, J. E. & Benton, M. J. (2010). The fossil record of early tetrapods: Worker effort and the end-Permian mass extinction. *Acta Palaeontol. Pol.*, **55**, 229–239, http://dx.doi.org/10.4202/app.2009.0025.

Berry, M. (2022). How to reduce fluorescence in Raman spectroscopy. *Edinburgh Instruments Ltd.*, 1-7, https://www.edinst.com/how-to-reduce-fluorescence-in-raman-spectroscopy/.

Blain, H.-A., Přikryl, T., Cáceres, I., Rodríguez-Salgado, P., Martínez-Monzón, A., Linares-Martín, A., Lozano-Fernández, I., Moreno-Ribas, E., Grandi, F., Oms, O., Agustí, J., Campeny Vall-Llosera, G. & Gómez de Soler, B. (2023). Skeletal taphonomy of the water frogs (Amphibia: Anura) from the Pit 7/8 of the Pliocene Camp dels Ninots site (Caldes de Malavella, NE Spain). *Hist. Biol.*, 1–28, https://doi.org/10.1080/08912963.2023.2237998.

Blumenstengel, H. (2004). 3.5 Tertiär. *In* Wansa, S. & Radzinski, K. (eds). *Erläuterungen zur Geologischen Karte 1:25 000 von Sachsen-Anhalt (GK 25), Blatt Mücheln (Geiseltal)*. Landesamt für Geologie und Bergwesen Sachsen-Anhalt, Halle (Saale), Germany, 143 pp.

Briggs, D. E. & Wilby, P. R. (1996). The role of the calcium carbonate-calcium phosphate switch in the mineralization of soft-bodied fossils. *J. Geol. Soc.*, **153**, 665–668, https://doi.org/10.1144/gsjgs.153.5.0665.

Briggs, D. E. G., Kear, A. J., Martill, D. M. & Wilby, P. R. (1993). Phosphatization of soft-tissue in experiments and fossils. *J. Geol. Soc.*, **150**, 1035–1038, https://doi.org/10.1144/gsjgs.150.6.1035.

Briggs, D. E. G. (1995). Experimental taphonomy. *Palaios*, **10**, 539–550, https://doi.org/10.2307/3515093.

Briggs, D. E. G. (2001). Chapter 3.4.1 - Exceptionally preserved fossils. 328–332. *In* Briggs, D. E. G. & Crowther, P. R. (eds). *Palaeobiology II*. Blackwell Science Ltd., 608 pp., https://doi.org/10.1002/9780470999295.ch76.

Briggs, D. E. G. (2003). The role of decay and mineralization in the preservation of soft-bodied fossils. *Annu. Rev. Earth Planet. Sci.*, **31**, 275–301, https://doi.org/10.1146/annurev.earth.31.100901.144746.

Briggs, D. E. G. (2014). Konservat-Lagerstätten 40 years on: the exceptional becomes mainstream. *Paleontol. Soc. Pap.*, **20**, 1–14, https://doi.org/10.1017/S1089332600002771.

Briggs, D. E. G. & McMahon, S. (2016). The role of experiments in investigating the taphonomy of exceptional preservation. *Palaeontology*, **59**, 1–11, https://doi.org/10.1111/pala.12219.

Brocklehurst, N., Upchurch, P., Mannion, P. D. & O'Connor, J. (2012). The completeness of the fossil record of Mesozoic birds: implications for early avian evolution. *PLOS ONE*, **7**, 1–21, e39056, https://doi.org/10.1371/journal.pone.0039056.

Brocklehurst, N. & Fröbisch, J. (2014). Current and historical perspectives on the completeness of the fossil record of pelycosaurian-grade synapsids. *Palaeogeogr. Palaeoclimatol. Palaeoecol.*, **399**, 114–126, https://doi.org/10.1016/j.palaeo.2014.02.006.

Brown, C. M., Henderson, D. M., Vinther, J., Fletcher, I., Sistiaga, A., Herrera, J. & Summons, R. E. (2017). An exceptionally preserved three-dimensional armored dinosaur reveals insights into coloration and cretaceous predator-prey dynamics. *Curr. Biol.*, **27**, 2514–2521, https://doi.org/10.1016/j.cub.2017.06.071.

Bruch, A., Utescher, T., Olivares, C. A., Doláková, N., Ivanov, D. & Mosbrugger, V. (2004). Middle and Late Miocene spatial temperature patterns and gradients in Europe-preliminary results based on palaeobotanical climate reconstructions. *Cour. Forschungsinst. Senckenberg*, **249**, 15–27.

Buchanan, B. W. (1993). Effects of enhanced lighting on the behaviour of nocturnal frogs. *Animal behaviour*, **45**, 893–899, https://doi.org/10.1006/anbe.1993.1109.

Bunaciu, A. A., Udriştioiu, E. g. & Aboul-Enein, H. Y. (2015). X-Ray diffraction: instrumentation and applications. *Crit. Rev. Anal. Chem.*, **45**, 289–299, https://doi.org/10.1080/10408347.2014.949616.

Buscalioni, Á. D. & Fregenal-Martínez, M. (2010). A holistic approach to the palaeoecology of Las Hoyas Konservat-Lagerstätte (La Huérguina Formation, Lower Cretaceous, Iberian Ranges, Spain). *J. Iber. Geol.*, **36**, 297–326, http://dx.doi.org/10.5209/rev_JIGE.2010.v36.n2.13.

Butterfield, N. J. (1990). Organic preservation of non-mineralizing organisms and the taphonomy of the Burgess Shale. *Paleobiology*, **16**, 272–286, https://doi.org/10.1017/S0094837300009994.

Butts, S. H. (2014). Silicification. *Paleontol. Soc. Pap.*, **20**, 15–34, https://doi.org/10.1017/S1089332600002783.

Cappellini, E., Prohaska, A., Racimo, F., Welker, F., Pedersen, M. W., Allentoft, M. E., de Barros Damgaard, P., Gutenbrunner, P., Dunne, J., Hammann, S., Roffet-Salque, M., Ilardo, M., Moreno-Mayar, J. V., Wang, Y., Sikora, M., Vinner, L., Cox, J., Evershed, R. P. & Willerslev, E. (2018). Ancient biomolecules and evolutionary inference. *Annu. Rev. Biochem.*, **87**, 1029–1060, https://doi.org/10.1146/annurev-biochem-062917-012002.

Carlisle, E. M., Jobbins, M., Pankhania, V., Cunningham, J. A. & Donoghue, P. C. J. (2021). Experimental taphonomy of organelles and the fossil record of early eukaryote evolution. *Sci. Adv.*, **7**, 1–8, eabe9487, https://doi.org/10.1126/sciadv.abe9487.

Carney, R. M., Vinther, J., Shawkey, M. D., D'Alba, L. & Ackermann, J. (2012). New evidence on the colour and nature of the isolated Archaeopteryx feather. *Nat. Commun.*, **3**, 1–6, 637, https://doi.org/10.1038/ncomms1642.

Carson, G. A. (1991). Silicification of fossils. 455–499. *In* Allison, P. A. & Briggs, D. E. G. (eds). *Taphonomy: releasing the data locked in the fossil record*. Plenum Press, New York, 560 pp, https://doi.org/10.1126/science.254.5037.1530.b.

Carter, D. O. & Tibbett, M. (2006). Microbial decomposition of skeletal muscle tissue (*Ovis aries*) in a sandy loam soil at different temperatures. *Soil Biol. Biochem.*, **38**, 1139–1145, https://doi.org/10.1016/j.soilbio.2005.09.014.

Carter, D. O., Yellowlees, D. & Tibbett, M. (2008). Temperature affects microbial decomposition of cadavers (*Rattus rattus*) in contrasting soils. *Appl. Soil Eco.*, **40**, 129–137, https://doi.org/10.1016/j.apsoil.2008.03.010.

Cashmore, D. D. & Butler, R. J. (2019). Skeletal completeness of the non-avian theropod dinosaur fossil record. *Palaeontology*, **62**, 951–981, https://doi.org/10.1111/pala.12436.

Cashmore, D. D., Mannion, P. D., Upchurch, P. & Butler, R. J. (2020). Ten more years of discovery: revisiting the quality of the sauropodomorph dinosaur fossil record. *Palaeontology*, **63**, 951–978, https://doi.org/10.1111/pala.12496.

Čerňanský, A., Stanley, E. L., Daza, J. D., Bolet, A., Arias, J. S., Bauer, A. M., Vidal-García, M., Bevitt, J. J., Peretti, A. M., Aung, N. N. & Evans, S. E. (2022). A new Early Cretaceous lizard in Myanmar amber with exceptionally preserved integument. *Sci. Rep.*, **12**, 1–12, 1660, https://doi.org/10.1038/s41598-022-05735-5.

Channing, A., Schweitzer, M. H., Horner, J. R. & McEneaney, T. (2005). A silicified bird from Quaternary hot spring deposits. *Proc. R. Soc. B*, **272**, 905–911, https://doi.org/10.1098/rspb.2004.2989.

Cincotta, A., Nguyen Tu, T. T., Colaux, J. L., Terwagne, G., Derenne, S., Godefroit, P., Carleer, R., Anquetil, C. & Yans, J. (2020). Chemical preservation of tail feathers from *Anchiornis huxleyi*, a theropod dinosaur from the Tiaojishan Formation (Upper Jurassic, China). *Palaeontology*, **63**, 841–863, https://doi.org/10.1111/pala.12494.

Cincotta, A., Nicolaï, M., Campos, H. B. N., McNamara, M. E., D'Alba, L., Shawkey, M. D., Kischlat, E.-E., Yans, J., Carleer, R., Escuillié, F. & Godefroit, P. (2022). Pterosaur melanosomes support signaling functions for early feathers. *Nature*, **604**, 684–688, https://doi.org/10.1038/s41586-022-04622-3.

Clarke, R. J. & Oprysa, A. (2004). Fluorescence and light scattering. *J. Chem. Educ.*, **81**, 705–707, https://doi.org/10.1021/ed081p705.

Cleary, T. J., Moon, B. C., Dunhill, A. M. & Benton, M. J. (2015). The fossil record of ichthyosaurs, completeness metrics and sampling biases. *Palaeontology*, **58**, 521–536, https://doi.org/10.1111/pala.12158.

Clements, T. & Gabbott, S. (2021). Exceptional preservation of fossil soft tissues. *eLS*, **2**, 1–10, https://doi.org/10.1002/9780470015902.a0029468.

Coates, M. (1996). The Devonian tetrapod *Acanthostega gunnari* Jarvik: postcranial anatomy, basal tetrapod interrelationships and patterns of skeletal evolution. *Earth Environ. Sci. Trans. R. Soc. Edinburgh*, **87**, 363–421, https://doi.org/10.1017/S0263593300006787.

Cody, G. D., Gupta, N. S., Briggs, D. E. G., Kilcoyne, A. L. D., Summons, R. E., Kenig, F., Plotnick, R. E. & Scott, A. C. (2011). Molecular signature of chitin-protein complex in Paleozoic arthropods. *Geology*, **39**, 255–258, https://doi.org/10.1130/G31648.1.

Colleary, C., Dolocan, A., Gardner, J., Singh, S., Wuttke, M., Rabenstein, R., Habersetzer, J., Schaal, S., Feseha, M., Clemens, M., Jacobs, B. F., Currano, E. D., Jacobs, L. L., Sylvestersen, R. L., Gabbott, S. E. & Vinther, J. (2015). Chemical, experimental, and morphological evidence for diagenetically altered melanin in exceptionally preserved fossils. *Proc. Natl. Acad. Sci.*, **112**, 12592–12597, https://doi.org/10.1073/pnas.1509831112.

Cotroneo, S., Schiffbauer, J. D., McCoy, V. E., Wortmann, U. G., Darroch, S. A. F., Peng, Y. & Laflamme, M. (2016). A new model of the formation of Pennsylvanian iron carbonate concretions hosting

exceptional soft-bodied fossils in Mazon Creek, Illinois. *Geobiology*, **14**, 543–555, https://doi.org/10.1111/gbi.12197.

D'Alba, L. & Shawkey, M. D. (2019). Melanosomes: biogenesis, properties, and evolution of an ancient organelle. *Physiol. Rev.*, **99**, 1–19, https://doi.org/10.1152/physrev.00059.2017.

Dang, M., Nowell, C., Nguyen, T., Bach, L., Sonne, C., Nørregaard, R., Stride, M. & Nowak, B. (2019). Characterisation and 3D structure of melanomacrophage centers in shorthorn sculpins (*Myoxocephalus scorpius*). *Tissue Cell*, **57**, 34–41, https://doi.org/10.1016/j.tice.2019.02.003.

Dean, C. D., Mannion, P. D. & Butler, R. J. (2016). Preservational bias controls the fossil record of pterosaurs. *Palaeontology*, **59**, 225–247, https://doi.org/10.1111/pala.12225.

Delsett, L. L., Friis, H., Kölbl-Ebert, M. & Hurum, J. H. (2022). The soft tissue and skeletal anatomy of two Late Jurassic ichthyosaur specimens from the Solnhofen archipelago. *PeerJ*, **10**, 1–24, e13173. https://doi.org/10.7717/peerj.13173.

DeSantis, L. R. G., Crites, J. M., Feranec, R. S., Fox-Dobbs, K., Farrell, A. B., Harris, J. M., Takeuchi, G. T. & Cerling, T. E. (2019). Causes and consequences of Pleistocene megafaunal extinctions as revealed from Rancho La Brea mammals. *Curr. Biol.*, **29**, 2488–2495, https://doi.org/10.1016/j.cub.2019.06.059.

Di Mauro, E., Xu, R., Soliveri, G. & Santato, C. (2017). Natural melanin pigments and their interfaces with metal ions and oxides: emerging concepts and technologies. *MRS Commun.*, **7**, 141–151, https://doi.org/10.1557/mrc.2017.33.

Dietrich, D., Lampke, T. & Rößler, R. (2013). A microstructure study on silicified wood from the Permian Petrified Forest of Chemnitz. *PalZ*, **87**, 397–407, https://doi.org/10.1007/s12542-012-0162-0.

Dilcher, D. L., Pavlick, R. J. & Mitchell, J. (1970). Chlorophyll derivatives in Middle Eocene sediments. *Science*, **168**, 1447–1449, https://doi.org/10.1126/science.168.3938.1447.

Dixon, A. D., Cox, W. R., Everham, E. M. & Ceilley, D. W. (2011). Anurans as biological indicators of restoration success in the Greater Everglades ecosystem. *Southeast. Nat.*, **10**, 629–646, https://doi.org/10.1656/058.010.0404.

Dodson, P. (1973). The significance of small bones in paleoecological interpretation. *Rocky Mt. Geol.*, **12**, 15–19.

Dominici, S. (2004). Quantitative taphonomy in sandstones from an ancient fan delta system (Lower Pleistocene,Western Emilia, Italy). *Palaios*, **19**, 193–205, https://doi.org/10.1669/0883-1351(2004)019<0193:QTISFA>2.0.CO;2.

Dornbos, S. Q. (2011). Phosphatization through the Phanerozoic. 435–456. *In* Allison, P. A. & Bottjer, D. J. (eds). *Taphonomy*. Springer, 600 pp., https://doi.org/10.1007/978-90-481-8643-3_12.

Driscoll, D. A., Dunhill, A. M., Stubbs, T. L. & Benton, M. J. (2019). The mosasaur fossil record through the lens of fossil completeness. *Palaeontology*, **62**, 51–75, https://doi.org/10.1111/pala.12381.

Du, C., Cui, F. Z., Zhang, W., Feng, Q. L., Zhu, X. D. & de Groot, K. (2000). Formation of calcium phosphate/collagen composites through mineralization of collagen matrix. *J. Biomed. Mater. Res.*, **50**, 518–527, https://doi.org/10.1002/(sici)1097-4636(20000615)50:4%3C518::aid-jbm7%3E3.0.co;2-w.

Duellman, W. E. & Trueb, L. (1994). *Biology of amphibians*. John Hopkins University Press, Baltimore and London, 271 pp., https://doi.org/10.1126/science.232.4747.271.a.

Edwards, N. P., Barden, H. E., van Dongen, B. E., Manning, P. L., Larson, P. L., Bergmann, U., Sellers, W. I. & Wogelius, R. A. (2011). Infrared mapping resolves soft tissue preservation in 50 million year-old reptile skin. *Proc. R. Soc. B*, **278**, 3209–3218, https://doi.org/10.1098/rspb.2011.0135.

Edwards, N. P., van Veelen, A., Anné, J., Manning, P. L., Bergmann, U., Sellers, W. I., Egerton, V. M., Sokaras, D., Alonso-Mori, R., Wakamatsu, K., Ito, S. & Wogelius, R. A. (2016). Elemental characterisation of melanin in feathers via synchrotron X-ray imaging and absorption spectroscopy. *Sci. Rep.*, **6**, 1–10, 34002, https://doi.org/10.1038/srep34002.

Edwards, N. P., Webb, S. M., Krest, C. M., van Campen, D., Manning, P. L., Wogelius, R. A. & Bergmann, U. (2018). A new synchrotron rapid-scanning X-ray fluorescence (SRS-XRF) imaging station at SSRL beamline 6-2. *J. Synchrotron. Radiat.*, **25**, 1565–1573, https://doi.org/10.1107/s1600577518010202.

Efremov, J. A. (1940). Taphonomy: a new branch of geology. *Pan-American Geologist*, **74**, 81–93, https://de.scribd.com/document/620634947/TAPHONOMY-NEW-BRANCH-OF-PALEONTOLOGY-Efremov-1940.

Eissmann, L. (2002). Tertiary geology of the Saale-Elbe region. *Quat. Sci. Rev.*, **21**, 1245–1274, https://doi.org/10.1016/S0277-3791(98)00082-1.

Elder, R. L. & Smith, G. R. (1988). Fish taphonomy and environmental inference in paleolimnology. *Palaeogeogr. Palaeoclimatol. Palaeoecol.*, **62**, 577–592.

Eliason, C. M., Hudson, L., Watts, T., Garza, H. & Clarke, J. A. (2017). Exceptional preservation and the fossil record of tetrapod integument. *Proc. R. Soc. B.*, **284**, 1–10, 20170556, https://doi.org/10.1098/rspb.2017.0556.

Elkan, E. (1968). Mucopolysaccharides in the anuran defense against desiccation. *J. Zool.*, **155**, 19–53, https://doi.org/10.1111/j.1469-7998.1968.tb03028.x.

Elkan, E. (1976). Ground substance: an anuran defense against desiccation. *Physiology of the Amphibia*, **3**, 101–110.

Evans, S. E. & Borsuk-Białynick, M. (2009). The early Triassic stem-frog *Czatkobatrachus* from Poland. *Palaeontol. Pol.*, **65**, 79–105, https://www.researchgate.net/publication/228117686_The_Early_Triassic_stem-frog_Czatkobatrachus_from_Poland.

Evershed, R. P. & Lockheart, M. J. (2001). Chapter 3.1.3 - Lipids. 247–253. *In* Briggs, D. E. G. & Crowther, P. R. (eds). *Palaeobiology II*. Blackwell Science Ltd., 608 pp., https://doi.org/10.1002/9780470999295.ch54.

Fabbri, M., Wiemann, J., Manucci, F. & Briggs, D. E. G. (2019). Three-dimensional soft tissue preservation revealed in the skin of a non-avian dinosaur. *Palaeontology*, **63**, 185–193, https://doi.org/10.1111/pala.12470.

Fabrezi, M., Goldberg, J. & Chuliver Pereyra, M. (2017). Morphological variation in anuran limbs: constraints and novelties. *J. Exp. Zool. B*, **328**, 546–574.

Falk, D., McCoy, V. & Wings, O. (2019). Ichnofossils of the Eocene Fossillagerstätte Geiseltal (Saxony-Anhalt, Germany) *3rd International Conference of Continental Ichnology (ICCI 2019)*, Abstract Volume & Field Trip Guide, 15–18, https://public.bibliothek.uni-halle.de/hjgb/article/view/1834.

Falk, D. & Stache, M. (2021). Die eozänen Froschlurche der Geiseltal-Sammlung, Interdisziplinäre Zugänge zum Rätsel der Fossilerhaltung. 39–47. *In* Seidl, E., Steinheimer, F. & Weber, C. (eds). *Eine Frage der Perspektive, Objekte als Vermittler von Wissenschaft*. Gesellschaft für Universitätssammlungen e.V., Humboldt-Universität zu Berlin, 124 pp., http://dx.doi.org/10.18452/23915.

Falk, D., Grosse, W.-R., McNamara, M. & Wings, O. (2022a). Der mysteriöse Tod der Frösche des Geiseltales/Sachsen-Anhalt im Mitteleozän. *Jahresschrift für Feldherpetologie und Ichthyofaunistik in Sachsen*, **23/2022**, 86–95, https://sachsen.nabu.de/imperia/md/content/sachsen/230525-nabu-jahresschrift-feldherpetologie-2023.pdf.

Falk, D., Wings, O. & McNamara, M. E. (2022b). The skeletal taphonomy of anurans from the Eocene Geiseltal Konservat-Lagerstätte, Germany: insights into the controls on fossil anuran preservation. *Pap. Palaeontol.*, **8**, 1–34, e1453, https://doi.org/10.1002/spp2.1453.

Falk, D., Wings, O., Unitt, R., Wade, J. & McNamara, M. E. (2024). Fossilized anuran soft tissues reveal a new taphonomic model for the Eocene Geiseltal Konservat-Lagerstätte, Germany. *Sci. Rep.*, **14**, 1–14, 7876, https://doi.org/10.1038/s41598-024-55822-y.

Feng, Y.-J., Blackburn, D. C., Liang, D., Hillis, D. M., Wake, D. B., Cannatella, D. C. & Zhang, P. (2017). Phylogenomics reveals rapid, simultaneous diversification of three major clades of Gondwanan frogs at the Cretaceous–Paleogene boundary. *Proc. Natl. Acad. Sci.*, **114**, 5864–5870, https://doi.org/10.1073/pnas.1704632114.

Fountaine, T. M. R., Benton, M. J., Dyke, G. J. & Nudds, R. L. (2005). The quality of the fossil record of Mesozoic birds. *Proc. R. Soc. B.*, **272**, 289–294, https://doi.org/10.1098/rspb.2004.2923.

Franzen, J. L. & Haubold, H. (1987). The biostratigraphic and palaeoecological significance of the Middle Eocene locality Geiseltal near Halle (German Democratic Republic). *Münchner Geowiss. Abh. A*, **10**, 93–100.

Gäb, F., Ballhaus, C., Stinnesbeck, E., Kral, A. G., Janssen, K. & Bierbaum, G. (2020). Experimental taphonomy of fish – role of elevated pressure, salinity and pH. *Sci. Rep.*, **10**, 1–10, 7839, https://doi.org/10.1038/s41598-020-64651-8.

Gaines, R. R. (2014). Burgess Shale-type preservation and its distribution in space and time. *Paleontol. Soc. Pap.*, **20**, 123–146, https://doi.org/10.1017/S1089332600002837.

Gardner, J. D. (2016). The fossil record of tadpoles. *Foss. Imp.*, **72**, 17–44, http://dx.doi.org/10.14446/FI.2016.17.

Garwood, R. J., Oliver, H. & Spencer, A. R. (2020). An introduction to the Rhynie chert. *Geol. Mag.*, **157**, 47–64, https://doi.org/10.1017/S0016756819000670.

Gehling, J. G. (1999). Microbial mats in terminal Proterozoic siliciclastics: Ediacaran death masks. *Palaios*, **14**, 40–57, https://doi.org/10.2307/3515360.

Georgalis, G. L., Rabi, M. & Smith, K. T. (2021). Taxonomic revision of the snakes of the genera *Palaeopython* and *Paleryx* (Serpentes, Constrictores) from the Paleogene of Europe. *Swiss J. Palaeontol.*, **18**, 1–140, https://doi.org/10.1186/s13358-021-00224-0.

Georgalis, G. L., Prendini, E. & Roček, Z. (2023). New information on the Eocene frog *Thaumastosaurus* (Anura, Pyxicephalidae) from the Phosphorites du Quercy, France. *Zool. J. Linn. Soc.*, **199**, 744–770, https://doi.org/10.1093/zoolinnean/zlad047.

Glass, K., Ito, S., Wilby, P. R., Sota, T., Nakamura, A., Bowers, C. R., Vinther, J., Dutta, S., Summons, R., Briggs, D. E. G., Wakamatsu, K. & Simon, J. D. (2012). Direct chemical evidence for eumelanin pigment from the Jurassic period. *Proc. Natl. Acad. Sci.*, **109**, 10218–10223, http://doi.org/10.1073/pnas.1118448109.

Godefroit, P., Sinitsa, S. M., Cincotta, A., McNamara, M. E., Reshetova, S. A. & Dhouailly, D. (2020). Integumentary structures in *Kulindadromeus zabaikalicus*, a basal neornithischian dinosaur from the Jurassic of Siberia. 47–65. *In* Foth, C. & Rauhut, O. W. M. (eds). *The evolution of feathers: from their origin to the present*. Springer International Publishing, 243 pp., https://doi.org/10.1007/978-3-030-27223-4_4.

Goldstein, G., Flory, K. R., Browne, B. A., Majid, S., Ichida, J. M. & Burtt Jr, E. H. (2004). Bacterial degradation of black and white feathers. *Auk*, **121**, 656–659, https://doi.org/10.1093/auk/121.3.656.

Grandi, F., Del Valle, H., Cáceres, I., Rodríguez-Salgado, P., Oms, O., Fernández-Jalvo, Y., García, F., Campeny, G. & Gómez de Soler, B. (2023). Exceptional preservation of large fossil vertebrates in a volcanic setting (Camp dels Ninots, Spain). *Hist. Biol.*, **35**, 1234–1249, https://doi.org/10.1080/08912963.2022.2085570.

Grimaldi, D. A., Engel, M. S. & Nascimbene, P. C. (2002). Fossiliferous Cretaceous amber from Myanmar (Burma): its rediscovery, biotic diversity, and paleontological significance. *Am. Mus. Novit.*, **2002**, 1–71, https://doi.org/10.1206/0003-0082(2002)361%3C0001:FCAFMB%3E2.0.CO;2.

Gueriau, P., Réguer, S., Leclercq, N., Cupello, C., Brito, P. M., Jauvion, C., Morel, S., Charbonnier, S., Thiaudière, D. & Mocuta, C. (2020). Visualizing mineralization processes and fossil anatomy using synchronous synchrotron X-ray fluorescence and X-ray diffraction mapping. *J. R. Soc. Interface*, **17**, 1–10, 20200216, https://doi.org/10.1098/rsif.2020.0216.

Guo, L., Li, W., Gu, Z., Wang, L., Guo, L., Ma, S., Li, C., Sun, J., Han, B. & Chang, J. (2023). Recent advances and progress on melanin: from source to application. *Int. J. Mol. Sci.*, **24**, 1–26, 4360, https://doi.org/10.3390/ijms24054360.

Gupta, N. S., Michels, R., Briggs, D. E. G., Evershed, R. P. & Pancost, R. D. (2006). The organic preservation of fossil arthropods: an experimental study. *Proc. R. Soc. B.*, **273**, 2777–2783, https://doi.org/10.1098/rspb.2006.3646.

Gupta, N. S., Briggs, D. E. G., Landman, N. H., Tanabe, K. & Summons, R. E. (2008a). Molecular structure of organic components in cephalopods: evidence for oxidative cross linking in fossil marine invertebrates. *Org. Geochem.*, **39**, 1405–1414, https://doi.org/10.1016/j.orggeochem.2008.06.008.

Gupta, N. S., Cambra-Moo, O., Briggs, D. E. G., Love, G. D., Fregenal-Martinez, M. A. & Summons, R. E. (2008b). Molecular taphonomy of macrofossils from the Cretaceous Las Hoyas Formation, Spain. *Cretac. Res.*, **29**, 1–8, https://doi.org/10.1016/j.cretres.2006.12.009.

Gupta, N. S., Cody, G. D., Tetlie, O. E., Briggs, D. E. G. & Summons, R. E. (2009). Rapid incorporation of lipids into macromolecules during experimental decay of invertebrates: Initiation of geopolymer formation. *Org. Geochem.*, **40**, 589–594, https://doi.org/10.1016/j.orggeochem.2009.02.005.

Hammer, Ø., Harper, D. A. T. & Ryan, P. D. (2001). PAST: Paleontological statistics software package for education and data analysis. *Palaeontol. Electron.*, **4**, 1–9.

Hastings, A. K. & Hellmund, M. (2015a). Rare in situ preservation of adult crocodilian with eggs from the Middle Eocene of Geiseltal. *Palaios*, **30**, 446–461, http://dx.doi.org/10.2110/palo.2014.062.

Hastings, A. K. & Hellmund, M. (2015b). Gaining Ground: horse-hunting Crocodiles and Giant Birds; New research results on the Eocene world of Germany ca. 45 million years ago. Companion volume to the exhibition presented at the National Academy of Sciences Leopoldina from March 6th to May 29th, 2015 in Halle (Saale), Germany. Center for Natural Science Collections (ZNS), Halle (Saale), Germany, 120 pp, http://geiseltal-ausstellung.de/media/Katalog.pdf.

Haubold, H. & Krumbiegel, G. (1984). Typenkatalog der Wirbeltiere aus dem Eozän des Geiseltals, 1934-1984 - 50 Jahre Geiseltalmuseum an der Martin-Luther-Univ. Halle-Wittenberg, Halle (Saale). 67.

Haubold, H. (1995). Wirbeltiergrabung und -forschung im Geiseltaleozän. *Hallesches Jb. Geowiss. B*, **17**, 1–18.

Haubold, H. & Hellmund, M. (1998). The Geiseltalmuseum of the Institute of Geological Sciences, University Halle-Wittenberg – Epicontinental Triassic International Symposium – Excursions. *Hallesches Jb. Geowiss. B*, **6**, 11–18.

Hellmund, M. & Hastings, A. K. (2014). Messel and Geiseltal: highlights from the Cenozoic; Excursion Guide, Part II - The Eocene Geiseltal Fossillagerstätte (Central Germany) and its vertebrate fossil fauna with 13 figures and 1 table, 25–46. *In* Smith, K. T., Lehmann, T., Hellmund, M. & Hastings, A. K. (eds). *SVP 2014*. Senckenberg Research Institute and Natural History Museum Frankfurt, Berlin, 46 pp.

Hellmund, M. (2018). The former Geiseltal Museum (1934–2011), the Eocene Geiseltal Fossilagerstätte (Germany) and the scientific meaning of Ben Barnes as a pioneer of systematic quantitative vertebrate excavations in the Geiseltal lignites. *Anu. do Inst. de Geocienc.*, **41**, 108–119, https://dx.doi.org/10.11137/2018_1_108_119.

Hendy, A. J. W. (2011). Taphonomic overprints on Phanerozoic trends in biodiversity: lithification and other secular megabiases. 19–77. *In* Allison, P. A. & Bottjer, D. J. (eds). Aims & Scope Topics in Geobiology Book Series, *Taphonomy*. Springer Dordrecht, 600 pp., https://doi.org/10.1007/978-90-481-8643-3_2.

Henrici, A. C. & Fiorillo, A. R. (1993). Catastrophic death assemblage of *Chelomophrynus bayi* (Anura, Rhinophrynidae) from the middle Eocene Wagon Bed Formation of central Wyoming. *J. Paleontol.*, **67**, 1016–1026, https://doi.org/10.1017/S0022336000025348.

Henrici, A. C. (1998). A new pipoid anuran from the Late Jurassic Morrison Formation at Dinosaur National Monument, Utah. *J. Vertebr. Paleontol.*, **18**, 321–332, https://doi.org/10.1080/02724634.1998.10011060.

Hong, L. & Simon, J. D. (2007). Current understanding of the binding sites, capacity, affinity, and biological significance of metals in melanin. *J. Phys. Chem. B*, **111**, 7938–7947, https://doi.org/10.1021/jp071439h.

Hu, D.-N., Simon, J. D. & Sarna, T. (2008). Role of ocular melanin in ophthalmic physiology and pathology. *Photochem. Photobiol.*, **84**, 639–644, https://doi.org/10.1111/j.1751-1097.2008.00316.x.

Hu, D., Clarke, J. A., Eliason, C. M., Qiu, R., Li, Q., Shawkey, M. D., Zhao, C., D'Alba, L., Jiang, J. & Xu, X. (2018). A bony-crested Jurassic dinosaur with evidence of iridescent plumage highlights complexity in early paravian evolution. *Nat. Commun.*, **9**, 1–12, 217, https://doi.org/10.1038/s41467-017-02515-y.

Ito, S. & Wakamatsu, K. (2003). Quantitative analysis of eumelanin and pheomelanin in humans, mice, and other animals: a comparative review. *Pigment Cell Res.*, **16**, 523–531, https://doi.org/10.1034/j.1600-0749.2003.00072.x.

Ito, S., Miyake, S., Maruyama, S., Suzuki, I., Commo, S., Nakanishi, Y. & Wakamatsu, K. (2018). Acid hydrolysis reveals a low but constant level of pheomelanin in human black to brown hair. *Pigment Cell Melanoma Res.*, **31**, 393–403, https://doi.org/10.1111/pcmr.12673.

Izzo, T. J., Rodrigues, D. J., Menin, M., Lima, A. P. & Magnusson, W. E. (2012). Functional necrophilia: a profitable anuran reproductive strategy? *J. Nat. Hist.*, **46**, 2961–2967, https://doi.org/10.1080/00222933.2012.724720.

Janssen, K., Mähler, B., Rust, J., Bierbaum, G. & McCoy, V. E. (2022). The complex role of microbial metabolic activity in fossilization. *Biol. Rev.*, **97**, 449–465, https://doi.org/10.1111/brv.12806.

Jarenmark, M., Sjövall, P., Ito, S., Wakamatsu, K. & Lindgren, J. (2021). Chemical evaluation of eumelanin maturation by ToF-SIMS and alkaline peroxide oxidation HPLC analysis. *Int. J. Mol. Sci.*, **22**, 1–16, 161, https://doi.org/10.3390/ijms22010161.

Jasp Team (2024). JASP (Version 0.18.3). https://jasp-stats.org/.

Jenkins Jr., F. A. & Shubin, N. H. (1998). *Prosalirus bitis* and the anuran caudopelvic mechanism. *J. Vertebr. Paleontol.*, **18**, 495–510, https://doi.org/10.1080/02724634.1998.10011077.

Jeon, D.-J., Paik, S., Ji, S. & Yeo, J.-S. (2021). Melanin-based structural coloration of birds and its biomimetic applications. *Appl. Microsc.*, **51**, 1–11, https://doi.org/10.1186/s42649-021-00063-w.

Jerzmanska, A. (1977). The freshwater fishes from the Middle Eocene of Geiseltal. *Martin-Luther-Universität Halle-Wittenberg Wissenschaftliche Beiträge*, 41–65.

Jiang, H., Tomaschek, F., Drew Muscente, A., Niu, C., Nyunt, T. T., Fang, Y., Schmidt, U., Chen, J., Lönartz, M., Mähler, B., Wappler, T., Jarzembowski, E. A., Szwedo, J., Zhang, H., Rust, J. & Wang, B. (2022). Widespread mineralization of soft-bodied insects in Cretaceous amber. *Geobiology*, **20**, 363–376, https://doi.org/10.1111/gbi.12488.

Jurašeková, Z., Fabriciová, G., Silveira, L. F., Lee, Y.-N., Gutak, J. M., Ataabadi, M. M. & Kundrát, M. (2022). Raman spectra and ancient life: vibrational ID profiles of fossilized (bone) tissues. *Int. J. Mol. Sci.*, **23**, 10689, https://doi.org/10.3390/ijms231810689.

Kemp, R. A. & Unwin, D. M. (1997). The skeletal taphonomy of *Archaeopteryx*: a quantitative approach. *Lethaia*, **30**, 229–238, https://doi.org/10.1111/j.1502-3931.1997.tb00465.x.

Kidwell, S. M., Fürsich, F. T. & Aigner, T. (1986). Conceptual framework for the analysis and classification of fossil concentrations. *Palaios*, **1**, 228–238, https://doi.org/10.2307/3514687.

Kidwell, S. M. & Baumiller, T. (1990). Experimental disintegration of regular echinoids: Roles of temperature, oxygen, and decay thresholds. *Paleobiology*, **16**, 247–271, https://doi.org/10.1017/S0094837300009982.

Kidwell, S. M. (2001). Chapter 3.3.1 - Major biases in the fossil record. 297–303. *In* Briggs, D. E. G. & Crowther, P. R. (eds). *Palaeobiology II*. Blackwell Science Ltd., 608 pp. https://doi.org/10.1002/9780470999295.ch67.

Kielan-Jaworowska, Z. & Hurum, J. H. (2006). Limb posture in early mammals: sprawling or parasagittal. *Acta Palaeontol. Pol.*, **51**, 393–406, https://www.app.pan.pl/article/item/app51-393.html.

Kimmig, J. & Schiffbauer, J. D. (2023). Finding and describing the exceptional: a modern definition of Fossil-Lagerstätten. 51–52. *In* Reitner, J., Reich, M. & Duda, J.-P. (eds). *Fossillagerstätten and taphonomy - new ideas and approaches*. Göttingen, Germany, 103 pp., https://www.researchgate.net/publication/375774483.

Kimmig, J. & Schiffbauer, J. D. (2024). A modern definition of Fossil-Lagerstätten. *Trends Ecol. Evol.*, **39**, 621–624, https://doi.org/10.1016/j.tree.2024.04.004.

Kjær, K. H., Winther Pedersen, M., De Sanctis, B., De Cahsan, B., Korneliussen, T. S., Michelsen, C. S., Sand, K. K., Jelavić, S., Ruter, A. H., Schmidt, A. M. A., Kjeldsen, K. K., Tesakov, A. S., Snowball, I., Gosse, J. C., Alsos, I. G., Wang, Y., Dockter, C., Rasmussen, M., Jørgensen, M. E., Skadhauge, B., Prohaska, A., Kristensen, J. Å., Bjerager, M., Allentoft, M. E., Coissac, E., Alsos, I. G., Coissac, E., Rouillard, A., Simakova, A., Fernandez-Guerra, A., Bowler, C., Macias-Fauria, M., Vinner, L., Welch, J. J., Hidy, A. J., Sikora, M., Collins, M. J., Durbin, R., Larsen, N. K., Willerslev, E. & PhyloNorway, C. (2022). A 2-million-year-old ecosystem in Greenland uncovered by environmental DNA. *Nature*, **612**, 283–291, https://doi.org/10.1038/s41586-022-05453-y.

Klug, C., Meyer, E. P., Richter, U. & Korn, D. (2008). Soft-tissue imprints in fossil and recent cephalopod septa and septum formation. *Lethaia*, **41**, 477–492, https://doi.org/10.1111/j.1502-3931.2008.00100.x.

Kohring, R. & Hirsch, K. F. (1996). Crocodilian and avian eggshells from the Middle Eocene of the Geiseltal, Eastern Germany. *J. Vertebr. Paleontol.*, **16**, 67–80, https://doi.org/10.1080/02724634.1996.10011285.

Kootstra, A. M. J., Brilman, D. W. F. & Kersten, S. R. A. (2019). Dissolution of phosphate from pig manure ash using organic and mineral acids. *Waste Manage.*, **88**, 141–146, https://doi.org/10.1016/j.wasman.2019.03.038.

Kopittke, P. M., Punshon, T., Paterson, D. J., Tappero, R. V., Wang, P., Blamey, F. P. C., van der Ent, A. & Lombi, E. (2018). Synchrotron-based X-ray fluorescence microscopy as a technique for imaging of elements in plants. *Plant Physiol.*, **178**, 507–523, https://doi.org/10.1104/pp.18.00759.

Korytowski, W. & Sarna, T. (1990). Bleaching of melanin pigments. Role of copper ions and hydrogen peroxide in autooxidation and photooxidation of synthetic dopa-melanin. *J. Biol. Chem.*, **265**, 12410–12416, https://doi.org/10.1016/S0021-9258(19)38362-0.

Krumbiegel, G. (1962a). Ostracodenfunde im Tagebau Neumark-Süd (Geiseltal). *Geologie*, **11**, 334–353.

Krumbiegel, G. (1962b). Die Fossilfundstellen der mitteleozänen Braunkohle des Geiseltales. *Wiss. Z., Martin-Luther-Univ. Halle-Wittenberg*, **11**, 173–208.

Krumbiegel, G. (1975). Zur Palökologie der tertiären Fossilfundstellen des Geiseltales. *Hercynia, N.F.*, **12**, 400–417.

Krumbiegel, G. (1977). Genese, Palökologie und Biostratigraphie der Fossilfundstellen im Eozän des Geiseltales. *Kongreß und Tagungsberichte der Martin-Luther-Universität Halle-Wittenberg, Wissenschaftliche Beiträge*, **5**, 113–138.

Krumbiegel, G., Rüffle, L. & Haubold, H. (1983). Das eozäne Geiseltal: ein mitteleuropäisches Braunkohlenvorkommen und seine Pflanzen- und Tierwelt. A. Ziemsen Verlag, Die Neue Brehm-Bücherei, Wittenberg Lutherstadt, 227 pp.

Krutzsch, W., Blumenstengel, H., Kiesel, Y. & Rüffle, L. (1992). Paläobotanische Klimagliederung des Alttertiärs (Mitteleozän bis Oberoligozän) in Mitteldeutschland und das Problem der Verknüpfung mariner und kontinentaler Gliederungen. *Neues Jahrb. Geol. Paläontol.*, **186**, 137–253.

Krutzsch, W. (2011). Stratigrafie und Klima des Palaogens im Mitteldeutschen Ästuar im Vergleich zur marinen nordlichen Umrahmung. *Zeitschrift der Deutschen Gesellschaft für Geowissenschaften*, **162**, 19–47, https://doi.org/10.1127/1860-1804/2011/0162-0019.

Kuhn, O. (1941). Die eozänen Anura aus dem Geiseltale nebst einer Übersicht über die fossilen Gattungen. *Nova Acta Leopold. NF*, **10**, 345–376.

Küstermann, W., Rappsilber, I. & Thomae, M. (2008). Regionale und tektonische Voraussetzungen zur Bildung der Geiseltal-Senke. *Veröffentlichungen der Deutschen Gesellschaft für Geowissenschaften*, **235**, 12–21.

Lebon, M., Zazzo, A. & Reiche, I. (2014). Screening in situ bone and teeth preservation by ATR-FTIR mapping. *Palaeogeogr. Palaeoclimatol. Palaeoecol.*, **416**, 110–119, https://doi.org/10.1016/j.palaeo.2014.08.001.

Lee, Y.-C., Chiang, C.-C., Huang, P.-Y., Chung, C.-Y., Huang, T. D., Wang, C.-C., Chen, C.-I., Chang, R.-S., Liao, C.-H. & Reisz, R. R. (2017). Evidence of preserved collagen in an Early Jurassic sauropodomorph dinosaur revealed by synchrotron FTIR microspectroscopy. *Nat. Commun.*, **8**, 1–8, 14220, https://doi.org/10.1038/ncomms14220.

Leo, R. F. & Barghoorn, E. S. (1976). Silicification of wood. *Botanical Museum Leaflets, Harvard University*, **25**, 1–47, https://doi.org/10.5962/p.295209.

Li, Q., Clarke, J. A., Gao, K. Q., Zhou, C. F., Meng, Q., Li, D., D'Alba, L. & Shawkey, M. D. (2014). Melanosome evolution indicates a key physiological shift within feathered dinosaurs. *Nature*, **507**, 350–364, https://doi.org/10.1038/nature12973.

Liebig, K. (2001). Chapter 3.1.4 - Bacteria. 253–256. *In* Briggs, D. E. G. & Crowther, P. R. (eds). *Palaeobiology II*. Blackwell Science Ltd., 608 pp., https://doi.org/10.1002/9780470999295.ch55.

Liesegang, M. & Gee, C. T. (2020). Silica entry and accumulation in standing trees in a hot-spring environment: cellular pathways, rapid pace and fossilization potential. *Palaeontology*, **63**, 651–660, https://doi.org/10.1111/pala.12480.

Lin, F., Liu, Y., Yu, X., Cheng, L., Singer, A., Shpyrko, O. G., Xin, H. L., Tamura, N., Tian, C., Weng, T.-C., Yang, X.-Q., Meng, Y. S., Nordlund, D., Yang, W. & Doeff, M. M. (2017). Synchrotron X-ray analytical techniques for studying materials electrochemistry in rechargeable batteries. *Chem. Rev.*, **117**, 13123–13186, https://doi.org/10.1021/acs.chemrev.7b00007.

Lin, M., Jr, H. C. L. & Shmueli, G. (2013). Research commentary – Too big to fail: large samples and the p-value problem. *Inf. Syst. Res.*, **24**, 906–917, https://doi.org/10.1287/isre.2013.0480.

Lincke, L. (1977). Zur Geologie des Geiseltales. *Originalabhandlungen und Vorträge des Internationalen Kolloquiums vom 4.–5. November 1974 in Halle (Saale), Martin-Luther-Universität Halle-Wittenberg, Wissenschaftliche Beiträge 1977/2 (P5)*, 139–147.

Lindgren, J., Uvdal, P., Sjövall, P., Nilsson, D. E., Engdahl, A., Schultz, B. P. & Thiel, V. (2012). Molecular preservation of the pigment melanin in fossil melanosomes. *Nat. Commun.*, **3**, 1–7, http://dx.doi.org/10.1038/ncomms1819.

Lindgren, J., Sjövall, P., Carney, R. M., Cincotta, A., Uvdal, P., Hutcheson, S. W., Gustafsson, O., Lefèvre, U., Escuillié, F., Heimdal, J., Engdahl, A., Gren, J. A., Kear, B. P., Wakamatsu, K., Yans, J. & Godefroit, P. (2015). Molecular composition and ultrastructure of Jurassic paravian feathers. *Sci. Rep.*, **5**, 1–13, 13520, https://doi.org/10.1038/srep13520.

Lindgren, J., Sjövall, P., Thiel, V., Zheng, W., Ito, S., Wakamatsu, K., Hauff, R., Kear, B. P., Engdahl, A., Alwmark, C., Eriksson, M. E., Jarenmark, M., Sachs, S., Ahlberg, P. E., Marone, F., Kuriyama, T., Gustafsson, O., Malmberg, P., Thomen, A., Rodríguez-Meizoso, I., Uvdal, P., Ojika, M. & Schweitzer, M. H. (2018). Soft-tissue evidence for homeothermy and crypsis in a Jurassic ichthyosaur. *Nature*, **564**, 359–365, https://doi.org/10.1038/s41586-018-0775-x.

Lizana, M., Márquez, R. & Martín-Sánchez, R. (1994). Reproductive biology of *Pelobates cultripes* (Anura: Pelobatidae) in central Spain. *J. Herpetol.*, **28**, 19–27, https://doi.org/10.2307/1564675.

Llovet, X., Moy, A., Pinard, P. T. & Fournelle, J. H. (2021). Electron probe microanalysis: A review of recent developments and applications in materials science and engineering. *Prog. Mater. Sci.*, **116**, 100673, https://doi.org/10.1016/j.pmatsci.2020.100673.

Lönartz, M. I., McCoy, V. E., Gee, C. T. & Geisler, T. (2023). Palaeoenvironmental conditions for the natural vulcanization of the Eocene “monkeyhair” laticifers from Geiseltal, Germany, as elucidated by Raman spectroscopy. *Palaeobiodivers. Palaeoenviron.*, 1–13, https://doi.org/10.1007/s12549-022-00566-8.

MacDougall, M. J., Tabor, N. J., Woodhead, J., Daoust, A. R. & Reisz, R. R. (2017). The unique preservational environment of the Early Permian (Cisuralian) fossiliferous cave deposits of the Richards Spur locality, Oklahoma. *Palaeogeogr. Palaeoclimatol. Palaeoecol.*, **475**, 1–11, https://doi.org/10.1016/j.palaeo.2017.02.019.

Mangione, S., Garcia, G. & Cardozo, O. M. (2011). The Eberth–Katschenko layer in three species of ceratophryines anurans (Anura: Ceratophrydae). *Acta Zool.*, **92**, 21–26, https://doi.org/10.1111/j.1463-6395.2009.00442.x.

Manning, P. L., Edwards, N. P., Bergmann, U., Anné, J., Sellers, W. I., van Veelen, A., Sokaras, D., Egerton, V. M., Alonso-Mori, R., Ignatyev, K., van Dongen, B. E., Wakamatsu, K., Ito, S., Knoll, F. & Wogelius, R. A. (2019). Pheomelanin pigment remnants mapped in fossils of an extinct mammal. *Nat. Commun.*, **10**, 1–13, 2250, https://doi.org/10.1038/s41467-019-10087-2.

Mannion, P. D. & Upchurch, P. (2010). Completeness metrics and the quality of the sauropodomorph fossil record through geological and historical time. *Paleobiology*, **36**, 283–302, https://doi.org/10.1666/09008.1.

Márquez, R. (1995). Female choice in the midwife toads (*Alytes obstetricans* and *A. cisternasii*). *Behaviour*, **132**, 151–161, https://doi.org/10.1163/156853995X00342.

Martill, D. M. (1988). Preservation of fish in the Cretaceous Santana Formation Brazil. *Palaeontology*, **31**, 1–18, https://www.palass.org/sites/default/files/media/publications/palaeontology/volume_31/vol31_part1_pp1-18.pdf.

Martin, R. E. (1999). Cambridge Paleobiology Series. *Taphonomy. A process approach*. Cambridge University Press, Cambridge, 508 pp, https://doi.org/10.1017/CBO9780511612381.

Matthews, T., van Dijk, E., Roberts, D. L. & Smith, R. M. H. (2015). An early Pliocene (5.1 Ma) fossil frog community from Langebaanweg, south-western Cape, South Africa. *Afr. J. Herpetol.*, **64**, 39–53, https://doi.org/10.1080/21564574.2014.985261.

Maus, M. & Wuttke, M. (2002). Comparative anatomical-morphological and taphonomical examination of the larvae of *Pelobates decheni* TROSCHEL (1861) and *Eopelobates anthracinus* PARKER (1929) (Anura: Pelobatidae) found at the Upper Oligocene sites at Enspel (Westerwald/Germany) and Rott (Siebengebirge/Germany). *Cour. Forschungsinst. Senckenberg*, **237**, 129–138, https://www.researchgate.net/publication/287774998_Comparative_anatomical_and_taphonomical_examination_of_the_larvae_of_Pelobates_decheni_Troschel_1861_and_Eopelobates_anthracinus_Parker_1929_Anura_Pelobatidae_found_at_the_Upper_Oligocene_sites_at_Ens.

Mayr, G. (2020). An updated review of the middle Eocene avifauna from the Geiseltal (Germany), with comments on the unusual taphonomy of some bird remains. *Geobios*, **62**, 45–59, https://doi.org/10.1016/j.geobios.2020.06.011.

McCoy, V. E., Young, R. T. & Briggs, D. E. G. (2015). Factors controlling exceptional preservation in concretions. *Palaios*, **30**, 272–280, https://doi.org/10.2110/palo.2014.081.

McCoy, V. E., Boom, A., Wings, O., Wappler, T., Labandeira, C. C. & Gee, C. T. (2021). Fossilisation of the Eocene "monkeyhair" laticifer tree from Geiseltal, Germany: a deeper understanding using micro-CT and pyrolysis GC/MS. *Palaios*, **36**, 1–14, https://doi.org/10.2110/palo.2020.052.

McMahon, S., Anderson, R. P., Saupe, E. E. & Briggs, D. E. G. (2016). Experimental evidence that clay inhibits bacterial decomposers: implications for preservation of organic fossils. *Geology*, **44**, 867–870, https://doi.org/10.1130/G38454.1.

McNamara, M., Orr, P. J., Kearns, S. L., Alcalá, L., Anadón, P. & Peñalver-Mollá, E. (2010a). Organic preservation of fossil musculature with ultracellular detail. *Proc. R. Soc. B.*, **277**, 423–427, https://doi.org/10.1098/rspb.2009.1378.

McNamara, M. E. (2007). Comparative taphonomy of lacustrine-hosted exceptional faunas from the Miocene of NE Spain. Unpublished PhD thesis, University College Dublin, Ireland, 535 pp.

McNamara, M. E., Orr, P. J., Kearns, S. L., Alcalá, L., Anadón, P. & Penalver Molla, E. (2009). Soft-tissue preservation in Miocene frogs from Libros, Spain: insights into the genesis of decay microenvironments. *Palaios*, **24**, 104–117, https://doi.org/10.2110/palo.2008.p08-017r.

McNamara, M. E., Orr, P. J., Kearns, S. L., Alcalá, L., Anadón, P. & Peñalver-Mollá, E. (2010b). Exceptionally preserved tadpoles from the Miocene of Libros, Spain: ecomorphological reconstruction and the impact of ontogeny upon taphonomy. *Lethaia*, **43**, 290–306, https://doi.org/10.1111/j.1502-3931.2009.00192.x.

McNamara, M. E., Orr, P. J., Alcalá, L., Anadón, P. & Peñalver, E. (2012a). What controls the taphonomy of exceptionally preserved taxa – environment or biology? A case study using frogs from the Miocene Libros Konservat-Lagerstätte (Teruel, Spain). *Palaios*, **27**, 63–77, https://doi.org/10.2110/palo.2010.p10-126r.

McNamara, M. E., Orr, P. J., Manzocchi, T., Alcalá, L., Anadón, P. & Peñalver, E. (2012b). Biological controls upon the physical taphonomy of exceptionally preserved salamanders from the Miocene of Rubielos de Mora, northeast Spain. *Lethaia*, **45**, 210–226, https://doi.org/10.1111/j.1502-3931.2011.00274.x.

McNamara, M. E. (2013). The taphonomy of colour in fossil insects and feathers. *Palaeontology*, **56**, 557–575, https://doi.org/10.1111/pala.12044.

McNamara, M. E., Briggs, D. E. G., Orr, P. J., Field, D. J. & Wang, Z. (2013). Experimental maturation of feathers: implications for reconstructions of fossil feather colour. *Biol. Lett.*, **9**, 1–6, 20130184,

McNamara, M. E., Orr, P. J., Kearns, S. L., Alcalá, L., Anadón, P. & Peñalver, E. (2016a). Reconstructing carotenoid-based and structural coloration in fossil skin. *Curr. Biol.*, **26**, 1075–1082, https://doi.org/10.1016/j.cub.2016.02.038.

McNamara, M. E., van Dongen, B. E., Lockyer, N. P., Bull, I. D. & Orr, P. J. (2016b). Fossilization of melanosomes via sulfurization. *Palaeontology*, **59**, 337–350, https://doi.org/10.1111/pala.12238.

McNamara, M. E., Kaye, J. S., Benton, M. J., Orr, P. J., Rossi, V., Ito, S. & Wakamatsu, K. (2018). Non-integumentary melanosomes can bias reconstructions of the colours of fossil vertebrates. *Nat. Commun.*, **9**, 1–9, https://doi.org/10.1038/s41467-018-05148-x.

McNamara, M. E., Rossi, V., Slater, T. S., Rogers, C. S., Ducrest, A.-L., Dubey, S. & Roulin, A. (2021). Decoding the evolution of melanin in vertebrates. *Trends Ecol. Evol.*, **36**, 430–443, https://doi.org/10.1016/j.tree.2020.12.012.

Méndez-Tepepa, M., Morales-Cruz, C., García-Nieto, E. & Anaya-Hernández, A. (2023). A review of the reproductive system in anuran amphibians. *Zool. Lett.*, **9**, 1–17, https://doi.org/10.1186/s40851-023-00201-0.

Menin, M., Rodrigues, D. J. & Lima, A. P. (2006). The tadpole of *Rhinella proboscidea* (Anura: Bufonidae) with notes on adult reproductive behavior. *Zootaxa*, **1258**, 47–56, https://doi.org/10.5281/zenodo.173120.

Mertz, D. F. & Renne, P. R. (2005). A numerical age for the Messel fossil deposit (UNESCO World Heritage Site) derived from $^{40}Ar/^{39}Ar$ dating on a basaltic rock fragment. *Cour. Forschungsinst. Senckenberg*, **255**, 67–75, https://www.researchgate.net/publication/281579713_A_numerical_age_for_the_Messel_fossil_deposit_UNESCO_World_Heritage_Site_derived_from_40Ar39Ar_dating_on_a_basaltic_rock_fragment.

Miyashita, T., Coates, M. I., Farrar, R., Larson, P., Manning, P. L., Wogelius, R. A., Edwards, N. P., Anné, J., Bergmann, U., Palmer, A. R. & Currie, P. J. (2019). Hagfish from the Cretaceous Tethys Sea and a reconciliation of the morphological–molecular conflict in early vertebrate phylogeny. *Proc. Natl. Acad. Sci.*, **116**, 2146–2151, https://www.pnas.org/doi/abs/10.1073/pnas.1814794116.

Mohun, S. M. & Davies, W. I. L. (2019). The evolution of amphibian photoreception. *Front. Ecol. Evol.*, **7**, 1–12, 321, https://doi.org/10.3389/fevo.2019.00321.

Moore, J. R. & Norman, D. B. (2009). Quantitatively evaluating the sources of taphonomic biasing of skeletal element abundances in fossil assemblages. *Palaios*, **24**, 591–602, https://doi.org/10.2110/palo.2008.p08-135r.

Mörs, T., Reguero, M. & Vasilyan, D. (2020). First fossil frog from Antarctica: implications for Eocene high latitude climate conditions and Gondwanan cosmopolitanism of Australobatrachia. *Sci. Rep.*, **10**, 1–11, 5051, https://doi.org/10.1038/s41598-020-61973-5.

Mosbrugger, V., Utescher, T. & Dilcher, D. L. (2005). Cenozoic continental climatic evolution of central europe. *Proc. Natl. Acad. Sci.*, **102**, 14964–14969, https://doi.org/10.1073/pnas.0505267102.

Moyer, A. E., Zheng, W., Johnson, E. A., Lamanna, M. C., Li, D.-q., Lacovara, K. J. & Schweitzer, M. H. (2014). Melanosomes or microbes: testing an alternative hypothesis for the origin of microbodies in fossil feathers. *Sci. Rep.*, **4**, 1–9, 4233, https://doi.org/10.1038/srep04233.

Muramiya, Y., Yoshida, H., Katsuta, N., Kuma, R. & Mikami, T. (2024). Formation of ammonite concretions through organic decomposition in the iron-reduction zone. *J. Sediment. Res.*, **94**, 51–61, https://doi.org/10.2110/jsr.2023.078.

Muscente, A. D., Schiffbauer, J. D., Broce, J., Laflamme, M., O'Donnell, K., Boag, T. H., Meyer, M., Hawkins, A. D., Huntley, J. W., McNamara, M., MacKenzie, L. A., Stanley, G. D., Hinman, N. W., Hofmann, M. H. & Xiao, S. (2017). Exceptionally preserved fossil assemblages through geologic time and space. *Gondwana Res.*, **48**, 164–188, https://doi.org/10.1016/j.gr.2017.04.020.

Muscente, A. D., Vinnes, O., Sinha, S., Schiffbauer, J. D., Maxwell, E. E., Schweigert, G. & Martindale, R. C. (2023). What role does anoxia play in exceptional fossil preservation? Lessons from the taphonomy of the Posidonia Shale (Germany). *Earth-Sci. Rev.*, **238**, 1–36, 104323, https://doi.org/10.1016/j.earscirev.2023.104323.

Mustoe, G. E. (2023). Silicification of wood: an overview. *Minerals*, **13**, 1–47, 206, https://doi.org/10.3390/min13020206.

Norden, K. K., Faber, J. W., Babarović, F., Stubbs, T. L., Selly, T., Schiffbauer, J. D., Peharec Štefanić, P., Mayr, G., Smithwick, F. M. & Vinther, J. (2019). Melanosome diversity and convergence in the evolution of iridescent avian feathers – implications for paleocolor reconstruction. *Evol.*, **73**, 15–27, https://doi.org/10.1111/evo.13641.

Nudelman, F., Lausch, A. J., Sommerdijk, N. A. J. M. & Sone, E. D. (2013). In vitro models of collagen biomineralization. *J. Struct. Biol.*, **183**, 258–269, https://doi.org/10.1016/j.jsb.2013.04.003.

Nützel, A. & Schulbert, C. (2005). Facies of two important Early Triassic gastropod Lagerstätten: implications for diversity patterns in the aftermath of the end-Permian mass extinction. *Facies*, **51**, 480–500, https://doi.org/10.1007/s10347-005-0074-5.

Oda, F. H., Batista, V. G., Gambale, P. G., Mise, F. T., de Souza, F., Bellay, S., JC, G. O. & Takemoto, R. M. (2016). Anuran species richness, composition, and breeding habitat preferences: a comparison between forest remnants and agricultural landscapes in southern Brazil. *Zool. Stud.*, **55**, 1–14, e34, https://doi.org/10.6620%2FZS.2016.55-34.

Orr, P. J., Kearns, S. L. & Briggs, D. E. (2002). Backscattered electron imaging of fossils exceptionally-preserved as organic compressions. *Palaios*, **17**, 110–117, https://doi.org/10.1669/0883-1351(2002)017%3C0110:BEIOFE%3E2.0.CO;2.

Pan, Y., Hu, L. & Zhao, T. (2018). Applications of chemical imaging techniques in paleontology. *Natl. Sci. Rev.*, **6**, 1040–1053, https://doi.org/10.1093/nsr/nwy107.

Petrovich, R. (2001). Mechanisms of fossilization of the soft-bodied and lightly armored faunas of the Burgess Shale and of some other classical localities. *Am. J. Sci.*, **301**, 683–726, http://dx.doi.org/10.2475/ajs.301.8.683.

Pich, A. A. & Sanchez, C. R. (2017). Clinical challenge: the endolymphatic system in the Denny's tree frog (*Polypedates dennysi*). *J. Zoo Wildl. Med.*, **48**, 602–606, https://doi.org/10.1638/2016-0110.1.

Pickel, W. & Wolf, M. (1989). Kohlenpetrographische und geochemische Charakterisierung von Braunkohlen aus dem Geiseltal (DDR). *Erdöl, Kohle, Erdgas, Petrochem.*, **42**, 481–484.

Piga, G., Brunetti, A., Lasio, B., Malfatti, L., Galobart, À., Dalla Vecchia, F. M. & Enzo, S. (2015). New insights about the presence of celestite into fossil bones from Molí del Baró 1 site (Isona i Conca Dellá, Lleida, Spain). *Appl. Phys. A*, **118**, 487–496, https://doi.org/10.1007/s00339-014-8814-4.

Pilkington, J. & Simkiss, K. (1966). The mobilization of the calcium carbonate deposits in the endolymphatic sacs of metamorphosing frogs. *J. Exp. Biol.*, **45**, 329–341, https://doi.org/10.1242/jeb.45.2.329.

Ponssa, M. L., Barrionuevo, J. S., Pucci Alcaide, F. & Pucci Alcaide, A. (2017). Morphometric variations in the skin layers of frogs: an exploration into their relation with ecological parameters in *Leptodactylus* (Anura, Leptodactylidae), with an emphasis on the Eberth-Kastschenko layer. *Anat. Rec.*, **300**, 1895–1909, https://doi.org/10.1002/ar.23640.

Price, S. J., Howe, R. W., Hanowski, J. M., Regal, R. R., Niemi, G. J. & Smith, C. R. (2007). Are anurans of great lakes coastal wetlands reliable indicators of ecological condition? *J. Gt. Lakes Res.*, **33**, 211–223, https://doi.org/10.3394/0380-1330(2007)33[211:AAOGLC]2.0.CO;2.

Provencio, I., Jiang, G., De Grip, W. J., Hayes, W. P. & Rollag, M. D. (1998). Melanopsin: An opsin in melanophores, brain, and eye. *Proc. Natl. Acad. Sci.*, **95**, 340–345, https://doi.org/10.1073/pnas.95.1.340.

Purnell, M. A., Donoghue, P. J. C., Gabbott, S. E., McNamara, M. E., Murdock, D. J. E. & Sansom, R. S. (2018). Experimental analysis of soft-tissue fossilization: opening the black box. *Palaeontology*, **61**, 317–323, https://doi.org/10.1111/pala.12360.

Rage, J.-C. & Roček, Z. (2003). Evolution of anuran assemblages in the tertiary and quaternary of europe, in the context of palaeoclimate and palaeogeography. *Amphibia-Reptilia*, **24**, 133–167, https://doi.org/10.1163/156853803322390408.

Rage, J.-C. (2016). Frogs (Amphibia, Anura) from the Eocene and Oligocene of the phosphorites du Quercy (France). An overview. *Foss. Imp.*, **72**, 53–66, https://doi.org/10.14446/fi.2016.53.

Raupach, F. v. (1948). Beitrag zur Geiseltalforschung. 3–18. *In* Lange, P. D. E. (ed.) *Abhandlungen der Geologischen Landesanstalt Berlin, N.F.* Akademie-Verlag GmbH Berlin, Berlin, 28 pp.

Reilly, S. M. & Jorgensen, M. E. (2011). The evolution of jumping in frogs: morphological evidence for the basal anuran locomotor condition and the radiation of locomotor systems in crown group anurans. *J. Morphol.*, **272**, 149–168, https://doi.org/10.1002/jmor.10902.

Reisdorf, A. G. & Wuttke, M. (2012). Re-evaluating Moodie's opisthotonic-posture hypothesis in fossil vertebrates part I: Reptiles – the taphonomy of the bipedal dinosaurs *Compsognathus longipes* and *Juravenator starki* from the Solnhofen Archipelago (Jurassic, Germany). *Palaeobiodivers. Palaeoenviron.*, **92**, 119–168, https://doi.org/10.1007/s12549-011-0068-y.

Riley, P. A. (1997). Melanin. *Int. J. Biochem. Cell Biol.*, **29**, 1235–1239, https://doi.org/10.1016/S1357-2725(97)00013-7.

Ring, S. J., Bocherens, H., Wings, O. & Rabi, M. (2020). Divergent mammalian body size in a stable Eocene greenhouse climate. *Sci. Rep.*, **10**, 1–10, 3987, https://doi.org/10.1038/s41598-020-60379-7.

Roček, Z. & Rage, J. (2000). Tertiary anura of Europe, Africa, Asia, North America, and Australia. *Amphibian Biology*, **4**, 1332–1387, http://rocek.gli.cas.cz/Publications/Ro%C4%8Dek%20and%20Rage%202000-.pdf.

Roček, Z. (2003). Larval development in Oligocene palaeobatrachid frogs. *Acta Palaeontol. Pol.*, **48**, 595–607, https://www.app.pan.pl/article/item/app48-595.html.

Roček, Z. & Wuttke, M. (2010). Amphibia of Enspel (Late Oligocene, Germany). *Palaeobiodivers. Palaeoenviron.*, **90**, 321–340, https://doi.org/10.1007/s12549-010-0042-0.

Roček, Z. (2013). Mesozoic and Tertiary anura of Laurasia. *Palaeobiodivers. Palaeoenviron.*, **93**, 397–439, https://doi.org/10.1007/s12549-013-0131-y.

Roček, Z., Wuttke, M., Gardner, J. D. & Singh Bhullar, B.-A. (2014). The Euro-American genus *Eopelobates*, and a re-definition of the family Pelobatidae (Amphibia, Anura). *Palaeobiodivers. Palaeoenviron.*, **94**, 529–567, https://doi.org/10.1007/s12549-014-0169-5.

Rogers, C. S., Astrop, T. I., Webb, S. M., Ito, S., Wakamatsu, K. & McNamara, M. E. (2019). Synchrotron X-ray absorption spectroscopy of melanosomes in vertebrates and cephalopods: implications for the affinity of *Tullimonstrum*. *Proc. R. Soc. B.*, **286**, 20191649, https://doi.org/10.1098/rspb.2019.1649.

Rossi, V., McNamara, M. E., Webb, S. M., Ito, S. & Wakamatsu, K. (2019). Tissue-specific geometry and chemistry of modern and fossilized melanosomes reveal internal anatomy of extinct vertebrates. *Proc. Natl. Acad. Sci.*, **116**, 17880–17889, https://doi.org/10.1073/pnas.1820285116.

Rossi, V., Webb, S. M. & McNamara, M. E. (2020). Hierarchical biota-level and taxonomic controls on the chemistry of fossil melanosomes revealed using synchrotron X-ray fluorescence. *Sci. Rep.*, **10**, 1–10, 8970, https://doi.org/10.1038/s41598-020-65868-3.

Rossi, V., Webb, S. M. & McNamara, M. E. (2021). Maturation experiments reveal bias in the chemistry of fossil melanosomes. *Geology*, **49**, 784–788, https://doi.org/10.1130/G48696.1.

Rossi, V., Unitt, R., McNamara, M., Zorzin, R. & Carnevale, G. (2022). Skin patterning and internal anatomy in a fossil moonfish from the Eocene Bolca Lagerstätte illuminate the ecology of ancient reef fish communities. *Palaeontology*, **65**, 1–11, e12600, https://doi.org/10.1111/pala.12600.

Roy, A., Rogers, C. S., Clement, T., Pittman, M., Habimana, O., Martin, P. & Vinther, J. (2020). Fossil microbodies are melanosomes: evaluating and rejecting the "fossilised decay-associated microbes" hypothesis. *Bull. Am. Mus. Nat. Hist.*, **440**, 251–276, https://doi.org/10.5061/dryad.xgxd254dj.

Roy, P. V., Briggs, D. E. G. & Gaines, R. R. (2015). The Fezouata fossils of Morocco; an extraordinary record of marine life in the Early Ordovician. *J. Geol. Soc.*, **172**, 541–549, https://doi.org/10.1144/jgs2015-017.

Rüffle, L., Müller-Stoll, W. & Litke, R. (1976). Eozäne Floren des Geiseltales. *Abhandlungen des Zentralen Geologischen Institutes, Berlin*, **26**, 199–238, https://books.google.ie/books/about/Eoz%C3%A4ne_Floren_des_Geiseltales.html?id=6pWgzwEACAAJ&redir_esc=y.

Rüffle, L. & Litke, R. (2000). Ergänzungen zur Eozän-Flora des Geiseltales, Deutschland, und einiger weiterer Eozän-Fundstätten. *Feddes Repert.*, **111**, 449–463, https://doi.org/10.1002/fedr.20001110711.

Sagemann, J., Bale, S. J., Briggs, D. E. G. & Parkes, R. J. (1999). Controls on the formation of authigenic minerals in association with decaying organic matter: an experimental approach. *Geochim. Cosmochim. Acta*, **63**, 1083–1095, https://doi.org/10.1016/S0016-7037(99)00087-3.

Salamon, M. A., Gorzelak, P., Borszcz, T., Gajerski, A. & Kaźmierczak, J. (2009). A crinoid concentration Lagerstätte in the Turonian (Late Cretaceous) Conulus Bed (Miechów-Wolbrom area, Poland). *Geobios*, **42**, 351–357, https://doi.org/10.1016/j.geobios.2008.10.008.

Scheele, B. C., Pasmans, F., Skerratt, L. F., Berger, L., Martel, A., Beukema, W., Acevedo, A. A., Burrowes, P. A., Carvalho, T., Catenazzi, A., De la Riva, I., Fisher, M. C., Flechas, S. V., Foster, C. N., Frías-Álvarez, P., Garner, T. W. J., Gratwicke, B., Guayasamin, J. M., Hirschfeld, M., Kolby, J. E., Kosch, T. A., La Marca, E., Lindenmayer, D. B., Lips, K. R., Longo, A. V., Maneyro, R., McDonald, C. A., Mendelson, J., Palacios-Rodriguez, P., Parra-Olea, G., Richards-Zawacki, C. L., Rödel, M.-O., Rovito, S. M., Soto-Azat, C., Toledo, L. F., Voyles, J., Weldon, C., Whitfield, S. M., Wilkinson, M., Zamudio, K. R. & Canessa, S. (2019). Amphibian fungal panzootic causes catastrophic and ongoing loss of biodiversity. *Science*, **363**, 1459–1463, https://doi.org/10.1126/science.aav0379.

Schneider, C. A., Rasband, W. S. & Eliceiri, K. W. (2012). NIH Image to ImageJ: 25 years of image analysis. Nat. Methods, **9**, 671–675, https://doi.org/10.1038/nmeth.2089.

Schoch, R. R. (2022). Phylogeny of the amphibamiform temnospondyls: the relationship of taxa known by adults, larvae and neotenes. *J. Syst. Palaeontol.*, **20**, 1–30, https://doi.org/10.1080/14772019.2022.2113831.

Seilacher, A. (1970). Begriff und Bedeutung der Fossil-Lagerstätten. *Neues Jahrb. Geol. Paläontol.*, 34–39.

Seilacher, A. & Westphal, F. (1971). Fossil-Lagerstätten. 327–335. *International Sedimentological Congress*. Heidelberg, Germany.

Seilacher, A., Reif, W.-E., Westphal, F., Riding, R., Clarkson, E. N. K., Whittington, H. B., Whittington, H. B. & Morris, S. C. (1985). Sedimentological, ecological and temporal patterns of fossil Lagerstätten. *Phil. Trans. R. Soc. Lond. B*, **311**, 5–24, https://doi.org/10.1098/rstb.1985.0134.

Shubin, N. H. & Jenkins, F. A. (1995). An Early Jurassic jumping frog. *Nature*, **377**, 49–52, https://doi.org/10.1038/377049a0.

Simoneit, B. R. T., Otto, A., Menor-Sálvan, C., Oros, D. R., Wilde, V. & Riegel, W. (2020). Composition of resinites from the Eocene Geiseltal brown coal basin, Saxony-Anhalt, Germany and comparison to their possible botanical analogues. *Org. Geochem.*, **152**, 1–16, 104138, https://doi.org/10.1016/j.orggeochem.2020.104138.

Sinninghe Damsté, J. S., de las Heras, F. X. C., van Bergen, P. F. & de Leeuw, J. W. (1993). Characterization of Tertiary Catalan lacustrine oil shales: discovery of extremely organic sulphur-rich type I kerogens. *Geochim. Cosmochim. Acta*, **57**, 389–415, https://doi.org/10.1016/0016-7037(93)90439-4.

Sinninghe Damsté, J. S., Rijpstra, W. I. C., Coolen, M. J. L., Schouten, S. & Volkman, J. K. (2007). Rapid sulfurisation of highly branched isoprenoid (HBI) alkenes in sulfidic Holocene sediments from Ellis Fjord, Antarctica. *Org. Geochem.*, **38**, 128–139, https://doi.org/10.1016/j.orggeochem.2006.08.003.

Sitiwin, E., Madigan, M. C., Gratton, E., Cherepanoff, S., Conway, R. M., Whan, R. & Macmillan, A. (2019). Shedding light on melanins within *in situ* human eye melanocytes using 2-photon microscopy profiling techniques. *Sci. Rep.*, **9**, 1–18, 18585, https://doi.org/10.1038/s41598-019-54871-y.

Slater, T. S., McNamara, M. E., Orr, P. J., Foley, T. B., Ito, S. & Wakamatsu, K. (2020). Taphonomic experiments resolve controls on the preservation of melanosomes and keratinous tissues in feathers. *Palaeontology*, **63**, 103–115, https://doi.org/10.1111/pala.12445.

Slater, T. S., Edwards, N. P., Webb, S. M., Zhang, F. & McNamara, M. E. (2023a). Preservation of corneous β-proteins in Mesozoic feathers. *Nat. Ecol. Evol.*, **7**, 1706–1713, https://doi.org/10.1038/s41559-023-02177-8.

Slater, T. S., Ito, S., Wakamatsu, K., Zhang, F., Sjövall, P., Jarenmark, M., Lindgren, J. & McNamara, M. E. (2023b). Taphonomic experiments reveal authentic molecular signals for fossil melanins and verify preservation of phaeomelanin in fossils. *Nat. Commun.*, **14**, 1–15, 5651, https://doi.org/10.1038/s41467-023-40570-w.

Smith, E. & Dent, G. (2019). Chapter 3 - The theory of Raman spectroscopy. 77–99. *In* Smith, E. & Dent, G. (eds) *Modern Raman spectroscopy – a practical approach*. John Wiley & Sons Ltd., 256 pp., https://doi.org/10.1002/9781119440598.ch3.

Smith, E. A., Mayfield, C. I. & Wong, P. T. S. (1977). Physical and chemical characterization of selected natural apatites in synthetic and natural aqueous solutions. *Water Air Soil Pollut.*, **8**, 401–415, https://doi.org/10.1007/BF00228655.

Smith, G. R. & Elder, R. L. (1985). Environmental interpretation of burial and preservation of Clarkia fishes. 85–94. *In* Smiley, C. J. (ed.) *Late Cenozoic History of the Pacific Northwest*. American Association for the Advancement of Science Pacific Division, San Francisco, 417 pp.,

Smith, K. T. & Wuttke, M. (2012). From tree to shining sea: taphonomy of the arboreal lizard Geiseltaliellus maarius from Messel, Germany. *Palaeobiodivers. Palaeoenviron.*, **92**, 45–65, https://doi.org/10.1007/s12549-011-0064-2.

Smith, R. E., Martill, D. M., Longrich, N., Unwin, D. M., Ibrahim, N. & Zouhri, S. (2023). Comparative taphonomy of Kem Kem Group (Cretaceous) pterosaurs of southeast Morocco. *Evolving Earth*, **1**, 1–22, 100006, https://doi.org/10.1016/j.eve.2023.100006.

So, C., Pardo, J. D. & Mann, A. (2024). A new amphibamiform from the Early Permian of Texas elucidates patterns of cranial diversity among terrestrial amphibamiforms. *Zool. J. Linn. Soc.*, 1–15, zlae012, https://doi.org/10.1093/zoolinnean/zlae012.

Špinar, Z. V. (1972). *Tertiary frogs from central Europe*. W. Junk & Czechoslovak Academy of Sciences Prague, 286 pp., https://doi.org/10.1007/978-94-010-2932-2.

Stock, C. (1930). Rancho La Brea: a record of Pleistocene life in California. *Los Angeles County Museum of Natural History*, **Publication No. 1**, 1–84, https://authors.library.caltech.edu/records/05rtr-69j43.

Stocker, M. R., Nesbitt, S. J., Kligman, B. T., Paluh, D. J., Marsh, A. D., Blackburn, D. C. & Parker, W. G. (2019). The earliest equatorial record of frogs from the Late Triassic of Arizona. *Biol. Lett.*, **15**, 1–5, 20180922, https://doi.org/10.1098/rsbl.2018.0922.

Storrs, G. W., Oser, S. E. & Aull, M. (2012). Further analysis of a Late Jurassic dinosaur bone-bed from the Morrison Formation of Montana, USA, with a computed three-dimensional reconstruction. *Earth Environ. Sci. Trans. R. Soc. Edinburgh*, **103**, 443–458, https://doi.org/10.1017/S1755691013000248.

Stosik, M. P., Tokarz-Deptuła, B. & Deptuła, W. (2019). Melanomacrophages and melanomacrophage centres in Osteichthyes. *Cent. Eur. J. Immunol.*, **44**, 201–205, https://doi.org/10.5114/ceji.2019.87072.

Sues, H.-D. & Boy, J. A. (1988). A procynosuchid cynodont from central Europe. *Nature*, **331**, 523–524, https://doi.org/10.1038/331523a0.

Sutcliffe, O. E., Briggs, D. E. G. & Bartels, C. (1999). Ichnological evidence for the environmental setting of the Fossil-Lagerstätten in the Devonian Hunsrück Slate, Germany. *Geology*, **27**, 275–278, https://doi.org/10.1130/0091-7613(1999)027%3C0275:IEFTES%3E2.3.CO;2.

Syromyatnikova, E. V. (2018). Palaeobatrachid frog from the late Miocene of Northern Caucasus, Russia. *Palaeontol. Electron.*, **21**, 1–16, https://doi.org/10.26879/861.

Tahoun, M., Engeser, M., Namasivayam, V., Sander, P. M. & Müller, C. E. (2022). Chemistry and analysis of organic compounds in Dinosaurs. *Biology*, **11**, 1–25, 670, https://doi.org/10.3390/biology11050670.

Talavera, R. R., Bustillo, M.-Á. & Sanchiz, B. (2019). Paleobiological forensic study of an upper Miocene Pelobates tadpole (Anura, Pelobatidae) from the Tresjuncos Lagerstätte of central Spain. *J. Vertebr. Paleontol.*, **39**, 1–11, e1669615, https://doi.org/10.1080/02724634.2019.1669615.

Terrill, R. S. & Shultz, A. J. (2023). Feather function and the evolution of birds. *Biol. Rev.*, **98**, 540–566, https://doi.org/10.1111/brv.12918.

Tissier, J., Rage, J.-C. & Laurin, M. (2017). Exceptional soft tissues preservation in a mummified frog-eating Eocene salamander. *PeerJ*, **5**, 1–14, e3861, https://doi.org/10.7717/peerj.3861.

Todd, B. D., Luhring, T. M., Rothermel, B. B. & Gibbons, J. W. (2009). Effects of forest removal on amphibian migrations: implications for habitat and landscape connectivity. *J. Appl. Ecol.*, **46**, 554–561, https://doi.org/10.1111/j.1365-2664.2009.01645.x.

Toporski, J. K. W., Steele, A., Westall, F., Avci, R., Martill, D. M. & McKay, D. S. (2002a). Morphologic and spectral investigation of exceptionally well-preserved bacterial biofilms from the Oligocene Enspel Formation, Germany. *Geochim. Cosmochim. Acta*, **66**, 1773–1791, https://doi.org/10.1016/S0016-7037(01)00870-5.

Toporski, J. K. W., Steele, A., Westall, F., Thomas-Keprta, K. L. & McKay, D. S. (2002b). The simulated silicification of bacteria – new clues to the modes and timing of bacterial preservation and implications for the search for extraterrestrial microfossils. *Astrobiology*, **2**, 1–26, https://doi.org/10.1089/153110702753621312.

Trauth, S. E., McCallum, M. L. & Cartwright, M. E. (2000). Breeding mortality in the wood frog, *Rana sylvatica* (Anura: Ranidae), from Northcentral Arkansas. *JAAS*, **54**, 154–156.

Trinajstic, K., Marshall, C., Long, J. & Bifield, K. (2007). Exceptional preservation of nerve and muscle tissues in Late Devonian placoderm fish and their evolutionary implications. *Biol. Lett.*, **3**, 197–200, https://doi.org/10.1098/rsbl.2006.0604.

Trümper, S., Rößler, R. & Götze, J. (2018). Deciphering silicification pathways of fossil forests: case studies from the Late Paleozoic of central Europe. *Minerals*, **8**, 1–29, 432, https://doi.org/10.3390/min8100432.

Trümper, S., Götze, J. & Rößler, R. (2020). Siliceous petrifactions in the Permian of the Parnaíba Basin, Central-North Brazil: sedimentary environment and fossilization pathways. 1–45. *In* Iannuzzi, R., Rößler, R. & Kunzmann, L. (eds). *Brazilian paleofloras: from Paleozoic to Holocene*. Springer International Publishing, https://doi.org/10.1007/978-3-319-90913-4_10-1.

Tütken, T. (2014). Isotope compositions (C, O, Sr, Nd) of vertebrate fossils from the Middle Eocene oil shale of Messel, Germany: Implications for their taphonomy and palaeoenvironment. *Palaeogeogr. Palaeoclimatol. Palaeoecol.*, **416**, 92–109, https://doi.org/10.1016/j.palaeo.2014.08.005.

van der Valk, T., Pečnerová, P., Díez-del-Molino, D., Bergström, A., Oppenheimer, J., Hartmann, S., Xenikoudakis, G., Thomas, J. A., Dehasque, M., Sağlıcan, E., Fidan, F. R., Barnes, I., Liu, S., Somel, M., Heintzman, P. D., Nikolskiy, P., Shapiro, B., Skoglund, P., Hofreiter, M., Lister, A. M., Götherström, A. & Dalén, L. (2021). Million-year-old DNA sheds light on the genomic history of mammoths. *Nature*, **591**, 265–269, https://doi.org/10.1038/s41586-021-03224-9.

Varejão, F. G., Warren, L. V., Simões, M. G., Fürsich, F. T., Matos, S. A. & Assine, M. L. (2019). Exceptional preservation of soft tissues by microbial entombment: insights into the taphonomy of the Crato Konservat-Lagerstätte. *Palaios*, **34**, 331–348, https://doi.org/10.2110/palo.2019.041.

Verrell, P. A. & McCabe, N. (1986). Mating balls in the common toad, *Bufo bufo*. *Herpetol. Bull.*, **16**, 28–29, https://www.thebhs.org/publications/the-herpetological-bulletin/issue-number-16-summer-1986/2243-hb016-05/file.

Vinther, J., Briggs, D. E., Prum, R. O. & Saranathan, V. (2008). The colour of fossil feathers. *Biol. Lett.*, **4**, 522–525, https://doi.org/10.1098/rsbl.2008.0302.

Vinther, J. (2015). A guide to the field of palaeo colour. *BioEssays*, **37**, 643–656, https://doi.org/10.1002/bies.201500018.

Vinther, J. (2016). Fossil melanosomes or bacteria? A wealth of findings favours melanosomes. *BioEssays*, **38**, 220–225, https://doi.org/10.1002/bies.201500168.

Vinther, J. (2020). Reconstructing vertebrate paleocolor. *Annu. Rev. Earth Planet. Sci.*, **48**, 345–375, https://doi.org/10.1146/annurev-earth-073019-045641.

Vitt, L. J. & Caldwell, J. P. (2014). Chapter 17 - Frogs. 471–522. *In* Vitt, L. J. & Caldwell, J. P. (eds). *Herpetology, 4th edition*. Academic Press, San Diego, 776 pp., https://doi.org/10.1016/B978-0-12-386919-7.00017-4.

Voigt, E. (1933). Die Übertragung fossiler Wirbeltierleichen auf Zellulose-Filme, eine neue Bergungsmethode für Wirbeltiere aus der Braunkohle. *PalZ*, **15**, 72–78, https://doi.org/10.1007/bf03041642.

Voigt, E. (1934). Die Fische aus der mitteleozänen Braunkohle des Geiseltales mit besonderer Berücksichtigung der Weichteile. *Nova Acta Leopold. NF*, **2**, 21–146.

Voigt, E. (1935). Die Erhaltung von Epithelzellen mit Zellkernen, von Chromatophoren und Corium in fossiler Froschhaut aus der mitteleozänen Braunkohle des Geiseltales. *Nova Acta Leopold. NF*, **3**, 339–360.

Voigt, E. (1937). Weichteile an Fischen, Amphibien und Reptilien aus der eozänen Braunkohle des Geiseltales. *Nova Acta Leopold. NF*, **5**, 116–142.

Voigt, E. (1988). Preservation of soft tissues in the Eocene lignite of the Geiseltal near Halle (Saale). *Cour. Forschungsinst. Senckenberg*, **107**, 325–343.

von Bitter, P. H., Purnell, M. A., Tetreault, D. K. & Stott, C. A. (2007). Eramosa Lagerstätte – exceptionally preserved soft-bodied biotas with shallow-marine shelly and bioturbating organisms (Silurian, Ontario, Canada). *Geology*, **35**, 879–882, https://doi.org/10.1130/G23894A.1.

Wakamatsu, K., Ito, S. & Rees, J. L. (2002). The usefulness of 4-amino-3-hydroxyphenylalanine as a specific marker of pheomelanin. *Pigment Cell Res.*, **15**, 225–232, https://doi.org/10.1034/j.1600-0749.2002.02009.x.

Wake, M. H. & Dickie, R. (1998). Oviduct structure and function and reproductive modes in amphibians. *J. Exp. Zool.*, **282**, 477–506, https://doi.org/10.1002/(SICI)1097-010X(199811/12)282:4/5<477::AID-JEZ6>3.0.CO;2-#.

Wang, Y., Roček, Z. & Dong, L. (2018). A new pelobatoid frog from the lower Eocene of southern China. *Palaeobiodivers. Palaeoenviron.*, **98**, 225–242, https://doi.org/10.1007/s12549-017-0304-1.

Webb, S. M. (2011). The MicroAnalysis Toolkit: X-ray Fluorescence Image Processing Software. *AIP Conference Proceedings*, **1365**, 196–199, https://doi.org/10.1063/1.3625338.

Webster, M., Gaines, R. R. & Hughes, N. C. (2008). Microstratigraphy, trilobite biostratinomy, and depositional environment of the "Lower Cambrian" Ruin Wash Lagerstätte, Pioche Formation, Nevada. *Palaeogeogr. Palaeoclimatol. Palaeoecol.*, **264**, 100–122, https://doi.org/10.1016/j.palaeo.2008.04.002.

Wedmann, S. (2000). Die Insekten der oberoligozänen Fossillagerstätte Enspel (Westerwald, Deutschland): Systematik, Biostratinomie und Paläoökologie. Unpublished PhD thesis, Georg-August-Universität zu Göttingen, 154 pp.

Weigelt, J. (1933). Die Biostratonomie der 1932 auf der Grube Cecilie im mittleren Geiseltal ausgegrabenen Leichenfelder. *Nova Acta Leopold. NF*, **1**, 157–174.

Weigelt, J. (1934). Die Geiseltalgrabungen des Jahres 1933 und die Biostratonomie der Fundschichten. *Nova Acta Leopold. NF*, **1**, 552–660.

Weigelt, J. (1989). Chapter 3: Laws governing positions of recent and fossil vertebrate carcasses. 79–120. *In* Weigelt, J. (ed.) *Recent vertebrate carcasses and their paleobiological implications [Rezente Wirbeltierleichen und ihre palaeobiologische Bedeutung] translated by Judith Schaefer, foreword by Anna K. Behrensmeyer and Catherine Badgley*. University of Chicago Press, 204 pp., https://press.uchicago.edu/ucp/books/book/chicago/R/bo3618802.html.

Whitaker, A. F. & Kimmig, J. (2020). Anthropologically introduced biases in natural history collections, with a case study on the invertebrate paleontology collections from the middle Cambrian Spence Shale Lagerstätte. *Palaeontol. Electron.*, **23**, 1–26, https://palaeo-electronica.org/content/pdfs/1106.pdf.

Wiemann, J., Fabbri, M., Yang, T.-R., Stein, K., Sander, P. M., Norell, M. A. & Briggs, D. E. G. (2018). Fossilization transforms vertebrate hard tissue proteins into N-heterocyclic polymers. *Nat. Commun.*, **9**, 1–9, https://doi.org/10.1038/s41467-018-07013-3.

Wiemann, J. & Briggs, D. E. G. (2022). Raman spectroscopy is a powerful tool in molecular paleobiology: An analytical response to Alleon *et al.* (https://doi.org/10.1002/bies.202000295). *BioEssays*, **44**, 2100070, https://doi.org/10.1002/bies.202100070.

Wilby, P. R., Briggs, D. E. G., Bernier, P. & Gaillard, C. (1996). Role of microbial mats in the fossilization of soft tissues. *Geology*, **24**, 787–790, http://dx.doi.org/10.1130/0091-7613(1996)024<0787:ROMMIT>2.3.CO;2.

Wilde, V. (1995). Die Makroflora aus dem Mitteleozän des Geiseltalgebietes, kurze Übersicht und Vergleiche. *Hallesches Jb. Geowiss. B*, **17**, 121–138.

Wilde, V. & Hellmund, M. (2010). First record of gut contents from a middle Eocene equid from the Geiseltal near Halle (Saale), Sachsen-Anhalt, Central Germany. *Palaeobiodivers. Palaeoenviron.*, **90**, 153–162, https://doi.org/10.1007/s12549-010-0028-ymc.

Wilson, M. V. H. (2001). Chapter 4.3.1 - Taphonomic evidence. 467–470. *In* Briggs, D. E. G. & Crowther, P. R. (eds). *Palaeobiology II*. Blackwell Science Ltd., 608 pp., https://doi.org/10.1002/9780470999295.ch114.

Wings, O., Rabi, M., Schneider, J. W., Schwermann, L., Sun, G., Zhou, C.-F. & Joyce, W. G. (2012). An enormous Jurassic turtle bone bed from the Turpan Basin of Xinjiang, China. *Naturwissenschaften*, **99**, 925–935, https://doi.org/10.1007/s00114-012-0974-5.

Wogelius, R. A., Manning, P. L., Barden, H. E., Edwards, N. P., Webb, S. M., Sellers, W. I., Taylor, K. G., Larson, P. L., Dodson, P., You, H., Da-qing, L. & Bergmann, U. (2011). Trace metals as biomarkers for eumelanin pigment in the fossil record. *Science*, **333**, 1622–1626, https://doi.org/10.1126/science.1205748.

Wolnicka-Glubisz, A., Pecio, A., Podkowa, D., Kolodziejczyk, L. M. & Plonka, P. M. (2012). Pheomelanin in the skin of *Hymenochirus boettgeri* (Amphibia: Anura: Pipidae). *Exp. Dermatol.*, **21**, 537–540, https://doi.org/10.1111/j.1600-0625.2012.01511.x.

Wuttke, M. (1983a). Aktuopaläontologische Studien über den Zerfall von Wirbeltieren. Teil I: Anura. *Senckenbergiana Lethaea*, **64**, 529–560.

Wuttke, M. (1983b). Weichteilerhaltung durch lithifizierte Mikroorganismen bei mitteleozänen Vertebraten aus den Ölschiefern der 'Grube Messel' bei Darmstadt. *Senckenbergiana Lethaea*, **64**, 509–527.

Wuttke, M. (1988). Amphibien am Messelsee - Salamander und Frösche. 95–99. *In* Keller, T., Schaal, S., Schaal, S. & Ziegler, W. (eds). *Messel - Ein Schaufenster in die Geschichte der Erde und des Lebens, 2nd edition*. Verlag Waldemar Kramer, Frankfurt am Main, 315 pp.

Wuttke, M. & Poschmann, M. (2010). First finding of fish in the diet of a water-dwelling extinct frog *Palaeobatrachus* from the Upper Oligocene Fossil-Lagerstätte Enspel (Westerwald Mountains, Western Germany). *Palaeobiodivers. Palaeoenviron.*, **90**, 59–64, https://doi.org/10.1007/s12549-009-0019-z.

Wuttke, M., Přikryl, T., Ratnikov, V. Y., Dvořák, Z. & Roček, Z. (2012). Generic diversity and distributional dynamics of the Palaeobatrachidae (Amphibia: Anura). *Palaeobiodivers. Palaeoenviron.*, **92**, 367–395, https://doi.org/10.1007/s12549-012-0071-y.

Wuttke, M. & Reisdorf, A. G. (2012). Taphonomic processes in terrestrial and marine environments. *Palaeobiodivers. Palaeoenviron.*, **92**, 1–3, https://doi.org/10.1007/s12549-012-0070-z.

Wuttke, M. (2018). Chapter 9 Amphibians in Messel - in the Water and on Land. 113–119. *In* Smith, K. T., Schaal, S. F. & Habersetzer, J. (eds). *Messel - An Ancient Greenhouse Ecosystem, 1st edition*. Senckenberg Gesellschaft für Naturfoschung, Frankfurt am Main, Schweizerbart Science Publishers, Stuttgart, Germany, 355 pp., https://www.schweizerbart.de/publications/detail/isbn/9783510614110/Senckenberg_Buch_Nr_80_MESSEL_An_Anc .

Xiao, M., Shawkey, M. D. & Dhinojwala, A. (2020). Bioinspired melanin-based optically active materials. *Adv. Opt. Mater.*, **8**, 1–15, 2000932, https://doi.org/10.1002/adom.202000932.

Xing, L., McKellar, R. C., Xu, X., Li, G., Bai, M., Persons, W. S., Miyashita, T., Benton, M. J., Zhang, J. & Wolfe, A. P. (2016). A feathered dinosaur tail with primitive plumage trapped in mid-Cretaceous amber. *Curr. Biol.*, **26**, 3352–3360, https://doi.org/10.1016/j.cub.2016.10.008.

Xu, X., Zheng, X. & You, H. (2009). A new feather type in a nonavian theropod and the early evolution of feathers. *Proc. Natl. Acad. Sci.*, **106**, 832–834, https://doi.org/10.1073/pnas.0810055106.

Yamaguchi, Y. & Hearing, V. J. (2014). Melanocytes and their diseases. *Cold Spring Harb. Perspect. Med.*, **4**, 1–18, https://doi.org/10.1101/cshperspect.a017046.

Yang, S.-Y., Jiang, S.-Y., Mao, Q., Chen, Z.-Y., Rao, C., Li, X.-L., Li, W.-C., Yang, W.-Q., He, P.-L. & Li, X. (2022). Electron probe microanalysis in geosciences: analytical procedures and recent advances. *Atom. Spectrosc.*, **43**, 186–200, http://dx.doi.org/10.46770/AS.2021.912.

Yang, Z., Jiang, B., McNamara, M. E., Kearns, S. L., Pittman, M., Kaye, T. G., Orr, P. J., Xu, X. & Benton, M. J. (2019). Pterosaur integumentary structures with complex feather-like branching. *Nat. Ecol. Evol.*, **3**, 24–30, https://doi.org/10.1038/s41559-018-0728-7.

Yang, Z., Jiang, B., Xu, J. & McNamara, M. E. (2024). Cellular structure of dinosaur scales reveals retention of reptile-type skin during the evolutionary transition to feathers. *Nat. Commun.*, **15**, 1–12, 4063, https://doi.org/10.1038/s41467-024-48400-3.

Yasutomi, M. (1987). Migration of epidermal melanophores to the dermis through the basement membrane during metamorphosis in the frog, *Rana japonica*. *Pigment Cell Res.*, **1**, 181–187, https://doi.org/10.1111/j.1600-0749.1987.tb00411.x.

Yesares-García, J. & Aguirre, J. (2004). Quantitative taphonomic analysis and taphofacies in lower Pliocene temperate carbonate–siliciclastic mixed platform deposits (Almería-Níjar basin, SE Spain). *Palaeogeogr. Palaeoclimatol. Palaeoecol.*, **207**, 83–103, https://doi.org/10.1016/j.palaeo.2004.02.002.

Yovanovich, C. A. M., Koskela, S. M., Nevala, N., Kondrashev, S. L., Kelber, A. & Donner, K. (2017). The dual rod system of amphibians supports colour discrimination at the absolute visual threshold. *Phil. Trans. R. Soc. Lond. B*, **372**, 1–10, 20160066, http://dx.doi.org/10.1098/rstb.2016.0066.

Yovanovich, C. A. M., Grant, T. & Kelber, A. (2019). Differences in ocular media transmittance in classical frog and toad model species and its impact on visual sensitivity. *J. Exp. Biol.*, **222**, 1–5, https://doi.org/10.1242/jeb.204271.

Zanger, K., Schwinger, G. & Greven, H. (1995). Mechanical properties of the skin of *Rana esculenta* (Anura, Amphibia) with some notes on structures related to them. *Ann. Anat.*, **177**, 509–514, https://doi.org/10.1016/S0940-9602(11)80082-8.

Zhang, F., Kearns, S. L., Orr, P. J., Benton, M. J., Zhou, Z., Johnson, D., Xu, X. & Wang, X. (2010). Fossilized melanosomes and the colour of Cretaceous dinosaurs and birds. *Nature*, **463**, 1075–1078, https://doi.org/10.1038/nature08740.

Zhang, X. & Briggs, D. E. G. (2007). The nature and significance of the appendages of *Opabinia* from the Middle Cambrian Burgess Shale. *Lethaia*, **40**, 161–173, https://doi.org/10.1111/j.1502-3931.2007.00013.x.

Zuasti, A., Jiménez-Cervantes, C., García-Borrón, J. C. & Ferrer, C. (1998). The melanogenic system of *Xenopus laevis*. *Arch. Histol. Cytol.*, **61**, 305–316, https://doi.org/10.1679/aohc.61.305.

Appendix

Appendix I – Lists

Sample list: list of specimens and samples that were analysed in this thesis

Sample no.	Specimen no.	Sample type	Analysis	Storage	Remarks	Melanosomes	Order
6698-B1	GMH CeIII-6698-1932 (Pelobatidae)	soft tissue	SEM/Raman	Al stub	-	None	Anura
6698-B2		soft tissue	SEM/EDS	Al stub	-	Yes	Anura
6698-B3a		soft tissue	SEM	Al stub	-	None	Anura
6698-B3b		soft tissue	SEM	Al stub	-	None	Anura
6698-B4		soft tissue	SEM/EDS/Raman	Al stub	-	Yes	Anura
6698-B5a		soft tissue	SEM/EDS	Al stub	-	Yes	Anura
6698-B5b		soft tissue	SEM/EDS	Al stub	-	Yes	Anura
6698-B6		soft tissue	SEM/EDS	Al stub	Au sputter-coated	Yes	Anura
6698-B7		soft tissue	SEM	Al stub	-	None	Anura
6698-B8		soft tissue	SEM/EDS	Al stub	-	Yes	Anura
6698-B9		soft tissue/bone	SEM/EDS/Raman	Al stub	-	None	Anura
4983-D1	GMH CeIII-4983-1932 (Anura indet.)	soft tissue	SEM	Al stub	-	Yes	Anura
4983-D2		soft tissue	SEM	Al stub	-	None	Anura
4983-D3a		soft tissue	SEM	Al stub	-	Yes	Anura
4983-D3a1		soft tissue	UMT	plastic vial	in resin	Yes	Anura
4983-D3a1		soft tissue	UMT	glass slide	9 UMT slices	None	Anura
4983-D3b		soft tissue	SEM	Al stub	-	Yes	Anura
4983-D3b1		soft tissue	UMT	plastic vial	in resin	None	Anura
4983-D3b1		soft tissue	UMT	glass slide	6 UMT slices	None	Anura
4983-D4		soft tissue	SEM	Al stub	-	Yes	Anura
4983-D5		soft tissue	SEM	Al stub	fungi hyphae	None	Anura
4983-D6		sediment	SEM	Al stub	fungi hyphae	None	Anura
4936-a-AI-1	GMH CeIII-4936a-1932 (Pelobatidae)	soft tissue	SEM/Raman	Al stub	formerly 4936(1)	None	Anura
4936-a-AI-2		soft tissue	SEM/Raman	Al stub	formerly 4936(1)	Yes	Anura
4936-a-AI-3		soft tissue	SEM	Al stub	formerly 4936(1)	Yes	Anura
4936-a-AI-4a		soft tissue	SEM	Al stub	formerly 4936(1)	Yes	Anura
4936-a-AI-4b		soft tissue	SEM	Al stub	formerly 4936(1)	Yes	Anura
4936-a-AI-4c		soft tissue	SEM	Al stub	formerly 4936(1)	Yes	Anura
4936-a-AI-4d		soft tissue	SEM	Al stub	formerly 4936(1)	None	Anura
4936-a-AI-4e		soft tissue	SEM	Al stub	formerly 4936(1)	Yes	Anura
4936-a-AI-7		soft tissue	SEM	Al stub	formerly 4936(1)	None	Anura
4936-a-AI-8		soft tissue	SEM	Al stub	formerly 4936(1)	None	Anura
4936-a-AI-9		soft tissue	SEM	Al stub	formerly 4936(1)	None	Anura
4936-a-AI-10		resin	SEM	Al stub	formerly 4936(1)	None	Anura
4936-a-AI-11		sediment	SEM	Al stub	formerly 4936(1)	None	Anura
4936-a-AI-12		sediment	SEM	Al stub	formerly 4936(1)	None	Anura
4936-a-A1		soft tissue	SEM/EDS/EPMA/FTIR/Raman	Al stub	in resin, formerly 4936(1)	Yes	Anura
4936-a-A2		soft tissue	SEM/UMT	Al stub	in resin, formerly 4936(1)	Yes	Anura
4936-a-A3		soft tissue	SEM/EDS	Al stub	formerly 4936(1)	Yes	Anura
4936-a-A4		soft tissue	SEM	Al stub	formerly 4936(1)	None	Anura
4936-a-A5		soft tissue	SEM	Al stub	formerly 4936(1)	None	Anura
4936-a-A6		soft tissue	SEM	Al stub	formerly 4936(1)	None	Anura
4936-a-A7		soft tissue	SEM	Al stub	formerly 4936(1)	None	Anura
4936-a-A8		sediment	SEM	Al stub	formerly 4936(1)	None	Anura
4967-B1	GMH CeIII-4967-1932 (Pelobatidae)	soft tissue	SEM/EDS/Raman	Al stub	Au sputter-coated	None	Anura
4967-B2		sediment	SEM	Al stub	Au sputter-coated	None	Anura
4967-B3a		soft tissue	SEM	Al stub	Au sputter-coated	None	Anura
4967-B3b		soft tissue	SEM/EDS	Al stub	Au sputter-coated	Yes	Anura
4967-B3c		soft tissue	SEM/EDS	Al stub	Au sputter-coated	None	Anura
4967-B3d		soft tissue	SEM	Al stub	Au sputter-coated	None	Anura
4967-B3e		soft tissue	SEM/EDS	Al stub	Au sputter-coated	Yes	Anura
4967-B4		soft tissue	SEM/EDS	Al stub	Au sputter-coated	Yes	Anura
4967-B5		resin	SEM/EDS	Al stub	Au sputter-coated	None	Anura
4967-B6		soft tissue	SEM/EDS/Raman	Al stub	Au sputter-coated	Yes	Anura
6743-C1	GMH CeIII-6743-1932 (Pelobatidae)	soft tissue	SEM	Al stub	-	None	Anura
6743-C2		soft tissue	SEM	Al stub	-	None	Anura
6743-C3		soft tissue	SEM	Al stub	-	None	Anura
6743-C4a		soft tissue	SEM	Al stub	-	Yes	Anura
6743-C4b		soft tissue	SEM	Al stub	-	None	Anura
6743-C5		sediment	SEM	Al stub	-	None	Anura
6743-C6		sediment	SEM	Al stub	-	None	Anura
6743-C7		bone	SEM	Al stub	-	None	Anura
6743-C8		soft tissue	SEM/EDS	Al stub	fungi hyphae	Yes	Anura

6743-C8a	GMH CeIII-6743-1932 (Pelobatidae)	soft tissue	UMT	plastic vial	in resin	Yes	Anura
6743-C8a		soft tissue	UMT	glass slide	5 UMT slices	Yes	Anura
6743-C9		soft tissue	SEM	Al stub	-	Yes	Anura
XXXV-11a-C1a	GMH XXXV-11A-1970 (Anura indet.)	soft tissue	SEM	Al stub	-	Yes	Anura
XXXV-11a-C1b		soft tissue	SEM	Al stub	-	None	Anura
XXXV-11a-C1c		soft tissue	SEM	Al stub	-	None	Anura
XXXV-11a-C2a		soft tissue	SEM	Al stub	-	None	Anura
XXXV-11a-C2b		soft tissue	SEM	Al stub	-	Yes	Anura
XXXV-11a-C2b1		soft tissue	UMT	plastic vial	in resin	Yes	Anura
XXXV-11a-C3		soft tissue	SEM	Al stub	-	None	Anura
XXXV-11a-C4		soft tissue	SEM	Al stub	-	Yes	Anura
XXXV-11a-D		sediment	SEM	Al stub	pieces taken for resin embedding	None	Anura
4967	GMH CeIII-4967-1932 (Pelobatidae)	full specimen	SRS XRF	slab	full specimen	Yes	Anura
XXXV-11_polished_01	GMH XXXV-11A-1970	sediment	SEM/EDS	resin on Al stub	broken piece from Al stub sample	None	Anura
XXXV-11_polished_02	GMH XXXV-11A-1970	sediment	SEM/EDS	resin on Al stub	broken piece from Al stub sample	None	Anura
3012-s1	GMH CeV-3012-1934	sediment	XRD	glass vial	-	None	Anura
3012-s1-J		sediment	SEM	Al stub	right side of stub	None	Anura
3240-s1	GMH LeoIII-3240-1934	sediment	XRD	glass vial	-	None	Anura
3240-s1-J		sediment	SEM	Al stub	left side of stub	None	Anura
3477B-s1	GMH LeoV-3477B-1934	sediment	XRD	glass vial	-	None	Anura
3477B-s1-L		sediment	SEM	Al stub	right side of stub	None	Anura
4947-s1	GMH CeI-4947-1930	sediment	XRD	glass vial	-	None	Anura
4947-s1-K		sediment	SEM	Al stub	left side of stub	None	Anura
4947-s2		sediment	XRD	glass vial	-	None	Anura
4947-s2-K		sediment	SEM	Al stub	right side of stub	None	Anura
4971-s1	GMH CeIV-4971-1933	sediment	XRD	glass vial	-	None	Anura
4971-s1 -I		sediment	SEM	Al stub	left side of stub	None	Anura
4971-s2		sediment	XRD	glass vial	-	None	Anura
4971-s2-I		sediment	SEM	Al stub	right side of stub	None	Anura
4976A-s1	GMH CeVI-4976A-1934	sediment	XRD	glass vial	-	None	Anura
4976A-s1-L		sediment	SEM	Al stub	left side of stub	None	Anura
4990-s1	GMH CeIII-4990-1932	sediment	XRD	glass vial	-	None	Anura
4990-s1-H		sediment	SEM	Al stub	left side of stub	None	Anura
4990-s2		sediment	XRD	glass vial	-	None	Anura
4990-s2-H		sediment	SEM	Al stub	right side of stub	None	Anura
6706-s1	GMH CeII-6706-1930	sediment	XRD	glass vial	-	None	Anura
6706-s1-F		sediment	SEM/EDS	Al stub	right side of stub, gold-coated	None	Anura
6706-s2		sediment	XRD	glass vial	-	None	Anura
6706-s2-F		sediment	SEM	Al stub	left side of stub, gold-coated	None	Anura
6740-s1	GMH CeIII-6740-1933	sediment	XRD	glass vial	-	None	Anura
6740-s1-G		sediment	SEM/EDS	Al stub	left side of stub	None	Anura
6740-s2		sediment	XRD	glass vial	-	None	Anura
6740-s2-G		sediment	SEM/EDS	Al stub	right side of stub	None	Anura
XXXV-11A-s1	GMH XXXV-11A-1970	sediment	XRD	glass vial	-	None	Anura
XXXV-11A-s1-M		sediment	SEM/EDS	Al stub	right side of stub	None	Anura
1305-s1	GMH CeIII-1305-1933	sediment	XRD	glass vial	preparation artefact	None	Anura
6238-s1	GMH CeIII-6238-1931	sediment	XRD	glass vial	-	None	Fish
6238-s1-M1		sediment	SEM/EDS	Al stub	left side of stub	None	Fish
y-72-s1	GMH y-72	sediment	XRD	glass vial	-	None	Fish
y-72-s1-N		sediment	SEM/EDS	Al stub	left side of stub	None	Fish
y-72-s2		sediment	XRD	glass vial	-	None	Fish
y-72-s2-N		sediment	SEM	Al stub	right side of stub	None	Fish
1275-s1	GMH 1275	resin	N/A	glass vial	not in database; drawer 27/1 left	None	Fish
4917-s1	GMH CeIII-4917-1932	resin	N/A	glass vial	-	None	Fish
4947-s1	GMH CeI-4947-1930	paraffinum wax	N/A	glass vial	-	None	Anura

Geiseltal Collection specimen requests: Geiseltal specimens located in institutions other than the Geiseltal Museum

Museum Collection	Location	Country	Contact person	Geiseltal specimens	Remarks
BASEL: The Natural History Museum Basel (NMB)	Basel	Switzerland	Loic Costeur	Yes	several specimens, birds only, cast of mammal jaws (Anthracobunodon [Amphirhagatherium], Messelobunodon)
COBURG: Naturkunde-Museum Coburg - Palaeontological Collections	Coburg	Germany	Eckhard Mönnig	Yes	several ambers
DESSAU-ROSSLAU: Museum of Natural History and Prehistory—Palaeontological Collection	Dessau-Rosslau	Germany	Angelika Hesse	Yes	several specimens, but repatriated as long-term loan to Geiseltal Collection, MNVD-G 11470 *Palaeopelobates geiseltalensis* , MNVD-G 11471 snake, MNVD-G 11472 *Borkenia germanica* , MNVD-G 11473 *Geiselemys ptychogastroides* , MNVD-G 11474 *Lophiodon* sp. rib, MNVD-G 11475 Spermatophyta ind. leaves, MNVD-G 11476 Spermatophyta ind. leaf, MNVD-G 11477 Spermatophyta ind. leaves, MNVD-G 15328 Actinopterygii ind without head, MNVD-G 25394 Actinopterygii ind. 2 teeth, MNVD-G 25395 Crocodylia ind. 2 teeth, MNVD-G 25396 Crocodylia ind. tooth, MNVD-G 25397 Crocodylia ind. dorsal plate, MNVD-G 25398 Actinopterygii ind. tooth, MNVD-G 25399 Vertebrata ind. Bone fragment, MNVD-G 25400 Vertebrata ind. bone from foot
DRESDEN: Senckenberg Naturhistorische Sammlungen Dresden (SNSD), Museum für Mineralogie und Geologie	Dresden	Germany	Kahlke, John-Albrecht Keiler, Peter Königshof, Ottmar Kullmer	Yes	palaeobotany: few specimens from former collection (1980's) of D. H. Mai (MfN Berlin, deceased 2013); 2 anurans in gypsum = AnT 175 (until 1999 in Collection Zschiedrich) and NAT 172 in lacquer (bought from Krantz company)
GÖTTINGEN: The Palaeontological Collections of the Geoscience Museum at the Georg-August University in Göttingen	Göttingen	Germany	Alexander Gehler; Mike Reich; Joachim Reitner	Yes	sediment samples
HALLE: The Geiseltal Collection of Martin Luther University, Halle-Wittenberg	Halle	Germany	Frank D. Steinheimer; Roberto Rozzi (formerly Oliver Wings)	Yes	Geiseltal Collection, ca. 50000 specimens
KREFELD: Palaeobotanical and Palynological Collection at the Geological Survey North Rhine-Westphalia	Krefeld	Germany	Christoph Hartkopf-Fröder	Yes	palynology: specimens from the pit Cecilie, used for publication from Potonié (1931, 1934); lignite sample: pit Michel, Geiseltal, oligoc. [sic] borown coal, sender: Geol. Inst. Bonn, 1949, 1 sample, 8 grams
PRAGUE: National Museum Prague (Národní muzeum), ?Spinars Collection	Prague	Czech Republic	Jiří Frank	yes	several plant fossils from Geiseltal, most common species; no vertebrates
BAMBERG: The Palaeontological Collection at the Museum of Natural History in Bamberg (NKMB)	Bamberg	Germany	Matthias Mäuser	No	n/a
BERN: The Natural History Museum — An Institution of the Burgergemeinde of Bern	Bern	Austria	Ursula Menkveld-Gfeller	No	n/a
BIELEFELD: Palaeontological Collections of Small Museums: The Example of Bielefeld (North Rhine Westphalia, Germany)	Bielefeld	Germany	Mark Keiter	No	n/a
BILZINGSLEBEN: The Bilzingsleben Collection	Bilzingsleben	Germany	Clemens Pasda	No	n/a
BREMEN: The Palaeontological Research Collection of the Geosciences Collection of the University of Bremen	Bremen	Germany	Jens Lehmann	No	n/a
CHEMNITZ: Natural history museum in Chemnitz, Palaeontological Collection	Chemnitz	Germany	Ronny Rößler	No	n/a
COTTBUS: Museum of Natural History and Environment in Cottbus	Cottbus	Germany	Rolf Striegler; Ursula Striegler	No	n/a
DARMSTADT: The Palaeontological Collections of Hessisches Landesmuseum Darmstadt	Darmstadt	Germany	Gabriele Gruber, Oliver Sandrock, and Torsten Wappler	No	n/a
DORTMUND: Museum für Naturkunde der Stadt Dortmund	Dortmund	Germany	Jan-Michael Ilger; Oliver Adrian	No	n/a
DOTTERNHAUSEN: The Jurassic World of the Swabian Alb Region (South Germany): The Fossil Collection of the Werkforum and Fossil Museum of Dotternhausen	Dotternhausen	Germany	Annette Schmid-Röhl	No	n/a
FREIBERG: Technical University Bergakademie Freiberg, Geological Institute, Palaeontological Collection	Freiberg	Germany	Birgit Gaitzsch	No	n/a
EICHSTÄTT: The Jura-Museum Eichstätt	Eichstätt	Germany	Andreas Hecker	No	n/a
GÖRLITZ: Senckenberg Museum für Naturkunde Görlitz	Görlitz	Germany	Stephan Schaal, Krister Smith, Mónica M. Sólorzano Kraemer	No	n/a

WEIMAR: Senckenberg Forschungsstation für Quartärpaläontologie	Weimar	Germany	Martina Stebich, Olaf Tietz, and Markus Wilmsen	No	n/a
FRICK: Late Triassic Basal Sauropodomorph and Theropod Dinosaurs at the Sauriermuseum Frick, Switzerland	n/a	Switzerland	Andrea B. Oettl-Rieser; Marion Zahner	No	n/a
GOTHA: Museum der Natur, Stiftung Schloss Friedenstein Gotha	Gotha	Germany	Tom Hübner; Carsten Eckert	No	n/a
Hessisches Landesamt für Naturschutz, Umwelt und Geologie	Wiesbaden	Germany	Gudrun Radtke	No	n/a
HILDESHEIM: Roemer- and Pelizaeus-Museum	Hildesheim	Germany	Jürgen Vespermann, Antje Spiekermann	No	n/a
INGELFINGEN: Muschelkalkmuseum Hagdorn Stadt Ingelfingen	Ingelfingen	Germany	Hans Hagdorn	No	n/a
JENA: The Palaeontological Collections at the Phyletisches Museum in Jena	Jena	Germany	Dietrich von Knorre; Rolf G. Beutel; Stefan Arndt; Dr. Manuela	No	n/a
MAGDEBURG: Museum of Natural History Magdeburg	Magdeburg	Germany	Michael Buchwitz	No	n/a
MAUER: The Locality of Mauer and its Virtual Collection of Middle Pleistocene Mammal Fossils	Mauer	Germany	H. Dieter Schreiber, Kristina Eck, Volker Liebig	No	n/a
KÖLN: Geological Collections of the University of Cologne (GCC) (Geological and Palaeontological Collections of the Institute of Geology and Mineralogy, University of Cologne)	Cologne	Germany	Michael R. W. Amler; Hans-Georg Herbig	No	n/a
LINZ: The Palaeontological Collection of the Upper Austrian State Museum, Linz	Linz	Austria	Björn Berning	No	n/a
LÜBECK: Museum of Nature and Environment, Palaeontological Collections	Lübeck	Germany	Susanne Füting	No	n/a
MAINZ: Palaeontological Collections of the University of Mainz (Geoscientific Collections)	Mainz	Germany	Kirsten I. Grimm; Bernd R. Schöne	No	n/a
MANNHEIM: The Reiss-Engelhorn-Museen	Mannheim	Germany	Doris Döppes; Wilfried Rosendahl	No	n/a
MÜNSTER: Geomuseum of the WWU	Münster	Germany	Markus Bertling	No	n/a
SCHIFFWEILER (Landsweiler-Reden): Center for Biological Documentation (Zentrum für Biodokumention - ZfBS)	Schiffweiler	Germany	Edgar Müller	No	n/a
SCHLEUSINGEN: Naturhistorisches Museum Schloss Bertholdsburg Schleusingen (Thuringia, Germany) - Home of Permian and Triassic Fossils	Schleusingen	Germany	Ralf Werneburg	No	n/a
SIEGSDORF: The Siegsdorf Natural History and Mammoth Museum	Siegsdorf	Germany	Robert Darga	No	n/a
ST. GALLEN: Naturmuseum St. Gallen	St. Gallen	Switzerland	Matthias Meier	No	n/a
THALLICHTENBERG: POLLICHIA Geoscience Collections at the Urweltmuseum GEOSKOP, Thallichtenberg and Bad Dürkheim (Germany)	Thallichtenberg#	Germany	Sebastian Voigt; Jan Fischer	No	n/a
TÜBINGEN: The Palaeontologial Collection of Tübingen	Tübingen	Germany	Ingmar Werneburg; Madelaine Böhme; Thomas Lechner	No	n/a
ZURICH: The Geological-Palaeontological Collection at ETH Zurich	Zurich	Switzerland	Andreas D. Mueller, Rodney Eastwood, Stefan Ungricht, Iwan Stoessel	No	n/a
ZURICH: Palaeontological Museum of the University of Zurich	Zurich	Switzerland	Christian Klug; Beat Scheffold	No	?Cretaceous bryozoe from Geiseltal
KARLSRUHE: State Museum of Natural History Karlsruhe: Institute of Life and Earth Sciences	Karlsruhe	Germany	Julien Kimmig (formerly Eberhard Frey; H. Dieter Schreiber)	No	there may be Geiseltal specimens in-between Messel specimens
BERLIN: The Palaeontological Collections of the Museum für Naturkunde Berlin	Berlin	Germany	Florian Witzmann	No	anuran sepcimens from Rott, Stösschen, Orsberg, Markvartice (formerly Markersdorf), Libros / Teruel, Westeregeln, Seifhennersdorf and a lot of pleistocene specimens e.g. from Grabschütz, Burgtonna and Pisede

Open collection requests or collections to consider	Location	Country	Contact Person	Geiseltal specimens	Remarks
MÜNCHEN: The Fossil Collections of the Bavarian State Collections at Munich	Munich	Germany	Mike Reich; Gert Wörheide	?	potential Geiseltal specimens from University Würzburg Geiseltal now in Munich collections
MAINZ: Palaeontological Collections of the Landesamt für Geologie Und Bergbau Rheinland-Pfalz (Rhineland-Palatinate, Germany)	Mainz	Germany	Jürgen Gad; Winfried Kuhn; Peter Schäfer	?	n/a
BERLIN: The Geoscientific Collections of the Federal Institute for Geosciences and Natural Resources and the State Authority for Mining, Energy and Geology in Hannover and Berlin	Berlin	Germany	?	?	n/a
HANNOVER: The Geoscientific Collections of the Federal Institute for Geosciences and Natural Resources and the State Authority for Mining, Energy and Geology in Hannover and Berlin	Hannover	Germany	Angela Ehling; Carmen Heunisch; Thomas Wiese; Jochen Erbacher	?	n/a
WIEN: The Palaeontological Collections of the Natural History Museum Vienna	Vienna	Austria	Mathias Harzhauser; Andreas Kroh	?	n/a
BONN: Goldfuß-Museum	Bonn	Germany	Georg Heumann, Martin Sander	?	n/a
BRAUNSCHWEIG: The Palaeontological Collection of the State Museum of Natural History (SNHM) in Braunschweig, Germany	Braunschweig	Germany	Ralf Kosma	?	n/a
ERLANGEN: The Erlangen Palaeobiology Collections	Erlangen	Germany	Michael Heinze	?	n/a
ESSEN: Ruhr Museum—Geological Collection	Essen	Germany	Ulrike Stottrop	?	n/a
FRANKFURT: Palaeontological collections of the Senckenberg Gesellschaft für Naturforschung (includes Marburg Collection)	Frankfurt	Germany	Michael Wuttke, D. Uhl	?	includes Marburg vertebrate collection
HALLE: The Palaeontological Collection of the Martin Luther University Halle-Wittenberg in Halle (Saale)	Halle	Germany	Norbert Hauschke	?	n/a
HAMBURG: Palaeontological Collections of the Center of Natural History, Universität Hamburg	Hamburg	Germany	Ulrich Kotthoff	?	n/a
HANNOVER: Niedersächsisches Landesmuseum Hannover—Lower Saxony State Museum Hannover	Hannover	Germany	Annette Richter	?	n/a
HOLZMADEN: Prehistoric Museum Hauff - A Fossil Museum Since 4 Generations (Urweltmuseum Hauff)	Holzmaden	Germany	Rolf Bernhard Hauff	?	n/a
NIERSTEIN: Paläontologisches Museum Nierstein	Nierstein	Germany	Lutz Kaecke	?	n/a
STUTTGART: Staatliches Museum für Naturkunde Stuttgart (SMNS)	Stuttgart	Germany	Rainer Schoch	?	n/a
WIESBADEN: Museum Wiesbaden, Natural History Collections	Wiesbaden	Germany	Fritz Geller-Grimm	?	n/a

Appendix II – Supplementary papers

Supplementary paper 1: Die eozänen Froschlurche der Geiseltal-Sammlung, Interdisziplinäre Zugänge zum Rätsel der Fossilerhaltung

This paper informs on historical information on the scientific excavations in the Geiseltal (central Germany) and on the formation of the Geiseltal Collection, the depository that holds the vast majority of the excavated specimens. The paper also provides information on the materials, approaches and techniques that were used to investigate the fossilised anurans from the Geiseltal Lagerstätte. The paper highlights the usefulness of historic fossil collections and the benefits of research activity for the Geiseltal Collection (e.g., the concurrent registration and digitalisation of specimens). The publication resulted from the workshop "Junges Forum 2020" at the Zentralmagazin Naturwissenschaftlicher Sammlungen (ZNS; Natural Sciences Collections) at the Martin-Luther-University Halle-Wittenberg in Halle (Saale), Germany (14.10.–15.10.2020). The peer-reviewed content of the paper contributes to the overall topic of the workshop "Eine Frage der Perspektive. Objekte als Vermittler von Wissenschaft" (A matter of perspective. Objects as transmitters of science). The paper is co-written in German language by two authors.

Falk, D. & Stache, M. (2021). Die eozänen Froschlurche der Geiseltal-Sammlung, Interdisziplinäre Zugänge zum Rätsel der Fossilerhaltung. 39–47. *In* Seidl, E., Steinheimer, F. & Weber, C. (eds). *Eine Frage der Perspektive, Objekte als Vermittler von Wissenschaft*. Gesellschaft für Universitätssammlungen e.V., Humboldt-Universität zu Berlin, 127 pp. http://dx.doi.org/10.18452/23915.

Candidate contribution to the study. DF contributed to the design of the study and performed a literature review on the Geiseltal anurans. MS provided historical information, access to the Geiseltal Collection and access to the Geiseltal Collection data base. DF contacted 54 international institutions for missing Geiseltal Collection specimens, in particular fossil anurans. MS registered the studied anuran specimens in the collection data base with assistance from DF. DF wrote the first draft of the paper, produced the figures and revised subsequent drafts in line with comments from MS. Following peer review, DF co-drafted the revisions to the paper with MS in accordance with comments from two reviewers.

Abstract (translated into English by DF). The Geiseltal Collection of the Natural Sciences Collections at the Martin-Luther-University Halle-Wittenberg represents a valuable geoscientific research resource and has been registered as nationally valuable cultural heritage since 2011. The fossils offer a detailed insight into the Eocene flora and fauna from 42.5–47.5 million years ago and into the geological deposits of a coastal swamp landscape. In the coal-dominated sediments of the Geiseltal (Saxony-Anhalt), commercial coal mining was combined with scientific excavations from the mid-1920s to the end of the 20th century. The Geiseltal Collection, which has been stored in Halle (Saale) for almost 100 years, combines scientific potential from a geoscientific, biological, chemical, museological and historical perspective. Fossil vertebrates are being examined as part of the German-Irish dissertation project "Taphonomy of the Eocene Geiseltal Konservat-Lagerstätte, Germany". In this article we present research approaches to better understand the extraordinary preservation of fossils. As an example, 180 anurans specimens were examined for their orientation in the sediment as well as for their skeletal completeness and articulation. Further investigations will involve chemical analyses of samples from potential soft tissue remains that are associated with the anurans and the sediment layers that embed the frogs. This article provides a historical overview of the Geiseltal Collection and presents the aforementioned research methods, preliminary results and the advantages that are associated with object-based research for the collection.

Die eozänen Froschlurche der Geiseltal-Sammlung: Interdisziplinäre Zugänge zum Rätsel der Fossilerhaltung

DANIEL FALK UND MICHAEL STACHE

Abstract

Die Geiseltal-Sammlung des Zentralmagazins Naturwissenschaftlicher Sammlungen (ZNS) der Martin-Luther-Universität Halle-Wittenberg stellt eine wertvolle geowissenschaftliche Forschungsressource dar und ist seit 2011 als national wertvolles Kulturgut eingetragen. Die Fossilien bieten einen detaillierten Einblick in die eozäne Tier- und Pflanzenwelt vor 42,5 bis 47,5 Millionen Jahren, aber auch auf den geologischen Ablagerungsraum einer küstennahen Sumpflandschaft. In den kohledominierten Sedimenten des Geiseltals (Sachsen-Anhalt) wurde von Mitte der 1920er Jahre bis zum Ende des 20. Jahrhunderts kommerzieller Braunkohlebergbau mit wissenschaftlichen Ausgrabungen kombiniert. Die seit fast 100 Jahren in Halle (Saale) gelagerte Geiseltal-Sammlung verbindet wissenschaftliches Potential aus geowissenschaftlicher, biologischer, chemischer, museologischer und historischer Sicht. Im Rahmen des deutsch-irischen Dissertationsprojektes „Taphonomy of the Eocene Geiseltal Konservat-Lagerstätte, Germany" werden die fossilen Wirbeltiere untersucht. In dem vorliegenden Beitrag präsentieren wir Forschungsansätze, um die außergewöhnliche Erhaltung der Fossilien besser zu verstehen. Es wurden hierfür exemplarisch 180 Anuren (Froschlurche) auf ihre Ausrichtung im Sediment sowie auf Skelettvollständigkeit und -artikulation untersucht. In weiteren Untersuchungen ist die chemische Analyse der beprobten, potentiellen Weichteilüberreste und der die Froschlurche einbettenden Sedimentschichten vorgesehen. Dieser Artikel gibt einen historischen Überblick zur Geiseltal-Sammlung und stellt die genannten Untersuchungsmethoden, vorläufige Resultate und die damit einhergehenden Vorzüge der Objektbearbeitung vor.

„Unter den Faunen fossiler Anura nehmen die […] des Geiseltales mit Abstand [weltweit] die erste Stelle ein was Reichhaltigkeit an Formen und Erhaltungszustand anbelangt."
(Kuhn 1941, 24)

Einleitung

Die Erhaltung der Fossilien der Geiseltal-Lagerstätte (47,5–42,5 Millionen Jahre), insbesondere die der Froschlurche (Anuren), wurde in der Vergangenheit mehrfach als bemerkenswert beschrieben (Kuhn 1941; Voigt 1935; Voigt 1988). Die Objekte weisen sowohl umfassende Hartteile (etwa Knochen) als auch Anzeiger für Weichteilerhaltung auf. Die Steuerungsmechanismen, die diese Erhaltung möglich machen, wurden für die Geiseltal-Anuren nie vollständig erforscht. Da sich der generelle Bauplan und die Lebensweise von Anuren seit dem Unteren Jura (rund 200 Millionen Jahre) nicht verändert haben (Roček 2013), lassen sich Ergebnisse aus Untersuchungen an fossilen Objekten mit den Ergebnissen von Untersuchungen an heutigen Froschlurchen vergleichen. Moderne Untersuchungsmethoden wie die detaillierte Analyse der Skelett-Taphonomie und geochemische Materialanalysen werden dazu beitragen, das Rätsel der äußerst detailreichen Fossilerhaltung zu lösen.

Die außergewöhnlichen Fossilien der Geiseltal-Sammlung

Mehr als 50.000 fossile Sammlungsobjekte befinden sich in der Geiseltal-Sammlung des Zentralmagazins Naturwissenschaftlicher Sammlungen (ZNS) der Martin-Luther-Universität Halle-Wittenberg in Halle (Saale); mehr als die Hälfte davon sind Überreste von Säugetieren, Vögeln, Reptilien, Fischen und Amphibien (Haubold & Krumbiegel 1984; Hellmund & Hastings 2014). Weiterhin treten Wirbellose (insbesondere Insekten), Pflanzen und Spurenfossilien (wie versteinerter Kot) in hoher Vielfalt auf (Krumbiegel, Rüffle & Haubold 1983). Besonderheiten stellen neben der Erhaltung von Hartteilen auch die teils mikroskopisch erhaltenen und/oder chemisch nachweisbaren Überreste einstiger Weichgewebe (etwa Hautzellen, Muskeln) und Farberhaltungen dar, von denen Voigt (1988) berichtet. Seit 2011 ist die Geiseltal-Sammlung als national wertvolles Kulturgut eingetragen.

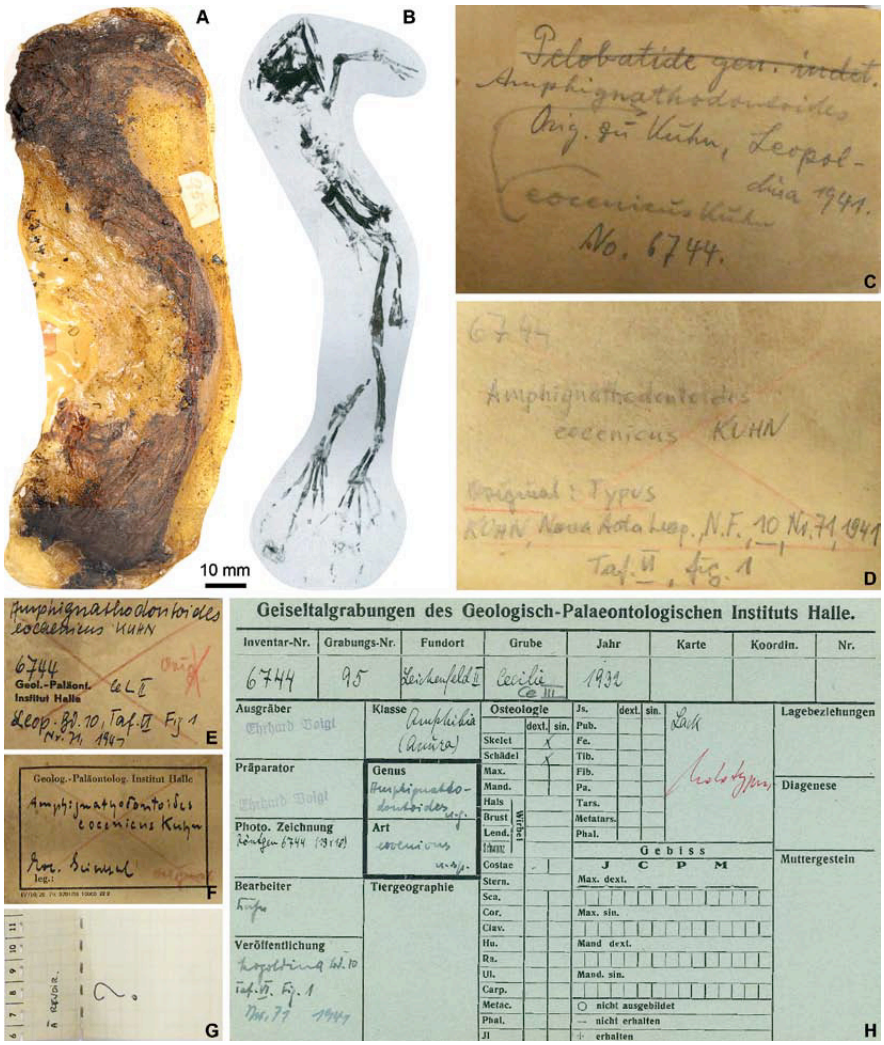


Abb. 1: Die Objekte und ihre Historie – sechs verschiedene Etiketten für diesen Froschlurch lassen auf mehrere Bearbeiter schließen, GMH Ce III-6744-1932, unbestimmt. A: Objektfotografie; das Skelett ist unvollständig und teilartikuliert, Lackfilm. B: Objekt als Röntgenaufnahme; die Knochen sind deutlich sichtbar; verändert aus Kuhn 1941. C: Etikett, Verfasser unbekannt. D: Etikett, Verfasser: Günter Krumbiegel. E: Etikett mit Hinweis zum Erstfund der Froschlurch-Art (Holotypus = rotes Kreuz), Verfasser: vermutlich Oskar Kuhn. F: Etikett, Verfasser unbekannt. G: Etikett mit französischem Hinweis „Ã REVOIR" (zur Überprüfung), Verfasser unbekannt. H: Inventarkarte mit Zusammenfassung aller Rohdaten zum Objekt, Verfasser: vermutlich u.a. Ehrhard Voigt und Oskar Kuhn. Fotos: A, C–G: Daniel Falk, H: Michael Stache; B: Röntgenaufnahme aus Kuhn 1941

Geologie und Stratigraphie

Beim Ablagerungsraum der fossilführenden Sedimente handelte es sich um ein subtropisches Sumpfgebiet. Die Sedimente wurden küstennah zur Paläo-Nordsee in einem ca. 75 km² erstreckenden Becken abgelagert (Blumenstengel 2004; Krumbiegel, Rüffle & Haubold 1983).

Die Ablagerungen der Geiseltal-Lagerstätte sind nicht für eine radiometrische Alterseinstufung geeignet. Dennoch lässt sich mithilfe des Vergleichs von Faunen aus der Messel-Fossillagerstätte (Mertz & Renne 2005) und der Eckfeld-Fossillagerstätte (Mertz, Swisher & Franzen u. a. 2000) sowie berechneter Sedimentationsraten (Franzen 2005) ein Alter von etwa 47,5 bis 42,5 Millionen Jahre (Lutetian, Mittleres Eozän) ableiten.

Grabungs- und Sammlungshistorie

Die Geiseltal-Fossillagerstätte ist eng mit einer Rohstofflagerstätte verbunden und befindet sich 20 Kilometer südwestlich von Halle (Saale) in Sachsen-Anhalt. In den ersten Jahren des 20. Jahrhunderts begann der industrielle Abbau der Braunkohle in Tagebauen. Der erste nachweisliche Fund eines fossilen Wirbeltieres – des „Lophiodons" (ein Vertreter aus der Tapirverwandtschaft) – wurde im Jahr 1908 gemacht und dem Geologischen Institut in Halle (Saale) übergeben. Ab Mitte der 1920er Jahre wurden detaillierte und quantitative Ausgrabungen unter Leitung des Institutsdirektors Johannes Walther (1860–1937) durchgeführt und in einer ersten Publikation von Benjamin E. Barnes (1903–1969) bekannt gemacht (Barnes 1926).

Im Jahr 1929 erhielt Johannes Weigelt (1890–1948) einen Ruf nach Halle (Saale) als Nachfolger seines Mentors Johannes Walther und wurde Direktor des Geologisch-Paläontologischen Instituts. Die Fossilausgrabungen wurden in der 1930er Jahren durch die von Ehrhard Voigt (1905–2004) beschriebenen Bergungsmethoden weiter ausgedehnt (siehe folgendes Kapitel). Dies führte zu zahlreichen Erstbeschreibungen (Holotypen, Abb. 1A–H) der fossilen Fauna im Geiseltal.

In den Jahren 1938 bis 1949 mussten die Fossilgrabungen im Geiseltal erst aufgrund der Priorisierung einer anderen Grabungsstelle durch das Hallenser Institut und dann durch den Ausbruch des zweiten Weltkriegs eingestellt werden.

Ab dem Jahr 1949 wurden unter der Institutsleitung von E. W. Hans-Friedrich Gallwitz (1896–1958) und später durch seinen Nachfolger Horst W. Matthes (1912–1986) die Grabungsaktivitäten wieder aufgenommen und die Forschung wiederbelebt (Haubold & Hellmund 1998), mit einem Höhepunkt an Fossilbergungen um die 1960er Jahre. Dennoch wurden vermutlich viele tausend Objekte während des jahrzehntelangen Bergbaubetriebes unabsichtlich zerstört (Hastings & Hellmund 2015).

Die Ausgrabungsaktivitäten nahmen in den 1980er Jahren, bedingt durch die Verlagerung des Kohleabbaus in den westlichen Teil der Lagerstätte mit deutlich geringerem Fossilienaufkommen, verstärkt ab.

Die letzten Ausgrabungsaktivitäten endeten im Sommer des Jahres 1993 (Hellmund 1997), gleichzeitig kam es auch zur endgültigen Einstellung der bergbaulichen Aktivitäten im Geiseltal. Insgesamt wurden während der 68-jährigen Grabungsperiode im Geiseltal, mit Unterbrechungen, ca. 86 Fundstellen unterschieden (Haubold & Krumbiegel 1984).

Im Jahr 2000 wurden letzte größere Geländearbeiten für eine Forschungsstudie zu stratigraphischen Fragen und zur Geochemie der Braunkohlen durchgeführt (Hellmund & Wilde 2001). Im Sommer 1993 begann die Rekultivierung des bergbaulichen Geländes. Mit der Flutung des Reviers (2003–2011) entstand das größte Gewässer in Mitteldeutschland – der Geiseltalsee.

Die Geiseltal-Sammlung war bereits von Johannes Weigelt und Ehrhard Voigt in der von Kardinal Albrecht II. von Brandenburg (1514–1545) erbauten Allerheiligenkapelle im Nordflügel der Neuen Residenz untergebracht worden und ist in Teilen seit 1934 im dortigen „Geiseltalmuseum" ausgestellt. Einzelne Pflanzenfossilien befinden sich zudem im Museum für Naturkunde Berlin.

Bergungs- und Konservierungsmethoden

Die Geiseltalfossilien zeichnen sich durch eine ungewöhnlich gute Erhaltung aus. Durch den hohen Wassergehalt der Braunkohle gestaltete sich deren Ausgrabung ausgesprochen schwierig. Ohne Vorbehandlung zerfielen die fragilen

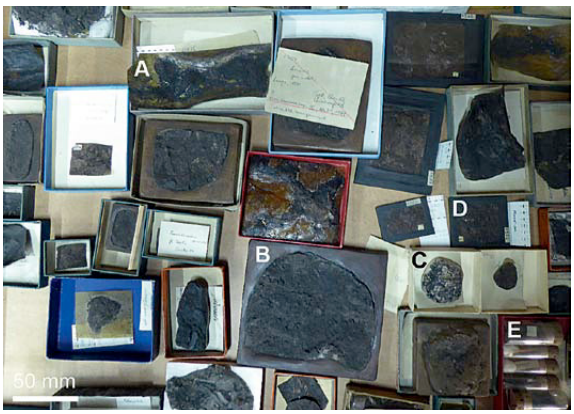


Abb. 2: Blick in eine Schublade mit den fossilen Froschlurchen der Geiseltal-Sammlung. Es sind verschiedene Aufbewahrungsmedien der Fossilien erkennbar. A – Lackfilm; B – Paraffin mit Gipsrahmen; C – Gips mit Lackfilmüberzug; D – Lackfilm, in Glaskästchen; E – Lackfilm in Glasviole mit Korkverschluss. Foto: Daniel Falk

Knochen zusammen mit den sie umgebenden kohligen Sedimenten beim Trocknen. Für die Bergung der Geiseltalfossilien kamen verschiedene Transfertechniken zum Einsatz (Abb. 2A–C): (1) Die Paraffin-Methode (Abb. 2B) wurde bei größeren, zusammenhängenden Skeletten angewendet. Das Fossil ist dabei mit einem Wall aus Ton umgeben worden, um anschließend geschmolzenes Paraffin auf das freigelegte Objekt zu gießen. Nach Abkühlen des Paraffinblockes wurde der Tonwall entfernt und eine Stützkappe aus Gips angefertigt. (2) Die Lackfilm-Methode (Abb. 1A, 2A, 4A) wurde von Ehrhard Voigt erstmalig als Weiterentwicklung von (1) beschrieben (Voigt 1933), unter Benutzung des Klebstoffs Nitrozellulose – ein gut verfügbarer Kunststoff der damaligen Zeit: Der Nitrozelluloselack wurde auf das freigelegte Fossil und auf das umgebende Sediment aufgetragen. Der verfestigte Film konnte wie ein Abziehbild vom Substrat gelöst werden. Zur Stabilisierung wurde bei den ersten Versuchen noch eine Gipskappe auf dem Lackfilm aufgetragen (Abb. 2C), später kam zumeist eine Holzplatte als Trägermaterial zum Einsatz. Bei beiden Methoden wurde nach der Bergung der Objekte die ehemals untenliegende Seite im Labor freipräpariert. Die Lackfilm-Methode ermöglichte, äußerst fragile Fossilien, so von Fischen, Fröschen und anderen kleinen Tieren, in großer Zahl zu bergen (Abb. 2A). (3) Die Gipsmantel-Methode (1950er Jahre) kam bei größeren Fossilienfunden zum Einsatz. Im Unterschied zur Lackfilm-Methode wurden hier nur die fossilen Knochen mit Nitrozelluloselack getränkt und anschließend für die Bergung in eine Gipskalotte verpackt, um sie im Labor frei zu präparieren.

Nitrozelluloselack ist nach heutigem Wissensstand nicht alterungsbeständig und zersetzt sich selbst. Daher müssen die entsprechenden Objekte der Geiseltal-Sammlung restauriert werden. Bei der heutigen Restaurierung wird oberflächlich der Nitrozelluloselack entfernt und durch das alterungsbeständige Polyvinylbutyral ersetzt.

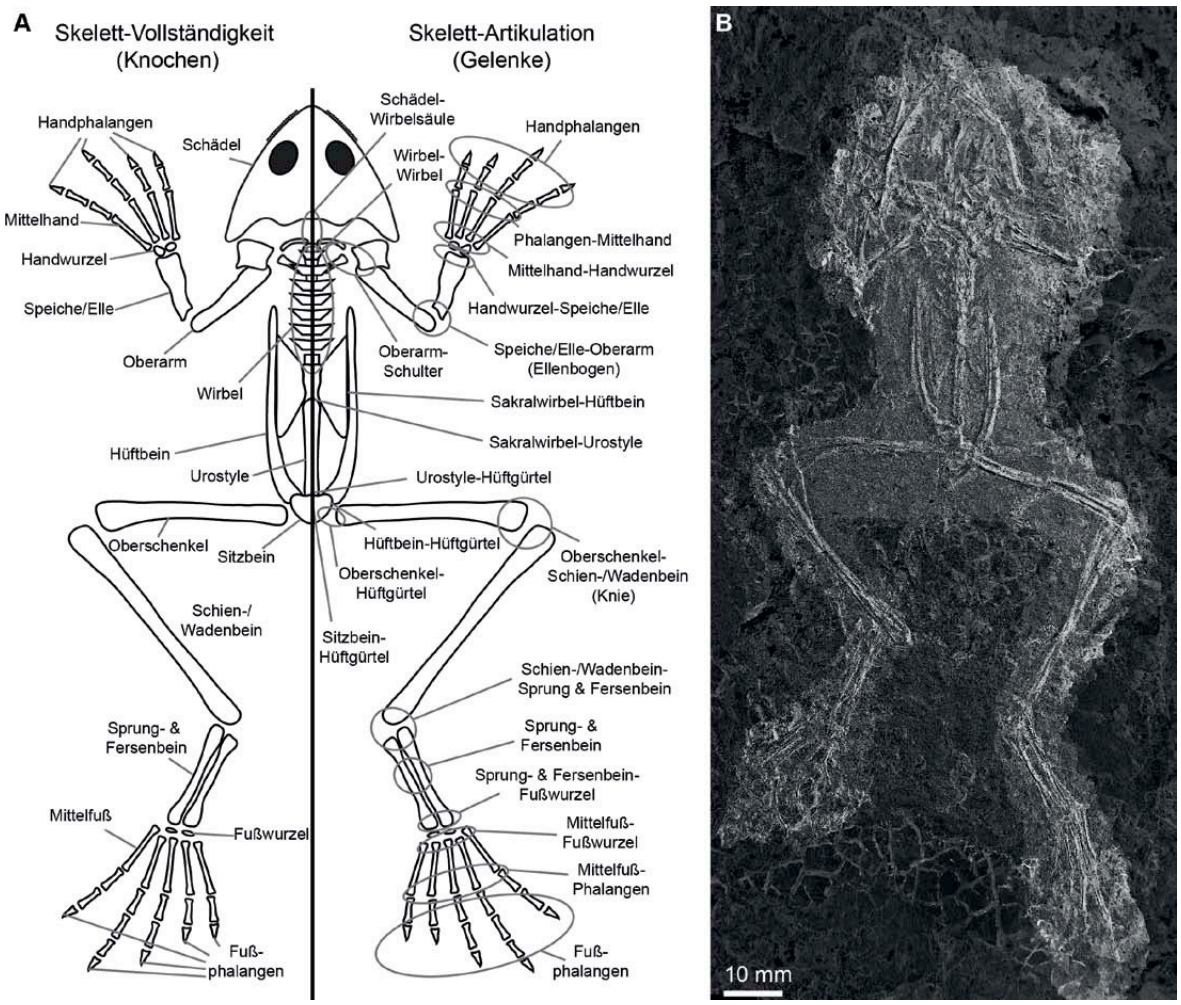


Abb. 3: Erläuterung der Skelett-Taphonomie. A: Schematisches Froschskelett. Untersuchung der beschrifteten Knochen und Gelenke zur Bestimmung der Vollständigkeit bzw. Artikulation des Skelettes; die Auswertung der Daten kann für einzelne Knochen, Gelenke oder das Objekt erfolgen. B: Froschlurch (Pelobatide) in Falschfarben, in Paraffin; dieses Exemplar zeigt eine außerordentlich hohe Vollständigkeit und Artikulation. Es ist der größte Froschlurch in der Sammlung, GMH Ce II-4949-1930. Skizze und Foto: Daniel Falk

Die eozänen Froschlurche des Geiseltals

Die eozänen Froschlurche (Anuren) der Geiseltal-Sammlung wurden parallel zum Abbau von Braunkohle entdeckt und aus den kohligen Sedimenten ausgegraben. Sie stammen von zwölf Grabungsstellen.

Eine erste detaillierte Beschreibung erfolgte durch Kuhn (1941) (Abb. 1B, E, H), der die Geiseltal-Anuren in eine Vielzahl von Arten unterteilte. Nach neueren Untersuchungen handelt es sich bei den Geiseltal-Froschlurchen um zwei bis drei Familien – die Pelobatidae (Schaufelfußkröten), die Palaeobatrachidae (ausgestorben, vermutlich mit den Krallenfröschen verwandt) (Roček 2013; Roček & Rage 2000) und möglicherweise auch die Discoglossidae (Scheibenzüngler) (Roček 2013; Roček & Rage 2003). Exemplare der letzteren Familie wurden für das Geiseltal noch nicht detailliert beschrieben. Die überwiegende Mehrheit der Objekte kann den Pelobatiden zugeordnet werden (Abb. 1A–B, 3B, 4A–C). Adulte Pelobatiden folgen mehrheitlich einem terrestrischen Lebensstil, mit Ausnahme der Fortpflanzungszeit, in der sie zu Wasserflächen migrieren (Lizana, Márquez & Martín-Sánchez 1994). Weniger Exemplare gehören zu den Palaeobatrachiden, die fast vollständig aquatisch lebten und nur eingeschränkt migrieren konnten (Wuttke, Přikryl & Ratnikov u. a. 2012).

In der Geiseltal-Sammlung sind 180 Objekte den Anuren (Stand Februar 2020) zugeordnet. Historische Quellen berichten von über 200 Anuren, die ausgegraben wurden, und von Hunderten von Objekten, die bei der Ausgrabung oder der Entnahme unbeabsichtigt zerstört worden sind (Krumbiegel, Rüffle & Haubold 1983).

Die fossilen Froschlurche sind entweder auf Nitrozelluloselack, in Paraffin oder einer Kombination aus Lack und Gips konserviert und unterschiedlich aufbewahrt worden (Abb. 2A–E). Objekte in Paraffin weisen häufig deutliche Mengen des kohligen, feinkörnigen Einbettungssediments auf. Bei Lackpräparaten ist oft nur wenig Sediment vorhanden.

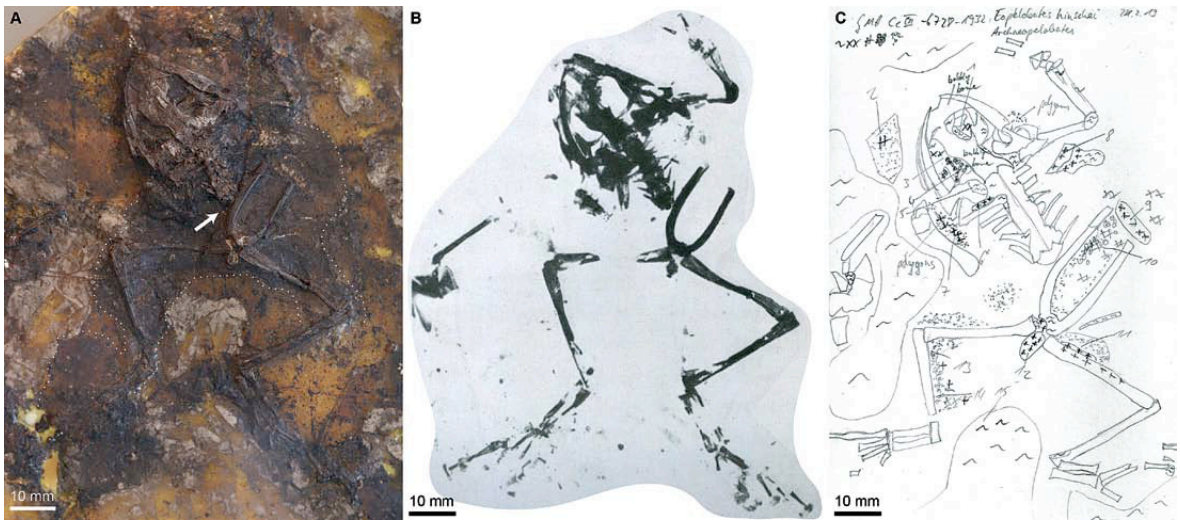


Abb. 4: Gut erhaltener Geiseltal-Froschlurch (Pelobatide), GMH Ce III-6728-1932. A: Objektfotografie, ein dunkler Schatten (Punktlinie) umgibt Knochen und deutet vermutlich auf Weichteilerhaltung hin; Unterkörper durch Versatz des Sakralwirbels und der Urostyle verschoben (Pfeil). B: Objekt als Röntgenaufnahme, aus Kuhn 1941. C: Objekt als schematische Handskizze zur Identifizierung und Nachbereitung von Vollständigkeit, Artikulation und unterschiedlichen Strukturen. Foto/Scan: Daniel Falk; Röntgenaufnahme aus Kuhn 1941

Nach der Ausgrabung und Präparation wurden die Froschlurche in Hinsicht auf die Artenvielfalt (Kuhn 1941), die Funktionsmorphologie (etwa Proportionen von Knochen und Rückschlüsse auf Lebensweise) (Hinsche 1941) und die Weichteilerhaltung (Voigt 1935) bearbeitet. Im institutseigenen Röntgengerät wurden zudem von einer Auswahl von Objekten Röntgenaufnahmen erzeugt (Abb. 1B, Abb. 4B). Zur Weichteilanalyse schnitt Voigt (1935) bis zu einem Zentimeter große Proben aus den fossilen Anuren, die er als „Mikropräparate" auf einen Objektträger klebte und mikroskopisch fotografierte (bis zu 840-fache Vergrößerung) (Voigt 1935; Voigt 1988). Weiterhin führte er Brennexperimente mit fossilem Material durch und untersuchte die mineralogische Zusammensetzung der Brennrückstände, die sich nach seiner Aussage als silikatisch erweisen. Er schlussfolgerte, dass die Erhaltung der Zellen durch einen Austausch der organischen Masse mit Kieselsäure erklärt werden kann. Nach heutigem Wissensstand wäre diese Art der Erhaltung bei fossilen Froschlurchen weltweit einmalig. Um die Hypothese der Silikaterhaltung zu prüfen und zu verstehen, bedarf es daher einer Untersuchung mit interdisziplinären Methoden der Gegenwart.

Methoden

Es werden zwei verschiedene methodische Ansätze zur Untersuchung der Objekte beschrieben, die die Grundlage zur Interpretation der Fossilerhaltung bilden werden.

Skelett-Taphonomie

Die Analyse der Skelett-Taphonomie von Objekten wird verwendet, um festzustellen, welche Prozesse auf einen Kadaver vor und während der Einbettung einwirkten und ob ein Zusammenhang zwischen der Skeletterhaltung und den Weichgewebeüberresten besteht.

Bei der Skelett-Taphonomie werden Vollständigkeit und Artikulation der Hartteile der Wirbeltiere (Knochen) untersucht (Abb. 3A). Zudem wird die dorsale oder ventrale Orientierung der einzelnen Skelette bestimmt. Damit kann die Orientierung des Kadavers bei der Einbettung nachvollzogen werden.

Von den 180 Anuren wurden insgesamt 40 Kaulquappen und unbestimmbare Objekte von der Analyse ausgeschlossen. Jeder Knochen der 140 Skelette wurde im Auflichtmikroskop betrachtet und gezeichnet; ggf. vorhandene Sedimente und/oder Strukturen wurden auf diesen Zeichnungen schematisch dokumentiert (Abb. 4C). Die Dokumentation wurde durch Fotografien unterstützt (Abb. 4A). Zeichnungen und Fotos bildeten die Grundlage für eine tabellarische Erfassung der bei einem vollständigen Objekt insgesamt 91 Einzelknochen. Ein Skelettelement gilt als vorhanden, wenn es auf dem Objekt sichtbar ist. Weil einige Skelettelemente sich häufig überlagern, fragmentarisch vorlagen oder sehr klein sind und daher einzeln nicht zuverlässig zu bestimmen waren, wurden sie in Gruppen von Knochen zusammengefasst (etwa für die Handphalangen: 0, 1–3, 4–6, 7–9 oder 10 vorhandene Phalangen), gemeinsam als ein Skelettelement betrachtet (wie Schädel, Hand-/Fußwurzelknochen) oder aus der Analyse ausgeschlossen (z. B. Schulterblätter, Rabenbeine, Brustbein).

Weiterhin wurde die Artikulation (Abb. 3B) bzw. Disartikulation (Abb. 4A) von bis zu 98 Gelenken (vollständiges Skelett) bestimmt (Abb. 3A). Die Artikulation konnte nur für Gelenke ausgeführt werden, deren dazugehörige Knochen vorhanden waren. Da einige Skelettelemente sich häufig überlagern, fragmentarisch vorlagen oder sehr klein sind

und daher einzeln nicht zuverlässig bestimmbar waren, wurden die dazugehörigen Gelenke in Gruppen zusammengefasst (z. B. für die Handphalangen: 0, 1–2, 2–3, oder 4–6 artikulierte Gelenke).

76 Prozent der bearbeiteten Skelette sind trunkiert, d.h. mindestens ein Knochen ist am Rande des Transfermediums oder an der Kante des Objektes abgeschnitten (z. B. durch die Bergungsmethode). Die Knochen jenseits des trunkierten Knochens wurden aus der Analyse ausgeschlossen, da es sich nicht bestimmen lässt, ob jene Knochen am (untrunkierten) Objekt vor der Ausgrabung vorhanden waren oder nicht (Falk, Wings & McNamara, im Erscheinen). Die Tabellenwerte der Skelett-Taphonomie können pro Skelettelement und Objekt mathematisch ausgewertet werden.

Weichteilanalyse

An zahlreichen Objekten berichtete Voigt (1935) über mikroskopische Nachweise von Weichteilüberresten, insbesondere über verschiedene Hautschichten. Zudem wurden auch fossile Bakterien beschrieben (Mrugowsky 1936). Mit modernen geochemischen Analysemethoden lassen sich diese Nachweise detaillierter bestimmen und ggf. verschiedenen Hautschichten, Pigmentzellen und/oder inneren Organen zuzuordnen (Rogers, Astrop & Webb u. a. 2019; Rossi, McNamara & Webb u. a. 2019).

Unterschiede in Farbgebung, Geometrie, Textur und Oberflächenmorphologien von potentiellen Weichteilüberresten lassen sich bereits mit dem Auflichtmikroskop erkennen und mittels vorhandener Literatur bestimmen (McNamara, Orr & Kearns u. a. 2009).

Mit dem Rasterelektronenmikroskop (REM) können Oberflächen und Geometrien im Mikrometerbereich abgebildet und charakterisiert werden. Der am REM angeschlossene Detektor zur Energiedispersiven Röntgenspektroskopie (EDS) misst fast gleichzeitig die elementare Zusammensetzung der analysierten Oberflächen.

Weitere Untersuchungsmethoden, die u. a. Rückschlüsse auf die Bindungskräfte zwischen Elementen, die Bestimmung von Mineralphasen oder die Verbreitung von Spurenmetallen am Objekt möglich machen, sind die Fourier-Transformations-Infrarotspektroskopie (FTIR), die RAMAN-Spektroskopie und die Röntgenabsorptionsspektroskopie (XAS). Für letztere wird die Untersuchung in einem Teilchenbeschleuniger wie dem der „Stanford Synchrotron Radiation Lightsource (SSRL)"-Einrichtung in Stanford (Kalifornien, USA) durchgeführt (Wogelius, Manning & Barden u. a. 2011).

Als Probenmenge wird normalerweise nicht mehr als 1 mm³ Untersuchungsmaterial benötigt. Weil die meisten Analysen die Probe nicht beschädigen (z. B. REM, EDS, FTIR), kann diese auch für weitere Analysen dienen und/oder als Objekt in die Sammlung mit aufgenommen werden.

Erste Resultate

Die Skelette der Anuren weisen eine sehr unterschiedliche Vollständigkeit auf. Eine erste Auswertung von Vollständigkeit ergab, dass die am häufigsten vorhandenen Skelettelemente Schädel, Femur und Wirbel sind. Sitzbein, Handwurzelknochen und Handphalangen sind jeweils bei nur knapp der Hälfte der Anuren vorhanden. Die Fußwurzelknochen sind nur selten überliefert.

Die Vollständigkeit nimmt in den Vorder- und Hintergliedmaßen in Richtung der Phalangen ab. Die Skelettelemente der hinteren Gliedmaßen sind tendenziell vollständiger als gleichartige Elemente der Vordergliedmaßen. Die Werte für die Vollständigkeit von Elementen der linken und rechten Skelettkörperseite sind vergleichbar.

Die meisten Skelette sind im Allgemeinen gut artikuliert. Auch für sehr unvollständige Skelette gilt, dass vorhandene Gelenke üblicherweise artikuliert sind. Die höchsten Artikulationswerte treten an den Gelenken der mittleren und äußeren Gliedmaßen und der Rückenwirbel auf. Die Verbindung von Halswirbel und Schädel, die körpernahen Gelenke der Gliedmaßen und die Gelenke in der Hüftregion weisen geringere Werte auf. Obwohl Handwurzelknochen und Fußwurzelknochen oft nicht vorhanden sind, sind die umliegenden Knochen – wenn vorhanden – üblicherweise artikuliert.

In der Gegenüberstellung von Vollständigkeit und Artikulation weisen die Objekte eine Bandbreite von Vollständigkeitswerten auf, aber nur sehr wenige Objekte davon sind stark disartikuliert. Fast alle Skelette weisen eine entweder dorsale oder ventrale Orientierung auf.

Körperferne Knochen wie die Phalangen sind relativ selten vorhanden (im Vergleich zu körpernahen Knochen), dann jedoch meist artikuliert. Dies könnte ein Resultat bodennaher Strömungen im Wasserkörper vor der endgültigen Einbettung des Froschlurchkadavers sein. Die kleinen, leichten, körperfernen Knochen sind exponiert und von wenig stützendem Weichgewebe umgeben. Ist letzteres zersetzt, folgt abhängig von der Stärke der Unterwasserströmungen eine Separierung dieser Knochen vom Skelett (d. h. Disartikulation) bis hin zum Abtransport und damit Verlust (Dodson 1973; McNamara, Orr & Kearns u. a. 2009). Die dorsale oder ventrale Orientierung eines Skelettes ist zudem die hydrodynamisch stabilste Position, weil die Extremitäten nahezu in horizontaler Ebene mit dem restlichen Körper liegen (McNamara, Orr & Alcalá u. a. 2012). In den nur wenige Meter tiefen Wasserkörpern des Geiseltals sind bodennahe Strömungen daher anzunehmen. Für einige Fundstellen ist zudem über verschiedene Vorzugsorientierungen für Froschlurchskelette berichtet worden (Weigelt 1933), die während des Transports des Kadavers und/oder durch Bodenströmungen generiert wurden.

Bei der Untersuchung der Objekte mit dem Binokular werden vorläufig vier unterschiedliche Schichten, die zwi-

schen und um die Knochen herum auftreten, als Weichteilerhaltung vermutet; eine nähere Untersuchung mit den oben genannten geochemischen Untersuchungsmethoden steht noch aus. Die von Voigt (1935) als Hohlräume von Schleimdrüsen bezeichnete Schicht ähnelt in ihrer sieb- und gitterförmigen, orangefarbenen Struktur der in den fossilen Fröschen der Libros-Fossillagerstätte (Miozän, Spanien) nachgewiesenen Eberth-Kastschenko-Hautschicht (McNamara, Orr & Kearns u. a. 2009). Die Geometrien in den dunkelbraunen, feinkörnigen Schichten in den Augenhöhlen könnten zudem auf fossile Melanosome (Rossi, McNamara & Webb u. a. 2019) anstelle von Bakterien (Mrugowsky 1936) hindeuten. Die geochemischen Analysen werden Lösungsansätze zur Erklärung dieser Auffälligkeiten bieten.

Verzerrung des Sammlungsbildes

Um Fehlinterpretationen zu verhindern, wurden die Skelettelemente distal der trunkierten Knochen von der Studie ausgeschlossen, was zu einer künstlichen Erhöhung der Vollständigkeitswerte für betroffene Skelettelemente und Skelette führen kann (siehe Methodik, Falk, Wings & McNamara, im Erscheinen). Zudem ist eine Verzerrung des Sammlungsbildes etwa durch nachweislich nicht geborgene Anurenreste und dokumentarisch belegte, aber derzeit unauffindbare Objekte möglich.

Die Ausgräber standen durch den zügig voranschreitenden Braunkohleabbau unter starkem Zeitdruck. Dieser könnte zur Priorisierung bei der Fossilbergung, abhängig vom wissenschaftlichen Interesse, geführt haben. Zudem ist denkbar, dass bevorzugt artikulierte Objekte gesammelt und aufbewahrt wurden.

Objektforschung als treibende Kraft: Nebeneffekte und Ausblick

Bei der wissenschaftlichen Bearbeitung der Objekte aus der Geiseltal-Sammlung ergeben sich direkte und indirekte Vorteile für die Sammlung. Mit dem Wissen um die Ökologie einer Lebenswelt von vor mehr als 45 Millionen Jahren lassen sich Analogien zur heutigen Entwicklung von Lebensräumen herstellen. Die mitteleozäne Geiseltalflora und -fauna ist zudem Puzzlestück im schleichenden Klimawandel von der Warmzeit (eisfreie Polkappen) im Eozän zur Eiszeit (vereiste Polkappen) im Oligozän (Mosbrugger, Utescher & Dilcher 2005) und kann zur Erforschung der Auswirkungen von klimatischen Veränderungen beitragen.

Für Sammlungen sorgen auch die fortschreitende Inventarisierung und Digitalisierung parallel zur wissenschaftlichen Bearbeitung für Vorteile (Falk, Lechner & Fuhrmann 2018). Im Falle der Geiseltal-Sammlung wurde durch Ehrhard Voigt schon frühzeitig ein Inventarsystem eingeführt. Die ca. 22.000 Inventarkarten wurden digitalisiert und in eine Datenbank eingefügt (Software „Claris FileMaker"). Die Karteikarten selbst sind inzwischen Sammlungsobjekte (Abb. 1H). Die vorhandenen Dokumentationen werden durch 3D-Scans von den Fossilien der Geiseltal-Sammlung ergänzt und mögliche Fehlstellen in der Datenbank im Laufe der wissenschaftlichen Objektbearbeitung korrigiert. Einige Objekte fehlen in der Sammlung. Diese mögen durch Kriegswirren, unprotokollierte Leihvorgänge oder Geschenke in anderen Institutionen liegen. Eine Anfrage an mehr als 54 Museen wird derzeit durchgeführt und brachte bereits erste Erfolge.

In naher Zukunft wird die Forschung an den Objekten der Geiseltal-Sammlung weiter ausgebaut werden. Neben der detaillierten Bearbeitung der Weichteilrückstände an den fossilen Anuren sollen die Daten für andere fossile Tiergruppen der Sammlung (z. B. Fische, Fledermäuse) erfasst und untereinander verglichen werden.

Fazit

Von 180 eozänen Froschlurch-Objekten in der Geiseltal-Sammlung (Stand Februar 2020) wurden 140 Skelette auf ihre Orientierung, Vollständigkeit und Artikulation (Skelett-Taphonomie) untersucht. Die Mehrheit der Skelette ist trunkiert. Körperferne und kleinere Skelettelemente sind weniger häufig vorhanden, verglichen mit größeren und körpernahen Elementen. Vorhandene Skelettelemente sind üblicherweise artikuliert. Mit weiteren Untersuchungsmethoden (z. B. REM, EDS, FTIR, Raman Spektroskopie, XAS) werden zukünftig potentielle Weichteilüberreste analysiert. Dies kann dazu beitragen, die Steuerungsmechanismen der Fossilerhaltung zu ergründen.

Die Geiseltal-Anuren stellen nur einen Bruchteil der Objekte der Geiseltal-Sammlung dar und bilden den Anfang zur Erforschung des Rätsels der Fossilerhaltung und vieler weiterer Fragestellungen.

Danksagungen

Daniel Falk bedankt sich bei Prof. Dr. Maria E. McNamara (University College Cork) und Dr. Oliver Wings (ZNS), dem derzeitigen Kurator der Geiseltal-Sammlung, für die Unterstützung und die gemeinsame Ausarbeitung des Projektes. Michael Stache bedankt sich bei Christoph Koehn, dem ehemaligen Präparator der Geiseltal-Sammlung, für das geteilte Wissen um die Sammlung und die damit verbundenen Präparationsmethoden.

Wir bedanken uns bei allen früheren Bearbeiter:innen des Geiseltal-Materials für die aufwendige Präparation, Inventarisierung und Dokumentation. Daniel Falk bedankt sich beim Irish Research Council (IRC) für die Finanzierung des Projektes durch ein Government of Ireland Postgraduate Scholarship (GOIPG/2018/3354). Zugleich sei den Organisatoren des Jungen Forums, insbesondere Prof. Dr. Cornelia Weber, für die Einladung gedankt, ebenso wie den Gastge-

bern der Tagung 2020 im Zentralmagazin Naturwissenschaftlicher Sammlungen (ZNS) der Martin-Luther-Universität Halle-Wittenberg, namentlich Bianca Bernstein, Arila-Maria Perl und Dr. Frank D. Steinheimer.

Literatur

Barnes, B. 1926. Eine eozäne Wirbeltier-Fauna aus der Braunkohle des Geiseltales. *Jahrbuch des Halleschen Verbandes für die Erforschung der mitteldeutschen Bodenschätze* 6: 5–24

Blumenstengel, H. 2004. Kapitel 3.5 Tertiär. In: Wansa, S.; Radzinski, K. (Hg.). *Erläuterungen zur Geologischen Karte 1:25 000 von Sachsen-Anhalt (GK 25), Blatt Mücheln (Geiseltal), 4636*. Halle (Saale): Landesamt für Geologie und Bergwesen Sachsen-Anhalt: 48–61

Dodson, P. 1973. The significance of small bones in paleoecological interpretation. *Rocky Mountain Geology* 12: 15–19

Falk, D.; Lechner, T.; Fuhrmann, A. 2018. Sammeln für die Ewigkeit – Ideen zur nachhaltigen Inventarisierung von geowissenschaftlichen Objekten. *Staatliches Museum für Naturkunde Karlsruhe, Carolinea* 76: 5–19

Falk, D.; Wings, O.; McNamara, M. E. The skeletal taphonomy of anurans from the Eocene Geiseltal Konservat-Lagerstätte, Germany. *Papers in Palaeontology* (im Erscheinen)

Franzen, J. L. 2005. The implications of the numerical dating of the Messel fossil deposit (Eocene, Germany) for mammalian biochronology. *Annales de Paléontologie* 91: 329–335

Hastings, A. K.; Hellmund, M. 2015. Rare in situ preservation of adult crocodilian with eggs from the Middle Eocene of Geiseltal. *Palaios* 30: 446–461

Haubold, H.; Hellmund, M. 1998. Die Fossillagerstätte Geiseltal bei Halle (Saale) und ihre Bedeutung für das terrestrische Mitteleozän Europas. *Terra Nostra* 98: 122–123

Haubold, H.; Krumbiegel, G. 1984. *Typenkatalog der Wirbeltiere aus dem Eozän des Geiseltals, 1934–1984 – 50 Jahre Geiseltalmuseum*, Halle (Saale): Martin-Luther-Universität Halle-Wittenberg

Hellmund, M. 1997. Letzte Grabungsaktivitäten im südwestlichen Geiseltal bei Halle (Deutschland). *Hercynia N.F.* 30: 163–176

Hellmund, M.; Hastings, A. K. 2014. Messel and Geiseltal: highlights from the Cenozoic; excursion guide, part II – the Eocene Geiseltal Fossillagerstätte (Central Germany) and its vertebrate fossil fauna with 13 figures and 1 table. In: Smith, K. T., Lehmann, T., Hellmund, M.; Hastings, A. K. (Hg.). *SVP 2014 Berlin*. Berlin: Senckenberg Research Institute and Natural History Museum Frankfurt: 25–46

Hellmund, M.; Wilde, V. 2001. Neue wissenschaftliche Aktivitäten im Bereich des ehemaligen Tagebaues Mücheln-Westfeld (Geiseltal, Sachsen-Anhalt, Deutschland). *Halleshes Jahrbuch für Geowissenschaften B, Beiheft*, 13: 3–17

Hinsche, G. 1941. Untersuchungen zum funktionellen Aufbau der Anuren mit besonderer Berücksichtigung der eozänen Geiseltalfunde. *Nova Acta Leopoldina N.F.* 10: 313–343

Krumbiegel, G.; Rüffle, L.; Haubold, H. 1983. *Das eozäne Geiseltal: ein mitteleuropäisches Braunkohlenvorkommen und seine Pflanzen- und Tierwelt*. Wittenberg: A. Ziemsen Verlag

Kuhn, O. 1941. Die eozänen Anura aus dem Geiseltale nebst einer Übersicht über die fossilen Gattungen. *Nova Acta Leopoldina N.F.* 10: 345–376

Lizana, M.; Márquez, R.; Martín-Sánchez, R. 1994. Reproductive Biology of *Pelobates cultripes* (Anura: Pelobatidae) in Central Spain. *Journal of Herpetology* 28: 19–27

McNamara, M. E.; Orr, P. J.; Alacalá, L.; Anadón, P.; Penalver, E. 2012. What controls the taphonomy of exceptionally preserved taxa – environment or biology? A case study using frogs from the Miocene Libros Konservat-Lagerstätte (Teruel, Spain). *Palaios* 27: 63–77

McNamara, M. E.; Orr, P. J.; Kearns, S. L.; Alacalá, L.; Anadón, P.; Penalver Mollá, E. 2009. Soft-tissue preservation in Miocene frogs from Libros, Spain: insights into the genesis of decay microenvironments. *Palaios* 24: 104–117

Mertz, D. F.; Renne, P. R. 2005. A numerical age for the Messel fossil deposit (UNESCO World Heritage Site) derived from $^{40}Ar/^{39}Ar$ dating on a basaltic rock fragment. *Courier Forschungsinstitut Senckenberg* 255: 67–75

Mertz, D. F.; Swisher, C. C.; Franzen, J. L.; Neuffer, F. O.; Lutz, H. 2000. Numerical dating of the Eckfeld maar fossil site, Eifel, Germany: a calibration mark for the Eocene time scale. *Naturwissenschaften* 87: 270–274

Mosbrugger, V.; Utescher, T.; Dilcher, D. L. 2005. Cenozoic continental climatic evolution of Central Europe. *Proceedings of the National Academy of Sciences* 102: 14964–14969

Mrugowsky, J. 1936. Über fossile Bakterien aus dem Mitteleozän des Geiseltales. *Nova Acta Leopoldina N. F.* 3, 597–603

Roček, Z. 2013. Mesozoic and Tertiary Anura of Laurasia. *Palaeobiodiversity and Palaeoenvironments* 93: 397–439

Roček, Z.; Rage, J.-C. 2003. Evolution of anuran assemblages in the Tertiary and Quaternary of Europe, in the context of palaeoclimate and palaeogeography. *Amphibia-Reptilia* 24: 133

Roček, Z.; Rage, J. 2000. Tertiary Anura of Europe, Africa, Asia, North America, and Australia. *Amphibian Biology* 4: 1332–1387

Rogers, C. S.; Astrop, T. I.; Webb, S. M.; Ito, S.; Wakamatsu, K.; McNamara, M. E. 2019. Synchrotron X-ray absorption spectroscopy of melanosomes in vertebrates and cephalopods: implications for the affinity of *Tullimonstrum*. *Proceedings of the Royal Society B* 286: 20191649

Rossi, V.; McNamara, M. E.; Webb; S. M.; Ito, S.; Wakamatsu, K. 2019. Tissue-specific geometry and chemistry of modern and fossilized melanosomes reveal internal anatomy of extinct vertebrates. *Proceedings of the National Academy of Sciences* 116: 17880–17889.

Voigt, E. 1933. Die Übertragung fossiler Wirbeltierleichen auf Zellulose-Filme, eine neue Bergungsmethode für Wirbeltiere aus der Braunkohle. *Palaeontologische Zeitschrift* 15: 72–78

Voigt, E. 1935. Die Erhaltung von Epithelzellen mit Zellkernen, von Chromatophoren und Corium in fossiler Froschhaut aus der mitteleozänen Braunkohle des Geiseltales. *Nova Acta Leopoldina N.F.* 3: 339–360

Voigt, E. 1988. Preservation of soft tissues in the Eocene lignite of the Geiseltal near Halle (Saale). *Courier Forschungsinstitut Senckenberg* 107: 325–343

Weigelt, J. 1933. Die Biostratonomie der 1932 auf der Grube Cecilie im mittleren Geiseltal ausgegrabenen Leichenfelder. *Nova Acta Leopoldina, N.F.* 1: 157–174

Wogelius, R. A.; Manning, P. L.; Barden, H. E.; Edwards, N. P.; Webb, S. M.; Seller, W. I.; Taylor, K. G.; Larson, P. L.; Dodson, P.; You, H.; Da-Qing, L.; Bergmann, U. 2011. Trace metals as biomarkers for eumelanin pigment in the fossil record. *Science* 333: 1622–1626

Wuttke, M.; Přikryl; T., Ratnikov, V. Y.; Dvořák, Z.; Roček, Z. 2012. Generic diversity and distributional dynamics of the Palaeobatrachidae (Amphibia: Anura). *Palaeobiodiversity and Palaeoenvironments* 92: 367–395

Zu den Autoren

Daniel Falk studierte Geowissenschaften (Schwerpunkt Paläontologie) an der TU Bergakademie Freiberg (Sachsen). Bevor er ein zweijähriges wissenschaftliches Volontariat am Staatlichen Museum für Naturkunde Karlsruhe absolvierte (2016–2018), war er im Rahmen von ingenieurgeologischen Arbeiten, insbesondere zur Erzprospektion, im In- und Ausland tätig. Seit Ende 2018 promoviert er als Stipendiat am University College Cork in Irland zum Thema „Taphonomy of the Eocene Geiseltal Konservat-Lagerstätte, Germany".

Michael Stache ist ausgebildeter geowissenschaftlicher Präparator. Seit 1994 ist er der Geiseltal-Sammlung verbunden. Nach einer langjährigen Anstellung am Senckenberg Forschungsinstitut für Quartärpaläontologie in Weimar ist er seit 2012 am Zentralmagazin Naturwissenschaftlicher Sammlungen (ZNS) der Martin-Luther-Universität Halle-Wittenberg fest angestellt und für die konservatorischen Belange der Geiseltal- und der Haustierkunde-Sammlung zuständig.

Kontakt
Daniel Falk M.Sc.
University College Cork
School of Biological, Earth, and Environmental Sciences
Butler Building, Distillery Fields, North Mall
Cork, T23 TK30
Irland
daniel.falk[at]ucc.ie

Michael Stache
Martin-Luther-Universität Halle-Wittenberg
Zentralmagazin Naturwissenschaftlicher Sammlungen (ZNS)
Domplatz 4, 06108 Halle (Saale)
Deutschland
michael.stache[at]zns.uni.halle.de

Supplementary paper 2: Der mysteriöse Tod der Frösche des Geiseltales/Sachsen-Anhalt im Mitteleozän

This popular science article represents a report on mating-related deaths of extant anurans in two independent colonies in Halle (Saale), Germany. Further, a summary of the results and interpretations of Falk *et al.* (2022a) with focus on the mode of death of the Geiseltal anurans is given. The article shows that mating mortality is common in extant anuran colonies and supports the interpretation of the Eocene Geiseltal anuran die-offs as mating-related deaths. The article is published in the "*Jahresschrift für Feldherpetologie und Ichthyofaunistik in Sachsen"* (annual journal for field herpetology and ichthyo faunistics in Saxony) and is co-written in German language by four authors.

Falk, D., Grosse, W.-R., McNamara, M. & Wings, O. (2022). Der mysteriöse Tod der Frösche des Geiseltales/Sachsen-Anhalt im Mitteleozän. *Jahresschrift für Feldherpetologie und Ichthyofaunistik in Sachsen*, **23**, 86–95. https://sachsen.nabu.de/imperia/md/content/sachsen/230525-nabu-jahresschrift-feldherpetologie-2023.pdf

Candidate contribution to the study. DF contributed to the design of the study, supervised by MMN and OW, and performed a literature review on the Geiseltal anurans and on mating-related deaths in extant anurans. OW provided access to the Geiseltal Collection and access to the Geiseltal Collection data base. DF summarised and translated the key results regarding the mode of death of the Geiseltal anurans published in Falk *et al.* (2022a). WRG offered information on the behaviour of extant anurans and provided documentation on mating-related deaths in local anuran populations. DF wrote the first draft of the article, produced Figure 2 and revised subsequent drafts in line with comments from the other authors.

Abstract. The Eocene Geiseltal biota from Saxony-Anhalt (Germany) includes fossil skeletons of anurans, that were primarily assigned to Pelobatidae and Palaeobatrachidae. Most of those anurans probably represent mating-related deaths. Certain anurans may have died due to diseases and/or due to old age. The article provides a report on mating-related deaths in two independent colonies in Halle (Saale), Germany.

Jschr. Feldherpetol. u. Ichthyofaunistik Sachsen	23	82–91	Leipzig, 2022

Der mysteriöse Tod der Frösche des Geiseltales/Sachsen-Anhalt im Mitteleozän

Daniel Falk, Wolf-Rüdiger Grosse, Maria McNamara & Oliver Wings

Die mitteleozäne Fossillagerstätte Geiseltal (ca. 45 Millionen Jahre alt) befindet sich ca. 20 km südwestlich von Halle (Saale) in Sachsen-Anhalt und ist seit 100 Jahren von internationalem wissenschaftlichen Interesse (Barnes 1926, Falk & Stache 2021). Mit seinen tausenden Fossilien liefert das Geiseltal uns immer wieder neue Erkenntnisse zur Lebensweise und Evolution von Pflanzen und Tieren über mehrere Millionen Jahre hinweg. Im Eozän war die Erde deutlich wärmer und das Gebiet des heutigen Geiseltals ein sumpfiger subtropischer Küstenwald. Zu den Bewohnern dieser Sumpflandschaft zählten Vorfahren heutiger Pferde, Krokodile, Schlangen, Echsen und eine Vielzahl von Froschlurchen, die nun als Fossilien mit beeindruckender Erhaltung vorliegen (Voigt 1988). Die geologischen Aufschlüsse, in denen die Fossilien gefunden wurden, waren im 20. Jahrhundert Teil eines großräumigen Braunkohleabbaugebietes. Im Rahmen der Rekultivierung wurden sie geflutet und sind heute nicht mehr zugänglich (Abb. 1).



Abb. 1: Blick auf den Geiseltalsee im Jahr 2022. Im Vordergrund ist ein Amphibientümpel auf einer Hochterrasse am Weinberghang zu sehen, wo u.a. im Frühjahr die Knoblauchkröten als die „Nachfahren der fossilen Schaufelfußkröten“ anzutreffen sind. Foto: W.-R. Grosse

Die Mehrheit der fossilen Froschlurche und Kaulquappen wurden in den 1930er Jahren ausgegraben und präpariert. Die Fossilien werden in der Geiseltal-Sammlung des Zentralmagazins Naturwissenschaftlicher Sammlungen (ZNS) der Martin-Luther-Universität Halle-Wittenberg (MLU) aufbewahrt. Die öffentlich zugängliche Sammlung beinhaltet über 50.000 Fossilien der Geiseltal-Flora und -Fauna, darunter ca. 25.000 Wirbeltierreste. Rund 180 Objekte der Sammlung sind den Froschlurchen zuzuordnen.

Geiseltal Froschlurche

Im Rahmen einer Forschungskooperation des ZNS mit dem University College Cork (UCC), Irland wurden 168 fossile Froschlurchskelette aus dem Geiseltal untersucht (Falk & Stache 2021, Falk et al. 2022), unter anderen, um die Todesursache der Froschlurche zu ergründen.

Fossile Kaulquappen wurden von der Analyse ausgeschlossen (Falk et al. 2022). In historischen Grabungsdokumentationen werden die Funde hunderter Froschlurche in verschiedenen Grabungsstellen und Schichtflächen erwähnt, aber nur ca. 200 wurden erfolgreich geborgen und präpariert (Krumbiegel et al. 1983). Soweit diagnostisch möglich, konnten die Froschlurche mehrheitlich den überwiegend terrestrisch lebenden Pelobatiden (n = 54, Schaufelfußkröten, Abb. 2) und untergeordnet den aquatischen Palaeobatrachiden (n = 15, ausgestorben, vermutlich Pipimorpha) zugeordnet werden (Kuhn 1941, Roček & Rage 2000, Roček 2013, Roček et al. 2014, Roček et al. 2021). Zudem wird die Zuordnung einiger Fossilien zu den fossilen Discoglossiden (Scheibenzünglern) diskutiert (Rage & Roček 2003, Roček 2013). Die Skelette sind unterschiedlich vollständig und weisen meistens eine hohe Artikulationsrate auf, d.h. die Knochen befinden sich häufig noch im originalen Skelett-Zusammenhang.

Rezent ist die Familie der Schaufelfußkröten in Europa, West-Asien und Nord-Afrika mit der Gattung *Pelobates*, in Deutschland einheimisch die Knoblauchkröte *Pelobates fuscus*, vertreten. Zu der rezenten Scheibenzünglerverwandtschaft gehören die Familie der Bombinatoridae (Unkenverwandte, verbreitet von Westeuropa bis östliches Russland, Türkei, China, Korea und Vietnam) und die Familie Alytidae (Geburtshelferkröten und Scheibenzüngler, verbreitet in West-Europa, mediterranes Nord-Afrika, Israel und Syrien).

Todesursachen

In früheren Studien wurde vermutet, dass die Froschlurche des Geiseltals durch die Austrocknung ihrer Tümpel und/oder in Folge des Umkippens des Gewässers durch Sauerstoffmangel gestorben sind (Voigt 1934, Weigelt 1934). Dies erscheint unwahrscheinlich, da Froschlurche bei für sie ungünstigen Umweltbedingungen zu anderen Gewässern abwandern (Henrici & Fiorillo 1993, Todd et al. 2009). Zudem belegen unsere Daten aus der detaillierten Analyse der Skelette, dass die Froschkadaver zeitweise in der Wassersäule getrieben sind (Falk et al. 2022), was dem Austrocknen der Tümpel entgegensteht. Die Fundsituation und Sedimente, in denen die Froschlurchskelette gefunden wurden, deuten auf mehrere Massensterben hin.

Im Folgenden beschreiben wir alternative Todesursachen und in welchem Umfang diese zum

Tod der Froschlurche beigetragen haben (nach Falk et al. 2022):

(1) Erhöhte Salinität in den Gewässern wird durch salzliebende Farne (Barthel & Rüffle 1970) und Ostrakoden (Krumbiegel 1962) angedeutet. Vergleichbar mit der Austrocknungs-Hypothese, ist ein Tod der Froschlurche durch den Salzgehalt unwahrscheinlich, da die Individuen abgewandert wären. Zudem können heutige Pelobatiden zum Teil auch Brackwasser tolerieren (Stănescu et al. 2013).

(2) Hungertod. Ein Verhungern ist nicht plausibel, da die Froschlurche üblicherweise migrieren, wenn die Nahrung knapp wird (Buchacher 1993, Todd et al. 2009). Einige Geiseltalskelette wurden mit Koprolithen (versteinerter Kot) überliefert, was für eine zeitnahe Mahlzeit vor dem Tod spricht. Auch ein Verhungern während einer Winterstarre lässt sich ausschließen, da das Paläoklima nicht ausreichend kalt war (kaum bis überhaupt kein Frost, siehe Punkt 5), um eine anhaltende Winterstarre zu gewährleisten (Grein et al. 2011, Krutzsch 2011).

(3) Vergiftung durch Algenblüten. Es sind geologische Ablagerungen von Diatomiten und Dinoflagellaten vorhanden (Krumbiegel et al. 1983). Diese lassen auf Algenblüten schliessen, die für die aquatische Fauna toxisch gewesen sein könnten (Carty & Parrow 2015, López-Cortés et al. 2015, Watson et al. 2015). Die direkte Zuordnung dieser Algenablagerungen zu den erhaltenen Froschlurchskeletten ist nicht möglich, aber die terrestrische Lebensweise der Pelobatiden schließt einen wesentlichen Einfluss auf den Tod der Individuen aus (Lizana et al. 1994, Henrici & Fiorillo 1993).

(4) Sturm / Flutevents. Einige Individuen, insbesondere die, deren Skelette in einer Himmelsrichtung ausgerichtet sind (Weigelt 1933), könnten durch starke Wasserturbulenzen während Starkregen und Flutereignisse getötet worden sein (Duellman & Trueb 1994, La Marca 2021). Eine post mortem Orientierung der Skelette durch Strömungen kann dennoch nicht ausgeschlossen werden (Henrici & Fiorillo 1993).

(5) Erfrierung. Das eozäne Treibhausklima schließt äußerst seltene kurzzeitige Temperaturschwankungen von weit unter 0°C auch im Geiseltal nicht aus (Grein et al. 2011, Hu et al. 2018). Solche Schwankungen können für Froschlurche zur Gefahr werden, wenn ihre Gewässer auch in der Tiefe vereisen. Die Seen und Tümpel des Geiseltals waren mit mehreren Metern Tiefe vermutlich tief genug, um bodennah eisfrei zu bleiben und somit Palaeobatrachiden während Kälteperioden Schutz zu bieten (Manion & Brother Lawrence 1952, Voituron et al. 2009, Brattstrom 1968, Costanzo et al. 2013). Pelobatiden dagegen suchen außerhalb der Paarungszeit keine Gewässer auf (Swanson & Graves 1995, Costanzo & Lee 2013, Lizana et al. 1994) und sind daher nicht zum Schutz vor Erfrieren in die Tümpel und Seen migriert.

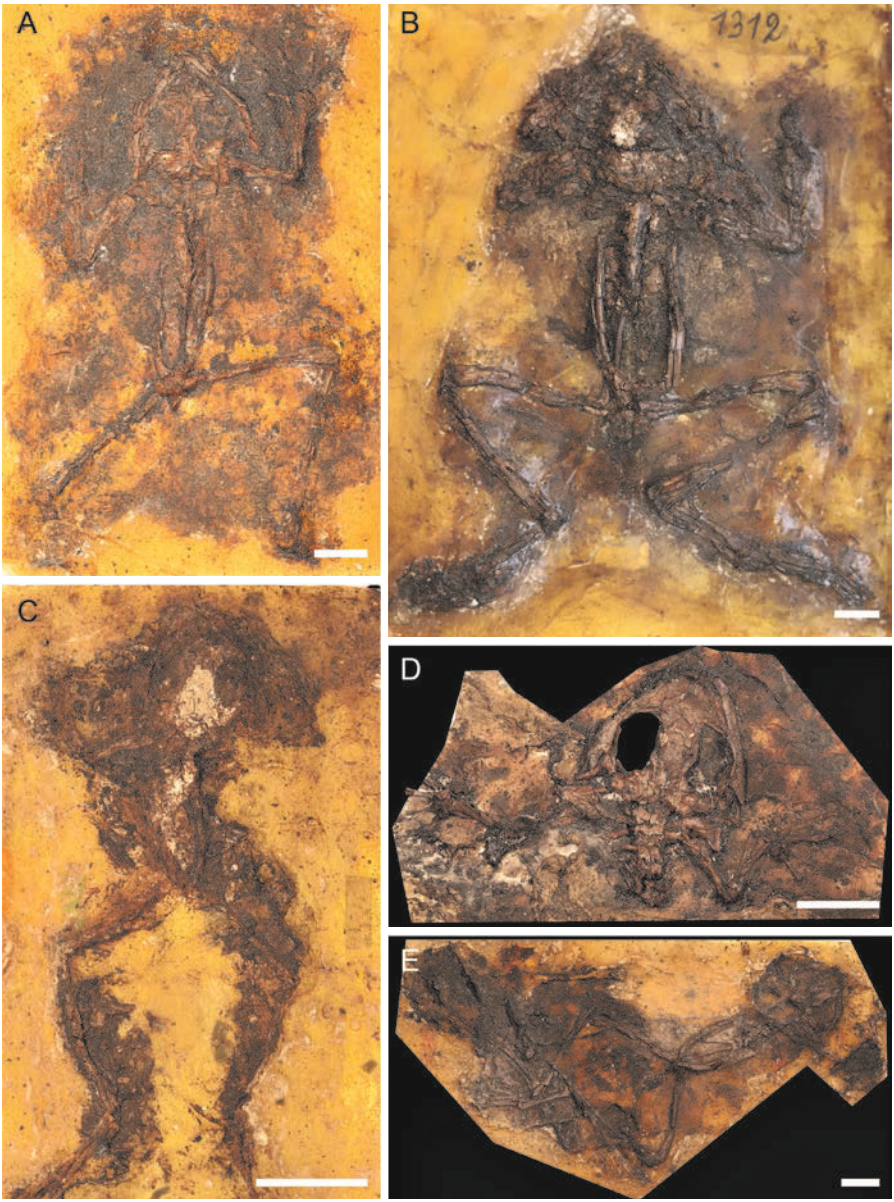


Abb. 2: Fossile Froschlurchskelette der Geiseltal Sammlung mit unterschiedlicher Skelettvollständigkeit und Skelettartikulation; A: Pelobatide, CeIII 6834-1932; B: Pelobatide, CeIII 1312-1932; C: Pelobatide, CeIV 6692-1933; D: Pelobatide CeIII 4965-1932; E: Pelobatide, CeIII 1301-1932; Maßstab: 1 cm. Fotos: D. Falk

(6) Krankheit. Das Massensterben könnte das Resultat von Seuchen sein (rezent z.B. Chytridiomykose (Lips 1999, Scheele et al. 2019) und Ranavirus (Price et al. 2017)). Eine Verifikation ist allerdings vermutlich unmöglich, da die Merkmale von Krankheiten normalerweise nicht im Fossilbericht überliefert sind (Densmore & Green 2007).
(7) Jagd und Raubfraß. Auch im eozänen Geiseltal hatten Amphibien eine große Anzahl Fressfeinde. Es gibt Belege an einzelnen Objekten auf Raubfraß (z.B. isolierte Körperhälften oder Mageninhalte von Fischen (Voigt 1934)), für die Mehrzahl der untersuchten Anurenskelette lässt sich aufgrund ihrer Vollständigkeit ein derartiger Einfluss aber ausschließen.
(8) Altersschwäche. Die Längendaten der Skelette sind normal verteilt, was auf eine breite Streuung von Größen und vermutlich Altersgruppen schließen lässt (auch, wenn ein statistischer Zusammenhang zwischen Größe und Alter nicht gesichert ist). Einige Froschlurche könnten an Altersschwäche gestorben sein, aber der natürliche, nahezu gleichzeitige Tod von mehreren hundert Individuen ist unwahrscheinlich.
(9) Paarung. Massensterben im Zusammenhang mit dem Paarungsverhalten ist bei rezenten Froschlurchen in der kurzen, aber explosiven Paarungszeit bekannt (Verrell & McCabe 1986, Trauth et al. 2000, Menin et al. 2006, Izzo et al. 2012). Insbesondere weibliche Exemplare haben ein relativ hohes Todesrisiko, wenn sie von mehreren männlichen Individuen während des kräfteraubenden Paarungsaktes unter Wasser gedrückt werden. Sie sterben an Erschöpfung oder ertrinken. Das Szenario ist auch für vornehmlich terrestrisch lebende Froschlurche anwendbar, da sie zur Reproduktion zu Gewässern migrieren (Lizana et al. 1994). Die Massensterben durch Paarung wurde auch an Froschfossilien aus anderen Ländern nachgewiesen (McNamara et al. 2012).

Beispiele misslungener Ablaichakte rezenter Amphibien

Im Frühjahr kommen viele Amphibien gleichzeitig verpaart oder unverpaart am Laichplatz an. Meist wimmelt es jedoch am Laichplatz von unverpaarten Männchen, auf der Suche nach einem Weibchen, die beispielsweise bei den Erdkröten meist stark in der Unterzahl sind. Unverpaarte Männchen versuchen deshalb, schon verpaarte Artgenossen von dem Weibchen zu trennen, was aber nur selten gelingt. Häufig kommt es dann zur Bildung von Paarungsknäueln, die aus mehreren Erdkröten bestehen. Eine derartige Beobachtung wurde am 26.03.2010 im Amphibienvorkommen Kreuzer Teiche in Halle/Sachsen-Anhalt gemacht (Abb. 3). Eine Massenvermehrung der Erdkröten führte in dem Jahr zu einem Geschlechterverhältnis von 10:1 (Männchen:Weibchen). Auch in dem Betonteich am

Palmenhaus des Botanischen Gartens in Halle konnten in den Jahren 2010–2012 derartige Paarungsknäueln beobachtet werden, wobei selbst Weibchen der Wechselkröte geklammert wurden. In solchen untergetauchten Knäueln ertrinken aufgrund Luftmangels viele Kröten; im Botanischen Garten führte das Verhalten der Erdkrötenmännchen sogar zum Erlöschen der Wechselkrötenpopulation, da diese Art an dem Standort weit in der Unterzahl war und sich in der Phase der Massenvermehrung der Erdkröten nicht mehr reproduzieren konnte. Auffällig war, dass die totgeklammerten Individuen in den ersten Tagen danach am Grund der Gewässer lagen, so wie es vielleicht auch ihren fossilen Vorfahren im Geiseltal ergangen sein könnte.



Abb. 3: Paarungsknäuel aus mehreren Erdkröten bestehend, 26.03.2010 Amphibienvorkommen Kreuzer Teiche in Halle/Sachsen-Anhalt. Foto: P. Fritzsche

Zusammenfassung

Die meisten Froschlurchskelette aus dem Geiseltal sind den Schaufelfußkröten zuzuordnen. Diese leben nur zur Paarungszeit in Gewässern. Durch das Ausschlussverfahren und die Annahme von Verhaltensweisen moderner Froschlurche für die eozänen Froschlurche ist die wahrscheinlichste Todesursache, dass viele Geiseltal Froschlurche in einer kurzen, explosiven Paarungszeit während des Aktes und / oder in der Paarungszeit gestorben sind. Wir können allerdings nicht ausschließen, dass der Tod im Paarungsgewässer auch durch Krankheit oder Altersschwäche eingetreten ist. Der Nachweis des Geschlechts an Skeletten ist nicht möglich. Nach dem Tod wurden die Kadaver durch Strömungen in tiefere Bereichen der Seen und Tümpel transportiert und durch normale taphonomische Prozesse konserviert.

Danksagung

Dank gilt allen aktuellen und ehemaligen BearbeiterInnen der Geiseltal Sammlung, den MitarbeiterInnen des ZNS und dem Irish Research Council (IRC) für die Finanzierung des Projektes durch ein Government of Ireland Postgraduate Scholarship (GOIPG/2018/3354).

Literatur

Barnes, B. (1926): Eine eozäne Wirbeltier-Fauna aus der Braunkohle des Geiseltales. – Jahrbuch des Halleschen Verbandes für die Erforschung der mitteldeutschen Bodenschätze, 6: 5–24.

Barthel, M. & L. Rüffle (1970): Vegetationsbilder aus dem Alttertiär (Eozän) der Braunkohle des Geiseltales. – Wissenschaftliche Zeitschrift der Humboldt-Universität zu Berlin / Mathematisch-Naturwissenschaftliche Reihe, XIX: 274–283.

Brattstrom, B. H. (1968): Thermal acclimation in anuran amphibians as a function of latitude and altitude. – Comparative Biochemistry and Physiology, 24: 93–111.

Buchacher, C. O. (1993): Field studies on the small Surinam toad, *Pipa arrabali*, near Manaus, Brazil. – Amphibia-Reptilia, 14: 59–69.

Carty, S. & M.W. Parrow (2015): Chapter 17 – Dinoflagellates. 773–807. In Wehr, J. D., Sheath, R. G. & J.P. Kociolek (Hrsg.): Freshwater Algae of North America. – Academic Press, Boston, 1066 S.

Costanzo, J. P., Do Amaral, M. C., Rosendale, A. J. & R. E. Jr. Lee (2013): Hibernation physiology, freezing adaptation and extreme freeze tolerance in a northern population of the wood frog. – Journal of Experimental Biology, 216: 3461–3473

Costanzo, J. P. & R. E. Jr. Lee (2013): Avoidance and tolerance of freezing in ectothermic vertebrates. – Journal of Experimental Biology, 216: 1961–1967.

Densmore, C. L. & D. E. Green (2007): Diseases of amphibians. – Institute for Laboratory Animal Research Journal, 48: 235–254.

Duellman, W. E. & L. Trueb (1994): Population Biology. 261–274. In Duellman, W. E. & L. Trueb (Hrsg.). Biology of amphibians. – John Hopkins University Press, Baltimore and London, 670 S.

Falk, D. & M. Stache (2021): Die eozänen Froschlurche der Geiseltal-Sammlung. S. 39–47. In Seidl, E., Steinheimer, F. & Weber, C. (Hrsg.): Eine Frage der Perspektive. Objekte als Vermittler von Wissenschaft. – Humboldt-Universität zu Berlin, Junges Forum für Sammlungs- und Objektforschung. Herausgegeben von der Gesellschaft für Universitätssammlungen e.V. Bd. V, 128 S.

Falk, D., Wings, O. & M.E. McNamara (2022): The skeletal taphonomy of anurans from the Eocene Geiseltal Konservat-Lagerstätte, Germany: insights into the controls on fossil anuran preservation. – Papers in Palaeontology, 8, e1453, 1–34.

Glandt, D. (2016): Amphibien und Reptilien. Herpetologie für Einsteiger. – Springer Spektrum, Berlin und Heidelberg, 246 S.

Grein, M., Utescher, T., Wilde, V. & A. Roth-Nebelsick (2011): Reconstruction of the Middle Eocene climate of Messel using palaeobotanical data. – Neues Jahrbuch für Geologie und Paläontologie – Abhandlungen, 260: 305–318.

Henrici, A. C. & A.R. Fiorillo (1993): Catastrophic death assemblage of Chelomophrynus bayi (Anura, Rhinophrynidae) from the middle Eocene Wagon Bed Formation of central Wyoming. – Journal of Paleontology, 67: 1016–1026.

Hu, Z., Cronin, T. W. & E. Tziperman (2018): Suppression of cold weather events over high-latitude continents in warm climates. – Journal of Climate, 31: 9625–9640.

Izzo, T. J., Rodrigues, D. J., Menin, M., Lima, A. P. & W.E. Magnusson (2012): Functional necrophilia: a profitable anuran reproductive strategy? – Journal of Natural History, 46: 2961–2967.

Krumbiegel, G., Rüffle, L. & H. Haubold (1983): Das eozäne Geiseltal: ein mitteleuropäisches Braunkohlenvorkommen und seine Pflanzen- und Tierwelt. – A. Ziemsen Verlag, Die Neue Brehm-Bücherei, Wittenberg Lutherstadt, 227 S.

Krumbiegel, G. (1962): Die Fossilfundstellen der mitteleozänen Braunkohle des Geiseltales. – Wissenschaftliche Zeitschrift der Martin-Luther-Universität in Halle, 11: 173–208.

Krutzsch, W. (2011): Stratigrafie und Klima des Palaogens im Mitteldeutschen Ästuar im Vergleich zur marinen nordlichen Umrahmung. – Zeitschrift der Deutschen Gesellschaft für Geowissenschaften, 162: 19–47.

Kuhn, O. (1941): Die eozänen Anura aus dem Geiseltale nebst einer Übersicht über die fossilen Gattungen. – Nova Acta Leopoldina, Neue Folge, 10: 345–376.

Lips, K. R. (1999): Mass mortality and population declines of anurans at an upland site in western Panama. – Conservation Biology, 13: 117–125.

La Marca, E. (2021): Action Plan for Atelopus oxyrhynchus. – https://www.amphibianark.org/wp-content/uploads/2020/06/Species-Action-Plan-Atelopus-oxyrhynchus.pdf, aufgerufen 18.10.2022.

Lizana, M., Márquez, R. & R. Martín-Sánchez (1994): Reproductive biology of *Pelobates cultripes* (anura: Pelobatidae) in Central Spain. – Journal of Herpetology, 28: 19–27.

López-Cortés, D. J., Núñez-Vázquez, E. J., Band-Schmidt, C. J., Gárate-Lizárraga, I., Hernández-Sandoval, F. E. & J.J. Bustillos-Guzmán (2015): Mass fish die-off during a diatom bloom in the Bahía de La Paz, Gulf of California. – Hidrobiológica, 25: 39–48.

Manion, J. J. & C. Brother Lawrence (1952): Winter kill of *Rana pipiens* in shallow ponds. – Herpetologica, 8: 32.

Menin, M., Rodrigues, D. J. & A.P. Lima (2006): The tadpole of *Rhinella proboscidea* (Anura: Bufonidae) with notes on adult reproductive behavior. – Zootaxa, 1258: 47–56.

McNamara, M. E., Orr, P. J., Alcalá, L., Anadón, P. & E. Peñalver (2012): What controls the taphonomy of exceptionally preserved taxa – environment or biology? A case study using frogs from the Miocene Libros Konservat-Lagerstätte (Teruel, Spain). – Palaios, 27: 63–77.

Price, S. J., Ariel, E., Maclaine, A., Rosa, G. M., Gray, M. J., Brunner, J. L. & T.W.J. Garner (2017): From fish to frogs and beyond: impact and host range of emergent ranaviruses. – Virology, 511: 272–279.

Roček, Z. (2013): Mesozoic and Tertiary Anura of Laurasia. – Palaeobiodiversity and Palaeoenvironments, 93: 397–439.

Roček, Z. & J. Rage (2000): Tertiary Anura of Europe, Africa, Asia, North America, and Australia. – Amphibian Biology, 4: 1332–1387.

Roček, Z., Rage, J.-C. & M. Venczel (2021): Fossil frogs of the genus *Palaeobatrachus* (Amphibia: Anura). – Abhandlungen der Senckenberg Gesellschaft für Naturforschung. Schweizerbart Science Publishers, Stuttgart, 151 pp.

Roček, Z., Wuttke, M., Gardner, J. D. & B.A. Singh Bhullar (2014): The Euro-American genus Eopelobates, and a re-definition of the family Pelobatidae (Amphibia, Anura). – Palaeobiodiversity and Palaeoenvironments, 94: 529–567.

Scheele, B. C., Pasmans, F., Skerratt, L. F., Berger, L., Martel, A., Beukema, W., Acevedo, A. A., Burrowes, P. A., Carvalho, T., Catenazzi, A., De La Riva, I., Fisher, M. C., Flechas, S. V., Foster, C. N., Frías-Álvarez, P., Garner, T. W. J., Gratwicke, B., Guayasamin, J. M., Hirschfeld, M., Kolby, J. E., Kosch, T. A., La Marca, E., Lindenmayer, D. B., Lips, K. R., Longo, A. V., Maneyro, R., McDonald, C. A., Mendelson, J., Palacios-Rodriguez, P., Parra-Olea, G., Richards-Zawacki, C. L., Rödel, M.-O., Rovito, S. M., Soto-Azat, C., Toledo, L. F., Voyles, J., Weldon, C., Whitfield, S. M., Wilkinson, M., Zamudio, K. R. & S. Canessa (2019): Amphibian fungal panzootic causes catastrophic and ongoing loss of biodiversity. – Science, 363: 1459–1463.

Stănescu, F., Iosif, R., Székely, D., Székely, P., Roşioru, D. & D. Cogălniceanu (2013): Salinity tolerance in Pelobates fuscus (Laurenti, 1768) tadpoles (Amphibia: Pelobatidae). – Travaux du Muséum National d'Histoire Naturelle "Grigore Antipa", 56: 103–108.

Swanson D. L. & Graves, B. M. (1995): Supercooling and freeze intolerance in overwintering juvenile spadefoot toads (*Scaphiopus bombifrons*). – Journal of Herpetology, 29: 280–285.

Trauth, S. E., McCallum, M. L. & M.E. Cartwright (2000): Breeding mortality in the wood frog, Rana sylvatica (Anura: Ranidae), from Northcentral Arkansas. – Journal of the Arkansas Academy of Science, 54: 154–156.

Todd, B. D., Luhring, T. M., Rothermel, B. B. & J.W. Gibbons (2009): Effects of forest removal on amphibian migrations: implications for habitat and landscape connectivity. – Journal of Applied Ecology, 46: 554–561.

Verrell, P. A. & N. McCabe (1986): Mating balls in the common toad, *Bufo bufo*. – British Herpetological Society Bulletin, 16: 28–29.

Voigt, E. (1934): Die Fische aus der mitteleozänen Braunkohle des Geiseltales mit besonderer Berücksichtigung der Weichteile. – Nova Acta Leopoldina, Neue Folge, 2: 21–146.

Voigt, E. (1988): Preservation of soft tissues in the Eocene lignite of the Geiseltal near Halle (Saale). – Courier Forschungsinstitut Senckenberg, 107: 325–343.

Voituron, Y., Barré, H., Ramløv, H. & C.J. Douady (2009): Freeze tolerance evolution among

anurans: frequency and timing of appearance. – Cryobiology, 58: 241–247.

Watson, S. B., Whitton, B. A., Higgins, S. N., Paerl, H. W., Brooks, B. W. & J.D. Wehr (2015): Harmful Algal Blooms. 873–920. – In Wehr, J. D., Sheath, R. G. & J.P. Kociolek (Hrsg.). – Freshwater Algae of North America. – Academic Press, Boston, 1066 S.

Weigelt, J. (1933): Die Biostratonomie der 1932 auf der Grube Cecilie im mittleren Geiseltal ausgegrabenen Leichenfelder. – Nova Acta Leopoldina, Neue Folge, 1: 157–174.

Weigelt, J. (1934): Die Geiseltalgrabungen des Jahres 1933 und die Biostratonomie der Fundschichten. – Nova Acta Leopoldina, Neue Folge, 1: 552–660.

Autoren:

Daniel Falk[1,2], Wolf-Rüdiger Grosse[3], Maria McNamara[1,2] & Oliver Wings[3,4]

[1] School of Biological, Earth and Environmental Sciences, University College Cork, Cork, Ireland; ORCiD ID: 0000-0001-7502-6844 (Daniel Falk); 0000-0003-0968-4624 (Maria E. McNamara); daniel.falk@ucc.ie

[2] Environmental Research Institute, University College Cork, Cork, Ireland.

[3] Zentralmagazin Naturwissenschaftlicher Sammlungen, Martin-Luther-Universität Halle-Wittenberg, Domplatz 4, 06108 Halle (Saale)

[4] Naturkundemuseum Bamberg, Fleischstr. 2, 96047 Bamberg; ORCiD ID: 0000-0002-6482-6683; *wings@snsb.de*

Kontakt zum Autor:

Daniel Falk
Wiesenweg 8c, 16515 Oranienburg
E-Mail: daniel.falk@ucc.ie

Appendix III – Datasets

Supplementary datasets 1–3

Falk, D., Wings, O. & McNamara, M. (2022). Data from: The skeletal taphonomy of anurans from the Eocene Geiseltal Konservat-Lagerstätte, Germany: insights into the controls on fossil anuran preservation [Dataset]. Dryad. https://doi.org/10.5061/dryad.2bvq83brt

SUPPLEMENTARY DATASET 1. Master dataset with skeletal taphonomic data for the Geiseltal anurans. Data are shown for each of 140 specimens used in the study and an additional 28 specimens that were excluded due to poor preservation (precluding confident identification of individual skeletal elements). Specimens lacking a full limb are identified on the basis of the absence of at least one humerus or femur and their respective distal limb elements. Specimens showing isolated limbs only are omitted from this analysis; specimens are also omitted where truncation (i.e. of the torso) prevents confidence of presence/absence of humeri and/or femura. Abbreviations: Ce, 'Cecilie' pit; IL, 'Geiselröhlitz' site; GMH, Geiseltalmuseum Halle; hyphen (-), unknown; indet., indetermined; Leo, 'Leonhard' pit; LMC, lower middle coal; LUC, lower upper coal; MC, middle coal; MUC, middle upper coal; Nw, 'Neumark-West' pit; N/A, not applicable; UHM, upper 'Hauptmittel' ('Hauptmittel': intercalated sandy and silty successions); UMC, upper middle coal; XXXV, most likely Neumark-Süd pit (NsXXXV).

museum prefix	site prefix	specimen number	year	anuran family	short description	snout-urostyle-length (mm)	Gaiselitsl-Taphonomic State (=truncated specimens only)	% completeness	% completeness (hands/feet omitted)	% completeness (phalanges omitted)	% completeness (distal to truncated = coded as 'not present')	% articulation	% articulation (hands/feet omitted)	% articulation (phalanges omitted)	%truncation	orientation (on embedding material)	truncated element(s)	specimen lacks full limb	potential coprolite	strata	embedding material
GMH	CeII	6709	1930	Pelobatidae	skeleton	N/A	2; 8; 9	42.5	92.9	59.4	42.5	86.0	88.5	85.3	0.0	dorso-ventral	N/A	no	no	LUC	paraffin wax (gypsum frame)
GMH	CeII	6687	1932	Palaeobatrachidae	skeleton	N/A	N/A	57.9	95.8	81.8	36.3	100.0	100.0	100.0	37.4	ventral	cranium, right humerus, right astragalus-calcaneum	no	no	LUC	nitrocellulose glue
GMH	CeIV	2893	1933	Anura indet.	disarticulated + accumulated, disarticulated bones	N/A	N/A	100.0	100.0	100.0	9.1	85.7	85.7	85.7	65.9	dorso-ventral	ilia, left and right femur, left astragalus calcaneum	no	no	UMC	nitrocellulose glue
GMH	CeII	4939	1932	Pelobatidae	skeleton	N/A	N/A	13.9	62.5	31.3	6.1	83.3	83.3	83.3	50.5	dorso-ventral	hip (no legs)	no	no	LUC	paraffin wax (gypsum frame)
GMH	CeII	4126	1932	?Pelobatidae	skeleton	N/A	3; 9	14.8	59.1	32.5	14.8	63.2	63.2	63.2	0.0	ventral	N/A	yes	no	LUC	nitrocellulose glue
GMH	Ce	9002	-	Pelobatidae	skeleton	31.5	N/A	69.0	95.5	88.6	44.0	94.3	100.0	93.9	36.3	ventral	right toes, left femur	no	no	-	paraffin wax
GMH	CeII	4935	1931	Pelobatidae	skeleton	37.6	2; 9	20.0	75.0	42.9	20.0	77.3	77.3	77.3	0.0	dorso-ventral	N/A	no	no	LUC	paraffin wax (gypsum frame)
GMH	CeII	6703	1930	Palaeobatrachidae	skeleton	N/A	2; 8; 9	27.5	60.0	51.2	27.5	77.4	81.3	87.5	0.0	dorso-ventral	N/A	yes	no	LUC	paraffin wax (gypsum frame)
GMH	CeII	4950	1930	Palaeobatrachidae	skeleton	40	2; 9	56.0	84.0	69.8	56.0	92.6	100.0	94.3	0.0	ventral	N/A	yes	no	LUC	paraffin wax (gypsum frame)
GMH	CeII	6700	1930	?Pelobatidae	skeleton	N/A	3; 9	35.2	68.0	60.5	35.2	81.8	93.3	80.0	0.0	dorso-ventral	N/A	no	no	LUC	paraffin wax (gypsum frame)
GMH	IL	17A	1969	Anura indet.	disarticulated bones	N/A	4; 9	36.0	36.0	36.0	36.0	37.5	37.5	37.5	0.0	N/A	N/A	no	no	LMC	nitrocellulose glue
GMH	IL	17C	1969	Anura indet.	disarticulated bones	N/A	N/A	100.0	100.0	100.0	9.9	75.0	75.0	75.0	90.1	N/A	vertebral column	N/A	no	LMC	nitrocellulose glue
GMH	CeII	6727	1932	Anura indet.	disarticulated bones	N/A	N/A	63.6	66.7	63.6	7.7	0.0	0.0	0.0	87.9	N/A	?femur/?tibiofibula	no	no	LUC	nitrocellulose glue on gypsum
GMH	CeII	6704	1930	Anura indet.	disarticulated bones	N/A	N/A	100.0	100.0	100.0	6.7	50.0	50.0	50.0	91.2	N/A	radioulna, ?humerus	no	no	LUC	paraffin wax (gypsum frame)
GMH	CeII	6762	1933	Pelobatidae	skeleton	N/A	N/A	38.1	100.0	67.4	35.2	97.1	100.0	97.0	7.7	dorsal	left metacarpals	no	yes	LUC	nitrocellulose glue
GMH	CeII	6718	1932	Pelobatidae	skeleton	N/A	4; 9	6.7	26.1	14.6	6.7	0.0	0.0	0.0	0.0	dorso-ventral	N/A	yes	no	LUC	nitrocellulose glue
GMH	CeII	4956	1932	Pelobatidae	skeleton	N/A	N/A	45.3	84.0	72.7	33.3	62.1	64.0	62.1	20.9	dorsal	cranium, right metatarsals	no	no	LUC	nitrocellulose glue
GMH	CeII	6708	1930	?Pelobatidae	skeleton	N/A	N/A	20.9	60.0	39.1	9.9	100.0	100.0	100.0	52.7	ventral	vertebral column (no sacral vertebrae)	yes	no	LUC	paraffin wax (gypsum frame)
GMH	CeI	4947	1930	Pelobatidae	skeleton	N/A	2; 9	30.3	73.9	51.2	30.3	93.8	100.0	100.0	0.0	dorsal	N/A	yes	no	UHM	paraffin wax (gypsum frame)
GMH	CeII	4975	1932	Pelobatidae	skeleton	N/A	N/A	32.2	33.3	39.4	22.1	81.3	40.0	75.0	29.7	dorso-ventral	cranium, left toes, right ?astragalus-calcaneum	yes	no	LUC	nitrocellulose glue
GMH	CeII	4940	1931	Anura indet.	disarticulated bones	N/A	N/A	100.0	100.0	100.0	4.5	100.0	100.0	100.0	93.4	N/A	left femur, left and right tibiofibula	no	no	LUC	paraffin wax
GMH	CeII	6725	1932	Anura indet.	skeleton (hindlimb only)	N/A	N/A	63.6	100.0	100.0	15.6	94.4	100.0	85.7	74.7	N/A	femur	N/A	no	LUC	nitrocellulose glue on gypsum
GMH	CeII	4944	1930	Pelobatidae	disarticulated bones	N/A	N/A	60.0	60.0	60.0	9.9	66.7	66.7	66.7	83.5	dorsal	cranium, vertebral column	no	no	LUC	paraffin wax
GMH	CeII	6720	1932	Anura indet.	skeleton (cranium+upper body)	N/A	3; 9	12.2	45.8	26.2	12.2	63.6	63.6	63.6	0.0	dorsal	N/A	yes	no	LUC	nitrocellulose glue on gypsum
GMH	CeVI	4976B	1934	Anura indet.	skeleton (hindlimbs only)	N/A	N/A	47.8	100.0	88.9	24.2	80.8	83.3	93.3	49.5	N/A	both femur	N/A	no	?UMC/?LUC	nitrocellulose glue
GMH	CeII	4968	1932	?Pelobatidae	skeleton	N/A	3; 9	45.5	88.0	74.4	45.5	94.7	95.7	97.0	0.0	dorsal	N/A	yes	no	LUC	nitrocellulose glue
GMH	CeII	4989	1932	Anura indet.	skeleton	N/A	N/A	22.2	36.4	30.8	9.6	71.4	71.4	71.4	51.6	N/A	cranium, right radioulna, left metatarsals, right astragalus-calcaneum	no	no	LUC	nitrocellulose glue
GMH	CeIV	4953	1933	Pelobatidae	accumulated, disarticulated bones	N/A	5; 9	25.8	47.1	38.1	25.8	33.3	33.3	33.3	0.0	N/A	N/A	no	no	UMC	nitrocellulose glue
GMH	CeII	4958	1933	?Pelobatidae	skeleton	N/A	2; 7; 9	36.3	72.0	62.8	36.3	80.0	65.0	76.7	0.0	dorso-ventral	N/A	yes	no	LUC	nitrocellulose glue
GMH	CeIV	4960	1933	Pelobatidae	accumulated, disarticulated bones	N/A	N/A	57.1	75.0	81.0	24.4	52.6	62.5	76.9	51.6	N/A	unidentified bone	no	no	UMC	nitrocellulose glue
GMH	CeIV	4955	1933	Anura indet.	skeleton	N/A	2; 7; 9	13.2	48.0	27.9	13.2	76.9	76.9	76.9	0.0	ventral	N/A	yes	no	UMC	nitrocellulose glue
GMH	CeIV	4957	1933	?Palaeobatrachidae	skeleton	N/A	1; 9	57.1	100.0	100.0	57.1	73.6	75.0	82.1	0.0	dorso-ventral	N/A	no	no	UMC	nitrocellulose glue
GMH	CeII	4967	1932	Pelobatidae	skeleton	N/A	N/A	37.0	95.2	66.7	22.0	100.0	100.0	100.0	40.7	ventral	right humerus, right femur	no	yes	LUC	nitrocellulose glue
GMH	CeII	6729	1932	Anura indet.	skeleton	?12.5	N/A	53.1	94.4	77.3	18.7	90.0	90.0	90.0	64.8	ventral	left radioulna, left tibiofibula, urostyle, hip (right hindlimb)	no	no	LUC	nitrocellulose glue
GMH	CeII	6761	1932	?Pelobatidae	skeleton	N/A	N/A	46.5	80.0	63.2	36.3	85.3	77.3	81.5	22.0	dorso-ventral	right phalanges, right astragalus-calcaneum	yes	no	LUC	nitrocellulose glue
GMH	CeIV	2895	1933	Anura indet.	disarticulated bones	N/A	5; 9	6.9	28.6	15.4	6.9	75.0	75.0	75.0	0.0	dorso-ventral	N/A	yes	no	UMC	nitrocellulose glue
GMH	CeII	1305	1933	Anura indet.	skeleton (hindlimbs only)	N/A	N/A	50.0	100.0	93.8	16.5	100.0	100.0	100.0	67.0	dorso-ventral	left and right tibiofibula, right metatarsals (missing upper body)	N/A	no	LUC	nitrocellulose glue
GMH	CeII	6748	1932	Anura indet.	skeleton	N/A	N/A	37.5	90.0	64.3	20.0	63.6	63.6	63.6	46.2	dorso-ventral	cranium, left and right tibiofibula	no	no	LUC	nitrocellulose glue
GMH	CeII	6747	1932	Anura indet.	skeleton	N/A	3; 9	9.0	4.5	3.3	9.0	83.3	0.0	0.0	0.0	dorso-ventral	N/A	yes	no	LUC	nitrocellulose glue
GMH	CeII	1307	1933	Anura indet.	disarticulated bones	N/A	N/A	50.0	66.7	68.2	26.3	76.2	54.5	70.6	41.8	dorso-ventral	?femur/?tibiofibula	no	no	LUC	nitrocellulose glue
GMH	CeII	4988	1932	Anura indet.	skeleton (hindlimbs only)	N/A	N/A	100.0	100.0	100.0	6.4	100.0	100.0	100.0	80.2	dorso-ventral	left toes, right astragalus-calcaneum, ?right toes	N/A	no	LUC	nitrocellulose glue
GMH	CeII	6740	1933	Anura indet.	skeleton (lower body only)	N/A	N/A	67.9	60.0	64.0	22.4	50.0	50.0	50.0	62.6	dorso-ventral	ilia, left toes, right metatarsals (no upper body, but vertebral column)	no	no	LUC	nitrocellulose glue
GMH	CeII	6743	1932	Pelobatidae	skeleton	?43.1	N/A	56.8	87.5	75.0	23.1	100.0	100.0	100.0	59.3	dorsal	right phalanges, hip (no legs)	yes	no	LUC	nitrocellulose glue
GMH	CeII	6754A	1933	Pelobatidae	skeleton	N/A	N/A	55.6	88.2	88.2	17.2	94.1	94.1	94.1	65.9	dorsal	cranium, right radioulna, hip (right femur present)	no	no	LUC	nitrocellulose glue
GMH	CeII	4990	1932	Pelobatidae	skeleton	N/A	N/A	25.3	58.3	42.9	23.3	61.9	42.9	57.9	7.7	dorso-ventral	left phalanges	yes	no	UMC	nitrocellulose glue
GMH	CeII	6745	1932	Pelobatidae	skeleton	N/A	N/A	75.9	100.0	100.0	24.2	96.7	94.4	95.7	68.1	dorsal	left humerus, right ilium, urostyle, hip (right femur present)	no	no	LUC	nitrocellulose glue
GMH	CeII	6754B	1933	?Discoglossidae/?Palaeoatrachidae	skeleton	32.3	N/A	57.9	83.3	72.7	36.7	81.6	86.4	82.1	36.3	ventral	left carpals, right astragalus-calcaneum, hip (no ischium)	no	no	LUC	nitrocellulose glue
GMH	NwXIV/?CeXIV	1275	1954	Anura indet.	skeleton	N/A	N/A	100.0	100.0	100.0	9.9	100.0	100.0	100.0	90.1	ventral	left and right ilium, urostyle (no vertebral column), left astragalus-calcaneum, right femur	no	no	-	nitrocellulose glue
GMH	CeII	6759	1932	Pelobatidae	skeleton	N/A	N/A	49.2	82.6	74.3	31.9	88.6	86.4	90.3	35.2	ventral	left metacarpals, right tibiofibula	yes	no	LUC	nitrocellulose glue
GMH	CeII	4978	1932	Pelobatidae	skeleton	N/A	N/A	60.9	86.4	77.1	46.2	83.0	90.9	87.1	24.2	ventral	cranium, left femur	no	no	LUC	nitrocellulose glue
GMH	CeII	6757	1932	Pelobatidae	skeleton	N/A	N/A	35.0	75.0	54.5	23.1	95.5	100.0	94.4	34.1	ventral	cranium, left phalanges, vertebral column (no ischium, no right leg)	no	no	LUC	nitrocellulose glue
GMH	CeII	6693	1933	Anura indet.	disarticulated + accumulated, disarticulated bones	N/A	N/A	100.0	100.0	100.0	9.3	100.0	100.0	100.0	85.7	N/A	left phalanges, no vertebral column (no sacral vertebrae/upper body)	no	no	LUC	nitrocellulose glue
GMH	CeII	6749	1932	?Palaeobatrachidae	skeleton	N/A	N/A	58.0	58.3	62.5	44.4	93.5	76.9	88.5	23.1	dorso-ventral	left metacarpals, right phalanges, right toes	no	no	LUC	nitrocellulose glue
GMH	CeI	4951	1930	Pelobatidae	skeleton	N/A	N/A	28.3	75.0	51.7	16.7	100.0	100.0	100.0	40.7	ventral	left humerus, right femur	yes	no	UHM	paraffin wax
GMH	CeII	7130	1931	?Palaeobatrachidae	skeleton (single hindlimb only)	N/A	N/A	92.9	100.0	87.5	14.3	100.0	100.0	100.0	84.6	N/A	toes, tibiofibula	N/A	no	LUC	paraffin wax
GMH	Ce	7197	-	Anura indet.	skeleton (cranium+spine)	N/A	4; 9	6.6	24.0	14.0	6.6	42.9	42.9	42.9	0.0	ventral	N/A	yes	no	-	paraffin wax
GMH	CeII	6750A	1933	?Pelobatidae	skeleton (big anuran)	N/A	N/A	43.4	75.0	71.1	36.7	84.4	100.0	80.0	15.4	ventral	?right radioulna	no	no	LUC	nitrocellulose glue
GMH	CeIV	4980	1933	Pelobatidae	accumulated, disarticulated bones	N/A	5; 9	41.2	100.0	100.0	41.2	66.7	66.7	66.7	0.0	N/A	N/A	no	no	UMC	nitrocellulose glue
GMH	CeII	4983	1932	?Pelobatidae	skeleton	N/A	N/A	56.9	80.0	75.8	41.1	93.9	83.3	90.5	27.5	dorsal	left metacarpals, vertebral column (partly present), left ilium, left and right toes	no	no	LUC	nitrocellulose glue
GMH	CeII	4991	1932	Pelobatidae	skeleton	N/A	2; 7; 8; 9	16.7	62.5	35.7	16.7	82.4	82.4	82.4	0.0	dorso-ventral	N/A	yes	no	LUC	nitrocellulose glue
GMH	CeII	4987	1933	Anura indet.	skeleton	N/A	N/A	50.0	69.6	69.4	34.1	100.0	100.0	100.0	31.9	ventral	left toes and right tibiofibula	no	no	LUC	nitrocellulose glue
GMH	CeV	3012	1934	Anura indet.	skeleton	N/A	3; 9	26.1	59.1	42.5	26.1	53.8	57.1	66.7	0.0	dorso-ventral	N/A	yes	no	MUC	nitrocellulose glue
GMH	LeoV	3477A	1934	Pelobatidae	skeleton	N/A	N/A	75.4	100.0	88.1	53.8	88.2	77.8	85.0	28.6	ventral	left toes and right metatarsals	no	no	MC	nitrocellulose glue
GMH	CeII	4983	1932	Anura indet.	skeleton (cranium only)	N/A	N/A	27.3	27.3	27.3	3.3	100.0	100.0	100.0	87.9	dorsal	vertebral column (after few vertebrae)	no	no	LUC	nitrocellulose glue
GMH	CeII	6751	1932	?Palaeobatrachidae	skeleton	17.3	1; 9	41.8	100.0	81.4	41.8	82.9	96.4	82.1	0.0	ventral	N/A	no	no	LUC	nitrocellulose glue
GMH	CeII	6739	1932	Anura indet.	skeleton	N/A	2; 9	17.8	85.7	40.0	17.8	81.8	100.0	87.5	0.0	ventral	N/A	no	no	LUC	nitrocellulose glue
GMH	CeII	6733	1932	Pelobatidae	skeleton	N/A	N/A	32.4	85.7	64.7	24.4	88.9	87.0	88.9	24.2	ventral	left femur	no	no	LUC	nitrocellulose glue
GMH	CeII	6711	1933	Anura indet.	skeleton	20.5	3; 9	14.4	54.2	31.0	14.4	100.0	100.0	100.0	0.0	dorso-ventral	N/A	yes	no	LUC	nitrocellulose glue
GMH	CeII	6738	1932	Anura indet.	skeleton (upper body only)	N/A	N/A	51.6	90.0	72.2	17.6	100.0	100.0	100.0	65.9	ventral	left phalanges, vertebral column	no	no	LUC	nitrocellulose glue
GMH	CeII	6736	1932	Anura indet.	skeleton (single lower hindlimb only)	N/A	N/A	77.3	100.0	100.0	18.7	100.0	100.0	100.0	75.8	dorso-ventral	tibiofibula	N/A	no	LUC	nitrocellulose glue
GMH	CeII	6737	1932	Anura indet.	skeleton (single lower hindlimb only)	N/A	6; 9	17.6	8.0	16.3	17.6	100.0	100.0	100.0	0.0	dorso-ventral	N/A	N/A	no	LUC	nitrocellulose glue
GMH	CeII	4998	1932	Anura indet.	skeleton (single hindlimb without foot)	N/A	N/A	100.0	100.0	100.0	8.1	45.5	100.0	62.5	86.8	N/A	femur	N/A	no	LUC	nitrocellulose glue
GMH	CeII	6717	1933	Anura indet.	disarticulated bones	N/A	N/A	75.0	75.0	75.0	9.9	75.0	75.0	75.0	86.8	dorso-ventral	vertebral column	N/A	no	LUC	nitrocellulose glue
GMH	CeII	6731	1932	Anura indet.	skeleton	?26.0	N/A	35.3	81.8	66.7	20.7	100.0	100.0	100.0	39.6	ventral	cranium, right radioulna, right femur	no	no	LUC	nitrocellulose glue
GMH	CeII	6735	1932	Pelobatidae	skeleton	23.4	N/A	89.1	100.0	100.0	45.1	100.0	100.0	100.0	49.5	ventral	right humerus (no radioulna, but hand), left and right femur	no	no	LUC	nitrocellulose glue
GMH	CeII	4997	1932	Pelobatidae	skeleton	N/A	N/A	56.8	89.5	77.8	23.6	95.8	100.0	95.8	57.1	dorso-ventral	left and right tibiofibula, left phalanges	yes	no	LUC	nitrocellulose glue
GMH	CeII	4996	1932	Anura indet.	skeleton	N/A	N/A	22.6	48.0	36.4	16.7	60.0	60.0	60.0	20.9	dorso-ventral	left metatarsals (but probably one toe present), right astragalus-calcaneum	yes	no	LUC	nitrocellulose glue
GMH	CeII	6732	1932	?Palaeobatrachidae	skeleton	N/A	N/A	30.8	69.6	51.2	27.0	84.0	77.8	82.6	12.1	dorso-ventral	left toes	yes	no	LUC	nitrocellulose glue
GMH	CeII	4999	1932	Anura indet.	disarticulated bones	N/A	N/A	100.0	100.0	100.0	7.9	25.0	25.0	25.0	90.1	dorso-ventral	left and right ?astragalus-calcaneum	no	no	LUC	nitrocellulose glue
GMH	CeII	4994	1932	Anura indet.	skeleton	N/A	3; 9	12.2	41.7	26.2	12.2	85.7	90.9	85.7	0.0	dorso-ventral	N/A	yes	no	LUC	nitrocellulose glue
GMH	CeIV	6688	1933	?Palaeobatrachidae	skeleton	N/A	N/A	43.8	60.0	67.4	38.5	94.6	100.0	92.6	12.1	dorso-ventral	left metatarsals, left toes	yes	no	UMC	nitrocellulose glue
GMH	CeII	6716	1932	?Palaeobatrachidae	skeleton (lower body only)	N/A	N/A	71.1	88.9	92.9	35.2	100.0	100.0	100.0	50.5	dorso-ventral	right toes, vertebral column (no shoulder)	no	no	LUC	nitrocellulose glue
GMH	CeII	4992	1932	Pelobatidae	skeleton	N/A	N/A	50.9	90.5	76.5	32.2	87.9	90.5	85.7	36.3	dorso-ventral	right toes, left femur	no	no	LUC	nitrocellulose glue
GMH	CeII	6723(1)	1933	Anura indet.	skeleton	35.1	N/A	100.0	100.0	100.0	20.3	88.2	85.7	90.9	69.2	dorso-ventral	cranium, left humerus, right phalanges, left and right femur	no	no	LUC	nitrocellulose glue
GMH	CeII	6760	1932	?Discoglossidae/?Pelobatidae	skeleton	41.8	N/A	39.7	60.9	53.7	34.4	89.7	85.7	87.0	13.2	ventral	left and right phalanges, hip (no ischium, but legs)	no	no	LUC	nitrocellulose glue
GMH	CeII	4995	1932	?Discoglossidae/?Pelobatidae	skeleton	N/A	N/A	53.3	100.0	80.0	17.6	93.8	93.3	93.8	67.0	ventral	right shoulder (no right arm), vertebral column (no hip/right leg, but left femur and tibiofibula), left tibiofibula	no	no	LUC	nitrocellulose glue
GMH	CeII	4962	1932	Palaeobatrachidae	skeleton	34.9	N/A	100.0	100.0	100.0	48.4	95.8	96.2	94.7	51.6	ventral	left tibiofibula, left and right metacarpals, right toes	no	no	LUC	nitrocellulose glue
GMH	CeII	4942	1930	?Palaeobatrachidae	skeleton	36	N/A	77.0	100.0	100.0	51.6	96.0	95.7	97.3	33.0	ventral	left toes, right femur	no	no	LUC	paraffin wax (gypsum frame)
GMH	CeIV	6699	1933	?Palaeobatrachidae	skeleton	N/A	N/A	66.1	31.8	58.3	52.7	96.6	83.3	90.9	16.5	ventral	right phalanges, left toes	no	no	UMC	nitrocellulose glue
GMH	CeII	4959	1932	Anura indet.	skeleton (hindlimbs only)	N/A	N/A	79.5	100.0	100.0	36.0	71.9	33.3	30.8	51.6	dorso-ventral	femur, left toes	N/A	no	LUC	nitrocellulose glue
GMH	CeIV	4961	1933	?Pelobatidae	skeleton	N/A	3; 7; 8; 9	16.9	60.0	39.1	16.9	63.2	57.1	63.2	0.0	dorso-ventral	N/A	yes	no	UMC	nitrocellulose glue

GMH	CeIV	6696	1933	Pelobatidae	skeleton	38.2	N/A	67.2	95.8	86.8	50.0	100.0	100.0	100.0	25.3	dorsal	left toes, right metatarsals	no	no	UMC	nitrocellulose glue
GMH	CeII	4936(1)	1932	Pelobatidae	skeleton	76.7	N/A	83.3	88.0	93.0	67.9	87.7	84.6	89.1	13.2	ventral	right phalanges, left toes	no	no	LUC	nitrocellulose glue
GMH	XXXV	11A	1970	Anura indet.	skeleton	N/A	N/A	100.0	100.0	100.0	37.3	76.2	100.0	76.2	37.4	dorso-ventral	?left radioulna, ?right humerus, hip (no right leg), left toes	no	no	UMC	sediment
GMH	LeoV	3477B	1934	Pelobatidae	skeleton	N/A	1; 7; 8; 9	39.6	92.0	69.8	39.6	75.6	95.0	86.2	0.0	dorso-ventral	N/A	no	no	MC	nitrocellulose glue
GMH	CeIII	1301	1932	Pelobatidae	skeleton	39	N/A	54.4	76.0	71.8	49.4	92.3	85.7	90.0	8.8	ventral	right toes	yes	no	LUC	nitrocellulose glue
GMH	CeIII	1302	1933	?Pelobatidae	skeleton	N/A	N/A	45.9	68.8	58.3	18.7	77.8	69.2	75.0	59.3	dorso-ventral	right phalanges, hip (no ischium, no urostyle, no legs but right femur)	yes	no	LUC	nitrocellulose glue
GMH	CeIII	1312	1932	Pelobatidae	skeleton	69	N/A	52.8	80.0	67.4	41.8	100.0	100.0	100.0	20.9	ventral	left&right toes	yes	no	-	nitrocellulose glue
GMH	CeIII	1537	1932	Pelobatidae	skeleton	33.7	N/A	22.4	50.0	36.4	17.0	88.9	81.8	85.7	23.1	ventral	left tibiofibula	no	no	LUC	nitrocellulose glue
GMH	CeI	4608	1931	Pelobatidae	skeleton	44.8	N/A	61.5	100.0	100.0	44.4	78.3	82.6	82.9	27.5	dorsal	left femur, right metatarsals	no	no	UHM	paraffin wax
GMH	CeIV	4665	1933	Pelobatidae	accumulated, disarticulated bones	N/A	N/A	70.0	60.0	70.0	16.3	75.0	75.0	75.0	72.5	N/A	several unidentified bones	no	no	UMC	nitrocellulose glue
GMH	CeII	4934	1930	Pelobatidae	skeleton	N/A	N/A	49.2	87.0	72.2	31.9	81.8	77.3	82.1	35.2	dorsal	left toes, right tibiofibula	yes	no	LUC	paraffin wax (gypsum frame)
GMH	CeIII	4936	1932	Palaeobatrachidae	skeleton	40	N/A	45.1	100.0	74.2	25.3	96.2	96.2	96.2	44.0	dorsal	left tibiofibula, right astragalus-calcaneum	no	no	LUC	paraffin wax (gypsum frame)
GMH	CeIII	4941	1931	Pelobatidae	skeleton	78.8	N/A	68.6	100.0	84.0	40.0	88.9	100.0	100.0	27.5	ventral	left femur, right tibiofibula (?metatarsals, ?toes present)	no	yes	LUC	paraffin wax (gypsum frame)
GMH	CeII	4943	1930	Pelobatidae	skeleton	N/A	N/A	77.8	95.2	96.2	31.5	82.8	78.3	82.8	58.2	ventral	cranium, right metacarpals, left astragalus-calcaneum, right tibiofibula	no	yes	LUC	paraffin wax (gypsum frame)
GMH	CeII	4946	1930	Pelobatidae	skeleton	37.9	2; 9	12.1	44.0	25.6	12.1	87.5	87.5	87.5	0.0	dorso-ventral	N/A	yes	no	LUC	paraffin wax (gypsum frame)
GMH	CeII	4948	1930	Palaeobatrachidae	skeleton	42.3	N/A	85.3	100.0	100.0	65.2	91.9	100.0	89.2	23.1	ventral	left ?tibiofibula	no	no	LUC	paraffin wax (gypsum frame)
GMH	CeII	4949	1930	Pelobatidae	skeleton	60.7	1; 9	86.8	100.0	100.0	86.8	98.7	100.0	100.0	0.0	ventral	N/A	no	no	LUC	paraffin wax (gypsum frame)
GMH	CeIII	4965	1932	Pelobatidae	skeleton	?29.3	N/A	85.2	93.8	96.9	56.1	95.9	90.9	94.9	30.8	dorsal	left metacarpals, left metatarsals and right toes	no	no	LUC	nitrocellulose glue
GMH	CeIV	4971	1933	Pelobatidae	skeleton	N/A	N/A	59.7	84.0	72.1	47.3	84.1	72.7	78.8	20.9	ventral	left and right toes	no	no	UMC	nitrocellulose glue
GMH	CeIII	4972	1932	?Pelobatidae	skeleton	N/A	N/A	29.3	40.9	44.7	23.0	52.9	44.4	52.9	17.6	dorso-ventral	left and right metatarsals, ?left toes	no	no	LUC	nitrocellulose glue
GMH	CeIII	4973	1931	Pelobatidae	skeleton	N/A	N/A	38.5	75.0	60.0	16.5	75.0	75.0	75.0	57.1	ventral	left and right humerus, right femur	yes	no	LUC	nitrocellulose glue
GMH	CeIII	4977	1932	Pelobatidae	skeleton	N/A	N/A	86.2	77.8	82.6	27.8	73.7	69.2	70.6	67.0	dorso-ventral	left metacarpals, right metacarpals, left and right femur	no	no	LUC	nitrocellulose glue
GMH	CeIII	4979	1931	?Pelobatidae	skeleton	N/A	N/A	23.3	66.7	43.5	12.3	63.6	63.6	63.6	41.8	dorso-ventral	left and right astragalus-calcanium	yes	no	LUC	nitrocellulose glue
GMH	CeIII	4981	1932	Palaeobatrachidae	skeleton	51.5	N/A	45.8	72.7	68.6	39.8	86.7	77.8	84.6	12.1	ventral	left toes	yes	no	LUC	nitrocellulose glue
GMH	CeIII	4984	1933	Palaeobatrachidae	skeleton	N/A	N/A	89.6	87.5	87.2	47.3	87.5	79.2	84.8	47.3	ventral	left and right phalanges, right humerus (no radioulna), left toes + right metatarsals	no	no	LUC	nitrocellulose glue
GMH	CeIII	4985	1932	Palaeobatrachidae	skeleton	N/A	N/A	68.8	95.8	84.4	38.8	100.0	100.0	100.0	40.7	dorsal	left phalanges, left astragalus-calcanium, right metatarsals	no	no	LUC	nitrocellulose glue
GMH	CeIV	6685	1933	Palaeobatrachidae	skeleton	N/A	N/A	35.7	65.2	55.6	23.8	71.4	68.8	71.4	30.8	dorso-ventral	left metatarsals and right metatarsals	yes	no	UMC	nitrocellulose glue
GMH	CeIII	6686	1932	Anura indet.	skeleton	16	N/A	37.5	91.3	65.6	23.1	82.6	82.6	82.6	38.5	ventral	left radioulna, right tibiofibula	no	no	LUC	nitrocellulose glue
GMH	CeIII	6689	1933	?Pelobatidae	skeleton	N/A	N/A	31.0	53.8	41.9	27.8	64.0	71.4	81.8	8.8	N/A	cranium, left toes	yes	no	LUC	nitrocellulose glue
GMH	CeIV	6691	1933	Palaeobatrachidae	skeleton	40.5	N/A	66.7	100.0	96.0	33.0	94.1	100.0	96.4	50.5	ventral	right femur, hip (no left leg)	no	no	UMC	nitrocellulose glue
GMH	CeIV	6692	1933	Pelobatidae	skeleton	N/A	N/A	35.7	52.0	48.8	33.0	90.3	84.6	91.3	7.7	dorsal	left phalanges	yes	no	UMC	nitrocellulose glue
GMH	CeIV	6697	1933	Pelobatidae	skeleton (upper body only)	N/A	N/A	75.0	100.0	88.2	46.2	100.0	100.0	100.0	38.5	dorsal	left toes, right metacarpals, right femur	no	no	UMC	nitrocellulose glue
GMH	CeIII	6698	1932	Pelobatidae	skeleton	54.5	N/A	35.6	56.0	46.5	32.1	92.9	83.3	90.0	8.8	ventral	left toes	yes	no	LUC	nitrocellulose glue
GMH	CeIII	6701	1930	Pelobatidae	skeleton (single lower hindlimb only)	N/A	N/A	100.0	100.0	100.0	17.6	100.0	N/A	100.0	82.4	N/A	toes, astragalus-calcaneum	N/A	no	LUC	paraffin wax (gypsum frame)
GMH	CeII	6706	1930	Pelobatidae	skeleton	N/A	N/A	45.0	93.8	75.0	20.7	81.0	93.3	94.4	51.6	ventral	ilia, hip (no legs)	no	no	LUC	paraffin wax (gypsum frame)
GMH	CeII	6707	1930	Pelobatidae	skeleton	N/A	1; 7; 9	29.9	76.0	59.0	29.9	96.3	94.7	96.0	0.0	ventral	N/A	no	no	LUC	paraffin wax (gypsum frame)
GMH	CeIII	6715	1932	?Pelobatidae	skeleton	N/A	N/A	20.9	60.0	39.1	10.1	61.5	61.5	61.5	50.5	ventral	hip (no legs)	yes	no	LUC	nitrocellulose glue
GMH	CeIII	6719	1932	?Pelobatidae	skeleton	?33.0	N/A	97.7	96.0	97.1	48.8	95.7	92.9	95.1	47.3	ventral	left radioulna, left toes, right phalanges, right toes	no	no	LUC	nitrocellulose glue
GMH	CeIII	6721	1932	?Palaeobatrachidae	skeleton (hindlimb only)	N/A	N/A	50.0	100.0	100.0	12.1	100.0	100.0	100.0	75.8	N/A	tibiofibula (no femur)	N/A	no	LUC	nitrocellulose glue on gypsum
GMH	CeIII	6722	1932	Anura indet.	skeleton	N/A	N/A	27.5	91.7	55.0	14.1	87.5	87.5	87.5	41.8	dorso-ventral	left and right astragalus-calcaneum	no	no	LUC	nitrocellulose glue on gypsum
GMH	CeIII	6726	1932	Palaeobatrachidae	skeleton	N/A	N/A	67.4	100.0	84.8	40.8	100.0	100.0	100.0	33.0	dorsal	?left metacarpals, left metatarsals, right astragalus-calcaneum	no	no	LUC	nitrocellulose glue on gypsum
GMH	CeIII	6728	1932	Pelobatidae	skeleton	N/A	1; 7; 8; 9	52.2	100.0	90.5	52.2	74.5	88.9	91.1	0.0	dorsal	N/A	no	yes	LUC	nitrocellulose glue
GMH	CeIII	6742	1932	Palaeobatrachidae	skeleton (upper body only)	N/A	N/A	100.0	100.0	100.0	24.2	100.0	100.0	100.0	75.8	ventral	left humerus, right phalanges, hip (no legs)	no	no	LUC	nitrocellulose glue
GMH	CeIII	6744	1932	?Pelobatidae	skeleton	N/A	N/A	88.1	92.3	90.3	65.8	90.4	72.7	90.0	22.0	dorso-ventral	cranium, left phalanges, left and right toes	no	no	LUC	nitrocellulose glue
GMH	CeIII	6755	1932	Palaeobatrachidae	skeleton	N/A	N/A	47.8	80.0	70.3	35.2	91.4	87.0	90.0	26.4	dorsal	cranium, left radioulna, right metatarsals	no	no	LUC	nitrocellulose glue
GMH	CeIII	6756	1933	Palaeobatrachidae	skeleton	?4.10	N/A	38.2	83.3	69.0	32.2	100.0	100.0	100.0	15.4	dorsal	right metatarsals	yes	no	LUC	nitrocellulose glue
GMH	CeIII	6834	1932	Pelobatidae	skeleton	54.5	N/A	97.4	95.7	96.7	41.8	86.7	100.0	97.1	57.1	ventral	left metacarpals, right phalanges, left tibiofibula, right astragalus-calcaneum	no	no	LUC	nitrocellulose glue
GMH	CeII	7136	1930	Pelobatidae	skeleton	N/A	3; 9	12.1	44.0	25.6	12.1	92.9	92.9	92.9	0.0	dorso-ventral	N/A	yes	no	LUC	paraffin wax (gypsum frame)
GMH	CeIII	7189	-	Anura indet.	skeleton (hindlimb only)	N/A	6; 9	9.9	16.0	20.9	9.9	100.0	100.0	100.0	0.0	N/A	N/A	N/A	no	-	paraffin wax (gypsum frame)
GMH	CeIII	4664	1933	?Pelobatidae	omitted specimen											N/A				LUC	nitrocellulose glue
GMH	-	4432A	-	Anura indet.	omitted specimen											N/A				-	nitrocellulose glue
GMH	CeIV	4121	1932	Anura indet.	omitted specimen											dorso-ventral				UMC	nitrocellulose glue
GMH	CeIV	4661	1933	Anura indet.	omitted specimen											N/A				UMC	nitrocellulose glue
GMH	CeIV	4660	-	Anura indet.	omitted specimen											N/A				UMC	nitrocellulose glue
GMH	CeIV	4669	1933	Anura indet.	omitted specimen											N/A				UMC	nitrocellulose glue
GMH	CeIV	4656	1933	Anura indet.	omitted specimen											N/A				UMC	nitrocellulose glue
GMH	IL	17B	1969	Anura indet.	omitted specimen											N/A				LMC	nitrocellulose glue
GMH	CeII	6710	1930	Anura indet.	omitted specimen											N/A				LUC	paraffin wax (gypsum frame)
GMH	CeIII	6724	1932	Anura indet.	omitted specimen											N/A				LUC	nitrocellulose glue on gypsum
GMH	CeIII	1311	1931	Anura indet.	omitted specimen											N/A				LUC	nitrocellulose glue on gypsum
GMH	CeVI	4976A	1934	Anura indet.	omitted specimen											N/A				?UMC/?LUC	nitrocellulose glue
GMH	CeIII	6723	1932	Anura indet.	omitted specimen											N/A				LUC	nitrocellulose glue on gypsum
GMH	CeIV	4657	1933	?Palaeobatrachidae	omitted specimen											N/A				UMC	nitrocellulose glue
GMH	CeIV	4952	1933	?Pelobatidae	omitted specimen											dorsal				UMC	nitrocellulose glue
GMH	CeIV	4954	1933	Anura indet.	omitted specimen											N/A				UMC	nitrocellulose glue
GMH	CeIII	1308	1932	Anura indet.	omitted specimen											N/A				LUC	nitrocellulose glue
GMH	CeIV	4663	1933	Anura indet.	omitted specimen											N/A				UMC	nitrocellulose glue
GMH	CeIV	1303	1933	Anura indet.	omitted specimen											N/A				UMC	nitrocellulose glue
GMH	CeIII	1306	-	Anura indet.	omitted specimen											N/A				LUC	nitrocellulose glue
GMH	CeIV	1304	1933	Anura indet.	omitted specimen											N/A				UMC	nitrocellulose glue
GMH	CeIII	6752	1933	Anura indet.	omitted specimen											N/A				LUC	nitrocellulose glue
GMH	CeIII	4986	1933	Anura indet.	omitted specimen											N/A				LUC	nitrocellulose glue
GMH	CeIII	4982	1932	Anura indet.	omitted specimen											dorso-ventral				LUC	nitrocellulose glue
GMH	LeoII	3240	1934	Anura indet.	omitted specimen											N/A				UMC	nitrocellulose glue
GMH	CeIV	6712	1932	Anura indet.	omitted specimen											dorso-ventral				UMC	nitrocellulose glue
GMH	CeII	4974	1932	?Palaeobatrachidae	omitted specimen											N/A				LUC	nitrocellulose glue
GMH	CeI	6702	1930	Anura indet.	omitted specimen											N/A				UHM	paraffin wax (gypsum frame)

SUPPLEMENTARY DATASET 2. Completeness data. Completeness data for each skeletal element in each specimen. Absence and presence of an element represented by a single bone (e.g. left humerus) are coded ‘0’ and ‘1’, respectively. Completeness categories for multi-bone elements (e.g. left phalanges) are defined in the main text and in the table column header. Abbreviations: Ce, ‘Cecilie’ pit; IL, ‘Geiselröhlitz’ site; GMH, Geiseltalmuseum Halle; hyphen (-), unknown; Leo, ‘Leonhard’ pit; Nw, ‘Neumark-West’ pit; N/A, not applicable (e.g. if the element in question is distal to a truncated element); Trunc#, element truncated, but up to # bones present; xx, not confident; XXXV, most likely Neumark-Süd pit (NsXXXV).

Specimen data				Element completeness																											Specimen completeness				Specimen completeness - missing elements distal to truncated elements coded as 'not present'			Specimen completeness - hands/feet omitted				Specimen completeness - phalanges omitted			
museum prefix	site prefix	specimen number	year	cranium: 0, 1	categories for left forelimb phalanges: 0, 3, 6, 9, 10	left metacarpals: 0, 1, 2, 3, 4	left carpals: 0, 1	left radiolina: 0, 1	left humerus: 0, 1	categories for right forelimb phalanges: 0, 3, 6, 9, 10	right metacarpals: 0, 1, 2, 3, 4	right carpals: 0, 1	right radiolina: 0, 1	right humerus: 0, 1	categories for vertebrae: 0, 3, 6, 9	urostyle: 0, 1	ischium: 0, 1	left ilium: 0, 1	right ilium: 0, 1	left femur: 0, 1	left tibiofibula: 0, 1	left astragalus-calcaneum: 0, 1, 2	left tarsals: 0, 1	left metatarsals: 0, 1, 2, 3, 4, 5	categories for left hindlimb phalanges: 0, 3, 6, 9, 12, 14	right femur: 0, 1	right tibiofibula: 0, 1	right astragalus-calcaneum: 0, 1, 2	right tarsals: 0, 1	right metatarsals: 0, 1, 2, 3, 4, 5	categories for right hindlimb phalanges: 0, 3, 6, 9, 12, 14	number of bones for complete specimen (excluding carpals, tarsals, cranium)	number of bones present in specimen (excluding carpals, tarsals, cranium)	number of bones omitted from calculation (N/A, xx)	number of bones per specimen used for calculation (excluding carpals, tarsals, cranium)	number of bones present in specimen (excluding carpals, tarsals, cranium)	number of bones omitted from calculation (xx)	number of bones per specimen used for calculation (excluding carpals, tarsals, cranium)	number of bones for complete specimen (excluding carpals, tarsals, cranium, hands/feet)	number of bones present in specimen (excluding carpals, tarsals, cranium, hands/feet)	number of bones omitted from calculation (N/A, xx)	number of bones per specimen used for calculation (excluding carpals, tarsals, cranium, hands/feet)	number of bones for complete specimen (excluding carpals, tarsals, cranium, phalanges)	number of bones present in specimen (excluding carpals, tarsals, cranium, phalanges)	number of bones omitted from calculation (N/A, xx)	number of bones per specimen used for calculation (excluding carpals, tarsals, cranium, phalanges)
GMH	CelI	6709	1930	1	0	0	0	xx	1	6	1	0	0	1	xx	1	xx	1	1	1	1	2	1	5	9	1	1	2	0	0	0	91	34	11	80	34	11	80	25	13	11	14	43	19	11	32
GMH	CelII	6687	1932	1	0	0	0	0	1	N/A	N/A	N/A	N/A	1	9	1	1	1	1	1	1	2	0	4	6	1	1	2	N/A	N/A	N/A	91	33	34	57	33	0	91	25	23	1	24	43	27	10	33
GMH	CelV	2893	1933	N/A	N/A	N/A	N/A	N/A	N/A	N/A	N/A	N/A	N/A	N/A	N/A	xx	xx	xx	xx	1	1	2	N/A	N/A	N/A	1	1	xx	0	xx	xx	91	6	85	6	6	25	66	25	6	19	6	43	6	37	6
GMH	CelII	4939	1932	1	0	0	0	0	1	0	0	0	1	1	xx	0	0	1	1	N/A	N/A	N/A	N/A	N/A	N/A	N/A	N/A	N/A	N/A	N/A	N/A	91	5	55	36	5	9	82	25	5	17	8	43	5	27	16
GMH	CelII	4126	1932	1	0	0	0	0	1	0	0	0	xx	xx	9	1	0	1	xx	0	0	0	0	0	0	1	0	0	0	0	0	91	13	3	88	13	3	88	25	13	3	22	43	13	3	40
GMH	Ce	9002	-	1	6	2	0	0	1	0	4	1	1	1	9	1	1	1	1	1	N/A	N/A	N/A	N/A	N/A	1	1	2	0	4	Trunc3	91	40	33	58	40	0	91	25	21	3	22	43	31	8	35
GMH	CelII	4935	1931	1	0	0	0	1	1	0	0	0	1	xx	9	1	1	1	1	1	0	0	0	0	0	1	0	0	0	0	0	91	18	1	90	18	1	90	25	18	1	24	43	18	1	42
GMH	CelI	6703	1930	N/A	0	0	0	0	0	0	2	1	1	1	6	1	0	0	0	1	1	2	0	5	3	1	1	0	0	0	0	91	25	0	91	25	0	91	25	15	0	25	43	22	0	43
GMH	CelI	4950	1930	1	9	4	1	1	1	0	0	0	0	0	9	1	1	1	1	1	1	0	0	0	0	1	1	2	1	5	12	91	51	0	91	51	0	91	25	21	0	25	43	30	0	43
GMH	CelI	6700	1930	N/A	0	4	0	1	1	0	0	0	0	1	3	1	0	1	1	1	1	2	0	0	0	1	1	2	1	5	6	91	32	0	91	32	0	91	25	17	0	25	43	26	0	43
GMH	IL	17A	1969	xx	xx	xx	xx	xx	0	0	xx	xx	xx	0	9	0	0	0	0	0	0	0	0	xx	xx	0	0	0	xx	xx	xx	91	9	66	25	9	66	25	25	9	0	25	43	9	18	25
GMH	IL	17C	1969	N/A	N/A	N/A	N/A	N/A	N/A	N/A	N/A	N/A	N/A	N/A	9	N/A	N/A	N/A	N/A	N/A	N/A	N/A	N/A	N/A	N/A	N/A	N/A	N/A	N/A	N/A	N/A	91	9	82	9	9	0	91	25	9	16	9	43	9	34	9
GMH	CelII	6727	1932	N/A	N/A	N/A	N/A	N/A	N/A	N/A	N/A	N/A	N/A	N/A	N/A	N/A	N/A	N/A	N/A	1	1	N/A	N/A	N/A	N/A	1	1	0	0	3	N/A	91	7	80	11	7	0	91	25	4	19	6	43	7	32	11
GMH	CelI	6704	1930	N/A	N/A	N/A	N/A	1	1	N/A	N/A	N/A	N/A	N/A	N/A	N/A	N/A	N/A	N/A	1	1	xx	N/A	N/A	N/A	1	1	N/A	N/A	N/A	N/A	91	6	85	6	6	2	89	25	6	19	6	43	6	37	6
GMH	CelII	6762	1933	1	Trunc3	4	1	1	1	0	0	0	1	1	9	1	1	1	1	1	1	2	0	0	0	1	1	2	0	0	0	91	32	7	84	32	0	91	25	25	0	25	43	29	0	43
GMH	CelII	6718	1932	1	0	0	0	xx	0	0	0	0	xx	1	3	0	0	0	1	1	0	0	0	0	0	0	0	0	0	0	0	91	6	2	89	6	2	89	25	6	2	23	43	6	2	41
GMH	CelII	4956	1932	1	0	0	0	1	1	0	3	1	1	1	6	1	0	1	1	1	1	2	xx	xx	xx	1	1	2	N/A	N/A	N/A	91	24	38	53	24	19	72	25	21	0	25	43	24	10	33
GMH	CelI	6708	1930	1	0	0	0	0	0	0	0	0	0	0	9	N/A	N/A	0	0	N/A	N/A	N/A	N/A	N/A	N/A	N/A	N/A	N/A	N/A	N/A	N/A	91	9	48	43	9	0	91	25	9	10	15	43	9	20	23
GMH	CeI	4947	1930	1	0	0	0	0	0	6	4	1	1	1	9	xx	xx	1	1	1	1	0	0	0	0	1	1	0	0	0	0	91	27	2	89	27	2	89	25	17	2	23	43	21	2	41
GMH	CelII	4975	1932	1	0	xx	0	1	1	0	0	0	0	0	0	0	xx	0	0	1	1	2	0	5	Trunc6	0	0	2	N/A	N/A	N/A	91	19	32	59	19	5	86	25	8	1	24	43	13	10	33
GMH	CelI	4940	1931	N/A	N/A	N/A	N/A	N/A	N/A	N/A	N/A	N/A	N/A	N/A	N/A	N/A	N/A	N/A	N/A	1	1	xx	N/A	N/A	N/A	1	1	N/A	N/A	N/A	N/A	91	4	87	4	4	2	89	25	4	21	4	43	4	39	4
GMH	CelII	6725	1932	N/A	N/A	N/A	N/A	N/A	N/A	N/A	N/A	N/A	N/A	N/A	N/A	N/A	N/A	N/A	N/A	xx	1	2	0	5	6	N/A	N/A	N/A	N/A	N/A	N/A	91	14	69	22	14	1	90	25	3	22	3	43	8	35	8
GMH	CelI	4944	1930	1	N/A	N/A	N/A	1	1	N/A	N/A	N/A	N/A	N/A	3	N/A	N/A	N/A	N/A	N/A	N/A	N/A	N/A	N/A	N/A	1	1	2	0	N/A	N/A	91	9	76	15	9	0	91	25	9	10	15	43	9	28	15
GMH	CelII	6720	1932	1	0	0	0	0	xx	0	0	0	0	1	9	0	0	0	1	0	0	0	0	0	0	0	0	0	0	0	0	91	11	1	90	11	1	90	25	11	1	24	43	11	1	42
GMH	CeVI	4976B	1934	N/A	N/A	N/A	N/A	N/A	N/A	N/A	N/A	N/A	N/A	N/A	N/A	N/A	N/A	N/A	N/A	1	1	2	0	3	0	1	1	2	0	5	6	91	22	45	46	22	0	91	25	8	17	8	43	16	25	18
GMH	CelII	4968	1932	xx	0	0	0	1	1	0	0	0	0	0	9	1	0	1	1	1	1	2	0	5	xx	1	1	2	0	5	3	91	35	14	77	25	22	0	25	43	32	0	43
GMH	CelII	4989	1932	1	0	0	0	0	1	N/A	N/A	N/A	1	1	0	0	0	0	0	1	1	2	N/A	xx	N/A	xx	1	xx	N/A	N/A	N/A	91	8	55	36	8	8	83	25	8	3	22	43	8	17	26
GMH	CelV	4953	1933	1	xx	xx	xx	xx	xx	0	0	0	1	0	3	xx	xx	0	0	1	1	xx	xx	xx	xx	1	1	xx	0	xx	xx	91	8	60	31	8	60	31	25	8	8	17	43	8	22	21
GMH	CelII	4958	1933	1	0	0	0	0	0	6	4	1	1	1	9	1	1	1	0	1	1	2	0	5	0	0	0	0	0	0	0	91	33	0	91	33	0	91	25	18	0	25	43	27	0	43
GMH	CelV	4960	1933	1	N/A	xx	N/A	N/A	xx	N/A	xx	N/A	N/A	N/A	6	N/A	1	1	1	1	1	1	0	5	3	N/A	N/A	N/A	N/A	N/A	N/A	91	20	56	35	20	9	82	25	12	9	16	43	17	22	21
GMH	CelV	4955	1933	1	0	0	0	0	1	0	0	0	0	0	3	1	1	1	1	1	1	1	0	0	0	1	0	0	0	0	0	91	12	0	91	12	0	91	25	12	0	25	43	12	0	43
GMH	CelV	4957	1933	xx	3	4	1	1	1	3	4	1	1	1	9	1	xx	xx	1	1	1	2	0	5	3	1	1	2	0	xx	3	91	48	7	84	48	7	84	25	23	2	23	43	36	7	36
GMH	CelII	4967	1932	1	0	0	0	0	1	N/A	N/A	N/A	N/A	1	9	1	1	1	1	1	1	2	0	0	0	1	N/A	N/A	N/A	N/A	N/A	91	20	37	54	20	0	91	25	20	4	21	43	20	13	30
GMH	CelII	6729	1932	1	N/A	N/A	N/A	1	1	0	0	0	0	1	9	1	N/A	1	1	1	1	N/A	N/A	N/A	N/A	N/A	N/A	N/A	N/A	N/A	N/A	91	17	59	32	17	0	91	25	17	7	18	43	17	21	22
GMH	CelII	6761	1932	1	0	0	0	0	1	Trunc9	4	1	1	1	9	1	1	1	1	0	0	0	0	0	0	1	1	2	N/A	N/A	N/A	91	33	20	71	33	0	91	25	20	0	25	43	24	5	38
GMH	CelV	2895	1933	xx	0	0	0	0	0	0	0	0	0	0	0	0	0	xx	xx	1	1	2	0	0	0	xx	xx	2	0	0	0	91	6	4	87	6	4	87	25	6	4	21	43	6	4	39
GMH	CelII	1305	1933	N/A	N/A	N/A	N/A	N/A	N/A	N/A	N/A	N/A	N/A	N/A	N/A	N/A	N/A	N/A	N/A	N/A	1	2	0	4	0	N/A	1	2	0	5	N/A	91	15	61	30	15	0	91	25	6	19	6	43	15	27	16
GMH	CelII	6748	1932	1	0	0	0	1	1	0	0	0	0	xx	9	1	0	1	1	1	1	N/A	N/A	N/A	N/A	1	1	N/A	N/A	N/A	N/A	91	18	43	48	18	1	90	25	18	5	20	43	18	15	28
GMH	CelII	6747	1932	1	0	0	0	0	0	0	0	0	0	0	0	0	0	0	0	xx	1	0	0	xx	3	xx	xx	0	0	xx	3	91	7	13	78	7	13	78	25	1	3	22	43	1	13	30
GMH	CelII	1307	1933	N/A	3	3	1	1	1	3	xx	0	1	1	3	1	1	1	1	1	N/A	xx	N/A	xx	N/A	N/A	N/A	N/A	N/A	N/A	N/A	91	21	49	42	21	11	80	25	12	7	18	43	15	21	22
GMH	CelII	4988	1932	N/A	N/A	N/A	N/A	N/A	N/A	N/A	N/A	N/A	N/A	N/A	N/A	N/A	N/A	N/A	N/A	1	1	2	0	xx	N/A	xx	1	xx	N/A	xx	N/A	91	5	86	5	5	13	78	25	5	20	5	43	5	38	5
GMH	CelII	6740	1933	N/A	N/A	N/A	N/A	N/A	N/A	N/A	N/A	N/A	N/A	N/A	3	xx	1	1	1	1	1	2	0	4	Trunc3	1	1	0	0	xx	N/A	91	19	63	28	19	6	85	25	12	5	20	43	16	18	25
GMH	CelII	6743	1932	1	0	0	0	0	0	Trunc3	4	1	1	1	9	1	N/A	1	1	N/A	N/A	N/A	N/A	N/A	N/A	N/A	N/A	N/A	N/A	N/A	N/A	91	21	54	37	21	0	91	25	14	9	16	43	18	19	24
GMH	CelII	6754A	1933	1	0	xx	0	0	0	N/A	N/A	N/A	1	1	9	1	N/A	1	1	N/A	N/A	N/A	N/A	N/A	N/A	1	N/A	N/A	N/A	N/A	N/A	91	15	64	27	15	4	87	25	15	8	17	43	15	26	17
GMH	CelII	4990	1932	1	Trunc3	4	1	1	1	0	0	0	0	xx	9	1	0	1	1	0	0	0	0	0	0	0	0	0	0	0	0	91	21	8	83	21	1	90	25	14	1	24	43	18	1	42
GMH	CelII	6745	1932	1	N/A	N/A	N/A	N/A	N/A	1	3	4	1	1	9	1	N/A	N/A	1	N/A	N/A	N/A	N/A	N/A	N/A	1	N/A	N/A	N/A	N/A	N/A	91	22	62	29	22	0	91	25	15	10	15	43	19	24	19
GMH	CelII	6754B	1933	1	N/A	N/A	1	1	1	9	4	1	1	1	9	1	xx	0	1	1	0	0	0	0	0	1	1	2	N/A	N/A	N/A	91	33	34	57	33	1	90	25	20	1	24	43	24	10	33
GMH	CeXIV	1275	1954	N/A	N/A	N/A	N/A	N/A	N/A	N/A	N/A	N/A	N/A	N/A	N/A	1	1	1	1	1	1	2	N/A	N/A	N/A	1	N/A	N/A	N/A	N/A	N/A	91	9	82	9	9	0	91	25	9	16	9	43	9	34	9
GMH	CelII	6759	1932	1	N/A	Trunc3	xx	1	1	3	4	1	1	1	9	1	1	1	1	0	0	0	0	0	0	1	1	N/A	N/A	N/A	N/A	91	29	32	59	29	0	91	25	19	2	23	43	26	8	35
GMH	CelII	4978	1932	1	6	4	1	1	1	9	4	0	1	1	9	1	1	1	1	1	N/A	N/A	N/A	N/A	N/A	1	0	0	0	0	0	91	42	22	69	42	0	91	25	19	3	22	43	27	8	35
GMH	CelII	6757	1932	1	Trunc3	3	1	1	1	0	0	0	1	1	9	0	N/A	1	0	1	0	0	0	0	0	N/A	N/A	N/A	N/A	N/A	N/A	91	21	31	60	21	0	91	25	15	5	20	43	18	10	33
GMH	CelII	6693	1933	1	Trunc3	xx	0	1	1	N/A	N/A	N/A	N/A	N/A	N/A	N/A	N/A	1	N/A	1	1	N/A	N/A	N/A	N/A	xx	N/A	N/A	N/A	N/A	N/A	91	8	83	8	8	5	86	25	5	20	5	43	5	38	5
GMH	CelII	6749	1932	1	N/A	Trunc2	1	1	0	Trunc6	4	1	1	xx	3	1	0	1	0	0	1	2	0	0	0	1	1	2	0	5	Trunc9	91	40	22	69	40	1	90	25	14	1	24	43	25	3	40
GMH	CeI	4951	1930	1	N/A	N/A	N/A	N/A	1	0	0	0	0	1	9	1	xx	1	1	0	0	0	0	0	0	1	N/A	N/A	N/A	N/A	N/A	91	15	38	53	15	1	90	25	15	5	20	43	15	14	29
GMH	CelI	7130	1931	N/A	N/A	N/A	N/A	N/A	N/A	N/A	N/A	N/A	N/A	N/A	N/A	N/A	N/A	N/A	N/A	N/A	1	2	1	4	Trunc6	N/A	N/A	N/A	N/A	N/A	N/A	91	13	77	14	13	0	91	25	3	22	3	43	7	35	8
GMH	Ce	7197	-	1	0	0	0	0	0	0	0	0	0	0	6	0	0	0	0	0	0	0	0	0	0	0	0	0	0	0	0	91	6	0	91	6	0	91	25	6	0	25	43	6	0	43

| | | |

SUPPLEMENTARY DATASET 3. Articulation data. Articulation data for each joint in each specimen. Disarticulation and articulation of a single joint (e.g. left radioulna-humerus) are coded ‘0’ and ‘1’, respectively. Articulation categories for multi-joint elements (e.g. left phalanges) are defined in the main text and in the table column header. Abbreviations: Ce, ‘Cecilie’ pit; IL, ‘Geiselröhlitz’ site; GMH, Geiseltalmuseum Halle; hyphen (-), unknown; Leo, ‘Leonhard’ pit; Nw, ‘Neumark-West’ pit; N/A, not applicable (e.g. if the element in question is distal to a truncated element); Trunc#, element truncated, but up to # bones present; xx, not confident; XXXV, most likely Neumark-Süd pit (NsXXXV).

| Specimen data | | | | Element articulation | | | |

| | | |